

SAMUEL RODRIGUES DOS SANTOS JÚNIOR

Biodistribuição De Nanopartículas De Quitosana Complexadas Com O Peptídeo Imunomodulador P10 E Avaliação De Sua Associação Com Anticorpos Monoclonais Sintéticos No Tratamento Da Paracoccidiodomicose Em Modelo Experimental Murino.

Tese apresentada ao Programa de Pós-Graduação em Microbiologia do Instituto de Ciências Biomédicas da Universidade de São Paulo, para obtenção do Título de Doutor em Ciências.

São Paulo

2022

SAMUEL RODRIGUES DOS SANTOS JÚNIOR

Biodistribuição De Nanopartículas De Quitosana Complexadas Com O Peptídeo Imunomodulador P10 E Avaliação De Sua Associação Com Anticorpos Monoclonais Sintéticos No Tratamento Da Paracoccidioidomicose Em Modelo Experimental Murino.

Tese apresentada ao Programa de Pós-Graduação em Microbiologia do Instituto de Ciências Biomédicas da Universidade de São Paulo, para obtenção do Título de Doutor em Ciências.

Área de concentração: Microbiologia

Orientador: Prof Dr. Carlos Pelleschi Taborda

Coorientador: Prof Dr. André Corrêa Amaral

Versão Original

São Paulo

2022

CATALOGAÇÃO NA PUBLICAÇÃO (CIP)

Serviço de Biblioteca e informação Biomédica do Instituto de Ciências Biomédicas
da Universidade de São Paulo

Ficha Catalográfica elaborada pelo(a) autor(a)

Rodrigues Dos Santos Júnior, Samuel

Biodistribuição De Nanopartículas De Quitosana Complexadas Com O Peptídeo Imunomodulador P10 E Avaliação De Sua Associação Com Anticorpos Monoclonais Sintéticos No Tratamento Da Paracoccidiodomicose Em Modelo Experimental Murino. / Samuel Rodrigues Dos Santos Júnior; orientador Carlos Pelleschi Taborda; coorientador André Corrêa Amaral. -- São Paulo, 2022. p.87

Tese (Doutorado) - Universidade de São Paulo, Instituto de Ciências Biomédicas.

1. PCM. 2. Nanopartículas de quitosana. 3. Biodistribuição . 4. Fluorescência . 5. Vacina Intranasal . I. Pelleschi Taborda, Carlos, orientador. II. Corrêa Amaral, André , coorientador. III. Título.

UNIVERSIDADE DE SÃO PAULO
INSTITUTO DE CIÊNCIAS BIOMÉDICAS

Candidato: Samuel Rodrigues Dos Santos Júnior

Título da Tese: **Biodistribuição De Nanopartículas De Quitosana Complexadas Com O Peptídeo Imunomodulador P10 E Avaliação De Sua Associação Com Anticorpos Monoclonais Sintéticos No Tratamento Da Paracoccidioidomicose Em Modelo Experimental Murino.**

Orientador: Carlos Pelleschi Taborda

Coorientador: André Corrêa Amaral

A Comissão Julgadora dos trabalhos de Defesa de Tese de Doutorado em sessão pública realizada em dia/mês/ano, considerou o candidato

() Aprovado () Reprovado

Examinador(a): Assinatura:

Nome:

Instituição:

Examinador(a): Assinatura:

Nome:

Instituição:

Examinador(a): Assinatura:

Nome:

Instituição:

CERTIFICADO

Certificamos que a proposta intitulada "Biodistribuição de nanopartículas de quitosana complexadas com o peptídeo imunomodulador P10 e avaliação de sua associação com anticorpos monoclonais sintéticos no tratamento da paracoccidiodomicose em modelo experimental murino.", protocolada sob o CEUA nº 3654290618, sob a responsabilidade de **Carlos Pelleschi Taborda** e equipe; *Samuel Rodrigues dos Santos Júnior* - que envolve a produção, manutenção e/ou utilização de animais pertencentes ao filo Chordata, subfilo Vertebrata (exceto o homem), para fins de pesquisa científica ou ensino - está de acordo com os preceitos da Lei 11.794 de 8 de outubro de 2008, com o Decreto 6.899 de 15 de julho de 2009, bem como com as normas editadas pelo Conselho Nacional de Controle da Experimentação Animal (CONCEA), e foi **aprovada** pela Comissão de Ética no Uso de Animais da Instituto de Ciências Biomédicas (Universidade de São Paulo) (CEUA-ICB/USP) na reunião de 22/04/2019.

We certify that the proposal "Biodistribution of chitosan nanoparticles complexed with the P10 immunomodulatory peptide and evaluation of its association with synthetic monoclonal antibodies in the treatment of paracoccidiodomycosis in a murine experimental model.", utilizing 480 isogenics mice (480 males), protocol number CEUA 3654290618, under the responsibility of **Carlos Pelleschi Taborda** and team; *Samuel Rodrigues dos Santos Júnior* - which involves the production, maintenance and/or use of animals belonging to the phylum Chordata, subphylum Vertebrata (except human beings), for scientific research purposes or teaching - is in accordance with Law 11.794 of October 8, 2008, Decree 6899 of July 15, 2009, as well as with the rules issued by the National Council for Control of Animal Experimentation (CONCEA), and was **approved** by the Ethic Committee on Animal Use of the Biomedical Sciences Institute (University of São Paulo) (CEUA-ICB/USP) in the meeting of 04/22/2019.

Finalidade da Proposta: **Pesquisa (Acadêmica)**

Vigência da Proposta: **48 meses**

Depto/Setor: **Microbiologia**

Origem: **Biotério Central FMUSP**

Espécie: **Camundongos isogênicos**

sexo: **Machos**

Idade ou peso: **6 a 8 semanas**

Linhagem: **BALB/c**

N amostral: **465**

Origem: **Biotério Central FMUSP**

Espécie: **Camundongos isogênicos**

sexo: **Machos**

Idade ou peso: **6 a 8 semanas**

Linhagem: **BALB/c Nude**

N amostral: **15**

São Paulo, 12 de agosto de 2019



Prof. Dra. Luciane Valéria Sita

Coordenadora da Comissão de Ética no Uso de Animais
Instituto de Ciências Biomédicas (Universidade de São Paulo)



Dr. Alexandre Ceroni

Vice-Coodenador da Comissão de Ética no Uso de Animais
Instituto de Ciências Biomédicas (Universidade de São Paulo)

À minha família e amigos pelo apoio e incentivo em todas as horas.

AGRADECIMENTOS

Agradeço ao meu orientador Prof. Dr. Carlos Pelleschi Taborda, pela oportunidade de ter realizado este trabalho, pela confiança em deixar uma pesquisa de tamanha relevância em minhas mãos, pelos ensinamentos e aprendizados que obtive ao longo destes 6 anos, principalmente na área da microbiologia com ênfase em micologia e por estar presente para dar conselhos e achar soluções e alternativas para diversos problemas.

Agradeço ao Prof. Dr. André Corrêa Amaral, por ter aceitado ser meu coorientador e por ter embarcado na parceria de desenvolver uma vacina com bases nanotecnológicas para o tratamento da paracoccidiodomicose. Agradeço também por estar presente para dar conselhos e achar soluções e alternativas para diversos problemas.

Agradeço os colegas de Laboratório de Fungos Dimórficos Patogênicos (LFDP) pelos auxílios, amizades e companheirismo.

Agradeço ao Prof. Dr. Arturo Casadevall, por ter me recebido por cerca de 16 meses em seu laboratório na *Johns Hopkins University Bloomberg School of Public Health* em Baltimore, Maryland - USA, para a realização de meu doutorado sanduíche.

Agradeço a Dra. Livia Liporagi Lopes, colega no laboratório de Prof. Arturo Casadevall, amiga e inspiração, por ter me recebido e ensinado praticamente tudo o que hoje sei sobre o cultivo e cuidado de *Cryptococcus Neoformans*, entre outros experimentos, sem os quais a conclusão do meu projeto não seria possível.

Agradeço os colegas do Laboratório do Prof. Arturo (Casadevalles), pelos ensinamentos, amizades e companheirismo.

Agradeço a Zita Maria de Oliveira Gregório, pela disposição, paciência e amizade que demonstrou por mim desde a primeira vez que vim ao laboratório.

Agradeço ao Msc. Shahab Zaki Pour e ao Dr. Marielton dos Passos Cunha, pelo auxílio nos ensaios de PCR e pela ajuda na análise de dados do sequenciamento do RNA total.

Agradeço a equipe do Laboratório de análises genômicas e sequenciamento da *Johns Hopkins University: Bloomberg School of Public Health* em Baltimore, Maryland - USA, Anne Jedlicka e Amanda Dziedzic. Pelo auxílio com o sequenciamento do RNA total e controle de qualidade.

Agradeço aos funcionários das secretarias da pós-graduação pelo suporte e serviços prestados durante o período do doutorado.

Agradeço a minha família pelo apoio e carinho.

AGRADECIMENTO AS AGÊNCIAS DE FOMENTO

Agradeço a Fundação de Amparo à Pesquisa do Estado de São Paulo (FAPESP 2016/08730-6), Conselho Nacional de Desenvolvimento Científico e Tecnológico (CNPq 420480/2018-8 e 134424/2016-6) e Coordenação de Aperfeiçoamento de Pessoal de Nível Superior–Brasil (CAPES 88882.333055/2019-01) pelo apoio financeiro.

This is the way

Din Djarin, The Mandalorian-Disney+, 2019

RESUMO

A Paracoccidioidomicose (PCM) é uma doença fúngica causada pelos fungos termodimórficos do gênero *Paracoccidioides* spp. Esta micose inicia-se pela inalação de propágulos fúngicos que, ao atingirem o pulmão, se transformam nas leveduras patogênicas, causando a doença. A PCM é uma doença granulomatosa e que pode apresentar duas formas clínicas principais, aguda/subaguda ou crônica. A evolução ou a contenção da doença depende da resposta imunológica gerada pelo hospedeiro. A forma aguda/subaguda acomete geralmente crianças, adolescentes, e jovens adultos; pessoas imunocomprometidas também podem ser afetadas. A forma crônica acomete principalmente homens com idade acima dos 30 anos, devido a um declínio da robustez do sistema imunológico, focos antigos podem ser reativados fazendo com que as leveduras contidas nos granulomas, principalmente nos pulmões, se espalhem gerando uma doença disseminada ou fiquem contidas em um único órgão. O tratamento da PCM é feito com quimioterápicos, mas uma significativa parte dos pacientes acabam abandonando o tratamento, devido aos efeitos colaterais e ao prolongado período de tratamento. O uso de anticorpos monoclonais no controle da PCM foi estudado experimentalmente sendo alguns destes anticorpos promissores no controle da doença. A terapia baseada em anticorpos monoclonais ainda é restrita, mesmo em pesquisas científicas, devido ao alto custo de produção e o nível de especialização necessário para produzi-lo e purificá-lo, gerando assim grande demanda para novas formas de expressão heterólogas, possíveis somente pelo sequenciamento dos genes responsáveis pela produção dos anticorpos. O uso de vacinas (terapêuticas) que promovam resposta imune celular robusta, principalmente dos tipos Th₁ e Th₁₇, pode ser uma alternativa combinada ao tratamento convencional. Ao longo do tempo já foi demonstrado que o peptídeo P10 de *P.brasiliensis* é capaz de promover a resposta imune Th₁ e Th₁₇ levando a redução da carga fúngica, mas seu uso ainda precisa ser otimizado sendo complexado ou co-administrado com nanopartículas de quitosana pela via intranasal. A utilização de nanopartículas de quitosana reduziu a quantidade de peptídeo P10 utilizado para a estimulação do sistema imune. O número de doses necessárias efetivas para ativação da resposta celular e redução da carga fúngica foram alvo de nosso estudo. A utilização de nanopartículas de quitosana fluorescentes demonstrou que uma significativa quantidade de nanopartículas ficam aderidas nas mucosas das vias aéreas superiores, estimulando o

sistema imune a promover uma resposta celular do tipo Th₁ e Th₁₇, reduzindo a carga fúngica dos pulmões e se provando como uma excelente candidata para o tratamento da PCM.

Palavras-chave: 1. PCM. 2. Nanopartículas de quitosana. 3. Biodistribuição. 4. Fluorescência. 5. Vacina Intranasal.

ABSTRACT

Paracoccidioidomycosis (PCM) is a fungal disease caused by thermally dimorphic fungi of the genus *Paracoccidioides*. This mycosis begins by inhaling fungal propagules that, upon reaching the lung, turn into pathogenic yeasts, causing the disease. PCM is a granulomatous disease and may present two main clinical forms, acute/subacute or chronic. The evolution or containment of the disease depends on the immune response generated by the host. The acute/subacute form usually affects children, adolescents, and young adults and immunocompromised people may also be affected. The chronic form mainly affects men over the age of 30, due to a decline in the robustness of the immune system when the fungi in the ancient *foci* can be reactivated causing the yeasts contained in the granulomas, especially in the lungs, to spread generating a disseminated disease or to be contained in a single organ. The treatment of PCM is usually done with chemotherapy drugs, but most patients end up abandoning the treatment, due to the enormous side effects and prolonged treatment. The use of monoclonal antibodies in the fight against PCM was analyzed and some of these antibodies showed good fungal load reduction, but their use is still restricted, even in scientific research, due to the high cost of production and the level of specialization necessary to produce and purify them, thus generating great demand for new heterologous forms of expression, possible only by sequencing the genes responsible to produce antibodies. Another way to treat PCM would be with the use of vaccines that promote a robust cellular immune response, mainly of the Th₁ and Th₁₇ types, which would be a way to improve or replace the existing treatment. Over time, it has been demonstrated that the P10 peptide is able to promote the desired immune response, leading to a reduction in the fungal load, but its use is still being optimized. Its optimization took place through its use complexed or co-administered within chitosan nanoparticles via the intranasal route. With the use of chitosan nanoparticles it was possible to reduce the amount of P10 peptide used to stimulate the immune system, the possibility of reducing the number of vaccine doses was demonstrated, the use of adjuvants was discarded, since chitosan nanoparticles exert this function and it was also verified by fluorescent nanoparticles that, most of the nanoparticles are adhered to the mucosa of the upper airways, stimulating the immune system to promote a cellular response of the Th₁ and Th₁₇ type, reducing the fungal load of the lungs and proving itself as a an excellent candidate for the treatment of PCM.

Keywords: 1. PCM. 2. Chitosan nanoparticles. 3. Biodistribution. 4. Fluorescence. 5. Intranasal Vaccine

LISTA DE FIGURAS

- Figura 1.** Lista de fungos de interesse médico de média prioridade divulgada pela organização mundial da saúde em 2022. 24
- Figura 2.** Mapa da distribuição epidemiológica da PCM nas américas, mostrando as principais zonas epidemiológicas, com destaque para o Brasil (vermelho), Colômbia, Venezuela e norte da Argentina..... 25
- Figura 3.** Mapa epidemiológico da PCM mostrando as principais zonas epidemiológicas no Brasil. Os estados que classicamente são mais acometidos pela PCM encontram-se na região centro sul do país, mas ultimamente devido ao desmatamento da floresta amazônica a região norte se tornou uma área de hiperendemicidade..... 26
- Figura 4.** Protocolo para PCR com as temperaturas e ciclagens da *nasted* PCR para as cadeias pesadas e leves dos anticorpos..... 40
- Figura 5.** Fluxograma de trabalho para montagem e análise das sequências obtidas por meio de softwares de bioinformática..... 42
- Figura 6.** Código em python do programa Bowtie2 utilizado para fazer o alinhamento e montagem das sequências do mRNA sequenciado. 43
- Figura 7.** Código em python do programa SPAdes V3.14 .1 utilizado para fazer o alinhamento e montagem de novo das sequências do mRNA sequenciado. 44
- Figura 8.** Eletroforese eletrônica do RNA ScreenTape mostrando a qualidade da extração do RNA total (sem arraste), e com a presença de bandas bem definidas, principalmente as bandas relacionadas com a maior porção de RNA presente nas células (RNA ribossomal 28s e 18s). [nt] = Quantidade de nucleotídeos do lader, A0(L) = lader, A1 = RNA total do hibridoma 3E e B1 = RNA total do hibridoma F1.4..... 45
- Figura 9.** Gráfico de intensidade do RNA ScreenTape mostrando a intensidade das moléculas de RNA total extraídas dos hibridomas, com a presença de bandas bem picos bem definidos, como os picos relacionadas com a maior porção de RNA presente nas células (RNA ribossomal 28s e 18s). 45
- Figura 10.** Representação das sequências e mapas montados pelos softwares de bioinformática para o hibridoma 3E, mostrando cerca de 10 milhões de sequências com até 17000 bases..... 46
- Figura 11.** Representação das sequências e mapas montados para o hibridoma 3E, mostrando cerca de 2600 sequências com até 1900 bases..... 47
- Figura 12.** Imagem da fluorescência obtida com IVIS Spectrum mostrando os camundongos posicionados em decúbito ventral, mostrando a fluorescência na via aérea superior do BALB/c nude após a inoculação de 5 µL por narina das nanopartículas fluorescentes de quitosana Cy5.5 em 0 horas (C+) inoculado apenas com o fluorocromo (Cy5.5), (C-) inoculado com PBS e (NP) inoculado com as nanopartículas fluorescentes. 53

Figura 13. Imagem da fluorescência obtida com IVIS Spectrum mostrando os camundongos posicionados em decúbito dorsal, mostrando a fluorescência na via aérea superior do camundongo BALB/c nude após inoculação de 5 µL por narina das nanopartículas fluorescentes de quitosana Cy5.5 em 0 horas (C+) inoculado apenas com o fluorocromo (Cy5.5), (C-) inoculado com PBS e (NP) inoculado com as nanopartículas fluorescentes.	54
Figura 14 Imagem da fluorescência obtida com IVIS Spectrum mostrando os camundongos posicionados em decúbito dorsal mostrando a fluorescência na via aérea superior do camundongo BALB/c nude após inoculação de 5 µL por narina das nanopartículas de quitosana Cy5.5 fluorescentes em 96 horas. (C+) inoculado apenas com o fluorocromo (Cy5.5), (C-) inoculado com PBS e (NP) inoculado com as nanopartículas fluorescentes.	55
Figura 15. Imagem da fluorescência obtida com IVIS Spectrum mostrando os camundongos posicionados em decúbito dorsal mostrando a fluorescência na via aérea superior do camundongo BALB/c nude após inoculação de 5 µL por narina das nanopartículas de quitosana Cy5.5 fluorescentes em 96 horas. (C+) inoculado apenas com o fluorocromo (Cy5.5), (C-) inoculado com PBS e (NP) inoculado com as nanopartículas fluorescentes.	55
Figura 16. Imagem da fluorescência obtida com IVIS Spectrum mostrando o pulmão (P), traqueia (T) e estômago (E), após inoculação de 5 µL por narina das nanopartículas fluorescentes de quitosana Cy5.5 (NP) em 0 horas.	56
Figura 17. Imagem da fluorescência obtida com IVIS Spectrum mostrando o pulmão (P), traqueia (T) e estômago (E) e cérebro (C), após inoculação de 5 µL por narina das nanopartículas fluorescentes de quitosana Cy5.5 em 96 horas.	57
Figura 18. Imagem da fluorescência obtida com IVIS Spectrum mostrando o pulmão (P), traqueia (T) e estômago (E), cérebro (C), fígado (F) e intestinos (I) após inoculação de 5 µL por narina de PBS em 0 horas.	57
Figura 19. Imagem da fluorescência obtida com IVIS Spectrum mostrando o pulmão (P), traqueia (T) e estômago (E) e cérebro (C), após inoculação de 5 µL por narina PBS em 96 horas.	58
Figura 20. Intensidade fluorescente da região de interesse (ROI) ao longo do tempo, mostrando que a fluorescência foi estável durante todos os momentos para o grupo NP, e uma redução significativa da fluorescência para o grupo C+ nas primeiras 24 horas $p < 0,001$	58
Figura 21. Fagocitose das nanopartículas de quitosana marcadas com FITC por macrófagos alveolares em 0 e 8 horas, mostrando as nanopartículas dentro dos lisossomos celulares após 8 horas. O filtro DAPI mostra os núcleos, o filtro FITC mostra as nanopartículas e o filtro RFP indica os lisossomos.	59
Figura 22. Fagocitose das nanopartículas de quitosana marcadas com FITC por macrófagos alveolares, mostrando as nanopartículas dentro dos lisossomos celulares após 8 horas. O filtro DAPI mostra os núcleos, o filtro FITC mostra as nanopartículas e o filtro RFP indica os lisossomos.	60

- Figura 23.** Fagocitose das nanopartículas de quitosana marcadas com FITC por macrófagos peritoneais em 0 e 8 horas, mostrando as nanopartículas dentro dos lisossomos celulares em 8 horas. O filtro DAPI mostra os núcleos, o filtro FITC mostra as nanopartículas e o filtro RFP indica os lisossomos..... 61
- Figura 24.** Fagocitose das nanopartículas de quitosana marcadas com FITC por macrófagos peritoneais, mostrando as nanopartículas dentro dos lisossomos celulares após 8 horas. O filtro DAPI mostra os núcleos, o filtro FITC mostra as nanopartículas e o filtro RFP indica os lisossomos. 62
- Figura 25.** Gráfico demonstrativo do tamanho e PDI das nanopartículas de quitosana vazias. 67
- Figura 26.** Gráfico demonstrativo do tamanho e PDI das nanopartículas de quitosana complexadas com o peptídeo P10. 67
- Figura 27.** Peso dos pulmões após a eutanásia (51 dias após a infecção). Houve aumento significativo do peso pulmonar dos animais infectados quando comparados ao grupo **SHAM**. **SHAM** (não infectado e não tratado), **Pb18** (infectado e não tratado), **Comp** (infectado e tratado com as nanopartículas complexadas com P10) e **Ncomp** (infectado e tratado com o P10 associado às nanopartículas vazias). * = $p < 0,05$ e ** = $p < 0,01$ 68
- Figura 28.** UFC por grama de pulmão dos camundongos 51 dias após a infecção. Os animais tratados com as nanopartículas tiveram uma redução significativa nas células viáveis de Paracoccidoides em comparação com o grupo **Pb 18**. **Pb18** (infectado e não tratado), **Comp** (infectado e tratado com as nanopartículas complexadas com P10) e **Ncomp** (infectado e tratado com P10 e com nanopartículas vazias). ** = $p < 0,01$ 69
- Figura 29.** Produção de citocinas Th₁ 51 dias após a infecção. Não foi detectada IL-2, e IL-12 e IFN- γ foram significativamente aumentados, quando comparados ao grupo **Pb18**. **SHAM** (não infectado e não tratado), **Pb18** (infectado e não tratado), **Comp** (infectado e tratado com as nanopartículas complexadas com P10) e **Ncomp** (infectado e tratado com o P10 coadministrado com nanopartículas vazias). * = $p < 0,05$; ** = $p < 0,01$ e **** = $p < 0,0001$ 70
- Figura 30.** Produção de citocinas Th₂ 51 dias após a infecção. A IL-4 foi significativamente diminuída e a IL-10 foi significativamente aumentada para ambos os grupos tratados com nanopartículas quando comparados ao grupo **Pb18**. **SHAM** (não infectado e não tratado), **Pb18** (infectado e não tratado), **Comp** (infectado e tratado com as nanopartículas complexadas com P10) e **Ncomp** (infectado e tratado com o P10 coadministrado com nanopartículas vazias). * = $p < 0,05$ e ** = $p < 0,01$ 70
- Figura 31.** Th₁₇ induziu a produção de citocinas 51 dias após a infecção. Não foram detectadas alterações nos níveis de IL-1 β , mas a IL-23 foi significativamente aumentada para ambos os grupos de tratamento com nanopartículas quando comparado ao grupo **Pb18**. **SHAM** (não infectado e não tratado), **Pb18** (infectado e não tratado), **Comp** (infectado e tratado com as nanopartículas complexadas com P10) e **Ncomp** (infectado e tratado com o P10 coadministrado com nanopartículas vazias). * = $p < 0,05$ e ** = $p < 0,01$ 71

Figura 32. Peso dos pulmões após a eutanásia (51 dias após a infecção). Houve aumento significativo do peso pulmonar dos animais infectados, quando comparados ao grupo **SHAM**. **SHAM** (não infectado e não tratado), **Pb18** (infectado e não tratado), **1D** (infectado e tratado com uma dose das nanopartículas complexadas com P10), **2D** (infectado e tratado com duas doses das nanopartículas complexadas com P10) e **3D** (infectado e tratado com três doses das nanopartículas complexadas com P10). * = $p < 0,05$ e ** = $p < 0,01$ 72

Figura 33. UFC dos pulmões 51 dias após a infecção. As nanopartículas complexadas com P10 reduziram significativamente o número de células viáveis de *Paracoccidioides* quando comparadas ao grupo **Pb 18**. **SHAM** (não infectado e não tratado), **Pb18** (infectado e não tratado), **1D** (infectado e tratado com uma dose das nanopartículas complexadas com P10), **2D** (infectado e tratado com duas doses das nanopartículas complexadas com P10) e **3D** (infectado e tratado com três doses das nanopartículas complexadas com P10). ** = $p < 0,01$ e *** = $p < 0,001$ 72

LISTA DE TABELAS

Tabela 1. Primers para amplificação e sequenciamento das cadeias leves e pesadas dos anticorpos. 39

Tabela 2. Produção de citocinas Th₁, Th₂ e Th₁₇ 51 dias após a infecção. 73

LISTA DE SIGLAS

°C – Grau Celsius	mV – Milivolt
ANOVA – Análise de variância	nm – Nanômetro
BHI – Infusão de coração e cérebro	P10 – Peptídeo 10
BR – Brasil	Pb – <i>Paracoccidioides brasiliensis</i>
CEUA – Comissão de Ética no Uso de Animais	PBS – Tampão fosfato de sódio
DMEM – Dulbecco's Modified Eagle's Medium	PCM – Paracoccidioidomicose
RPMI – Roswell Park Memorial Institute	PDI – Índice de polidispersão
DMSO – Dimetilsulfóxido	PGA – Ácido Poli-Glicólico
DNA – Ácido desoxirribonucleico	PLA – Ácido Poli-Lático
FMUSP – Faculdade de Medicina Universidade de São Paulo	PLGA – Poli(Ácido Lático-Co-Ácido Glicólico)
HSP – Proteína de choque térmico	q.s.p – Quantidade suficiente para
ICB – Instituto de Ciências Biomédicas	RNA – Ácido ribonucleico
IFN-γ – Interferon gama	mRNA – Ácido ribonucleico mensageiro
IL-2 – Interleucina 2	rpm – Rotações por minuto
IL-4 – Interleucina 4	SFB – Soro Fetal Bovino
IL-10 – Interleucina 10	Th₁ – T helper 1
IL-12 – Interleucina 12	Th₂ – T helper 2
IL-23 – Interleucina 23	Th₉ – T helper 9
IL-1β – Interleucina 1 β	Th₁₇ – T helper 17
Ltda – Limitada	Th₂₂ – T helper 22
mM – milimolar	TPP – Tripolifosfato
mg – Miligrama	UFC – Unidade formadora de colônia
milli Q – Água deionizada	EUA – Estados Unidos da América
mL – Mililitro	USP – Universidade de São Paulo
	VLP – Partícula de tipo viral

μg – Micrograma

μL – Microlitro

SUMÁRIO

CAPÍTULO 1: INTRODUÇÃO GERAL E OBJETIVOS	24
1. INTRODUÇÃO:	24
1.1 Paracoccidiodomicose	24
1.2 Fungo	27
1.3 Modulação da imunidade	28
1.4 Tratamento medicamentoso	29
1.5 Vacinas em desenvolvimento contra a PCM	30
1.6 Anticorpos monoclonais ou policlonais contra a PCM	32
1.7 Anticorpos e hibridomas 3E e F14	33
1.8 Nanopartículas aplicadas na produção de vacinas contra a PCM	34
1.9 Quitosana e nanopartículas de quitosana	34
2. JUSTIFICATIVA	35
3. OBJETIVOS:	36
3.1 Objetivo geral	36
3.2 Objetivos específicos	36
CAPÍTULO 2: SEQUENCIAMENTO DOS ANTICORPOS 3E E F1.4 POR TÉCNICAS CLÁSSICAS E MODERNAS	37
1. MATERIAIS E MÉTODOS	37
1.1 Cultivo e manutenção dos Hibridomas 3E e F1.4	37
1.2 Extração do mRNA total dos hibridomas 3E e F1.4	37
1.3 Produção do cDNA e PCR das cadeias pesadas	38
1.4 Sequenciamento do RNA total	40
1.5 Removendo os adaptadores e “aparando” as sequências	42
1.6 Montagem de novo	44
2. RESULTADOS	44
2.1 Extração do mRNA total dos hibridomas 3E e F1.4	44
2.1 Montagem e análise dos mapas e sequências obtidas após análises de bioinformática	46
3. DISCUÇÃO	47
4. CONCLUSÃO	48
CAPÍTULO 3: PRODUÇÃO, CARACTERIZAÇÃO E BIODISTRIBUIÇÃO DE NANOPARTÍCULAS DE QUITOSANA MARCADAS COM FLUOROCROMOS (CY5.5 OU FITC)	49
1. MATERIAIS E MÉTODOS	49
1.1 Produção da quitosana fluorescente	49
1.2 Preparação das nanopartículas	49

1.3	Caracterização físico-química das nanopartículas	50
1.4	Comitê de ética	50
1.5	Delineamento experimental	50
1.6	Detecção das nanopartículas de quitosana fluorescente <i>In Vivo</i>	51
1.7	Ensaio de fagocitose das nanopartículas.....	51
1.8	Análise estatística	52
2.	RESULTADOS	52
2.1	Caracterização das nanopartículas	52
2.2	Biodistribuição utilizando equipamento IVIS Spectrum	52
2.3	Ensaio de fagocitose das nanopartículas.....	59
3.	DISCUSSÃO	62
4.	CONCLUSÃO	63
	CAPÍTULO 4: PRODUÇÃO, CARACTERIZAÇÃO, AVALIAÇÃO DO NÚMERO DE DOSES VACINAIS E EFEITO ADJUVANTE DAS NANOPARTÍCULAS DE QUITOSANA NO TRATAMENTO DA PARACOCCIDIOIDOMICOSE	64
1.	MATERIAIS E MÉTODOS	64
1.1	Preparação das nanopartículas	64
1.2	Caracterização físico-química das nanopartículas	64
1.3	Comitê de ética	65
1.4	Leveduras	65
1.5	Delineamento experimental	65
1.6	Infecção intratraqueal	66
1.7	Esquema de tratamento.....	66
1.8	Avaliação do UFC (Unidade Formadora de Colônia) e Citocinas	66
1.9	Análise estatística	66
2.	RESULTADOS	67
2.1	Caracterização das nanopartículas	67
2.2	Análise do UFC após 51 dias de infecção.....	68
2.3	Análise das citocinas presentes no pulmão dos animais utilizados para a verificação do efeito adjuvante da quitosana.....	69
2.4	Análise de UFC após 51 dias de infecção	71
2.5	Análise das citocinas presentes no pulmão dos animais utilizados para a verificação do efeito do número de doses vacinais no tratamento da PCM.	72
3.	DISCUSSÃO	73
4.	CONCLUSÃO	75
	BIBLIOGRAFIA	77
	ANEXOS	95

Produção científica.....	95
Trabalhos apresentados em eventos científicos.....	96
Outras atividades.....	98
LISTA DE REAGENTES.....	98
TAMPÃO FOSFATO DE SÓDIO (PBS).....	98
MEIO DE CULTURA FAVA-NETTO.....	98
MEIO DE CULTURA BHI.....	99
ANEXO A – Certificado de realização do curso de treinamento em biossegurança.	100
ANEXO B – Certificado de realização do curso de uso de animais em experimentação.....	101
ANEXO C – Certificado de realização do curso de armazenamento, manuseio e descarte de produtos químicos.....	101
Artigos e capítulos de livros publicados durante o período do doutorado.....	102

CAPÍTULO 1: INTRODUÇÃO GERAL E OBJETIVOS

1. INTRODUÇÃO

1.1 Paracoccidioidomicose

A paracoccidioidomicose (PCM) é uma micose sistêmica que atinge primariamente os pulmões, podendo posteriormente se disseminar pelo organismo. A PCM é causada por fungos termodimórficos do gênero *Paracoccidioides*, sendo atualmente reconhecidas cinco espécies desse fungo: *P.brasiliensis strictu sensu*, *P.americana*, *P.restrepiensis*, *P.venezuelensis* e *P.lutzii* (1,2).

Estudos ambientais indicam que fungos vem aumentando gradativamente seus mecanismos de virulência e resistência devido ao aumento da temperatura global, uso de fungicidas de forma indiscriminada pela agricultura, desmatamento de florestas nativas e o aumento de desastres naturais como enchentes e queimadas (3–5). Estes fatores levaram a Organização Mundial de Saúde a publicar uma lista de fungos potencialmente patogênicos (Figura 1) e que podem vir no futuro causar grandes pandemias, incluindo *Paracoccidioides* (3).

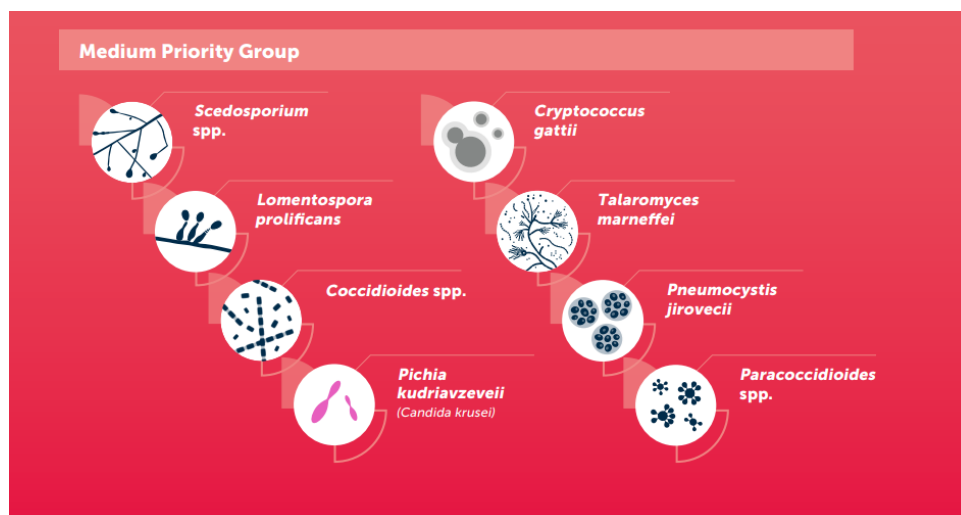


Figura 1. Lista de fungos de interesse médico de média prioridade divulgada pela organização mundial da saúde em 2022.

Registros de infecção por *Paracoccidioides* spp. podem ser encontrados em quase todos os países da América Latina (Figura 2), se estendendo do México até a Argentina excluindo as ilhas do caribe e países como Suriname e Chile (4). Os países com mais

casos registrados são o Brasil, com cerca de 80% dos casos, seguidos da Colômbia, Venezuela e Argentina (5,6).

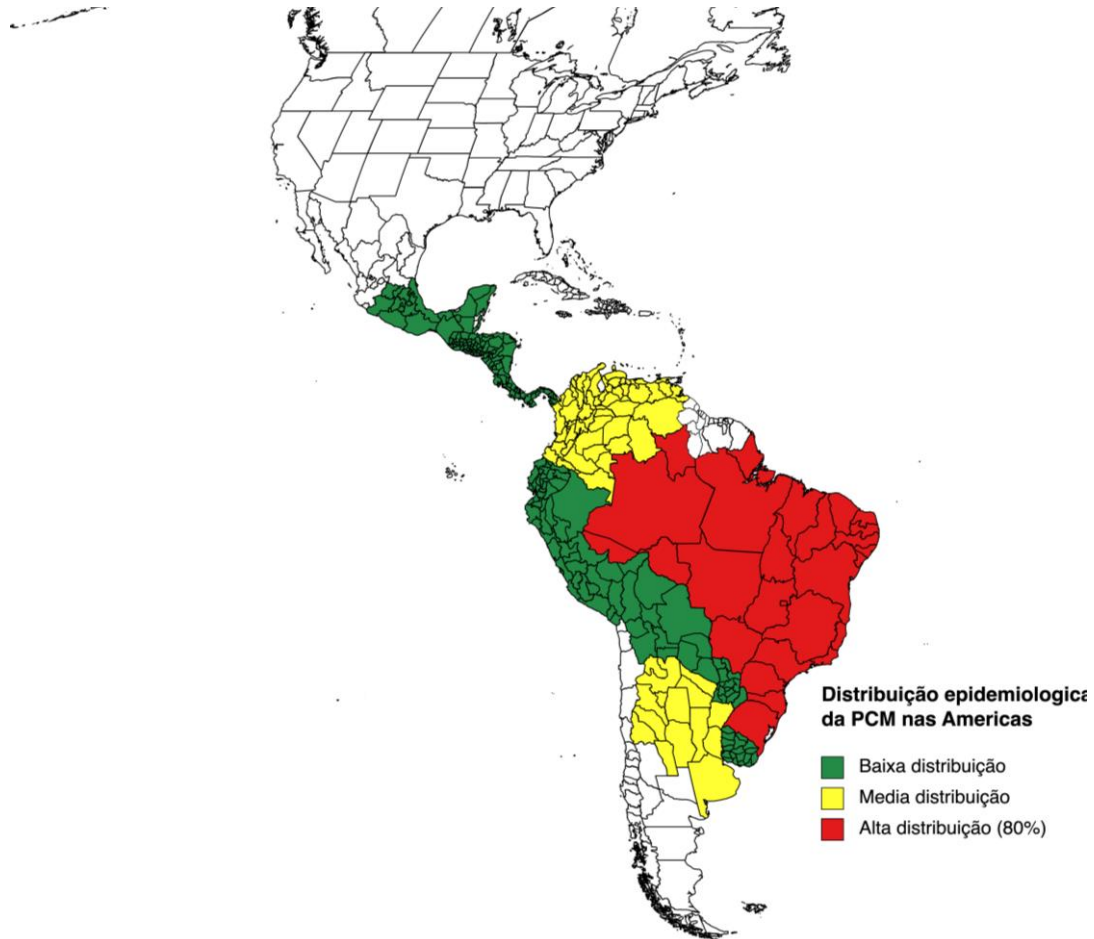


Figura 2. Mapa da distribuição epidemiológica da PCM nas Américas, mostrando as principais zonas epidemiológicas, com destaque para o Brasil (vermelho), Colômbia, Venezuela e norte da Argentina.

No Brasil, os principais relatos epidemiológicos da doença concentram-se nas regiões Centro-Sul do país (5,6) apesar da distribuição em todo o território nacional (Figura 3).



Created with mapchart.net

Figura 3. Mapa epidemiológico da PCM mostrando as principais zonas epidemiológicas no Brasil. Os estados que classicamente são mais acometidos pela PCM encontram-se na região centro sul do país, mas ultimamente devido ao desmatamento da floresta amazônica a região norte se tornou uma área de hiperendemicidade.

Devido à falta de dados oficiais (DATA SUS e ministério da Saúde) o estudo da epidemiologia da PCM no Brasil é feito por pesquisadores independentes. No ano de 2020 o ministro da saúde Luiz Henrique Mandetta publicou por meio do diário oficial a portaria do ministério da saúde nº 264, de 17 de fevereiro de 2020 que colocava a PCM como uma doença de notificação compulsória, mas em maio de 2020 o ministro interino Eduardo Pazuello, revogou a portaria nº 264, de 17 de fevereiro de 2020 com a portaria nº 1.061, de 18 de maio de 2020, dificultando a coleta de dados para estudos epidemiológicos das doenças fúngicas sistêmicas/subcutâneas como a PCM, criptococose e a esporotricose humana. Com a revogação da portaria ficou a cargo dos Estados e Municípios a notificação de doenças sistêmicas fúngicas, sendo o Estado do Mato Grosso

do Sul um dos únicos que tornaram a notificação compulsória com a divulgação da nota técnica 02/2021.

A PCM pode ser classificada em: PCM infecção ou doença, onde a PCM infecção não apresenta manifestações clínicas e a PCM doença é classificada em três formas clínicas: juvenil/aguda e subaguda, adulto/crônica e sequelar (7). Quando a doença se manifesta na forma juvenil, apresenta uma característica sistêmica sem distinção entre os sexos dos hospedeiros, acometendo principalmente crianças, adolescentes e jovens adultos. Na forma adulta a doença se manifesta principalmente nos pulmões, podendo ter disseminação para outros tecidos e acomete principalmente homens entre 30 - 60 anos (4,8).

Pacientes acometidos pela PCM geralmente apresentam sequelas pós-tratamento, pois a infecção costuma gerar lesões extensas em regiões como os pulmões, tecidos mucosos, tecido linfático, tecido digestório/excretor e sistema nervoso (7).

A infecção pelo fungo ocorre por meio da inalação de conídios ou propágulos fúngicos, que após adentrarem no hospedeiro se depositam nas vias aéreas inferiores, principalmente no parênquima pulmonar, e caso não seja contido em granulomas ou eliminado pelo sistema imune do hospedeiro pode se disseminar pelo organismo por meio do sistema linfático (7,9). A disseminação pode ocorrer também caso o fungo consiga escapar dos granulomas devido a uma redução da competência imunológica do hospedeiro (9).

O diagnóstico da PCM é feito por meio de exames clínicos e de imagens para avaliar as lesões, exame direto de amostras clínicas como biópsias ou lavado bronco alveolar para detectar a presença do fungo por microscopia; cultivo de biópsias ou lavado bronco alveolar para verificar a presença do fungo devido ao seu crescimento em meio de cultura; exames sorológicos em busca de antígenos e principalmente anticorpos contra os antígenos de *Paracoccidioides* e por meio de testes moleculares (5,7,9).

O diagnóstico diferencial é essencial para distinguir a PCM de outras doenças como a tuberculose, leishmaniose, cromoblastomicose e alguns tipos de neoplasia (5,7,9).

1.2 Fungo

Paracoccidioides spp. é um fungo termodimórfico, que na natureza em temperatura ambiente, com média de 24 °C, apresenta características filamentosas e forma de vida saprofítica (10). Ao entrar em contato com o ambiente interno do

hospedeiro, com temperatura média variando de 35 °C a 37 °C, o fungo passa da forma micelial para levedura causadora da doença (11–13).

Fatores hormonais estão associados com a prevalência da doença em homens, uma vez que o hormônio estrogênio, presente em maiores quantidades em mulheres, inibe a conversão do micélio em levedura (14).

Além de hospedeiros humanos, o fungo também pode infectar outros animais como preguiças, tatus, cachorros e cavalos (15,16). Acredita-se que *Paracoccidioides* infecta de forma não intencional animais silvestres ou mesmo domésticos, já que o fungo tem natureza saprofítica sendo seu habitat natural o solo (16,17).

1.3 Modulação da imunidade

O controle eficaz da PCM requer uma resposta imune do tipo Th₁ com a produção de IFN- γ e IL-2 responsáveis por estimular a fagocitose e formação de granulomas epitelióides. Entretanto, a resposta imune dos pacientes é do tipo mista (Th₁ e Th₂) sendo que nos casos mais graves a resposta Th₂ é prevalente (18,19). A formação do granuloma desempenha papel fundamental no combate ao fungo, pois impede a disseminação do patógeno (17,18).

Em pacientes imunocomprometidos ou que apresentam formas mais graves da doença, uma resposta do tipo Th₂ é encontrada predominantemente, onde os títulos dos anticorpos estão ligados diretamente com o grau de severidade que o paciente se encontra (20,21).

Recentemente foi demonstrado a importância da resposta imune celular do tipo Th₁₇, para a contenção e ou eliminação de infecções fúngicas. Este tipo de resposta é bastante associado com resposta danosa de hiperinflamação principalmente em mucosas, devido ao estímulo e liberação de espécies reativas de oxigênio e nitrogênio, um dos principais mecanismos de eliminação do fungo (9,22–24).

A competência imunológica do hospedeiro e a carga fúngica inalada estão diretamente associadas à progressão da doença (25–29). Em pessoas imunodeficientes a prevalência da resposta de células T dos subtipos Th₂ e Th₉ acaba fazendo com que o hospedeiro tenha a forma aguda e mais grave da doença com a disseminação dos fungos pelo organismo, hospedeiros imunocompetentes respondem de maneira mais eficiente a infecção, fazendo com que o fungo seja contido em granulomas caso prevaleça uma

resposta imune de células T dos subtipos Th₁₇ e Th₂₂, ou a completa eliminação do fungo caso o organismo produza uma resposta imune de células T subtipo Th₁ (25–29).

Foi demonstrado que neutrófilos são uma das primeiras linhas de defesa contra a PCM, por sua capacidade de fagocitar e eliminar o fungo por meio da produção de explosões de espécies oxidativas, eles também são de extrema importância durante a resposta imune estimulada por vacinas (30).

Outros grupos celulares que estão entre a primeira linha de defesa do organismo são as células “*natural killers*” (NK) com mecanismos de ação parecidos com os dos linfócitos T CD8 e os monócitos/macrófagos que são extremamente eficientes em fagocitar as leveduras de *Paracoccidioides*, mas precisam de estímulos para eliminar as células internalizadas, uma vez que o fungo, pode sobreviver no interior dos fagolisossomos (25–29).

A formação do granuloma também está associado à competência imunológica do hospedeiro e com a carga de propágulos fúngicos inalados (25–29,31,32). Caso o hospedeiro esteja com o sistema imune competente haverá o recrutamento de macrófagos que formaram células gigantes multinucleares com posterior recrutamento de células NKs, neutrófilos, eosinófilos linfócitos T e B, formando um pré-granuloma (25–29,31,32). Fibroblastos são então recrutados promovendo a deposição de fibras colágenas do tipo 2 e 3 formando um granuloma bem definido com contornos regulares e mais firme (25–29,31,32). Em hospedeiros imunodeficientes o granuloma fica frouxo e multifocado, permitindo que o fungo sobreviva e escape do granuloma podendo disseminar pelo organismo (25–29,31,32).

1.4 Tratamento medicamentoso

O tratamento para a PCM ocorre em duas etapas, a primeira etapa consiste em um tratamento de ataque inicial para controlar rapidamente a infecção e a segunda etapa consiste em um tratamento para inibir a proliferação dos fungos remanescentes até níveis que impeçam a recorrência da doença (21).

Os principais medicamentos para o tratamento da PCM são quimioterápicos poliênicos como a anfotericina B, compostos sulfanilamídicos como a sulfadiazina e drogas azólicas como o itraconazol (7). Apesar de essas drogas serem bastante eficazes no tratamento da PCM e de outras micoses, elas apresentam importantes efeitos adversos

a serem observados tanto comuns como cefaléias, distúrbios gástricos eritemas e erupções cutâneas até nefrotoxicidade no caso da anfotericina B (33,34).

Nos últimos anos diversos estudos vem buscando fármacos sintéticos ou naturais como alternativas ou em conjunto com os fármacos clássico para o tratamento da PCM, estes fármacos são em sua maioria novos compostos mas há também a presença de moléculas que foram reposicionadas, algumas das principais moléculas com grau terapêutico são galatos de alquila inibidor da N-glicosilação o tiosemicarbazona lapachol, luliconazol, butaconazol inibidores da biossíntese do ergosterol, peptídeos antimicrobianos como o MK58911, dentre outros compostos (35,36).

Extratos vegetais com propriedades antifúngicas como argetilactona derivada de *Hyptis ovalifolia*, enoteína B derivada de *Eugenia uniflora*, ésteres metílicos de ácidos graxos e compostos derivados de óleos essenciais de *Annona cornifolia*, extratos hidroalcoólicos das espécies *Piper regnellii* e *Baccharis dracunculifolia*, curcumina de *Curcuma longa*, o ajoeno, derivado do *Allium sativum*, dentre outros compostos também apresentaram efeito inibidor de crescimento contra leveduras de *Paracoccidioides* PCM, (35,36).

1.5 Vacinas em desenvolvimento contra a PCM

Uma alternativa para tratar/prevenir a PCM é o uso de vacinas para a geração de resposta imune tipo Th₁ e Th₁₇, fundamental para controle da doença.

Diversos grupos testaram, em modelo experimental, alternativas vacinais, tais como o uso de leveduras de *P.brasiliensis* atenuadas por radiação (37), uso de leveduras de *Saccharomyces cerevisiae* geneticamente modificadas para expressar a molécula gp43(38), utilização de porções proteicas purificadas de extrato de parede como as porções F0 e FII (39), vacinas de DNA (40–44), vacinas recombinantes (45), além de vacinas que utilizam nanopartículas como forma de liberação e proteção de moléculas ativas (46).

Um dos candidatos vacinais mais estudado é a vacina baseada no peptídeo P10 derivado da glicoproteína de 43 kDa de *P. brasiliensis* que apresenta 15 aminoácidos em sua estrutura cuja sequência é QTLIAIHTLAIRYAN (47).

O peptídeo P10 foi selecionado entre um conjunto de peptídeos derivados da gp43 por ter sido capaz de promover uma linfoproliferação mais acentuada em relação aos

peptídeos comparados além de possuir a capacidade de estimular a produção de citocinas como o IFN- γ , levando a uma resposta imunológica predominante do tipo Th₁ (47).

Devido à baixa estabilidade e rápida degradação do peptídeo P10 novas formulações e novas formas de utilização foram testadas e os resultados foram bastante promissores (48).

Vacinas de DNA utilizando-se plasmídeos para a expressão do peptídeo P10 sozinho ou em conjunto com a expressão de IL-12 mostraram-se eficazes na redução da carga fúngica, na preservação da estrutura pulmonar e estimularam a produção de citocinas do tipo Th₁ (44,49).

Vacinas quiméricas também foram utilizadas para tentar melhorar o efeito imunogênico do peptídeo P10. Foram feitas fusões do peptídeo P10 ou da proteína gp43 de *P.brasiliensis* com a proteína flagelina (FliC) de *Salmonella entérica* (45). Foi demonstrado que a antigenicidade da fusão entre a FliC e o P10 foram eficazes na redução da carga fúngica, na preservação da estrutura pulmonar e estimularam a produção de citocinas do tipo Th₁ (45).

Partículas do tipo viral VLPs (do inglês: *virus like particles*) também foram utilizadas como forma de melhorar a estimulação da resposta imune do peptídeo P10 (50). O peptídeo P10 foi fusionado com proteínas do capsídeo viral da hepatite B, essa fusão foi eficaz na redução da carga fúngica, na preservação da estrutura pulmonar e estimulou a produção de citocinas do tipo Th₁ (50).

Buscando uma forma mais eficiente de promover a apresentação antigênica do peptídeo P10 e a ativação de células T, foram utilizadas células dendríticas tratadas (pulsadas) previamente com o peptídeo P10 (51,52). Os estudos utilizaram camundongos imunocompetentes e imunossuprimidos com dexametasona. Em ambos, as células dendríticas tratadas previamente com o peptídeo P10 foram capazes de reduzir a carga fúngica no pulmão dos animais infectados, além de promoverem a proliferação de células T e a produção de citocinas como IL-12 e IFN- γ (51,52).

Foram utilizados lipídeos catiônicos como o DDA/TDB (Dioctadecil Dimetil Amônio e Dibehenato de Trealose (CAF01) e o DODAB (Brometo de Bioctadecil Dimetil Amônio) como novos adjuvantes (30,53). Ambas as formulações foram eficazes na redução da carga fúngica, na preservação da estrutura pulmonar e estimularam a produção de citocinas do tipo Th₁

Nanopartículas de PLGA e de quitosana também foram utilizadas como forma de proteção e carreamento do peptídeo P10 mostrando-se altamente eficientes na redução da carga fúngica e estimulação da resposta imune no combate a PCM (11,54).

A utilização de anticorpos monoclonais também já foi avaliada frente a PCM com resultados encorajadores na redução da carga fúngica, mostrando que anticorpos específicos também podem ser utilizados para o tratamento de doenças infecciosas fúngicas (55–58).

1.6 Anticorpos monoclonais ou policlonais contra a PCM.

Anticorpos são glicoproteínas produzidas pelas células de defesa com a finalidade de proteger o organismo através de diferentes mecanismos de ação, desde ação direta contra o corpo estranho, até a facilitação da fagocitose deste corpo estranho por diferentes células (59).

No caso de infecções fúngicas a presença de anticorpos foi considerada por muito tempo como indicador de malignidade, já que aparentemente não apresentavam função protetora na resolução da infecção (60–63).

Na PCM os anticorpos séricos são utilizados para averiguar o grau de severidade da doença, já que as formas mais graves estão associadas com a predominância de resposta Th₂ (7,56)

Após estudos demonstrarem o efeito protetor dos anticorpos monoclonais no controle de infecções fúngicas, o interesse terapêutico aumentou de forma exponencial (60–63).

Diversos grupos demonstraram que anticorpos policlonais ou monoclonais possuem a capacidade de reduzir a carga fúngica e proteger os animais infectados com *P.brasiliensise P.lutzii* através do aumento da fagocitose por macrófagos e elevação dos índices de IFN- γ (64).

Um dos primeiros trabalhos utilizando-se anticorpos monoclonais avaliou o efeito de dois anticorpos monoclonais anti gp70 de *P. brasiliensis*, estes anticorpos foram capazes de reduzir a carga fúngica em animais infectados além de reduzirem o dano tecidual causado pela infecção (55). *P. brasiliensis* apresenta como fator de virulência a capacidade de produzir melanina e foi demonstrado *in vitro* um aumento da fagocitose das leveduras de *Paracoccidioides* ao se utilizar anticorpos policlonais anti-melanina (65,66).

Anticorpos policlonais contra glicolipídios de *Paracoccidioides* também já foram estudados e foi demonstrado que estes anticorpos ao serem utilizados em desafios profiláticos ou terapêuticos foram capazes de reduzir a carga fúngica dos animais, também reduziram o dano tecidual causado pela infecção e foi demonstrado *in vitro* aumento da fagocitose e aumento da produção de espécies reativas de oxigênio (67).

Outros trabalhos utilizando-se anticorpos monoclonais contra *P. brasiliensis* focaram seus alvos na parede celular e na principal molécula antigênica do fungo a glicoproteína gp43, estes anticorpos e os seus hibridomas serão discutidos com detalhes no tópico a seguir (56,57).

1.7 Anticorpos e hibridomas 3E e F14

O hibridoma produtor do anticorpo 3E é proveniente da fusão de esplenócitos de camundongos BALB/c com células de mieloma da linhagem SP-2.Ag14 (produzido pela Profa. Rosana Puccia – UNIFESP). Para a geração dos esplenócitos produtores de anticorpo contra *P.brasiliensis* foi feita a imunização dos camundongos com a glicoproteína gp43 purificada de extratos de cultura e parede de *P. brasiliensis*. Os animais receberam 50 µg do antígeno pela via subcutânea a cada 15 dias junto com o adjuvante completo de Freund's na primeira dose e incompleto nas doses subsequentes. Por meio de testes bioquímicos foi determinado que este anticorpo pertence a classe das IgG2β e que sua cadeia leve do tipo kappa (κ). Este anticorpo se mostrou eficaz na redução da carga fúngica do pulmão dos animais infectados com o *P.brasiliensis*, bem como aumentou os níveis de citocinas pró-inflamatórias do tipo Th₁ e os níveis de espécies reativas de oxigênio (57,58,68).

O hibridoma produtor do anticorpo F1.4 (produzido em colaboração com Prof. Joshua Nosanchuk no setor de facilidades AECOM/NY). Para a geração dos esplenócitos produtores de anticorpo contra *P.brasiliensis* foi feita a imunização dos camundongos com extratos de cultura e parede celular. Por meio de testes bioquímicos foi determinado que o anticorpo F1.4 reconhecia epítomos de β-glucana presentes na parede celular de *P.brasiliensis* e que este anticorpo pertence a classe das IgG1 e que sua cadeia leve do tipo kappa (κ). Este anticorpo se mostrou eficaz na redução da carga fúngica do pulmão dos animais infectados com *P. brasiliensis*, bem como aumentou os níveis de citocinas pró-inflamatórias do tipo Th₁ e os níveis de espécies reativas de oxigênio (69).

1.8 Nanopartículas aplicadas na produção de vacinas contra a PCM

Existem diversos tipos de nanopartículas poliméricas feitas de diferentes materiais. As características físicas e químicas destas nanopartículas são definidas a partir de qual ou quais materiais (monômeros e ou polímeros) utilizados e da concentração deles. Os monômeros mais utilizados são quitosana, PLA (Ácido Poli-Lático), PGA (Ácido Poli-Glicólico), PLGA (Poli(Ácido Lático-Co-Ácido Glicólico)), alginato, entre outros (70–73).

A eficácia do uso de nanopartículas para *delivery* e liberação sustentada do peptídeo P10, fármacos e até porções de anticorpos (scFv) contra a PCM, já foi comprovado em diversos estudos, os quais mostraram a redução considerável da molécula carregada e a manutenção sustentada do mesmo por um longo período de tempo (11,54,74,75).

Diversos estudos já demonstraram que o uso das nanopartículas de quitosana, como adjuvantes ou como carreador de fármacos, DNA/ RNA, peptídeos ou proteínas, aumentou significativamente o efeito desejado para o qual as nanopartículas foram empregadas, e isso se deve às características físico/químicas que a associação destes compostos com estas nanopartículas apresentaram (76–78)

A característica mais marcante nas nanopartículas de quitosana é a sua capacidade de ser mucoadesiva, mas há outras propriedades relevantes, tais como biocompatibilidade, fácil obtenção e preparação das nanopartículas por necessitar de poucos processos (54).

Em estudos anteriores do nosso grupo foi demonstrado que as nanopartículas de quitosana administradas pela via intranasal dos camundongos foram extremamente eficazes na redução da carga fúngica, e na redução da quantidade de peptídeo necessário para se gerar uma resposta imune que fosse capaz de eliminar leveduras de *P.brasiliensis* dos pulmões dos animais infectados (54). Estes resultados animadores demonstram que as nanopartículas de quitosana podem ser futuramente empregadas no tratamento de doenças fúngicas como a PCM.

1.9 Quitosana e nanopartículas de quitosana

A quitosana é um polímero derivado da quitina, que é encontrada em diferentes espécies de animais, como os insetos, crustáceos e também como um dos principais constituintes da parede celular de fungos, e é a partir da desacetilação da quitina que se obtém a quitosana (79–81).

As nanopartículas de quitosana tem diversas aplicações, podendo ser usada na cicatrização de feridas (82,83), como adjuvante vacinal devido à sua capacidade de estimular a resposta imune Th₁ e Th₁₇ (84–86) e como carreadores para *delivery* vacinal contra doenças em aves, porcos e gado (87–91).

As nanopartículas de quitosana também demonstraram eficiência como carreador de fármacos, DNA/ RNA, peptídeos ou proteínas para doenças que acometem os seres humanos (54,78,92,93).

A característica que mais chama a atenção nas nanopartículas de quitosana é a sua capacidade de ser mucoadesiva. Esta capacidade é essencial em formulação para aplicação em mucosas, já que nas regiões de mucosa ocorrem fenômenos de degradação e *clearance* causados pelo deslocamento de partículas estranhas pelas paredes das mucosas (54,94–96).

Esta mucoadesividade promove a aderência das nanopartículas, aumentando o tempo de contato das nanopartículas com o organismo e levando assim a uma melhor resposta (54,94–96). A presença de grupamentos amina em toda a estrutura da quitosana deixa a molécula com uma carga elétrica positiva, já a mucina apresenta carga elétrica negativa, devido à grande quantidade de glicoproteínas ligadas por pontes de sulfeto e radicais OH⁻ (97–99). A diferença entre as cargas é a responsável pela mucoadesividade da quitosana (97–99).

2. JUSTIFICATIVA

Devido ao alto custo de produção de anticorpos monoclonais por meio de hibridomas, faz-se necessário a otimização de novas técnicas de produção. O sequenciamento dos genes responsáveis pela formação dos anticorpos com a finalidade de se os expressar de maneira heteróloga e ou facilitar sua humanização é uma das tecnologias mais promissoras na área, pois permite a redução significativa dos custos de produção.

Para aprovação do uso de um novo fármaco ou imunobiológico a descrição da atividade farmacológica ou imunológica é essencial. Recentemente nosso grupo depositou junto à agência USP de inovação e o INPI a patente da formulação em nanopartículas de quitosana do peptídeo P10 para tratamento da paracoccidiodomicose (SANTOS JÚNIOR, 2018) sob o número: BR 10 2019 012313 3 A2.

Os resultados obtidos foram promissores e por isso temos como objetivo inicial descrever como estas nanopartículas são dispersas pelos órgãos e o mecanismo de

ativação envolvido. Para isso, a concentração mínima da molécula ativa, o número de doses, o possível efeito adjuvante e a localização da célula responsável pela sua captação e transporte é essencial, para aprimoramento do processo de *delivery* e a liberação sustentada de moléculas de forma mais específica e eficiente.

3. OBJETIVOS

3.1 Objetivo geral

Sequenciar RNA dos hibridomas produtores dos anticorpos monoclonais 3E e F1.4, contra gp43 e beta glucana de *P. brasiliensis* respectivamente, produzir e avaliar diferentes formulações vacinais baseadas em nanopartículas de quitosana contra *P. brasiliensis* e avaliar a biodistribuição das nanopartículas de quitosana administradas pela via intranasal.

3.2 Objetivos específicos

- Extrair o RNA total dos Hibridomas responsáveis pela produção dos anticorpos monoclonais 3E e F1.4.
- Transformar o mRNA em cDNA por meio de reações de PCR.
- Amplificar as regiões codificadoras das cadeias pesadas e leves dos anticorpos por meio de reações de PCR.
- Sequenciar o RNA total e o mRNA por meio de técnicas de sequenciamento de nova geração.
- Montar as sequências de RNA total e mRNA e identificar as sequências responsáveis pela produção dos anticorpos monoclonais 3E e F1.4.
- Verificar a biodistribuição das nanopartículas de quitosana complexadas com o peptídeo P10 administradas pela via intranasal.
- Verificar a localização das nanopartículas de quitosana complexadas com o peptídeo P10 na célula por meio de ensaios de fagocitose.
- Verificar a necessidade de complexação do P10 com as nanopartículas de quitosana para a redução da carga fúngica.
- Verificar a quantidade de doses vacinais para a redução da carga fúngica utilizando-se nanopartículas de quitosana complexadas com o peptídeo P10.

CAPÍTULO 2: SEQUENCIAMENTO DOS ANTICORPOS 3E E F1.4 POR TÉCNICAS CLÁSSICAS E MODERNAS

1. MATERIAIS E MÉTODOS

1.1 Cultivo e manutenção dos Hibridomas 3E e F1.4

Os hibridomas foram descongelados dos estoques armazenados em um freezer a -80 °C. Os tubos criogênicos consistiam em: 500 µL de Soro Fetal Bovino (SFB, Gibco, Thermo Fisher Scientific, Waltham, Massachusetts, EUA), 400 µL de meio RPMI-1640 (LGC Biotecnologia, Cotia, São Paulo, Brasil), 100 µL de Dimetilsulfóxido (DMSO, Sigma-Aldrich, St. Louis, MO, EUA) e os hibridomas estavam na concentração de 1×10^6 células/mL, foi-se realizado o rápido descongelamento dos hibridomas (banho maria a 37 °C) e as células foram colocadas em placas de 6 poços em um volume de 500 µL de células e 1,5 mL de meio de manutenção e cultivo por poço.

O meio de manutenção e cultivo era composto por 20% de SFB (Gibco, Thermo Fisher Scientific) ou 10% de SFB na presença de 10% de NCTC 109 (Thermo Fisher Scientific, Waltham, Massachusetts, EUA), 1% de solução de penicilina/estreptomicina/ (pen/strp, Gibco, Thermo Fisher Scientific, Waltham, Massachusetts, EUA), 2 mM de L-glutamina (concentração final) (Gibco, Thermo Fisher Scientific, Waltham, Massachusetts, EUA) ou 1% de solução de penicilina/estreptomicina/L-glutamina (Gibco, Thermo Fisher Scientific, Waltham, Massachusetts, EUA), 0,8% de 100× aminoácidos não essenciais (Gibco, Thermo Fisher Scientific, Waltham, Massachusetts, EUA), 25mM de Hepes (concentração final) (Gibco, Thermo Fisher Scientific, Waltham, Massachusetts, EUA), 2 mM de piruvato (concentração final) (Gibco, Thermo Fisher Scientific, Waltham, Massachusetts, EUA) e RPMI-1640 (LGC Biotecnologia) q.s.p 500 mL.

As células foram mantidas em estufas de cultivo celular a 37 °C com 5% CO₂, o meio era trocado a cada 48 horas ou conforme a necessidade das células. Após a confluência das células no fundo dos poços elas foram realocadas para garrafas de cultura de células de 4 mL e foram mantidas nas mesmas condições.

1.2 Extração do mRNA total dos hibridomas 3E e F1.4

O RNA total foi extraído com TRIzol™ Reagent (Invitrogen™, Waltham, Massachusetts, EUA) de acordo com o protocolo estabelecido pelo fabricante.

Brevemente, as células foram coletadas das garrafas e centrifugadas a 300 g por 10 minutos a 4 °C, o *pellet* foi coletado e o sobrenadante foi descartado, 750 µL de TRIzol™ (Invitrogen™) foi adicionado para uma concentração de aproximadamente 10×10^6 células/mL em microtubos de 1 mL, a mistura foi homogeneizada diversas vezes posteriormente foi deixada incubando a temperatura ambiente por 5 minutos.

Posteriormente a mistura de células lisadas e TRIzol™ (Invitrogen™) foi centrifugada a 12,000 g por 5 minutos a 4 °C, o sobrenadante foi transferido para um novo microtubo e o lisado de células foi descartado. Foi adicionado ao tubo com sobrenadante 200 µL de clorofórmio (Synth São Paulo, Brasil) e a nova mistura foi incubada a temperatura ambiente por 2 minutos, após a incubação a mistura foi centrifugada a 12.000 g por 15 minutos a 4 °C, após a centrifugação foi possível verificar a formação de três fases uma inferior avermelhada composta por uma mistura de clorofórmio, fenol e DNA, uma camada intermediária esbranquiçada formada por proteínas e uma camada superficial transparente e aquosa na qual está o RNA total extraído.

A fase aquosa foi transferida para um novo microtubo onde foram acrescentados 5 µg de RNase-free glycogen (Invitrogen™, Waltham, Massachusetts, EUA) utilizado como carreador para a precipitação do RNA total, também foram adicionados 500 µL de isopropanol para cada 1 mL de e TRIzol™ (Invitrogen™). A mistura foi incubada a temperatura ambiente por 10 minutos, após a incubação a mistura foi centrifugada a 12.000 g por 10 minutos a 4 °C, após a centrifugação é possível verificar a formação de um *pellet* branco de RNA no fundo do microtubo.

O sobrenadante foi descartado e o RNA total foi ressuspensionado em 1 mL de etanol 75% por 1 mL de TRIzol™ (Invitrogen™). A nova mistura foi centrifugada a 7.500 g por 10 minutos a 4 °C, o sobrenadante foi descartado e o RNA total foi “secado” por cerca de 10 minutos dentro da cabine de segurança biológica. Após a “secagem” o RNA total foi ressuspensionado em 50 µL of RNase-free water (Invitrogen™, Waltham, Massachusetts, EUA) e armazenado em um freezer a -20 °C até o uso.

1.3 Produção do cDNA e PCR das cadeias pesadas

O cDNA foi produzido com o kit High-Capacity cDNA Reverse Transcription Kit (Applied Biosystems™ Waltham, Massachusetts, EUA) de acordo com o protocolo estabelecido pelo fabricante.

As ampliações por PCR das sequências de interesse foram realizadas com o kit Platinum™ Taq DNA Polymerase High Fidelity (Invitrogen™ Waltham, Massachusetts, EUA) de acordo com o protocolo estabelecido pelo fabricante.

Devido à alta variabilidade e rearranjo dos genes responsáveis pela produção de anticorpos, diversos primers (Tabela 1) foram utilizados baseados no trabalho de Tiller, Thomas; 2009 (100) para a amplificação das sequências de interesse para o posterior sequenciamento destas sequências.

Foi utilizada uma técnica chamada *nested* PCR que consiste em usar o produto de uma PCR para se realizar outra amplificação interna por PCR, esta técnica é utilizada quando a amostra original apresenta uma baixa concentração das sequências alvo. Para isso foram utilizadas diferentes temperaturas e ciclagens para as cadeias pesadas e leves (Figura 4).

Os anticorpos 3E e F1.4 foram descritos anteriormente por Puccia, Rosana; 1991 e Boniche, Camila; 2020 (68,101) como sendo pertencentes às classes de IgG2β e IgG1, respectivamente, pela análise de suas cadeias pesadas por métodos bioquímicos e ambos apresentam como cadeia leve a variante kappa (κ) (mais comum), também identificada por métodos bioquímicos.

Tabela 1. Primers para amplificação e sequenciamento das cadeias leves e pesadas dos anticorpos.

Passo da PCR	Nome do Primer	Sequência dos nucleotídeos 5'–3'
Igh 1° PCR	5' MsVHE	GGGAATTCGAGGTGCAGCTGCAGGAGTCTGG
	3' Cγ2b outer	GGAAGGTGTGCACACTGCTGGAC
	3' Cγ1 outer	GGAAGGTGTGCACACCGCTGGAC
Igh 2° PCR	5' MsVHE	GGGAATTCGAGGTGCAGCTGCAGGAGTCTGG
	3' Cγ2b inner	ACTCAGGGAAGTAGCCCTTGAC
	3' Cγ1 inner	GCTCAGGGAATAGCCCTTGAC
Igk 1° PCR	5' L-Vκ_3	TGCTGCTGCTCTGGGTTCCAG
	5' L-Vκ_4	ATTWTCAGCTTCCTGCTAATC
	5' L-Vκ_5	TTTGCTTTTCTGGATTYCAG
	5' L-Vκ_6	TCGTGTTKCTSTGGTTGTCTG
	5' L-Vκ_6,8,9	ATGGAATCACAGRCYCWGG
	5' L-Vκ_14	TCTTGTTGCTCTGGTTYCCAG
	5' L-Vκ_19	CAGTTCCTGGGGCTCTTGTTGTTC
	5' L-Vκ_20	CTCACTAGCTCTTCTCCTC
	3' mCκ	GATGGTGGGAAGATGGATACAGTT
Igk 2° PCR	5' mVκappa	GAYATTGTGMTSACMCARWCTMCA

3' BsiWI P-mJK01	GCCACCGTACGTTTGTATTCCAGCTTGGTG
3' BsiWI P-mJK02	GCCACCGTACGTTTTATTCCAGCTTGGTC
3' BsiWI P-mJK03	GCCACCGTACGTTTTATTCCAACCTTGTGTC
3' BsiWI P-mJK04	GCCACCGTACGTTTCAGCTCCAGCTTGGTG

Igh = cadeia pesada do anticorpo, **Igk** = cadeia leve do anticorpo, **Cy2b** = IgG2 β , **Cy1** = IgG1.

1ª PCR

Igh	Igk	Igl
94 °C 2 min	94 °C 2 min	94 °C 2 min
94 °C 15 s (Desnaturação)	94 °C 15 s (Desnaturação)	94 °C 15 s (Desnaturação)
56 °C 30 s (Anelamento)	50 °C 30 s (Anelamento)	58 °C 30 s (Anelamento)
68 °C 55 s (Elongação)	68 °C 55 s (Elongação)	68 °C 55 s (Elongação)
68 °C 10 min	68 °C 10 min	68 °C 10 min
4 °C ∞	4 °C ∞	4 °C ∞

50 X

2ª PCR

Igh	Igk	Igl
94 °C 2 min	94 °C 2 min	94 °C 2 min
94 °C 15 s (Desnaturação)	94 °C 15 s (Desnaturação)	94 °C 15 s (Desnaturação)
56 °C 30 s (Anelamento)	56 °C 30 s (Anelamento)	56 °C 30 s (Anelamento)
68 °C 55 s (Elongação)	68 °C 55 s (Elongação)	68 °C 55 s (Elongação)
68 °C 10 min	68 °C 10 min	68 °C 10 min
4 °C ∞	4 °C ∞	4 °C ∞

50 X

Figura 4. Protocolo para PCR com as temperaturas e ciclagens da *nasted* PCR para as cadeias pesadas e leves dos anticorpos.

1.4 Sequenciamento do RNA total

Após a verificação de que não seria possível se obter as sequências de interesse por meio dos métodos tradicionais de PCR foi realizada a tentativa de sequenciamento e montagem das sequências alvo por meio de tecnologias de sequenciamento de nova geração.

O sequenciamento foi realizado pela equipe do laboratório de análises genômicas e sequenciamento da *Johns Hopkins University: Bloomberg School of Public Health* em Baltimore, Maryland - USA, as montagens e análise de dados foram realizadas pela

equipe do Laboratório de Evolução Molecular e Bioinformática da Universidade de São Paulo, Instituto de Ciências Biomédicas 2, São Paulo, São Paulo - Brasil.

Utilizou-se o seguinte protocolo: após a extração do RNA total, foi realizada sua quantificação com o kit Qubit BR RNA Assay e Qubit Flex Fluorometer (Invitrogen/ThermoFisher, Waltham, Massachusetts, EUA), e a avaliação da qualidade foi realizada pela análise do RNA total em uma RNA *ScreenTape* (Agilent, Santa Clara, Califórnia, EUA) e a leitura foi realizada no Agilent *TapeStation 2200* (Agilent).

Bibliotecas exclusivas de código de barras de índice duplo para RNA-Seq foram preparadas a partir de 100 ng de RNA total usando o kit Universal Plus Total RNA-Seq com *NuQuant Library* (Tecan Genomics, Redwood City, CA, EUA), de acordo com o protocolo recomendado pelo fabricante. O número do ciclo para amplificação da biblioteca (16 ciclos) foi otimizado por qPCR. A qualidade das bibliotecas foi avaliada por *High Sensitivity DNA Lab Chips* em um Agilent BioAnalyzer 2100 (Agilent, Santa Clara, Califórnia, EUA). A quantificação foi realizada com reagente NuQuant e confirmada pelo ensaio Qubit *High Sensitivity DNA*, em Qubit 4 e Qubit *Flex Fluorometers* (Invitrogen/ThermoFisher). As bibliotecas foram diluídas e os *pools* equimolares preparados, de acordo com o protocolo do fabricante para o sequenciador apropriado. Um sequenciador Illumina iSeq (Illumina, San Diego, CA, USA) e o kit iSeq100 i1 V2 300 (Illumina, San Diego, CA, USA) foram utilizados para avaliação final da qualidade do conjunto de bibliotecas e para sequenciamento de alto rendimento do RNA total.

Um *pipeline* confiável foi projetado e utilizado para a preparação e análises das sequências obtidas (Figura 5). Ao verificar os dados brutos provenientes do sequenciamento de alto rendimento, podemos analisar que as saídas Fastq foram avaliadas quanto à sua qualidade usando FastQC V0.11.6 (Babraham *Bioinformatics*, Cambridge, UK). Foram verificados o total de sequências (leituras), comprimento de sequência, qualidade de sequência por base, conteúdo de GC (guanina e citosina) por sequência, distribuição de comprimento de sequência, sequências sobrerrepresentadas e conteúdo do adaptador.

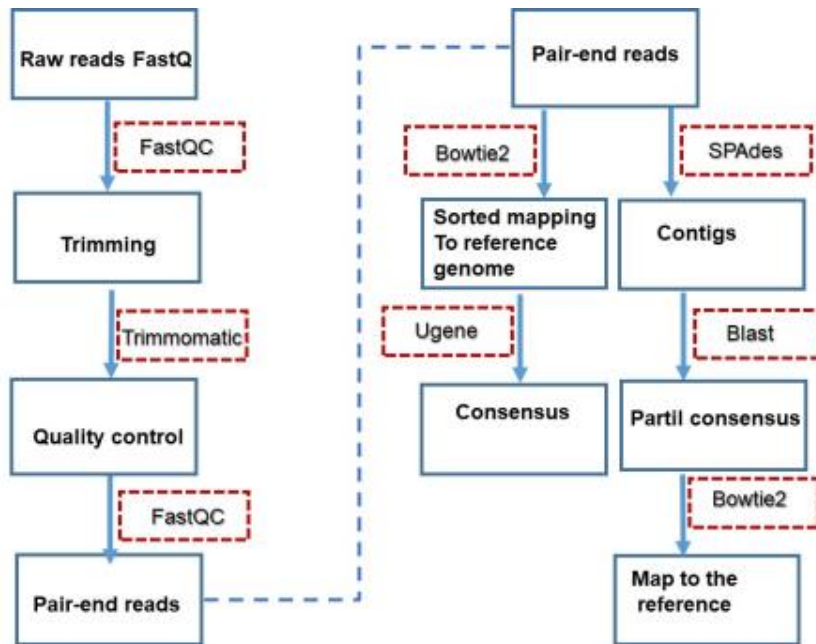


Figura 5. Fluxograma de trabalho para montagem e análise das sequências obtidas por meio de softwares de bioinformática.

1.5 Removendo os adaptadores e “aparando” as sequências

Sequências de baixa qualidade ou técnicas, como adaptadores, foram removidas usando Trimmomatic V 0.39. (102). Este software inclui uma variedade de etapas de processamento e algoritmos para aparar e diferentes filtragens, como tamanho e qualidade. Algumas opções e fatores que implementamos no *script* principal para melhores resultados. Para obter as melhores opções, executamos o mesmo grupo de leituras de sequência usando diferentes opções para processamento de dados *downstream*. Por exemplo, alguns desses fatores podem ser observados abaixo:

- a) As pontuações de qualidade foram definidas para Phred 33 (Probabilidade de um erro em 1000) como uma espécie de normalização para outras bases de aparagem.
- b) Para cada kit utilizado para preparação da biblioteca (neste caso TruSeq3-PE), os adaptadores foram removidos e verificados para garantir a remoção bem-sucedida.
- c) *Leading 20*: Cortar bases de baixa qualidade ou N abaixo de um limite de qualidade desde o início das leituras. O padrão era 3, mas usamos 20 por ter uma melhor qualidade nas leituras.
- d) *Trailing*: Corte de baixa qualidade ou N bases abaixo de um limite de qualidade a partir do final das leituras. O padrão era 3, mas usamos 20 para ter uma melhor qualidade de leitura
- e) *JANELA DESLIZANTE*: Executa um recorte de janela deslizante, cortando uma vez que a qualidade média dentro da janela cai abaixo de um limite. O padrão era

4:15, mas alteramos para 4:25. Isso significa que o programa verifica as leituras com uma janela deslizante de 4 bases de largura, reduzindo a qualidade média por base abaixo de 25.

f) MINLEN: Esta opção foi utilizada como valor padrão de 36. Com esta opção, as sequências menores que 31 bp foram eliminadas.

Como resultado de todos esses métodos de corte de base na qualidade e tamanho, terminamos com arquivos contendo dois conjuntos de dados de extremidade única e dois de extremidade de par. Mais uma vez, após o *trimming*, a qualidade das leituras foi verificada pelo FastQC (Babraham *Bioinformatics*, Cambridge, UK)

As leituras foram montadas por mapeamento para o genoma de referência utilizando o software de alinhamento de leitura Bowtie2 V2.2.5. (Figura 6) (103). Os conjuntos resultantes foram verificados usando programas Ugene (102).

```
#!/bin/bash
#QC control
$/FastQC/fastqc -o ./fastqc_after -t 4 --nogroup *.fq
#Trimming low quality bases and also barcodes
$java -jar /Trimmomatic-0.39/trimmomatic-0.39.jar PE -threads 2 -phred33 ./seq_R1.fastq
./seq_R2.fastq seq_PE_1.fq seq_SR_1.fq seq_PE_2.fq seq_SR_2.fq
ILLUMINAACLIP:/home/shahab/Downloads/software/Trimmomatic-0.39/adapters/TruSeq3-
PE.fa:2:30:10 LEADING:20 TRAILING:20 SLIDINGWINDOW:4:25 MINLEN:36
#Second QC control to assure everything is Ok
$/FastQC/fastqc -o ./fastqc_after -t 4 --nogroup *.fq
#Quality stats
$fastx_quality_stats -Q 33 -i seq_PE_1.fq -o seq_PE_1.txt
$fastx_quality_stats -Q 33 -i seq_PE_2.fq -o seq_PE_2.txt
$cat *.txt | awk '{sum += $2} END {print sum}' > seq.quality_bases.txt
#Genome assembly against provided references
#First, building the reference (index)
$bowtie2-build reference.fasta reference
#Then, Bowtie2 mapping
$bowtie2 -p 2 --no-unal -x reference -1 seq_PE_1.fq -2 seq_PE_2.fq -S seq.sam
#sam to bam
$samtools view -bS seq.sam > seq.bam
#sorted.bam
$samtools sort seq.bam -o seq.sorted.bam
$samtools index seq.sorted.bam
#stats
$samtools depth seq.sorted.bam | awk '{sum+=$3} END {print "Average= ", sum/NR}' >
seq.average.txt
#de novo assembly with SPAdes-3
$/SPAdes-3.14.1-Linux/bin/spades.py --pe1-1 seq_PE_1.fq --pe1-2 seq_PE_2.fq -o
spades_output
$cd spades_output
$grep '^>' contigs.fasta -c > number_of_contigs.txt
```

Figura 6. Código em python do programa Bowtie2 utilizado para fazer o alinhamento e montagem das sequências do mRNA sequenciado.

1.6 Montagem de novo

A montagem de novo foi feita pelo SPAdes V3.14 .1 (104) (Figura 7), que é um módulo interativo de montagem do genoma de leitura curta, com base no valor de K -mer, selecionado com base no comprimento da leitura e no tipo de conjunto de dados.

```
#!/bin/bash#Assembly para a amostra seqgunzip *.gzcat *R1*.fastq > seq_R1.fastqcat
*R2*.fastq > seq_R2.fastqchmod 755
/home/shahab/Downloads/software/FastQC/fastqcmkdir fastqc_beforemkdir
fastqc_after/home/shahab/Downloads/software/FastQC/fastqc -o ./fastqc_before -t 4 --
nogroup *.fastqchmod 755 /home/shahab/Downloads/software/Trimmomatic-
0.38/trimmomatic-0.38.jarjava -jar /home/shahab/Downloads/software/Trimmomatic-
0.38/trimmomatic-0.38.jar PE -threads 2 -phred33 ./seq_R1.fastq ./seq_R2.fastq
seq_PE_1.fq seq_SR_1.fq seq_PE_2.fq seq_SR_2.fq LEADING:20 TRAILING:20
SLIDINGWINDOW:4:25 MINLEN:36/home/shahab/Downloads/software/FastQC/fastqc -o
./fastqc_after -t 4 --nogroup *.fqfastx_quality_stats -Q 33 -i seq_PE_1.fq -o
seq_PE_1.txtfastx_quality_stats -Q 33 -i seq_PE_2.fq -o seq_PE_2.txtcat *.txt | awk '{sum
+= $2} END {print sum}' > seq.quality_bases.txtbowtie2-build reference.fasta
referencebowtie2 -p 2 --no-unal -x reference -1 seq_PE_1.fq -2 seq_PE_2.fq -S
seq.samsamtools view -bS seq.sam > seq.bamsamtools sort seq.bam seq.sortedsamtools
index seq.sorted.bamsamtools depth seq.sorted.bam | awk '{sum+= $3} END {print
"Average= ", sum/NR}' >
seq.average.txt/home/shahab/Downloads/software/sam2fasta.py reference.fasta
seq.sam consensus.fasta/home/shahab/Downloads/software/SPAdes-3.13.0-
Linux/bin/spades.py --pe1-1 seq_PE_1.fq --pe1-2 seq_PE_2.fq -o spades_outputcd
spades_outputgrep '^>' contigs.fasta -c > number_of_contigs.txt
```

Figura 7. Código em python do programa *SPAdes V3.14 .1* utilizado para fazer o alinhamento e montagem de novo das sequências do mRNA sequenciado.

2. RESULTADOS

2.1 Extração do mRNA total dos hibridomas 3E e F1.4

Foi possível observar que a extração do RNA total utilizando TRIzol™ (Invitrogen™) foi satisfatória, uma vez que é possível verificar a qualidade do RNA total, onde não foi observado arraste e somente bandas bem definidas (Figura 8), também foi possível observar a presença de grande quantidade de RNA ribossomal além de uma menor concentração de outros RNAs (mensageiro, interferência, transportador, etc...) (Figura 9).

Infelizmente não foram observados produtos de PCR após inúmeras tentativas de amplificação das regiões de interesse por meio das técnicas clássicas de PCR convencional.

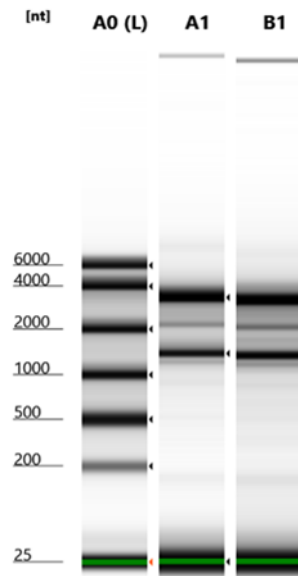


Figura 8. Eletroforese eletrônica do RNA *ScreenTape* mostrando a qualidade da extração do RNA total (sem arraste), e com a presença de bandas bem definidas, principalmente as bandas relacionadas com a maior porção de RNA presente nas células (RNA ribossomal 28s e 18s). [nt] = Quantidade de nucleotídeos do *lader*, A0(L) = *lader*, A1 = RNA total do hibridoma 3E e B1 = RNA total do hibridoma F1.4.

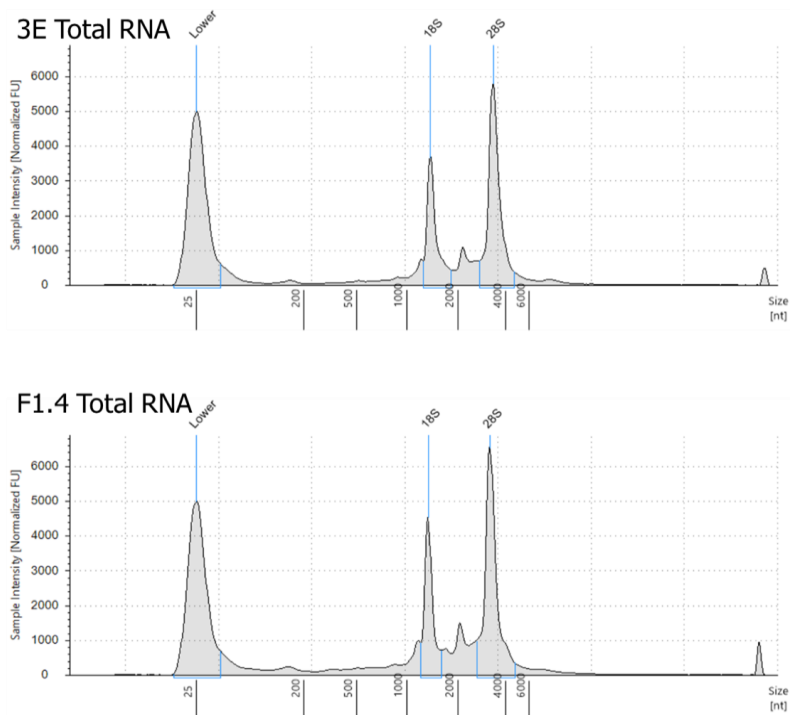


Figura 9. Gráfico de intensidade do RNA *ScreenTape* mostrando a intensidade das moléculas de RNA total extraídas dos hibridomas, com a presença de bandas bem picos bem definidos, como os picos relacionadas com a maior porção de RNA presente nas células (RNA ribossomal 28s e 18s).

2.1 Montagem e análise dos mapas e sequências obtidas após análises de bioinformática

Pelas análises de dados e montagens de sequências e mapas de sequências pelos *softwares* de bioinformática (Bowtie2 V2.2.5 e SPAdes V3.14 .1) foi possível observar que o sequenciamento e as montagens foram bem sucedidas, uma vez que mais de 10 milhões de sequências (Figura 10) com até 17000 bases, foram visualizadas tanto para o híbridoma 3E como para o F1.4.

Mesmo após uma análise de curadoria das sequências e dos mapas, reduzindo as sequências para até 1900 bases, reduzindo as 10 milhões de sequências para cerca de 2600 sequências (Figura 11), não foi possível identificar a presença do mRNA responsável pela produção dos anticorpos para os dois híbridomas.



Figura 10. Representação das sequências e mapas montados pelos *softwares* de bioinformática para o híbridoma 3E, mostrando cerca de 10 milhões de sequências com até 17000 bases.

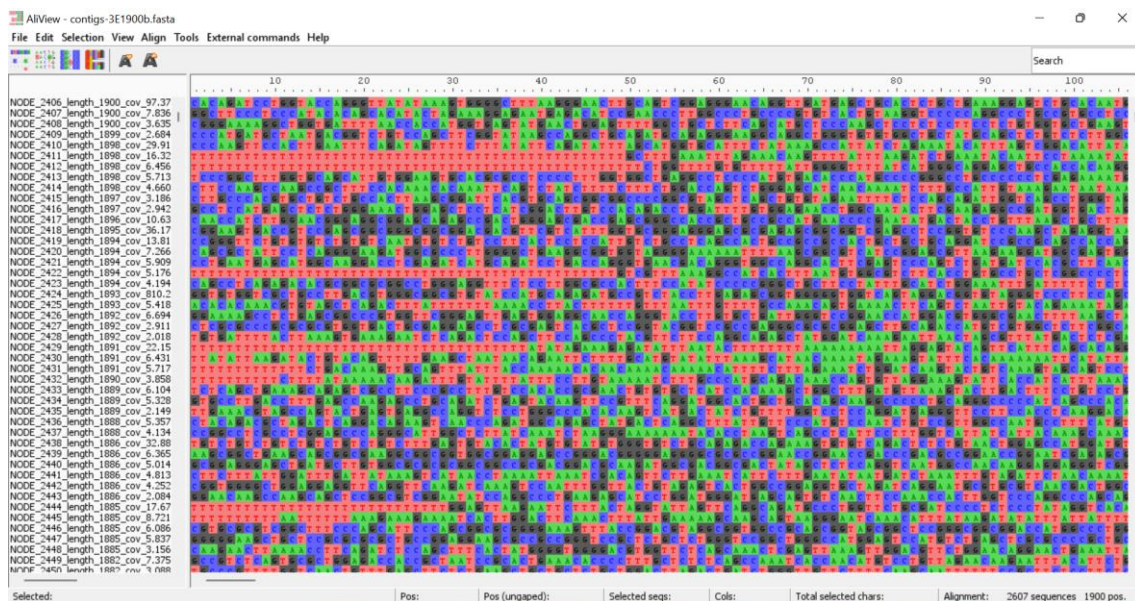


Figura 11. Representação das sequências e mapas montados para o hibridoma 3E, mostrando cerca de 2600 sequências com até 1900 bases.

Não foi possível obter-se as sequências gênicas responsáveis pela expressão dos anticorpos monoclonais até o momento. Devido à grande variabilidade genética, aos processos pré-transcricionais, pós-traducionais e as diferentes localizações dos genes em diferentes cromossomos, o sequenciamento dos anticorpos é uma tarefa complicada e árdua de serem realizadas, tanto por meios clássicos os como a por PCR, como por meios modernos como os utilizando sequenciamentos de nova geração. Mesmo assim o sequenciamento do mRNA é a única forma de se saber com 100% de certeza a sequência de uma proteína, neste caso os anticorpos. O sequenciamento dos anticorpos por meio de técnicas de espectrometria de massa é uma forma mais simples para se obter a sequência, mas possui diversas falhas já que não é possível de se afirmar que as sequências obtidas pelas técnicas são 100% acuradas no quesito de sequência de aminoácidos.

3. DISCUSSÃO

A pequena quantidade de mRNA responsável pela expressão dos anticorpos pode ter sido um dos responsáveis pela dificuldade em se obter a sequência dos anticorpos, mesmo sabendo que as células estavam produzindo anticorpos, a quantidade e a volatilidade do mRNA torna difícil seu sequenciamento. Para os próximos experimentos, o estímulo das células com IL-2 ou co-cultivo com células apresentadoras de antígenos, na presença de seus respectivos antígenos, para promover a super-expressão dos anticorpos pode ser um fator positivo, pois com o aumento da expressão dos anticorpos

os níveis de mRNA presentes após a extração do RNA total estará aumentado, facilitando assim seu sequenciamento.

Outro fator que pode estar relacionado a dificuldade de obtenção das sequências dos anticorpos pode ter sido o fato de se ter extraído e utilizado o RNA total das células, causando uma diluição não intencional das sequências de mRNA necessárias para o sequenciamento dos anticorpos. O uso de kits de extração pode ser uma alternativa para este problema, uma vez que os kits permitem a separação e concentração do mRNA presentes nas células.

A combinação do uso dos kits de extração e da estimulação da super-expressão dos anticorpos, pode ser uma alternativa ainda mais poderosa para se auxiliar no sequenciamento dos anticorpos monoclonais no futuro. O projeto não será abandonado e deverá ser continuado em uma etapa posterior.

4. CONCLUSÃO

- A extração do RNA total dos hibridomas responsáveis pela produção dos anticorpos monoclonais 3E e F1.4 foi realizada com sucesso e sua qualidade foi considerada ótima.
- Não foi possível transformar o mRNA em cDNA por meio de reações de PCR.
- Não foi possível amplificar as regiões codificadoras das cadeias pesadas e leves dos anticorpos por meio de reações de PCR.
- O sequenciamento do RNA total e do mRNA por meio de técnicas de sequenciamento de nova geração foi realizada com sucesso e sua qualidade foi considerada ótima.
- Foram montados diferentes mapas das sequências de RNA total e mRNA, mas não foi possível identificar as sequências responsáveis pela produção dos anticorpos monoclonais 3E e F1.4.

CAPÍTULO 3: PRODUÇÃO, CARACTERIZAÇÃO E BIODISTRIBUIÇÃO DE NANOPARTÍCULAS DE QUITOSANA MARCADAS COM FLUOROCROMOS (CY5.5 OU FITC)

1. MATERIAIS E MÉTODOS

1.1 Produção da quitosana fluorescente

Para produzir as nanopartículas fluorescentes, a quitosana foi conjugada com os fluorocromos FITC (Sigma-Aldrich) ou Cy5.5 NHS éster (Abcam, Cambridge Biomedical Campus, Cambridge, UK) usando protocolo adaptado de Kwangmeyung Kim, 2010 e Min Huang, 2002 (105,106).

Para a conjugação da quitosana com o FITC, foi necessário dissolver 15 mg do fluorocromo (FITC) em 15 mL de DMSO, enquanto a quitosana (2 mg/mL) foi dissolvida com 1% de ácido acético (concentração final) em água ultrapura sob agitação magnética por 1h em temperatura ambiente. O pH da quitosana foi então ajustado para aproximadamente 4,4 usando NaOH 0,1 M. A solução de fluorocromo e a de quitosana foram misturadas sob agitação magnética por 3-4 horas à temperatura ambiente ou durante a noite a 4 °C. Após a agitação, a quitosana fluorescente foi precipitada aumentando-se o pH para 10 com NaOH 0,5 M.

Para a conjugação da quitosana com o Cy5.5, foi necessário dissolver 1 mg do fluorocromo (Cy5.5) em 1,5 mL de DMSO, 2 mg/mL de quitosana foi solubilizada em 15 mL de água MiliQ, e o pH foi ajustado para 8,3-8,5 com NaHCO₃. A solução de fluorocromo e a de quitosana foram misturadas sob agitação magnética por 3-4 horas à temperatura ambiente ou durante a noite a 4 °C.

Após a conjugação, as quitosanas fluorescentes (FITC ou Cy5.5) foram dialisadas por 3 dias usando uma membrana de 10 kDa e posteriormente liofilizadas e armazenadas no escuro.

1.2 Preparação das nanopartículas

As nanopartículas foram preparadas de acordo com nosso protocolo previamente padronizado (54). Em resumo, uma solução de quitosana (quitosana de baixo peso molecular, Sigma-Aldrich, St. Louis, MO, EUA) foi misturada gota a gota com uma solução de tripolifosfato de sódio (TPP; Sigma-Aldrich) com ou sem peptídeo P10 (GenOne Biotech, Rio de Janeiro, RJ, Brasil). A primeira solução era composta por 2 mg/mL de quitosana, preparada pela dissolução da quitosana com 1% de ácido acético

(concentração final) em água ultrapura sob agitação magnética por 1h em temperatura ambiente. O pH da solução de quitosana foi então ajustado para aproximadamente 4,4 usando NaOH 0,1 M. A segunda solução era composta por 1 mg/mL de TPP e 5 µg (massa final) do peptídeo P10 solubilizado para as nanopartículas complexadas ou sem o peptídeo P10 para as nanopartículas vazias.

A segunda solução (TPP+P10 ou TPP) foi misturada gota a gota na primeira solução sob agitação magnética por 90 minutos à temperatura ambiente. As nanopartículas foram lavadas com água ultrapura e centrifugadas a 13.200 rpm, 4 °C por 1 h, por três vezes. As nanopartículas foram então ressuspensas em água ultrapura para sua caracterização físico-química, em PBS (veículo vacinal), ou DMEM (LGC Biotecnologia, Cotia, São Paulo, Brasil) (ensaio de fagocitose).

1.3 Caracterização físico-química das nanopartículas

Os tamanhos das nanopartículas e os índices de polidispersividade (PDI) foram determinados por espalhamento dinâmico de luz e o potencial Zeta foi medido por eletroforese capilar usando um equipamento Zetasizer nano Zs (Malvern Panalytical Ltd, Reino Unido).

1.4 Comitê de ética

Camundongos BALB/c nude e BALB/c, machos, livres de patógenos com idade entre 6-8 semanas, foram utilizados de acordo com a aprovação do comitê de ética da Universidade de São Paulo (CEUA ICB n° 3654290618).

1.5 Delineamento experimental

Os camundongos BALB/c nude foram aleatoriamente organizados nos seguintes grupos: **(C+)** – Um camundongo inoculado apenas com o fluorocromo (Cy5.5); **(C-)** – Um camundongo inoculado com PBS; e **(NP)** – Três camundongos inoculados com as nanopartículas fluorescentes (Cy5.5) (15 animais no total foram utilizados).

Os camundongos BALB/c foram distribuídos aleatoriamente nos seguintes grupos: **(C+)** – Um camundongo inoculado apenas com o fluorocromo (FITC); **(C-)** – Um camundongo inoculado com PBS; e **(NP)** – Três camundongos inoculados com as nanopartículas fluorescentes (FITC). Pulmões, traqueia, estômago, intestinos e cérebro foram coletados em cada intervalo de análise (75 animais no total foram utilizados).

1.6 Detecção das nanopartículas de quitosana fluorescente *In Vivo*

Cinco microlitros de fluorocromo, PBS ou nanopartícula fluorescente foram inoculados em cada narina dos camundongos BALB/c nude e BALB/c de acordo com os grupos relatados anteriormente. As nanopartículas fluorescentes (Cy5.5) foram utilizadas para visualizar a biodistribuição *in vivo* nos camundongos BALB/c nude. Para avaliar a presença das nanopartículas nos órgãos dos animais foram utilizados os camundongos BALB/c. As imagens foram obtidas com o IVIS Spectrum (PerkinElmer, Waltham, Massachusetts, EUA) localizado no Centro de Pesquisas (CEFAP – Instituto de Ciências Biomédicas IV, Universidade de São Paulo, São Paulo, SP, Brasil). Os animais ou órgãos foram analisados em diferentes tempos (0, 24, 48, 72 e 96 horas) após a inoculação das nanopartículas de quitosana fluorescentes.

1.7 Ensaio de fagocitose das nanopartículas

Macrófagos alveolares e peritoneais foram coletados de camundongos não inoculados, seguindo um protocolo modificado de Herb, M. 2019; Zhang, X. 2008; e Busch, C. 2019 (107–109). Macrófagos alveolares foram coletados usando tampão BAL (lavagem bronco alveolar) composto por PBS, EDTA 2 mM (concentração final) e 0,5% de soro fetal bovino (SFB, Gibco, Thermo Fisher Scientific, Waltham, Massachusetts, EUA). O tampão BAL e as células coletadas foram mantidos a 37 °C. Os macrófagos peritoneais foram coletados e mantidos em PBS frio.

Após a coleta, as células foram centrifugadas a 3.000 rpm a 4 ° C por 5 min e semeados em placas de 6 poços com lamínulas de vidro redondas na parte inferior dos poços. Os macrófagos alveolares foram mantidos com DMEM suplementado com 10% SFB, 1% (vol/vol) penicilina/estreptomicina (pen/strp, Gibco, Thermo Fisher Scientific), 30 ng de GM – CSF (Thermo Fisher Scientific) e 2% de piruvato (Thermo Fisher Scientific). As células peritoneais foram mantidas com DMEM suplementado com 10% de SFB, 1% (vol/vol) pen/strp e 2% de piruvato (Thermo Fisher Scientific). Ambas as células foram mantidas em incubadoras de células a 37 ° C e 5% de CO₂ até que apresentassem confluência celular completa sobre as lamínulas.

Após a confluência celular completa das lamínulas, as nanopartículas fluorescentes (FITC) foram centrifugadas, ressuspensas em 1 mL de DMEM e adicionadas às células. As células foram analisadas em diferentes tempos (2, 4, 6 e 8 horas) após a adição das nanopartículas de quitosana fluorescentes.

O kit de coloração lisossomal - fluorescência vermelha (RFP) - Cytopainter (Abcam) foi utilizado para fornecer a co-localização das nanopartículas e o fluorocromo DAPI (Sigma-Aldrich) foi para corar o núcleo.

As células foram visualizadas no microscópio EVOS Cell Imaging Systems (Thermo Fisher Scientific) usando como meio de montagem 100 µL de PBS 10× em 900 µL de glicerol.

1.8 Análise estatística

Foi realizada análise de variância (ANOVA) ou teste de Student seguido de pós-teste de Tukey ou Dunnett utilizando Graph Pad Prism 8. Os valores de p foram considerados significativos quando $< 0,05$, as barras de erro foram expressas como o erro padrão da média (SEM).

Todos os experimentos foram feitos em triplicata.

2. RESULTADOS

2.1 Caracterização das nanopartículas

O diâmetro e distribuição do tamanho das nanopartículas conjugadas com fluorocromo complexadas com P10 estavam em torno de 350 nm com PDI $< 0,5$. O potencial Z ficou em torno de +20 mV para todas as partículas testadas.

2.2 Biodistribuição utilizando equipamento IVIS Spectrum

A biodistribuição das nanopartículas marcadas com Cy5.5, após a inoculação nos camundongos BALB/c nude, foi avaliada por até 96 horas (5 dias) (0 hora e 96 horas são mostradas). As imagens do IVIS Spectrum foram obtidas com os camundongos posicionados em decúbito ventral (Figuras 12 e 14) e em decúbito dorsal (Figuras 13 e 15). Uma diminuição na área de fluorescência foi observada ao longo do tempo, sugerindo que as nanopartículas estavam sendo fagocitadas e processadas. Ao utilizar o IVIS Spectrum para visualizar as nanopartículas fluorescentes (Cy5.5), foi possível observar que as nanopartículas permanecem principalmente nas vias aérea superiores e apresentaram uma intensidade fluorescente estável em todos os períodos avaliados, diferente do controle positivo (C+) em que uma perda significativa da intensidade de fluorescência da região de interesse (ROI) nas primeiras 24 horas (Figura 20).

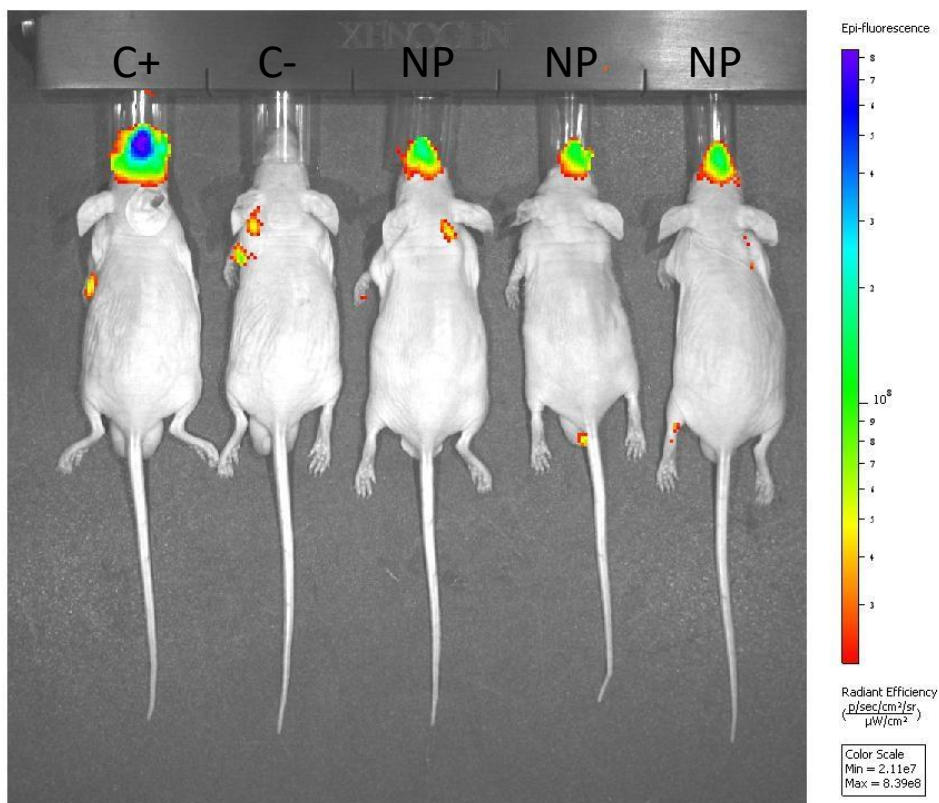


Figura 12. Imagem da fluorescência obtida com IVIS Spectrum mostrando os camundongos posicionados em decúbito ventral, mostrando a fluorescência na via aérea superior do BALB/c nude após a inoculação de 5 μ L por narina das nanopartículas fluorescentes de quitosana Cy5.5 em 0 horas (C+) inoculado apenas com o fluorocromo (Cy5.5), (C-) inoculado com PBS e (NP) inoculado com as nanopartículas fluorescentes.

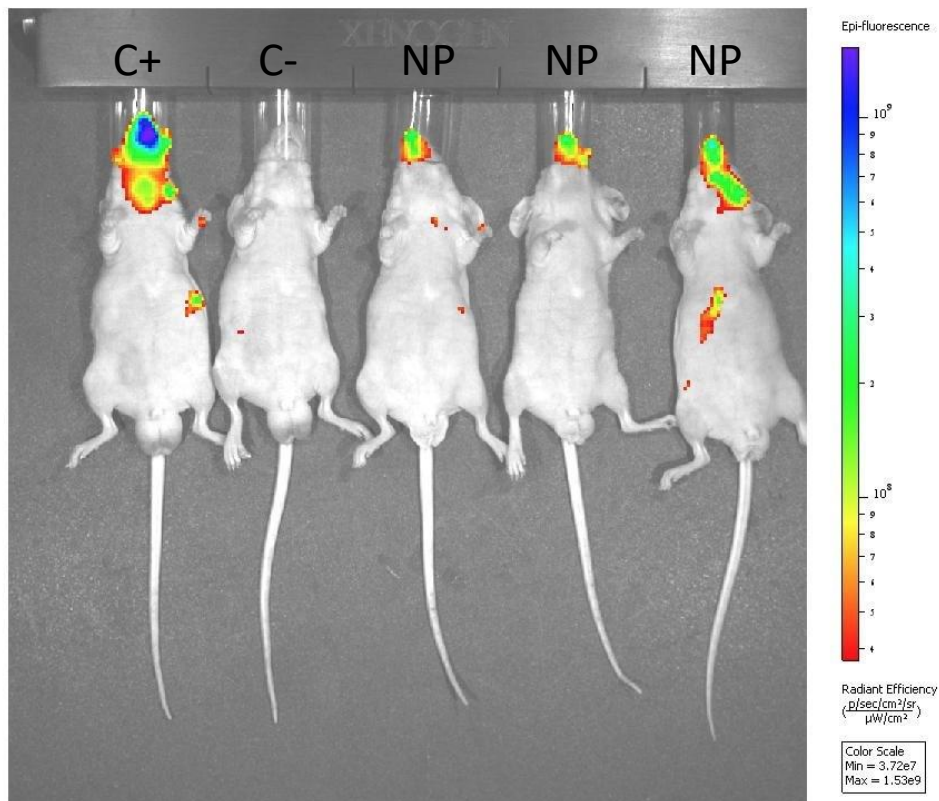


Figura 13. Imagem da fluorescência obtida com IVIS Spectrum mostrando os camundongos posicionados em decúbito dorsal, mostrando a fluorescência na via aérea superior do camundongo BALB/c nude após inoculação de 5 μ L por narina das nanopartículas fluorescentes de quitosana Cy5.5 em 0 horas (C+) inoculado apenas com o fluorocromo (Cy5.5), (C-) inoculado com PBS e (NP) inoculado com as nanopartículas fluorescentes.

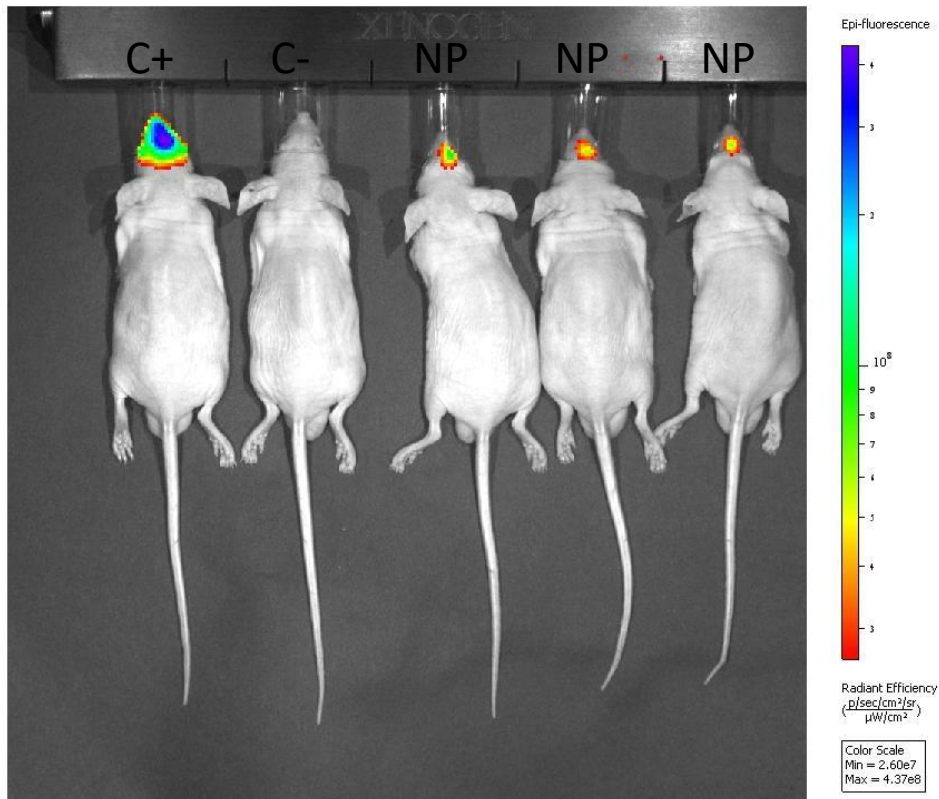


Figura 14 Imagem da fluorescência obtida com IVIS Spectrum mostrando os camundongos posicionados em decúbito dorsal mostrando a fluorescência na via aérea superior do camundongo BALB/c nude após inoculação de 5 μ L por narina das nanopartículas de quitosana Cy5.5 fluorescentes em 96 horas. (C+) inoculado apenas com o fluorocromo (Cy5.5), (C-) inoculado com PBS e (NP) inoculado com as nanopartículas fluorescentes.

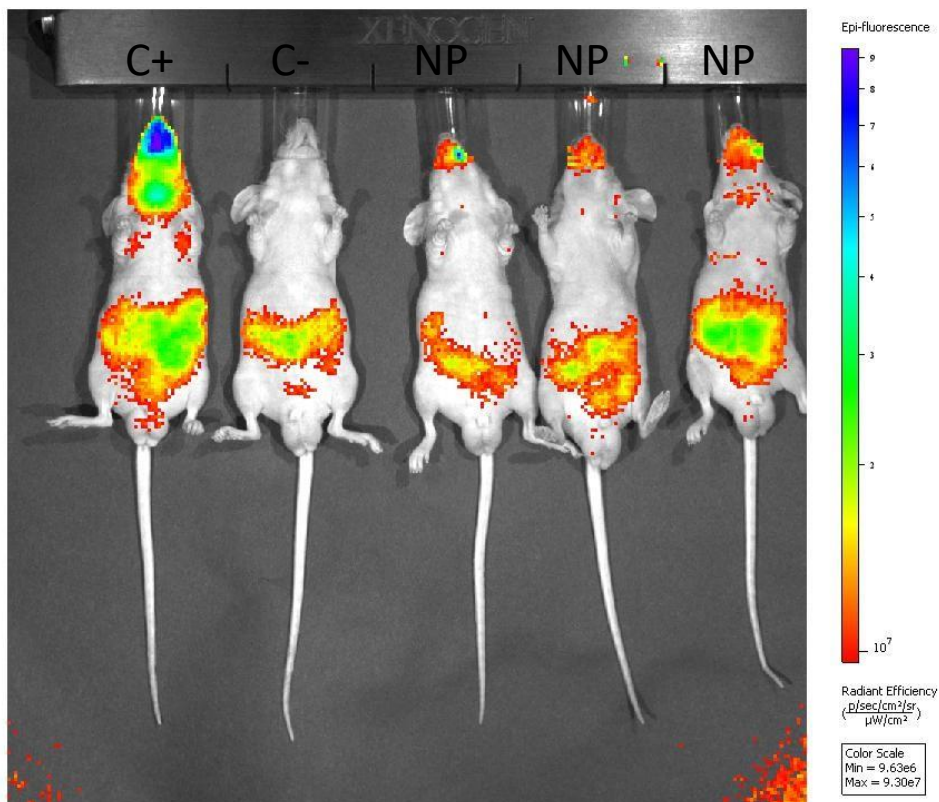


Figura 15. Imagem da fluorescência obtida com IVIS Spectrum mostrando os camundongos posicionados em decúbito dorsal mostrando a fluorescência na via aérea superior do camundongo BALB/c nude após

inoculação de 5 μL por narina das nanopartículas de quitosana Cy5.5 fluorescentes em 96 horas. (C+) inoculado apenas com o fluorocromo (Cy5.5), (C-) inoculado com PBS e (NP) inoculado com as nanopartículas fluorescentes.

Para analisar a fluorescência nos órgãos dos camundongos, o inóculo de nanopartículas teve que ser concentrado três vezes (o volume inoculado não foi alterado).

A fluorescência foi observada por 96 horas (5 dias) (0 hora e 96 horas são mostradas). Antes da aquisição da imagem, os camundongos foram eutanasiados e seus órgãos foram colhidos, em cada período analisado. Algumas das nanopartículas estavam presentes na traqueia e pulmões dos camundongos (Figura 16), mas sua fluorescência diminuiu ao longo do tempo (Figura 17). Estômago e intestinos apresentaram autofluorescência, demonstrada pela fluorescência no grupo C- (Figura 18 e Figura 19).

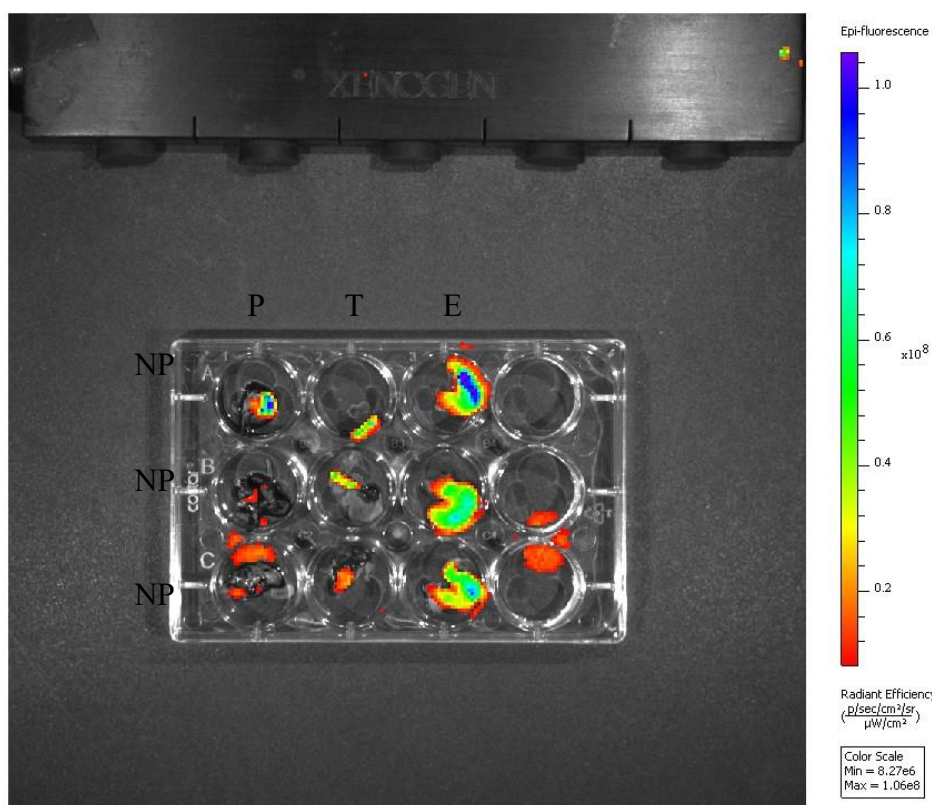


Figura 16. Imagem da fluorescência obtida com IVIS Spectrum mostrando o pulmão (P), traqueia (T) e estômago (E), após inoculação de 5 μL por narina das nanopartículas fluorescentes de quitosana Cy5.5 (NP) em 0 horas.

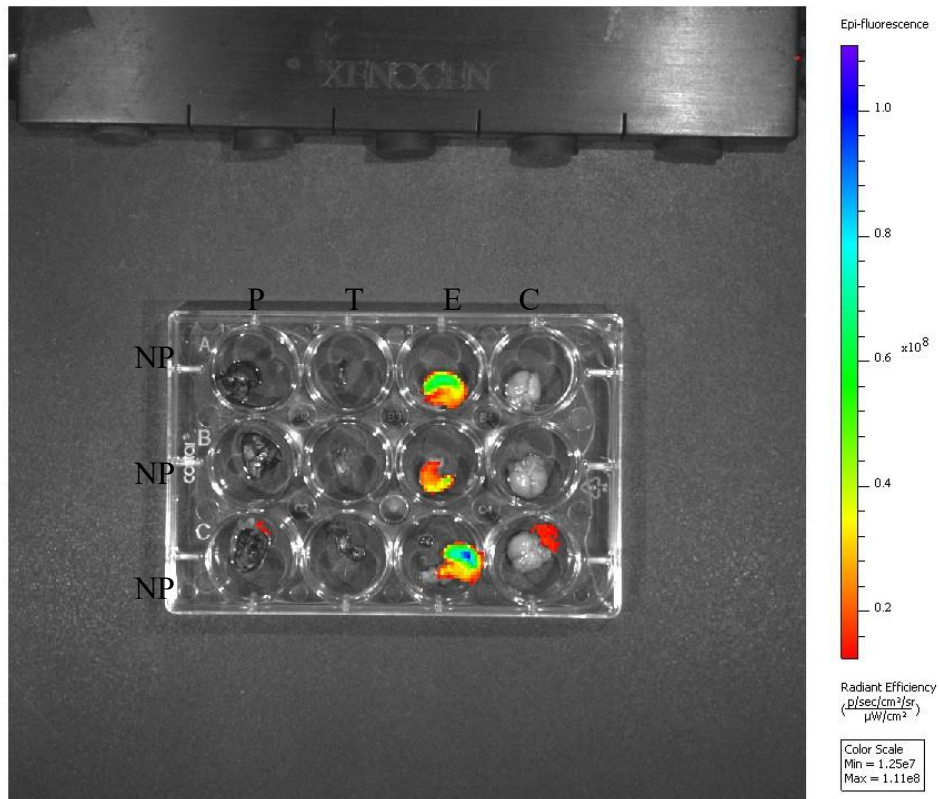


Figura 17. Imagem da fluorescência obtida com IVIS Spectrum mostrando o pulmão (P), traqueia (T) e estômago (E) e cérebro (C), após inoculação de 5 μL por narina das nanopartículas fluorescentes de quitosana Cy5.5 em 96 horas.

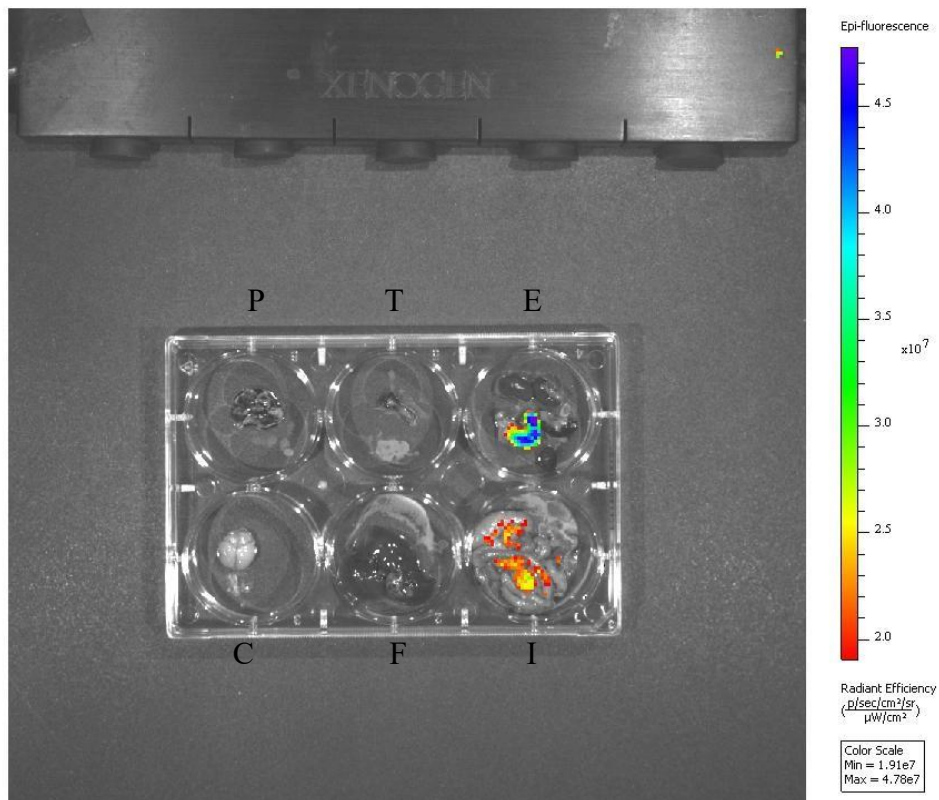


Figura 18. Imagem da fluorescência obtida com IVIS Spectrum mostrando o pulmão (P), traqueia (T) e estômago (E), cérebro (C), fígado (F) e intestinos (I) após inoculação de 5 μL por narina de PBS em 0 horas

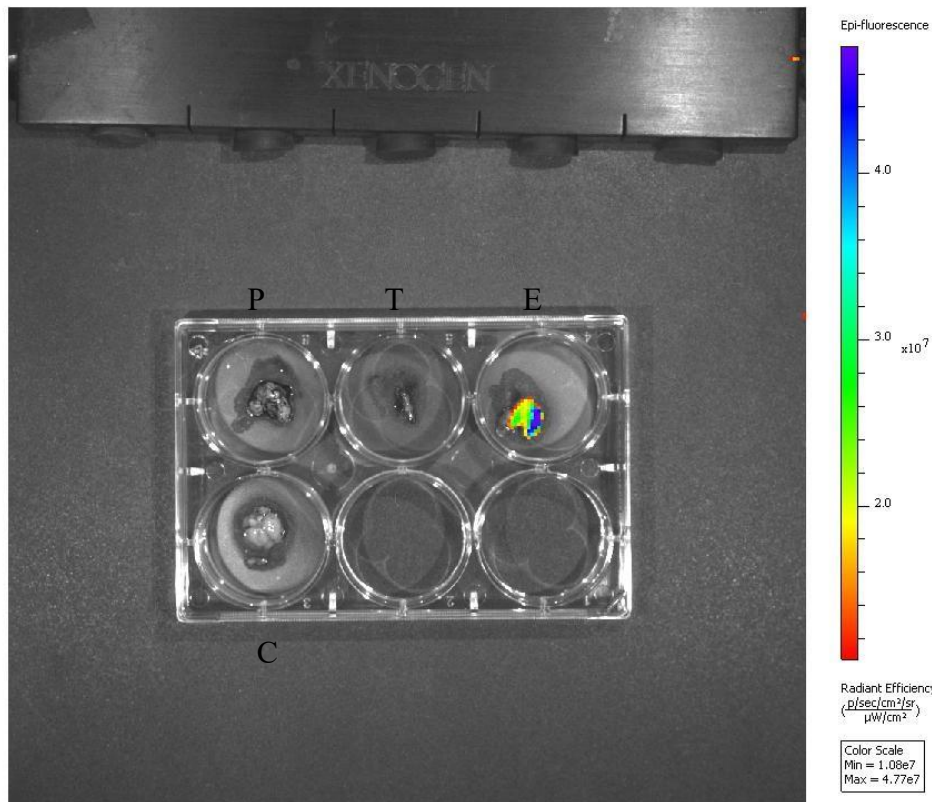


Figura 19. Imagem da fluorescência obtida com IVIS Spectrum mostrando o pulmão (P), traqueia (T) e estômago (E) e cérebro (C), após inoculação de 5 µL por narina PBS em 96 horas.

A presença de fluorescência no estômago e intestino dos camundongos pode ser explicada pela autofluorescência no alimento dos camundongos (110–114).

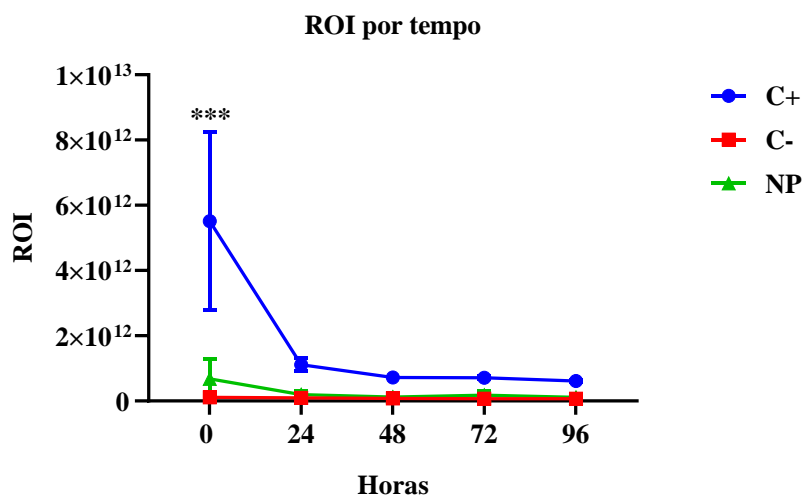


Figura 20. Intensidade fluorescente da região de interesse (ROI) ao longo do tempo, mostrando que a fluorescência foi estável durante todos os momentos para o grupo NP, e uma redução significativa da fluorescência para o grupo C+ nas primeiras 24 horas $p < 0,001$.

2.3 Ensaio de fagocitose das nanopartículas

As nanopartículas de quitosana marcadas com FITC foram fagocitadas por macrófagos alveolares (Figura 21 e 22) ou peritoneais (Figura 23 e 24) em 6 horas (dados não mostrados) e a fagocitose máxima ocorreu em 8 horas.

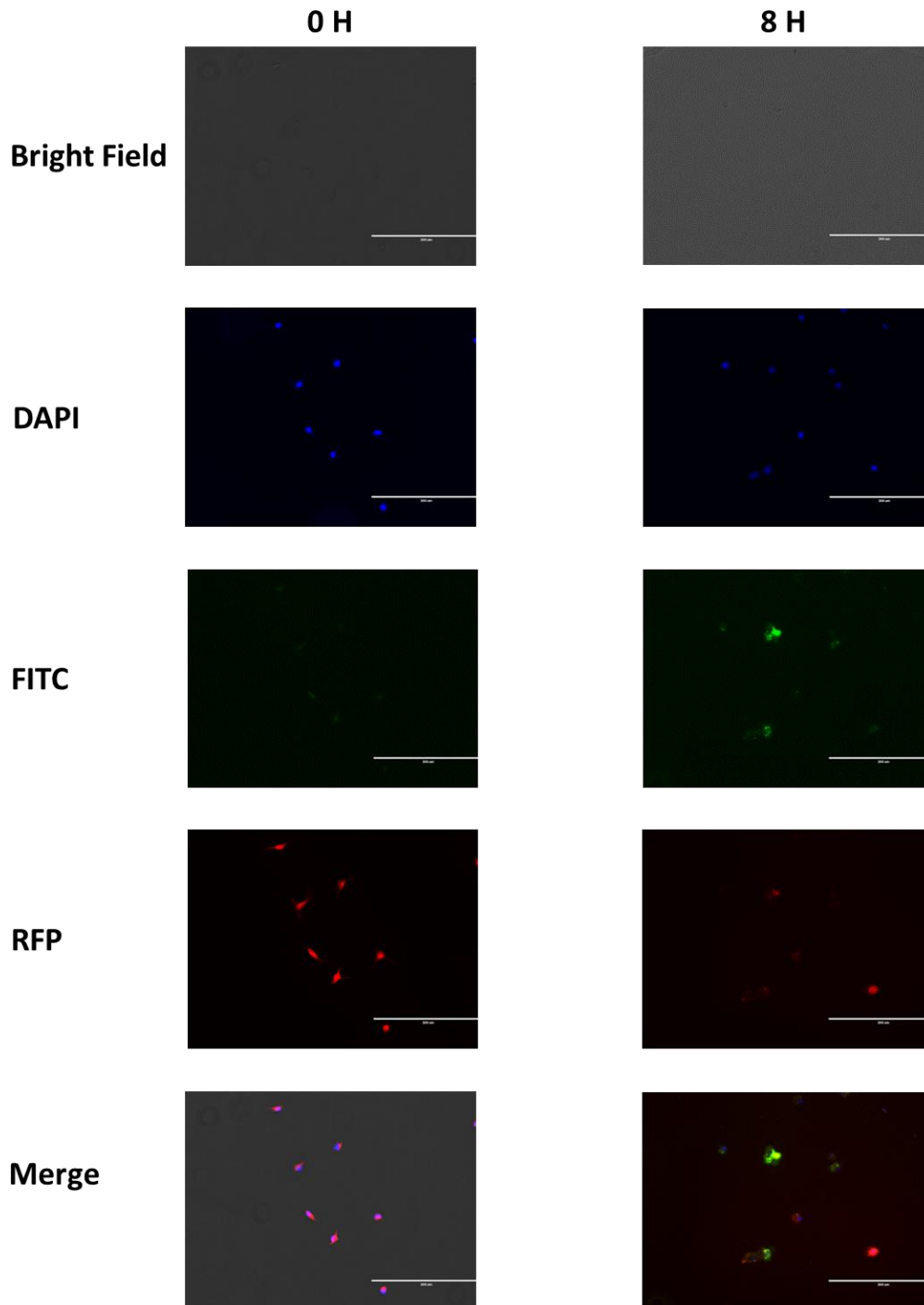


Figura 21. Fagocitose das nanopartículas de quitosana marcadas com FITC por macrófagos alveolares em 0 e 8 horas, mostrando as nanopartículas dentro dos lisossomos celulares após 8 horas. O filtro DAPI mostra os núcleos, o filtro FITC mostra as nanopartículas e o filtro RFP indica os lisossomos.

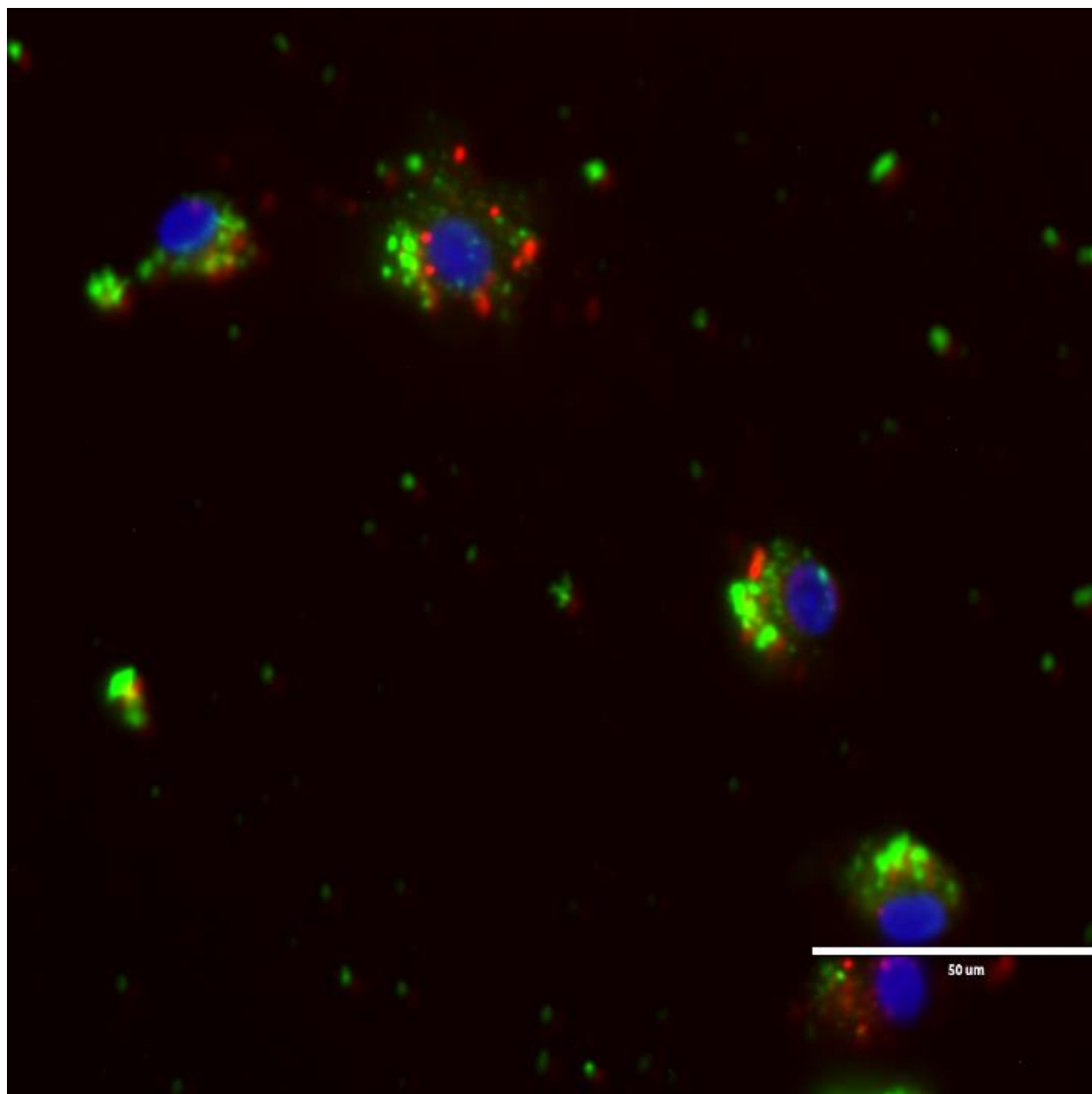


Figura 22. Fagocitose das nanopartículas de quitosana marcadas com FITC por macrófagos alveolares, mostrando as nanopartículas dentro dos lisossomos celulares após 8 horas. O filtro DAPI mostra os núcleos, o filtro FITC mostra as nanopartículas e o filtro RFP indica os lisossomos.

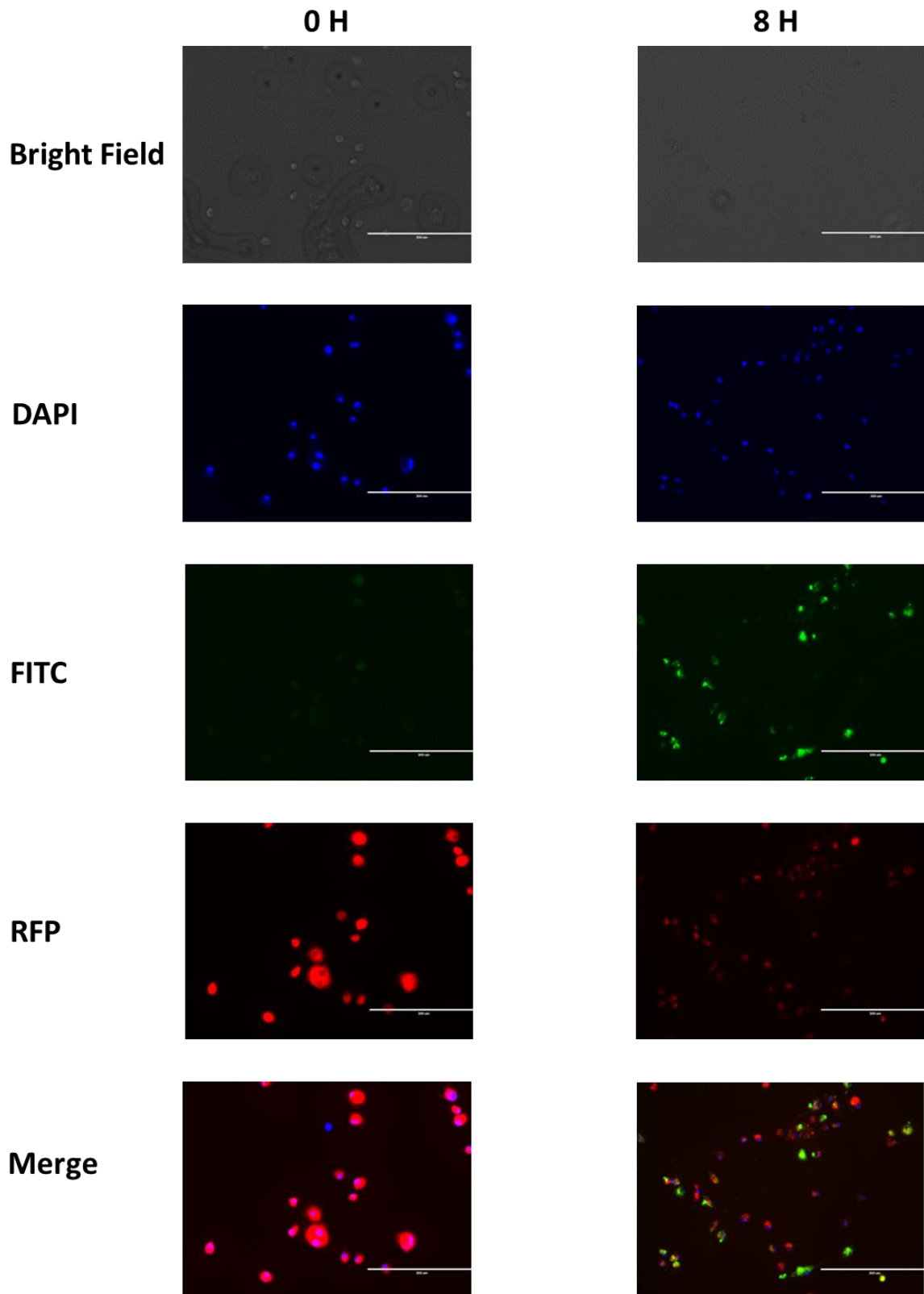


Figura 23. Fagocitose das nanopartículas de quitosana marcadas com FITC por macrófagos peritoneais em 0 e 8 horas, mostrando as nanopartículas dentro dos lisossomos celulares em 8 horas. O filtro DAPI mostra os núcleos, o filtro FITC mostra as nanopartículas e o filtro RFP indica os lisossomos.

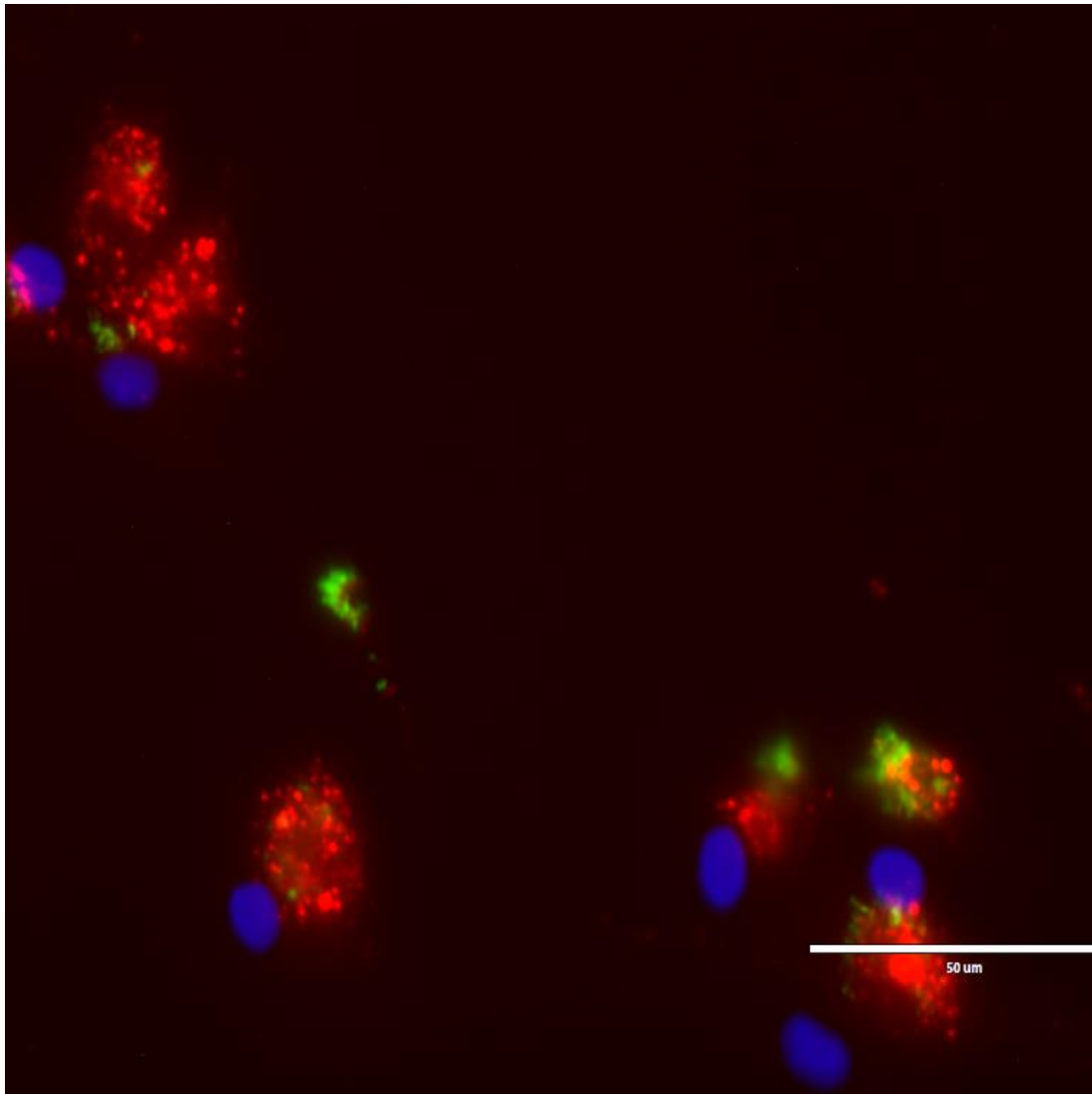


Figura 24. Fagocitose das nanopartículas de quitosana marcadas com FITC por macrófagos peritoneais, mostrando as nanopartículas dentro dos lisossomos celulares após 8 horas. O filtro DAPI mostra os núcleos, o filtro FITC mostra as nanopartículas e o filtro RFP indica os lisossomos.

3. DISCUSSÃO

Realizamos ensaios de biodistribuição a fim de otimizar ainda mais a entrega do peptídeo P10 usando nanopartículas de quitosana. Observamos que as nanopartículas foram fagocitadas nas primeiras 4 a 6 horas de interação com as células e que a maioria das nanopartículas estava aderida à mucosa do trato respiratório superior, sendo que quantidades menores foram detectadas na traqueia e pulmões onde permaneceram por pelo menos uma semana. Esses achados são consistentes com as características conferidas pelas nanopartículas de quitosana devido à sua capacidade mucoadesiva (94,95,115).

A fluorescência no estômago dos animais é causada pela presença de alfafa e seus derivados na ração dos camundongos, essas substâncias apresentam autofluorescência

que é captada pelo equipamento nas mesmas frequências de excitação e emissão do Cy5.5 (110–114).

A distribuição de vacinas administradas por via intranasal pode influenciar na localização final dessas partículas (trato respiratório ou trato gastrointestinal), conforme demonstrado na bibliografia atual, o volume de inoculação, indução da anestesia e posição do animal durante e após a vacinação são fatores que afetam a distribuição e localização de nanopartículas após a administração intranasal (116–118)

Em nosso delineamento experimental tentamos reduzir ao máximo as variáveis que pudessem influenciar na localização correta das nanopartículas, pois a ração dos animais apresentava fluorescência semelhante à do fluorocromo utilizado, mesmo com esses cuidados não podemos descartar a possibilidade de que uma pequena quantidade da vacina pode ter sido ingerida (112–116, 118–120).

As nanopartículas de quitosana utilizadas neste estudo não foram feitas com a finalidade de resistir ao baixo pH e nem a enzimas proteolíticas ou peptídicas presentes em certas regiões do trato gastrointestinal dos animais, mas se algumas das nanopartículas complexadas ou co-administradas com peptídeo passarem ilesas pelo trato gastrointestinal dos animais, acreditamos que células imunes relacionadas ao tecido linfóide associado ao intestino GALT (do inglês: *gut-associated lymphoid tissue*) possam ter capturado as nanopartículas e o peptídeo gerando uma resposta imune sistêmica, que foi eficaz na redução da carga fúngica nos pulmões dos animais (91,119,120)

4. CONCLUSÃO

- Demonstramos que as nanopartículas de quitosana complexadas com o peptídeo P10 permanecem principalmente na via aérea superior dos camundongos quando administradas por via intranasal com uma quantidade menor encontrada na traqueia e pulmões.
- As nanopartículas de quitosana complexadas com o peptídeo P10 foram fagocitadas nas primeiras 4 a 6 horas, sendo o pico de internalização das nanopartículas em 8 horas.

CAPÍTULO 4: PRODUÇÃO, CARACTERIZAÇÃO, AVALIAÇÃO DO NÚMERO DE DOSES VACINAIS E EFEITO ADJUVANTE DAS NANOPARTÍCULAS DE QUITOSANA NO TRATAMENTO DA PARACOCCIDIOIDOMICOSE

1. MATERIAIS E MÉTODOS

1.1 Preparação das nanopartículas

As nanopartículas foram preparadas de acordo com nosso protocolo previamente padronizado (54). Em resumo, uma solução de quitosana (quitosana de baixo peso molecular, Sigma-Aldrich, St. Louis, MO, EUA) foi misturada gota a gota com uma solução de tripolifosfato de sódio (TPP; Sigma-Aldrich) com ou sem peptídeo P10 (GenOne Biotech, Rio de Janeiro, RJ, Brasil). A primeira solução era composta por 2 mg/mL de quitosana, preparada pela dissolução da quitosana com 1% de ácido acético (concentração final) em água ultrapura sob agitação magnética por 1h em temperatura ambiente. O pH da solução de quitosana foi então ajustado para aproximadamente 4,4 usando NaOH 0,1 M. A segunda solução era composta por 1 mg/mL de TPP e 5 µg (massa final) do peptídeo P10 solubilizado para as nanopartículas complexadas ou sem o peptídeo P10 para as nanopartículas vazias.

A segunda solução (TPP+P10 ou TPP) foi misturada gota a gota na primeira solução sob agitação magnética por 90 minutos à temperatura ambiente. As nanopartículas foram lavadas com água ultrapura e centrifugadas a 13.200 rpm, 4 °C por 1 h, por três vezes. As nanopartículas foram então ressuspendidas em água ultrapura para sua caracterização físico-química, em PBS (veículo vacinal), ou DMEM (LGC Biotecnologia, Cotia, São Paulo, Brasil) (ensaio de fagocitose).

1.2 Caracterização físico-química das nanopartículas

Os tamanhos das nanopartículas e os índices de polidispersividade (PDI) foram determinados por espalhamento dinâmico de luz e o potencial Zeta foi medido por eletroforese capilar usando um equipamento Zetasizer nano Zs (Malvern Panalytical Ltd, Reino Unido).

1.3 Comitê de ética

Camundongos BALB/c nude e BALB, machos, livres de patógenos com idade entre 6-8 semanas, foram utilizados de acordo com a aprovação do comitê de ética da Universidade de São Paulo (CEUA ICB n° 3654290618).

1.4 Leveduras

P. brasiliensis cepa Pb 18 foi mantido na forma de levedura em meio sólido Fava Netto (121). As leveduras foram transferidas para meio líquido BHI (Brain Heart Infusion, Bacto™, BD, Franklin Lakes, New Jersey, EUA) suplementado com 4% de SFB, 4% de glicose (Difco™, BD) e cultivadas a 37 °C e 150 rpm de cinco a sete dias antes da infecção. As leveduras foram coletadas e lavadas por três vezes usando com PBS 1× e centrifugação a 3.000 rpm por dez minutos. As leveduras foram ressuspensas em 5 mL de PBS e a viabilidade das células fúngicas foi avaliada pela contagem de leveduras em uma câmara de Neubauer usando azul de tripan (Gibco, Thermo Fisher Scientific).

1.5 Delineamento experimental

Camundongos BALB/c (dez animais por grupo) foram organizados aleatoriamente nos seguintes grupos. Para a avaliação da atividade adjuvante entre a nanopartícula de quitosana e o peptídeo 10 foram utilizados os seguintes grupos: (**Pb 18**) – controle positivo, infectado sem tratamento; Nanopartículas associadas (**Ncomp**) – infectados e tratados com 3 doses de nanopartículas vazias co-administradas com 5µg/10µL de peptídeo P10; Complexado (**Comp**) – infectado e tratado com 3 doses de nanopartículas complexadas com 5µg/10µL de peptídeo P10; e (**SHAM**) – controle negativo, não infectado e não tratado (foram utilizados 120 animais no total).

Para o experimento testando diferenças entre uma única ou múltiplas doses do tratamento com nanopartículas de quitosana complexadas com o peptídeo P10 foram utilizados os seguintes grupos: (**Pb 18**) – controle positivo, infectado sem tratamento; (**1D**) – infectados e tratados com uma dose das nanopartículas complexadas com 5µg/10µL de peptídeo P10; (**2D**) – infectados e tratados com duas doses das nanopartículas complexadas com 5µg/10µL de peptídeo P10; (**3D**) – infectados e tratados com três doses das nanopartículas complexadas com 5µg/10µL de peptídeo P10; e (**SHAM**) – controle negativo, não infectado e não tratado. Embora **Comp** e **3D** sejam o mesmo regime, eles são nomeados de forma diferente para maior clareza nas diferentes abordagens experimentais (foram utilizados 150 animais no total).

1.6 Infecção intratraqueal

Para simular uma infecção causada por *P. brasiliensis*, camundongos BALB/c foram infectados com leveduras de Pb 18 na concentração de 3×10^5 levedura/50 μ L. Os animais foram anestesiados pela via peritoneal com 200 μ L de solução que continha 80 mg kg⁻¹ de cetamina e 10 mg kg⁻¹ de xilazina, foi feita uma incisão na traqueia e 50 μ L da suspensão de leveduras foram inoculadas. Após a infecção, a incisão foi suturada e o camundongo observado e mantido aquecido até a completa recuperação do animal.

1.7 Esquema de tratamento

Trinta dias após a infecção, as vacinas de nanopartículas foram administradas aos camundongos por via intranasal. 5 μ L de cada formulação vacinal foi em cada narina. Para camundongos que receberam mais de uma única inoculação, as nanopartículas foram administradas uma vez por semana.

1.8 Avaliação do UFC (Unidade Formadora de Colônia) e Citocinas

Para determinar os efeitos da vacinação, os camundongos foram eutanasiados 51 dias após a infecção e os pulmões foram removidos. Os pulmões foram macerados manualmente em 2 mL de PBS e 100 μ L do tecido foram plaqueados em meio sólido BHI, suplementado com 4% (vol/vol) SFB, 4% (vol/vol) glicose e 1% (vol/vol) pen/strp. As placas foram incubadas a 37 °C e as colônias foram contadas por até 21 dias.

Para avaliação das citocinas, 500 μ L dos macerados pulmonares foram aliqüotados em microtubos, que continham 500 μ L de inibidor de protease cOmplete™ (Roche, Suíça). A análise de citocinas foi realizada por Enzyme-Linked Immunosorbent Assay (ELISA) usando kits comerciais para as seguintes citocinas IL-2, IL-4, IL-10, IL-12 e IFN- γ (BD OptEIA™, BD) e IL -1 β e IL-23 Ensaio de Imunoadsorção Enzimática (ELISA) (Thermo Fisher Scientific). As absorvâncias foram avaliadas usando o equipamento Epoch 2 Microplate Spectrophotometer (BioTek Instruments, Inc. Winooski, Vermont, EUA).

1.9 Análise estatística

Foi realizada análise de variância (ANOVA) ou teste de Student seguido de pós-teste de Tukey ou Dunnett utilizando Graph Pad Prism 8. Os valores de p foram considerados significativos quando $< 0,05$, as barras de erro foram expressas como o erro padrão da média (SEM).

Todos os experimentos foram feitos em triplicata.

2. RESULTADOS

2.1 Caracterização das nanopartículas

O diâmetro e distribuição de tamanho, bem como o potencial Z das nanopartículas apresentaram as qualidades desejadas e esperadas para este tipo de polímero, de modo que os tamanhos das nanopartículas vazias ficaram em torno de 230 nm (Figura 25) com um PDI < 0,5 e as nanopartículas complexadas em torno de 330 nm (Figura 26) e com PDI < 0,5. O potencial Z ficou em torno de +20 mV para todas as partículas testadas.

	Size (d.nm...)	% Intensity:	St Dev (d.n...
Z-Average (d.nm): 238,4	Peak 1: 301,4	95,3	145,3
Pdl: 0,344	Peak 2: 4493	4,7	883,2
Intercept: 0,937	Peak 3: 0,000	0,0	0,000

Result quality Good

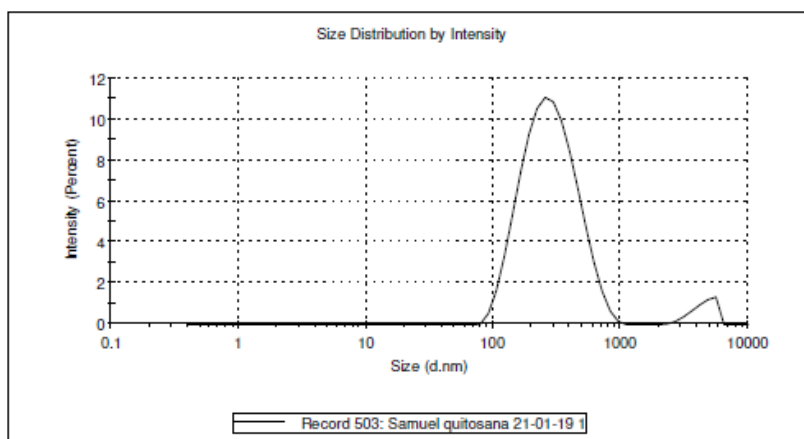


Figura 25. Gráfico demonstrativo do tamanho e PDI das nanopartículas de quitosana vazias.

	Size (d.nm...)	% Intensity:	St Dev (d.n...
Z-Average (d.nm): 341,3	Peak 1: 305,1	100,0	92,55
Pdl: 0,383	Peak 2: 0,000	0,0	0,000
Intercept: 0,963	Peak 3: 0,000	0,0	0,000

Result quality Good

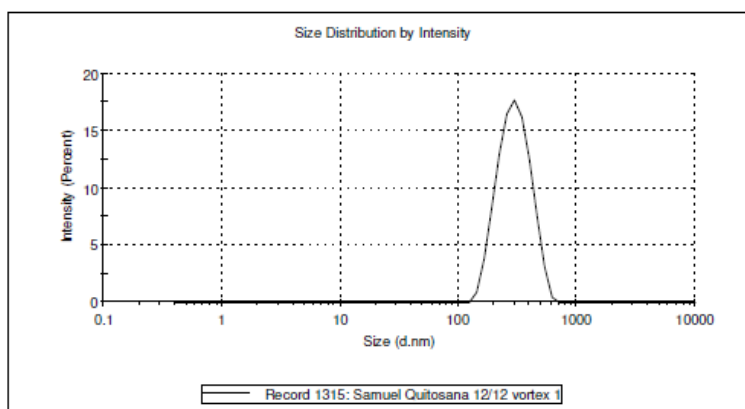


Figura 26. Gráfico demonstrativo do tamanho e PDI das nanopartículas de quitosana complexadas com o peptídeo P10.

2.2 Análise do UFC após 51 dias de infecção

Os animais foram eutanasiados após 51 dias de infecção durante os quais não foram tratados durante os primeiros 30 dias (estabelecimento da doença) e então tratados com nanopartículas ou deixados sem tratamento (**Pb 18**, controle infectado). Após a eutanásia os pulmões foram coletados assepticamente, macerados e alíquotas plaqueadas para avaliar a eficácia das nanopartículas de quitosana complexadas com peptídeo P10 e o efeito adjuvante das nanopartículas de quitosana vazias co-administradas com o peptídeo P10. Os pulmões dos animais infectados dos grupos **Pb18**, **Comp** e **Ncomp** foram significativamente mais pesados que os pulmões dos animais controle (**SHAM**, não infectados e não tratados), indicando o sucesso da infecção (Figura 27). As contagens de UFC mostraram uma diminuição significativa das leveduras viáveis de *Paracoccidioides* dos pulmões de ambos os grupos de camundongos tratados com nanopartículas em comparação com o grupo não tratado (Figura 28). As UFC foram semelhantes entre os camundongos tratados com nanopartículas complexadas com P10 e os animais que receberam nanopartículas vazias de quitosana co-administradas com P10.

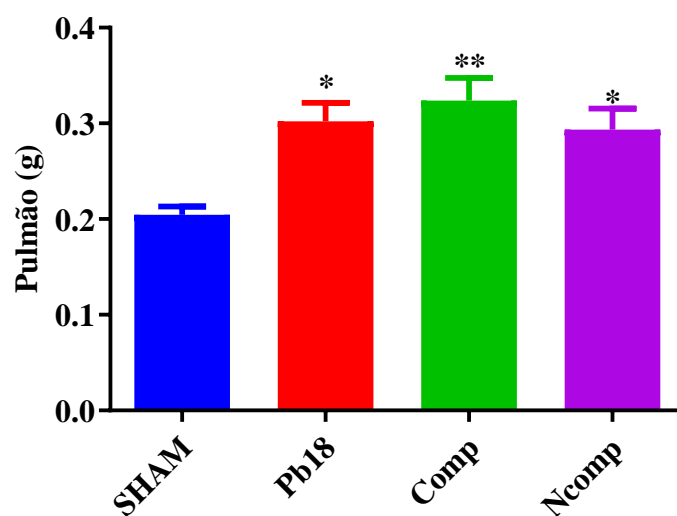


Figura 27. Peso dos pulmões após a eutanásia (51 dias após a infecção). Houve aumento significativo do peso pulmonar dos animais infectados quando comparados ao grupo **SHAM**. **SHAM** (não infectado e não tratado), **Pb18** (infectado e não tratado), **Comp** (infectado e tratado com as nanopartículas complexadas com P10) e **Ncomp** (infectado e tratado com o P10 associado às nanopartículas vazias). * = $p < 0,05$ e ** = $p < 0,01$.

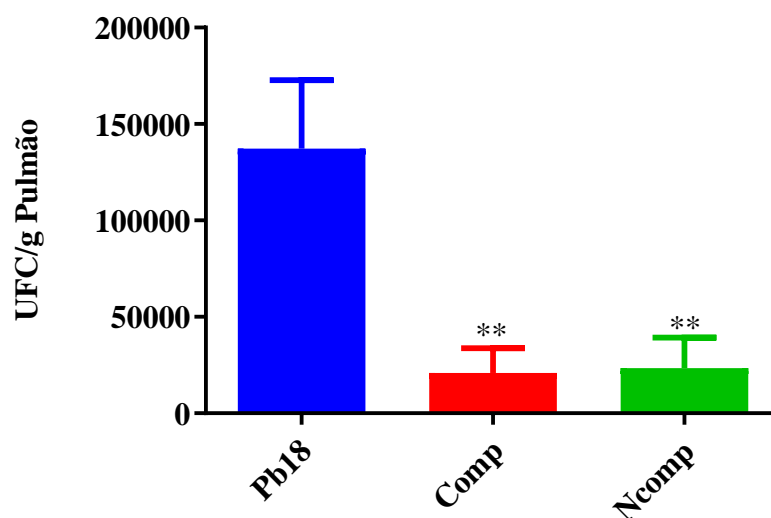


Figura 28. UFC por grama de pulmão dos camundongos 51 dias após a infecção. Os animais tratados com as nanopartículas tiveram uma redução significativa nas células viáveis de *Paracoccidioides* em comparação com o grupo **Pb 18**. **Pb18** (infetado e não tratado), **Comp** (infetado e tratado com nanopartículas complexadas com P10) e **Ncomp** (infetado e tratado com P10 e com nanopartículas vazias). ** = $p < 0,01$.

2.3 Análise das citocinas presentes no pulmão dos animais utilizados para a verificação do efeito adjuvante da quitosana.

A produção de citocinas foi avaliada 51 dias após a infecção utilizando os mesmos animais estudados para a contagem de UFC. Os macerados pulmonares desses camundongos foram armazenados em freezer $-20\text{ }^{\circ}\text{C}$ em microtubos que continham um inibidor de proteinase até serem utilizados para análise de citocinas por ELISA. Concentramos nossa análise em citocinas associadas a populações de células T do tipo Th_1 (Figura 29), Th_2 (Figura 30) e Th_{17} (Figura 31). Verificamos que as nanopartículas induziram uma ativação Th_1 e Th_{17} , embora também houvesse uma pequena, mas não ausente, resposta Th_2 .

Não foi detectada IL-2 nos pulmões dos animais analisados enquanto os níveis de IL-12 e IFN- γ foram significativamente aumentados, quando comparados ao grupo **Pb18**. Os níveis de IL-12 foram maiores no grupo **Ncomp** quando comparado ao grupo **Comp**. A IL-4 foi significativamente diminuída e a IL-10 foi significativamente aumentada para ambos os grupos tratados com nanopartículas quando comparados ao grupo **Pb18**. Não foram detectadas alterações nos níveis de IL-1 β , mas a IL-23 foi significativamente

aumentada para ambos os grupos de tratamento com nanopartículas quando comparado ao grupo **Pb18**.

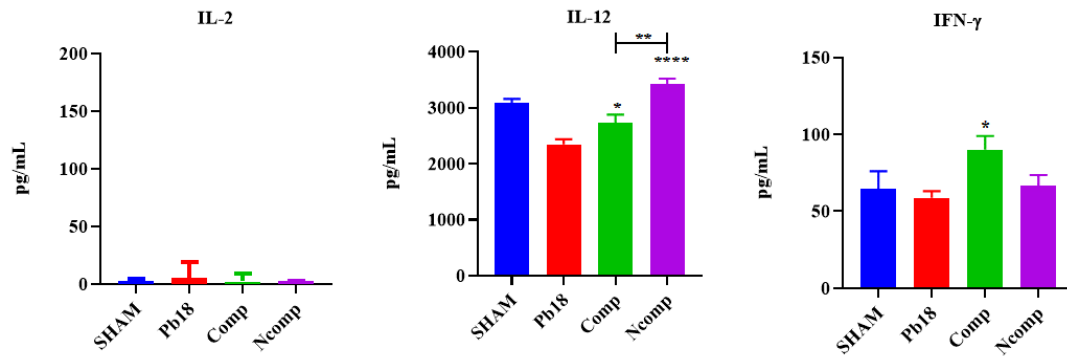


Figura 29. Produção de citocinas Th₁ 51 dias após a infecção. Não foi detectada IL-2, e IL-12 e IFN-γ foram significativamente aumentados, quando comparados ao grupo **Pb18**. **SHAM** (não infectado e não tratado), **Pb18** (infectado e não tratado), **Comp** (infectado e tratado com as nanopartículas complexadas com P10) e **Ncomp** (infectado e tratado com o P10 coadministrado com nanopartículas vazias). * = p<0,05; ** = p<0,01 e **** = p<0,0001.

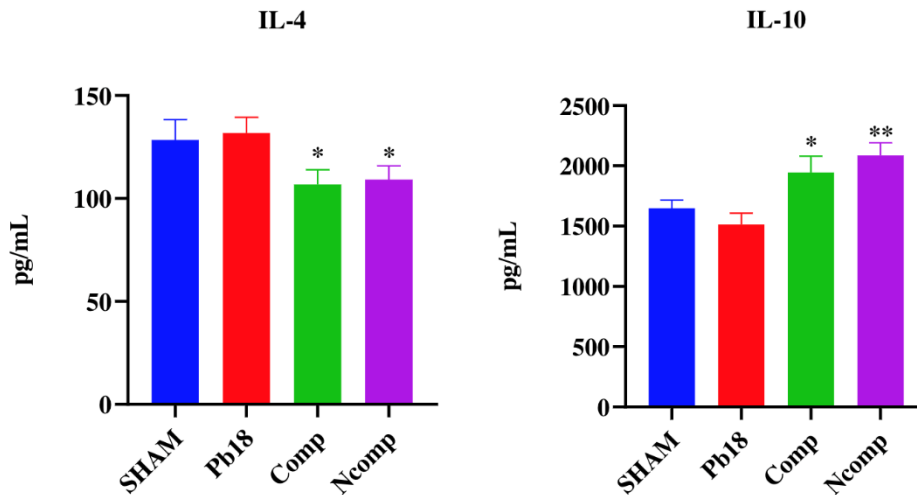


Figura 30. Produção de citocinas Th₂ 51 dias após a infecção. A IL-4 foi significativamente diminuída e a IL-10 foi significativamente aumentada para ambos os grupos tratados com nanopartículas quando comparados ao grupo **Pb18**. **SHAM** (não infectado e não tratado), **Pb18** (infectado e não tratado), **Comp** (infectado e tratado com as nanopartículas complexadas com P10) e **Ncomp** (infectado e tratado com o P10 coadministrado com nanopartículas vazias). * = p<0,05 e ** = p<0,01.

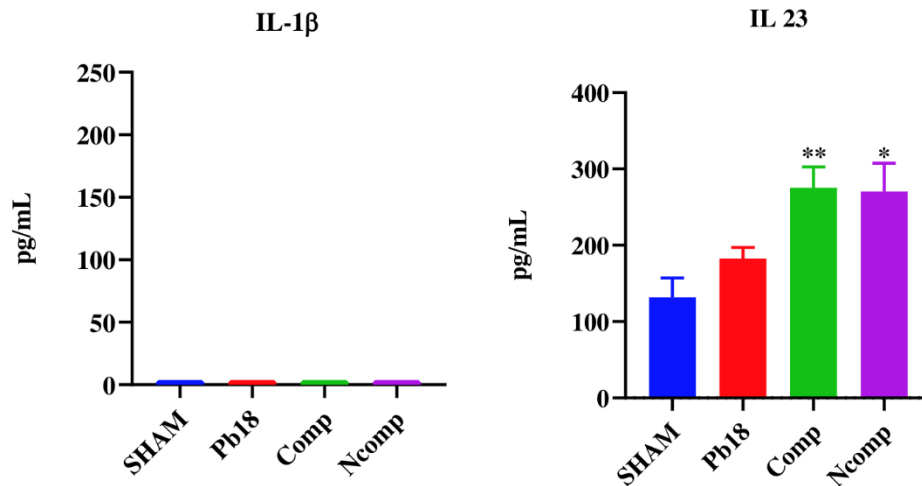


Figura 31. Th₁₇ induziu a produção de citocinas 51 dias após a infecção. Não foram detectadas alterações nos níveis de IL-1 β , mas a IL-23 foi significativamente aumentada para ambos os grupos de tratamento com nanopartículas quando comparado ao grupo Pb18. **SHAM** (não infectado e não tratado), **Pb18** (infectado e não tratado), **Comp** (infectado e tratado com as nanopartículas complexadas com P10) e **Ncomp** (infectado e tratado com o P10 coadministrado com nanopartículas vazias). * = p<0,05 e ** = p<0,01.

2.4 Análise de UFC após 51 dias de infecção

Os pulmões dos animais infectados (**Pb18, 1D, 2D e 3D**) foram significativamente mais pesados que os pulmões dos camundongos do grupo não infectado e não tratado (**SHAM**) (Figura 32), demonstrando sucesso na infecção dos animais pela via intratraqueal. As UFC foram significativamente menores nos animais tratados com nanopartículas complexadas com P10 em comparação com os camundongos infectados e não tratados (Figura 33). Notavelmente, não houve diferenças entre um único tratamento com as nanopartículas e uma segunda ou terceira administração dos compostos com uma semana de intervalo.

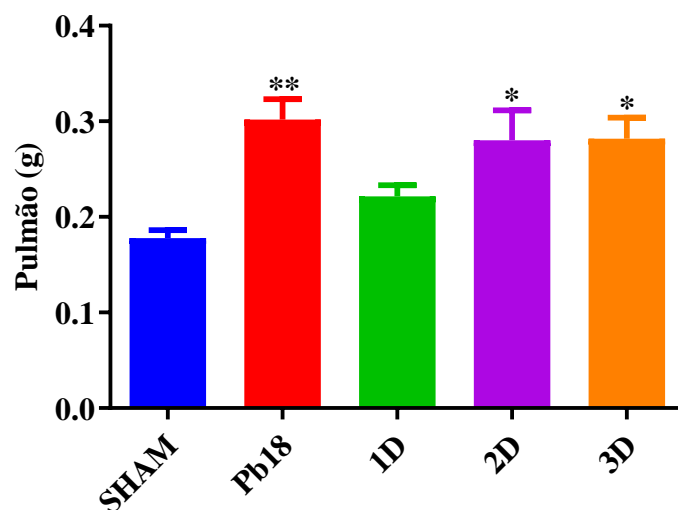


Figura 32. Peso dos pulmões após a eutanásia (51 dias após a infecção). Houve aumento significativo do peso pulmonar dos animais infectados, quando comparados ao grupo **SHAM**. **SHAM** (não infectado e não tratado), **Pb18** (infectado e não tratado), **1D** (infectado e tratado com uma dose das nanopartículas complexadas com P10), **2D** (infectado e tratado com duas doses das nanopartículas complexadas com P10) e **3D** (infectado e tratado com três doses das nanopartículas complexadas com P10). * = $p < 0,05$ e ** = $p < 0,01$.

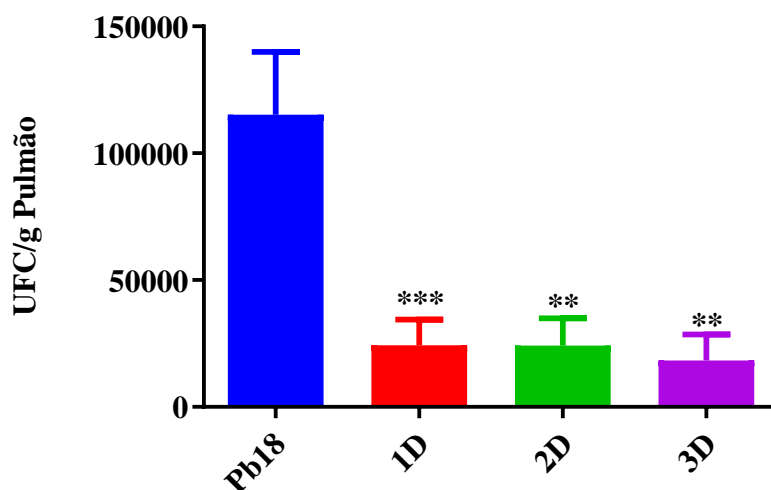


Figura 33. UFC dos pulmões 51 dias após a infecção. As nanopartículas complexadas com P10 reduziram significativamente o número de células viáveis de *Paracoccidioides* quando comparadas ao grupo **Pb 18**. **SHAM** (não infectado e não tratado), **Pb18** (infectado e não tratado), **1D** (infectado e tratado com uma dose das nanopartículas complexadas com P10), **2D** (infectado e tratado com duas doses das nanopartículas complexadas com P10) e **3D** (infectado e tratado com três doses das nanopartículas complexadas com P10). ** = $p < 0,01$ e *** = $p < 0,001$

2.5 Análise das citocinas presentes no pulmão dos animais utilizados para a verificação do efeito do número de doses vacinais no tratamento da PCM.

Com base na redução de UFC foi avaliada a produção de citocinas pulmonares somente nos grupos **P18**, **Sham** e **1D**, novamente o foco foi voltado para as citocinas associadas à população de células T do tipo Th₁, Th₂ e Th₁₇ (Tabela 2). Identificamos uma ativação Th₁ e Th₁₇ juntamente com uma pequena, mas não ausente, resposta Th₂.

Não foi detectada IL-2 nos pulmões dos animais analisados enquanto os níveis de IL-12 estavam significativamente aumentados no grupo **1D**, quando comparado ao grupo **Pb18**. Os níveis de IFN- γ estavam significativamente aumentados no grupo **1D**, quando comparados ao grupo **Pb18**. IL-4 e IL-10 estavam significativamente aumentados no grupo **1D**, quando comparados ao grupo **Pb18**. Nenhuma alteração significativa foi observada para a IL-1 β , e a IL-23 foi significativamente aumentada em todos os diferentes grupos de doses, quando comparado ao grupo **Pb18**.

Tabela 2. Produção de citocinas Th₁, Th₂ e Th₁₇ 51 dias após a infecção.

Grup os	Citocinas						
	Th ₁		Th ₂			Th ₁₇	
	IL-2	IL-12	IFN- γ	IL-4	IL-10	IL-1 β	IL-23
Sham	0	2605 \pm 480,1	80,96 \pm 22	148,4 \pm 57,84	1965 \pm 297,8	0	339,4 \pm 208,9
Pb 18	0	2491 \pm 502,8	66,80 \pm 9,9	140,4 \pm 37,61	2000 \pm 387,7	0	117,0 \pm 107,2
1D	0	3168 \pm 438,5 ***	92,84 \pm 29,38 *	193,6 \pm 47,72 **	2418 \pm 299,8 **	0	232,4 \pm 87,20 **

Produção de citocinas Th₁, Th₂ e Th₁₇ quando comparado ao grupo Pb18. Números em itálico = SD, * = p<0,05; ** = p<0,01 e *** = p<0,001.

3. DISCUSSÃO

A PCM é uma das doenças fúngicas mais prevalentes e negligenciadas na América Latina, especialmente no Brasil. Novas formas de tratamento são uma questão importante, pois, devido ao tempo de tratamento e toxicidades, é comum o abandono do tratamento e o ressurgimento da infecção (7). Além das drogas antifúngicas tradicionais, novas abordagens para prevenir ou tratar as doenças fúngicas se fazem importantes, principalmente as que propõem a indução de respostas imunes celulares que foram demonstradas como ideais para a eliminação ou contenção de infecções fúngicas (48,122).

Nosso grupo demonstrou com sucesso que o uso de nanopartículas poliméricas é vantajoso para o tratamento da PCM (11,54). O uso de nanopartículas permite a redução da carga da molécula ativa, além de servir como adjuvante em vacinas, o que pode levar a um aumento na relação custo-benefício e eficácia de uma vacina (11,54).

O peptídeo P10 vem sendo estudado há várias décadas, e seu efeito imunomodulador é bem descrito, mas seu uso como terapêutico não é otimizado, pois há a necessidade de grandes concentrações do peptídeo e adjuvantes fortes, que às vezes podem interferir na modulação da resposta imune, para gerar uma resposta protetora do hospedeiro a PCM (11,54,123).

A redução da carga fúngica em camundongos infectados tratados com P10 complexado às nanopartículas já era esperada devido a trabalhos anteriores do nosso grupo de pesquisa utilizando nanopartículas de quitosana como vacina intranasal para tratar a PCM (54). A inovação deste novo trabalho foi a redução do número de doses e a redução da concentração do peptídeo P10 quando co-administrado com nanopartículas de quitosana vazias, demonstrando os efeitos adjuvante e imunomodulador das nanopartículas de quitosana (84,124–129).

A redução do número de doses vacinais e a concentração de P10 estão diretamente relacionadas com a redução de custo. Aqui mostramos a redução da quantidade total de peptídeo P10 que normalmente era utilizado como padrão (60 µg em três doses) para 12 vezes menos (5 µg em uma única dose) para as nanopartículas complexadas e para 4 vezes menos quando o peptídeo foi utilizado co-administrado com as nanopartículas vazias (11,54,130).

O efeito adjuvante da quitosana a torna uma escolha ideal para uso em vacinas que visam induzir respostas imunes com ênfase no recrutamento celular e não humoral (84,124–129).

A quitosana estimula células fagocíticas, como macrófagos e células dendríticas, a produzir interferons tipo 1 e interleucinas, principalmente IL-1β, e essa estimulação é baseada na interação da quitosana com receptores TLR-4, estimulação do inflamassoma NLRP3 (necessário para combater e ou conter *Paracoccidioides*), e ativação de vias de sinalização celular STING (estimulador de genes de interferon), que funciona como um detector de ácido nucleico e cGAS (sintase de dinucleotídeos cíclicos de guanina e adenina) co-estimulador de STING (84,124–129).

A imunidade da mucosa é outro fator chave relacionado à redução da carga fúngica potencializada pelo efeito adjuvante das nanopartículas de quitosana (131,132). A mucosa das vias aéreas superiores é conhecida como um dos principais fatores relacionados à prevenção de infecções (133). É possível encontrar na região nasal diferentes mecanismos relacionados à imunidade inata e adaptativa, como o próprio muco, repleto de enzimas e proteínas relacionadas à degradação, inativação e opsonização de partículas ou microrganismos potencialmente perigosos (134). Células fagocitárias e células apresentadoras de antígeno também são encontradas na mucosa das vias aéreas superiores, estas células podem ser as responsáveis pela captação das nanopartículas de quitosana (131,132,135). Após a captação, o efeito adjuvante da quitosana é ativado

levando à estimulação ou re-estimulação do mecanismo efetor responsável por conter ou eliminar as leveduras de *Paracoccidioides* nos pulmões (22,23,25). Devido à esperada resposta imune induzida por nanopartículas e ao tipo de resposta imune elicitada pela infecção, analisamos os grupos de citocinas associadas à resposta protetora no combate a infecções fúngicas. Essas citocinas pertencem aos subconjuntos de células T Th₁ e Th₁₇, que são responsáveis por coordenar a eliminação ou contenção das leveduras (9).

As vacinas de nanopartículas de quitosana complexadas ou co-administradas foram capazes de aumentar os níveis de IL-12 e IFN- γ , importantes citocinas Th₁ relacionadas à inflamação e eliminação de *Paracoccidioides*, embora não tenha sido detectada IL-2, provavelmente porque sua liberação ocorre nas primeiras 24 horas de estimulação (9,18,41,136). Os níveis de IL-4 foram reduzidos e os níveis de IL-10 ligeiramente aumentados, essas citocinas Th₂ provavelmente estão relacionadas ao controle da inflamação, reparo tecidual ou reorganização celular, importantes para a formação do granuloma (9,18). Nenhuma IL-1 β foi significativamente detectada, mas os níveis de IL-23 foram aumentados apontando para uma possível presença do subconjunto de células T Th₁₇ (9,18,23).

Resultados semelhantes de citocinas foram observados no grupo da vacina de dose única, mostrando níveis aumentados de citocinas relacionadas a Th₁ e Th₁₇ e presença aumentada de citocinas Th₂ (9,18,23)

Observamos um aumento nos níveis das citocinas IL-12, IFN- γ , IL-4 e IL-10 do grupo tratado (1D) em relação aos grupos controles (SHAM e Pb18), e a análise estatística foi realizada comparando o grupo 1D com o grupo infectado com Pb 18 (9,18,23).

Pequenas variações nos níveis de citocinas foram detectadas entre lotes de camundongos, mesmo sendo animais isogênicos e livres de patógenos, no entanto o padrão geral de resposta foi semelhante nos diferentes experimentos (9,18,23).

Com base em nossos achados, podemos inferir que as nanopartículas de quitosana aderidas à mucosa estão sendo fagocitadas constante e lentamente, induzindo a produção de citocinas inflamatórias associada a células do tipo T Th₁ e Th₁₇, reduzindo a carga fúngica nos pulmões.

4. CONCLUSÃO

- As nanopartículas de quitosana mostraram potencial como adjuvante para vacinas que envolvem resposta imune Th₁ e Th₁₇, ideais para combater infecções fúngicas,

pois não foi necessária a complexação das nanopartículas com o peptídeo P10 para reduzir a carga fúngica no pulmão dos animais.

- As nanopartículas de quitosana mostraram que é possível reduzir o número de doses vacinais para se obter a redução das leveduras de *Paracoccidioides* nos pulmões dos animais.

BIBLIOGRAFIA

1. Travassos LR, Taborda CP. Paracoccidioidomycosis vaccine. Hum Vaccin Immunother [Internet]. 2012 Oct 16;8(10):1450–3. Available from: <http://www.tandfonline.com/doi/abs/10.4161/hv.21283>
2. Turissini DA, Gomez OM, Teixeira MM, McEwen JG, Matute DR. Species boundaries in the human pathogen *Paracoccidioides*. Fungal Genet Biol [Internet]. 2017;106(April):9–25. Available from: <http://www.sciencedirect.com/science/article/pii/S1087184517300932>
3. WHO fungal priority pathogens list to guide research, development and public health action [Internet]. Geneva: World Health Organization: World Health Organization; 2022 [cited 2022 Nov 19]. 48 p. Available from: <https://www.who.int/publications/i/item/9789240060241>
4. Palmeiro M, Cherubini K, Yurgel LS. Paracoccidioidomicose – Revisão da Literatura. Sci Medica, Porto Alegre PUCRS. 2005;15(4):274–8.
5. Peçanha PM, Peçanha-Pietrobon PM, Grão-Velloso TR, Rosa Júnior M, Falqueto A, Gonçalves SS. Paracoccidioidomycosis: What We Know and What Is New in Epidemiology, Diagnosis, and Treatment. J Fungi [Internet]. 2022 Oct 1 [cited 2022 Nov 19];8(10):1098. Available from: [/pmc/articles/PMC9605487/](https://pubmed.ncbi.nlm.nih.gov/33826630/)
6. Mattos K, Cocio TA, Chaves EGA, Borges CL, Venturini J, de Carvalho LR, et al. An update on the occurrence of *Paracoccidioides* species in the Midwest region, Brazil: Molecular epidemiology, clinical aspects and serological profile of patients from Mato Grosso do Sul State. PLoS Negl Trop Dis [Internet]. 2021 Apr 1 [cited 2022 Nov 19];15(4). Available from: <https://pubmed.ncbi.nlm.nih.gov/33826630/>
7. Shikanai-Yasuda MA, Mendes RP, Colombo AL, de Queiroz-Telles F, Kono ASG, Paniago AMM, et al. Brazilian guidelines for the clinical management of paracoccidioidomycosis. Rev Soc Bras Med Trop. 2017;50(5):715–40.
8. Restrepo A, Gómez BL, Tobón A. Paracoccidioidomycosis: Latin America's own fungal disorder. Curr Fungal Infect Rep. 2012;6(4):303–11.
9. Taborda CP, Travassos LR, Benard G. Paracoccidioidomycosis. In: Encyclopedia

- of Mycology [Internet]. Elsevier; 2021 [cited 2021 Sep 28]. p. 654–75. Available from: <https://linkinghub.elsevier.com/retrieve/pii/B9780128199909000019>
10. Terçarioli GR, Bagagli E, Reis GM, Theodoro RC, Bosco SDMG, Macoris SADG, et al. Ecological study of *Paracoccidioides brasiliensis* in soil: Growth ability, conidia production and molecular detection. *BMC Microbiol.* 2007;7:1–8.
 11. Amaral AC, Marques AF, Muñoz JE, Bocca AL, Simioni AR, Tedesco AC, et al. Poly(lactic acid-glycolic acid) nanoparticles markedly improve immunological protection provided by peptide P10 against murine paracoccidioidomycosis. *Br J Pharmacol* [Internet]. 2010 Mar;159(5):1126–32. Available from: <http://doi.wiley.com/10.1111/j.1476-5381.2009.00617.x>
 12. Gegembauer G, Araujo LM, Pereira EF, Rodrigues AM, Paniago AMM, Hahn RC, et al. Serology of Paracoccidioidomycosis Due to *Paracoccidioides lutzii*. *PLoS Negl Trop Dis.* 2014;8(7).
 13. De Melo Teixeira M, Theodoro RC, Freire F, De Oliveira M, Machado GC, Hahn RC, et al. *Paracoccidioides lutzii* sp. nov.: biological and clinical implications. *Med Mycol.* 2014;52(June 2013):19–28.
 14. Aristizábal BH, Clemons K V., Cock AM, Restrepo A, Stevens DA. Experimental *Paracoccidioides brasiliensis* infection in mice: influence of the hormonal status of the host on tissue responses. *Med Mycol.* 2002 Jan;40(2):169–78.
 15. Restrepo a, McEwen JG, Castañeda E. The habitat of *Paracoccidioides brasiliensis*: how far from solving the riddle? *Med Mycol.* 2001;39(3):233–41.
 16. Mendes JF, Klafke GB, Albano APN, Cabana ÂL, Teles AJ, de Camargo ZP, et al. Paracoccidioidomycosis infection in domestic and wild mammals by *Paracoccidioides lutzii*. *Mycoses* [Internet]. 2017;(November 2016):1–5. Available from: <http://doi.wiley.com/10.1111/myc.12608>
<http://www.ncbi.nlm.nih.gov/pubmed/28295653>
 17. Teixeira MM, Theodoro RC, de Carvalho MJA, Fernandes L, Paes HC, Hahn RC, et al. Phylogenetic analysis reveals a high level of speciation in the

- Paracoccidioides genus. *Mol Phylogenet Evol* [Internet]. 2009;52(2):273–83. Available from: <http://dx.doi.org/10.1016/j.ympev.2009.04.005>
18. Benard G. An overview of the immunopathology of human paracoccidioidomycosis. *Mycopathologia*. 2008;165:209–21.
 19. Calich VLG, Mamoni RL, Loures F V. Regulatory T cells in paracoccidioidomycosis. *Virulence* [Internet]. 2019 Jan 1 [cited 2022 Nov 19];10(1):810. Available from: </pmc/articles/PMC6779406/>
 20. Bocca AL, Amaral AC, Teixeira MM, Sato PK, Sato P, Shikanai-Yasuda MA, et al. Paracoccidioidomycosis: eco-epidemiology, taxonomy and clinical and therapeutic issues. *Future Microbiol* [Internet]. 2013;8(9):1177–91. Available from: <http://www.ncbi.nlm.nih.gov/pubmed/24020744>
 21. Shikanai-yasuda MA, Queiroz F De, Filho T, Mendes RP, Colombo AL, Moretti ML, et al. Consenso em paracoccidioidomicose Guidelines in paracoccidioidomycosis. *Rev Soc Bras Med Trop*. 2006;39(3):297–310.
 22. Khader SA, Gaffen SL, Kolls JK. Th17 cells at the crossroads of innate and adaptive immunity against infectious diseases at the mucosa. *Mucosal Immunol* [Internet]. 2009 Sep 8;2(5):403–11. Available from: www.nature.com/mi
 23. Kolls JK, Khader SA. The role of Th17 cytokines in primary mucosal immunity. *Cytokine Growth Factor Rev* [Internet]. 2010 Dec;21(6):443–8. Available from: <https://linkinghub.elsevier.com/retrieve/pii/S1359610110000808>
 24. Paulovičová L, Paulovičová E, Bystrický S. Immunological basis of anti- *Candida* vaccines focused on synthetically prepared cell wall mannan-derived manno-oligomers. *Microbiol Immunol* [Internet]. 2014 Oct;58(10):545–51. Available from: <http://doi.wiley.com/10.1111/1348-0421.12195>
 25. Burger E. Paracoccidioidomycosis Protective Immunity. *J Fungi* [Internet]. 2021 Feb [cited 2022 Nov 21];7(2). Available from: </pmc/articles/PMC7918802/>
 26. de Castro LF, Ferreira MC, da Silva RM, Blotta MH de SL, Longhi LNA, Mamoni RL. Characterization of the immune response in human paracoccidioidomycosis.

- J Infect [Internet]. 2013 Nov [cited 2022 Nov 21];67(5):470–85. Available from: <https://pubmed.ncbi.nlm.nih.gov/23872208/>
27. De Oliveira HC, Assato PA, Marcos CM, Scorzoni L, De Paula E Silva ACA, Da Silva J de F, et al. Paracoccidioides-host interaction: An overview on recent advances in the paracoccidioidomycosis. *Front Microbiol*. 2015;6(NOV):1319.
 28. Alves CCS, Azevedo ALS, Rodrigues MF, Machado RP, Souza MA, Machado MA, et al. Cellular and humoral immune responses during intrathoracic paracoccidioidomycosis in BALB/c mice. *Comp Immunol Microbiol Infect Dis* [Internet]. 2009 [cited 2022 Nov 21];32:513–25. Available from: www.elsevier.com/locate/cimid Available online at www.sciencedirect.com
 29. Calich VLG, da Costa TA, Felonato M, Arruda C, Bernardino S, Loures FV, et al. Innate immunity to *Paracoccidioides brasiliensis* infection. *Mycopathologia* [Internet]. 2008 Apr 24 [cited 2022 Nov 21];165(4–5):223–36. Available from: <http://link.springer.com/10.1007/s11046-007-9048-1>
 30. Dias L dos S, Silva LBR, Nosanchuk JD, Taborda CP. Neutrophil Cells Are Essential for The Efficacy of a Therapeutic Vaccine against Paracoccidioidomycosis. *J Fungi* 2021, Vol 7, Page 416 [Internet]. 2021 May 26 [cited 2022 Nov 21];7(6):416. Available from: <https://www.mdpi.com/2309-608X/7/6/416/htm>
 31. Pagán AJ, Ramakrishnan L. The Formation and Function of Granulomas. *Annu Rev Immunol* [Internet]. 2018 Apr 26 [cited 2022 Nov 21];36(1):639–65. Available from: <https://pubmed.ncbi.nlm.nih.gov/29400999/>
 32. Cock AM, Cano LE, Vélez D, Aristizábal BH, Trujillo J, Restrepo A. Fibrotic sequelae in pulmonary paracoccidioidomycosis: Histopathological aspects in BALB/c mice infected with viable and non-viable *Paracoccidioides brasiliensis* propagules. *Rev Inst Med Trop Sao Paulo*. 2000;42(2):59–66.
 33. Restrepo A, Arango MD. In vitro susceptibility testing of *Paracoccidioides brasiliensis* to sulfonamides. *Antimicrob Agents Chemother*. 1980;18(1):190–4.
 34. Borges SRC, Da Silva GMS, Da Costa Chambela M, De Vasconcellos De CRO,

- Costa RLB, Wanke B, et al. Itraconazole vs. trimethoprim-sulfamethoxazole: A comparative cohort study of 200 patients with paracoccidioidomycosis. *Med Mycol.* 2014;52(3):303–10.
35. Kioshima ES, de Mendonça P de SB, Teixeira M de M, Capoci IRG, Amaral A, Rodrigues-Vendramini FAV, et al. One Century of Study: What We Learned about Paracoccidioides and How This Pathogen Contributed to Advances in Antifungal Therapy. *J Fungi* 2021, Vol 7, Page 106 [Internet]. 2021 Feb 2 [cited 2022 Nov 19];7(2):106. Available from: <https://www.mdpi.com/2309-608X/7/2/106/htm>
 36. Silva LDC, de Oliveira AA, de Souza DR, Barbosa KLB, E Silva KSF, Carvalho Júnior MAB, et al. Overview of Antifungal Drugs against Paracoccidioidomycosis: How Do We Start, Where Are We, and Where Are We Going? *J Fungi* 2020, Vol 6, Page 300 [Internet]. 2020 Nov 19 [cited 2022 Nov 19];6(4):300. Available from: <https://www.mdpi.com/2309-608X/6/4/300/htm>
 37. Nascimento EM, Sgarbi B, Cristina V, Costa S, Miranda A, Silva A, et al. Immunization with radioattenuated yeast cells of *Paracoccidioides brasiliensis* induces a long lasting protection in BALB / c mice. *Vaccine.* 2007;25:7893–9.
 38. Assis-marques MA, Oliveira AF, Ruas LP, Reis F, Roque-barreira MC, Sergio P, et al. *Saccharomyces cerevisiae* Expressing gp43 Protects Mice against *Paracoccidioides brasiliensis* Infection. *PLoS One.* 2015;1–13.
 39. Diniz SN, Reis BS, Goes TS, Zouain CS, Leite MF, Goes AM. Protective immunity induced in mice by F0 and FII antigens purified from *Paracoccidioides brasiliensis*. *Vaccine* [Internet]. 2004 Jan;22(3–4):485–92. Available from: <http://linkinghub.elsevier.com/retrieve/pii/S0264410X03006078>
 40. Pinto AR, Puccia R, Diniz SN, Franco MF, Travassos R. DNA-based vaccination against murine paracoccidioidomycosis using the gp43 gene from *Paracoccidioides brasiliensis*. *Vaccine.* 2000;18:3050–8.
 41. Ribeiro AM, Bocca AL, Amaral AC, Faccioli LH, Galetti FCS, Zárata-Bladés CR, et al. DNAhsp65 vaccination induces protection in mice against *Paracoccidioides brasiliensis* infection. *Vaccine* [Internet]. 2009 Jan;27(4):606–13. Available from: <http://linkinghub.elsevier.com/retrieve/pii/S0264410X08013819>

42. Ribeiro AM, Souza ACO, Amaral AC, Vasconcelos NM, Jerônimo MS, Carneiro FP, et al. Nanobiotechnological Approaches to Delivery of DNA Vaccine Against Fungal Infection. *J Biomed Nanotechnol* [Internet]. 2013 Feb 1;9(2):221–30. Available from: <http://openurl.ingenta.com/content/xref?genre=article&issn=1550-7033&volume=9&issue=2&spage=221>
43. Ribeiro AM, Bocca AL, Amaral AC, Souza ACCO, Faccioli LH, Coelho-Castelo AAM, et al. HSP65 DNA as therapeutic strategy to treat experimental paracoccidioidomycosis. *Vaccine* [Internet]. 2010 Feb;28(6):1528–34. Available from: <http://linkinghub.elsevier.com/retrieve/pii/S0264410X09018659>
44. Amorim J de, Magalhães A, Muñoz JE, Rittner GMG, Nosanchuk JD, Travassos LR, et al. DNA vaccine encoding peptide P10 against experimental paracoccidioidomycosis induces long-term protection in presence of regulatory T cells. *Microbes Infect* [Internet]. 2013 Mar;15(3):181–91. Available from: <http://linkinghub.elsevier.com/retrieve/pii/S1286457912003073>
45. Braga CJMM, Rittner GMGG, Henao JEMM, Teixeira AF, Massis LM, Sbrogio-Almeida ME, et al. Paracoccidioides brasiliensis vaccine formulations based on the gp43-derived P10 sequence and the Salmonella enterica FliC flagellin. *Infect Immun*. 2009;77(4):1700–7.
46. dos Santos Junior SR, Amaral AC, Taborda CP. Application of Nanoparticles to Invasive Fungal Infections. In: *Nanotechnology for Infectious Diseases* [Internet]. Singapore: Springer Singapore; 2022 [cited 2022 Aug 15]. p. 151–73. Available from: https://link.springer.com/chapter/10.1007/978-981-16-9190-4_7
47. Taborda CP, Juliano MA, Puccia R, Franco M, Travassos LR. Mapping of the T-cell epitope in the major 43-kilodalton glycoprotein of Paracoccidioides brasiliensis which induces a Th-1 response protective against fungal infection in BALB/c mice. *Infect Immun*. 1998;66(2):786–93.
48. TABORDA CP, URÁN ME, NOSANCHUK JD, TRAVASSOS LR. PARACOCCIDIOIDOMYCOSIS: CHALLENGES IN THE DEVELOPMENT OF A VACCINE AGAINST AN ENDEMIC MYCOSIS IN THE AMERICAS.

- Rev Inst Med Trop Sao Paulo [Internet]. 2015 Sep;57(suppl 19):21–4. Available from: http://www.scielo.br/scielo.php?script=sci_arttext&pid=S0036-46652015000800021&lng=en&tlng=en
49. Rittner GMG, Muñoz JE, Marques AF, Nosanchuk JD, Taborda CP, Travassos LR. Therapeutic DNA Vaccine Encoding Peptide P10 against Experimental Paracoccidioidomycosis. Bethony JM, editor. PLoS Negl Trop Dis [Internet]. 2012 Feb 28;6(2):e1519. Available from: <http://dx.plos.org/10.1371/journal.pntd.0001519>
 50. Holanda RA, Muñoz JE, Dias LS, Silva LBR, Santos JRA, Pagliari S, et al. Recombinant vaccines of a CD4+ T-cell epitope promote efficient control of Paracoccidioides brasiliensis burden by restraining primary organ infection. Al-Salem WS, editor. PLoS Negl Trop Dis [Internet]. 2017 Sep 22;11(9):e0005927. Available from: <http://dx.plos.org/10.1371/journal.pntd.0005927>
 51. Magalhães A, Ferreira KS, Almeida SR, Nosanchuk JD, Travassos LR, Taborda CP. Prophylactic and Therapeutic Vaccination Using Dendritic Cells Primed with Peptide 10 Derived from the 43-Kilodalton Glycoprotein of Paracoccidioides brasiliensis. Clin Vaccine Immunol [Internet]. 2012 Jan;19(1):23–9. Available from: <http://cvi.asm.org/lookup/doi/10.1128/CVI.05414-11>
 52. Silva LBR, Dias LS, Rittner GMG, Muñoz JE, Souza ACO, Nosanchuk JD, et al. Dendritic Cells Primed with Paracoccidioides brasiliensis Peptide P10 Are Therapeutic in Immunosuppressed Mice with Paracoccidioidomycosis. Front Microbiol [Internet]. 2017 Jun 14;8(JUN):1–10. Available from: <http://journal.frontiersin.org/article/10.3389/fmicb.2017.01057/full>
 53. de Araújo MV, Santos Júnior SR Dos, Nosanchuk JD, Taborda CP. Therapeutic vaccination with cationic liposomes formulated with dioctadecyldimethylammonium and trehalose dibehenate (Caf01) and peptide p10 is protective in mice infected with paracoccidioides brasiliensis. J Fungi. 2020;6(4):1–16.
 54. Rodrigues Dos Santos Junior S, Kelley Lopes da Silva F, Santos Dias L, Oliveira Souza AC, Valdemir de Araujo M, Buffoni Roque da Silva L, et al. Intranasal

- Vaccine Using P10 Peptide Complexed within Chitosan Polymeric Nanoparticles as Experimental Therapy for Paracoccidioidomycosis in Murine Model. *J Fungi* [Internet]. 2020 Sep 2;6(3):160. Available from: <https://www.mdpi.com/2309-608X/6/3/160>
55. De Mattos Grosso D, De Almeida SR, Mariano M, Lopes JD. Characterization of gp70 and Anti-gp70 Monoclonal Antibodies in *Paracoccidioides brasiliensis* Pathogenesis. *Infect Immun* [Internet]. 2003 Nov [cited 2022 Nov 19];71(11):6534–42. Available from: <https://journals.asm.org/doi/10.1128/IAI.71.11.6534-6542.2003>
 56. Thomaz L, Nosanchuk JD, Rossi DCP, Travassos LR, Taborda CP. Monoclonal antibodies to heat shock protein 60 induce a protective immune response against experimental *Paracoccidioides lutzii*. *Microbes Infect* [Internet]. 2014 Sep;16(9):788–95. Available from: <http://dx.doi.org/10.1016/j.micinf.2014.08.004>
 57. Buissa-Filho R, Puccia R, Marques AF, Pinto FA, Munoz JE, Nosanchuk JD, et al. The Monoclonal Antibody against the Major Diagnostic Antigen of *Paracoccidioides brasiliensis* Mediates Immune Protection in Infected BALB/c Mice Challenged Intratracheally with the Fungus. *Infect Immun* [Internet]. 2008 Jul 1;76(7):3321–8. Available from: <http://iai.asm.org/cgi/doi/10.1128/IAI.00349-08>
 58. Gesztesi J-Ll, Puccia R, Travassos Lr, Vicentini Ap, De Moraes Jz FM. Monoclonal antibodies against the 43,000 Da glycoprotein from *Paracoccidioides brasiliensis* modulate laminin-mediated fungal adhesion to epithelial cells and pathogenesis. *Hybridoma*. 1996 Dec;15(6):415–22.
 59. Schroeder HW, Cavacini L. Structure and function of immunoglobulins. *J Allergy Clin Immunol* [Internet]. 2010 Feb;125(2):S41–52. Available from: <http://linkinghub.elsevier.com/retrieve/pii/S0091674909014651>
 60. Casadevall A. Antibody immunity and invasive fungal infections. *Infect Immun* [Internet]. 1995 [cited 2020 Nov 7];63(11):4211–8. Available from: <https://www.ncbi.nlm.nih.gov/pmc/articles/PMC173598/>

61. Casadevall A, Pirofski L. Insights into Mechanisms of Antibody-Mediated Immunity from Studies with *Cryptococcus neoformans*. *Curr Mol Med* [Internet]. 2005 Jun 1;5(4):421–33. Available from: <http://www.ncbi.nlm.nih.gov/pubmed/15977998>
62. Casadevall A, Feldmesser M, Pirofski LA. Induced humoral immunity and vaccination against major human fungal pathogens. *Curr Opin Microbiol*. 2002;5(4):386–91.
63. Nosanchuk J. Protective Antibodies and Endemic Dimorphic Fungi. *Curr Mol Med* [Internet]. 2005;5(4):435–42. Available from: <http://www.eurekaselect.com/openurl/content.php?genre=article&issn=1566-5240&volume=5&issue=4&spage=435>
64. Boniche C, Rossi SA, Kischkel B, Barbalho FV, Moura ÁND, Nosanchuk JD, et al. Immunotherapy against Systemic Fungal Infections Based on Monoclonal Antibodies. *J fungi (Basel, Switzerland)* [Internet]. 2020 Mar 1 [cited 2022 Nov 19];6(1). Available from: <https://pubmed.ncbi.nlm.nih.gov/32121415/>
65. Urán ME, Nosanchuk JD, Restrepo A, Hamilton AJ, Gómez BL, Cano LE. Detection of Antibodies against *Paracoccidioides brasiliensis* Melanin in In Vitro and In Vivo Studies during Infection. *Clin VACCINE Immunol*. 2011;18(10):1680–8.
66. da Silva MB, Marques AF, Nosanchuk JD, Casadevall A, Travassos LR, Tabora CP. Melanin in the dimorphic fungal pathogen *Paracoccidioides brasiliensis*: effects on phagocytosis, intracellular resistance and drug susceptibility. *Microbes Infect*. 2006 Jan;8(1):197–205.
67. Bueno RA, Thomaz L, Muñoz JE, Da Silva CJ, Nosanchuk JD, Pinto MR, et al. Antibodies against glycolipids enhance antifungal activity of macrophages and reduce fungal burden after infection with *Paracoccidioides brasiliensis*. *Front Microbiol*. 2016 Feb 3;7(FEB):1–10.
68. Puccia R, Travassos LR. The 43-kDa glycoprotein from the human pathogen *Paracoccidioides brasiliensis* and its deglycosylated form: Excretion and susceptibility to proteolysis. *Arch Biochem Biophys*. 1991 Aug;289(1):298–302.

69. Thomaz L. Proteção ou exacerbação de anticorpos monoclonais gerados contra antígenos de *Paracoccidioides brasiliensis* na infecção experimental. [Internet]. Instituto de Ciências Biomédicas 2, Universidade de São Paulo; 2012. Available from: https://www.teses.usp.br/teses/disponiveis/42/42132/tde-30012013-105937/publico/LucianaThomaz_Doutorado.PDF%0Ahttp://www.teses.usp.br/teses/disponiveis/42/42132/tde-30012013-105937/
70. Ahmed TA, Aljaeid BM. Preparation , characterization , and potential application of chitosan , chitosan derivatives , and chitosan metal nanoparticles in pharmaceutical drug delivery. *Drug Des Devel Ther.* 2016;10:483–507.
71. Bolhassani A, Javanzad S, Saleh T, Hashemi M, Aghasadeghi MR, Sadat SM. Polymeric nanoparticles Potent vectors for vaccine delivery targeting cancer and infectious diseases. *Hum Vaccines Immunother.* 2014;10(2):321–3.
72. Carcaboso AM, Hernandez RM, Igartua M, Rosas JE, Patarroyo ME, Pedraz JL. Potent, long lasting systemic antibody levels and mixed Th1/Th2 immune response after nasal immunization with malaria antigen loaded PLGA microparticles. *Vaccine.* 2004;22(11–12):1423–32.
73. Csaba N, Garcia-Fuentes M, Alonso MJ. Nanoparticles for nasal vaccination. *Adv Drug Deliv Rev* [Internet]. 2009;61(2):140–57. Available from: <http://dx.doi.org/10.1016/j.addr.2008.09.005>
74. Amaral AC, Bocca AL, Ribeiro AM, Nunes J, Peixoto DLGG, Simioni AR, et al. Amphotericin B in poly(lactic-co-glycolic acid) (PLGA) and dimercaptosuccinic acid (DMSA) nanoparticles against paracoccidioidomycosis. *J Antimicrob Chemother* [Internet]. 2009 Jan 15;63(3):526–33. Available from: <https://academic.oup.com/jac/article-lookup/doi/10.1093/jac/dkn539>
75. Jannuzzi GP, Souza N de A, Françoso KS, Pereira RH, Santos RP, Kaihami GH, et al. Therapeutic treatment with scFv–PLGA nanoparticles decreases pulmonary fungal load in a murine model of paracoccidioidomycosis. *Microbes Infect* [Internet]. 2018 Jan;20(1):48–56. Available from: <https://linkinghub.elsevier.com/retrieve/pii/S1286457917301478>
76. Kheiri A, Moosawi Jorf SA, Malhipour A, Saremi H, Nikkhah M. Synthesis and

- characterization of chitosan nanoparticles and their effect on *Fusarium* head blight and oxidative activity in wheat. *Int J Biol Macromol* [Internet]. 2017 Sep;102:526–38. Available from: <http://dx.doi.org/10.1016/j.ijbiomac.2017.04.034>
77. Dananjaya SHS, Erandani WKC, Kim C-H, Nikapitiya C, Lee J, De Zoysa M. Comparative study on antifungal activities of chitosan nanoparticles and chitosan silver nano composites against *Fusarium oxysporum* species complex. *Int J Biol Macromol* [Internet]. 2017 Dec;105:478–88. Available from: <http://dx.doi.org/10.1016/j.ijbiomac.2017.07.056>
 78. Read RC, Naylor SC, Potter CW, Bond J, Jabbal-Gill I, Fisher A, et al. Effective nasal influenza vaccine delivery using chitosan. *Vaccine*. 2005;23(35):4367–74.
 79. da Silva FKL, de Sa Alexandre AR, Casas AA, Ribeiro MC, de Souza KMC, Soares ES, et al. Increased production of chitinase by a *Paenibacillus illinoisensis* isolated from Brazilian coastal soil when immobilized in alginate beads. *Folia Microbiol (Praha)* [Internet]. 2022 Jul 18 [cited 2022 Nov 19];67(6):935–45. Available from: <https://link.springer.com/article/10.1007/s12223-022-00992-3>
 80. Signini R, Campana Filho SP. Purificação e caracterização de quitosana comercial. *Polímeros Ciência e Tecnol*. 1998;8(4):63–8.
 81. Battisti M V., Campana-Filho SP. Obtenção e caracterização de a-quitina e quitosanas de cascas de *Macrobrachium rosenbergii*. *Quim Nova*. 2008;31(8):2014–9.
 82. Ribeiro MC, Correa VLR, Silva FKL da, Casas AA, Chagas A de L das, Oliveira LP de, et al. Wound healing treatment using insulin within polymeric nanoparticles in the diabetes animal model. *Eur J Pharm Sci*. 2020 Jul 1;150:105330.
 83. Bano I, Arshad M, Yasin T, Ghauri MA, Younus M. Chitosan: A potential biopolymer for wound management. *Int J Biol Macromol* [Internet]. 2017;102:380–3. Available from: <http://dx.doi.org/10.1016/j.ijbiomac.2017.04.047>
 84. Carroll EC, Jin L, Mori A, Muñoz-Wolf N, Oleszycka E, Moran HBT, et al. The Vaccine Adjuvant Chitosan Promotes Cellular Immunity via DNA Sensor cGAS-

- STING-Dependent Induction of Type I Interferons. *Immunity* [Internet]. 2016 Mar 15 [cited 2022 Aug 15];44(3):597–608. Available from: <https://pubmed.ncbi.nlm.nih.gov/26944200/>
85. Muzzarelli R. Chitins and Chitosans as Immunoadjuvants and Non-Allergenic Drug Carriers. *Mar Drugs* [Internet]. 2010 Feb 21;8(2):292–312. Available from: <http://www.mdpi.com/1660-3397/8/2/292>
 86. Riteau N, Sher A. Chitosan: An Adjuvant with an Unanticipated STING. *Immunity* [Internet]. 2016;44(3):522–4. Available from: <http://dx.doi.org/10.1016/j.immuni.2016.03.002>
 87. Zhao K, Zhang Y, Zhang X, Shi C, Wang X, Wang X, et al. Chitosan-coated poly(lactic-co-glycolic) acid nanoparticles as an efficient delivery system for Newcastle disease virus DNA vaccine. *Int J Nanomedicine* [Internet]. 2014;9(1):4609–19. Available from: [https://www.dovepress.com/chitosan-coated-poly\(lactic-co-glycolic-acid-nanoparticles-as-an-efficient-delivery-system-for-newcastle-disease-virus-dna-vaccine-peer-reviewed-article-IJN](https://www.dovepress.com/chitosan-coated-poly(lactic-co-glycolic-acid-nanoparticles-as-an-efficient-delivery-system-for-newcastle-disease-virus-dna-vaccine-peer-reviewed-article-IJN)
 88. Khalili I, Ghadimipour R, Sadigh Eteghad S, Fathi Najafi M, Ebrahimi MM, Godsian N, et al. Evaluation of Immune Response Against Inactivated Avian Influenza (H9N2) Vaccine, by Using Chitosan Nanoparticles. *Jundishapur J Microbiol* [Internet]. 2015;8(12):10–4. Available from: http://www.jjmicrobiol.com/?page=article&article_id=27035
 89. da Silva MB, Thomaz L, Marques AF, Svidzinski AE, Nosanchuk JD, Casadevall A, et al. Resistance of melanized yeast cells of *Paracoccidioides brasiliensis* to antimicrobial oxidants and inhibition of phagocytosis using carbohydrates and monoclonal antibody to CD18. *Mem Inst Oswaldo Cruz*. 2009;104(4):644–8.
 90. Renu S, Renukaradhya GJ. Chitosan Nanoparticle Based Mucosal Vaccines Delivered Against Infectious Diseases of Poultry and Pigs. *Front Bioeng Biotechnol*. 2020 Nov 13;8:1316.
 91. Pan L, Zhang Z, Lv J, Zhou P, Hu W, Fang Y, et al. Induction of mucosal immune responses and protection of cattle against direct-contact challenge by intranasal delivery with foot-and-mouth disease virus antigen mediated by nanoparticles. *Int J Nanomedicine*. 2014;9(1):5603–18.

92. Lebre F, Borchard G, Faneca H, Pedroso De Lima MC, Borges O. Intranasal Administration of Novel Chitosan Nanoparticle/DNA Complexes Induces Antibody Response to Hepatitis B Surface Antigen in Mice. *Mol Pharm* [Internet]. 2016;13(2):472–82. Available from: <http://www.embase.com/search/results?subaction=viewrecord&from=export&id=L608002633>
93. Jesus S, Soares E, Costa J, Borchard G, Borges O. Immune response elicited by an intranasally delivered HBsAg low-dose adsorbed to poly- ϵ -caprolactone based nanoparticles. *Int J Pharm* [Internet]. 2016;504(1–2):59–69. Available from: <http://linkinghub.elsevier.com/retrieve/pii/S0378517316302125>
94. Raj PM, Raj R, Kaul A, Mishra AK, Ram A. Biodistribution and targeting potential assessment of mucoadhesive chitosan nanoparticles designed for ulcerative colitis via scintigraphy. *RSC Adv* [Internet]. 2018 Jun 5 [cited 2022 Aug 15];8(37):20809–21. Available from: <https://pubs.rsc.org/en/content/articlehtml/2018/ra/c8ra01898g>
95. Shim S, Soh SH, Im Y Bin, Park HE, Cho CS, Kim S, et al. Elicitation of Th1/Th2 related responses in mice by chitosan nanoparticles loaded with *Brucella abortus* malate dehydrogenase, outer membrane proteins 10 and 19. *Int J Med Microbiol*. 2020 Jan 1;310(1):151362.
96. Fernandes Costa A, Evangelista Araujo D, Santos Cabral M, Teles Brito I, Borges de Menezes Leite L, Pereira M, et al. Development, characterization, and in vitro–in vivo evaluation of polymeric nanoparticles containing miconazole and farnesol for treatment of vulvovaginal candidiasis. *Med Mycol* [Internet]. 2019 Jan 1;57(1):52–62. Available from: <https://academic.oup.com/mmy/article/57/1/52/4817017>
97. Menchicchi B, Fuenzalida JP, Bobbili KB, Hensel A, Swamy MJ, Goycoolea FM. Structure of Chitosan determines its interactions with mucin. *Biomacromolecules* [Internet]. 2014 Oct 13 [cited 2022 Nov 27];15(10):3550–8. Available from: <https://pubs.acs.org/doi/abs/10.1021/bm5007954>
98. Szilágyi BÁ, Mammadova A, Gyarmati B, Szilágyi A. Mucoadhesive interactions

- between synthetic polyaspartamides and porcine gastric mucin on the colloid size scale. *Colloids Surfaces B Biointerfaces*. 2020 Oct 1;194:111219.
99. Collado-González M, Espinosa YG, Goycoolea FM. Interaction Between Chitosan and Mucin: Fundamentals and Applications. *Biomimetics* 2019, Vol 4, Page 32 [Internet]. 2019 Apr 25 [cited 2022 Nov 27];4(2):32. Available from: <https://www.mdpi.com/2313-7673/4/2/32/htm>
 100. Tiller T, Busse CE, Wardemann H. Cloning and expression of murine Ig genes from single B cells. *J Immunol Methods* [Internet]. 2009 Oct 31 [cited 2022 Oct 6];350(1–2):183–93. Available from: <https://linkinghub.elsevier.com/retrieve/pii/S0022175909002634>
 101. Boniche C, Rossi SA, Kischkel B, Barbalho FV, Moura ÁND, Nosanchuk JD, et al. Immunotherapy against systemic fungal infections based on monoclonal antibodies [Internet]. Vol. 6, *Journal of Fungi*. MDPI AG; 2020 [cited 2020 Nov 7]. Available from: </pmc/articles/PMC7151209/?report=abstract>
 102. Okonechnikov K, Golosova O, Fursov M, Varlamov A, Vaskin Y, Efremov I, et al. Unipro UGENE: a unified bioinformatics toolkit. *Bioinformatics* [Internet]. 2012 Apr 15 [cited 2022 Nov 19];28(8):1166–7. Available from: <https://academic.oup.com/bioinformatics/article/28/8/1166/195474>
 103. Langmead B, Salzberg SL. Fast gapped-read alignment with Bowtie 2. *Nat Methods* [Internet]. 2012 Apr 4 [cited 2022 Nov 19];9(4):357–9. Available from: <https://www.nature.com/articles/nmeth.1923>
 104. Bushmanova E, Antipov D, Lapidus A, Prjibelski AD. rnaSPAdes: a de novo transcriptome assembler and its application to RNA-Seq data. *Gigascience* [Internet]. 2019 Sep 1 [cited 2022 Nov 19];8(9):1–13. Available from: <http://orcid.org/0000-0003-2816-4608>
 105. Kim K, Kim JH, Park H, Kim YS, Park K, Nam H, et al. Tumor-homing multifunctional nanoparticles for cancer theragnosis: Simultaneous diagnosis, drug delivery, and therapeutic monitoring. *J Control Release*. 2010 Sep 1;146(2):219–27.

106. Huang M, Ma Z, Khor E, Lim LY. Uptake of FITC-chitosan nanoparticles by A549 cells. *Pharm Res.* 2002;19(10):1488–94.
107. Herb M, Farid A, Gluschko A, Krönke M, Schramm M. Highly Efficient Transfection of Primary Macrophages with In Vitro Transcribed mRNA. *J Vis Exp* [Internet]. 2019 Nov 9 [cited 2022 Aug 13];2019(153):e60143. Available from: <https://www.jove.com/v/60143/highly-efficient-transfection-primary-macrophages-with-vitro>
108. Zhang X, Goncalves R, Mosser DM. The Isolation and Characterization of Murine Macrophages. *Curr Protoc Immunol* [Internet]. 2008 Nov 15 [cited 2022 Aug 13];83(1). Available from: <https://onlinelibrary.wiley.com/doi/10.1002/0471142735.im1401s83>
109. Busch C, Favret J, Geirsdóttir L, Molawi K, Sieweke M. Isolation and Long-term Cultivation of Mouse Alveolar Macrophages. *BIO-PROTOCOL.* 2019;9(14).
110. Del Rosal B, Villa I, Jaque D, Sanz-Rodríguez F. In vivo autofluorescence in the biological windows: the role of pigmentation. *J Biophotonics* [Internet]. 2016 Oct 1 [cited 2022 Aug 14];9(10):1059–67. Available from: <https://onlinelibrary.wiley.com/doi/full/10.1002/jbio.201500271>
111. Kwon S, Davies-Venn C, Sevick-Muraca EM. In vivo dynamic imaging of intestinal motions using diet-related autofluorescence. *Neurogastroenterol Motil* [Internet]. 2012 May 1 [cited 2022 Aug 14];24(5):494–7. Available from: <https://onlinelibrary.wiley.com/doi/full/10.1111/j.1365-2982.2012.01886.x>
112. del Rosal B, Benayas A. Strategies to Overcome Autofluorescence in Nanoprobe-Driven In Vivo Fluorescence Imaging. *Small Methods.* 2018 Sep;2(9):1800075.
113. Bhaumik S, Depuy J, Klimash J. Strategies to minimize background autofluorescence in live mice during noninvasive fluorescence optical imaging. *Lab Anim* 2007 368 [Internet]. 2007 Sep [cited 2022 Aug 14];36(8):40–3. Available from: <https://www.nature.com/articles/lab0907-40>
114. Inoue Y, Izawa K, Kiryu S, Tojo A, Ohtomo K. Diet and Abdominal Autofluorescence Detected by in Vivo Fluorescence Imaging of Living Mice. *Mol*

- Imaging [Internet]. 2008 Jan [cited 2022 Aug 14];7(1):7290.2008.0003. Available from: <http://journals.sagepub.com/doi/10.2310/7290.2008.0003>
115. Rençber S, Karavana SY, Yılmaz FF, Eraç B, Nenni M, Ozbal S, et al. Development, characterization, and in vivo assessment of mucoadhesive nanoparticles containing fluconazole for the local treatment of oral candidiasis. *Int J Nanomedicine* [Internet]. 2016 Jun;11:2641. Available from: <https://www.dovepress.com/development-characterization-and-in-vivo-assessment-of-mucoadhesive-na-peer-reviewed-article-IJN>
 116. Southam DS, Dolovich M, O’Byrne PM, Inman MD. Distribution of intranasal instillations in mice: effects of volume, time, body position, and anesthesia. *Am J Physiol Cell Mol Physiol* [Internet]. 2002 Apr 1 [cited 2022 Nov 17];282(4):L833–9. Available from: <http://www.ajplung.org/l833>
 117. Miller MA, Stabenow JM, Parvathareddy J, Wodowski AJ, Fabrizio TP, Bina XR, et al. Visualization of Murine Intranasal Dosing Efficiency Using Luminescent *Francisella tularensis*: Effect of Instillation Volume and Form of Anesthesia. Kaushal D, editor. *PLoS One* [Internet]. 2012 Feb 24 [cited 2022 Nov 17];7(2):e31359. Available from: www.niaid.nih.gov/
 118. VISWESWARAIAH A. Tracking the tissue distribution of marker dye following intranasal delivery in mice and chinchillas: a multifactorial analysis of parameters affecting nasal retention. *Vaccine* [Internet]. 2002 Aug 19 [cited 2022 Nov 17];20(25–26):3209–20. Available from: <https://pubmed.ncbi.nlm.nih.gov/12163273/>
 119. Xia Y, Fan Q, Hao D, Wu J, Ma G, Su Z. Chitosan-based mucosal adjuvants: Sunrise on the ocean. *Vaccine* [Internet]. 2015 Nov;33(44):5997–6010. Available from: <http://dx.doi.org/10.1016/j.vaccine.2015.07.101>
 120. Chadwick S, Kriegel C, Amiji M. Nanotechnology solutions for mucosal immunization. *Adv Drug Deliv Rev* [Internet]. 2010;62(4–5):394–407. Available from: <http://dx.doi.org/10.1016/j.addr.2009.11.012>
 121. Netto CF, Vegas VS, Sciannaméa IM, Guarnieri DB. [The polysaccharidic antigen from *Paracoccidioides brasiliensis*. Study of the time of cultivation necessary for

- the preparation of the antigen]. *Rev Inst Med Trop Sao Paulo* [Internet]. 1969;11(3):177–81. Available from: <http://www.ncbi.nlm.nih.gov/pubmed/5824780>
122. Almeida F, Rodrigues ML, Coelho C. The Still Underestimated Problem of Fungal Diseases Worldwide. *Front Microbiol* [Internet]. 2019 Feb 12;10(FEB):1–5. Available from: <https://www.frontiersin.org/article/10.3389/fmicb.2019.00214/full>
 123. Mayorga O, Munoz JE, Travassos LR, Carlos P. The role of adjuvants in therapeutic protection against paracoccidioidomycosis after immunization with the P10 peptide. 2012;3(May):1–6.
 124. Swanson K V., Deng M, Ting JPY. The NLRP3 inflammasome: molecular activation and regulation to therapeutics. *Nat Rev Immunol* [Internet]. 2019 Aug 1 [cited 2022 Aug 15];19(8):477–89. Available from: <https://pubmed.ncbi.nlm.nih.gov/31036962/>
 125. Dubensky TW, Kanne DB, Leong ML. Rationale, progress and development of vaccines utilizing STING-activating cyclic dinucleotide adjuvants. *Ther Adv vaccines* [Internet]. 2013 Nov [cited 2022 Aug 15];1(4):131–43. Available from: <https://pubmed.ncbi.nlm.nih.gov/24757520/>
 126. Villiers C, Chevallet M, Diemer H, Couderc R, Freitas H, Van Dorsselaer A, et al. From secretome analysis to immunology: chitosan induces major alterations in the activation of dendritic cells via a TLR4-dependent mechanism. *Mol Cell Proteomics* [Internet]. 2009 [cited 2022 Aug 15];8(6):1252–64. Available from: <https://pubmed.ncbi.nlm.nih.gov/19279042/>
 127. Bueter CL, Lee CK, Wang JP, Ostroff GR, Specht CA, Levitz SM. Spectrum and Mechanisms of Inflammasome Activation by Chitosan. *J Immunol*. 2014 Jun 15;192(12):5943–51.
 128. Bueter CL, Lee CK, Rathinam VAK, Healy GJ, Taron CH, Specht CA, et al. Chitosan but not chitin activates the inflammasome by a mechanism dependent upon phagocytosis. *J Biol Chem*. 2011 Oct 14;286(41):35447–55.

129. Mori A, Oleszycka E, Sharp FA, Coleman M, Ozasa Y, Singh M, et al. The vaccine adjuvant alum inhibits IL-12 by promoting PI3 kinase signaling while chitosan does not inhibit IL-12 and enhances Th1 and Th17 responses. *Eur J Immunol*. 2012 Oct;42(10):2709–19.
130. Travassos LR, Taborda CP. New advances in the development of a vaccine against paracoccidioidomycosis. *Front Microbiol*. 2012;3(JUN):1–6.
131. Lavelle EC, Ward RW. Mucosal vaccines — fortifying the frontiers. *Nat Rev Immunol* [Internet]. 2022 Apr 26;22(4):236–50. Available from: <https://doi.org/10.1038/>
132. Holmgren J, Czerkinsky C. Mucosal immunity and vaccines. *Nat Med* [Internet]. 2005 Apr 5 [cited 2022 Sep 20];11(S4):S45–53. Available from: <http://www.nature.com/naturemedicine>
133. Marttin E, Schipper NGM, Coos Verhoef J, Merkus FWHM. Nasal mucociliary clearance as a factor in nasal drug delivery. *Adv Drug Deliv Rev*. 1998;29(1–2):13–38.
134. Kyd JM, Foxwell AR, Cripps AW. Mucosal immunity in the lung and upper airway. *Vaccine*. 2001;19:2527–33.
135. Ogra PL, Faden H, Welliver RC. Vaccination Strategies for Mucosal Immune Responses. *Clin Microbiol Rev* [Internet]. 2001 Apr;14(2):430–45. Available from: <https://journals.asm.org/journal/cmvr>
136. Sojka DK, Bruniquel D, Schwartz RH, Singh NJ. IL-2 Secretion by CD4 + T Cells In Vivo Is Rapid, Transient, and Influenced by TCR-Specific Competition. *J Immunol* [Internet]. 2004 May 15;172(10):6136–43. Available from: <http://www.jimmunol.org/content/172/10/6136.abstract>

ANEXOS

Produção científica

Deposito de patente no INPI com número BR 10 2019 012313-3 de 14.06.2019

Trabalhos apresentados em eventos científicos

Trabalho apresentado na forma de pôster no 30º Congresso Brasileiro de Microbiologia

<https://www.sbmicrobiologia.org.br/30cbm-anais/resumos/R0067-1.pdf>

TITLE: P10 PEPTIDE COMPLEXED IN POLYMERIC NANOPARTICLES AS INTRANASAL THERAPEUTIC VACCINE FOR THE TREATMENT OF PARACOCCIDIOIDOMYCOSIS IN MURINE MODEL.

AUTHORS: SANTOS JÚNIOR, S.R.¹ ; LOPES, F.K.² ; DIAS, L.S.¹ ; SOUZA, A.C.O.¹ ; ARAUJO, M.V.¹ ; AMARAL, A.C.² ; TABORDA, C.P.^{1,3} .

INSTITUTION: ¹UNIVERSIDADE DE SÃO PAULO: INSTITUTO DE CIÊNCIAS BIOLÓGICAS DEPARTAMENTO DE MICROBIOLOGIA; ²UNIVERSIDADE FEDERAL DE GOIÁS: INSTITUTO DE PATOLOGIA TROPICAL E SAÚDE PÚBLICA DEPARTAMENTO DE BIOTECNOLOGIA; ³UNIVERSIDADE DE SÃO PAULO: INSTITUTO DE MEDICINA TROPICAL.

ABSTRACT:

Paracoccidiodomycosis (PCM) is a systemic fungal disease, caused by the thermomorphic fungal *Paracoccidioides* spp., that mainly affects the lungs. PCM therapy is usually prescribed, depending on the gravity of infection, in two steps, firstly an initial attack for the rapid control of the infection, and secondly a treatment to prevent the proliferation of possible remaining yeasts, avoiding the recurrence of the disease. The main drugs for the treatment of PCM are polyene chemotherapeutics, sulfanilamide compounds and azoles drugs. As an alternative for treating and / or preventing PCM, the use of vaccines has been explored, promoting the production of IFN- γ , inducing this way an Th1 immune response, ideal for the control of the disease. One of the most studied vaccine candidates is the P10 peptide-based vaccine, consisting of 15 mer amino acids, provenient from the 43 kDa glycoprotein of *P. brasiliensis*. Studies using P10-based strategies for vaccination have been demonstrating really significant results, nevertheless, the P10 peptide short lifetime impairs its effectiveness, due to premature degradation. An alternative to overcome this problem is by its complexation within nanoparticles in order

to protect and improve the immunomodulatory effect of the peptide. For the P10 peptide complexation chitosan was chosen due its physico-chemical and biological characteristics, such as: biocompatibility, mucoadhesiveness and relative low cost. The nanoparticles complexed with P10 peptide at different concentrations were produced by the ionic gelation technique, their poly dispersion index (PDI), size, and Zeta potential (Z potential) were analyzed. The encapsulation efficiency was assessed using the Qubit™ Protein Assay Kit and the toxicity verified by hemolysis and cell viability assays with murine J774.16 macrophages. The nanoparticles obtained presented a size of approximately 220 nm, PDI below 0.5 and Zeta potential of approximately + 20 mV. The encapsulation efficiency was greater than 90% and there were no cytotoxicity effects in the first 48 hours. Treatment with the nanoparticles containing different concentrations of P10 peptide was efficient in reducing lung fungal load during murine PCM and as able to reduce from 4 to 20 the usual standard concentration of the peptide P10 peptide. These results show that the nanoparticle is stable and presents the physico-chemical characteristics desirable for an intranasal vaccine using chitosan as polymer.

Keywords: Paracoccidioidomycosis, Paracoccidioides spp, Nanoparticles, Chitosan, P10 peptide, Intranasal vaccine.

Funding Agencies: CNPq, FAPESP, CAPES.



Outras atividades

Prêmio de melhor trabalho área de Micologia em formato de pôster no 30º Congresso Brasileiro de Microbiologia



LISTA DE REAGENTES

TAMPÃO FOSFATO DE SÓDIO (PBS)

REAGENTES	PBS - 1x	PBS - 10x
NaCl	8 g	80 g
KCl	0,2 g	2 g
Na ₂ HPO ₄	1,44 g	14,4 g
KH ₂ PO ₄	0,24g	2,4 g
H ₂ O d q.s.p	1000 mL	1000 mL

Solução autoclavada a 120 °C por 20 minutos.

MEIO DE CULTURA FAVA-NETTO

REAGENTES	Líquido	Sólido
-----------	---------	--------

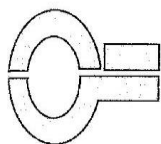
Protease peptona	3 g	3 g
Peptona	10 g	10 g
Extrato de carne	5 g	5 g
NaCl	5 g	5 g
Extrato de levedura	5 g	5 g
Dextrose	40 g	40 g
Agar	-	18 g
H₂O d q.s.p	1000 mL	1000 mL

Meio autoclavado a 120 °C por 20 minutos.

MEIO DE CULTURA BHI

REAGENTES	Líquido	Sólido
BHI Caldo	37 g	37 g
Agar	-	15 g
BHI Agar	-	-
H₂O d q.s.p	1000 mL	1000 mL
Glicose*	40 mg (4%)	40 mg (4%)
SFB*	40 mL (4%)	40 mL (4%)
FPb 192*#	-	50 mL (5%)

*Meio Suplementado; #Meio UFC. Meio autoclavado a 120 °C por 20 minutos.



Certificado



Certificamos que **Samuel Rodrigues dos Santos Junior** participou do Treinamento em Biossegurança realizado no Departamento de Microbiologia/ICB-USP, no dia 30 de novembro de 2016, com carga horária total de 6 horas.

Prof. Dr. Gabriel Padilla
Responsável pelo Treinamento

Veridiana Munford
Técnica Responsável pelo Treinamento

ANEXO B – Certificado de realização do curso de uso de animais em experimentação.



Uso de animais
para experimentação



DECLARAÇÃO

Declaramos para os devidos fins que

Samuel Rodrigues dos Santos Júnior

participou do Curso “Uso de Animais em Experimentação” com carga horária total de 10 horas, em formato ensino a distância, realizado pela Comissão de Biotérios do Instituto de Ciências Biomédicas da Universidade de São Paulo.

São Paulo, 13 julho 2017
Comissão de Biotérios
ICB USP

Instituto de Ciências Biomédicas | USP
Av. Prof. Lineu Prestes, 2415 • Cidade Universitária “Armando Salles Oliveira” • Butantã – São Paulo – SP • CEP 05508-900

ANEXO C – Certificado de realização do curso de armazenamento, manuseio e descarte de produtos químicos.



Declaro, para os devidos fins, que

Samuel Rodrigues dos Santos Júnior

concluiu o Curso "Armazenamento, Manuseio e Descarte de Produtos Químicos",
realizado no Instituto de Ciências Biomédicas da Universidade de São Paulo.

São Paulo, 13 julho 2017

(Declaração válida por 5 anos)

Helayne Freitas
Presidente da Comissão de Resíduos Químicos

Prof. Dr. Jackson Cioni Bittencourt
Diretor do ICB

Instituto de Ciências Biomédicas | USP
Av. Prof. Lineu Prestes, 2415 • Cidade Universitária "Armando Salles Oliveira" • Butantã – São Paulo – SP • CEP 05508-900

Article

Biodistribution and Adjuvant Effect of an Intranasal Vaccine Based on Chitosan Nanoparticles against Paracoccidioidomycosis

Samuel Rodrigues Dos Santos Júnior ^{1,*} , Filipe Vieira Barbalho ¹, Joshua D. Nosanchuk ², Andre Correa Amaral ³ and Carlos Pelleschi Taborda ^{1,4,*} 

- ¹ Laboratory of Pathogenic Dimorphic Fungi, Department of Microbiology, Institute of Biomedical Sciences, University of São Paulo, São Paulo 05508000, Brazil
- ² Department of Medicine and Department of Microbiology and Immunology—The Bronx, Albert Einstein College of Medicine, New York, NY 10461, USA
- ³ Laboratory of Nano&Biotechnology, Department of Biotechnology, Institute of Tropical Pathology and Public Health, Federal University of Goiás, Goiânia 74605050, Brazil
- ⁴ Laboratory of Medical Mycology, School of Medicine/IMT/SP-LIM53, University of São Paulo, São Paulo 05403000, Brazil
- * Correspondence: samuelmicrobio@usp.br (S.R.D.S.J.); taborda@usp.br (C.P.T.)

Abstract: Paracoccidioidomycosis (PCM) is a fungal infection caused by the thermodimorphic *Paracoccidioides* sp. PCM mainly affects the lungs, but, if it is not contained by the immune response, the disease can spread systemically. An immune response derived predominantly from Th1 and Th17 T cell subsets facilitates the elimination of *Paracoccidioides* cells. In the present work, we evaluated the biodistribution of a prototype vaccine based on the immunodominant and protective *P. brasiliensis* P10 peptide within chitosan nanoparticles in BALB/c mice infected with *P. brasiliensis* strain 18 (Pb18). The generated fluorescent (FITC or Cy5.5) or non-fluorescent chitosan nanoparticles ranged in diameter from 230 to 350 nm, and both displayed a Z potential of +20 mV. Most chitosan nanoparticles were found in the upper airway, with smaller amounts localized in the trachea and lungs. The nanoparticles complexed or associated with the P10 peptide were able to reduce the fungal load, and the use of the chitosan nanoparticles reduced the necessary number of doses to achieve fungal reduction. Both vaccines were able to induce a Th1 and Th17 immune response. These data demonstrates that the chitosan P10 nanoparticles are an excellent candidate vaccine for the treatment of PCM.

Keywords: PCM; intranasal vaccine; chitosan nanoparticles; adjuvant nanoparticles; fluorescent nanoparticles



Citation: Santos Júnior, S.R.D.; Barbalho, F.V.; Nosanchuk, J.D.; Amaral, A.C.; Taborda, C.P. Biodistribution and Adjuvant Effect of an Intranasal Vaccine Based on Chitosan Nanoparticles against Paracoccidioidomycosis. *J. Fungi* **2023**, *9*, 245. <https://doi.org/10.3390/jof9020245>

Academic Editor: Maria Mendes Giannini

Received: 18 November 2022
Revised: 26 November 2022
Accepted: 3 December 2022
Published: 12 February 2023



Copyright: © 2023 by the authors. Licensee MDPI, Basel, Switzerland. This article is an open access article distributed under the terms and conditions of the Creative Commons Attribution (CC BY) license (<https://creativecommons.org/licenses/by/4.0/>).

1. Introduction

Paracoccidioidomycosis (PCM) is a mycosis that mainly affects the lungs but can lead to disseminated disease when the immune response is inadequate to control the spread of the fungus. PCM can be classified as a PCM infection and a PCM disease, in which PCM infection has no clinical manifestations and PCM disease is classified into two sub-forms: juvenile/acute/subacute or adult/chronic disease [1–3].

PCM is caused by thermodimorphic fungi of the genus *Paracoccidioides*, which is currently comprised by five known species: *P. brasiliensis*, *P. americana*, *P. restrepiensis*, *P. venezuelensis* and *P. lutzzi*. These fungi are found in almost every country in Latin America [4,5].

The effective control of PCM requires a Th1 and Th17 immune response with the production of IL-2, IL-12, IFN- γ , IL-17 and IL-23, which are responsible for stimulating phagocytosis and the formation of epithelioid granulomas [6,7]. In contrast, a Th2 response is prevalent in the most severe cases, usually in immunosuppressed patients [6,7].

The main drugs to treat PCM are polyene drugs (e.g., amphotericin B), sulfanilamide compounds (e.g., sulfadiazine), and azole drugs (e.g., itraconazole) [2,3,8]. Although these drugs are quite effective in treating PCM, they have numerous adverse effects, such as amphotericin B causing headaches, liver and kidney toxicity, and skin rashes [9].

A promising strategy to treat PCM is to use a therapeutic vaccine to generate a strong Th1 and Th17 immune response. One of the most researched candidate vaccines is based on the P10 peptide that has 15 amino acids (QTLIAHTLAIRYAN) derived from the immunodominant glycoprotein Gp 43 of *P. brasiliensis* [1,6,10,11]. Additionally, P10 peptide nanoparticles using polymers such as PLGA (poly(lactic-co-glycolic acid)) and chitosan can deliver a sustained release of the peptide resulting in significant protection from, and improvement of, PCM disease [12–16].

An important feature of chitosan nanoparticles is their ability to be mucoadhesive. This mucoadhesiveness promotes the attachment of nanoparticles to tissues, increasing their time of contact with cells and, potentially, leading to a better immune response [17–21]. For vaccine development, it is important to define the path taken by nanoparticles after administration, their location inside the cell, and which cells are responsible for their uptake, as this information facilitates subsequent improvements in the methods of nanoparticle delivery and provides insights into modifications to the particles that can vary the release of the P10 peptide [22–26].

When studying nanoparticles vaccines, several factors can affect the delivery, biodistribution and effect of the preparation. One of the most important factors is the complexation, or not, of the active molecule. This distinction can alter the time of processing of the vaccine, the presentation of the antigen and the lifetime of the antigen as well as the protection of the active molecule from degradation in the physiological environment of the live organism [22–26].

To evaluate the biodistribution, the necessity of complexation, adjuvant effect and the number of doses required to reduce the fungal load of the *P. brasiliensis* strain 18 (Pb18), we evaluated the administration of different chitosan nanoparticles vaccine formulations and dosing approaches.

2. Materials and Methods

2.1. Non-Fluorescent Nanoparticles Preparation

The nanoparticles were prepared according to our published protocol [14]. In brief, a solution of chitosan (Chitosan Low Molecular Weight, Sigma-Aldrich, St. Louis, MO, USA) was mixed dropwise with a solution of sodium tripolyphosphate (TPP; Sigma-Aldrich) with or without P10 peptide (GenOne Biotech, Rio de Janeiro, RJ, Brazil). The first solution was composed of 2 mg/mL of chitosan prepared by dissolving the chitosan with 1% of acetic acid (final concentration) in ultrapure water under magnetic stirring for 1 h at room temperature. The pH of the chitosan solution was then adjusted to approximately 4.4 using NaOH 0.1 M. The second solution was composed of 1 mg/mL of TPP and 5 µg (final mass) of the solubilized P10 peptide for the complexed nanoparticles, or without the P10 peptide for the empty nanoparticles.

The second solution (TPP + P10 or TPP) was mixed dropwise in the first solution under magnetic stirring for 90 min at room temperature. After the nanoparticle formation, the nanoparticles were washed with ultra-pure water and centrifuged at 13,200 rpm, 4 °C for 1 h. The washing and centrifugation steps were performed three times. The nanoparticles were then suspended in ultra-pure water for characterization, and then in PBS (vaccine vehicle) or DMEM media (LGC Biotecnologia, Cotia, São Paulo, Brazil) (phagocytosis assay).

2.2. Preparation of Fluorescent Nanoparticles

To produce fluorescent nanoparticles, the chitosan was conjugated with the fluorochromes FITC (Sigma-Aldrich) or Cy5.5 NHS ester (Abcam, Cambridge Biomedical Campus, Cambridge, UK) using a protocol adapted from Kwangmeyung Kim, 2010 and

Min Huang, 2002 [27,28]. For the FITC conjugation, 15 mg of the fluorochrome was dissolved in 15 mL of DMSO and the chitosan was solubilized with 1% of acetic acid (final concentration) in ultrapure water under magnetic stirring for 1 h at room temperature. The pH of the chitosan was then adjusted to approximately 4.4 using NaOH 0.1 M. The fluorochrome and chitosan solution were then mixed under magnetic stirring for 3–4 h at room temperature or overnight at 4 °C. After stirring, the fluorescent chitosan was precipitated by increasing the pH to 10 with NaOH 0.5 M. For the Cy5.5 conjugation, 1 mg of the fluorochrome was dissolved in 1.5 mL of DMSO, the chitosan was placed in 15 mL of ultra-pure water, and the pH was adjusted to 8.3–8.5 with NaHCO₃. The fluorochrome and chitosan solution were then mixed under magnetic stirring for 3–4 h at room temperature or overnight at 4 °C. Both the FITC and Cy5.5 fluorescent chitosan were dialyzed for 3 days using a 10 kDa membrane and then lyophilized in the dark until used.

2.3. Physical-Chemical Characterization of the Nanoparticles

The sizes of the nanoparticles and polydispersity indexes (PDI) were determined by dynamic light scattering and Zeta Potential (Z potential) was measured by capillary electrophoresis using a Zetasizer nano Zs equipment (Malvern Panalytical Ltd., UK).

2.4. Animal Approvals

Pathogen-free male BALB/c nude mice and BALB/c mice, aged 6–8 weeks, were used according to the approval of the ethics committee of the University of São Paulo (CEUA ICB n ° 3654290618).

2.5. Experimental Design Used in the Biodistribution Protocol

BALB/c nude mice were randomly organized in the following groups: (C+)—one mouse was inoculated with the fluorochrome only (Cy5.5); (C−)—one mouse was inoculated with PBS; and (NP)—three mice were inoculated with the fluorescent nanoparticles (15 animals in total were utilized).

The BALB/c mice were similarly randomly assigned in the following groups: (C+)—one mouse was inoculated with the fluorochrome only (FITC); (C−)—one mouse was inoculated with PBS; and (NP)—three mice were inoculated with the fluorescent nanoparticles. Lungs, trachea, stomach, bowels and brain were collected (75 animals in total were utilized).

The BALB/c nude and BALB/c mice were anesthetized intraperitoneally with 200 µL of 80 mg kg^{−1} of ketamine and 10 mg kg^{−1} of xylazine prior the administration of 5 µL in each nostril (10 µL in total volume) according to the groups described. The fluorescent Cy5.5 nanoparticles were used to visualize the *in vivo* biodistribution in the BALB/c nude mice and to evaluate the presence of the nanoparticles in the organs of the BALB/c animals. Images were obtained with the IVIS Spectrum (PerkinElmer, Waltham, MA, USA) located on the Research Facility Center (CEFAP—Institute of Biomedical Science IV, University of São Paulo, São Paulo, SP, Brazil). The animals, or the organs, were analyzed at different times (0, 24, 48, 72 and 96 h) after the inoculation of the fluorescent chitosan nanoparticles.

2.6. Nanoparticles Phagocytosis Assay

Alveolar and peritoneal macrophages were collected from non-inoculated mice following a protocol modified from Herb, M. 2019; Zhang, X. 2008; and Busch, C. 2019 [29–31]. Alveolar macrophages were collected using BAL (bronchoalveolar lavage) buffer composed of PBS, EDTA 2 mM (final concentration) and 0.5% Fetal Bovine Serum (FBS, Gibco, Thermo Fisher Scientific, Waltham, MA, USA). The BAL buffer and the collected cells were maintained at 37 °C. The peritoneal macrophages were collected and maintained using cold PBS. After collection, both cell types were centrifuged at 3000 rpm at 4 °C for 5 min and seeded in 6-well plates with round glass coverslips at the bottom. The alveolar macrophages were maintained with DMEM supplemented with 10% FBS, 1% (vol/vol) penicillin/streptomycin (pen/strp, Gibco, Thermo Fisher Scientific), 30 ng of GM-CSF

(Thermo Fisher Scientific) and 2% pyruvate (Thermo Fisher Scientific). The peritoneal cells were maintained with DMEM supplemented with 10% FBS, 1% (vol/vol) pen/strep and 2% pyruvate (Thermo Fisher Scientific). Both cell types were maintained in cell incubators at 37 °C and 5% CO₂ until they produced full cell confluence over the coverslips.

The cells were grown in 6-wells plate, each time point in one well. The nanoparticles were added at the same time (0 h).

After full cell confluence of the coverslips, the FITC fluorescent nanoparticles were centrifuged, suspended in 1 mL of DMEM, and added to the cells. The cells were analyzed at different times (0, 2, 4, 6 and 8 h) after the addition of the fluorescent chitosan nanoparticles. Lysosomal Staining Kit—Red Fluorescence (RFP)—Cytointer (Abcam) was used to provide co-localization of the nanoparticles and the DAPI fluorochrome (Sigma-Aldrich) was used to stain the nucleus. The cells were visualized using a mounting media of 100 µL of 10 × PBS with 900 µL of glycerol in the EVOS Cell Imaging System (Thermo Fisher Scientific).

2.7. Yeast Cells

The *P. brasiliensis* strain Pb 18 was maintained as yeast cells in Fava Netto solid media [32]. The yeast cells were transferred to liquid BHI medium (Brain Heart Infusion, Bacto™, BD, Franklin Lakes, NJ, USA) supplemented with 4% FBS, 4% glucose (Difico™, BD) and cultivated at 37 °C and 150 rpm for five to seven days prior to infection. The yeast cells were collected and washed three times using PBS, then centrifuged at 3000 rpm for ten minutes. The yeast cells were suspended in 5 mL of PBS and the viability of the fungal cells was assessed by counting the yeast cells in a Neubauer's chamber using trypan blue (Gibco, Thermo Fisher Scientific).

2.8. Experimental Design Used in the Infection Protocol

BALB/c mice (ten animals per group) were randomly organized in following groups for the two different protocols. For the assessment of activity between the P10 complexed chitosan nanoparticle and the P10 co-administered with the empty particle: (a) Pb 18—positive control, infected without treatment. (b) Associated nanoparticles (Ncomp)—infected and treated weekly with three doses of empty nanoparticles co-administered with 5 µg/10 µL of P10 peptide. (c) Complexed (Comp)—infected and treated weekly with three doses of nanoparticles complexed with 5 µg/10 µL of P10 peptide. (d) SHAM—negative control, uninfected and untreated. 120 animals in total were utilized.

For the experiment testing differences between a single or multiple treatments with P10 complexed with chitosan nanoparticles: (a) Pb 18—positive control, infected without treatment. (b) 1D—infected and treated with one dose of the nanoparticles complexed with 5 µg/10 µL of P10 peptide. (c) 2D—infected and treated with two doses of the nanoparticles complexed with 5 µg/10 µL of P10 peptide. (d) 3D—infected and treated with three doses of the nanoparticles complexed with 5 µg/10 µL of P10 peptide. (e) SHAM—negative control, uninfected and untreated. Although Comp and 3D are the same regimen, they are named differently for clarity within the different experimental approaches. 150 animals in total were utilized.

2.9. Intratracheal Infection and Immunization

To simulate a natural infection caused by the *P. brasiliensis*, BALB/c mice were intratracheally infected with Pb 18 yeast cells at a concentration of 3×10^5 yeast/50 µL. The animals were anesthetized intraperitoneally with 200 µL of 80 mg kg⁻¹ of ketamine and 10 mg kg⁻¹ of xylazine, an incision was made in the trachea, and 50 µL of the yeast cells suspension was inoculated [14]. After infection, the incision was sutured, and the mice observed and kept warm until complete recovery was documented.

Thirty days after infection, the nanoparticle vaccines were administered to the mice intranasally. Five microliters of the specific formulation were administered into each nostril.

For mice receiving more than a single inoculation, the nanoparticles were administered once per week.

2.10. Antifungal and Cytokine Evaluation

To determine the effects of vaccination, mice were euthanized 51 days after infection and the lungs were removed. The lungs were macerated manually in 2 mL of PBS, and 100 μ L of the tissue was plated on BHI solid media, supplemented with 4% (vol/vol) FBS, 4% (vol/vol) Glucose and 1% (vol/vol) pen/strep. The plates were incubated at 37 °C and the CFU/g of lung were counted 21 days later.

For evaluation of cytokines, 500 μ L of the lung macerates were aliquoted into microtubes that contained 500 μ L of cOmplete™ protease inhibitor (Roche, Switzerland). Cytokine analysis was performed by Enzyme-Linked Immunosorbent Assay (ELISA) using commercial kits for the following cytokines IL-2, IL-4, IL-10, IL-12, and IFN- γ (BD OptEIA™, BD), and IL-1 β and IL-23 Enzyme-Linked Immunosorbent Assays (ELISA) (Thermo Fisher Scientific). The ODs were assessed using the Epoch 2 Microplate Spectrophotometer (BioTek Instruments, Inc. Winooski, Vermont, EUA).

2.11. Statistical Analysis

Analysis of variance (ANOVA) or Student's *t* test were performed followed by Tukey or Dunnett post-tests using Graph Pad Prism 8. *P* values were considered significant when <0.05 . Error bars were expressed as the standard error of the mean (SEM). All experiments were performed in triplicates.

3. Results

3.1. Nanoparticles Preparation and Characterization

The diameter and size distribution as well as the Z potential of the non-fluorescent nanoparticles presented the desired qualities expected for this type of polymer such that the sizes of the empty nanoparticles were around 230 nm with a PDI less <0.5 , and the complexed nanoparticles around 330 nm, also with a PDI <0.5 . Similarly, the fluorochrome conjugated nanoparticles complexed with P10 were around 350 nm with a PDI <0.5 . The Z potential was around +20 mV for all particles tested.

3.2. Biodistribution using the IVIS Spectrum

The fluorescence biodistribution of the Cy5.5-labeled nanoparticles after administration to the BALB/c nude mice were followed for 96 h (5 days; 0 h and 96 h are shown). The IVIS spectrum images were obtained both with the mice positioned in the prone position (Figure 1A,B) and supine position (Figure 1C,D (individual figures can be found in the Supplementary material). A decrease in the fluorescent area was observed over time, suggesting that the nanoparticles were phagocytosed and processed over the interval of 0 and 96 h. By using the IVIS Spectrum to visualize the fluorescent Cy5.5 nanoparticles, we determined that the nanoparticles remained mainly in the upper airway and showed a stable fluorescent intensity at all of the time points, which was different from the control in which there was a significant loss of fluorescent intensity of the region of interest (ROI) in the first 24 h (Figure 2) and (Table 1).

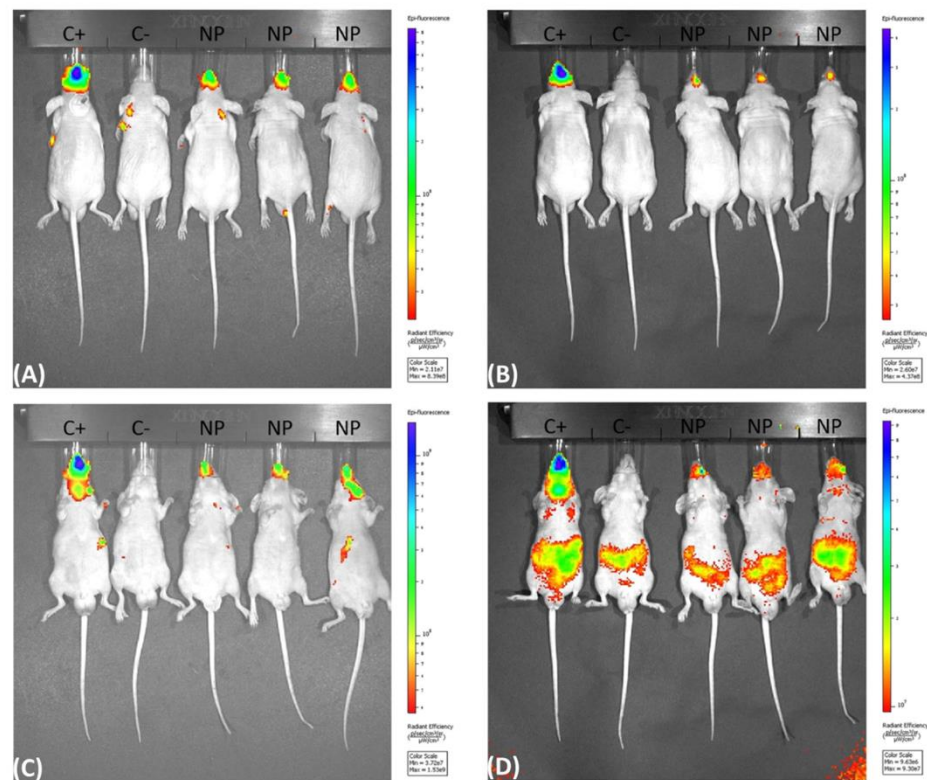


Figure 1. IVIS spectrum fluorescence obtained with the mice positioned in the prone (A,B) and supine (C,D) position, showing the fluorescence in the upper air way of the BABL/c nude mice after inoculation of 5 μ L per nostril of the fluorescent Cy5.5 chitosan nanoparticles at 0 h (A,C) and at 96 h (B,D). (C+) inoculated with the fluorochrome only (Cy5.5), (C-) inoculated with PBS and (NP) inoculated with the fluorescent nanoparticles.

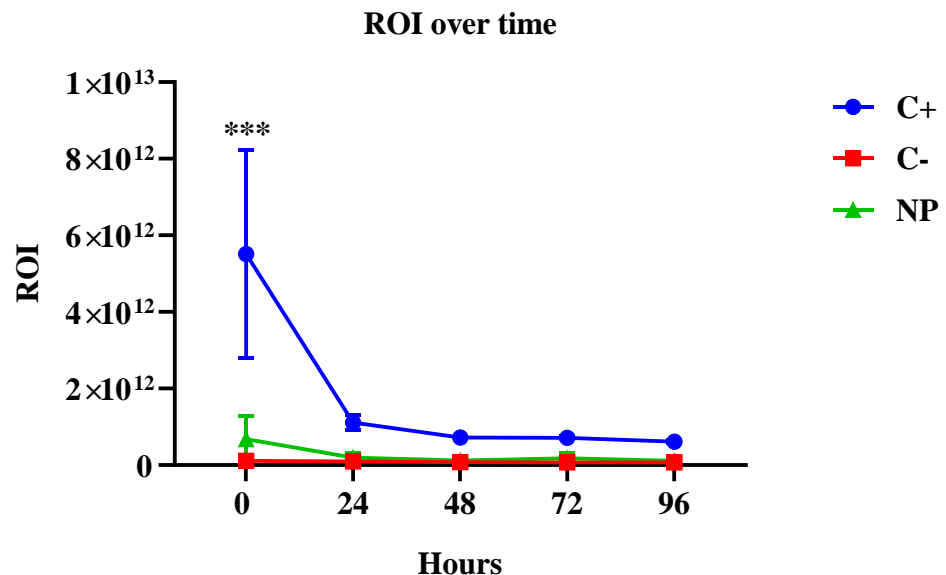


Figure 2. Fluorescent intensity of the region of interest (ROI) over time, showing that the fluorescence was stable during all time points for the NP group, and a significant reduction of the fluorescence for the C+ group in the first 24 h $p < 0.001$.

Table 1. Fluorescent intensity of the region of interest (ROI) over time, showing the specific average values of the fluorescence intensity for all time points.

Hours	Fluorescent Intensity of the Region of Interest (ROI)		
	C+	C–	NP
0	5.5×10^{12}	1.0×10^{11}	6.7×10^{11}
24	1.1×10^{12}	9.3×10^{10}	1.9×10^{11}
48	7.2×10^{11}	7.6×10^{10}	1.1×10^{11}
72	7.1×10^{11}	7.3×10^{10}	1.7×10^{11}
96	6.0×10^{11}	7.2×10^{10}	1.1×10^{11}

(C+) inoculated with the fluorochrome only (Cy5.5), (C–) inoculated with PBS and (NP) inoculated with the fluorescent nanoparticles.

To analyze fluorescence in the organs of the mice, the nanoparticle inoculum had to be concentrated three times (the inoculated volume was not altered). The fluorescence was followed for 96 h (5 days; 0 h and 96 h are shown). Prior to image acquisition, mice were euthanized, and their organs were harvested at each time point. Some of the nanoparticles were present in the trachea and lungs of the mice (Figure S1), but their fluorescence was reduced over time (Figure S2). Stomach and bowels presented background noise fluorescence demonstrated by the fluorescence in the C– group (Figures S3 and S4).

The fluorescence signals in the stomach and bowels of the mice can be explained by the autofluorescence in the mice food, which is well established in the literature [33–37].

In the control animal (PBS), no fluorescence was observed in the upper airway area but we observed fluorescence in the stomach of the animal, although they received PBS only. In the Supplementary material (Figure S3) it is possible to observe stomach and bowels fluorescence in the PBS group from 0 h, and in all mice before the inoculation of any substance (Figure S5).

3.3. Nanoparticles Phagocytosis Assay

The FITC labeled chitosan nanoparticles were phagocytosed by alveolar (Figure 3) and peritoneal (Figure 4) macrophages by 6 h (data not shown) and the maximal phagocytosis occurred by 8 h.

3.4. CFU from the Complexed or Co-Administered Nanoparticle Immunizations

The animals were euthanized after 51 days of infection during which they were untreated for the first 30 days (establishment of the disease) and then treated with nanoparticles or left untreated (Pb 18, control infected). Then, their lungs were aseptically collected, macerated and aliquots plated to evaluate the efficacy of chitosan nanoparticles complexed with P10 peptide and the adjuvant effect of empty chitosan nanoparticles co-administered with the P10 peptide. The lungs of infected animals in groups Pb18, Comp and Ncomp were significantly heavier than the lungs of control animals (SHAM, not infected and not treated), indicating the success of infection (Figure S6). The CFU determinations showed a significant decrease in viable *Paracoccidioides* cells from the lungs of both groups of nanoparticle-treated mice compared with the untreated group (Figure 5). The CFUs were similar between the P10 complexed nanoparticle-treated mice and the animals that received empty chitosan nanoparticles co-administered with P10.

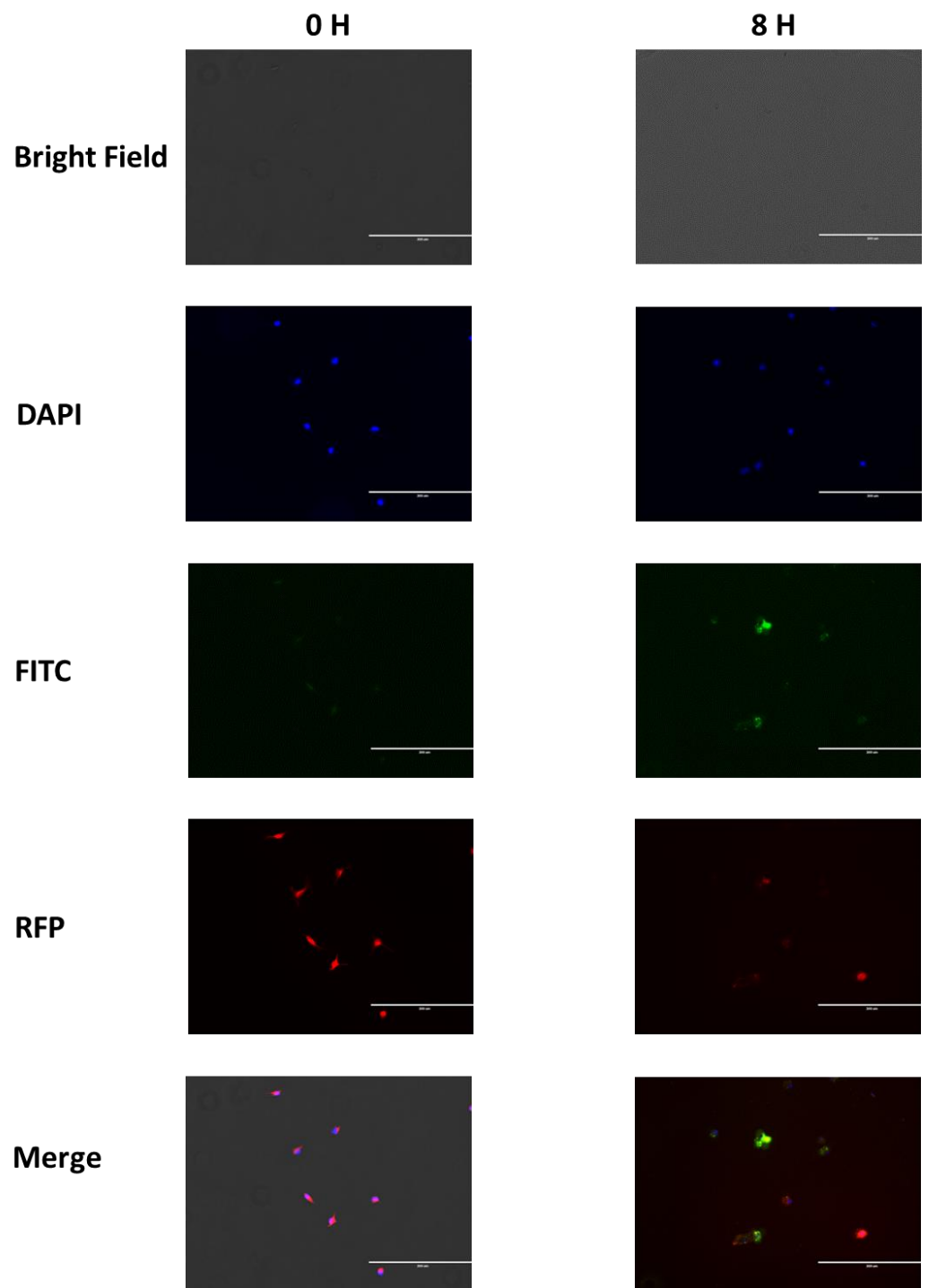


Figure 3. Alveolar macrophage phagocytosis of FITC chitosan nanoparticles at 0 and 8 h showing the nanoparticles inside of cell lysosomes at 8 h. The DAPI filter shows the nuclei, the FITC filter demonstrates the nanoparticles, and the RFP filter indicates the lysosomes.

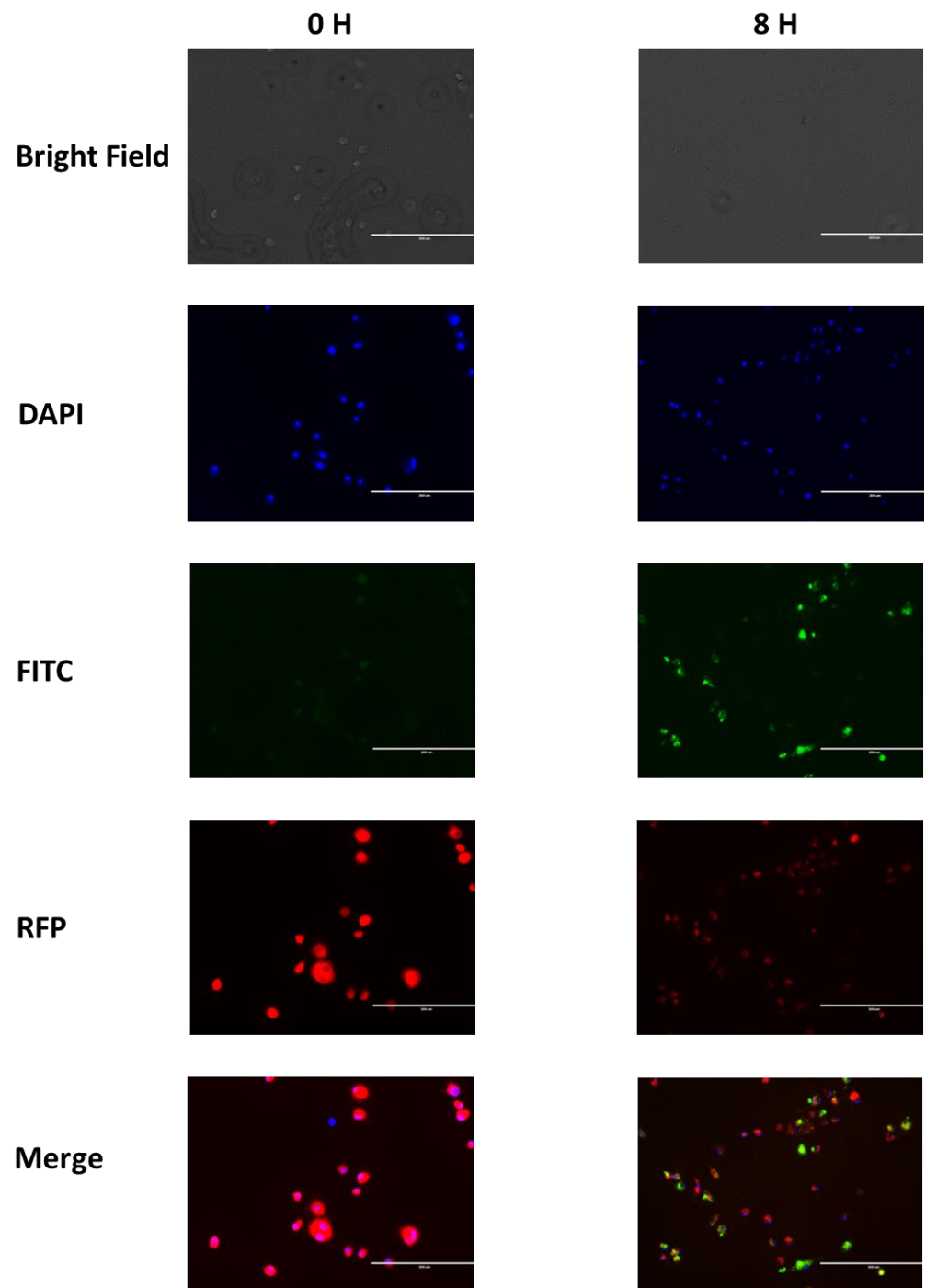


Figure 4. Peritoneal macrophage phagocytosis of FITC chitosan nanoparticles at 0 and 8 h showing the nanoparticles inside of cell lysosomes at 8 h. The DAPI filter shows the nuclei, the FITC filter demonstrates the nanoparticles, and the RFP filter indicates the lysosomes.

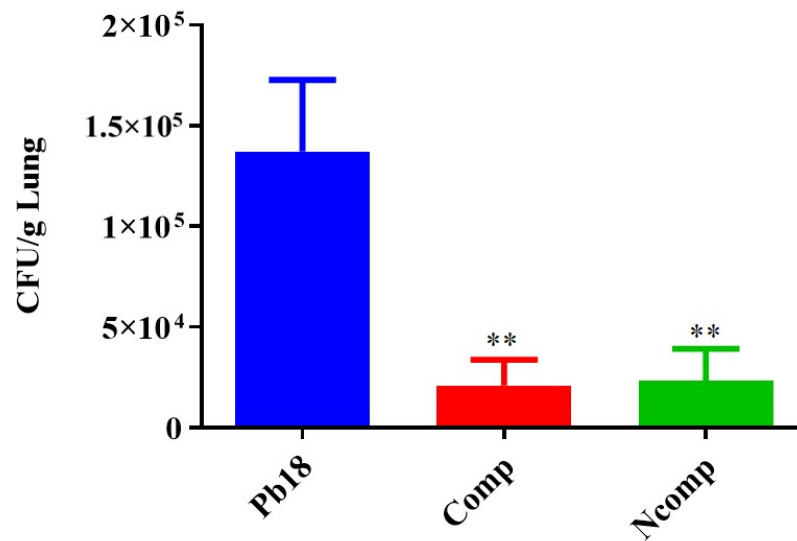


Figure 5. CFU of mice 51 days post infection. The nanoparticle-treated animals had a significant reduction in viable *Paracoccidioides* cells compared to the Pb 18 group. Pb18 (infected and non-treated), Comp (infected and treated with the P10 complexed nanoparticles) and Ncomp (infected and treated with P10 and with empty nanoparticles). ** = $p < 0.01$.

Our intention was to verify if the immune response was generated by the complexation of the peptide, and if the chitosan nanoparticles possess an adjuvant effect, since the chitosan itself does not possess immunostimulatory effects alone, as with the peptide. In combination, the chitosan and the peptide (complexed or not) were phagocytized by macrophages and dendritic cells and stimulated an Th1 and Th17 cells immune response.

3.5. Cytokines from the Complexed or Co-Administered Nanoparticle Immunizations

Cytokine production was evaluated 51 days post infection using the same animals as studied for CFUs. The lung macerates from these mice were stored in a $-20\text{ }^{\circ}\text{C}$ freezer in microtubes that contained a proteinase inhibitor until they were used for cytokine analysis by ELISA. We focused our evaluation on cytokines associated with the Th1 (Figure 6), Th2 (Figure 7) and Th17 (Figure 8) T cells subset population. We determined that the nanoparticles induced Th1 and Th17 activation, although there was also a small, but not absent, Th2 response.

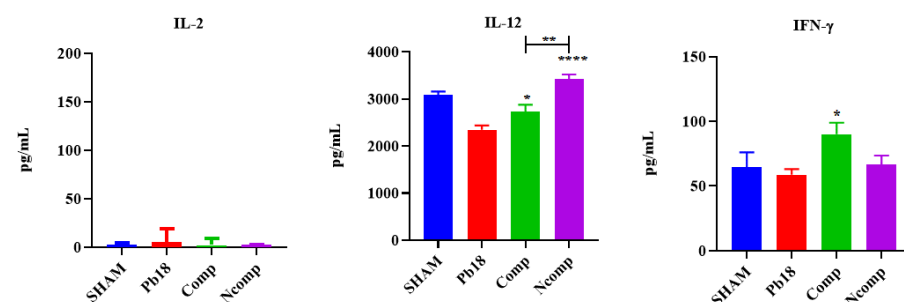


Figure 6. Th1 cytokine production 51 days post infection. No IL-2 was detected, and the IL-12 and IFN- γ were significantly increased, when compared to the Pb18 group. SHAM (non-infected and non-treated), Pb18 (infected and non-treated), Comp (infected and treated with the P10 complexed nanoparticles) and Ncomp (infected and treated with the P10 co-administered with empty nanoparticles). * = $p < 0.05$; ** = $p < 0.01$ and **** = $p < 0.0001$.

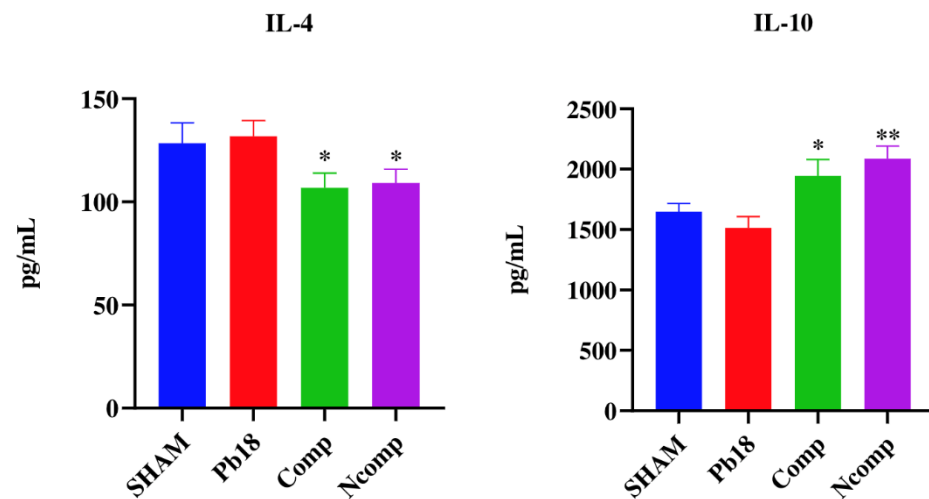


Figure 7. Th2 cytokine production 51 days post infection. IL-4 was significantly decreased, and the IL-10 was significantly increased, for both nanoparticles treated groups when compared to the Pb18 group. SHAM (non-infected and non-treated), Pb18 (infected and non-treated), Comp (infected and treated with the P10 complexed nanoparticles) and Ncomp (infected and treated with the P10 co-administered with empty nanoparticles). * = $p < 0.05$ and ** = $p < 0.01$.

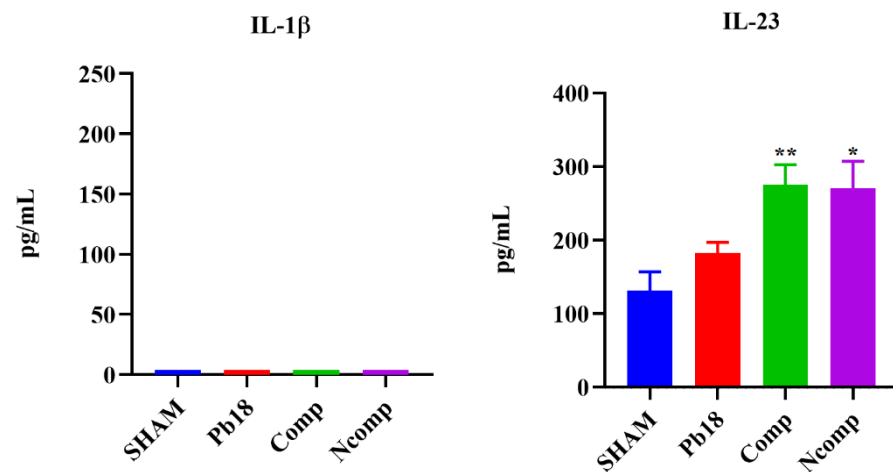


Figure 8. Th17-induced cytokine production 51 days post infection. No changes in IL-1 β levels were detected, but IL-23 was significantly increased for both nanoparticles treatment groups when compared to the Pb18 group. SHAM (non-infected and non-treated), Pb18 (infected and non-treated), Comp (infected and treated with the P10 complexed nanoparticles) and Ncomp (infected and treated with the P10 co-administered with empty nanoparticles). * = $p < 0.05$ and ** = $p < 0.01$.

No IL-2 was detected, and the IL-12 and IFN- γ were significantly increased, when compared to the Pb18 group. IL-12 was higher in the Ncomp group when compared with the Comp group. IL-4 was significantly decreased, and the IL-10 was significantly increased, for both nanoparticle-treated groups when compared to the Pb18 group. No changes in IL-1 β levels were detected, but IL-23 was significantly increased for both nanoparticles treatment groups when compared to the Pb18 group.

3.6. CFU from the Immunization with Different Doses of Nanoparticles

The lungs of infected animals (Pb18, 1D, 2D and 3D) were significantly heavier than the lungs of mice from the non-infected and untreated group (SHAM) (Figure S7), showing a successfully infection of the animals by the intratracheal route. The CFUs were significantly lower in the P10 complexed nanoparticle treated animals compared to the infected and untreated mice (Figure 9). Notably, there were no differences between a single treatment

with the nanoparticles and either a second or third administration of the compounds one week apart.

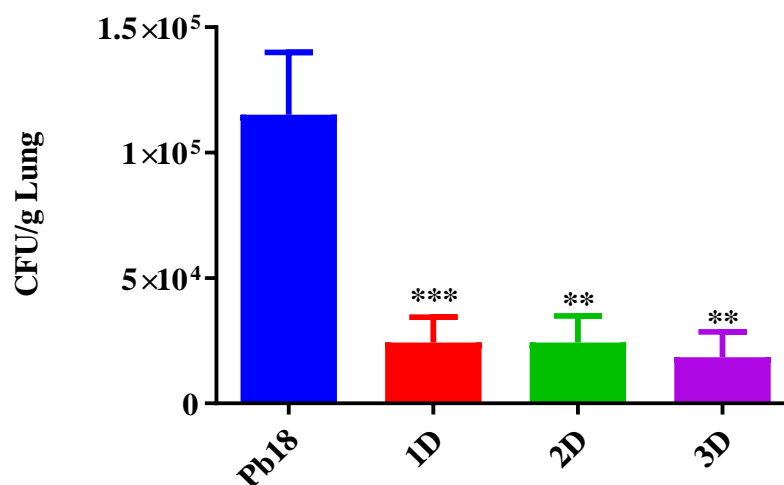


Figure 9. CFU of the lungs 51 days post infection. The P10 complexed nanoparticles significantly reduced the number of the viable *Paracoccidioides* cells when compared to the Pb 18 group. Pb18 (infected and non-treated), 1D (infected and treated with one dose of the P10 complexed nanoparticles), 2D (infected and treated with two doses) and 3D (infected and treated with three doses). ** = $p < 0.01$ and *** = $p < 0.001$.

3.7. Cytokines from the Immunization with Different Doses of Nanoparticles

Based on the reduction of CFUs with only one dose, the pulmonary cytokine production was evaluated in the P18, Sham and 1D groups for responses associated with the Th1, Th2 and Th17 T cells subset population (Table 2). We identified a Th1 and Th17 activation together with a small, but not absent, Th2 response.

Table 2. Th1, Th2 and Th17 cytokine production 51 days post infection.

Groups	Cytokines						
	Th1			Th2		Th17	
	IL-2	IL-12	IFN- γ	IL-4	IL-10	IL-1 β	IL-23
Sham	0	2605 \pm 480.1	80.96 \pm 22	148.4 \pm 57.84	1965 \pm 297.8	0	339.4 \pm 208.9
Pb 18	0	2491 \pm 502.8	66.80 \pm 9.9	140.4 \pm 37.61	2000 \pm 387.7	0	117.0 \pm 107.2
1D	0	3168 \pm 438.5 ***	92.84 \pm 29.38 *	193.6 \pm 47.72 **	2418 \pm 299.8 **	0	232.4 \pm 87.20 **

Th1, Th2 and Th17 cytokine production when compared to Pb18 group. Numbers in italic = SD, * = $p < 0.05$; ** = $p < 0.01$ and *** = $p < 0.001$.

No IL-2 was detected, and the IL-12 were significantly increased in the 1D, when compared to the Pb18 group. The IFN- γ were significantly increased in the 1D when compared to the Pb18 group. IL-4 and IL-10 were significantly increased in the 1D group when compared to the Pb18 group. No significant change was observed for the IL-1 β , and the IL-23 was significantly increased in all the different doses groups, when compared to the Pb18 group.

4. Discussion

PCM is one of the most prevalent yet neglected fungal disease in Latin America, especially in Brazil. New forms of treatment are an important issue since, due to costs and toxicity, the abandonment of treatment and the resurgence of infection is common [3]. In addition to traditional antifungal drugs, novel approaches for preventing or treating fungal diseases have focused on the induction of specific cellular responses that have been demonstrated as ideal for the elimination or containment of fungal infections [10,38]. Our

group has successfully demonstrated that the use of polymeric nanoparticles is advantageous for treating PCM disease, and is an exciting new approach to improving current treatment regimens [12,14]. The use of nanoparticles allows for the reduction of the load of the active molecule while serving as adjuvants in vaccines, which can lead to an increase in the cost-effectiveness and efficacy of a vaccine [12,14].

The P10 peptide has been studied for several decades, and its immunomodulatory effect is well described, but its use as a therapeutic has not been optimized as there has been a requirement for large concentrations of the peptide and strong adjuvants, which can sometimes interfere with the modulation of the immune response, to generate a protective host response to PCM disease [12,14,39]. We demonstrated in our studies with nanoparticles that this type of delivery platform can reduce the amount needed to effectively modify the immune response to the benefit of the host [12,14].

To further optimize the delivery of the P10 peptide using chitosan nanoparticles, we performed biodistribution assays. We observed that the nanoparticles were phagocytosed in the first 4 to 6 h of interaction with the cells, and that most of the nanoparticles adhered to the mucosa of the upper respiratory tract; smaller amounts were detected in the trachea and lung where they remained for at least one week. These findings are consistent with characteristics conferred by chitosan nanoparticles due to their mucoadhesive capacity [24,40,41].

IVIS experiments are complicated by the background fluorescence in the stomach and bowels of the mice. This background fluorescence is a consequence of the presence of chlorophyll-containing alfalfa and its derivatives in mouse food. These substances present autofluorescence in the same frequencies of excitation and emission of near infrared fluorochromes [33–37]. For compliance with animal welfare requirements, the mice in our experiments received food and water ad libitum.

As demonstrated by different researchers, the volume of inoculation, anesthesia induction status and position of the animal during and after vaccination, are factors that may affect the correct localization of the vaccines based in nanoparticles or not after intranasal administration [42–44].

In our experimental design we tried to reduce as much as possible the variables that could influence the correct location of the nanoparticles, since the animals' food presented fluorescence similar to that of the fluorochrome used. Even with these precautions, we cannot rule out the possibility that a small amount of the vaccine could have been swallowed, even though it was designed for degradation in the airway mucosa and can be partially degraded in the low pH of the stomach or peptidases in the intestinal tract [33–37,42–44].

The reduction of the fungal load in infected mice treated with P10 complexed to the nanoparticles was expected based on previous work from our research group using chitosan nanoparticles as an intranasal vaccine to treat PCM disease [14]. The innovation of this new work was the reduction of the number of doses and the reduction of the concentration of the P10 peptide when co-administered with empty chitosan nanoparticles, demonstrating the adjuvant and immunomodulatory effects of the chitosan nanoparticles [45–51].

The reduction of the necessary vaccine doses and the P10 concentration are directly related to a reduction of cost. Here, we show the reduction of the total amount of P10 peptide is usually used as standard (60 µg in three doses) to 12 times less (5 µg in one single dose) for the complexed nanoparticles, and to 4 times less when the peptide co-administrated with the empty nanoparticles [1,12,14].

The adjuvant effect of chitosan makes it an ideal choice for use in vaccines that aim to induce immune responses with an emphasis on cellular and non-humoral recruitment [45–51].

In our previous work we demonstrated that the chitosan nanoparticles alone had no immunomodulatory effect [14].

Chitosan stimulates phagocytic cells such as macrophages and dendritic cells to produce type 1 interferons and interleukins, especially IL-1β, and this stimulation is based on the interaction of chitosan with TLR-4 receptors, stimulation of the NLRP3 inflammasome

(necessary for combating and or containing *Paracoccidioides* [6]), and activation of cell signaling pathways (STING: stimulator of interferon genes) that function as a nucleic acid detector, and cGAS (guanine and adenine cyclic dinucleotides synthase) that is a precursor and co-stimulator of STING [45–51].

Mucosal immunity is another key factor related to the reduction of the fungal load enhanced by the adjuvant effect of the chitosan nanoparticles [52,53]. The upper airway mucosa is known as one of the main factors related to prevent infections [54]. The nasal region has different mechanisms related to innate and adaptative immunity, such as the mucus itself, which is full of enzymes and proteins related to degradation, inactivation and opsonization of dangerous particles or microorganisms [19]. Phagocytic cells and antigen present cells are also found in the mucosa of the upper airway, and these cells may be responsible for the uptake of the chitosan nanoparticles [52,53,55]. After uptake, the adjuvant effect of the chitosan is activated leading to the stimulation or re-stimulation of the effector mechanism responsible to contain or eliminate the *Paracoccidioides* in the lungs [56–58]. Due to the expected nanoparticle-induced immune response, and the type of immune response elicited by the infection, we analyzed the group of cytokines mainly associated with a protective response to fight fungal infections. These cytokines belong to Th1 and Th17 cell subsets, which are the responsible for coordinating the clearance of PCM disease [6].

The complexed vs co-administered formulation experiment was designed to verify if the chitosan nanoparticles act as an adjuvant when utilized without complexation with the peptide (co-administrated), and also to validate if this adjuvant effect would work with smaller amounts of the peptide in relation to our previous work [14].

Our model of infection (30 days prior treatment) was designed to simulate the chronic granulomatous PCM [6,7,59,60]. Increase of these cytokines can be observed in the early days of infection, or later during the adaptative immune response to the infection with granuloma formation. After the granuloma formation, the immune response is reduced to prevent tissue damage. This is one of the most remarkable characteristics of PCM [6,7,59,60].

The complexed and co-administrated nanoparticle chitosan vaccines were able to increase the levels of IL-12 and IFN- γ , which are important Th1 cytokines related to inflammation and elimination of the *Paracoccidioides*; however, no IL-2 was detected, probably because its release occurs in the first 24 h of stimulation [6,7,59,60]. The levels of IL-4 were reduced and the levels of IL-10 was slightly increased. These Th2 cytokines are related with inflammation control, associated with tissue repair or cell reorganization, and are important to the regulation of granuloma formation [6,7]. No IL-1 β was detected, but the levels of IL-23 were increased, pointing to a possible presence of the Th17 T cell subset [6,7,56].

Similar cytokines results were observed in the single dose vaccine group, showing increased levels of Th1 and Th17-related cytokines and the increased presence of Th2 cytokines. We observed an increase in the IL-12, IFN- γ , IL-4 and IL-10 cytokine levels of the treated group (1D) in relation to the controls groups (SHAM and Pb18), and statistical analysis was performed in comparison with the 1D group and infected with Pb 18 group [6,7,56]. Small variations in cytokine levels were detected between batches of mice, even though they were SPF animals; however, the general pattern of response was similar across the different experiments [6,7,56].

Based on our findings, we concluded that the chitosan nanoparticles adhered to the mucosa were constantly and slowly phagocytosed, inducing the production of inflammatory cytokines type Th1 and Th17, reducing the fungal load in the lungs.

5. Conclusion

We demonstrated that our chitosan nanoparticles remained mostly in the upper airway of the mice when administered intranasally, with a smaller amount localizing in the trachea and lungs due to chitosan muco-adhesiveness; the nanoparticles were phagocytized after 4 to 6 h. The chitosan nanoparticles show strong potential as an adjuvant for vaccines effectively inducing Th1 and Th17 immune responses, which are ideal for fighting fungal

infections. The nanoparticles also reduced the need for multiple doses to significantly reduce the fungal burdens in the lungs of infected animals.

6. Patents

INPI: BR 10 2019 012313 3 A2.

Supplementary Materials: The following supporting information can be downloaded at: <https://www.mdpi.com/article/10.3390/jof9020245/s1>, Figure S1: IVIS spectrum fluorescence of lung (L), trachea (T) and stomach (S), after inoculation of 5 μ L per nostril of the fluorescent Cy5.5 chitosan nanoparticles (NP) at 0 h; Figure S2: IVIS spectrum fluorescence of lung (L), trachea (T), stomach (S) and brain (B), after inoculation of 5 μ L per nostril of the fluorescent Cy5.5 chitosan nanoparticles (NP) at 96 h; Figure S3: IVIS spectrum fluorescence of lung (L), trachea (T), stomach (S), brain (Br), liver (L) and bowels (Bo) after inoculation of 5 μ L per nostril of PBS at 0 h; Figure S4: IVIS spectrum fluorescence of lung (L), trachea (T), stomach (S) and brain (Br), after 96 h of the inoculation of 5 μ L per nostril of PBS; Figure S5: IVIS spectrum fluorescence obtained with the mice positioned in supine position showing the fluorescence in the gastrointestinal tract of the BABL/c nude mice before the inoculation of any substance; Figure S6: Weight of the lungs after euthanasia (51 days post infection). There was a significant increase of the lung weight from infected animals when compared to the SHAM group. SHAM (non-infected and non-treated), Pb18 (infected and non-treated), Comp (infected and treated with the P10 complexed nanoparticles) and Ncomp (infected and treated with the P10 associated with empty nanoparticles). * = $p < 0.05$ and ** = $p < 0.01$; Figure S7: Weight of the lungs after euthanasia (51 days post infection). There was a significant increase of the lung weight from infected animals, when compared to the SHAM group. SHAM (non-infected and non-treated), Pb18 (infected and non-treated), 1D (infected and treated with one dose of the P10 complexed nanoparticles), 2D (infected and treated with two doses of the P10 complexed nanoparticles) and 3D (infected and treated with three doses of the P10 complexed nanoparticles). * = $p < 0.05$ and ** = $p < 0.01$.

Author Contributions: Conceptualization, S.R.D.S.J., A.C.A. and C.P.T.; data curation, S.R.D.S.J., A.C.A. and C.P.T.; formal analysis, S.R.D.S.J., A.C.A. and C.P.T.; funding acquisition, C.P.T.; Investigation, S.R.D.S.J. and F.V.B.; Methodology, S.R.D.S.J. and F.V.B.; project administration, A.C.A. and C.P.T.; Supervision, A.C.A. and C.P.T.; writing—original draft, S.R.D.S.J.; writing—review & editing, J.D.N., A.C.A. and C.P.T. All authors have read and agreed to the published version of the manuscript.

Funding: This research was funded by Fundação de Amparo à Pesquisa do Estado de São Paulo (FAPESP 2016/08730-6), Conselho Nacional de Desenvolvimento Científico e Tecnológico (CNPq 420480/2018-8 and 134424/2016-6) and Coordenação de Aperfeiçoamento de Pessoal de Nível Superior—Brasil (CAPES 88882.333055/2019-01).

Institutional Review Board Statement: The animal study protocol was approved by the Institutional Ethics Committee of the University of São Paulo; Institute of Biomedical Sciences (CEUA ICB n^o 3654290618 in 08/12/2019).

Informed Consent Statement: Not applicable.

Data Availability Statement: Not applicable.

Conflicts of Interest: There are no conflict of interest to declare.

References

1. Travassos, L.R.; Tabora, C.P. New advances in the development of a vaccine against paracoccidioidomycosis. *Front. Microbiol.* **2012**, *3*, 212. [CrossRef]
2. Shikanai-yasuda, M.A.; De Queiroz, F.; Filho, T.; Mendes, R.P.; Colombo, A.L.; Moretti, M.L.; Consultores, D. Consenso em paracoccidioidomicose Guideliness in paracoccidioidomycosis. *Rev. Soc. Bras. Med. Trop.* **2006**, *39*, 297–310. [CrossRef] [PubMed]
3. Shikanai-Yasuda, M.A.; Mendes, R.P.; Colombo, A.L.; de Queiroz-Telles, F.; Kono, A.S.G.; Paniago, A.M.M.; Nathan, A.; do Valle, A.C.F.; Bagagli, E.; Benard, G.; et al. Brazilian guidelines for the clinical management of paracoccidioidomycosis. *Rev. Soc. Bras. Med. Trop.* **2017**, *50*, 715–740. [CrossRef] [PubMed]
4. Turissini, D.A.; Gomez, O.M.; Teixeira, M.M.; McEwen, J.G.; Matute, D.R. Species boundaries in the human pathogen *Paracoccidioides*. *Fungal Genet. Biol.* **2017**, *106*, 9–25. [CrossRef] [PubMed]

5. Souza, A.C.O.; Taborda, C.P. Epidemiology of Dimorphic Fungi. In *Encyclopedia of Mycology*; Elsevier: Amsterdam, The Netherlands, 2021; pp. 613–623; ISBN 9780323851800.
6. Taborda, C.P.; Travassos, L.R.; Benard, G. Paracoccidioidomycosis. In *Encyclopedia of Mycology*; Elsevier: Amsterdam, The Netherlands, 2021; pp. 654–675.
7. Benard, G. An overview of the immunopathology of human paracoccidioidomycosis. *Mycopathologia* **2008**, *165*, 209–221. [[CrossRef](#)] [[PubMed](#)]
8. Bocca, A.L.; Amaral, A.C.; Teixeira, M.M.; Sato, P.K.; Sato, P.; Shikanai-Yasuda, M.A.; Soares Felipe, M.S. Paracoccidioidomycosis: Eco-epidemiology, taxonomy and clinical and therapeutic issues. *Future Microbiol.* **2013**, *8*, 1177–1191. [[CrossRef](#)]
9. Amaral, A.C.; Bocca, A.L.; Ribeiro, A.M.; Nunes, J.; Peixoto, D.L.G.G.; Simioni, A.R.; Primo, F.L.; Lacava, Z.G.M.M.; Bentes, R.; Titze-de-Almeida, R.; et al. Amphotericin B in poly(lactic-co-glycolic acid) (PLGA) and dimercaptosuccinic acid (DMSA) nanoparticles against paracoccidioidomycosis. *J. Antimicrob. Chemother.* **2009**, *63*, 526–533. [[CrossRef](#)]
10. Taborda, C.P.; Urán, M.E.; Nosanchuk, J.D.; Travassos, L.R. Paracoccidioidomycosis: Challenges in the development of a vaccine against an endemic mycosis in the Americas. *Rev. Inst. Med. Trop. Sao Paulo* **2015**, *57*, 21–24. [[CrossRef](#)]
11. Taborda, C.P.; Juliano, M.A.; Puccia, R.; Franco, M.; Travassos, L.R. Mapping of the T-cell epitope in the major 43-kilodalton glycoprotein of Paracoccidioides brasiliensis which induces a Th-1 response protective against fungal infection in BALB/c mice. *Infect. Immun.* **1998**, *66*, 786–793. [[CrossRef](#)]
12. Amaral, A.C.; Marques, A.F.; Muñoz, J.E.; Bocca, A.L.; Simioni, A.R.; Tedesco, A.C.; Morais, P.C.; Travassos, L.R.; Taborda, C.P.; Felipe, M.S.S. Poly(lactic acid-glycolic acid) nanoparticles markedly improve immunological protection provided by peptide P10 against murine paracoccidioidomycosis. *Br. J. Pharmacol.* **2010**, *159*, 1126–1132. [[CrossRef](#)]
13. Jannuzzi, G.P.; Souza, N.d.A.; Franoso, K.S.; Pereira, R.H.; Santos, R.P.; Kaihami, G.H.; de Almeida, J.R.F.; Batista, W.L.; Amaral, A.C.; Maranhão, A.Q.; et al. Therapeutic treatment with scFv–PLGA nanoparticles decreases pulmonary fungal load in a murine model of paracoccidioidomycosis. *Microbes Infect.* **2018**, *20*, 48–56. [[CrossRef](#)] [[PubMed](#)]
14. Rodrigues Dos Santos Junior, S.; Kelley Lopes da Silva, F.; Santos Dias, L.; Oliveira Souza, A.C.; Valdemir de Araujo, M.; Buffoni Roque da Silva, L.; Travassos, L.R.; Correa Amaral, A.; Taborda, C.P. Intranasal Vaccine Using P10 Peptide Complexed within Chitosan Polymeric Nanoparticles as Experimental Therapy for Paracoccidioidomycosis in Murine Model. *J. Fungi* **2020**, *6*, 160. [[CrossRef](#)]
15. Kischkel, B.; Rossi, S.A.; Santos, S.R.; Nosanchuk, J.D.; Travassos, L.R.; Taborda, C.P. Therapies and Vaccines Based on Nanoparticles for the Treatment of Systemic Fungal Infections. *Front. Cell. Infect. Microbiol.* **2020**, *10*, 463. [[CrossRef](#)]
16. dos Santos Junior, S.R.; Amaral, A.C.; Taborda, C.P. Application of Nanoparticles to Invasive Fungal Infections. In *Nanotechnology for Infectious Diseases*; Springer: Singapore, 2022; pp. 151–173.
17. Van der Lubben, I.M.; Verhoef, J.C.; Borchard, G.; Junginger, H.E. Chitosan for mucosal vaccination. *Adv. Drug Deliv. Rev.* **2001**, *52*, 139–144. [[CrossRef](#)] [[PubMed](#)]
18. Pan, L.; Zhang, Z.; Lv, J.; Zhou, P.; Hu, W.; Fang, Y.; Chen, H.; Liu, X.; Shao, J.; Zhao, F.; et al. Induction of mucosal immune responses and protection of cattle against direct-contact challenge by intranasal delivery with foot-and-mouth disease virus antigen mediated by nanoparticles. *Int. J. Nanomed.* **2014**, *9*, 5603–5618. [[CrossRef](#)] [[PubMed](#)]
19. Kyd, J.M.; Foxwell, A.R.; Cripps, A.W. Mucosal immunity in the lung and upper airway. *Vaccine* **2001**, *19*, 2527–2533. [[CrossRef](#)]
20. Xia, Y.; Fan, Q.; Hao, D.; Wu, J.; Ma, G.; Su, Z. Chitosan-based mucosal adjuvants: Sunrise on the ocean. *Vaccine* **2015**, *33*, 5997–6010. [[CrossRef](#)]
21. Chadwick, S.; Kriegel, C.; Amiji, M. Nanotechnology solutions for mucosal immunization. *Adv. Drug Deliv. Rev.* **2010**, *62*, 394–407. [[CrossRef](#)]
22. Banerjee, T.; Mitra, S.; Kumar Singh, A.; Kumar Sharma, R.; Maitra, A. Preparation, characterization and biodistribution of ultrafine chitosan nanoparticles. *Int. J. Pharm.* **2002**, *243*, 93–105. [[CrossRef](#)] [[PubMed](#)]
23. Sonin, D.; Pochkaeva, E.; Zhuravskii, S.; Postnov, V.; Korolev, D.; Vasina, L.; Kostina, D.; Mukhametdinova, D.; Zelinskaya, I.; Skorik, Y.; et al. Biological Safety and Biodistribution of Chitosan Nanoparticles. *Nanomaterials* **2020**, *10*, 810. [[CrossRef](#)]
24. Raj, P.M.; Raj, R.; Kaul, A.; Mishra, A.K.; Ram, A. Biodistribution and targeting potential assessment of mucoadhesive chitosan nanoparticles designed for ulcerative colitis via scintigraphy. *RSC Adv.* **2018**, *8*, 20809–20821. [[CrossRef](#)] [[PubMed](#)]
25. Suri, S.; Ruan, G.; Winter, J.; Schmidt, C.E. Microparticles and Nanoparticles. In *Biomaterials Science: An Introduction to Materials in Medicine*, 3rd ed.; Academic Press: Cambridge, MA, USA, 2013; pp. 360–388. [[CrossRef](#)]
26. Buzea, C.; Pacheco, I. Toxicity of nanoparticles. In *Nanotechnology in Eco-Efficient Construction: Materials, Processes and Applications*; Woodhead Publishing: Soston, UK, 2018; pp. 705–754. [[CrossRef](#)]
27. Kim, K.; Kim, J.H.; Park, H.; Kim, Y.S.; Park, K.; Nam, H.; Lee, S.; Park, J.H.; Park, R.W.; Kim, I.S.; et al. Tumor-homing multifunctional nanoparticles for cancer theragnosis: Simultaneous diagnosis, drug delivery, and therapeutic monitoring. *J. Control. Release* **2010**, *146*, 219–227. [[CrossRef](#)]
28. Huang, M.; Ma, Z.; Khor, E.; Lim, L.Y. Uptake of FITC-chitosan nanoparticles by A549 cells. *Pharm. Res.* **2002**, *19*, 1488–1494. [[CrossRef](#)]
29. Herb, M.; Farid, A.; Gluschko, A.; Krönke, M.; Schramm, M. Highly Efficient Transfection of Primary Macrophages with In Vitro Transcribed mRNA. *J. Vis. Exp.* **2019**, *2019*, e60143. [[CrossRef](#)]
30. Zhang, X.; Goncalves, R.; Mosser, D.M. The Isolation and Characterization of Murine Macrophages. *Curr. Protoc. Immunol.* **2008**, *83*, 14. [[CrossRef](#)]




31. Busch, C.; Favret, J.; Geirsdóttir, L.; Molawi, K.; Sieweke, M. Isolation and Long-term Cultivation of Mouse Alveolar Macrophages. *Bio-Protocol* **2019**, *9*, e3302. [[CrossRef](#)] [[PubMed](#)]
32. Netto, C.F.; Vegas, V.S.; Sciannaméa, I.M.; Guarnieri, D.B. The polysaccharidic antigen from *Paracoccidioides brasiliensis*. Study of the time of cultivation necessary for the preparation of the antigen. *Rev. Inst. Med. Trop. Sao Paulo* **1969**, *11*, 177–181. [[PubMed](#)]
33. Del Rosal, B.; Villa, I.; Jaque, D.; Sanz-Rodríguez, F. In vivo autofluorescence in the biological windows: The role of pigmentation. *J. Biophotonics* **2016**, *9*, 1059–1067. [[CrossRef](#)]
34. Kwon, S.; Davies-Venn, C.; Sevick-Muraca, E.M. In vivo dynamic imaging of intestinal motions using diet-related autofluorescence. *Neurogastroenterol. Motil.* **2012**, *24*, 494–497. [[CrossRef](#)] [[PubMed](#)]
35. del Rosal, B.; Benayas, A. Strategies to Overcome Autofluorescence in Nanoprobe-Driven In Vivo Fluorescence Imaging. *Small Methods* **2018**, *2*, 1800075. [[CrossRef](#)]
36. Bhaumik, S.; Depuy, J.; Klimash, J. Strategies to minimize background autofluorescence in live mice during noninvasive fluorescence optical imaging. *Lab Anim.* **2007**, *36*, 40–43. [[CrossRef](#)] [[PubMed](#)]
37. Inoue, Y.; Izawa, K.; Kiryu, S.; Tojo, A.; Ohtomo, K. Diet and Abdominal Autofluorescence Detected by In Vivo Fluorescence Imaging of Living Mice. *Mol. Imaging* **2008**, *7*, 21–27. [[CrossRef](#)] [[PubMed](#)]
38. Almeida, F.; Rodrigues, M.L.; Coelho, C. The Still Underestimated Problem of Fungal Diseases Worldwide. *Front. Microbiol.* **2019**, *10*, 214. [[CrossRef](#)]
39. Mayorga, O.; Munoz, J.E.; Travassos, L.R.; Carlos, P. The role of adjuvants in therapeutic protection against paracoccidioidomycosis after immunization with the P10 peptide. *Front. Microbiol.* **2012**, *3*, 154. [[CrossRef](#)]
40. Shim, S.; Soh, S.H.; Bin Im, Y.; Park, H.E.; Cho, C.S.; Kim, S.; Yoo, H.S. Elicitation of Th1/Th2 related responses in mice by chitosan nanoparticles loaded with *Brucella abortus* malate dehydrogenase, outer membrane proteins 10 and 19. *Int. J. Med. Microbiol.* **2020**, *310*, 151362. [[CrossRef](#)]
41. Rençber, S.; Karavana, S.Y.; Yılmaz, F.F.; Eraç, B.; Nenni, M.; Ozbal, S.; Pekçetin, Ç.; Gurer-Orhan, H.; Hoşgör Limoncu, M.; Güneri, P.; et al. Development, characterization, and in vivo assessment of mucoadhesive nanoparticles containing fluconazole for the local treatment of oral candidiasis. *Int. J. Nanomed.* **2016**, *11*, 2641. [[CrossRef](#)]
42. Southam, D.S.; Dolovich, M.; O’Byrne, P.M.; Inman, M.D. Distribution of intranasal instillations in mice: Effects of volume, time, body position, and anesthesia. *Am. J. Physiol. Cell. Mol. Physiol.* **2002**, *282*, L833–L839. [[CrossRef](#)]
43. Miller, M.A.; Stabenow, J.M.; Parvathareddy, J.; Wodowski, A.J.; Fabrizio, T.P.; Bina, X.R.; Zalduondo, L.; Bina, J.E. Visualization of Murine Intranasal Dosing Efficiency Using Luminescent *Francisella tularensis*: Effect of Instillation Volume and Form of Anesthesia. *PLoS ONE* **2012**, *7*, e31359. [[CrossRef](#)] [[PubMed](#)]
44. Visweswaraiah, A. Tracking the tissue distribution of marker dye following intranasal delivery in mice and chinchillas: A multifactorial analysis of parameters affecting nasal retention. *Vaccine* **2002**, *20*, 3209–3220. [[CrossRef](#)]
45. Swanson, K.V.; Deng, M.; Ting, J.P.Y. The NLRP3 inflammasome: Molecular activation and regulation to therapeutics. *Nat. Rev. Immunol.* **2019**, *19*, 477–489. [[CrossRef](#)]
46. Carroll, E.C.; Jin, L.; Mori, A.; Muñoz-Wolf, N.; Oleszycka, E.; Moran, H.B.T.; Mansouri, S.; McEntee, C.P.; Lambe, E.; Agger, E.M.; et al. The Vaccine Adjuvant Chitosan Promotes Cellular Immunity via DNA Sensor cGAS-STING-Dependent Induction of Type I Interferons. *Immunity* **2016**, *44*, 597–608. [[CrossRef](#)]
47. Dubensky, T.W.; Kanne, D.B.; Leong, M.L. Rationale, progress and development of vaccines utilizing STING-activating cyclic dinucleotide adjuvants. *Ther. Adv. Vaccines* **2013**, *1*, 131–143. [[CrossRef](#)]
48. Villiers, C.; Chevallet, M.; Diemer, H.; Couderc, R.; Freitas, H.; Van Dorsselaer, A.; Marche, P.N.; Rabilloud, T. From secretome analysis to immunology: Chitosan induces major alterations in the activation of dendritic cells via a TLR4-dependent mechanism. *Mol. Cell. Proteom.* **2009**, *8*, 1252–1264. [[CrossRef](#)] [[PubMed](#)]
49. Bueter, C.L.; Lee, C.K.; Wang, J.P.; Ostroff, G.R.; Specht, C.A.; Levitz, S.M. Spectrum and Mechanisms of Inflammasome Activation by Chitosan. *J. Immunol.* **2014**, *192*, 5943–5951. [[CrossRef](#)] [[PubMed](#)]
50. Bueter, C.L.; Lee, C.K.; Rathinam, V.A.K.; Healy, G.J.; Taron, C.H.; Specht, C.A.; Levitz, S.M. Chitosan but not chitin activates the inflammasome by a mechanism dependent upon phagocytosis. *J. Biol. Chem.* **2011**, *286*, 35447–35455. [[CrossRef](#)]
51. Mori, A.; Oleszycka, E.; Sharp, F.A.; Coleman, M.; Ozasa, Y.; Singh, M.; O’Hagan, D.T.; Tajber, L.; Corrigan, O.I.; McNeela, E.A.; et al. The vaccine adjuvant alum inhibits IL-12 by promoting PI3 kinase signaling while chitosan does not inhibit IL-12 and enhances Th1 and Th17 responses. *Eur. J. Immunol.* **2012**, *42*, 2709–2719. [[CrossRef](#)] [[PubMed](#)]
52. Lavelle, E.C.; Ward, R.W. Mucosal vaccines—Fortifying the frontiers. *Nat. Rev. Immunol.* **2022**, *22*, 236–250. [[CrossRef](#)]
53. Holmgren, J.; Czerkinsky, C. Mucosal immunity and vaccines. *Nat. Med.* **2005**, *11*, S45–S53. [[CrossRef](#)]
54. Marttin, E.; Schipper, N.G.M.; Coos Verhoef, J.; Merkus, F.W.H.M. Nasal mucociliary clearance as a factor in nasal drug delivery. *Adv. Drug Deliv. Rev.* **1998**, *29*, 13–38. [[CrossRef](#)]
55. Ogra, P.L.; Faden, H.; Welliver, R.C. Vaccination Strategies for Mucosal Immune Responses. *Clin. Microbiol. Rev.* **2001**, *14*, 430–445. [[CrossRef](#)]
56. Kolls, J.K.; Khader, S.A. The role of Th17 cytokines in primary mucosal immunity. *Cytokine Growth Factor Rev.* **2010**, *21*, 443–448. [[CrossRef](#)] [[PubMed](#)]
57. Khader, S.A.; Gaffen, S.L.; Kolls, J.K. Th17 cells at the crossroads of innate and adaptive immunity against infectious diseases at the mucosa. *Mucosal Immunol.* **2009**, *2*, 403–411. [[CrossRef](#)] [[PubMed](#)]
58. Burger, E. Paracoccidioidomycosis Protective Immunity. *J. Fungi* **2021**, *7*, 137. [[CrossRef](#)] [[PubMed](#)]

59. Ribeiro, A.M.; Bocca, A.L.; Amaral, A.C.; Faccioli, L.H.; Galetti, F.C.S.; Zárata-Bladés, C.R.; Figueiredo, F.; Silva, C.L.; Felipe, M.S.S. DNAhsp65 vaccination induces protection in mice against *Paracoccidioides brasiliensis* infection. *Vaccine* **2009**, *27*, 606–613. [[CrossRef](#)]
60. Sojka, D.K.; Bruniquel, D.; Schwartz, R.H.; Singh, N.J. IL-2 Secretion by CD4 + T Cells In Vivo Is Rapid, Transient, and Influenced by TCR-Specific Competition. *J. Immunol.* **2004**, *172*, 6136–6143. [[CrossRef](#)] [[PubMed](#)]

Disclaimer/Publisher’s Note: The statements, opinions and data contained in all publications are solely those of the individual author(s) and contributor(s) and not of MDPI and/or the editor(s). MDPI and/or the editor(s) disclaim responsibility for any injury to people or property resulting from any ideas, methods, instructions or products referred to in the content.

Article

Intranasal Vaccine Using P10 Peptide Complexed within Chitosan Polymeric Nanoparticles as Experimental Therapy for Paracoccidioidomycosis in Murine Model

Samuel Rodrigues Dos Santos Junior ^{1,*}, Francenya Kelley Lopes da Silva ²,
Lucas Santos Dias ^{1,†}, Ana Camila Oliveira Souza ^{1,‡}, Marcelo Valdemir de Araujo ¹,
Leandro Buffoni Roque da Silva ¹, Luiz R. Travassos ^{3,§}, Andre Correa Amaral ² and
Carlos P. Taborda ^{1,4}

¹ Departamento de Microbiologia, Instituto de Ciências Biológicas, Universidade de São Paulo, São Paulo, SP 05508-000, Brazil; dossantosdia@wisc.edu (L.S.D.); aolivei5@uthsc.edu (A.C.O.S.); marceloaraujo@usp.br (M.V.d.A.); leandrobr87@usp.br (L.B.R.d.S.); taborda@usp.br (C.P.T.)

² Laboratório de Nano & Biotecnologia, Departamento de Biotecnologia, Instituto de Patologia Tropical e Saúde Pública, Universidade Federal de Goiás, Goiânia, GO 74605-050, Brazil; francenya@hotmail.com (F.K.L.d.S.); amaral.nanobiotech@gmail.com (A.C.A.)

³ Departamento de Microbiologia, Imunologia e Parasitologia, Universidade Federal de São Paulo, São Paulo, SP 04023-062, Brazil; travassos@unifesp.br

⁴ Departamento de Dermatologia, Instituto de Medicina Tropical de São Paulo, Faculdade de Medicina, Universidade de São Paulo, São Paulo, SP 05403-000, Brazil

* Correspondence: samuelmicrobio@usp.br

† Current address: Departments of Pediatrics, School of Medicine and Public Health University of Wisconsin, Madison, WI 53706, USA.

‡ Current address: Health Science Center, The University of Tennessee, Memphis, TN 38163, USA.

§ Deceased.

Received: 13 August 2020; Accepted: 25 August 2020; Published: 2 September 2020



Abstract: Paracoccidioidomycosis (PCM) is a granulomatous fungal disease caused by the dimorphic fungal species of *Paracoccidioides*, which mainly affects the lungs. Modern strategies for the treatment and/or prevention of PCM are based on a Th1-type immune response, which is important for controlling the disease. One of the most studied candidates for a vaccine is the P10 peptide, derived from the 43 kDa glycoprotein of *Paracoccidioides brasiliensis*. In order to improve its immune modulatory effect, the P10 peptide was associated with a chitosan-conjugated nanoparticle. The nanoparticles presented 220 nm medium size, poly dispersion index (PDI) below 0.5, zeta potential of +20 mV and encapsulation efficiency around 90%. The nanoparticles' non-toxicity was verified by hemolytic test and cell viability using murine macrophages. The nanoparticles were stable and presented physicochemical characteristics desirable for biological applications, reducing the fungal load and the usual standard concentration of the peptide from 4 to 20 times.

Keywords: paracoccidioidomycosis; P10 peptide; nanovaccine; polymeric nanoparticles; antifungal therapy

1. Introduction

Paracoccidioidomycosis (PCM) is a granulomatous disease caused by the thermo-dimorphic fungi belonging to the genus *Paracoccidioides*, endemic in Latin America, spreading from southern Mexico to the north of Argentina [1,2]. Although the affected organs are most frequently the lungs, PCM can also be a systemic disease [3].

This mycosis is characterized by skin and oral mucosa lesions, and the formation of granulomas, as a result of the lung infection and tissue damage. The liver and spleen can also be affected, leading to hepatosplenomegaly, which can cause organ malfunction [3,4]. Infection initiates when the host inhales fungal propagules dispersed in the atmosphere, which can then reach the alveoli. At the physiological temperature 37 °C, the fungus switches to a pathogenic yeast form [5,6].

The treatment of PCM is based on the patients' clinical conditions and requires the use of chemotherapeutics, such as sulfamethoxazole trimethoprim, itraconazole and amphotericin B [3,7]. Some of these, however, can cause unwanted adverse side effects, for instance a long-term treatment or liver and kidney toxicity [8,9]. One of the alternative therapies that could be used to treat or prevent PCM is an immunomodulatory vaccine that increases the production of interferon gamma (IFN- γ) to stimulate a protective cell-mediated (Th1) immune response [10,11]. Different vaccine proposals, ranging from attenuated fungal particles to DNA-based vaccines have been investigated [12–14]. One of the most promising candidates for PCM is based on a 15-amino acid peptide (QTLIAIHTLAIRYAN) derived from the 43 kDa glycoprotein (GP43) of *Paracoccidioides brasiliensis* [15,16]. The P10 peptide stimulates the production of cytokines, such as IFN- γ , leading to a predominant Th1 immune response [15].

Although the P10 peptide is a promising vaccine candidate, a major drawback is its instability—similar to many other short peptides for in vivo application. An efficient approach used for the delivery of peptide vaccines actively being studied is the encapsulation or entrapment of the antigen within polymeric nanoparticles, which allows increased bioavailability of the immunogenic peptide [17,18].

Chitosan is a cationic, natural and low-cost polymer used to prepare these types of nanoparticles. The most striking feature of chitosan nanoparticles is their ability to be mucoadhesive. Given that PCM fungi are lined with mucus at the site of infection, this property of nanoparticles is essential for interactions in the respiratory tract, where degradation and displacement of particles takes place [19–22].

The objective of this study was to investigate an intranasal vaccine for the treatment of PCM using chitosan nanoparticles as a carrier for the P10 peptide.

2. Methods

2.1. P10-Chitosan Nanoparticles Preparation and Characterization

The nanoparticles were prepared according to modifications on the ionotronic gelation technique described by Calvo et al. [23,24]. Initially, 60 mg of chitosan (Chitosan Low Molecular Weight Sigma-Aldrich, St. Louis, MO, USA), deacetylation degree $\geq 75\%$ and viscosity 20–300 cps ($c = 1\%$ in 1% of acetic acid) were diluted in 20 mL of ultrapure water and 174 μL of 0.1 M acetic acid (final concentration). The polymer was dissolved in a magnetic stirrer for approximately 1 h at room temperature. The pH of the solution was adjusted to 4.4 using NaOH 0.1 M and the final volume was adjusted to 30 mL with ultrapure water. For the sodium tripolyphosphate (TPP; Sigma-Aldrich, St. Louis, MO, USA) solution, 14 mg of TPP was dissolved in 14 mL of ultrapure water.

Complexed nanoparticles formation used 250 μL of P10 peptide at concentration of 20 $\mu\text{g}/10 \mu\text{L}$ mixed with 1.13 mL of TPP solution. The TPP + P10 was slowly dripped into 2.12 mL of chitosan solution with magnetic stirring at 50–75 rpm for one hour at room temperature. The nanoparticles were then centrifuged for one hour at 13,200 rpm at 4 °C and the supernatant was collected and used for P10 association efficiency analysis. The empty nanoparticles were prepared following the same protocol but replacing the P10 peptide solution with 250 μL of ultra-pure water with 20% DMSO.

The pellet containing the empty or complexed nanoparticles was resuspended in 1 mL of PBS and stored at 4 °C for a week.

Prior to administration, the nanoparticles were diluted in PBS to achieve concentrations of 1 $\mu\text{g}/10 \mu\text{L}$ and 5 $\mu\text{g}/10 \mu\text{L}$ of P10 peptide.

2.2. Physical-Chemical Characterization of Nanoparticles

The size (given as z-average), size distribution (given as polydispersity index (PDI) and surface charge (given as zeta potential) of the nanoparticles were determined using the Zetasizer Nano Zs equipment (Malvern Panalytical Ltd. Enigma Business Park. Grovewood Road. Malvern. WR14 1XZ. United Kingdom). All measurements were done at 25 °C. The association efficiency (AE) of P10 within chitosan nanoparticles was assessed by quantification of the non-complexed P10 peptide present in the supernatant using the Qubit™ Protein Assay Kit (Thermo Fisher Scientific, Waltham, MA, USA). The supernatant of the empty nanoparticles was used as the blank control in the measurements. AE was calculated using the Equation (1):

$$AE = \frac{\text{Total P10} - \text{Free P10 on supernatant}}{\text{Total P10}} \times 100 \quad (1)$$

All physiochemical characterizations were assessed using the complexed nanoparticles with the highest concentration of the P10 peptide 20 µg/10 µL.

2.3. Nanoparticles Safety Assays

In order to evaluate the cytotoxicity of the empty or P10-complexed nanoparticles, cell viability was measured using the MTT 3-(4,5-dimethylthiazole bromide-2-yl)-2,5-diphenyltetrazolium bromide (Sigma-Aldrich, St. Louis, MO, USA) method and a hemolysis assay was performed according to [9].

2.3.1. Hemolysis

Fresh blood was collected from healthy volunteers. Red blood cells (RBCs) were separated by centrifugation at 5000 rpm for 10 min, the supernatant was discarded, and the cells were washed three times with PBS. RBCs were then diluted in PBS (3:11). For the assay, 20 µL of RBC were distributed in the wells of a 96-well microplate containing 180 µL of empty or complexed P10 nanoparticles. Sterilized water was used as positive control (100% hemolysis) and 1× PBS was used for negative control (no hemolysis). P10-complexed nanoparticles were used at the concentrations of 0, 0.5, 1, 1.5, 2, 2.5 and 3 mg/mL. For empty nanoparticles, 2-fold serial dilutions of the initial concentration of nanoparticles (1×) were performed, where the dilutions (*n*) are represented as two to the power of *n* (2^{-*n*}). Thus, the dilutions of the empty nanoparticles ranged from 1× (initial concentration after preparation) to 2⁻⁶×.

The samples were incubated for two or six hours at 37 °C and 5% CO₂. After the incubation, the plates were centrifuged at 5000 rpm for 10 min at room temperature. The supernatant was transferred to another 96-well microplate and left at room temperature for 30 min to oxidize the hemoglobin of the lysed erythrocytes. The absorbance of the supernatants was then measured using a plate spectrophotometer reader at 540 nm.

The percentage of hemolysis was calculated using the following Equation (2),

$$\% \text{ of hemolysis} = \frac{(100 \times AH)}{AdH_2O} \quad (2)$$

where AH: Absorbance of sample, AdH₂O: Mean of sample absorbances treated with distilled water.

2.3.2. Cell Viability

Murine macrophage lineage J774.16 was also used to assess the cytotoxicity of the nanoparticles. Macrophages were maintained in DMEM medium (Gibco, Thermo Fisher Scientific, Waltham, MA, USA) supplemented with 10% FBS (Fetal Bovine Serum, LGC Biotecnologia, Cotia, Sao Paulo, Brazil). First, 180 µL of DMEM supplemented with 10% FBS, containing nanoparticles with different amounts of P10 ranging from 400 µg to 0.19 µg were distributed in 96-well plates. Then, 20 µL of a suspension containing 5 × 10⁴ cells/mL was added to each well.

After 24, 48 and 72 h of incubation with the nanoparticles, 20 μL of 5 mg/mL MTT was added to each well and incubated at 37 °C and 5% CO_2 for 4 h. The supernatants were then discarded and 100 μL of DMSO (dimethylsulfoxide, Sigma-Aldrich, St. Louis, MO, USA) was added to each well. Then, the absorbance of the supernatants was measured at 540 nm using a plate spectrophotometer reader. The percentage of live cells was calculated using the following Equation (3),

$$\% \text{ of live cells} = \frac{(100 \times A_v)}{\text{ADMEM}} \quad (3)$$

where: A_v : Absorbance of sample, ADMEM: Average absorbance of samples treated with DMEM (control).

2.4. In Vivo P10-Nanoparticles Vaccine Evaluation PBS

2.4.1. Yeast

P. brasiliensis strain Pb 18 was maintained as yeast in Fava Neto solid medium. The yeasts were then transferred to the Brain Heart Infusion (BHI, BACTO™, BD Franklin Lakes, NJ, USA) liquid medium supplemented with 4% fetal bovine serum (FBS), 4% glucose (DIFCO™, BD Franklin Lakes, NJ, USA) and kept in a shaker at 37 °C and 150 rpm for five to seven days prior to infection. The yeast was then collected and washed three times using 1 \times and centrifuged at 3000 rpm for ten minutes. The yeast was resuspended in 5 mL of PBS and the viability of the fungal cells was assessed by counting in Neubauer's chamber using the Janus green dye 1:1 (Sigma-Aldrich, St. Louis, MO, USA) and adjusted to 3 \times 10⁵ yeast/50 μL .

2.4.2. Animals

Male BALB/c mice, free of pathogens, aged six to eight weeks, were used according to the Animal Use Ethics Committee: CEUA ICB #65/2016 (10/11/216). The animals were kept in the animal facility of the Microbiology Department of the Biomedical Science Institute and had access to water and food *ad libitum*. The animals were randomly organized accordingly: Group (i) positive control infected, without treatment (Pb 18); group (ii) infected and treated with a co-administered vaccine (empty nanoparticles + 20 μg /10 μL free-form of P10 peptide) (Nano + P10); group (iii) infected and treated with empty nanoparticles (0 μg); group (iv) infected and treated with the nanoparticles complexed with 1 μg /10 μL of P10 (1 μg); group (v) infected and treated with complexed nanoparticles with 5 μg /10 μL of P10 (5 μg); group (vi) infected and treated with nanoparticles complexed with 20 μg /10 μL of P10 (20 μg); group (vi) sham (uninfected and untreated).

2.4.3. Intratracheal Infection

In order to simulate the infection caused by *P. brasiliensis*, BALB/c mice were infected with Pb18 yeasts through intratracheal inoculation. Briefly, animals were anesthetized intraperitoneally with 80 mg kg^{-1} of ketamine and 10 mg kg^{-1} of xylazine, and when the animals showed no reaction to any stimulus, indicating the anesthetic effect, an incision was made in the animal's neck to expose the trachea in which 50 μL containing 3 \times 10⁵ yeasts were inoculated. After infection, the mice were sutured and kept warm until full recovery.

2.4.4. Immunization and Treatment

After 30 days of infection the mice received the nanoparticle vaccines intranasally, empty, complexed or co-administered, once a week for three weeks. Five microliters of the vaccine were administered into each nostril, resulting in 30 μL of vaccine per mouse at the end of treatment. Mice were euthanized 7 days after the last vaccination (51 days after infection was initiated).

2.4.5. Evaluation of Treatment

The treatment efficacy was evaluated by counting colony forming units (CFU) from viable yeasts present in the lungs after 51 days of infection.

After euthanasia, the lungs were aseptically removed, transversal sections of the tissue were randomly collected for histological processing, and the remaining tissue was weighted. The lungs were homogenized in 2 mL of PBS and 100 μ L was plated in BHI agar supplemented with 4% (*v/v*) FBS, 4% (*v/v*) glucose, 5% (*v/v*) culture filtrate of *P. brasiliensis* strain 192 and 20 μ g/mL gentamicin sulphate. After 21 days of incubation at 37 °C, colony forming units were counted.

2.4.6. Cytokine Production Evaluation

For cytokine quantification, lung homogenate (500 μ L) was aliquoted into microtubes, which contained 500 μ L of protease inhibitor (Protease Inhibitor Panel (INHIB1) Sigma-Aldrich, St. Louis, MO, USA). The following recipe was used: Pepstatin A (P5318)—50 μ g/mL, Benzamidine HCl (B6506)—50 mg/mL, N-Ethylmaleimide (E3876)—15.5 mg, EDTA (ED2SS)—1 mL—100 mM and distilled water q.s.p for 100 mL of protease inhibitor.

Cytokine analysis was performed by Enzyme-Linked Immunosorbent Assay (ELISA) using commercial kits (BD OptEIA™, BD Franklin Lakes, NJ, USA) for the following cytokines IL-4, IL-6, IL-10, IL-12, and IFN- γ .

2.4.7. Lung Histology

In order to evaluate the cellular preservation of the organ after treatment, lung transversal sections were fixed in 10% buffered formalin and embedded in paraffin using standard protocol. Histological slides were stained with haematoxylin and eosin (HE) for evaluation of the cellular structure of the organ.

2.5. Statistical Analysis

Analysis of variance (ANOVA) or student *t* test was performed followed by Tukey or Dunnett post-tests, using Graph Pad Prism 6. *p* values were considered significant when $p \leq 0.05$ and error bars were used representing the standard error of the mean (SEM).

3. Results

3.1. P10-Based Chitosan Nanoparticles Vaccine

The sizes and Zeta potential presented the expected values (Table 1) for this type of formulation, taking into account the preparation method and the materials used.

Table 1. Physio-chemical characteristics of empty NP (nanoparticles without P10) and complex NP (nanoparticles complexed with 20 μ g/10 μ L of P10 peptide).

Characteristics	Empty	Complexed
PDI	0.52 \pm 0.06	0.454 \pm 0.04
Size	338 \pm 8 nm	226 \pm 14 nm
Zeta potential	41.14 \pm 1.4 mV	19.6 \pm 3.5 mV

Both nanoparticles (empty and complexed) were smaller than 350 nm, presented a PDI below 0.5 indicating homogeneity in particle size, and a positive zeta potential ideal for muco-adhesiveness. The encapsulation efficiency of the peptide was above 90%.

3.2. Cytotoxicity

Neither the empty nor complex nanoparticles showed any hemolytic effect at 2 and 6 h (Figure 1) at the different concentrations analyzed.

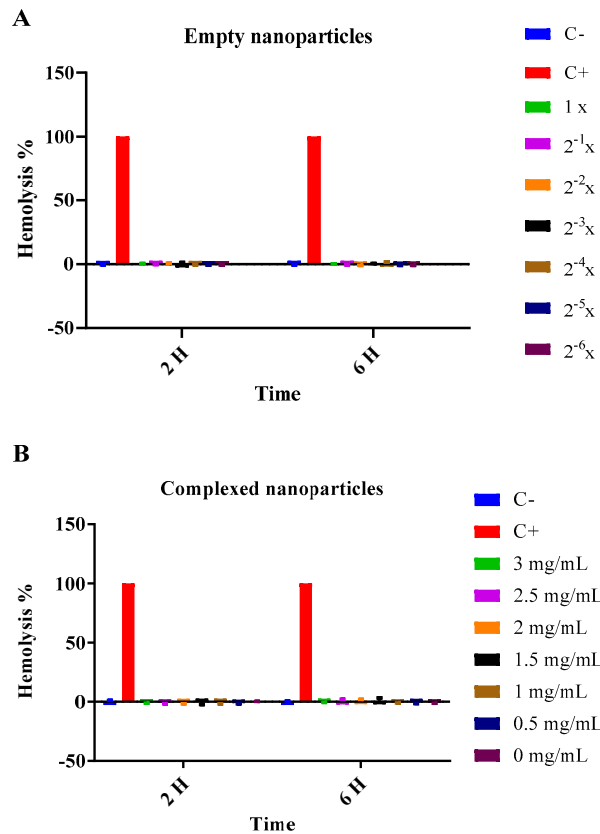


Figure 1. Hemolysis assay with empty or P10-complexed chitosan nanoparticles. Red Blood Cells were incubated with nanoparticles for 2 and 6 h and hemolysis was determined by absorbance measurement at 540 nm. Empty chitosan nanoparticles; (A) were serial diluted and concentrations ranged from 1× to 2⁻⁶×, with 1× being the initial concentration after preparation of the nanoparticles. The concentrations of P10-complexed chitosan nanoparticles; (B) varied from 3 mg/mL to 0 mg/mL. PBS was used as negative control (C−) (0% hemolysis) and autoclaved distilled water was used as positive control (C+) (100% hemolysis).

In the J774.16 cell viability assay, no cytotoxicity was observed in the first 24-h; in the 48-h period (Figure 2) only the highest concentration of P10 nanoparticles showed cytotoxicity. After 72-h of incubation, almost all concentrations of the P10 nanoparticles showed some degree of toxicity but none caused more than 50% cytotoxicity.

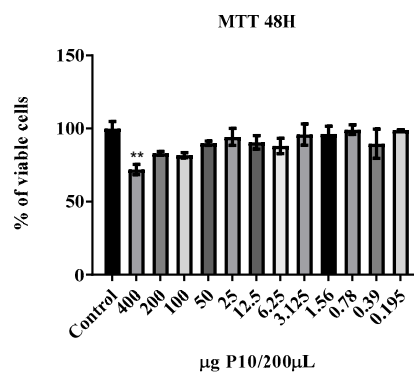


Figure 2. Cont.

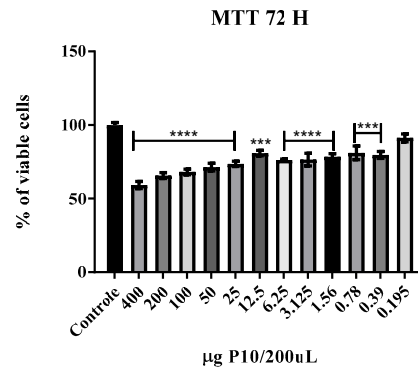


Figure 2. Cytotoxicity of P10-complexed chitosan nanoparticles in J774.16 macrophages with the aid of MTT colorimetric assay after 48 h and 72 h of co-incubation. At 48 h of incubation, only the concentration of 400 µg P10/200 µL showed toxicity to the cells ($p \leq 0.01$) compared to control using only DMEM medium. At 72 h, a cytotoxicity pattern was shown for almost all the concentrations tested. Data are represented as mean SEM and were analyzed by ANOVA statistical test with ** $p \leq 0.01$, *** $p \leq 0.001$ and **** $p \leq 0.0001$ in comparison to the control group (DMEM).

3.3. In Vivo Antifungal Efficacy of P10-Complexed Chitosan Nanoparticles

The antifungal efficacy of the P10-complexed nanoparticles was evaluated 51 days after infection, corresponding to 30 days of infection and 21 days of therapy. In order to evaluate the therapeutic effectiveness, quantification of colony forming units (CFU) recovered from the lungs of the animals was performed. Both treatments with P10-complexed nanoparticles in different doses and empty nanoparticles mixed with the free P10 were effective in reducing the fungal load (Figure 3). P10-complexed nanoparticles were effective at even lower doses (1 and 5 µg).

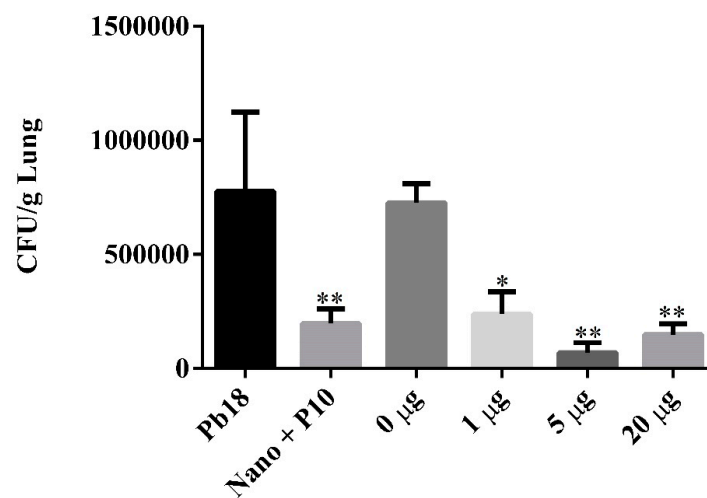


Figure 3. Fungal burden assessed by quantification of colony forming units per gram of lung tissue (CFU/g) in BALB/c mice after 51 days of *P. brasiliensis* infection. Mice were infected and randomly distributed in the following groups: Pb 18: non-treated; Nano + P10: co-administered vaccine (empty nanoparticles + 20 µg/10 µL free-form of P10 peptide); 0 µg: treated with empty nanoparticles; 1 µg: treated with P10-complexed nanoparticles containing 1 µg of P10/10 µL nanoparticles; 5 µg: treated with complexed nanoparticles containing 5 µg/10 µL of P10; 20 µg: treated with complexed nanoparticles containing 20 µg/10 µL of P10. Data are represented as mean SEM and were analyzed by ANOVA statistical test with * $p \leq 0.05$ and ** $p \leq 0.01$ in comparison to non-treated mice (Pb18). There was no statistical difference when comparing the groups Nano + P10, 1 µg, 5 µg and 20 µg.

3.4. Cytokine Production Induced by P10-Complexed Chitosan Nanoparticles

The cytokine profile was investigated in the mouse lung macerate by quantifying the Th1 cytokines IL-12 and IFN- γ or Th2 cytokines IL-4 and IL-6. Figure 4 shows the cytokine profile representing a diverse Th1 and Th2 immune response, which was not expected based on the type of nanoparticle used and the known immunomodulatory characteristics of the P10 peptide.

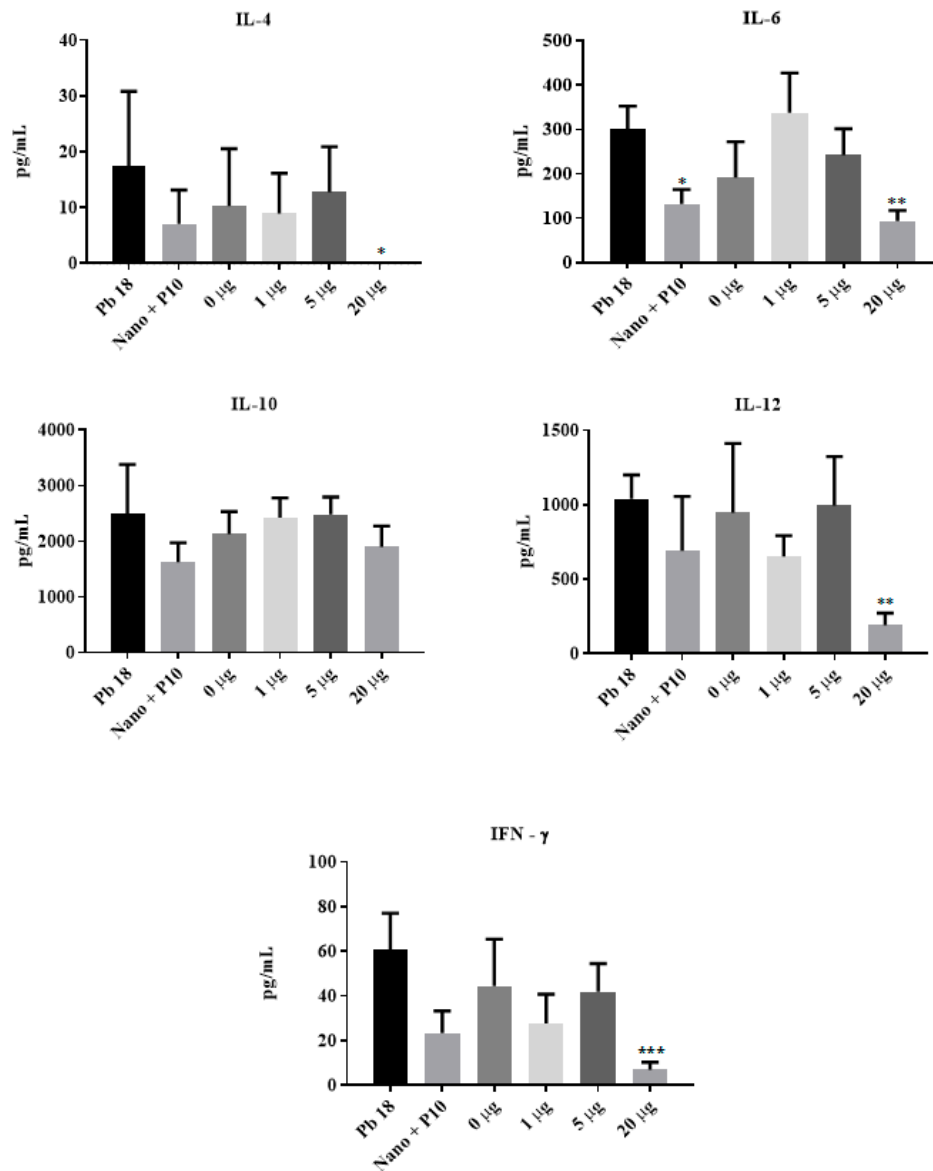


Figure 4. Determination of cytokine production in lung homogenat of BALB/c mice after 51 days of infection with *P. brasiliensis*. Mice were infected and randomly distributed in the following groups: Pb 18: non-treated; Nano + P10: co-administered vaccine (empty nanoparticles + 20 $\mu\text{g}/10 \mu\text{L}$ free-form of P10 peptide); 0 μg : treated with empty nanoparticles; 1 μg : treated with P10-complexed nanoparticles containing 1 μg of P10/ $10 \mu\text{L}$ nanoparticles; 5 μg : treated with complexed nanoparticles containing 5 $\mu\text{g}/10 \mu\text{L}$ of P10; 20 μg : treated with complexed nanoparticles containing 20 $\mu\text{g}/10 \mu\text{L}$ of P10. The cytokines showed a tendency of mixed immune response, where the anti-inflammatory and pro-inflammatory cytokines appear to be in balance when compared to the control group (Pb 18). The group treated with nanoparticles complexed with 20 μg of P10 had a significant reduction in the cytokines IL-4, IL-6, IL-12 and IFN- γ . Data are represented as mean SEM and were analyzed by ANOVA statistical test with * $p \leq 0.05$, ** $p \leq 0.01$ and *** $p \leq 0.001$ in comparison to non-treated mice (Pb18).

Mice that received 20 µg of P10 complexed within chitosan nanoparticles showed significant reduction in the cytokines IL-4, IL-6, IL-12, and IFN-γ. IL-6 levels were also lower in mice co-administered with empty nanoparticles and free P10. Other cytokine levels were not altered after treatment with free P10 mixed with empty chitosan nanoparticles or with lower doses of P10 encapsulated in the chitosan nanoparticles (1 and 5 µg).

3.5. Lung Histopathology of P10-Complexed Nanoparticles Treated Animals

The lung histology of the infected and untreated mice (Figure 5C,D) showed a disorganized granuloma and inflammatory cell infiltrate. The group treated with empty nanoparticles (Figure 5G,H) presented a mixture of loose and defined granulomas. The groups treated with P10 associated with empty nanoparticles (Figure 5E,F), or P10-complexed nanoparticles at 1 µg (Figure 5I,J), 5 µg (Figure 5K,L) or 20 µg (Figure 5M,N) also presented granulomatous lesions; however, those lesions were more defined and organized. Additionally, the pulmonary structure was better preserved in these P10-treated animals when compared to the untreated group.

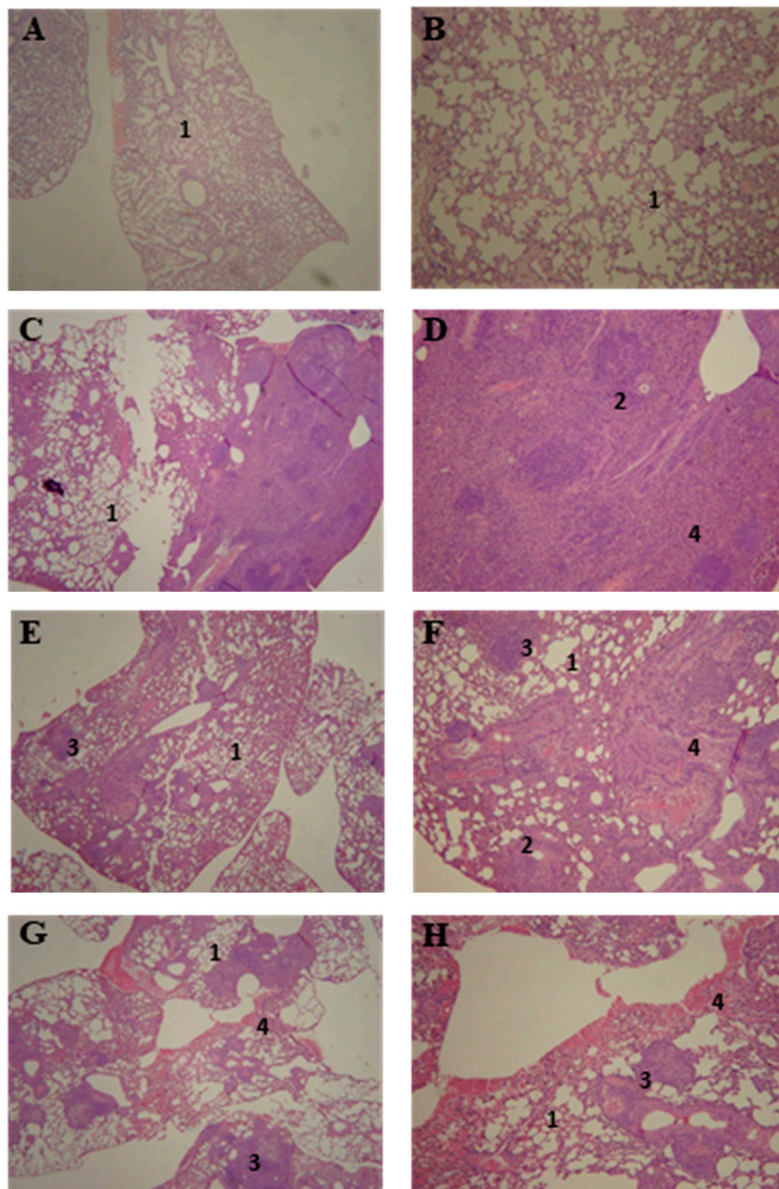


Figure 5. *Cont.*

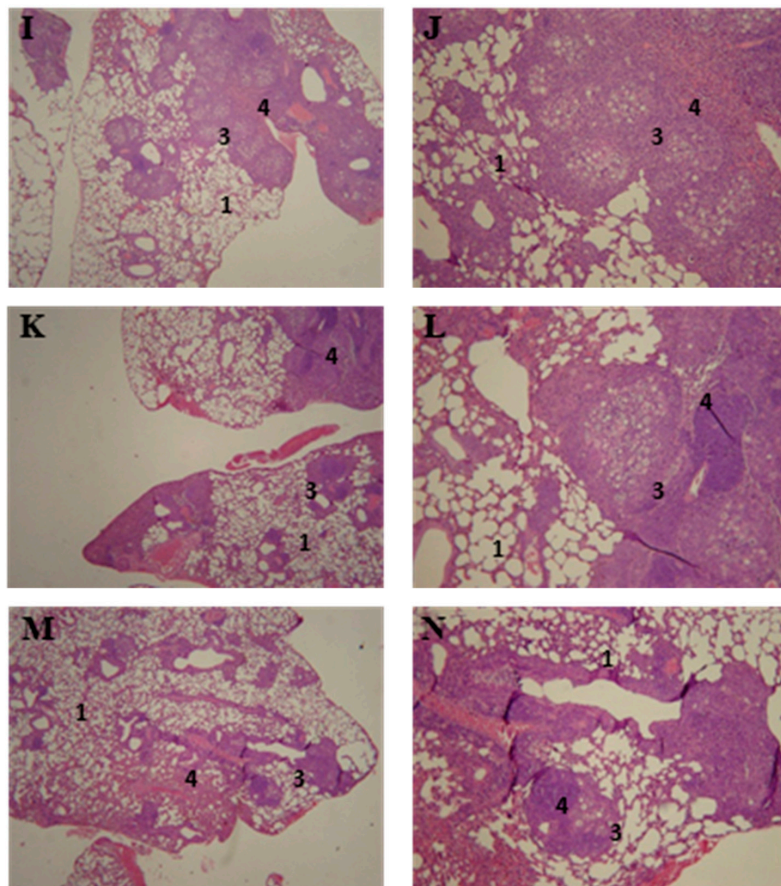


Figure 5. BALB/c mice lung histology (HE-stain) after 51 days of infection with *P. brasiliensis*. Findings include; (1) preserved lung tissue, (2) loose granulomas, (3) well defined granulomas and (4) presence of inflammatory infiltrates. Figures depict (A,B) non-infected mice and: infected and (C,D) non-treated, (E,F) treated with empty nanoparticles and 20 μg of free form of P10, (G,H) treated with empty nanoparticles and treated with P10-complexed nanoparticles with (I,J) 1 μg of P10, (K,L) 5 μg of P10 and (M,N) 20 μg of P10. (A,C,E,G,I,K,M) bear 8 \times magnification; (B,D,F,H,J,L,N) bear 20 \times magnification.

4. Discussion

The prolonged treatment time, relapses, and continuous medical follow-up that occur in PCM reveal how crucial the development of new therapeutic alternatives for the treatment of infection, in order to improve both, clinical conditions and the well-being of patients. Among these new alternatives, it is worth highlighting the use of the immunotherapy, particularly the P10 peptide, which exerts an important effect of reducing the fungal load in different forms of murine PCM [15,18].

Although the P10 peptide represents an advance in the experimental treatment of PCM, the P10 peptide itself does not have efficacy when used without an adjuvant in the animal model. While, it has strong immunomodulatory effects in cultured cells [25], improvements in this therapeutic strategy are needed. One of the approaches is to protect P10 from in vivo degradation through complexation within polymeric nanoparticles such as those made of PLGA or chitosan [18,26].

The use of nanoparticles to carry the peptide P10 was first evaluated in previous studies by our research group. P10-PLGA nanoparticles with dimercaptosuccinic acid (DMSA) were used to treat PCM in a murine model [18]. Both studies showed the capacity to reduce the fungal load and the concentration of the peptide P10 used. The advantages of our chitosan nanoparticles over PLGA nanoparticles are that it can be administered intranasally instead of intraperitoneally, and that the local delivery to the airways avoids the necessity to incorporate other molecules, such as DMSA, to induce tropism to the respiratory system.

Studies have found that using a DNA vaccine based on the heat shock protein of *Mycobacterium leprae* (HSP 65) loaded on PLGA nanoparticles or liposomes reduced the fungal load of *P. brasiliensis* [27]. In both cases, the use of PLGA nanoparticles and liposomes containing the P10 peptide or the DNA vaccine (HSP 65 of *Mycobacterium leprae*) induced an immune response with a Th1 pattern with increased production of IL-12 cytokines and or IFN- γ [18,28].

Chitosan nanoparticles have already been used as fungicides or fungistatics that cause morphological changes in cell walls and/or membranes [29,30]. Their efficacy as carriers and deliverers of molecules, such as antifungals has also been verified [31].

To the best of our knowledge, this is the first study that utilizes chitosan nanoparticles as carriers for an intranasal vaccine against fungi, although chitosan nanoparticles have already been used in intranasal vaccines against viral infections [32–35].

In this work, the P10 peptide was incorporated within chitosan nanoparticles. Physicochemical characterization indicated the size, PDI and zeta potential were suitable for in vivo administration, as suggested in other studies on the same topic [36,37]. The PDI mean value was less than 0.5, indicating a monodisperse nanoparticle size, and the positive zeta potential allows a greater interaction with the negative cell membrane [37–39].

In our results, the difference between the sizes of the empty nanoparticles, and the nanoparticles complexed with the P10 peptide, can be explained by the interaction of the peptide with chitosan and TPP [36]. The neutral residual charge of the P10 peptide and its hydrophobicity explains the interaction with the TPP negative charges and with the positive charge of the chitosan. The same interaction of charges also explains the reduction of the zeta potential of the complexed nanoparticles [36].

The hemolysis assays corroborate the data from literature that confirm the biocompatibility of chitosan nanoparticles with or without the P10 peptide [19,40,41]. In the cell viability assays, it was observed that after 72 h there was a cytotoxic effect caused by nanoparticles complexed with the P10. Possible explanations for cytotoxicity, include the presence of dimethyl sulfoxide, which is necessary for solubilization of P10, and the peptide's strong immunomodulatory ability, which could lead to cell activation and death [42].

The use of the chitosan nanoparticles complexed or co-administered with the P10 peptide provided a significant reduction in the fungal load. Further, complexation in chitosan nanoparticles allowed a decrease of 4 (5 μg) to 20 (1 μg) times the usual dose of P10 peptide (20 μg) used to generate an effective immune response [18,26].

Complexation of nanoparticles allows a significant reduction of the P10 peptide concentration used in the vaccine, and we believe this benefit is mainly contributed by the adjuvanting effect of nanoparticles. Previous studies of our group where P10 peptide was administered with different adjuvants showed the lowest amount of P10 peptide required to elicit a productive immune response in infected mice was 20 μg [18,26].

We believe that complexed or co-administered chitosan nanoparticles act as adjuvants favoring the immune response, and reducing the needed peptide concentrations to generate this type of stimulus. [18]. No tests were carried out using empty nanoparticles with concentrations of the p10 peptide other than 20 $\mu\text{g}/10 \mu\text{L}$, as this result was not expected.

In this study, the results indicate that the use of chitosan nanoparticles, complexed or associated with the P10 peptide, promotes a mixed pattern of immune response with both Th1 and Th2 type cytokines. These data corroborate other studies in which authors describe that chitosan has the ability to modulate both, Th1 or Th2 and induce a mixture of Th1/Th2 cytokines [43–46]. In contrast, a previous study from our group showed modulation towards a Th1-type immune response with increased production of IL-2, IL-12 and IFN- γ and reduction of IL-4 and IL-10 [10,11,26]. The reduction of the cytokines IL-4, IL-6, IL-12 and IFN- γ during treatment with complexed nanoparticles containing 20 $\mu\text{g}/10 \mu\text{L}$ of P10 was an unexpected result and may indicate the beginning of the process of a serological cure [3,4]. Although the timeframe chosen to assess cytokine production was based on previous experiments, 51 days post-infection and 21 days post-treatment could potentially not be the

ideal time to determine modulation of cytokine production in this model. Therefore, the timepoint, use of a new kind of nanoparticle, and the route of immunization (intranasal) could account for these observations.

5. Conclusions

The chitosan nanoparticles presented appropriate physical and chemical characteristics for mucosal administration of P10. They allowed a 4 to 20-fold reduction in the dose of P10 peptide compared to other immunization strategies studied by our research group, and were able to promote a significant reduction in pulmonary fungal load. The treatment induced a mixed Th1 and Th2 immune response. Moreover, the histological analysis of the lungs of infected mice, treated with P10-complexed to chitosan nanoparticles, revealed more preserved structures in comparison to untreated mice.

Author Contributions: Conceptualization, S.R.D.S.J., C.P.T. and A.C.A.; formal analysis, S.R.D.S.J. and F.K.L.d.S.; funding acquisition, C.P.T.; investigation, S.R.D.S.J., F.K.L.d.S., L.S.D., A.C.O.S., M.V.d.A. and L.B.R.d.S.; methodology, S.R.D.S.J., F.K.L.d.S., L.S.D., A.C.O.S., M.V.d.A. and A.C.A.; supervision, C.P.T. and A.C.A.; writing—original draft, S.R.D.S.J.; writing—review and editing, S.R.D.S.J., L.S.D., A.C.O.S., L.R.T., C.P.T. and A.C.A. All authors have read and agreed to the published version of the manuscript.

Funding: This research was funded by Fundacao de Amparo a Pesquisa do Estado de Sao Paulo (FAPESP 2016/08730-6), Conselho Nacional de Desenvolvimento Cientifico e Tecnologico (CNPq 420480/2018-8 and 134424/2016-6) and Coordenação de Aperfeiçoamento de Pessoal de Nível Superior–Brasil (CAPES).

Conflicts of Interest: There are no conflicts of interest to declare.

References

- Martinez, R. Epidemiology of Paracoccidioidomycosis. *Rev. Inst. Med. Trop. São Paulo* **2015**, *57* (Suppl. 1), 11–20. [[CrossRef](#)]
- Martinez, R. New Trends in Paracoccidioidomycosis Epidemiology. *J. Fungi* **2017**, *3*, 1. [[CrossRef](#)]
- Shikanai-Yasuda, M.A.; Mendes, R.P.; Colombo, A.L.; de Queiroz-Telles, F.; Kono, A.S.G.; Paniago, A.M.M.; Nathan, A.; do Valle, A.C.F.; Bagagli, E.; Benard, G.; et al. Brazilian guidelines for the clinical management of paracoccidioidomycosis. *Rev. Soc. Bras. Med. Trop.* **2017**, *50*, 715–740. [[CrossRef](#)]
- Shikanai-yasuda, M.A.; Queiroz, F.D.; Filho, T.; Mendes, R.P.; Colombo, A.L.; Moretti, M.L.; Consultores, D. Consenso em paracoccidioidomycose Guideliness in paracoccidioidomycosis. *Rev. Soc. Bras. Med. Trop.* **2006**, *39*, 297–310. [[CrossRef](#)]
- Restrepo, A.; Gómez, B.L.; Tobón, A. Paracoccidioidomycosis: Latin America's own fungal disorder. *Curr. Fungal Infect. Rep.* **2012**, *6*, 303–311. [[CrossRef](#)]
- Bocca, A.L.; Amaral, A.C.; Teixeira, M.M.; Sato, P.K.; Sato, P.; Shikanai-Yasuda, M.A.; Soares Felipe, M.S. Paracoccidioidomycosis: Eco-epidemiology, taxonomy and clinical and therapeutic issues. *Future Microbiol.* **2013**, *8*, 1177–1191. [[CrossRef](#)] [[PubMed](#)]
- Borges, S.R.C.; da Silva, G.M.S.; da Costa Chambela, M.; de Vasconcellos De, C.R.O.; Costa, R.L.B.; Wanke, B.; Do Valle, A.C.F. Itraconazole vs. trimethoprim-sulfamethoxazole: A comparative cohort study of 200 patients with paracoccidioidomycosis. *Med. Mycol.* **2014**, *52*, 303–310. [[CrossRef](#)] [[PubMed](#)]
- Amaral, A.C.; Bocca, A.L.A.L.; Ribeiro, A.M.; Nunes, J.; Peixoto, D.L.G.G.; Simioni, A.R.; Primo, F.L.; Lacava, Z.G.M.M.; Bentes, R.; Titze-de-Almeida, R.; et al. Amphotericin B in poly(lactic-co-glycolic acid) (PLGA) and dimercaptosuccinic acid (DMSA) nanoparticles against paracoccidioidomycosis. *J. Antimicrob. Chemother.* **2009**, *63*, 526–533. [[CrossRef](#)] [[PubMed](#)]
- Souza, A.C.O.; Nascimento, A.L.L.; de Vasconcelos, N.M.M.; Jerônimo, M.S.S.; Siqueira, I.M.M.; R-Santos, L.; Cintra, D.O.S.O.S.; Fuscaldi, L.L.L.; Pires Júnior, O.R.R.; Titze-de-Almeida, R.; et al. Activity and in vivo tracking of Amphotericin B loaded PLGA nanoparticles. *Eur. J. Med. Chem.* **2015**, *95*, 267–276. [[CrossRef](#)] [[PubMed](#)]
- Taborda, C.P.; Urán, M.E.; Nosanchuk, J.D.; Travassos, L.R. Paracoccidioidomycosis: Challenges in the development of a vaccine against an endemic mycosis in the Americas. *Rev. Inst. Med. Trop. Sao Paulo* **2015**, *57*, 21–24. [[CrossRef](#)] [[PubMed](#)]

11. Travassos, L.R.; Taborda, C.P. Paracoccidioidomycosis vaccine. *Hum. Vaccines Immunother.* **2012**, *8*, 1450–1453. [[CrossRef](#)] [[PubMed](#)]
12. Nascimento, E.M.; Sgarbi, B.; Cristina, V.; Costa, S.; Miranda, A.; Silva, A.; Andrade, R. De Immunization with radioattenuated yeast cells of *Paracoccidioides brasiliensis* induces a long lasting protection in BALB/c mice. *Vaccine* **2007**, *25*, 7893–7899. [[CrossRef](#)]
13. Pinto, A.R.; Puccia, R.; Diniz, S.N.; Franco, M.F.; Travassos, R. DNA-based vaccination against murine paracoccidioidomycosis using the gp43 gene from *Paracoccidioides brasiliensis*. *Vaccine* **2000**, *18*, 3050–3058. [[CrossRef](#)]
14. Ribeiro, A.M.; Bocca, A.L.; Amaral, A.C.; Faccioli, L.H.; Galetti, F.C.S.; Zárata-Bladés, C.R.; Figueiredo, F.; Silva, C.L.; Felipe, M.S.S. DNAhsp65 vaccination induces protection in mice against *Paracoccidioides brasiliensis* infection. *Vaccine* **2009**, *27*, 606–613. [[CrossRef](#)] [[PubMed](#)]
15. Taborda, C.P.; Juliano, M.A.; Puccia, R.; Franco, M.; Travassos, L.R. Mapping of the T-cell epitope in the major 43-kilodalton glycoprotein of *Paracoccidioides brasiliensis* which induces a Th-1 response protective against fungal infection in BALB/c mice. *Infect. Immun.* **1998**, *66*, 786–793. [[CrossRef](#)]
16. Cisalpino, P.S.; Puccia, R.; Yamauchi, L.M.; Cano, M.I.N.; da Silveira, J.F.; Travassos, L.R. Cloning, characterization, and epitope expression of the major diagnostic antigen of *Paracoccidioides brasiliensis*. *J. Biol. Chem.* **1996**, *271*, 4553–4560. [[CrossRef](#)]
17. Jannuzzi, G.P.; de Araújo Souza, N.; Françoso, K.S.; Pereira, R.H.; Santos, R.P.; Kaihama, G.H.; de Almeida, J.R.F.; Batista, W.L.; Amaral, A.C.; Maranhao, A.Q.; et al. Therapeutic treatment with scFv–PLGA nanoparticles decreases pulmonary fungal load in a murine model of paracoccidioidomycosis. *Microbes Infect.* **2018**, *20*, 48–56. [[CrossRef](#)]
18. Amaral, A.C.; Marques, A.F.; Muñoz, J.E.; Bocca, A.L.; Simioni, A.R.; Tedesco, A.C.; Morais, P.C.; Travassos, L.R.; Taborda, C.P.; Felipe, M.S.S. Poly(lactic acid-glycolic acid) nanoparticles markedly improve immunological protection provided by peptide P10 against murine paracoccidioidomycosis. *Br. J. Pharmacol.* **2010**, *159*, 1126–1132. [[CrossRef](#)]
19. Casettari, L.; Illum, L. Chitosan in nasal delivery systems for therapeutic drugs. *J. Control. Release* **2014**, *190*, 189–200. [[CrossRef](#)]
20. Read, R.C.; Naylor, S.C.; Potter, C.W.; Bond, J.; Jabbal-Gill, I.; Fisher, A.; Illum, L.; Jennings, R. Effective nasal influenza vaccine delivery using chitosan. *Vaccine* **2005**, *23*, 4367–4374. [[CrossRef](#)]
21. Bernstein, J.M. Mucosal Immunology of the Uper Respiratory Tract. *Respiration* **1992**, *59*, 3–13. [[CrossRef](#)] [[PubMed](#)]
22. Mygind, N.; Dahl, R. Anatomy, physiology and function of the nasal cavities in health and disease. *Adv. Drug Deliv. Rev.* **1998**, *29*, 3–12. [[CrossRef](#)]
23. Calvo, P.; Remuñan-López, C.; Vila-Jato, J.L.; Alonso, M.J. Chitosan and chitosan/ethylene oxide-propylene oxide block copolymer nanoparticles as novel carriers for proteins and vaccines. *Pharm. Res.* **1997**, *14*, 1431–1436. [[CrossRef](#)] [[PubMed](#)]
24. Neves, A.L.D.P.; Milioli, C.C.; Müller, L.; Riella, H.G.; Kuhnen, N.C.; Stulzer, H.K. Factorial design as tool in chitosan nanoparticles development by ionic gelation technique. *Colloids Surf. A Physicochem. Eng. Asp.* **2014**, *445*, 34–39. [[CrossRef](#)]
25. Mayorga, O.; Munoz, J.E.; Travassos, L.R.; Carlos, P. The role of adjuvants in therapeutic protection against paracoccidioidomycosis after immunization with the P10 peptide. *Front. Microbiol.* **2012**, *3*, 1–6. [[CrossRef](#)]
26. Travassos, L.R.; Taborda, C.P. Linear epitopes of *Paracoccidioides brasiliensis* and other fungal agents of human systemic mycoses as vaccine candidates. *Front. Immunol.* **2017**, *8*, 1–11. [[CrossRef](#)]
27. Ribeiro, A.M.; Souza, A.C.O.; Amaral, A.C.; Vasconcelos, N.M.; Jerônimo, M.S.; Carneiro, F.P.; Faccioli, L.H.; Felipe, M.S.S.; Silva, C.L.; Bocca, A.L. Nanobiotechnological Approaches to Delivery of DNA Vaccine Against Fungal Infection. *J. Biomed. Nanotechnol.* **2013**, *9*, 221–230. [[CrossRef](#)]
28. Ribeiro, A.M.; Bocca, A.L.; Amaral, A.C.; Souza, A.C.C.O.; Faccioli, L.H.; Coelho-Castelo, A.A.M.; Figueiredo, F.; Silva, C.L.; Felipe, M.S.S. HSP65 DNA as therapeutic strategy to treat experimental paracoccidioidomycosis. *Vaccine* **2010**, *28*, 1528–1534. [[CrossRef](#)]
29. Dananjaya, S.H.S.; Erandani, W.K.C.U.; Kim, C.-H.; Nikapitiya, C.; Lee, J.; De Zoysa, M. Comparative study on antifungal activities of chitosan nanoparticles and chitosan silver nano composites against *Fusarium oxysporum* species complex. *Int. J. Biol. Macromol.* **2017**, *105*, 478–488. [[CrossRef](#)]



30. Xing, K.; Shen, X.; Zhu, X.; Ju, X.; Miao, X.; Tian, J.; Feng, Z.; Peng, X.; Jiang, J.; Qin, S. Synthesis and in vitro antifungal efficacy of oleoyl-chitosan nanoparticles against plant pathogenic fungi. *Int. J. Biol. Macromol.* **2016**, *82*, 830–836. [[CrossRef](#)]
31. Souza, A.C.O.; Amaral, A.C. Antifungal Therapy for Systemic Mycosis and the Nanobiotechnology Era: Improving Efficacy, Biodistribution and Toxicity. *Front. Microbiol.* **2017**, *8*, 1–13. [[CrossRef](#)] [[PubMed](#)]
32. Zhao, K.; Zhang, Y.; Zhang, X.; Shi, C.; Wang, X.; Wang, X.; Jin, Z.; Cui, S. Chitosan-coated poly(lactic-co-glycolic) acid nanoparticles as an efficient delivery system for Newcastle disease virus DNA vaccine. *Int. J. Nanomed.* **2014**, *9*, 4609–4619. [[CrossRef](#)] [[PubMed](#)]
33. Van der Lubben, I.M.; Verhoef, J.C.; Borchard, G.; Junginger, H.E. Chitosan for mucosal vaccination. *Adv. Drug Deliv. Rev.* **2001**, *52*, 139–144. [[CrossRef](#)]
34. Khalili, I.; Ghadimipour, R.; Sadigh Eteghad, S.; Fathi Najafi, M.; Ebrahimi, M.M.; Godsian, N.; Sefidi Heris, Y.; Khalili, M.T. Evaluation of Immune Response Against Inactivated Avian Influenza (H9N2) Vaccine, by Using Chitosan Nanoparticles. *Jundishapur J. Microbiol.* **2015**, *8*, 10–14. [[CrossRef](#)] [[PubMed](#)]
35. Pan, L.; Zhang, Z.; Lv, J.; Zhou, P.; Hu, W.; Fang, Y.; Chen, H.; Liu, X.; Shao, J.; Zhao, F.; et al. Induction of mucosal immune responses and protection of cattle against direct-contact challenge by intranasal delivery with foot-and-mouth disease virus antigen mediated by nanoparticles. *Int. J. Nanomed.* **2014**, *9*, 5603–5618. [[CrossRef](#)] [[PubMed](#)]
36. Berthold, A.; Cremer, K. Preparation and characterization of chitosan microspheres as drug carrier for prednisolone sodium phosphate as model for anti-inflammatory drugs. *J. Control. Release* **1996**, *39*, 17–25. [[CrossRef](#)]
37. Mohammadpour, D.N.; Eskandari, R.; Zolfagharian, H.; Mohammad, M. Preparation and in vitro characterization of chitosan nanoparticles containing Mesobuthus eupeus scorpion venom as an antigen delivery system. *J. Venom. Anim. Toxins Incl. Trop. Dis.* **2012**, *18*, 44–52. [[CrossRef](#)]
38. He, C.; Hu, Y.; Yin, L.; Tang, C.; Yin, C. Effects of particle size and surface charge on cellular uptake and biodistribution of polymeric nanoparticles. *Biomaterials* **2010**, *31*, 3657–3666. [[CrossRef](#)]
39. Masarudin, M.J.; Cutts, S.M.; Evison, B.J.; Phillips, D.R.; Pigram, P.J. Factors determining the stability, size distribution, and cellular accumulation of small, monodisperse chitosan nanoparticles as candidate vectors for anticancer drug delivery: Application to the passive encapsulation of [14C]-doxorubicin. *Nanotechnol. Sci. Appl.* **2015**, *8*, 67. [[CrossRef](#)]
40. Xia, Y.; Fan, Q.; Hao, D.; Wu, J.; Ma, G.; Su, Z. Chitosan-based mucosal adjuvants: Sunrise on the ocean. *Vaccine* **2015**, *33*, 5997–6010. [[CrossRef](#)]
41. Carroll, E.C.; Jin, L.; Fitzgerald, K.A.; Bowie, A.G.; Lavelle, E.C.; Oleszycka, E.; Moran, H.B.T. The Vaccine Adjuvant Chitosan Promotes Cellular Immunity via DNA Sensor cGAS-STING-Dependent Induction of Type I Interferons Article the Vaccine Adjuvant Chitosan Promotes Cellular Immunity via DNA Sensor cGAS-STING-Dependent Induction of Type I Interfero. *Immunity* **2016**, *44*, 597–608. [[CrossRef](#)] [[PubMed](#)]
42. De Melo, F.M.; Braga, C.J.; Pereira, F.V.; Maricato, J.T.; Origassa, C.S.; Souza, M.F.; Melo, A.C.; Silva, P.; Tomaz, S.L.; Gimenes, K.P.; et al. Anti-metastatic immunotherapy based on mucosal administration of flagellin and immunomodulatory P10. *Immunol. Cell Biol.* **2015**, *93*, 86–98. [[CrossRef](#)] [[PubMed](#)]
43. Wen, Z.S.; Xu, Y.L.; Zou, X.T.; Xu, Z.R. Chitosan nanoparticles act as an adjuvant to promote both Th1 and Th2 immune responses induced by ovalbumin in mice. *Mar. Drugs* **2011**, *9*, 1038–1055. [[CrossRef](#)] [[PubMed](#)]
44. Riteau, N.; Sher, A. Chitosan: An Adjuvant with an Unanticipated STING. *Immunity* **2016**, *44*, 522–524. [[CrossRef](#)]
45. Shim, S.; Soh, S.H.; Im, Y.B.; Park, H.E.; Cho, C.S.; Kim, S.; Yoo, H.S. Elicitation of Th1/Th2 related responses in mice by chitosan nanoparticles loaded with Brucella abortus malate dehydrogenase, outer membrane proteins 10 and 19. *Int. J. Med. Microbiol.* **2020**, *310*, 151362. [[CrossRef](#)]
46. Muzzarelli, R. Chitins and Chitosans as Immunoadjuvants and Non-Allergenic Drug Carriers. *Mar. Drugs* **2010**, *8*, 292–312. [[CrossRef](#)]





Application of Nanoparticles to Invasive Fungal Infections

7

Samuel Rodrigues dos Santos Junior , Andre Correa Amaral , and Carlos Pelleschi Taborda 

Abstract

The present chapter provides an overview of the applications of nanoparticles in Medical Mycology. Nanoparticles possess sizes between 1 and 400 nm with different chemical and physical properties. The aim of the present chapter is to describe studies and applications with drugs and peptides into different types of nanoparticles with the objective of reducing fungal infection by stimulation of the immune system or acting directly on the fungus.

Keywords

Nanoparticles · Systemic mycosis · Fungal infections · Medical Mycology · *Candida* · *Aspergillus* · *Cryptococcus* · *Paracoccidioides*

S. R. dos Santos Junior

Department of Microbiology, Institute of Biomedical Sciences, University of Sao Paulo, Sao Paulo, SP, Brazil

e-mail: samuelmicrobio@usp.br

A. C. Amaral

Nano & Biotechnology Laboratory, Department of Biotechnology, Institute of Tropical Pathology and Public Health, Federal University of Goias, Goiania, GO, Brazil

e-mail: andre_amaral@ufg.br

C. P. Taborda (✉)

Department of Microbiology, Institute of Biomedical Sciences, University of Sao Paulo, Sao Paulo, SP, Brazil

Institute of Tropical Medicine of Sao Paulo, Department of Dermatology, Faculty of Medicine, University of Sao Paulo, Sao Paulo, SP, Brazil

e-mail: taborda@usp.br

7.1 Introduction

Fungi can be found in different habitats on the planet (Blackwell 2011), and it is assumed that there are about five million species of fungi distributed around the globe (Kohler et al. 2015; Fisher et al. 2020), of which about 100,000 are known and only a few hundred are pathogenic to humans (Blackwell 2011; Kohler et al. 2015). Fungi are mostly saprophytes and can be found in the soil or be part of the microbiota of plants and animals (Casadevall 2005; Casadevall and Damman 2020). These microorganisms can become pathogenic and cause disease to the host (Pires et al. 2014; Casadevall 2018; Chaturvedi et al. 2018).

Mycoses are caused by different fungi (Table 7.1), which are classified into opportunistic or “true pathogenic fungi” (Staab and Wong 2014). Opportunistic fungi are those that take advantage of biological or environmental changes to colonize the host (Lionakis and Kontoyiannis 2003; Schmiedel and Zimmerli 2016; Tabora et al. 2018; Sanguinetti et al. 2019; Dantas et al. 2021). These mycoses are usually associated with alterations in the host’s immune response and may occur mostly as systemic disease. The most common fungal genus involved are *Aspergillus* sp., *Candida* sp., *Cryptococcus* sp., *Pneumocystis* sp., and *Fusarium* sp. (Schmiedel and Zimmerli 2016).

Although infections caused by true pathogenic fungi do not necessarily depend on changes in the host’s immune response, these diseases are usually more severe in immunocompromised patients. These mycoses are classified as cutaneous, subcutaneous, and systemic (Aditya et al. 2005; Degreef 2008; Vermout et al. 2008; Pires et al. 2014; Laniosz and Wetter 2014). Cutaneous, or superficial mycoses, are the most common mycoses among the population and are caused by a wide variety of fungi (Aditya et al. 2005; Degreef 2008; Vermout et al. 2008; Pires et al. 2014; Laniosz and Wetter 2014). Subcutaneous and systemic mycoses are caused by fungi of the genus *Sporothrix* sp., *Blastomyces* sp., *Coccidioides* sp., *Histoplasma* sp., and

Table 7.1 Mycoses and their etiological agents

Pathogenic potential	Form	Gender	Mycosis
Opportunistic	Mycelium	<i>Aspergillus</i>	Aspergillosis
		<i>Fusarium</i>	Fusarioses
		<i>Cryptococcus</i>	Cryptococcosis
	Yeast	<i>Candida</i>	Candidiasis (systemic and cutaneous)
		<i>Pneumocystis</i>	Pneumocystosis
True pathogens	Dimorphic fungi	<i>Blastomyces</i>	Blastomycosis
		<i>Coccidioides</i>	Coccidioidomycosis
		<i>Histoplasma</i>	Histoplasmosis
		<i>Sporothrix</i>	Sporotrichosis
		<i>Paracoccidioides</i>	Paracoccidioidomycosis

Paracoccidioides sp., among others (Staab and Wong 2014; Kohler et al. 2015; Fisher et al. 2016, 2020; Almeida et al. 2019; Dantas et al. 2021).

Since the 1980s, there has been a significant increase in the number of cases of systemic mycoses (Casadevall 2018; Sanguinetti et al. 2019; Firacative 2020; Dantas et al. 2021). This is related to the increasing number of people with some type of immunodeficiency, such as those caused by the human immunodeficiency virus (HIV), use of compounds such as broad-spectrum antibiotics or corticosteroids, drugs to prevent organ transplant rejection, hematopoietic diseases, and cancer (Lionakis and Kontoyiannis 2003; Enoch et al. 2006, 2017; Streinu-Cercel 2012; Schmiedel and Zimmerli 2016; Taborda et al. 2018; Sanguinetti et al. 2019; Firacative 2020; Dantas et al. 2021).

It is also important to highlight the importance of the progressive devastation of tropical forests changing the entire balance of nature (Taborda et al. 2018). Considering the debilitated condition of the patients, systemic mycoses are difficult to be treated and usually lead to the death of the patient (Enoch et al. 2006, 2017; Streinu-Cercel 2012; Firacative 2020).

7.2 Antifungal Therapy

The therapeutic approach for mycoses (Table 7.2) is based on azole compounds, pyrimidine analogues, polyenes, and echinocandins (Gubbins and Anaissie 2009; Shoham et al. 2010; Laniosz and Wetter 2014; McManus 2015; Scorzoni et al. 2017). These molecules (Fig. 7.1) can be used topically in the treatment of cutaneous and subcutaneous mycoses, presenting low toxicity and orally or parenterally against systemic mycoses, causing significant toxic effects (Aditya et al. 2005; Enoch et al. 2006; Degreef 2008; Gubbins and Anaissie 2009; Shoham et al. 2010; Staab and

Table 7.2 Antifungal compounds and targets of action

Antifungal family	Target	Name	Route of administration
Azoles	14- α -demethylase (Ergosterol biosynthesis)	Ketoconazole	Oral/IV
		Fluconazole	Oral/IV
		Itraconazole	Oral/IV
		Voriconazole	Oral/IV
		Posaconazole	Oral/IV
Polyenes	Membrane ergosterol	Nystatin	Topical
		Amphotericin B	Oral/IV
Pyrimidine analogues	DNA/RNA	5-Fluocytosine	Oral
Echinocandins	β -1,3-glucan synthase (β -glucan biosynthesis)	Caspofungin	IV
		Anidulafungin	IV
		Micafungin	IV

IV intravenous

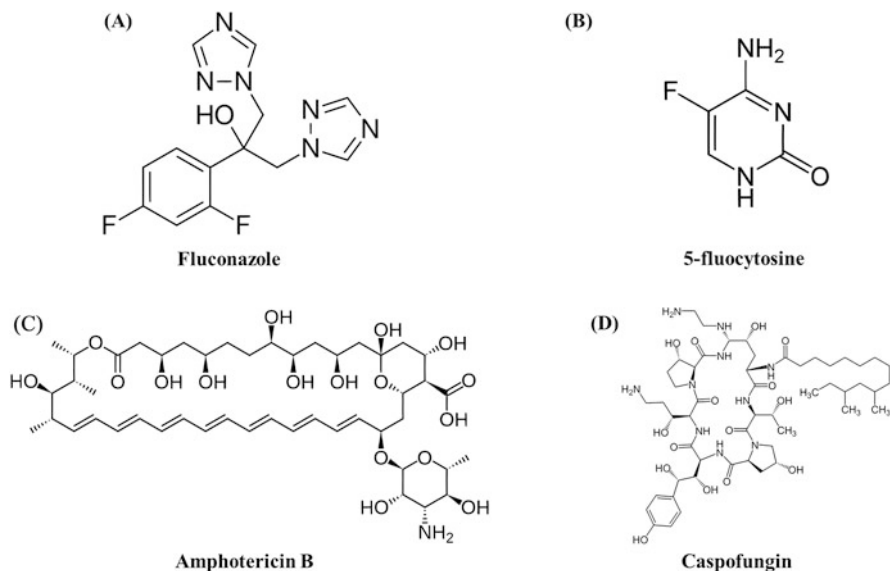


Fig. 7.1 Leading antifungal compounds used to treat invasive mycosis; (a) Fluconazole, (b) 5-fluorocytosine, (c) Amphotericin B, (d) Caspofungin

Wong 2014; Pires et al. 2014; Laniosz and Wetter 2014; McManus 2015; Schmiedel and Zimmerli 2016; Scorzoni et al. 2017; Sanguinetti et al. 2019).

7.2.1 Azole Compounds

The main azole compounds are ketoconazole, fluconazole (Fig. 7.1a), itraconazole, voriconazole, and posaconazole. The mechanism of action of these compounds occurs by interference in ergosterol synthesis by inhibition of the enzyme 14- α -demethylase P450 cytochrome-dependent. This inhibition prevents the conversion of lanosterol into ergosterol, leading to dysfunction of the fungus plasma membrane and accumulation of toxic compounds to the cell (Gubbins and Anaissie 2009; Shoham et al. 2010; Laniosz and Wetter 2014; McManus 2015; Scorzoni et al. 2017).

7.2.2 Pyrimidine Analogous

The 5-fluorocytosine (Fig. 7.1b) is the only compound of the molecules analogous to pyrimidine. It is administered orally and has low toxicity (Gubbins and Anaissie 2009; Shoham et al. 2010; Laniosz and Wetter 2014; McManus 2015; Scorzoni et al. 2017). The 5-fluorocytosine is transported into the fungal cell facilitated by the enzyme cytosine permease and then converted to 5-fluorouracil by the cytosine deaminase,

causing interruption of DNA and or RNA synthesis (Gubbins and Anaissie 2009; Shoham et al. 2010; Laniosz and Wetter 2014; McManus 2015; Scorzoni et al. 2017).

7.2.3 Polyenes

Nystatin and Amphotericin B are antifungals of the polyene class, the latter being considered the gold standard drug in the treatment of mycosis, used orally or parenterally. This drug interacts with ergosterol, a component of the fungal membrane which corresponds to the cholesterol present in the human membranes. This interaction results in rupture of the fungus plasma membrane (Gubbins and Anaissie 2009; Shoham et al. 2010; Laniosz and Wetter 2014; McManus 2015; Scorzoni et al. 2017).

The mechanism of action of Amphotericin B (Fig. 7.1c) is based on its binding to ergosterol forming pores that lead to membrane depolarization and extravasation of cytosol content. However, although in lesser intensity, Amphotericin B is also able to interact with cholesterol and, therefore, presents a high level of toxicity, mainly for the kidneys (Amaral et al. 2009; Souza et al. 2015).

In an attempt to circumvent the toxic adverse effects of this drug, different drug formulations have been proposed to reduce these problems. Drug delivery formulation in nanoscale such as Amphotericin B lipid complex (Abelcet[®]), Amphotericin B colloidal dispersion (Amphotec[®]), and Amphotericin B liposomal (AmBisome[®]) are safer than the conventional Amphotericin B deoxycholate (Fungizone[®]) (Gubbins and Anaissie 2009; Amaral et al. 2009; Shoham et al. 2010; Souza et al. 2015).

7.2.4 Echinocandins

Echinocandins are synthetic lipopeptides representing the most modern group of antifungals. The main drugs in this class are caspofungin (Fig. 7.1d), micafungin, and anidulafungin. The mechanism of action of these drugs is by inhibiting the synthesis of β 1,3-glucan, a molecule essential to the cell wall composition of the fungus and, since it is not present in animal cells, causes lower toxicity to the patient. The inhibition in the synthesis of this cell component causes an increase in cell wall permeability leading to its subsequent rupture (Gubbins and Anaissie 2009; Shoham et al. 2010; Laniosz and Wetter 2014; McManus 2015; Scorzoni et al. 2017).

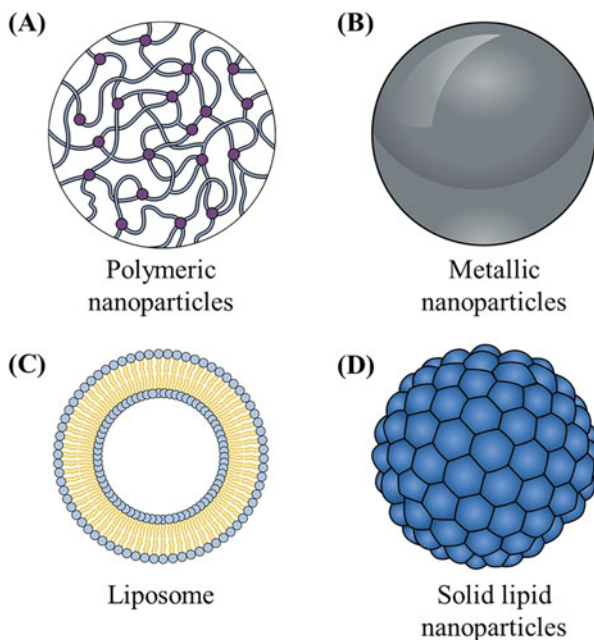
7.3 Nanoformulations for Antifungal Therapy

The successful use of Amphotericin B within nanoparticles has motivated the development of different nanoscale formulations for classical drugs and molecules with antifungal effects (Table 7.3). There are important advantages to develop these formulations on a nanoscale. Considering the possibility of using biodegradable

Table 7.3 Examples of nanoparticles development for invasive fungal infections

Pathogen	Class of nanoparticle	Material	Active compounds	Tests in vivo (+) or in vitro (++)	Reference	
<i>Candida</i>	Polymeric	Chitosan	Amphotericin B	+ / ++	Park et al. (2017)	
		Chitosan	Miconazole/ Farnesol	+ / ++	Fernandes Costa et al. (2019)	
		PLGA	Amphotericin B	+ / ++	Liu et al. (2014)	
		Chitosan	Fluconazole	+ / ++	Reñber et al. (2016)	
		Eudragit S100	Osthol/Fluconazole	+ / ++	Li et al. (2018)	
		Poloxamer P407/P188	Amphotericin B	+ / ++	Ci et al. (2018)	
		Alginate	Miltefosine	+ / ++	Spadari et al. (2019)	
		Poly-ε-caprolactone	2-Amino-thiophene	++	Neves et al. (2020)	
		MPEG-PCL	Amphotericin B	+ / ++	Zhang et al. (2017)	
		Chitosan-PLGA	Natamycin/ Clotrimazole	+ / ++	Cui et al. (2021)	
	Lipid		Solid lipid	Amphotericin B	+ / ++	Riaz et al. (2020)
			Cholesterol conjugated	CG3R6TAT	+ / ++	Xu et al. (2011b)
			Solid lipid	Miconazole	+ / ++	Aljaeid and Hosny (2016)
		Cubosome	Amphotericin B	+ / ++	Xu et al. (2014)	
		Solid lipid	Eugenol	+ / ++	Garg and Singh (2011)	
		Solid lipid	Uncharacterized	+ / ++	Vidal Bonifácio et al. (2015)	
<i>Aspergillus</i>		Encochleated	Amphotericin B	+ / ++	Santangelo et al. (2000)	
	Polymeric	PLGA	Amphotericin B	+ / ++	Van de Ven et al. (2012)	
		Chitosan	Voriconazole	+ / ++	Kaur et al. (2021)	
		B-polymethacrylic	Amphotericin B	+ / ++	Shirkhani et al. (2015)	
		Poly-ε-caprolactone	2-Amino-thiophene	++	Neves et al. (2020)	
<i>Cryptococcus</i>		Alginate	Miltefosine	+ / ++	Spadari et al. (2019)	
		PLA-b-PEG	Amphotericin B	+	Ren et al. (2009)	

Fig. 7.2 Most studied nanoparticles for treating invasive fungal infections. (a) Polymeric nanoparticles, (b) Metallic nanoparticles, (c) Liposomes, (d) Solid lipids nanoparticles. (Image created using the Mind the graph website)



materials, it is possible to promote the sustained release of compounds associated with nanoparticles. Next, instead of applying multiple doses or high concentrations of the drug to reach the therapeutic level, a large amount of the antifungal can be encapsulated in the nanoparticles to be released over time (Couvreur and Vauthier 2006; Peek et al. 2008; das Neves et al. 2010; Etheridge et al. 2013; Thorley and Tetley 2013).

It is also possible to direct the drugs to act in specific treatment locations, linking molecules on the surface of these structures that present tropism by specific tissues or organs of the body (Csaba et al. 2009; Gupta and Vyas 2012; Gregory et al. 2013; Melkoumov et al. 2013; Nazarian et al. 2014; Zhao et al. 2014; Yan et al. 2014; Sharma et al. 2015; Spadari et al. 2019; Riaz et al. 2020). Drugs or molecules can also be protected against degradation by enzymes present in the biological environment. These nanoscale drug delivery systems can be prepared using a variety of nanoparticles (Fig. 7.2), such as polymers, metals, and phospholipids (Csaba et al. 2009; Gupta and Vyas 2012; Gregory et al. 2013; Melkoumov et al. 2013; Nazarian et al. 2014; Zhao et al. 2014; Yan et al. 2014; Sharma et al. 2015; Spadari et al. 2019; Riaz et al. 2020).

7.3.1 Polymeric Nanoparticles

Polymeric nanoparticles (Fig. 7.2a) are prepared based on different types of polymers, both natural and synthetic (Carcaboso et al. 2004; Csaba et al. 2009;

Garcia-Fuentes and Alonso 2012; Bolhassani et al. 2014; Ahmed and Aljaeid 2016). The physical and chemical properties of nanoparticles are defined according to the characteristics of the materials used in its preparation, such as concentration of the monomers and/or polymers, charge, and hydrophilicity (Carcaboso et al. 2004; Csaba et al. 2009; Garcia-Fuentes and Alonso 2012; Bolhassani et al. 2014; Ahmed and Aljaeid 2016). The polymers most commonly used, but not restricted, to prepare polymeric nanoparticles are chitosan, polylactic acid (PLA), polyglycolic acid (PGA), poly (lactic acid-*co*-glycolic acid) (PLGA), and alginate (Carcaboso et al. 2004; Csaba et al. 2009; Garcia-Fuentes and Alonso 2012; Bolhassani et al. 2014; Ahmed and Aljaeid 2016).

7.3.2 Metallic Nanoparticles

Metallic nanoparticles (Fig. 7.2b) are very small structures that can be obtained using metals such as gold, silver, titanium, zinc, copper, and iron (Mody et al. 2010; Schröfel et al. 2014; Govindrao Jamkhande et al. 2019; Marinescu et al. 2020). These types of nanoparticles are widely studied because of their chemical and physical characteristics that can be used in nanocarriers of different types of molecules, including antimicrobials and bioactive molecules (Schröfel et al. 2014; Marinescu et al. 2020). The main mechanism of action of metallic nanoparticles with antimicrobial action is the interference of these nanoparticles in the cellular homeostasis, and the disruption of the flow of electrons inside and around the cell's membranes, leading the cells to apoptosis (Mody et al. 2010; Schröfel et al. 2014; Aderibigbe 2017).

7.3.3 Lipid Nanoparticles

Lipid nanoparticles can be classified into liposomes/micelle (Fig. 7.2c), solid lipid nanoparticles (Fig. 7.2d), and nanoemulsions (Gupta and Vyas 2012). The liposomes/micelles are spherical with an aqueous or oily nucleus in a lipid shell. Depending on the phospholipid used in the preparation of these nanoparticles, micelles can be formed, which contain only a lipid layer or liposomes with a double lipid layer, mimicking a biological membrane (Lambros et al. 1998; Bolhassani et al. 2014; De Serrano and Burkhart 2017; Zhang et al. 2017). Solid lipid nanoparticles are a class of lipid blocks forming a matrix and may be fluid or rigid depending on the type of lipid used (Jain et al. 2010; Gupta and Vyas 2012; Vaghasiya et al. 2013). In the same category, nanoemulsions, which are dispersions of two immiscible solutions, widely used for topical applications (Mirza et al. 2013; Soriano-Ruiz et al. 2019; do Carmo Silva et al. 2020).

7.4 Systemic Mycoses and Nanotechnology

Despite their medical relevance and the need for more efficient and less toxic therapy based on the clinical situation of the patient, the researchers are focused on developing a more sophisticated therapy for systemic mycoses (Dantas et al. 2021).

7.4.1 *Candida* sp.

Candidiasis are fungal diseases responsible for causing various types of infections: superficially such as onychomycosis, candidiasis related to sexually transmitted infections (STIs), and the systemic candidiasis, which is the most severe form and occurs when the fungus spreads and colonizes the host through the circulatory system leading to sepsis and death (Enoch et al. 2006; Giri and Kindo 2012; Quindós 2014; Pappas et al. 2018; Sanguinetti et al. 2019; Firacative 2020).

Candida sp. are saprophytic microorganisms that colonize the epithelial microbiota of animals. The onset of systemic candidiasis occurs when there is a lesion of the epithelial tissue allowing the contact of the fungus with the bloodstream (Giri and Kindo 2012; Quindós 2014; Scorzoni et al. 2017; Pappas et al. 2018). One of the main causes of systemic candidiasis is the contamination in hospitals, making systemic candidiasis one of the main nosocomial fungal infections with a high mortality rate along with aspergillosis (Enoch et al. 2006; Giri and Kindo 2012; Quindós 2014; Pappas et al. 2018).

There are about 15 species of *Candida* with pathogenic potential; *C. albicans* is the main species causing candidiasis, followed by *C. glabrata*, *C. tropicalis*, *C. parapsilosis*, and *C. krusei*. The pathogenic importance varies according to the geographical location and factors such as the main antifungal compound used to combat fungal infections (Giri and Kindo 2012; Quindós 2014; Scorzoni et al. 2017; Pappas et al. 2018). In recent years, a species that has been attracting the attention of researchers is the newly identified *C. auris*, which presented resistance to several types of antifungal compounds (Giri and Kindo 2012; Quindós 2014; Scorzoni et al. 2017; Pappas et al. 2018; Singh et al. 2020).

The main antifungals used in the treatment of invasive candidiasis are fluconazole, Amphotericin B, and echinocandins, but due to its toxicity, the use of nanoparticles is highly recommended (Giri and Kindo 2012; Quindós 2014; Scorzoni et al. 2017; Pappas et al. 2018).

7.4.1.1 Polymeric Nanoparticles

Xiaolong Tang et al. 2014 prepared a formulation for the use of Amphotericin B with PLGA nanoparticles, improving bioavailability and reducing toxicity and fungal load in mice models (Tang et al. 2014).

Seda Rençber et al. 2016 prepared a formulation of fluconazole within chitosan nanoparticles for the treatment of oral candidiasis in rabbit, and they demonstrated that it is possible to use this treatment for local application due to the bioadhesive characteristics of chitosan (Rençber et al. 2016).

Seong-Cheol Park et al. 2017 prepared a combination of Amphotericin B and the antifungal peptide histatin 5 within chitosan nanoparticles targeting the nanoparticle to the fungus cell, reducing Amphotericin B toxicity and fungal load in mice models (Park et al. 2017).

Peipei Zhang et al. 2017 showed that an Amphotericin B formulation in MPEG-PCL (poly(ethylene poly(ϵ -caprolactone))) used in starch tablets were able to reduce oral candidiasis and Amphotericin B toxicity in mice models (Zhang et al. 2017).

Lin-peng Li et al. 2018 evaluated the *Cnidium monnier* secondary metabolite Osthol interaction with fluconazole for evaluation of the metabolite fungicidal capacity in fluconazole-resistant strains. The delivery of the osthol was made by Eudragit S100 nanoparticles. They showed a reduction of the fungal load of the fluconazole resistant strains in mice models (Li et al. 2018).

Tianyuan Ci et al. 2018 prepared a new formulation made by nanosuspensions of Amphotericin B in a p407/P188 poloxamer thermogel for the treatment of vulvovaginal candidiasis in mice. The formulation demonstrated a better efficiency, gradually releasing the Amphotericin B and reducing the fungal load when compared with a commercial Amphotericin B effervescent tablet used as a control (Ci et al. 2018).

Adelaide Fernandes Costa et al. 2019 used chitosan nanoparticles as a farnesol and miconazole carrier to treat mice vulvovaginal candidiasis, showing reduced fungal proliferation and tissue inflammation (Fernandes Costa et al. 2019).

Cristina de Castro Spadari et al. 2019 prepared a new formulation of the redirected compound miltefosine within alginate nanoparticles. They showed that the formulation was able to reduce the miltefosine toxicity and the fungal load of the *Candida* yeast in mice models (Spadari et al. 2019).

Wendell Wons Neves et al. 2020 prepared a formulation of the secondary metabolite 2-amino-thiophene (6CN10) in 2-hydroxy nanocarriers propyl- β -cyclodextrin within nanocapsules or nanospheres of poly- ϵ -caprolactone to access biofilm reduction and fungal susceptibility. The formulations worked against *Cryptococcus* and not against *Candida* (Neves et al. 2020).

Xiaoming Cui et al. 2021 created a formulation with Natamycin and Clotrimazole in PLGA and chitosan nanoparticles to treat keratitis caused by *Candida*. They showed an increase in the solubility, bioavailability, and a reduction of toxic effect and reduction of the infection in rabbits (Cui et al. 2021).

7.4.1.2 Lipid Nanoparticles

Kaijin Xu et al. 2011 showed a reduction of the fungal load by using an antimicrobial peptide conjugated with cholesterol molecules for the automatic formation of lipopeptide nanoparticles to treat meningitis caused by *Candida* in rabbit (Xu et al. 2011b).

Anuj Garg and Sanjay Kumar Singh, 2011 demonstrated an increase of the solubilization, bioavailability, and antifungal activity of the eugenol when formulated in solid lipid nanoparticles associated with a carbopol matrix for the treatment of oral candidiasis in immunosuppressed mice (Garg and Singh 2011).

Zhiwen Yang et al. 2014 prepared a formulation of Amphotericin B in cubosomes (lipid nanoparticles in cubic form) that increased the bioavailability of the compound by oral administration showing reduction of fungal load only in the kidney of the animals (Xu et al. 2014).

Bruna Vidal Boniface et al. 2015 showed that a formulation of hydroethanolic extracts of *Astronium* in solid lipid nanoparticles reduced the fungal load in the treatment of vulvovaginal candidiasis in comparison with free extract and Amphotericin B in mice models (Vidal Bonifácio et al. 2015).

Bader Mubarak Aljaeid Khaled and Mohamed Hosny 2016 prepared a formulation of miconazole in solid lipid nanoparticles for oral application, increasing the solubility of the compound and reducing the fungal load in comparison to the encapsulated formulation available in the market used as a control in mice models (Aljaeid and Hosny 2016).

Amina Riaz et al. 2020 prepared a formulation of Amphotericin B in a lipid nanocarrier that showed reduction of the Amphotericin B toxicity and reduction of the cutaneous leishmaniasis and vulvovaginal candidiasis in mice models (Riaz et al. 2020).

Rosaria Santangelo et al. 2000 prepared an Amphotericin B formulation in curly lipid nanoparticles (Encochleated) for oral administration and evaluation of the bioavailability and toxicity of the compound. They demonstrated an increase in the survival rate and reduction of the fungal load in mice models of systemic candidiasis (Santangelo et al. 2000).

7.4.2 *Aspergillus* sp.

Aspergillosis is a fungal disease and may present mild manifestations such as allergies, and in severe cases, such as invasive aspergillosis. The host immunological condition is a determining factor driving the level of severity of the infection (Enoch et al. 2006; Zmeili and Soubani 2007; Kousha et al. 2011; Thompson and Patterson 2011; Streinu-Cercel 2012; Kosmidis and Denning 2015; Schmiedel and Zimmerli 2016; Firacative 2020).

Aspergillus sp. is a ubiquitous fungus, being found everywhere by transposing virtually all types of barriers. Due to its presence in any given place, several cases of nosocomial infections by *Aspergillus* are reported annually, and these numbers continue to grow as more people become immunocompromised due to increased cases of cancer, organ transplants autoimmune diseases, and immunodeficiencies conditions such as AIDS (Zmeili and Soubani 2007; Kousha et al. 2011; Thompson and Patterson 2011; Kosmidis and Denning 2015).

The frequent fungus causing invasive aspergillosis is *A. fumigatus*, and in most cases, infection occurs when fungal particles are inhaled and subsequently deposited in the lower part of the respiratory tract of the patient (Zmeili and Soubani 2007; Kousha et al. 2011; Thompson and Patterson 2011; Kosmidis and Denning 2015). As occurs in the treatment for candidiasis and other systemic mycosis, the main compounds used in the treatment of invasive aspergillosis are fluconazole,

Amphotericin B and echinocandins, but due to its toxicity, the use of nanoparticles is once again highly recommended (Zmeili and Soubani 2007; Kousha et al. 2011; Thompson and Patterson 2011; Kosmidis and Denning 2015).

7.4.2.1 Polymeric Nanoparticles

Helene Van de Ven et al. 2012—Preparation of a formulation of Amphotericin B in PLGA nanoparticles and nanosuspensions to reduce the toxic effects of the compound in addition to evaluating the efficacy of the formulation in reducing fungal load in mice models (Van de Ven et al. 2012).

Khojasteh Shirkhani et al. 2015 prepared an Amphotericin B formulation in polymethacrylate nanoparticles for prophylactic administration in immunosuppressed mice to mimic organ transplant-related immunosuppression. The trials showed that the formulation presented low toxicity and great efficacy in reducing fungal infection in mice models (Shirkhani et al. 2015).

Ranjot Kaur et al. 2021 developed a voriconazole solution in chitosan nanoparticles functionalized with dipalmitoylphosphatidylcholine (DPPC) for nebulization, allowing greater retention and bioavailability of the formulation in the lung. In vitro assays have demonstrated efficacy reducing the fungal load, and in vivo assays have demonstrated the retention capacity and greater bioavailability of the compound in mice models (Kaur et al. 2021).

7.4.3 *Cryptococcus* sp.

Cryptococcosis is a globally disseminated systemic fungal disease (Srikanta et al. 2014; Gushiken et al. 2021). The main organs affected by cryptococcosis are the lungs and brain due to the tropism that the fungus presents to the central nervous system (CNS) (Casadevall et al. 2018). The spread of *Cryptococcus* sp. through the body results from its main virulence mechanisms, corresponding to the presence of a polysaccharide capsule and production of melanin (Casadevall et al. 2018; Colombo et al. 2019; Cordero et al. 2020; Kuttel et al. 2020). Cryptococcosis is a disease that affects hosts with some type of immunodeficiency, mostly related to AIDS (Casadevall et al. 2018; Colombo et al. 2019; Cordero et al. 2020; Kuttel et al. 2020).

This co-infection dynamic was widely reported in the 1970s and 1980s during the dissemination of AIDS cases (Srikanta et al. 2014; May et al. 2016; Khatun et al. 2020).

Genus *Cryptococcus* are divided into two species complexes: *C. neoformans* and *C. gattii*; within these two complexes there are the species *C. neoformans* and *C. deneoformans* belonging to the neoformans complex and the species *C. gattii*, *C. deuterogattii*, *C. bacillisporus*, *C. tetragattii* and a hybrid species not yet classified (Danesi et al. 2021; Wang 2021; Montoya et al. 2021).

These species differ from each other due to the different serotypes, which are classified according to the polysaccharide composition of the capsule (Zaragoza et al. 2009; Casadevall et al. 2019; Crawford et al. 2020). The *Cryptococcus* capsule consists of different branches and basically two amounts of sugars:

glucuronoxylomannan (GXM) and galactoxilomanana (GalXM). Due to these variations of sugars and branches, it is possible to classify the strains and species of *Cryptococcus* in five different serotypes: A, B, C, D, and AD (Zaragoza et al. 2009; Casadevall et al. 2019; Crawford et al. 2020).

Another important virulence factor is the ability of *Cryptococcus* to produce melanin. Melanin is associated with the fungus ability to resist to environmental stresses and escape from the human immune system (Chrissian et al. 2020; Cordero et al. 2020; de Sousa et al. 2021).

The main antifungals for the treatment of cryptococcosis are the polyene compounds such as Amphotericin B, pyrimidine-like analogue compounds such as 5-fluorocytosine and azole compounds, such as fluconazole, but due to its toxicity, the use of nanoparticles is once again highly recommended (Gushiken et al. 2021).

7.4.3.1 Polymeric Nanoparticles

Tianbin Ren et al. 2009 prepared an Amphotericin B formulation in PLA-b-PEG poly(lactic acid)-b-poly(ethylene glycol) nanoparticles, functionalized with polysorbate 80, that allowed greater bioavailability of the compound in the central nervous system through the passage of nanoparticles by the blood–brain barrier, reducing the toxicity of the compound and the fungal load in mice models (Ren et al. 2009).

Nan Xu et al. 2011 created a formulation of Amphotericin B in b-polybutylcyanoacrylate nanoparticles functionalized with Polysorbate 80 that also allowed greater bioavailability of the compound in the central nervous system through the passage of nanoparticles by the blood–brain barrier, reducing the toxicity of the compound and the fungal load in mice models (Xu et al. 2011a).

Cristina de Castro Spadari et al. 2019 prepared a new formulation of the redirected compound miltefosine within alginate nanoparticles. They showed that the formulation was able to reduce the miltefosine toxicity and the fungal load of the *Cryptococcus* yeast in mice models (Spadari et al. 2019).

Wendell Wons Neves et al. 2020 prepared a formulation of the secondary metabolite 2-amino-thiophene (6CN10) in 2-hydroxy nanocarriers propyl- β -cyclodextrin within nanocapsules or nanospheres of poly- ϵ -caprolactone to access biofilm reduction and fungal susceptibility. The formulations worked against *Cryptococcus* and not against *Candida* (Neves et al. 2020).

7.4.3.2 Metallic Nanoparticles

Chao Zhang et al. 2016 evaluated the combination of the fungicidal action of metallic nanoparticles with Amphotericin B and showed synergism of the formulation in mice models (Zhang et al. 2016).

7.4.3.3 Lipid Nanoparticles

Huaying Wang et al. 2010 used antimicrobial peptides conjugated with cholesterol molecules for the automatic formation of lipopeptide nanoparticles for the treatment of Cryptococcosis meningitis. They showed a reduction of the fungal load in the brain due to the nanoparticles cross of the blood–brain barrier in rabbits (Wang et al. 2010).

Ruying Lu et al. 2019 prepared a formulation of Amphotericin B in curly lipid nanoparticles (Encocchleated) for oral administration of the compound. They demonstrated increasing in the bioavailability and toxicity reduction of the compound and showed efficiency of the formulation against Cryptococcosis meningitis in association with 5-fluocytosine in mice model (Lu et al. 2019).

Natália Kronbauer Oliveira et al. 2021 prepared a formulation of amiodarone (blocker of calcium channels) in lipid nucleus nanoparticles for intranasal and or intraperitoneal application. They showed that this compound only reduced the infection and fungal load when inside the nanoparticle in mice models (Oliveira et al. 2021).

7.4.4 *Paracoccidioides* sp.

Paracoccidioidomycosis (PCM) is a systemic mycosis that primarily affects the lungs and may later disseminate throughout the body (Travassos and Tabora 2012). PCM is caused by dimorphic fungi of the genus *Paracoccidioides*, and five species of this fungus are currently recognized, *P. brasiliensis strictu* sensu, *P. americana*, *P. restrepiensis*, *P. venezuelensis*, *P. lutzii* (Turissini et al. 2017).

This fungus presents at room temperature around 24 °C, a filamentous and saprophytic characteristic (Travassos and Tabora 2012). The most frequent form of infection of humans and animals by the fungus is by inhaling conidia or fungal propagules that settle primarily in the lungs and can spread throughout the body through the lymphatic system, with the increase of temperature around 37 °C, the fungus changes from the mycelial to pathogenic yeast form (Amaral et al. 2010; De Melo et al. 2014; Gegembauer et al. 2014).

These fungi can be found in almost all Latin American countries, from Mexico to Argentina, excluding Suriname, Chile, and the Caribbean islands (Palmeiro et al. 2005).

PCM can be classified as: PCM infection or disease, in which PCM infection does not present clinical manifestations and PCM disease is classified into two clinical forms: juvenile/acute and subacute or adult/chronic (Shikanai-Yasuda et al. 2017). When the disease manifests in the juvenile phase it has a systemic characteristic and has no distinction between the sexes of the hosts. In the adult form, the disease manifests mainly in the lungs and especially in men between 20 and 50 years old (Palmeiro et al. 2005; Restrepo et al. 2012; Tabora et al. 2021).

The treatment of PCM occurs in two phases. The first consists of an initial attack treatment to quickly control the infection and the second phase consists of a treatment to inhibit the proliferation of the remaining fungi to prevent the recurrence of the disease (Shikanai-yasuda et al. 2006).

The main drugs for the treatment of PCM are Amphotericin B, sulfadiazine, and itraconazole (Shikanai-Yasuda et al. 2017). Although these compounds are very effective in the treatment of PCM and other mycoses, they present important adverse effects to be observed: common headaches, gastric disorders, and rashes until

nephrotoxicity in the case of Amphotericin B (Borges et al. 2014; Taborda et al. 2021).

Nanotechnology has been demonstrating a role of great importance to improve the adverse effects because it allows not only to reduce the concentration of the drug used, but also to allow sustained release (Amaral et al. 2009).

7.4.4.1 Polymeric Nanoparticles

Andre Correa Amaral et al. 2009 prepared a formulation of Amphotericin B in PLGA nanoparticles functionalized with DMSA (dimercaptosuccinic acid), a molecule that presents tropism by the lungs, showing reduction of the toxic effects of the compound and reducing fungal load in mice models (Amaral et al. 2009).

Polymeric Nanoparticles Used in Vaccines

Andre Correa Amaral et al. 2010 produced a formulation composed of the complexation of an immunomodulatory peptide in PLGA nanoparticles associated with chemotherapy compounds (Bactrim) for the development of a therapeutic vaccine against PCM. They reduced the fungal load in mice models (Amaral et al. 2010).

Grasielle Pereira Jannuzzi et al. 2018 developed a vaccine formulation composed of the complexation of the variable fractions of the light and heavy chains (scFv) of a mimetic antibody to Gp43 in PLGA nanoparticles. They showed a reduction in fungal load and an increase of IFN-g and IL-12 cytokine production by using the vaccine as a prophylactic or therapeutic treatment for PCM in mice models (Jannuzzi et al. 2018).

Santos Junior et al. 2020 produced a vaccine formulation composed of the complexation of an immunomodulatory peptide in chitosan nanoparticles for the development of an intranasal therapeutic vaccine against PCM. They showed that the intranasal vaccine was effective, reducing mice lung fungal load (Rodrigues Dos Santos Junior et al. 2020).

7.4.4.2 Metallic Nanoparticles

Camila Arruda Saldanha et al. 2016 prepared a formulation of Amphotericin B within magnetite nanoparticles (Fe_3O_4) functionalized in a lipid bilayer of uric acid. They showed reduction of toxic effects of the compound and an increase of the effectiveness of the formulation in reducing fungal load in mice models (Saldanha et al. 2016).

7.4.4.3 Lipid Nanoparticles

Junya de Lacorte Singulani et al. 2018 created a formulation of dodecyl gallate (secondary metabolite) in solid lipid nanoparticles. They demonstrated an increase bioavailability and toxicity reduction of the compound and reduction of the fungal infection in the treatment of PCM in mice models (de Singulani et al. 2018).

Kaila Medina-Alarcón et al. 2020 prepared a formulation of 2-hydroxyccalcone (precursor of secondary metabolites) in a nanoemulsion, showing increase in the bioavailability and toxicity reduction of the compound, in addition to reducing the

viability of *Paracoccidioides brasiliensis* in mice models (Medina-Alarcón et al. 2020).

7.5 Conclusion

Nanotechnology has brought enormous advantages in drug treatment by reducing the cytotoxicity of antifungal agents or in the formulation of vaccines. An important point that we highlight is that most studies are still in the experimental phase. We believe that nanotechnology may soon be included in clinical trials and its effectiveness will be proven.

References

- Aderibigbe B (2017) Metal-based nanoparticles for the treatment of infectious diseases. *Molecules* 22:1370. <https://doi.org/10.3390/molecules22081370>
- Aditya KG, Jennifer ER, Melody C, Elizabeth AC (2005) Dermatophytosis: the management of fungal infections. *Skinmed* 4:305–310. <https://doi.org/10.1111/j.1540-9740.2005.03435.x>
- Ahmed TA, Aljaeid BM (2016) Preparation, characterization, and potential application of chitosan, chitosan derivatives, and chitosan metal nanoparticles in pharmaceutical drug delivery. *Drug Des Devel Ther* 10:483–507. <https://doi.org/10.2147/DDDT.S99651>
- Aljaeid B, Hosny KM (2016) Miconazole-loaded solid lipid nanoparticles: formulation and evaluation of a novel formula with high bioavailability and antifungal activity. *Int J Nanomedicine* 11:441. <https://doi.org/10.2147/IJN.S100625>
- Almeida F, Rodrigues ML, Coelho C (2019) The still underestimated problem of fungal diseases worldwide. *Front Microbiol* 10:1–5. <https://doi.org/10.3389/fmicb.2019.00214>
- Amaral AC, Bocca AL, Ribeiro AM et al (2009) Amphotericin B in poly(lactic-co-glycolic acid) (PLGA) and dimercaptosuccinic acid (DMSA) nanoparticles against paracoccidioidomycosis. *J Antimicrob Chemother* 63:526–533. <https://doi.org/10.1093/jac/dkn539>
- Amaral AC, Marques AF, Muñoz JE et al (2010) Poly(lactic acid-glycolic acid) nanoparticles markedly improve immunological protection provided by peptide P10 against murine paracoccidioidomycosis. *Br J Pharmacol* 159:1126–1132. <https://doi.org/10.1111/j.1476-5381.2009.00617.x>
- Blackwell M (2011) The fungi: 1, 2, 3 ... 5.1 million species? *Am J Bot* 98:426–438. <https://doi.org/10.3732/ajb.1000298>
- Bolhassani A, Javanad S, Saleh T et al (2014) Polymeric nanoparticles potent vectors for vaccine delivery targeting cancer and infectious diseases. *Hum Vaccines Immunother* 10:321–323. <https://doi.org/10.4161/hv.26796>
- Borges SRC, Da Silva GMS, Da Costa Chambela M et al (2014) Itraconazole vs. trimethoprim-sulfamethoxazole: a comparative cohort study of 200 patients with paracoccidioidomycosis. *Med Mycol* 52:303–310. <https://doi.org/10.1093/mmy/myt012>
- Carcaboso AM, Hernández RM, Igartua M et al (2004) Potent, long lasting systemic antibody levels and mixed Th1/Th2 immune response after nasal immunization with malaria antigen loaded PLGA microparticles. *Vaccine* 22:1423–1432. <https://doi.org/10.1016/j.vaccine.2003.10.020>
- Casadevall A (2005) Fungal virulence, vertebrate endothermy, and dinosaur extinction: is there a connection? *Fungal Genet Biol* 42:98–106. <https://doi.org/10.1016/j.fgb.2004.11.008>
- Casadevall A (2018) Fungal diseases in the 21st century: the near and far horizons. *Pathog Immun* 3:183. <https://doi.org/10.20411/pai.v3i2.249>

- Casadevall A, Damman C (2020) Updating the fungal infection-mammalian selection hypothesis at the end of the Cretaceous Period. *PLoS Pathog* 16:e1008451. <https://doi.org/10.1371/journal.ppat.1008451>
- Casadevall A, Coelho C, Alanio A (2018) Mechanisms of *Cryptococcus neoformans*-mediated host damage. *Front Immunol* 9:1–8. <https://doi.org/10.3389/fimmu.2018.00855>
- Casadevall A, Coelho C, Cordero RJB et al (2019) The capsule of *Cryptococcus neoformans*. *Virulence* 10:822–831. <https://doi.org/10.1080/21505594.2018.1431087>
- Chaturvedi V, Bouchara J-P, Hagen F et al (2018) Eighty years of mycopathologia: a retrospective analysis of progress made in understanding human and animal fungal pathogens. *Mycopathologia* 183:859–877. <https://doi.org/10.1007/s11046-018-0306-1>
- Chrissian C, Camacho E, Fu MS et al (2020) Melanin deposition in two *Cryptococcus* species depends on cell-wall composition and flexibility. *J Biol Chem* 295:1815–1828. <https://doi.org/10.1074/jbc.RA119.011949>
- Ci T, Yuan L, Bao X et al (2018) Development and anti-Candida evaluation of the vaginal delivery system of amphotericin B nanosuspension-loaded thermogel. *J Drug Target* 26:829–839. <https://doi.org/10.1080/1061186X.2018.1434660>
- Colombo AC, Rella A, Normile T et al (2019) *Cryptococcus neoformans* glucuronoxylomannan and sterylglucoside are required for host protection in an animal vaccination model. *MBio* 10:1–22. <https://doi.org/10.1128/mBio.02909-18>
- Cordero RJB, Camacho E, Casadevall A (2020) Melanization in *Cryptococcus neoformans* requires complex regulation. *MBio* 11:1–4. <https://doi.org/10.1128/mBio.03313-19>
- Couvreur P, Vauthier C (2006) Nanotechnology: intelligent design to treat complex disease. *Pharm Res* 23(7):1417–1450
- Crawford CJ, Cordero RJB, Guazzelli L et al (2020) Exploring *Cryptococcus neoformans* capsule structure and assembly with a hydroxylamine-armed fluorescent probe. *J Biol Chem* 295:4327–4340. <https://doi.org/10.1074/jbc.RA119.012251>
- Csaba N, Garcia-Fuentes M, Alonso MJ (2009) Nanoparticles for nasal vaccination. *Adv Drug Deliv Rev* 61:140–157. <https://doi.org/10.1016/j.addr.2008.09.005>
- Cui X, Li X, Xu Z et al (2021) Fabrication and characterization of chitosan/poly(lactic-co-glycolic acid) core-shell nanoparticles by coaxial electrospray technology for dual delivery of natamycin and clotrimazole. *Front Bioeng Biotechnol* 9:1–13. <https://doi.org/10.3389/fbioe.2021.635485>
- Danesi P, Falcaro C, Schmettmann LJ et al (2021) *Cryptococcus* in wildlife and free-living mammals. *J Fungi* 7:29. <https://doi.org/10.3390/jof7010029>
- Dantas KC, Mauad T, de André CDS et al (2021) A single-centre, retrospective study of the incidence of invasive fungal infections during 85 years of autopsy service in Brazil. *Sci Rep* 11:3943. <https://doi.org/10.1038/s41598-021-83587-1>
- das Neves J, Amiji MM, Bahia MF, Sarmento B (2010) Nanotechnology-based systems for the treatment and prevention of HIV/AIDS. *Adv Drug Deliv Rev* 62:458–477. <https://doi.org/10.1016/j.addr.2009.11.017>
- De Melo Teixeira M, Theodoro RC, Freire F et al (2014) *Paracoccidioides lutzii* sp. nov.: biological and clinical implications. *Med Mycol* 52:19–28. <https://doi.org/10.3109/13693786.2013.794311>
- De Serrano LO, Burkhart DJ (2017) Liposomal vaccine formulations as prophylactic agents: design considerations for modern vaccines. *J Nanobiotechnol* 15:1–23. <https://doi.org/10.1186/s12951-017-0319-9>
- de Singulani JL, Scorzoni L, Lourencetti NMS et al (2018) Potential of the association of dodecyl gallate with nanostructured lipid system as a treatment for paracoccidioidomycosis: in vitro and in vivo efficacy and toxicity. *Int J Pharm* 547:630–636. <https://doi.org/10.1016/j.ijpharm.2018.06.013>
- de Sousa HR, de Frazão S, de Oliveira Júnior GP et al (2021) Cryptococcal virulence in humans: learning from translational studies with clinical isolates. *Front Cell Infect Microbiol* 11:1–8. <https://doi.org/10.3389/fcimb.2021.657502>

- Degreef H (2008) Clinical forms of dermatophytosis (ringworm infection). *Mycopathologia* 166: 257–265. <https://doi.org/10.1007/s11046-008-9101-8>
- do Carmo Silva L, Miranda MACM, de Freitas JV et al (2020) Antifungal activity of Copaíba resin oil in solution and nanoemulsion against *Paracoccidioides* spp. *Braz J Microbiol* 51:125–134. <https://doi.org/10.1007/s42770-019-00201-3>
- Enoch DA, Ludlam HA, Brown NM (2006) Invasive fungal infections: a review of epidemiology and management options. *J Med Microbiol* 55:809–818. <https://doi.org/10.1099/jmm.0.46548-0>
- Enoch DA, Yang H, Aliyu SH, Micallef C (2017) The changing epidemiology of invasive fungal infections. In: *Pediatric research*. Springer, New York, pp 17–65
- Etheridge ML, Campbell SA, Erdman AG et al (2013) The big picture on nanomedicine: the state of investigational and approved nanomedicine products. *Nanomedicine* 9:1–14. <https://doi.org/10.1016/j.nano.2012.05.013>
- Fernandes Costa A, Evangelista Araujo D, Santos Cabral M et al (2019) Development, characterization, and in vitro–in vivo evaluation of polymeric nanoparticles containing miconazole and farnesol for treatment of vulvovaginal candidiasis. *Med Mycol* 57:52–62. <https://doi.org/10.1093/mmy/myx155>
- Firacative C (2020) Invasive fungal disease in humans: are we aware of the real impact? *Mem Inst Oswaldo Cruz* 115:1–9. <https://doi.org/10.1590/0074-02760200430>
- Fisher MC, Gow NAR, Gurr SJ (2016) Tackling emerging fungal threats to animal health, food security and ecosystem resilience. *Philos Trans R Soc B Biol Sci* 371:20160332. <https://doi.org/10.1098/rstb.2016.0332>
- Fisher MC, Gurr SJ, Cuomo CA et al (2020) Threats posed by the fungal kingdom to humans, wildlife, and agriculture. *MBio* 11:1–17. <https://doi.org/10.1128/mBio.00449-20>
- García-Fuentes M, Alonso MJ (2012) Chitosan-based drug nanocarriers: where do we stand? *J Control Release* 161:496–504. <https://doi.org/10.1016/j.jconrel.2012.03.017>
- Garg A, Singh S (2011) Enhancement in antifungal activity of eugenol in immunosuppressed rats through lipid nanocarriers. *Colloids Surf B Biointerfaces* 87:280–288. <https://doi.org/10.1016/j.colsurfb.2011.05.030>
- Gegembauer G, Araujo LM, Pereira EF et al (2014) Serology of paracoccidioidomycosis due to *Paracoccidioides lutzii*. *PLoS Negl Trop Dis* 8:e2986. <https://doi.org/10.1371/journal.pntd.0002986>
- Giri S, Kindo A (2012) A review of *Candida* species causing blood stream infection. *Indian J Med Microbiol* 30:270–278. <https://doi.org/10.4103/0255-0857.99484>
- Govindrao Jamkhande P, Ghule NW, Haque Bamer A, Kalaskar MG (2019) Metal nanoparticles synthesis: an overview on methods of preparation, advantages and disadvantages, and applications. *J Drug Deliv Sci Technol*. <https://doi.org/10.1016/j.jddst.2019.101174>
- Gregory AE, Titball R, Williamson D (2013) Vaccine delivery using nanoparticles. *Front Cell Infect Microbiol* 3:13. <https://doi.org/10.3389/fcimb.2013.00013>
- Gubbins PO, Anaissie EJ (2009) Antifungal therapy. In: *Clinical mycology*. Elsevier, Amsterdam, pp 161–195
- Gupta M, Vyas SP (2012) Development, characterization and in vivo assessment of effective lipidic nanoparticles for dermal delivery of fluconazole against cutaneous candidiasis. *Chem Phys Lipids* 165:454–461. <https://doi.org/10.1016/j.chemphyslip.2012.01.006>
- Gushiken AC, Saharia KK, Baddley JW (2021) Cryptococcosis. *Infect Dis Clin N Am* 35:493–514. <https://doi.org/10.1016/j.idc.2021.03.012>
- Jain S, Jain S, Khare P et al (2010) Design and development of solid lipid nanoparticles for topical delivery of an anti-fungal agent. *Drug Deliv* 17:443–451. <https://doi.org/10.3109/10717544.2010.483252>
- Jannuzzi GP, de Araujo Souza N, Franoso KS et al (2018) Therapeutic treatment with scFv–PLGA nanoparticles decreases pulmonary fungal load in a murine model of paracoccidioidomycosis. *Microbes Infect* 20:48–56. <https://doi.org/10.1016/j.micinf.2017.09.003>

- Kaur R, Dennison SR, Burrow AJ et al (2021) Nebulised surface-active hybrid nanoparticles of voriconazole for pulmonary Aspergillosis demonstrate clathrin-mediated cellular uptake, improved antifungal efficacy and lung retention. *J Nanobiotechnol* 19:19. <https://doi.org/10.1186/s12951-020-00731-1>
- Khatun F, Toth I, Stephenson RJ (2020) Immunology of carbohydrate-based vaccines. *Adv Drug Deliv Rev* 165–166:117–126. <https://doi.org/10.1016/j.addr.2020.04.006>
- Kohler JR, Casadevall A, Perfect J (2015) The spectrum of fungi that infects humans. *Cold Spring Harb Perspect Med* 5:a019273. <https://doi.org/10.1101/cshperspect.a019273>
- Kosmidis C, Denning DW (2015) The clinical spectrum of pulmonary aspergillosis. *Thorax* 70:270–277. <https://doi.org/10.1136/thoraxjnl-2014-206291>
- Kousha M, Tadi R, Soubani AO (2011) Pulmonary aspergillosis: a clinical review. *Eur Respir Rev* 20:156–174. <https://doi.org/10.1183/09059180.00001011>
- Kuttel MM, Casadevall A, Oscarson S (2020) Cryptococcus neoformans capsular GXM conformation and epitope presentation: a molecular modelling study. *Molecules* 25:2651. <https://doi.org/10.3390/molecules25112651>
- Lambros MP, Schafer F, Blackstock R, Murphy JW (1998) Liposomes, a potential immunoadjuvant and carrier for a cryptococcal vaccine. *J Pharm Sci* 87:1144–1148. <https://doi.org/10.1021/js9704184>
- Lianosz V, Wetter D (2014) What's new in the treatment and diagnosis of dermatophytosis? *Semin Cutan Med Surg* 33:136–139. <https://doi.org/10.12788/j.sder.0110>
- Li L, Wang X, Zhang J-Y et al (2018) Antifungal activity of osthonol in vitro and enhancement in vivo through Eudragit S100 nanocarriers. *Virulence* 9:555–562. <https://doi.org/10.1080/21505594.2017.1356503>
- Lionakis MS, Kontoyiannis DP (2003) Glucocorticoids and invasive fungal infections. *Lancet* 362:1828–1838. [https://doi.org/10.1016/S0140-6736\(03\)14904-5](https://doi.org/10.1016/S0140-6736(03)14904-5)
- Lu R, Hollingsworth C, Qiu J et al (2019) Efficacy of oral encocleated amphotericin B in a mouse model of cryptococcal meningoencephalitis. *MBio* 10:e00724–e00719. <https://doi.org/10.1128/mBio.00724-19>
- Marinescu L, Ficai D, Oprea O et al (2020) Optimized synthesis approaches of metal nanoparticles with antimicrobial applications. *J Nanomater*. <https://doi.org/10.1155/2020/6651207>
- May RC, Stone NRH, Wiesner DL et al (2016) Cryptococcus: from environmental saprophyte to global pathogen. *Nat Rev Microbiol* 14:106–117. <https://doi.org/10.1038/nrmicro.2015.6>
- McManus DS (2015) Antifungal drugs. In: Side effects of drugs annual, 1st edn. Elsevier B.V, Amsterdam, pp 307–319
- Medina-Alarcón KP, de Singulani JL, Dutra LA et al (2020) Antifungal activity of 2'-hydroxychalcone loaded in nanoemulsion against Paracoccidioides spp. *Future Microbiol* 15:21–33. <https://doi.org/10.2217/fmb-2019-0095>
- Melkoumov A, Goupil M, Louhichi F et al (2013) Nystatin nanosizing enhances in vitro and in vivo antifungal activity against Candida albicans. *J Antimicrob Chemother* 68:2099–2105. <https://doi.org/10.1093/jac/dkt137>
- Mirza MA, Ahmad S, Mallick MN et al (2013) Development of a novel synergistic thermosensitive gel for vaginal candidiasis: an in vitro, in vivo evaluation. *Colloids Surf B Biointerfaces* 103:275–282. <https://doi.org/10.1016/j.colsurfb.2012.10.038>
- Mody V, Siwale R, Singh A, Mody H (2010) Introduction to metallic nanoparticles. *J Pharm Bioallied Sci* 2:282. <https://doi.org/10.4103/0975-7406.72127>
- Montoya MC, Magwene PM, Perfect JR (2021) Associations between Cryptococcus genotypes, phenotypes, and clinical parameters of human disease: a review. *J Fungi* 7:260. <https://doi.org/10.3390/jof7040260>
- Nazarian S, Gargari SLM, Rasooli I et al (2014) A PLGA-encapsulated chimeric protein protects against adherence and toxicity of enterotoxigenic Escherichia coli. *Microbiol Res* 169:205–212. <https://doi.org/10.1016/j.micres.2013.06.005>

- Neves WW, Neves RP, Macêdo DPC et al (2020) Incorporation of 2-amino-thiophene derivative in nanoparticles: enhancement of antifungal activity. *Braz J Microbiol* 51:647–655. <https://doi.org/10.1007/s42770-020-00248-7>
- Oliveira NK, Frank LA, Squizani ED et al (2021) New nanotechnological formulation based on amiodarone-loaded lipid core nanocapsules displays anticryptococcal effect. *Eur J Pharm Sci* 162:105816. <https://doi.org/10.1016/j.ejps.2021.105816>
- Palmeiro M, Cherubini K, Yurgel LS (2005) Paracoccidioidomycose – Revisão da Literatura. *Sci Medica* 15:274–278
- Pappas PG, Lionakis MS, Arendrup MC et al (2018) Invasive candidiasis. *Nat Rev Dis Prim* 4:18026. <https://doi.org/10.1038/nrdp.2018.26>
- Park S-C, Kim Y-M, Lee J-K et al (2017) Targeting and synergistic action of an antifungal peptide in an antibiotic drug-delivery system. *J Control Release* 256:46–55. <https://doi.org/10.1016/j.jconrel.2017.04.023>
- Peek LJ, Middaugh CR, Berkland C (2008) Nanotechnology in vaccine delivery. *Adv Drug Deliv Rev* 60:915–928. <https://doi.org/10.1016/j.addr.2007.05.017>
- Pires CAA, da Cruz NFS, Lobato AM et al (2014) Clinical, epidemiological, and therapeutic profile of dermatophytosis. *An Bras Dermatol* 89:259–264. <https://doi.org/10.1590/abd1806-4841.20142569>
- Quindós G (2014) Epidemiology of candidaemia and invasive candidiasis. A changing face. *Rev Iberoam Micol* 31:42–48. <https://doi.org/10.1016/j.riam.2013.10.001>
- Ren T, Xu N, Cao C et al (2009) Preparation and therapeutic efficacy of polysorbate-80-coated amphotericin B/PLA-b-PEG nanoparticles. *J Biomater Sci Polym Ed* 20:1369–1380. <https://doi.org/10.1163/092050609X12457418779185>
- Rençber S, Karavana SY, Yılmaz FF et al (2016) Development, characterization, and in vivo assessment of mucoadhesive nanoparticles containing fluconazole for the local treatment of oral candidiasis. *Int J Nanomedicine* 11:2641. <https://doi.org/10.2147/IJN.S103762>
- Restrepo A, Gómez BL, Tobón A (2012) Paracoccidioidomycosis: Latin America's own fungal disorder. *Curr Fungal Infect Rep* 6:303–311. <https://doi.org/10.1007/s12281-012-0114-x>
- Riaz A, Hendricks S, Elbrink K et al (2020) Preparation and characterization of nanostructured lipid carriers for improved topical drug delivery: evaluation in cutaneous Leishmaniasis and vaginal candidiasis animal models. *AAPS PharmSciTech* 21:185. <https://doi.org/10.1208/s12249-020-01717-w>
- Rodrigues Dos Santos Junior S, Lopes K, da Silva F, Santos Dias L et al (2020) Intranasal vaccine using P10 peptide complexed within chitosan polymeric nanoparticles as experimental therapy for paracoccidioidomycosis in murine model. *J Fungi* 6:160. <https://doi.org/10.3390/jof6030160>
- Saldanha CA, Garcia MP, Iocca DC et al (2016) Antifungal activity of amphotericin B conjugated to nanosized magnetite in the treatment of paracoccidioidomycosis. *PLoS Negl Trop Dis* 10:e0004754. <https://doi.org/10.1371/journal.pntd.0004754>
- Sanguinetti M, Posteraro B, Beigelman-Aubry C et al (2019) Diagnosis and treatment of invasive fungal infections: looking ahead. *J Antimicrob Chemother* 74:ii27–ii37. <https://doi.org/10.1093/jac/dkz041>
- Santangelo R, Paderu P, Delmas G et al (2000) Efficacy of oral coxlate-amphotericin B in a mouse model of systemic candidiasis. *Antimicrob Agents Chemother* 44:2356–2360. <https://doi.org/10.1128/AAC.44.9.2356-2360.2000>
- Schmiedel Y, Zimmerli S (2016) Common invasive fungal diseases: an overview of invasive candidiasis, aspergillosis, cryptococcosis, and Pneumocystis pneumonia. *Swiss Med Wkly* 146:w14281. <https://doi.org/10.4414/smw.2016.14281>
- Schröfel A, Kratošová G, Šafařík I et al (2014) Applications of biosynthesized metallic nanoparticles-a review. *Acta Biomater.* <https://doi.org/10.1016/j.actbio.2014.05.022>

- Scorzoni L, de Paula e Silva AC, Marcos CM et al (2017) Antifungal therapy: new advances in the understanding and treatment of mycosis. *Front Microbiol* 08:1–23. <https://doi.org/10.3389/fmicb.2017.00036>
- Sharma R, Agrawal U, Mody N, Vyas SP (2015) Polymer nanotechnology based approaches in mucosal vaccine delivery: challenges and opportunities. *Biotechnol Adv* 33:64–79. <https://doi.org/10.1016/j.biotechadv.2014.12.004>
- Shikanai-Yasuda MA, de Queiroz F, Filho T et al (2006) Consenso em paracoccidioidomicose Guidelines in paracoccidioidomycosis. *Rev Soc Bras Med Trop* 39:297–310
- Shikanai-Yasuda MA, Mendes RP, Colombo AL et al (2017) Brazilian guidelines for the clinical management of paracoccidioidomycosis. *Rev Soc Bras Med Trop* 50:715–740. <https://doi.org/10.1590/0037-8682-0230-2017>
- Shirkhani K, Teo I, Armstrong-James D, Shaunak S (2015) Nebulised amphotericin B-polymethacrylic acid nanoparticle prophylaxis prevents invasive aspergillosis. *Nanomed Nanotechnol Biol Med* 11:1217–1226. <https://doi.org/10.1016/j.nano.2015.02.012>
- Shoham S, Groll AH, Walsh TJ (2010) Antifungal agents. In: *Infectious diseases*, 3rd edn. Elsevier, Amsterdam, pp 1477–1489
- Singh DK, Tóth R, Gácsér A (2020) Mechanisms of pathogenic *Candida* species to evade the host complement attack. *Front Cell Infect Microbiol* 10:94. <https://doi.org/10.3389/fcimb.2020.00094>
- Soriano-Ruiz JL, Calpena-Capmany AC, Cañadas-Enrich C et al (2019) Biopharmaceutical profile of a clotrimazole nanoemulsion: evaluation on skin and mucosae as anticandidal agent. *Int J Pharm* 554:105–115. <https://doi.org/10.1016/j.ijpharm.2018.11.002>
- Souza ACO, Nascimento AL, de Vasconcelos NM et al (2015) Activity and in vivo tracking of Amphotericin B loaded PLGA nanoparticles. *Eur J Med Chem* 95:267–276. <https://doi.org/10.1016/j.ejmech.2015.03.022>
- Spadari CC, da Silva de Bastiani FWM, Lopes LB, Ishida K (2019) Alginate nanoparticles as non-toxic delivery system for miltefosine in the treatment of candidiasis and cryptococcosis. *Int J Nanomedicine* 14:5187–5199. <https://doi.org/10.2147/IJN.S205350>
- Srikanta D, Santiago-Tirado FH, Doering TL (2014) *Cryptococcus neoformans*: historical curiosity to modern pathogen. *Yeast* 31:47–60. <https://doi.org/10.1002/yea.2997>
- Staab JF, Wong B (2014) Fungal infections, systemic. In: *Reference module in biomedical sciences*, 4th edn. Elsevier, Amsterdam, pp 341–361
- Streinu-Cercel A (2012) Invasive fungal infections. *GERMS* 2:35. <https://doi.org/10.11599/germs.2012.1011>
- Taborda CP, Buccheri R, Benard G et al (2018) *Paracoccidioides* spp. and *Histoplasma capsulatum*: current and new perspectives for diagnosis and treatment. *Curr Top Med Chem* 18:1333–1348. <https://doi.org/10.2174/1568026618666181002112231>
- Taborda CP, Travassos LR, Benard G (2021) Paracoccidioidomycosis. In: *Encyclopedia of mycology*. Elsevier, Amsterdam, pp 654–675
- Tang X, Zhu H, Sun L et al (2014) Enhanced antifungal effects of amphotericin B-TPGS-b-(PCL-ran-PGA) nanoparticles in vitro and in vivo. *Int J Nanomedicine* 9:5403. <https://doi.org/10.2147/IJN.S71623>
- Thompson G, Patterson T (2011) Pulmonary aspergillosis: recent advances. *Semin Respir Crit Care Med* 32:673–681. <https://doi.org/10.1055/s-0031-1295715>
- Thorley AJ, Tetley TD (2013) New perspectives in nanomedicine. *Pharmacol Ther* 140:176–185. <https://doi.org/10.1016/j.pharmthera.2013.06.008>
- Travassos LR, Taborda CP (2012) Paracoccidioidomycosis vaccine. *Hum Vaccine Immunother* 8:1450–1453. <https://doi.org/10.4161/hv.21283>
- Turissini DA, Gomez U, Teixeira MM et al (2017) Species boundaries in the human pathogen *Paracoccidioides*. *Fungal Genet Biol* 106:9–25. <https://doi.org/10.1016/j.fgb.2017.05.007>
- Vaghasiya H, Kumar A, Sawant K (2013) Development of solid lipid nanoparticles based controlled release system for topical delivery of terbinafine hydrochloride. *Eur J Pharm Sci* 49:311–322. <https://doi.org/10.1016/j.ejps.2013.03.013>

- Van de Ven H, Paulussen C, Feijens PB et al (2012) PLGA nanoparticles and nanosuspensions with amphotericin B: potent in vitro and in vivo alternatives to Fungizone and AmBisome. *J Control Release* 161:795–803. <https://doi.org/10.1016/j.jconrel.2012.05.037>
- Vermout S, Tabart J, Baldo A et al (2008) Pathogenesis of dermatophytosis. *Mycopathologia* 166: 267–275. <https://doi.org/10.1007/s11046-008-9104-5>
- Vidal Bonifácio B, dos Santos Ramos MA, Silva P et al (2015) Nanostructured lipid system as a strategy to improve the anti-*Candida albicans* activity of Astronium sp. *Int J Nanomedicine* 10: 5081. <https://doi.org/10.2147/IJN.S79684>
- Wang P (2021) Genetic transformation in *Cryptococcus* species. *J Fungi* 7:56. <https://doi.org/10.3390/jof7010056>
- Wang H, Xu K, Liu L et al (2010) The efficacy of self-assembled cationic antimicrobial peptide nanoparticles against *Cryptococcus neoformans* for the treatment of meningitis. *Biomaterials* 31:2874–2881. <https://doi.org/10.1016/j.biomaterials.2009.12.042>
- Xu N, Julin G, Yuanjie Z et al (2011a) Efficacy of intravenous amphotericin B-polybutylcyanoacrylate nanoparticles against cryptococcal meningitis in mice. *Int J Nanomedicine* 6:905. <https://doi.org/10.2147/IJN.S17503>
- Xu K, Wang H, Liu L et al (2011b) Efficacy of CG3R6TAT nanoparticles self-assembled from a novel antimicrobial peptide for the treatment of *Candida albicans* meningitis in rabbits. *Chemotherapy* 57:417–425. <https://doi.org/10.1159/000330855>
- Xu P, Yang Z, Chen M et al (2014) Evaluating the potential of cubosomal nanoparticles for oral delivery of amphotericin B in treating fungal infection. *Int J Nanomedicine* 9:327. <https://doi.org/10.2147/IJN.S54967>
- Yan L, Yang Y, Zhang W, Chen X (2014) Advanced materials and nanotechnology for drug delivery. *Adv Mater*. <https://doi.org/10.1002/adma.201305683>
- Zaragoza O, Rodrigues ML, De Jesus M et al (2009) Chapter 4 The capsule of the fungal pathogen *Cryptococcus neoformans*. In: *Advances in applied microbiology*, 1st edn. Elsevier Inc., Amsterdam, pp 133–216
- Zhang C, Chen M, Wang G et al (2016) Pd@Ag Nanosheets in combination with amphotericin B exert a potent anti-cryptococcal fungicidal effect. *PLoS One* 11:e0157000. <https://doi.org/10.1371/journal.pone.0157000>
- Zhang P, Yang X, He Y et al (2017) Preparation, characterization and toxicity evaluation of amphotericin B loaded MPEG-PCL micelles and its application for buccal tablets. *Appl Microbiol Biotechnol* 101:7357–7370. <https://doi.org/10.1007/s00253-017-8463-6>
- Zhao K, Zhang Y, Zhang X et al (2014) Chitosan-coated poly(lactic-co-glycolic) acid nanoparticles as an efficient delivery system for Newcastle disease virus DNA vaccine. *Int J Nanomedicine* 9: 4609–4619. <https://doi.org/10.2147/IJN.S70633>
- Zmeili OS, Soubani AO (2007) Pulmonary aspergillosis: a clinical update. *QJM* 100:317–334. <https://doi.org/10.1093/qjmed/hcm035>

Article

Therapeutic Vaccination with Cationic Liposomes Formulated with Dioctadecyldimethylammonium and Trehalose Dibehenate (CAF01) and Peptide P10 Is Protective in Mice Infected with *Paracoccidioides brasiliensis*

Marcelo Valdemir de Araújo ¹, Samuel Rodrigues Dos Santos Júnior ¹,
Joshua D. Nosanchuk ² and Carlos Pelleschi Tabora ^{1,3,*}

- ¹ Departamento de Microbiologia, Instituto de Ciências Biomédicas, Universidade de São Paulo, São Paulo 05508-000, Brazil; marceloaraujo@usp.br (M.V.d.A.); samuelmicrobio@usp.br (S.R.D.S.J.)
- ² Departments of Medicine (Division of Infectious Disease), Microbiology and Immunology, Albert Einstein College of Medicine and Montefiore Medical Center, Bronx, NY 10461, USA; nosanchuk@gmail.com
- ³ Departamento de Dermatologia, Instituto de Medicina Tropical de São Paulo—LIM53, Faculdade de Medicina, Universidade de São Paulo, São Paulo 4023-062, Brazil
- * Correspondence: taborda@usp.br; Tel.: +55-11-3091-7351

Received: 16 October 2020; Accepted: 4 December 2020; Published: 8 December 2020



Abstract: The peptide P10 is a vaccine candidate for Paracoccidioidomycosis, a systemic mycosis caused by fungal species of the genus *Paracoccidioides* spp. We have previously shown that peptide P10 vaccination, in the presence of several different adjuvants, induced a protective cellular immune response mediated by CD4⁺ Th₁ lymphocytes that was associated with the increased production of IFN- γ in mice challenged with a virulent isolate of *Paracoccidioides brasiliensis*. Cationic liposomes formulated with dioctadecyldimethylammonium and trehalose dibehenate (DDA/TDB, termed also CAF01—cationic adjuvant formulation) have been developed for safe administration in humans and CAF01 liposomes are utilized as an adjuvant for modulating a robust Th₁/Th₁₇ cellular response. We evaluated the efficacy of the adsorption of peptide P10 to CAF01 cationic liposomes and used the generated liposomes to vaccinate C57Bl/6 mice infected with *P. brasiliensis*. Our results showed that P10 was efficiently adsorbed onto CAF01 liposomes. The vaccination of infected mice with cationic liposomes formulated with DDA/TDB 250/50 $\mu\text{g/mL}$ and 20 μg of P10 induced an effective cellular immune response with increased levels of Th₁₇ cytokines, which correlated with significant decreases in the fungal burdens in lungs and protective granulomatous tissue responses. Hence, cationic liposomes of DDA/TDB 250/50 $\mu\text{g/mL}$ with 20 μg of P10 are a promising therapeutic for safely and effectively improving the treatment of paracoccidioidomycosis.

Keywords: paracoccidioidomycosis; *P. brasiliensis*; peptide vaccine; adjuvant; CAF01; DDA/TDB; cationic liposome

1. Introduction

Paracoccidioidomycosis (PCM) is a systemic fungal disease that is due to infection by the thermally-dimorphic fungi of the genus *Paracoccidioides* [1]. These pathogens are found in soil as saprophyte mycelium [1]. Disturbances in the environment can aerosolize hyphal fragments or conidia, which can be inhaled and subsequently deposited in the alveoli where they undergo morphogenic transformation to a yeast phase [2]. *Paracoccidioides brasiliensis* was for many years considered as the

only species in the genus [3] until Teixeira et al. (2014) described a second species, known as *P. lutzii* [4]. However, further detailed molecular studies identified that there are five phylogenetic species in the genus *Paracoccidioides*: *P. lutzii* and four cryptic species of the *P. brasiliensis*: S1, PS2, PS3, and PS4 [5–8]. The formerly aggregated *P. brasiliensis* species are currently referred to as *P. brasiliensis* (S1), *P. americana* (PS2), *P. restrepensis* (PS3), *P. venezuelensis* (PS4), and *P. lutzii* [3].

PCM principally occurs from the south of Mexico to the north of Argentina, and it is considered one of the most important systemic fungal infections in the geographic region that corresponds to Latin America [1]. Antifungal treatment is essential for achieving a cure and durations of therapy are prolonged, frequently requiring 2 or more years of therapy [2,9]. Two clinical forms are well known. The acute form (juvenile type) is the more aggressive, frequently systemic manifestation, which affects children, adolescents, and young adults (30 to 40 years) and is homogenous between genders [2]. The chronic form (adult type) is significantly more common (74% to 96% of PCM cases) and affects adults between 30 a 60 years of age with males being more commonly afflicted [2].

An efficient cellular immune response is crucial in host defense against fungal pathogens such as *Paracoccidioides* spp. [10]. Therapeutic or prophylactic vaccines are important promising tools for the prevention or treatment of patients with fungal infections [11]. The peptide P10 (QTLIAIHTLAIRYAN) has been highlighted as a vaccine candidate against PCM [12]. Derived from a *P. brasiliensis* glycoprotein of 43kDa (gp43) [13], P10 is considered the main diagnostic antigen [14,15]. Although the orthology of a glycoprotein of 43kDa in *P. lutzii* (Plgp43) has only 80% of identity with gp43, both are structurally related to fungal exo-glucanases [16]. Previous studies have shown that the administration of P10 vaccine with different adjuvants can reduce the fungal burden and elicit a mixed cellular immune response characterized by a predominant Th₁ response with production of IFN- γ , TNF- α and IL-12 in murine infection models [11,17].

In general, peptides alone are poorly immunogenic and require adjuvants and delivery systems to be effective [18]. The use of an adjuvant combined with a specific antigen produces a more robust immune response in experimental PCM compared to the antigen alone [10]. Cationic liposomes can potentiate subunit vaccines in addition to helping to decrease the vaccine dose required for efficacy [19]. The amphiphilic synthetic lipid DODAB (dioctadecyldimethylammonium bromide) is a surfactant-based in ammonium quaternary (DDA), which can function as a cationic liposome that can be used as a carrier in a drug delivery system and as an adjuvant [20].

The level and quality of an immune response induced by DDA liposomes may be enhanced by the incorporation of an immunostimulatory compound, such as trehalose dibehenate (TDB) [21], a synthetic analogue of trehalose dimycolate (TDM), known as a cord factor. However, it is considered unacceptable for clinical use because it is an important factor in the granulomatous response of mycobacteria [21–24]. Therefore, TDB was modified by replacing long branched mycolic acid (>70 carbons) [25] for two long 22-carbon acyl chains (behenic acid) [21] resulting in a compound with lower toxicity that retains its adjuvant activity [26,27]. The modified TBD acts on the Mincle receptor by activating Syk-Card9 signaling in antigen-presenting cells (APCs) [25,28–30].

The combination of DDA with TDB results in the adjuvant known as CAF01 (*cationic adjuvant formulation*), which induces a potent immune response with production of high level with IFN- γ , IL-17, and low levels of IL-5 [21,31]. CAF01 has been tested in phase I clinical trial in humans volunteers against tuberculosis in combination with Ag85B and ESAT 6 (H1) antigen (H1:CAF01) [32].

In the current study, we have adsorbed the *P. brasiliensis* peptide P10 onto DDA/TDB adjuvant (CAF01). Our data shows that P10 with DDA/TDB is a promising adjuvant-boosted vaccine as it efficiently decreased fungal lung burden in C57Bl/6 mice infected with *P. brasiliensis* in a therapeutic study. Additionally, the vaccine increased the levels of pro-inflammatory cytokines, such as IL-17, in mice with PCM.

2. Materials and Methods

2.1. Animals

We obtained 6-to 8-week-old male C57BL/6, weighing between 25 to 30 g, from the Animal facility at Faculdade de Medicina da Universidade de São Paulo under Specific-Pathogen-Free conditions and transferred to the animal facility at Departamento de Microbiologia do Instituto de Ciências Biomédicas da Universidade de São Paulo. All procedures were performed according to the guidelines of National Council of Ethics with Animals (CONCEA) and the protocols were approved by the Ethical Committee for Animal Use from Institute of Biomedical Sciences at University of Sao Paulo (CEUA ICB USP certificates 101/2014, approved in 01/12/2014).

2.2. Peptide P10 Preparation

The peptide P10 (QTLIAIHTLAIRYAN) [12] was synthesized and purified by Aminotech (São Paulo, SP, Brazil) with a purity grade of >94% as confirmed by mass spectrometry and HPLC. The stock solution (1000 µg/mL) was prepared by adding 20% DMSO (Dimethyl sulfoxide) Sigma (St. Louis, MO, USA) and 80% 1 mM Tris-buffer (Carlsbad, CA, USA). The stock was aliquoted and stored in the freezer –20 °C until use. The peptide was thawed and just added to liposomes, described below, with an interaction time of 1 h at 25 °C [33].

The Mincle agonist D-(+) trehalose 6,6'-dibehenate (TDB) was obtained as a powder from Avanti Polar Lipids (Sigma, Alabaster, AL, USA) and stored at –20 °C according to manufacturer's instructions. The specified quantities were weighed at the time of preparation of liposomes and added to DDA. The cationic lipid dioctadecyldimethylammonium bromide (DODAB) was purchased from Sigma (St. Louis, MO, USA), at >98% purity as confirmed by TLC.

2.3. Preparation of Liposome

Unilamellar liposomes of DDA/TDB were prepared by the film hydration method [34,35]. The method consists of dilution of DDA/TDB (5:1) (1.25/0.5 mg/mL) in a mixed solution of chloroform/methanol (9:1). The removal of organic solvent was achieved by a rotary evaporator and the process was stopped when a film was observed on the bottom of the bottle. The liposomes were hydrated with 10 mM tris-buffer for 20 min at a temperature 10 °C above transition phase ($T_m = 47$ °C) until complete hydration occurred and then the liposomes were stored at 4 °C for up two weeks [35].

2.4. Determination of Diameter Size, Polydispersity and Zeta Potential of Liposomes

The diameters (Dz), polydispersity index (Pdi), and zeta potential (ζ) of the liposomes were determined using a Zetasizer (Nano ZS Malvern Instruments, Worcestershire, UK). The samples were dispersed with 1mM tris-buffer (pH: 7.4) with a dilution rate of 1:300. The refractive index of pure water (1.0) was used as a baseline [35,36].

2.5. Adsorption Efficiency

The adsorption efficiency of liposomes and antigen was estimated by the following Equation (1) [37,38]:

$$EE(\%) = \frac{\text{Total Antigen} - \text{Free Antigen}}{\text{Total Antigen}} \times 100\% \quad (1)$$

Free antigen was separated from liposomes by ultracentrifugation and quantified by Qubit protein assay (Invitrogen, Eugene, OR, USA). For separation, the samples (liposome plus peptide) were centrifuged at 36,000 rpm (100,000× g, Ultracentrifuge Beckman Coulter Optima XL-100K, rotor type 70.1Ti) for 60 min, 4 °C, and then the supernatant with free antigen was collected. The measurements were performed using 20 µL of samples in 180 µL of working solution (kit Qubit) incubated for 15 min and read on a Qubit fluorometer.

2.6. Determination of Liposomes Morphology by Transmission Electronic Microscopy (TEM)

The morphological analysis of unilamellar DDA/TDB liposomes was performed using a Jeol 1200EX transmission electron microscope with LaB6 filament operating at 80 kV voltage. For measurements, liposomes samples were diluted in 1 mM tris-buffer (pH: 7.4), 10 μ L were placed on a copper grid and dried at room temperature (approximately 2 min), then the excess was removed with a paper filter and 10 μ L of Uranyl was added. The mixture remained at room temperature for approximately 5 min, the excess was withdrawn with a paper filter [35].

2.7. Experimental Infection

The well-characterized, virulent isolate *P. brasiliensis* (Pb18) [39] was used to infect mice via intratracheal injection. The isolate was maintained by weekly passages on Fava Netto solid medium at 37 °C. After 7 to 10 days of growth, yeast cells were transferred to Brain Heart Infusion medium (Becton and Dickinson, Sparks, MD, USA) supplement with 4% fetal bovine serum (Gibco, Grand Island, NY, USA) and gentamicin 50,000 mg (Gibco, Grand Island, NY, USA) (40 μ g/mL) and then incubated with rotary shaking at 37 °C for 7 days. Yeast cells were collected, washed with Phosphate Buffered Saline (PBS), pH: 7.2, and passed through a 1 mL syringe attached to a 26-gauge hypodermic needle to dissociate clustered cells. The cell concentration was determined by counting using a Neubauer's chamber. Viability was determined by Trypan blue (Sigma, St. Louis, MO, USA) staining and was always higher than 90%. C57Bl/6 mice were intraperitoneally anesthetized with 300 μ L of a solution of Xylazine 2 g/100 mL and Ketamine 10 g/mL in PBS buffer (both from União Química Farmacêutica, São Paulo, Brazil). Then, the mice had their tracheas exposed for injection with a 50 μ L of a solution containing 3×10^5 yeasts of Pb18. The incisions were sutured with 4-0 silk, and the animals were rested until they recovered from the procedure.

2.8. Vaccination Protocols

Different concentrations of DDA/TDB liposome (250/50 μ g/mL, 312.5/62.5 μ g/mL and 500/100 μ g/mL) were combined with 20 μ g of peptide P10. The mixtures were kept for 20 min at room temperature. Five groups of mice (each one with 6 animals) received the vaccine formulation or control solutions (DDA/TDB alone). The animals received the first vaccination subcutaneously with 100 μ L of vaccine or controls solutions at the base of the tail 30 days after infection. In total, mice received 3 doses at 2 weeks intervals between them. Two weeks after the last vaccination, the animals were euthanized, and their lungs were excised and analyzed for fungal burden, histology, and levels of cytokines.

2.9. Determination of Fungal Burden

After euthanasia of mice, the lungs were excised and weighed immediately. The tissues were then manually homogenized in PBS buffer, adjusting to a volume of 2 mL. A portion of homogenate was plated in solid BHI medium, supplemented with 5% culture filtrate of *P. brasiliensis* isolate 192, plus 4% inactivated fetal bovine serum (Gibco, Grand Island, NY, USA), 1% streptomycin and penicillin (Sigma, St. Louis, Mo, USA). The plates were maintained at 37 °C for a period of 7 to 15 days. The number of Colony Forming Units (CFUs) was counted, and results were expressed per gram of tissue.

2.10. Quantification of Cytokines Levels of Homogenate Pulmonary for the ELISA Method

Cytokines were determined in the supernatants from lung homogenates by enzyme-linked immunosorbent assay (ELISA) as described [40]. The levels interleukin-4 (IL-4), interleukin-12 (IL-12), interferon-gamma (IFN- γ), interleukin-6 (IL-6), interleukin-10 (IL-10), and tumor necrosis factor-alpha (TNF- α) were determined using ELISA kits (BD Biosciences, San Diego, CA, USA). Interleukin-17 (IL-17) was measured using Biolegend's ELISA Max (San Diego, CA, USA).

2.11. Histopathological Lungs Analysis

A fraction of lung tissue was collected and fixed in formalin 10% (Merck, Darmstadt, Germany). The fragments were embedded in paraffin, and 4 to 5 μm sections were cut and stained with hematoxylin-eosin (H.E.). The images were acquired with an inverted microscope (Zeiss, Primovert, Gottingen, Germany) coupled to a digital camera system (Axiocam 105 color, Zeiss, Oberkochen, Germany) and processed by the Zeiss Software (Zen core, Oberkochen, Germany) in the Laboratory of the immunobiology of interaction Leishmania-macrophages of Instituto de Ciências Biomédicas da Universidade de São Paulo.

2.12. Statistical Analysis

The results were analyzed using GraphPad Prism 5.0 Software GraphPad Inc. (San Diego, CA, USA) and analysis of variance (ANOVA) was performed followed by the Bonferroni post-test. The results were considered significant when $p < 0.05$.

3. Results

3.1. The Effect of Peptide P10 Adsorption on DDA/TDB Liposomes

The physicochemical characteristics of DDA/TDB and DDA/TDB/P10 liposomes prepared by the film hydration method are demonstrated in Table 1. The liposomes alone (DDA/TDB) were dispersed in 1 mM Tris buffer and presented an average diameter size of 471.5 ± 2 nm. The stability of the suspension was maintained by the positive surface charge of liposomes (44.3 ± 2 mV). The polydispersity index (0.528) of the DDA/TDB liposomes is considered average and within pre-established parameters [41]. The adsorption of the peptide onto liposome was accomplished by the simple addition of peptide P10 into the solution for approximately 20 min at room temperature (25 °C). The adsorption of the peptide modified the diameter size of the liposome, increasing it to 667.9 ± 3 nm; furthermore, the Pdi value decreased to 0.302, this value is considered the better dispersity for liposomes, indicating a homogenous population of phospholipid liposomes [42–45] and the ζ potential of liposomes was 39 ± 3 mV. Interestingly, the changes in the concentrations of DDA/TDB in the formation of liposomes only modestly changed the diameter size, Pdi, or ζ potential, as shown in Table 1.

Table 1. Characterization of liposomal liposomes.

Description	Size (nm)	Polydispersity Index	Zeta Potential (mV)
DDA /TDB 250/50 μg	471.5 ± 2	0.528	44.3 ± 2
DDA/TDB 250/50 μg /P10 20 μg	667.9 ± 3	0.302	39 ± 3
DDA/TDB 312.5/62.5 μg /P10 20 μg	650.8 ± 5	0.369	44.7 ± 3
DDA/TDB 100/500 μg /P10 20 μg	639.2 ± 3	0.411	45.7 ± 4

Measurements of diameter size (Dz), polydispersity index (Pdi) and zeta potential (ζ). Results denote mean \pm S.D. from 3 different analysis.

3.2. Determination of Liposomes Morphology after P10 Adsorption by TEM

We used transmission electron microscopy (TEM) to investigate the structure of the liposome and check for possible changes in the liposome after the adsorption of the peptide to it. As shown in Figure 1, the liposomes formed by the film hydration method presented spherical with several sizes, and without signs of aggregation. The adsorption of peptide onto liposomes did not markedly modify its morphology, the liposomes plus peptide demonstrated spherical morphology resembling as liposome alone.

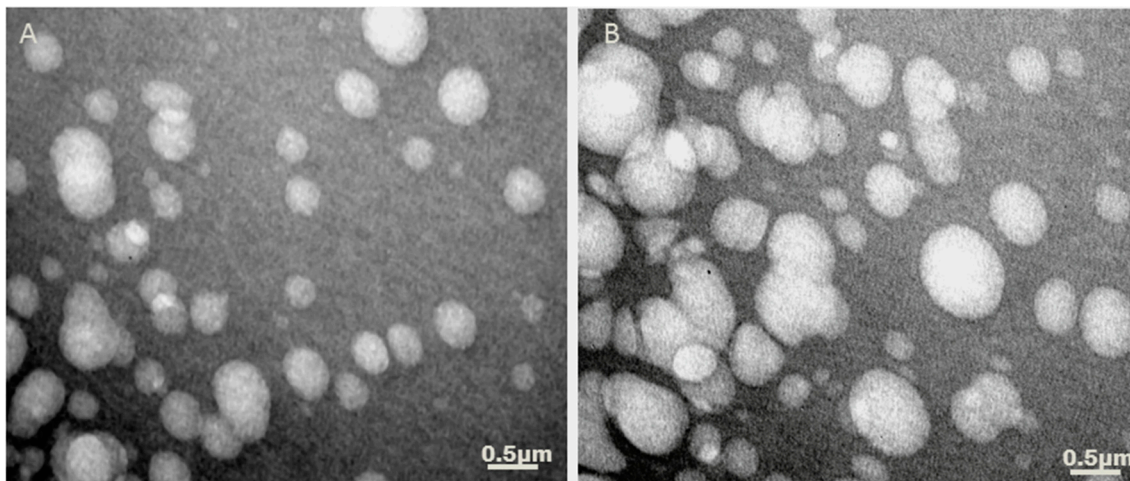


Figure 1. TEM of cationic liposomes. The liposomes were prepared by the film hydration method and fixed with Uranyl for morphological analyses. The micrographs show unilamellar liposomes of DDA/TDB alone (A); DDA/TDB plus P10 (B).

3.3. Adsorption of Peptide to Adjuvant Liposome

After the formation of the liposomes, the antigen was added to the structure and then the efficiency of P10 adsorption was evaluated by separating the free antigen by ultracentrifugation. As seen in Table 2, the peptide was efficiently adsorbed onto the liposome at a rate of 80%. The efficiency is consistent with the increase in the liposome/peptide diameter (667.9 nm) compared to the liposome alone (471.5 nm), indicating the accumulation of peptide.

Table 2. Adsorption efficiency of peptide P10 onto liposome of DDA/TDB.

Description	Adsorption Efficiency %
DDA/TDB 250/50 μg /P10 20 μg	84.5% (*)

*: The data represent three independent measurements. Protein (peptide) concentration refers to the concentration of peptide initially added to the liposome before the ultra-centrifugation process, and the final concentration refers to the amount of free peptide in the supernatant. These results represent the calculations performed according to the instructions of the Qubit kit manufacturer.

3.4. DDA/TDB/P10 Vaccination Controls Pulmonary Fungal Burden

The immunogenic effect of the different concentrations of DDA/TDB/P10 liposomes was evaluated two weeks after the last of third vaccination. The CFU from the lungs of infected mice is shown in Figure 2. The vaccination with DDA/TDB/P10 in the concentration of 250/50 $\mu\text{g}/\text{mL}$ plus 20 μg of P10 showed the best effect with a significant reduction of fungal burden in the lungs ($p < 0.001$), which is a decrease of about 15,000 CFU/g of tissue. This reduction was less pronounced in the formulation of 312.5/62.5 $\mu\text{g}/\text{mL}$ with P10 ($p < 0.05$), and DDA/TDB 500/100 $\mu\text{g}/\text{mL}$ with P10 did not significantly alter the fungal burden (Figure 2).

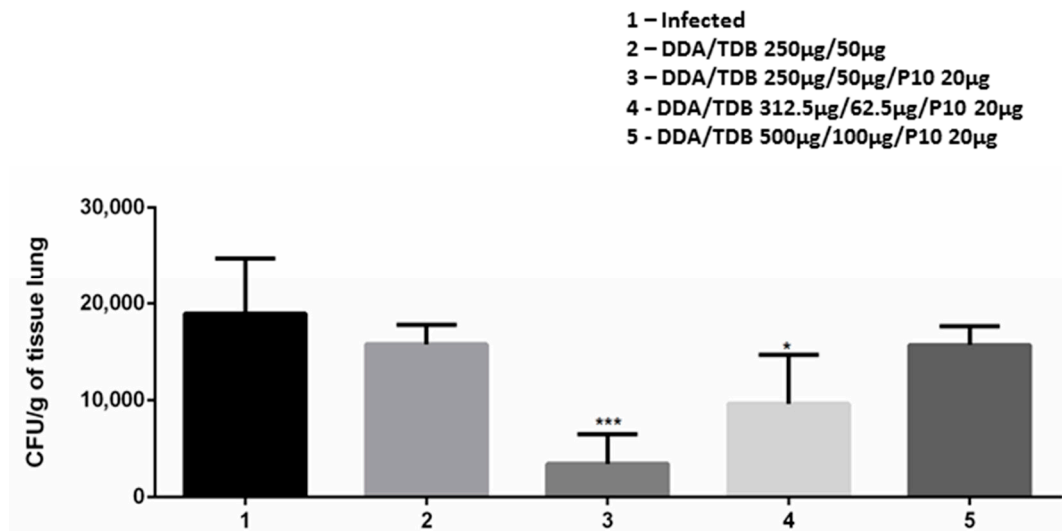


Figure 2. Vaccination with DDA/TDB/P10 decreases the fungal load. The fungal burden was measured in the lungs of mice infected with *P. brasiliensis* via Colony Forming Units (CFU) assay and the results were expressed as CFU/g of lung tissue. Infected animals either received PBS (1), DDA/TDB alone (2), or different formulations of DDA/TDB with P10 (3, 4, and 5). The data represent the mean and SD of results from 3 experiments using 6 mice per group. An asterisk (*) represents a statistically significant difference, *** $p < 0.001$ and * $p < 0.05$.

3.5. The Therapeutic Effect of DDA/TDB/P10 Vaccination Correlates with an IL-4/IL-17 Balance in the Lung Parenchyma

We evaluated whether the adsorption of the peptide onto the liposome altered the profile of cytokines in infected and immunized animals. For this, the cytokine levels corresponding to the Th₁, Th₂, and Th₁₇ immune responses of the pulmonary homogenate were evaluated by the ELISA method and the results are shown in Figure 3. As seen in the graphs, the therapeutic vaccination with DDA/TDB (250/50 µg/mL) plus P10 (20 µg) or liposome alone (250/50 µg/mL) in the *P. brasiliensis* infected mice, did not induce alterations of levels of cytokine associated with the Th₁ immune response. On the other hand, vaccination with the liposome alone, or peptide plus liposome, and with lower concentrations (250/50 and 312.5/62.5 µg/mL) of the liposome, led to decreased levels of IL-4 ($p < 0.01$); a cytokine associated with a Th₂-biased response. The induction of the Th₁₇ response in therapeutic vaccination with liposome associated P10 was also assessed in the pulmonary homogenate (Figure 3). The Th₁₇ signature cytokine, IL-17A, had higher levels only following vaccination performed with the formulation of the peptide P10 adsorbed to the liposome in low concentration (250/50 µg/mL) ($p < 0.01$). Notably, the levels of cytokine IL-6, associated with Th₁₇ polarization, increased only in mice treated with liposome alone ($p < 0.05$).

3.6. Lung Histology

We performed a histological analysis of lung tissue of all animals included in our protocol using hematoxylin-eosin staining to assess for the presence of granulomas and yeast cells (Figure 4). Lungs from mice infected, but untreated, showed a large number of yeast cells that were diffusely distributed and there was an absence of an organized cellular response (Figure 4B). Animals infected that received DDA/TDB developed well-delimited granulomas containing yeast cells (Figure 4C). Mice infected with *Paracoccidioides* and vaccinated with DDA/TDB 250/50 µg/P10-20 µg showed more compact granuloma with yeast cells inside and the granulomas were surrounded by a dense mass formed by inflammatory cells. Notably, the parenchyma adjacent to the granulomas appeared normal and there were no disseminated yeasts (Figure 4D). The two other DDA/TDB and P10 formulations

also induced granuloma formation; however, there was an increased number of yeast cells inside the granulomas and a less dense adjacent infiltration of immune cells (Figure 4E,F).

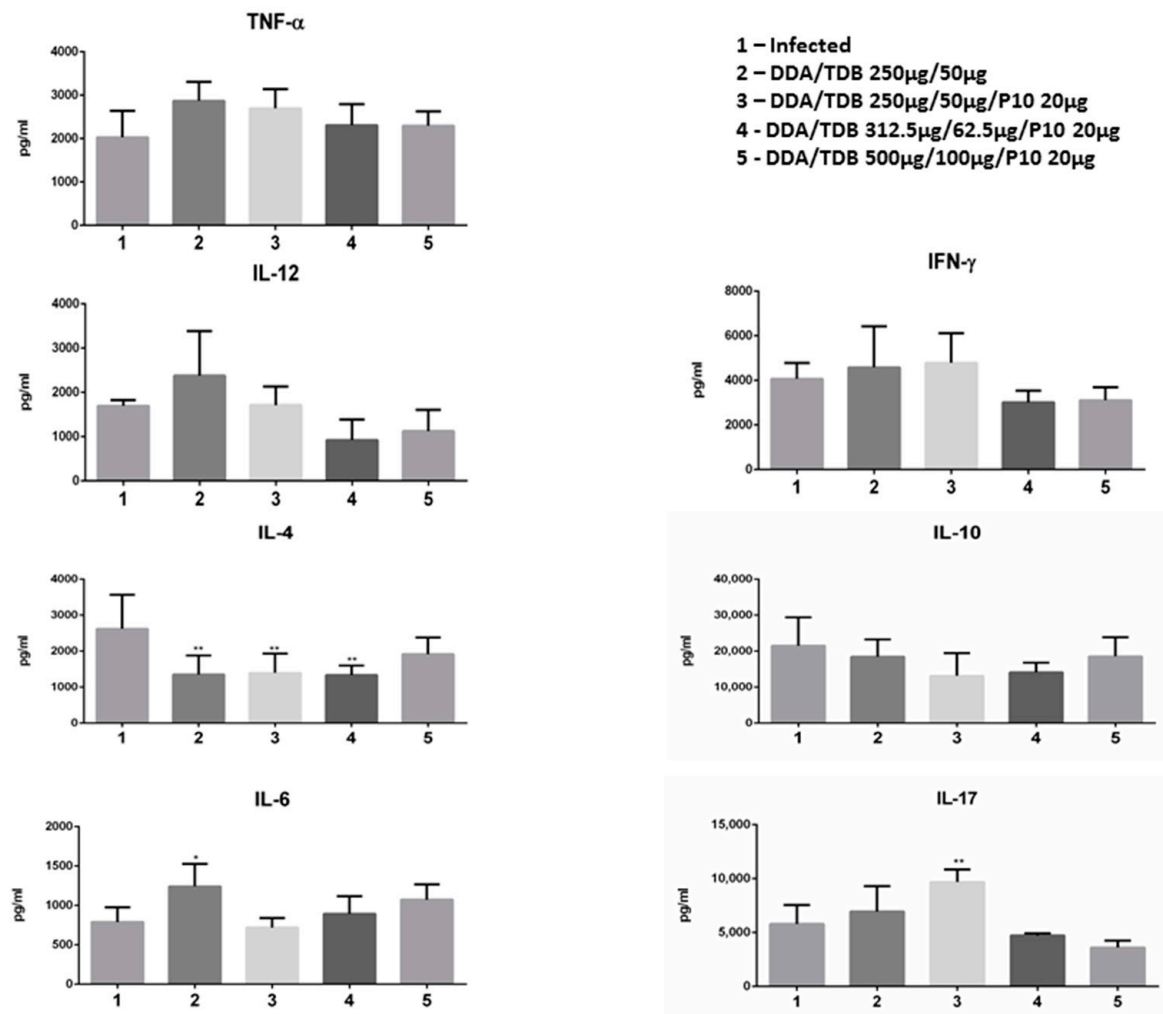


Figure 3. Evaluation of immune responses induced by P10 peptide adsorbed on DDA/TDB liposomes. Th₁, Th₂, and Th₁₇-associated cytokines were measured in pulmonary homogenates 75 days after infection by capture enzyme-linked immunosorbent assay (ELISA). Infected mice with *P. brasiliensis* received three doses of either PBS as a control (1), DDA/TDB alone (2), or different concentrations of DDA/TDB with P10 (3–5). The data are shown are the mean and SD of results from three independent experiments using 6 mice per group. The asterisk represents a statistically significant difference * $p < 0.05$ and ** $p < 0.01$.

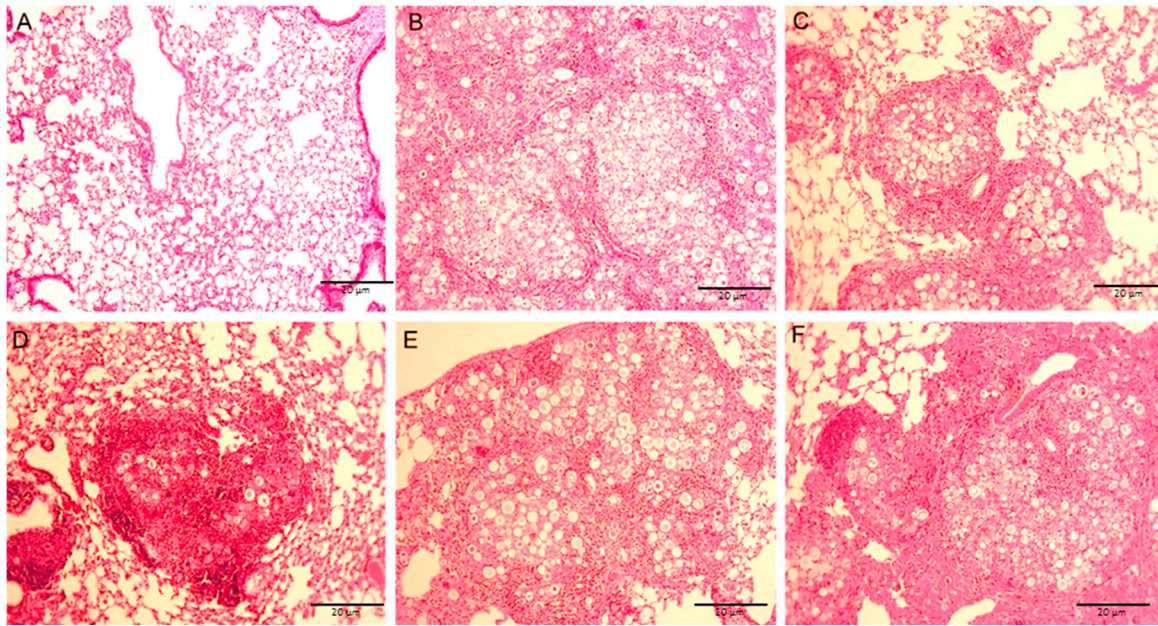


Figure 4. Photomicrographs of pulmonary tissues from C57BL/6 mice with or without *P. brasiliensis* infection. The lung sections were stained with Hematoxylin and Eosin to analyze the presence of inflammation. Uninfected lung tissue (A) is presented for comparison with *P. brasiliensis* infected lungs from mice that received PBS only (B), treated with DDA/TDB alone (C), or vaccinated with DDA: DDA/TDB 250/50 µg/P10 20 µg (D) DDA/TDB 312.5/62.5 µg/P10 20 µg (E) or DDA/TDB 500/100 µg/P10 20 µg (F). (10× magnification).

4. Discussion

In this study, we evaluated the immunomodulatory response of the P10 peptide adsorbed onto unilamellar liposome formed by the DDA/TDB adjuvant (CAF01) in an experimental PCM model using C57BL/6 mice infected with *P. brasiliensis* (Pb18). We previously published that other adjuvants, such as CFA (complete Freund's Adjuvant), associated with peptide P10 significantly reduced the fungal burden of mice infected with *P. brasiliensis* [46]. We also previously showed that dioctadecyldimethylammonium bromide (DODAB) associated with peptide P10 efficiently reduced lung fungal burden of mice infected with *P. brasiliensis* [17]. However, we have continued to seek an effective adjuvant that is deemed safe in humans.

The Cationic Adjuvant Formulation (CAF01 comprised by DDA/TDB) was developed as a safe adjuvant for humans and animals and its mechanism of action is through the triggering of Th₁ responses [31]. CAF adjuvant has been tested in either human or animals infections with Chikungunya virus [47], Influenza [48], *Chlamydia trachomatis* [49], *Mycobacterium tuberculosis* [50,51], *Plasmodium falciparum* [52], and *Streptococcus pyogenes* [53].

PCM requires prolonged antifungal treatment, with durations frequently extending past 2 years. This protracted therapy often leads to discontinuation of medications by the patient. Yet, even after prolonged treatment, relapses may occur [54]. Strategies that combine the use of antifungal drugs and therapeutic vaccines may help reduce treatment time, effective recovery of the immune system, and prevent sequelae, including relapses [54]. The ability of antifungal drugs combined with peptide P10 to improve outcomes in experimental PCM has been effectively demonstrated [54]. Hence, there is a solid scientific basis and an important clinical need for a therapeutic PCM vaccine based on P10.

The adsorption of P10 onto liposomes of DDA/TDB modified the physicochemical characteristics of adjuvant. The surface charge remained positive and higher than 30mV, which is essential for the repulsion between liposomes to minimize the likelihood of aggregation [18]. Notably, the adsorption of P10 onto the liposomes changed the diameter size of liposomes from 471.5 nm to 667.9 nm. The size

of a liposome may affect the development of specific immune responses, driving the cytokine profile towards a Th₁ or Th₂ response [26,55,56].

In our experiments, we observed that the concentration of DDA/TDB was critical for the efficiency of the vaccine preparation in modifying the pathobiology of experimental PCM. We tested three different formulations of DDA/TDB with 20 µg of peptide P10, which was the amount of peptide previously standardized by our group as an effective protective dose of P10 [12,46]. The preparations of liposomes with DDA/TDB 250/50 µg/mL and 312.5/62.5 µg/mL, but not 500/100 µg/mL, were able to significantly reduce pulmonary fungal burdens when the vaccine was administered to infected mice. However, DDA/TDB 250/50 µg/mL with P10-20 µg was significantly more efficient compared to the DDA/TDB 312.5/62.5 µg/mL and 500/100 µg/mL formulations.

The choice of these concentrations was based on the work of Van Dissel 2014 [32], which utilized different concentrations of DDA/TDB in a human trial evaluating the efficiency of prophylactic vaccination against tuberculosis with H1 protein. In their study, Van Dissel and collaborators showed that intermediate and higher concentrations of liposomes induced T cell memory, and this profile was responsive until 150 weeks after vaccination [32]. In our work, low concentrations of DDA/TDB significantly modulated protective immune response with P10, resulting in a significant decrease of burden fungal, an increase of cytokines Th₁₇-associated, and the formation of compact granulomas. Curiously, the intermediate and higher concentrations of liposomes did not modulate the immune response against fungal infection.

Our first hypothesis focused on the physical-chemical characteristics of liposomes, with intermediate and higher concentrations, whether these characteristics could increase responsiveness of the cells of the immune system. However, the analysis of diameter size and Pdi are associated with efficacy of liposomes and delivery systems. For better uptake of liposomes by antigen-presenting cells (APCs), the size of the liposome can vary between 500 to 1000 nm [57], in our study all the liposomes were approximately 650 nm (Table 1). The Pdi of liposomes indicated values within of parameters between 0.3 and 0.4. For a population to be considered homogeneous, Pdi values of 0.3 or less are required [41,43–45].

Then, we formulated the hypothesis that the amount of peptide in these formulations might not be enough to prime the dendritic cells and modulate the immune response. The rate of phagocytosis is dependent on the concentration of the liposome [58]. A study carried out by Allen 1991 [59] with mouse bone marrow-derived macrophages demonstrated that the uptake of liposomes by macrophages is greater with higher concentrations of the liposome [58,59]. These data were corroborated by Bose 2015 [60], who studied the influence of cationic lipid concentration (DOTAP) on the formation of nanospheres, and their uptake in vitro by HeLa cells, the increase in DOTAP concentration (from 6% to 24%) revealed a higher uptake rate cells (>85%). We hypothesize these concentrations of liposomes, intermediate and higher, of DDA/TDB, could require higher amounts of antigen to modulate immune response similar to the low concentration of liposome. As mentioned above, the amount of peptide used in this work was based on other works of our group [12,46] and indicated that 20 µg of the peptide was sufficient to elicit a protective immune response against PCM in those conditions. So, we hypothesize that lower concentrations of cationic liposome such as 62.5/25 µg/mL with 20 µg of P10, or less, could also modulate a protective immune response.

Once the liposomes of higher concentrations of DDA/TDB did not help in the modulation of immune response, we prioritize the DDA/TDB 250/50 µg/mL formulation to investigate the effect of the adsorption of peptide to liposome by adsorption efficiency. The P10 peptide was efficiently adsorbed onto DDA/TDB 250/50 µg/mL liposome with a rate higher than 80%. It is important to remember that the degree of adsorption depends on electrostatic forces between components (antigen and liposome). Antigens with an isoelectric point (pI) below 7.4 have a higher rate of adsorption when compared with protein antigens with pI above 7.4 [61–63]. The cationic characteristic of P10 peptide (pI = 9.95) (isoelectric.org) could lead to difficulties with adsorption onto liposomes. However, the process of

adsorption can be influenced by other features besides pI, like distribution of charge and flexibility of antigen, pH, ionic forces and composition of buffer [61].

Interestingly, the association of the P10 to the DDA/TDB induced an increase in the levels of IL-17A cytokine, while the levels of IL-6 cytokine did not change. However, the level of IL-6 cytokine was significantly increased in the mice group vaccinated with liposome alone. The cytokine IL-17A has the function of inducing granulopoiesis, inflammatory response, recruiting neutrophils, inducing fungicidal activity, inducing microbial peptides such as S100A7, S100A8 [64–67], and promotion of resistance to infection [68–70]. The Th₁₇ response induced by vaccination has been pointed out as particularly positively impactful in several studies with vaccine candidates against fungal infection. The importance of the Th₁₇ response has been demonstrated in a study of vaccination against three species of dimorphic fungi (*Coccidioides posadasii*, *Histoplasma capsulatum*, and *Blastomyces dermatitidis*) [71]. The Th₁₇ response was evaluated by neutralization of IL-17A with monoclonal antibodies, blocking of IL-17A with adenovirus overexpressing IL-17R: soluble Fc, and vaccination of knockout mice for the receptor by IL-17A (IL-17AR). In all experiments, the animals failed to generate resistance against infection by dimorphic fungi [71], underscoring the importance of the Th₁₇ response. In our study, the protective antifungal response induced by IL-17A led to a decrease in the fungal load of mice vaccinated with P10 plus liposome, probably due to the increased inflammatory cells demonstrated by lung histology.

Many cell types can produce IL-6 [72,73], and the association of IL-6 plus TGF- β cytokines is important for the induction of transcription factor ROR γ -t, which induces the differentiation of Th₁₇ cells [72,74,75]. Indeed, DDA/TDB induces potent CD4 Th₁ and Th₁₇ responses [31]. In this work, the rise of levels of cytokine IL-17 occurred without the concomitant rise of IL-6. One hypothesis is that the production of IL-6 cytokine may have occurred at earlier events or may have been consumed during Th₁₇ differentiation.

The reduction in the fungal load in the lungs of animals infected with *P. brasiliensis* and vaccinated with DDA/TDB/P10 was consistent with the increase in the level of IL-17A cytokine and decrease in IL-4 level. In tuberculosis and PCM, an effective CD4 T cell response was essential to control the diseases [76,77]. A prophylactic vaccine (started after 30 days of mice infection) with P10 in the presence of Complete Freund's Adjuvant in combination with simultaneous treatment with Trimethoprim-Sulfamethoxazole enhanced the efficacy of vaccination [46]. Also, the discontinuation of drug treatment in the group of vaccinated mice demonstrated that the immunological state of the mice was effective in preventing relapses [46]. In our current work, we show that DDA/TDB 250/50 μ g/P10-20 μ g generates an immunological response that leads to a significant reduction in the pulmonary fungal load, which did not occur in animals that received DDA/TDB only.

Granulomatous lesions are important structures in host defense against fungi [78]. This immune reaction functions to restrict the spread of the pathogen and this protective innate immune response is impaired in several forms of immune deficiencies such as HIV or due to drugs like prednisone [79]. Overall, our data are in agreement with studies carried out with knockout animals for IL-6 and IL-17 cytokines in an experimental PCM model, where it was demonstrated that the absence of these cytokines led to the formation of loose and poorly structured granulomas [78]. Moreover, the number of viable fungal cells in granulomas increased with increasing liposome concentrations, highlighting the failure to generate a protective immune response in these groups.

In our study, infected and untreated mice did not effectively form granuloma, whereas mice vaccinated with DDA/TDB alone or DDA/TDB 250/50 μ g/mL with P10-20 μ g developed well-delimited granuloma containing yeast cells. In particular, vaccination with DDA/TDB/P10 led to the formation of well structured, compact granuloma with the presence of cell infiltrates, showing that treatment was effective in producing a satisfactory response, and recruitment of cells of immune system to infection site.

5. Conclusions

Overall, our data suggest that the use of P10 peptide adsorbed onto the cationic liposome DDA/TDB (CAF01) maintains the immunomodulatory properties of DDA/TDB and the DDA/TDB 250/50 µg/P10-20 µg therapeutic vaccine markedly enhances the antifungal potency of the host response against *P. brasiliensis*. These data support ongoing efforts to translate a P10 vaccine from the bench to the bedside.

Author Contributions: Conceptualization, M.V.d.A., C.P.T.; formal analysis, M.V.d.A., funding acquisition, C.P.T.; investigation, M.V.d.A. and S.R.D.S.J.; methodology, M.V.d.A. and S.R.D.S.J.; supervision, C.P.T.; writing—original draft, M.V.d.A.; writing—review and editing, M.V.d.A., C.P.T. and J.D.N. All authors have read and agreed to the published version of the manuscript.

Funding: This research was funded by Fundação de Amparo à Pesquisa do Estado de São Paulo (FAPESP 2016/08730-6), Conselho Nacional de Desenvolvimento Científico e Tecnológico (CNPq 420480/2018-8 and 134424/2016-6) and Coordenação de Aperfeiçoamento de Pessoal de Nível Superior—Brasil (CAPES).

Conflicts of Interest: There are no conflict of interest to declare.

References

1. Souza, A.C.O.; Taborda, C.P. Epidemiology of Dimorphic Fungi. In *Reference Module in Life Sciences*; Elsevier BV: Amsterdam, The Netherlands, 2020.
2. Shikanai-Yasuda, M.A.; Mendes, P.R.; Colombo, A.L.; De Queiroz-Telles, F.; Kono, A.S.G.; Paniago, A.M.M.; Nathan, A.; Valle, A.C.F.D.; Bagagli, E.; Benard, G.; et al. Brazilian guidelines for the clinical management of paracoccidioidomycosis. *Rev. Soc. Bras. Med. Trop.* **2017**, *50*, 715–740. [[CrossRef](#)] [[PubMed](#)]
3. Turissini, D.A.; Gomez, O.M.; Teixeira, M.M.; McEwen, J.G.; Matute, D.R. Species boundaries in the human pathogen *Paracoccidioides*. *Fungal Genet. Biol.* **2017**, *106*, 9–25. [[CrossRef](#)] [[PubMed](#)]
4. Teixeira, M.D.M.; Theodoro, R.C.; De Oliveira, F.F.M.; Machado, G.C.; Hahn, R.C.; Bagagli, E.; San-Blas, G.; Felipe, M.S. *Paracoccidioides lutzii* sp. nov.: Biological and clinical implications. *Med. Mycol.* **2013**, *52*, 1–10. [[CrossRef](#)] [[PubMed](#)]
5. Matute, D.R.; McEwen, J.G.; Puccia, R.; Montes, B.A.; San-Blas, G.; Bagagli, E.; Rauscher, J.T.; Restrepo, A.; Morais, F.; Nino-Vega, G.; et al. Cryptic Speciation and Recombination in the Fungus *Paracoccidioides brasiliensis* as Revealed by Gene Genealogies. *Mol. Biol. Evol.* **2006**, *23*, 65–73. [[CrossRef](#)]
6. Teixeira, M.D.M.; Theodoro, R.C.; De Carvalho, M.J.; Fernandes, L.; Paes, H.C.; Hahn, R.C.; Mendoza, L.; Bagagli, E.; San-Blas, G.; Felipe, M.S.S. Phylogenetic analysis reveals a high level of speciation in the *Paracoccidioides* genus. *Mol. Phylogenet. Evol.* **2009**, *52*, 273–283. [[CrossRef](#)]
7. Teixeira, M.D.M.; Theodoro, R.C.; Derengowski, L.D.S.; Nicola, A.M.; Bagagli, E.; Felipe, M.S. Molecular and Morphological Data Support the Existence of a Sexual Cycle in Species of the Genus *Paracoccidioides*. *Eukaryot. Cell* **2013**, *12*, 380–389. [[CrossRef](#)]
8. Theodoro, R.C.; Teixeira, M.D.M.; Felipe, M.S.S.; Paduan, K.D.S.; Ribolla, P.M.; San-Blas, G.; Bagagli, E. Genus *Paracoccidioides*: Species Recognition and Biogeographic Aspects. *PLoS ONE* **2012**, *7*, e37694. [[CrossRef](#)]
9. Tobon, A.M.; Agudelo, C.A.; Osorio, M.L.; Alvarez, D.L.; Arango, M.; Cano, L.E.; Restrepo, A. Residual Pulmonary Abnormalities in Adult Patients with Chronic *Paracoccidioidomycosis*: Prolonged Follow-Up after Itraconazole Therapy. *Clin. Infect. Dis.* **2003**, *37*, 898–904. [[CrossRef](#)]
10. Travassos, L.R.; Taborda, C.P. Linear Epitopes of *Paracoccidioides brasiliensis* and Other Fungal Agents of Human Systemic Mycoses as Vaccine Candidates. *Front. Immunol.* **2017**, *8*, 224. [[CrossRef](#)]
11. Rossi, S.A.; De Araujo, M.V.; Taira, C.L.; Travassos, L.R.; Taborda, C.P. Vaccine Development to Systemic Mycoses by Thermally Dimorphic Fungi. *Curr. Trop. Med. Rep.* **2019**, *6*, 64–75. [[CrossRef](#)]
12. Taborda, C.P.; Juliano, M.A.; Puccia, R.; Franco, M.; Travassos, L.R. Mapping of the T-Cell Epitope in the Major 43-Kilodalton Glycoprotein of *Paracoccidioides brasiliensis* Which Induces a Th-1 Response Protective against Fungal Infection in BALB/c Mice. *Infect. Immun.* **1998**, *66*, 786–793. [[CrossRef](#)] [[PubMed](#)]
13. Puccia, R.; Travassos, L.R. The 43-kDa glycoprotein from the human pathogen *Paracoccidioides brasiliensis* and its deglycosylated form: Excretion and susceptibility to proteolysis. *Arch. Biochem. Biophys.* **1991**, *289*, 298–302. [[CrossRef](#)]

14. Da Silva, S.H.M.; Colombo, A.L.; Blotta, M.H.S.L.; Lopes, J.D.; Queiroz-Telles, F.; De Camargo, Z.P. Detection of Circulating gp43 Antigen in Serum, Cerebrospinal Fluid, and Bronchoalveolar Lavage Fluid of Patients with Paracoccidioidomycosis. *J. Clin. Microbiol.* **2003**, *41*, 3675–3680. [[CrossRef](#)]
15. De Camargo, Z.; Unterkircher, C.; Campoy, S.P.; Travassos, L.R. Production of Paracoccidioides brasiliensis exoantigens for immunodiffusion tests. *J. Clin. Microbiol.* **1988**, *26*, 2147–2151. [[CrossRef](#)] [[PubMed](#)]
16. Jr, N.P.L.; Vallejo, M.C.; Conceição, P.M.; Camargo, Z.P.; Hahn, R.; Puccia, R. Paracoccidioides lutzii Plp43 Is an Active Glucanase with Partial Antigenic Identity with P. brasiliensis gp43. *PLoS Negl. Trop. Dis.* **2014**, *8*, e3111. [[CrossRef](#)]
17. Emayorga, O.; Muñoz, J.E.; Lincopan, N.; Teixeira, A.F.; Ferreira, L.C.D.S.; Travassos, L.R.; Tabora, C.P. The role of adjuvants in therapeutic protection against paracoccidioidomycosis after immunization with the P10 peptide. *Front. Microbiol.* **2012**, *3*, 154. [[CrossRef](#)]
18. Li, W.; Joshi, M.D.; Singhanian, S.; Ramsey, K.H.; Murthy, A.K. Peptide Vaccine: Progress and Challenges. *Vaccines* **2014**, *2*, 515–536. [[CrossRef](#)]
19. Barnier-Quer, C.; Elsharkawy, A.; Romeijn, S.; Kros, A.; Jiskoot, W. Adjuvant Effect of Cationic Liposomes for Subunit Influenza Vaccine: Influence of Antigen Loading Method, Cholesterol and Immune Modulators. *Pharmaceutics* **2013**, *5*, 392–410. [[CrossRef](#)]
20. Souza, A.C.O.; Amaral, A.C. Antifungal Therapy for Systemic Mycosis and the Nanobiotechnology Era: Improving Efficacy, Biodistribution and Toxicity. *Front. Microbiol.* **2017**, *8*, 336. [[CrossRef](#)]
21. Christensen, D.; Korsholm, K.S.; Andersen, P.; Agger, E.M. Cationic liposomes as vaccine adjuvants. *Expert Rev. Vaccines* **2011**, *10*, 513–521. [[CrossRef](#)]
22. Hunter, R.; Olsen, M.; Jagannath, C.; Actor, J.K. Trehalose 6,6'-Dimycolate and Lipid in the Pathogenesis of Caseating Granulomas of Tuberculosis in Mice. *Am. J. Pathol.* **2006**, *168*, 1249–1261. [[CrossRef](#)] [[PubMed](#)]
23. Hunter, R.L.; Olsen, M.R.; Jagannath, C.; Actor, J.K. Multiple roles of cord factor in the pathogenesis of primary, secondary, and cavitary tuberculosis, including a revised description of the pathology of secondary disease. *Ann. Clin. Lab. Sci.* **2006**, *36*, 371–386. [[PubMed](#)]
24. Hunter, R.L.; Venkataprasad, N.; Olsen, M.R. The role of trehalose dimycolate (cord factor) on morphology of virulent M. tuberculosis in vitro. *Tuberculosis* **2006**, *86*, 349–356. [[CrossRef](#)] [[PubMed](#)]
25. Christensen, D. Development and Evaluation of CAF01. In *Immunopotentiators in Modern Vaccines*; Elsevier BV: Amsterdam, The Netherlands, 2017; pp. 333–345.
26. Henriksen-Lacey, M.; Devitt, A.; Perrie, Y. The vesicle size of DDA:TDB liposomal adjuvants plays a role in the cell-mediated immune response but has no significant effect on antibody production. *J. Control. Release* **2011**, *154*, 131–137. [[CrossRef](#)]
27. Sakurai, T.; Saiki, I.; Ishida, H.; Takeda, K.; Azuma, I. Lethal toxicity and adjuvant activities of synthetic TDM and its related compounds in mice. *Vaccine* **1989**, *7*, 269–274. [[CrossRef](#)]
28. Desel, C.; Werninghaus, K.; Ritter, M.; Jozefowski, K.; Wenzel, J.; Russkamp, N.; Schleicher, U.; Christensen, D.; Wirtz, S.; Kirschning, C.; et al. The Mincle-Activating Adjuvant TDB Induces MyD88-Dependent Th1 and Th17 Responses through IL-1R Signaling. *PLoS ONE* **2013**, *8*, e53531. [[CrossRef](#)]
29. Nordly, P.; Rose, F.; Christensen, D.; Nielsen, H.M.; Andersen, P.; Agger, E.M.; Foged, C. Immunity by formulation design: Induction of high CD8+ T-cell responses by poly(I:C) incorporated into the CAF01 adjuvant via a double emulsion method. *J. Control. Release* **2011**, *150*, 307–317. [[CrossRef](#)] [[PubMed](#)]
30. Werninghaus, K.; Babiak, A.; Groß, O.; Hölscher, C.; Dietrich, H.; Agger, E.M. Adjuvant activity of a synthetic cord factor analogue for subunit Mycobacterium tuberculosis vaccination requires FcRγ-Syk-Card9-dependent innate immune activation. *J. Exp. Med.* **2009**, *206*, 89–97. [[CrossRef](#)] [[PubMed](#)]
31. Pedersen, G.K.; Andersen, P.; Christensen, D. Immunocorrelates of CAF family adjuvants. *Semin. Immunol.* **2018**, *39*, 4–13. [[CrossRef](#)] [[PubMed](#)]
32. Van Dissel, J.T.; Joosten, S.A.; Hoff, S.T.; Soonawala, D.; Prins, C.; Hokey, D.A.; O'Dee, D.M.; Graves, A.J.; Thierry-Carstensen, B.; Andreasen, L.V.; et al. A novel liposomal adjuvant system, CAF01, promotes long-lived Mycobacterium tuberculosis-specific T-cell responses in human. *Vaccine* **2014**, *32*, 7098–7107. [[CrossRef](#)]
33. Lincopan, N.; Espíndola, N.M.; Vaz, A.J.; Da Costa, M.H.B.; Faquim-Mauro, E.L.; Carmona-Ribeiro, A.M. Novel immunoadjuvants based on cationic lipid: Preparation, characterization and activity in vivo. *Vaccine* **2009**, *27*, 5760–5771. [[CrossRef](#)] [[PubMed](#)]

34. Feitosa, E.; Barreleiro, P.; Olofsson, G. Phase transition in dioctadecyldimethylammonium bromide and chloride vesicles prepared by different methods. *Chem. Phys. Lipids* **2000**, *105*, 201–213. [[CrossRef](#)]
35. Davidsen, J.; Rosenkrands, I.; Christensen, D.; Vangala, A.; Kirby, D.; Perrie, Y.; Agger, E.M.; Andersen, P. Characterization of cationic liposomes based on dimethyldioctadecylammonium and synthetic cord factor from *M. tuberculosis* (trehalose 6,6'-dibehenate)—A novel adjuvant inducing both strong CMI and antibody responses. *Biochim. Biophys. Acta Biomembr.* **2005**, *1718*, 22–31. [[CrossRef](#)] [[PubMed](#)]
36. Hussain, M.J.; Wilkinson, A.; Bramwell, V.W.; Christensen, D.; Perrie, Y. Th1 immune responses can be modulated by varying dimethyldioctadecylammonium and distearoyl-sn-glycero-3-phosphocholine content in liposomal adjuvants. *J. Pharm. Pharmacol.* **2014**, *66*, 358–366. [[CrossRef](#)]
37. Wang, N.; Chen, M.; Wang, T. Liposomes used as a vaccine adjuvant-delivery system: From basics to clinical immunization. *J. Control. Release* **2019**, *303*, 130–150. [[CrossRef](#)]
38. Qu, W.; Li, N.; Yu, R.; Zuo, W.; Fu, T.; Fei, W.; Hou, Y.; Liu, Y.; Yang, J. Cationic DDA/TDB liposome as a mucosal vaccine adjuvant for uptake by dendritic cells in vitro induces potent humoral immunity. *Artif. Cells Nanomed. Biotechnol.* **2018**, *46*, 852–860. [[CrossRef](#)]
39. Singer-Vermes, L.M.; Burger, E.; Franco, M.F.; Di-Bacchi, M.M.; Mendes-Giannini, M.J.; Calich, V.L. Evaluation of the pathogenicity and immunogenicity of seven *Paracoccidioides brasiliensis* isolates in susceptible inbred mice. *J. Med. Veter. Mycol.* **1989**, *27*, 71–82. [[CrossRef](#)]
40. Muñoz, J.E.; Luft, V.D.; Amorim, J.; Magalhães, A.; Thomaz, L.; Nosanchuk, J.D.; Travassos, L.R.; Tabora, C.P. Immunization with P10 Peptide Increases Specific Immunity and Protects Immunosuppressed BALB/c Mice Infected with Virulent Yeasts of *Paracoccidioides brasiliensis*. *Mycopathologia* **2014**, *178*, 177–188. [[CrossRef](#)]
41. Danaei, M.; Dehghankhold, M.; Ataei, S.; Davarani, F.H.; Javanmard, R.; Dokhani, A.; Khorasani, S.; Mozafari, M. Impact of Particle Size and Polydispersity Index on the Clinical Applications of Lipidic Nanocarrier Systems. *Pharmaceutics* **2018**, *10*, 57. [[CrossRef](#)]
42. Clayton, K.N.; Salameh, J.W.; Wereley, S.T.; Kinzer-Ursem, T.L. Physical characterization of nanoparticle size and surface modification using particle scattering diffusometry. *Biomicrofluidics* **2016**, *10*, 054107. [[CrossRef](#)]
43. Badran, M. Formulation and in vitro evaluation of flufenamic acid loaded deformable liposomes for improved skin delivery. *Dig. J. Nanomater. Biostructures* **2014**, *9*, 83–91.
44. Chen, M.; Liu, X.; Fahr, A. Skin penetration and deposition of carboxyfluorescein and temoporfin from different lipid vesicular systems: In vitro study with finite and infinite dosage application. *Int. J. Pharm.* **2011**, *408*, 223–234. [[CrossRef](#)] [[PubMed](#)]
45. Putri, D.C.A.; Dwiastuti, R.; Marchaban, M.; Nugroho, A.K. Optimization of mixing temperature and sonication duration in liposome preparation. *J. Pharm. Sci. Commun.* **2017**, *14*, 79–85. [[CrossRef](#)]
46. Marques, A.F.; Da Silva, M.B.; Juliano, M.A.P.; Travassos, L.R.; Tabora, C.P. Peptide Immunization as an Adjuvant to Chemotherapy in Mice Challenged Intratracheally with Virulent Yeast Cells of *Paracoccidioides brasiliensis*. *Antimicrob. Agents Chemother.* **2006**, *50*, 2814–2819. [[CrossRef](#)] [[PubMed](#)]
47. Abeyratne, E.; Tharmarajah, K.; Freitas, J.R.; Mostafavi, H.; Mahalingam, S.; Zaid, A.; Zaman, M.; Taylor, A. Liposomal Delivery of the RNA Genome of a Live-Attenuated Chikungunya Virus Vaccine Candidate Provides Local, but Not Systemic Protection After One Dose. *Front. Immunol.* **2020**, *11*. [[CrossRef](#)]
48. Rosenkrands, I.; Vingsbo-Lundberg, C.; Bundgaard, T.J.; Lindenstrøm, T.; Enouf, V.; Van Der Werf, S.; Andersen, P.; Agger, E.M. Enhanced humoral and cell-mediated immune responses after immunization with trivalent influenza vaccine adjuvanted with cationic liposomes. *Vaccine* **2011**, *29*, 6283–6291. [[CrossRef](#)]
49. Nguyen, N.D.N.T.; Olsen, A.W.; Lorenzen, E.; Andersen, P.; Hvid, M.; Follmann, F.; Dietrich, J. Parenteral vaccination protects against transcervical infection with *Chlamydia trachomatis* and generate tissue-resident T cells post-challenge. *NPJ Vaccines* **2020**, *5*, 7–12. [[CrossRef](#)] [[PubMed](#)]
50. Riccomi, A.; Piccaro, G.; Christensen, D.; Palma, C.; Andersen, P.; Vendetti, S. Parenteral Vaccination with a Tuberculosis Subunit Vaccine in Presence of Retinoic Acid Provides Early but Transient Protection to *M. Tuberculosis* Infection. *Front. Immunol.* **2019**, *10*. [[CrossRef](#)]
51. Woodworth, J.S.; Christensen, D.; Cassidy, J.P.; Agger, E.M.; Mortensen, R.; Andersen, P. Mucosal boosting of H56:CAF01 immunization promotes lung-localized T cells and an accelerated pulmonary response to *Mycobacterium tuberculosis* infection without enhancing vaccine protection. *Mucosal Immunol.* **2019**, *12*, 816–826. [[CrossRef](#)]

52. Dejon-Agobe, J.C.; Ateba-Ngoa, U.; Lalremruata, A.; Homoet, A.; Engelhorn, J.; Nouatin, O.P.; Edoa, J.R.; Fernandes, J.F.; Esen, M.; Mouwenda, Y.D.; et al. Controlled Human Malaria Infection of Healthy Adults with Lifelong Malaria Exposure to Assess Safety, Immunogenicity, and Efficacy of the Asexual Blood Stage Malaria Vaccine Candidate GMZ2. *Clin. Infect. Dis.* **2019**, *69*, 1377–1384. [[CrossRef](#)]
53. Mortensen, R.; Christensen, D.; Hansen, L.B.; Christensen, J.P.; Andersen, P.; Dietrich, J. Local Th17/IgA immunity correlate with protection against intranasal infection with *Streptococcus pyogenes*. *PLoS ONE* **2017**, *12*, e0175707. [[CrossRef](#)]
54. Travassos, L.R.; Taborda, C.P.; Colombo, A.L. Treatment options for paracoccidioidomycosis and new strategies investigated. *Expert Rev. Anti-Infect. Ther.* **2008**, *6*, 251–262. [[CrossRef](#)]
55. Brewer, J.M.; Tetley, L.; Richmond, J.; Liew, F.Y.; Alexander, J. Lipid vesicle size determines the Th1 or Th2 response to entrapped antigen. *J. Immunol.* **1998**, *161*, 4000–4007. [[PubMed](#)]
56. Mann, J.F.S.; Shakir, E.; Carter, K.C.; Mullen, A.B.; Alexander, J.; Ferro, V.A. Lipid vesicle size of an oral influenza vaccine delivery vehicle influences the Th1/Th2 bias in the immune response and protection against infection. *Vaccine* **2009**, *27*, 3643–3649. [[CrossRef](#)]
57. Bachmann, M.F.; Jennings, G.T. Vaccine delivery: A matter of size, geometry, kinetics and molecular patterns. *Nat. Rev. Immunol.* **2010**, *10*, 787–796. [[CrossRef](#)] [[PubMed](#)]
58. Ahsan, F. Targeting to macrophages: Role of physicochemical properties of particulate carriers—liposomes and microspheres—on the phagocytosis by macrophages. *J. Control. Release* **2002**, *79*, 29–40. [[CrossRef](#)]
59. Allen, T.; Austin, G.; Chonn, A.; Lin, L.; Lee, K. Uptake of liposomes by cultured mouse bone marrow macrophages: Influence of liposome composition and size. *Biochim. Biophys. Acta Biomembr.* **1991**, *1061*, 56–64. [[CrossRef](#)]
60. Park, H.; Lee, S.-H.; Ahn, J.C.; Rajendiran, J.C.B.; Arai, Y. Influence of cationic lipid concentration on properties of lipid–polymer hybrid nanospheres for gene delivery. *Int. J. Nanomed.* **2015**, *10*, 5367. [[CrossRef](#)]
61. Hamborg, M.; Jorgensen, L.; Bojsen, A.R.; Christensen, D.; Foged, C. Protein Antigen Adsorption to the DDA/TDB Liposomal Adjuvant: Effect on Protein Structure, Stability, and Liposome Physicochemical Characteristics. *Pharm. Res.* **2013**, *30*, 140–155. [[CrossRef](#)]
62. Hamborg, M.; Rose, F.; Jorgensen, L.; Bjorklund, K.; Pedersen, H.B.; Christensen, D.; Foged, C. Elucidating the mechanisms of protein antigen adsorption to the CAF/NAF liposomal vaccine adjuvant systems: Effect of charge, fluidity and antigen-to-lipid ratio. *Biochim. Biophys. Acta Biomembr.* **2014**, *1838*, 2001–2010. [[CrossRef](#)]
63. Schmidt, S.T.; Foged, C.; Korsholm, K.S.; Rades, T.; Christensen, D. Liposome-Based Adjuvants for Subunit Vaccines: Formulation Strategies for Subunit Antigens and Immunostimulators. *Pharmaceutics* **2016**, *8*, 7. [[CrossRef](#)] [[PubMed](#)]
64. Chan, Y.R.; Liu, J.S.; Pociask, D.A.; Zheng, M.; Mietzner, T.A.; Berger, T.; Mak, T.W.; Clifton, M.C.; Strong, R.K.; Ray, P.; et al. Lipocalin 2 Is Required for Pulmonary Host Defense against *Klebsiella* Infection. *J. Immunol.* **2009**, *182*, 4947–4956. [[CrossRef](#)]
65. Ferreira, M.C.; Whibley, N.; Mamo, A.J.; Siebenlist, U.; Chan, Y.R.; Gaffen, S.L. Interleukin-17-Induced Protein Lipocalin 2 Is Dispensable for Immunity to Oral Candidiasis. *Infect. Immun.* **2013**, *82*, 1030–1035. [[CrossRef](#)] [[PubMed](#)]
66. Liang, S.C.; Tan, X.-Y.; Luxenberg, D.P.; Karim, R.; Dunussi-Joannopoulos, K.; Collins, M.; Fouser, L.A. Interleukin (IL)-22 and IL-17 are coexpressed by Th17 cells and cooperatively enhance expression of antimicrobial peptides. *J. Exp. Med.* **2006**, *203*, 2271–2279. [[CrossRef](#)] [[PubMed](#)]
67. Jiang, S. Immunity against Fungal Infections. *Immunol. Immunogenet. Insights* **2016**, *8*, S38707. [[CrossRef](#)]
68. Romani, L. Immunity to fungal infections. *Nat. Rev. Immunol.* **2011**, *11*, 275–288. [[CrossRef](#)]
69. Hernández-Santos, N.; Gaffen, S.L. Th17 Cells in Immunity to *Candida albicans*. *Cell Host Microbe* **2012**, *11*, 425–435. [[CrossRef](#)]
70. Perez-Nazario, N.; Rangel-Moreno, J.; O'Reilly, M.A.; Pasparakis, M.; Gigliotti, F.; Wright, T.W. Selective Ablation of Lung Epithelial IKK2 Impairs Pulmonary Th17 Responses and Delays the Clearance of *Pneumocystis*. *J. Immunol.* **2013**, *191*, 4720–4730. [[CrossRef](#)]
71. Wüthrich, M.; Gern, B.; Hung, C.Y.; Ersland, K.; Rocco, N.; Pick-Jacobs, J. Vaccine-induced protection against 3 systemic mycoses endemic to North America requires Th17 cells in mice. *J. Clin. Investig.* **2011**, *121*, 554–568. [[CrossRef](#)]
72. Kim, J.S.; Jordan, M.S. Diversity of IL-17-producing T lymphocytes. *Cell. Mol. Life Sci.* **2012**, *70*, 2271–2290. [[CrossRef](#)]

73. Taga, T.; Kishimoto, T. Gp 130 and the interleukin-6 family of cytokines. *Annu. Rev. Immunol.* **1997**, *15*, 797–819. [[CrossRef](#)]
74. Yang, X.O.; Pappu, B.P.; Nurieva, R.; Akimzhanov, A.; Kang, H.S.; Chung, Y.; Ma, L.; Shah, B.; Panopoulos, A.D.; Schluns, K.S.; et al. T Helper 17 Lineage Differentiation Is Programmed by Orphan Nuclear Receptors ROR α and ROR γ . *Immunity* **2008**, *28*, 29–39. [[CrossRef](#)]
75. Yang, X.O.; Panopoulos, A.D.; Nurieva, R.; Chang, S.H.; Wang, D.; Watowich, S.S.; Dong, C. STAT3 Regulates Cytokine-mediated Generation of Inflammatory Helper T Cells. *J. Biol. Chem.* **2007**, *282*, 9358–9363. [[CrossRef](#)] [[PubMed](#)]
76. Taborda, C.P.; Travassos, L.R. Peptide Vaccine Against Paracoccidioidomycosis. In *Methods in Molecular Biology*; Springer Science, Business Media, LLC: Berlin/Heidelberg, Germany, 2017; Volume 1625, pp. 113–128.
77. Woodworth, J.S.; Aagaard, C.S.; Hansen, P.R.; Cassidy, J.P.; Agger, E.M.; Andersen, P. Protective CD4 T Cells Targeting Cryptic Epitopes of Mycobacterium tuberculosis Resist Infection-Driven Terminal Differentiation. *J. Immunol.* **2014**, *192*, 3247–3258. [[CrossRef](#)]
78. Tristão, F.S.M.; Rocha, F.A.; Carlos, D.; Ketelut-Carneiro, N.; Souza, C.O.S.; Milanezi, C.M.; Silva, J.S. Th17-Inducing Cytokines IL-6 and IL-23 Are Crucial for Granuloma Formation during Experimental Paracoccidioidomycosis. *Front. Immunol.* **2017**, *8*, 949. [[CrossRef](#)]
79. Petersen, H.J.; Smith, A.M. The Role of the Innate Immune System in Granulomatous Disorders. *Front. Immunol.* **2013**, *4*, 120. [[CrossRef](#)]

Publisher’s Note: MDPI stays neutral with regard to jurisdictional claims in published maps and institutional affiliations.



© 2020 by the authors. Licensee MDPI, Basel, Switzerland. This article is an open access article distributed under the terms and conditions of the Creative Commons Attribution (CC BY) license (<http://creativecommons.org/licenses/by/4.0/>).



Therapies and Vaccines Based on Nanoparticles for the Treatment of Systemic Fungal Infections

Brenda Kischkel^{1,2*}, Suélen A. Rossi^{1,2}, Samuel R. Santos Junior^{1,2},
Joshua D. Nosanchuk³, Luiz R. Travassos⁴ and Carlos P. Taborda^{1,2*}

¹ Department of Microbiology, Institute of Biomedical Sciences, University of São Paulo, São Paulo, Brazil, ² Laboratory of Medical Mycology-Institute of Tropical Medicine of São Paulo/LIM53/Medical School, University of São Paulo, São Paulo, Brazil, ³ Departments of Medicine [Division of Infectious Diseases], Microbiology and Immunology, Albert Einstein College of Medicine and Montefiore Medical Center, Bronx, NY, United States, ⁴ Department of Microbiology, Immunology and Parasitology, Federal University of São Paulo, São Paulo, Brazil

OPEN ACCESS

Edited by:

James Bernard Konopka,
Stony Brook University, United States

Reviewed by:

Jose L. Lopez-Ribot,
University of Texas at San Antonio,
United States

Amir M. Farnoud,
Ohio University, United States

*Correspondence:

Brenda Kischkel
brendakischkel@usp.br
Carlos P. Taborda
taborda@usp.br

Specialty section:

This article was submitted to
Fungal Pathogenesis,
a section of the journal
Frontiers in Cellular and Infection
Microbiology

Received: 24 June 2020

Accepted: 28 July 2020

Published: 03 September 2020

Citation:

Kischkel B, Rossi SA,
Santos Junior SR, Nosanchuk JD,
Travassos LR and Taborda CP (2020)
Therapies and Vaccines Based on
Nanoparticles for the Treatment of
Systemic Fungal Infections.
Front. Cell. Infect. Microbiol. 10:463.
doi: 10.3389/fcimb.2020.00463

Treatment modalities for systemic mycoses are still limited. Currently, the main antifungal therapeutics include polyenes, azoles, and echinocandins. However, even in the setting of appropriate administration of antifungals, mortality rates remain unacceptably high. Moreover, antifungal therapy is expensive, treatment periods can range from weeks to years, and toxicity is also a serious concern. In recent years, the increased number of immunocompromised individuals has contributed to the high global incidence of systemic fungal infections. Given the high morbidity and mortality rates, the complexity of treatment strategies, drug toxicity, and the worldwide burden of disease, there is a need for new and efficient therapeutic means to combat invasive mycoses. One promising avenue that is actively being pursued is nanotechnology, to develop new antifungal therapies and efficient vaccines, since it allows for a targeted delivery of drugs and antigens, which can reduce toxicity and treatment costs. The goal of this review is to discuss studies using nanoparticles to develop new therapeutic options, including vaccination methods, to combat systemic mycoses caused by *Candida* sp., *Cryptococcus* sp., *Paracoccidioides* sp., *Histoplasma* sp., *Coccidioides* sp., and *Aspergillus* sp., in addition to providing important information on the use of different types of nanoparticles, nanocarriers and their corresponding mechanisms of action.

Keywords: drug delivery systems, vaccine adjuvant, antifungal therapy, mycosis, *Candida albicans*, *Cryptococcus* sp., *Histoplasma capsulatum*

INTRODUCTION

Fungal diseases are broadly classified according to the degree of interactions between the pathogen and the host tissue in superficial, subcutaneous, and systemic infections (Tiew et al., 2020). Superficial mycoses, which are estimated to occur in 25% of the world population, are the most common form of fungal infection. Systemic mycosis, however, is most severe since it is associated to a high mortality rate, significant morbidity, limited chemotherapeutic options, and the diagnosis is frequently difficult and complex (Kauffman, 2007; Brunet et al., 2018).

Opportunistic fungal infections usually occur in immunocompromised individuals as a result of subacute infection or the treatment itself. Infections of endogenous origin caused by pathogens such as *Candida albicans* can also occur (Colombo et al., 2017; Rautemaa-Richardson and Richardson, 2017). Species of *Aspergillus*, *Candida*, *Cryptococcus*, and *Trichosporon* are the main agents of opportunistic mycoses. Endemic fungal infections are usually caused by dimorphic fungi, found in the soil or in animal feces. Host acquisition occurs by inhalation of infectious spores/infective propagules (Rodríguez-Cerdeira et al., 2014). In the case of endemic mycoses, immunocompetent individuals dwelling in endemic areas may develop severe disease following inhalation of fungal particles, associated or not to a competent immune response (Edwards et al., 2013). The main species that cause endemic mycoses are *Blastomyces dermatitidis*, *Coccidioides immitis* and *Coccidioides posadasii*, *Histoplasma capsulatum*, *Paracoccidioides*, particularly *P. brasiliensis* and *P. lutzii*, *Sporothrix*, primarily *S. brasiliensis* and *S. schenckii*, and *Talaromyces marneffeii* (Brown et al., 2012; Limper et al., 2017).

In the second half of the 20th century, a worldwide, progressive increase in the number of immunocompromised individuals took place, paralleling the outcome of HIV epidemics as well as the expanded use of immunosuppressive drugs in cancer, autoimmune disease, and transplant patients (Coelho and Casadevall, 2016; Armstrong-James et al., 2017). As a consequence, systemic mycoses have been considered an emergent threat, because immunocompromised individuals are more susceptible to fungal infection (Lockhart, 2019). Cryptococcosis is an excellent example of the profound impact of fungal infections over time, in humans. The number of infections caused by *Cryptococcus* has increased from 300 cases in 1,950 to ~1 million cases in 2008 causing ~600,000 deaths per year in patients with HIV (Park et al., 2009; Del Poeta and Casadevall, 2012). Currently this number is closer to ~180,000 deaths annually (Rajasingham et al., 2017). Globally, the estimated number of deaths per year has been 6 million among invasive fungal infections (Stop neglecting fungi, 2017). In the case of invasive *Candida* and *Aspergillus* infections, the mortality rate could reach 60–80%, respectively (Perlroth et al., 2007; Moriyama et al., 2014). Bongomin et al. (2017) estimated the number of mycoses in the Leading International Fungal Education (LIFE) portal, which covers 80% of the world's population (5.7 billion people), and estimated that there occurred annually ~3,000,000 cases of pulmonary aspergillosis, ~250,000 of invasive aspergillosis, ~700,000 of invasive candidiasis, and ~500,000 of histoplasmosis of which ~100,000 were disseminated cases. The global estimate of *Paracoccidioides* and *Coccidioides* cases is 4,000 and 25,000, respectively. It must be emphasized that these are considered neglected diseases, therefore the number of reported cases can be an underestimate of the actual burden of the disease. In Brazil,

paracoccidioidomycosis (PCM) ranks as the 8th death causing infectious disease in patients without immunosuppression, surpassing histoplasmosis, or cryptococcosis in this group of patients. In fact, there is no compulsory notification of fungal infections in Brazil and the disease frequently occurs in rural and poor farmer populations. They frequently lack access to medical care, therefore the presumed incidence of the mycoses that differ from the real one (Shikanai-Yasuda and Mendes, 2007; Giacomazzi et al., 2016).

Fungal infections are often defined as difficult to treat, including the toxicity of antifungals and their interaction with other drugs (Westerberg and Voyack, 2013; Bicanic, 2014; Brunet et al., 2018). There is broad consensus that currently available antifungal therapy is limited and far from ideal (LaSenna and Tosti, 2015; Armstrong-James et al., 2017; Brunet et al., 2018). In the USA, fungal diseases may cost more than 7.0 billion dollars a year (Benedict et al., 2019), and the treatment of invasive fungal infections 70,000 dollars per patient (Ashley et al., 2012). Particularly in under resourced populations, the long periods and high costs of treatment contribute to patients abandoning their chemotherapy, when clinical symptoms may disappear, but are frequently followed by disease recurrences.

Systemic fungal infections are largely treated with polyenes, azoles or echinocandins, depending on the fungal pathogen and the clinical condition of the patient (Polvi et al., 2015; Souza and Amaral, 2017). The traditional antifungal agent is amphotericin B (AmB), a polyene with a broad spectrum of action, involving interaction with fungal ergosterol, destabilization of the cell membrane and, consequently, the death of the pathogen (Palacios et al., 2011). The drug interacts also with mammalian sterols, such as cholesterol, which can lead to treated patient collateral effects (Carmona and Limper, 2017). Azoles are widely prescribed against invasive fungal infections, mainly represented by fluconazole, voriconazole, itraconazole (ITZ), posaconazole, and isavuconazole (Gintjee et al., 2020). Azoles act by inhibiting lanosterol 14 α -demethylase (Erg11), which converts lanosterol into ergosterol (Di Mambro et al., 2019). Its activity is also associated to inhibition of cytochrome P450 with undesired side effects. Echinocandins, micafungin, caspofungin, and anidulafungin target, on the other hand, receptors that do not exist in human cells such as β (1,3)-D-glucan synthase, an enzyme responsible for the synthesis of β -1,3 glucan, a structural component of the fungal cell wall (Di Mambro et al., 2019). Such reactivity makes echinocandins more tolerable, with limited toxicity and drug interaction. However, a limited spectrum of action is exhibited toward certain yeasts and molds, with no activity against important opportunistic yeasts such as *Cryptococcus* sp. and dimorphic fungi (Lewis, 2011; Gintjee et al., 2020).

Azole resistance is well-recognized in *Aspergillus fumigatus*, *Cryptococcus neoformans*, *Coccidioides* spp., *H. capsulatum*, and *Candida* sp. (Wheat et al., 2001; Kriesel et al., 2008; Snelders et al., 2011; Vincent et al., 2013; Fontes et al., 2017). The resistance to azoles is mainly due to mutations in fungal DNA, which reduce the interactions between the drug and the cell target (Hagiwara et al., 2016). As examples, in *A. fumigatus* azole resistance mechanisms include the insertion of repeated

Abbreviations: AmB, Amphotericin B; ITZ, Itraconazole; NPs, nanoparticles; PLGA, Poly (lactic-co-glycolic acid); PEG, polyethylene glycol; NLCs, Nanostructured lipid carriers; SLNs, solid lipid Nanoparticles; PAMAM, poly (amidoamine); AgNPs, Silver nanoparticles; AuNPs, gold nanoparticles.

sequences in tandem into the *cyp51A* promoter, amino acid substitutions in the structure of the target Cyp51A protein, and overexpression of the ABC transporter Cdr1B (Hagiwara et al., 2016). Although rare, resistance to AmB can occur intrinsically or it may be induced. *Candida tropicalis* resists the action of AmB by reducing mitochondrial production of reactive oxygen species (ROS) (Vincent et al., 2013). In *Aspergillus terreus* the genes encoding catalase (CAT) and superoxide dismutase (SOD) are essential for intrinsic resistance, since the inhibition of these enzymes makes the isolates susceptible to treatment by the drug (Jukic et al., 2017). Low levels of β -1,3 glucan lead to the lack of efficacy of echinocandins against certain species, but resistance can also develop, primarily through hotspot mutations, such as changes in glucan synthase genes (Huang et al., 2016).

An intact immune system prevents the development of most invasive fungal infections. Hence, there is significant interest in stimulating the immune system to get a more effective response against pathogenic fungi primary or during treatment of the installed disease. Studies supported that therapeutic or prophylactic vaccines can stimulate the immune system in experimental mycosis models, even in immunosuppressed mice (Silva et al., 2017). The combination of vaccination and antifungal chemotherapy leads to improved treatment efficacy and reduction of treatment period, which would also potentially prevent relapses (Travassos and Taborda, 2017). Currently there is no licensed vaccine, prophylactic or therapeutic, to treat human systemic mycoses (Travassos and Taborda, 2017). Experimental vaccines have been developed for histoplasmosis, aspergillosis, candidiasis, cryptococcosis, coccidioidomycosis, and PCM (Brown et al., 2012), but none have progressed to market. Such delay is linked to a myriad of obstacles, which include lack of adequate formulation, high development costs, and lack of market interest (Cassone and Casadevall, 2012). In addition, the fact that some fungal diseases mainly affect immunocompromised individuals is an obstacle to the generation of an effective vaccine for this population. Currently, different research groups have focused on the development of a vaccine that can be used both in healthy patients and in immunodeficient ones or otherwise high-risk patients, providing protection without aggravating the patient's clinical condition (Spellberg, 2011; Cassone and Casadevall, 2012; Medici et al., 2015; Travassos and Taborda, 2017). Additionally, the identification of appropriate adjuvants has been a major obstacle for fungal vaccine development.

Nanotechnology is a field that has been widely explored as an innovative and low-cost strategy for the development of new antifungals and more efficient vaccines (Souza and Amaral, 2017). This application of nanotechnology in vaccine development has attracted the attention of researchers since nanotherapeutics can utilize low toxicity materials that allow for the slow and direct delivery of drugs and antigens to specific targets (Zhao et al., 2014). In relation to antifungal chemotherapy, nanoparticles (NPs) have been used due to their intrinsic antifungal activity or as a drug delivery vehicle with a focus on reducing the concentration of drug required for treatment (Zhao et al., 2014). In the formulation of vaccines, NPs can act as a delivery tool capable of improving the stability of antigens such as peptides and the immunogenicity of the

antigen, as well as possible immunostimulant adjuvants (Zhao et al., 2014).

In this review, we discuss the use of NPs in the development of new therapeutic approaches and vaccines against systemic mycoses, briefly commenting on the types of NPs used for this purpose and their mechanism of action. Finally, we present the current state of art of NPs for the development of new antifungal agents and vaccines aiming at systemic mycoses with a focus on *Candida* sp., *Cryptococcus* sp., *Paracoccidioides* sp., *Histoplasma* sp., *Coccidioides* sp., and *Aspergillus* sp..

NP AND THE DEVELOPMENT OF A NEW THERAPEUTIC APPROACH AND VACCINATION ALTERNATIVE

The treatment of systemic fungal infections has limitations since currently available antifungals exhibit low biodistribution and treatment effectiveness, with lack of selectivity, and serious side effects (Voltan et al., 2016). Nanotechnology appears as an alternative to these problems since NPs can function as a controlled and specific drug delivery system, which can improve mycosis treatment without impairing the patient's quality of life.

NPs can be obtained by physical, chemical, or biological methods. The synthetic process should consider constraints of large-scale production, stability, cost, and toxicity. Methodologies involving physical synthesis can be expensive, particularly due to the equipment used for electronic excitation (Haroon Anwar, 2018). Inorganic solvents used in the chemical reduction are highly toxic, including citrate, borohydride, thioglycerol, and 2-mercaptoethanol (Zhang X.-F. et al., 2016). The biological synthesis of NPs can significantly reduce the risk of producing toxic compounds by employing plant extracts, or bacterial and fungal metabolites with antimicrobial potential, acting as reducing agents, and/or stabilizers of NPs (Ahmed et al., 2018; Lakshmeesha et al., 2019). In addition to developing NPs appropriate for medical application, the nanoformulation is also essential since the efficacy of biological activity and cytotoxicity depends on the physicochemical properties exhibited by NPs, such as size, shape, surface area, solubility, aggregation, composition with coating reactivity of particles in solution, ion release efficiency, and type of the reducing agent used in the synthetic process (Carlson et al., 2008; Murdock et al., 2008; Lin et al., 2014).

NPs exhibit antimicrobial activity through different mechanisms. Nanometric particles can cross the cell interstitium and release metal ions from the surface of the NPs inside the cell, increasing the antimicrobial activity, due to their interaction with proteins, inhibiting their activity or causing damage to the cell wall, leading to pathogen death (Oberdörster et al., 2005; Reddy et al., 2012). Another mechanism of action is through oxidative stress, which can vary based on the specific chemical properties of the materials, such as the formation of surface groups that act as reactive sites. Active sites reacting with O₂ lead to the formation of ROS that increase tissue damage (Nel et al., 2006). Oxidation of fatty acid double bonds in cell membranes, may alter membrane permeability and increase the osmotic

stress resulting in cell death. In addition, ROS can damage the DNA, RNA, and proteins of the pathogen (Reddy et al., 2012; Huang et al., 2014; Rónavári et al., 2018; Rodrigues et al., 2019). Increased toxicity is inversely proportional to NPs size. Specifically, small NPs have a larger gravimetric specific surface area, which allows more molecules to be exposed for interaction and raising damage (Nel et al., 2006).

The antimicrobial activity of NPs against pathogens *in vitro* and *in vivo* has been extensively reported in the literature (Ambrosio et al., 2019; Lakshmeesha et al., 2019; Xue et al., 2019). Nanoformulations showing a broad spectrum of action by inhibiting the growth of different pathogens such as fungi, bacteria or viruses, such as silver NPs (AgNPs), have been described (Yah and Simate, 2015). Mohammed Fayaz et al. (2012) developed a method for coating polyurethane condoms with Ag and demonstrated that the product was able to inactivate HIV-1/2 and significantly inhibit the growth of bacteria (*Escherichia coli*, *Staphylococcus aureus*, *Micrococcus luteus*, and *Klebsiella pneumoniae*) and *Candida* (*C. tropicalis*, *C. krusei*, *C. glabrata*, and *C. albicans*). In addition, chitosan-carbon nanotube (Chitosan-CNT) hydrogels, exploited in medicine for dressing and drug administration applications, inhibited the growth of *S. aureus*, *E. coli*, and *C. tropicalis* (Venkatesan et al., 2014).

The ability to form a biofilm is an important virulence mechanism that microorganisms such as bacteria and fungi are able to build during infection, which is also associated with disease persistence as well as relapses (Wojtyczka et al., 2013; Sav et al., 2018). The antibiofilm activity of NPs has been studied and the potential of nanoformulations to disrupt these complex matrices have been reported (Khan et al., 2012; Gondim et al., 2018; Yang et al., 2019).

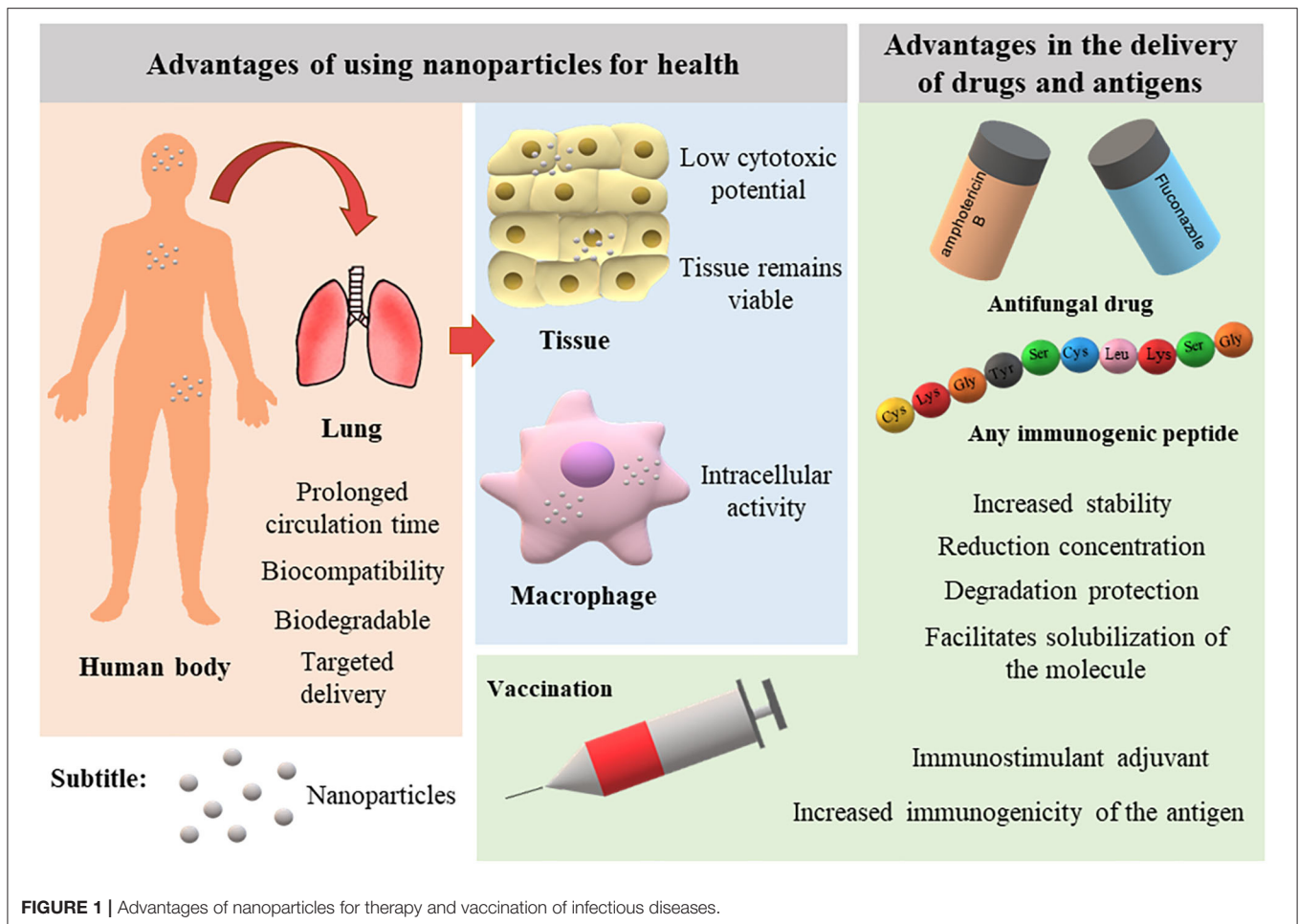
Nanotechnology effectively combat both extracellular and intracellular pathogens. In the case of extracellular pathogens, biocompatibility and the time spent in the bloodstream in adequate concentrations is essential for the successful treatment of systemic infections. Therapy for intracellular pathogens requires a more nuanced approach that includes the proper targeting of nanocarriers to infected cells through different ligands. In general, drugs targeting intracellular pathogens have to disrupt or transit the cell membrane and release and maintain the drug at the therapeutic level for the desired time inside the target cell. Certain nanocarriers enter the cell through endocytic mechanisms and remain stable within the endolysosomes until they gain access to the cytosol to release the drug. Otherwise, the release of the drug into the endolysosome could render it ineffective (Armstead and Li, 2011). The nanometric scale of particles allows for drug delivery into specific locations of the body, entering living cells to deliver drug or antigen payloads into macrophages and dendritic cells, which is particularly useful in the treatment of intracellular pathogens such as *H. capsulatum* (Couvreur, 2013; Dube et al., 2014). Dendritic cells are capable of absorbing particles of 20–200 nm, whereas particles of 0.5–5 μm are taken up by macrophages (Xiang et al., 2006). Receptors on these cells act, thus, to improve antigen processing and activate pathways that will enhance the immune response (Zhao et al., 2014). An example is β -1,3-glucan, a polysaccharide found in the cell wall of most fungi

that interacts directly with the Dectin-1 receptor present on the surface of macrophages (Brown et al., 2002). Activation of Dectin-1 enhances phagocytosis and consequently promote a greater absorption of NPs into macrophages (Goodridge et al., 2009). Several studies have validated that nanoparticles can target intracellular pathogens; however, most of these studies have targeted the bacterium *Mycobacterium tuberculosis* or the parasite *Leishmania brasiliensis* (Dube et al., 2014; Tukulula et al., 2015, 2018). Poly (lactic-co-glycolic acid) (PLGA) NPs made functional by β -1,3-glucan and carrying rifampin have shown promise for the treatment of tuberculosis, and these particles were not cytotoxic and were quickly recognized by macrophages (Tukulula et al., 2015, 2018). Chitosan—PLGA core-shell NPs with β -1,3 glucan and rifampin, increased the intracellular concentration of rifampin and showed an enhanced ability to modulate immune responses of human alveolar macrophages (Dube et al., 2014). In addition to β -glucan, other types of ligands such as antibodies can be incorporated on the surface of nanocarriers to target specific compartments of the target cell to act against intracellular pathogens. The use of pH-responsive polymers, which specifically release drugs in the presence of defined pHs, also represents an attractive alternative that can be explored against fungal pathogens (Armstead and Li, 2011). Interestingly, Mehta et al. (1997) suggested that the liposomal AmB synthesized by the authors in the 7:3 ratio of DMPC: DMPG (similar to Abelcet) is captured and retained by macrophages. These macrophages demonstrated enhanced killing of yeast cells, in this case *C. albicans*. However, this was not due to differential activation of the macrophages. The authors proposed that the candidicidal activity of the formulation occurred due to the macrophages retaining the liposomal AmB and releasing the drug to kill the yeast (i.e., drug delivery via macrophages).

Nanotechnology has advanced in recent decades with the development of innovative nanoscale products for various applications. **Figure 1** illustrates the main advantages of using NPs in the medical field. Currently, the nanomedicine market includes new approaches in the diagnosis, prevention, and therapy of diverse diseases. In 2006, these innovations sustained a market of US \$6.8 billion (Wagner et al., 2006). A recent study predicted an annual growth of 12.6% such that the market can reach up to US \$261 billion in 2023 (reviewed by Marques et al., 2019).

TYPES OF NANOCARRIERS

Several types of nanostructures are currently being investigated for the delivery of antifungal drugs and improve their ability to serve as adjuvants for vaccine delivery (Ribeiro et al., 2013; Souza and Amaral, 2017). These nanostructures can be classified according to their composition into (Soliman, 2017): polymeric NPs, phospholipid-based vesicles, nanostructured lipid carriers (NLCs), dendrimers, nano-emulsions (NE), and metallic and magnetic NPs. Below, we briefly present the types of nanocarriers that can be used in formulations for systemic administration of antifungals and antigen delivery.



Polymeric Nanoparticles

The most common materials used for nano-carrier development are polymers (Bolhassani et al., 2014). Polymeric NPs are formed by chains of identical chemical structures, called monomers. Polymers are generated by the union of several monomers (Sahoo et al., 2007). Polymers and monomers may be extracted from nature or chemically synthesized. The main polymers used in the production of NPs for mycosis treatment are alginate, chitosan, and PLGA (Italia et al., 2011; Yang et al., 2011; Spadari et al., 2017; Fernandes Costa et al., 2019).

Alginate is a natural polymer found mainly in the cell wall of algae of the Phylum *Phaeophyta*, and it is formed by the junction of two monomers, α -L-guluronic acid (G block), and β -D-mannuronic acid (M block) (Jain and Bar-Shalom, 2014). The difference in concentrations between the monomers and the variations in their arrangement defines how rigid the polymer structure will be, and consequently the NPs (Jain and Bar-Shalom, 2014). Alginate NPs can be obtained through different techniques that work in basically the same way, with alginate interacting with calcium salts and promoting polymer folding to form NPs (Jain and Bar-Shalom, 2014; Lopes et al., 2017). Alginate is a water-soluble polymer, and alginate-based NPs

have biocompatible mucoadhesive characteristics and are non-cytotoxic (Yehia et al., 2009).

Chitosan is a polymer obtained from the deacetylation of chitin, which is widely distributed in nature, particularly in the animal and fungal kingdoms. In the animal kingdom, chitin is present in insect, arachnid, and crustacean exoskeletons, whereas fungal chitin is a cell wall component in most fungi (Frank et al., 2020). Chitosan may be used for the production of nanogels, nano-emulsions, and NPs. Among the different applications of chitosan are food supplementation, wound healing, and immunomodulation (Dai et al., 2011; Ahmed and Aljaeid, 2016). Due to its hydrophobic character and positive charge, chitosan is ideal for the production of NPs and delivery of different types of molecules in mucous membranes (Frank et al., 2020). DNA/RNA, peptides, proteins, and drugs (Illum, 2003; Riteau and Sher, 2016) are effectively delivered by chitosan NPs. Since chitosan is biocompatible, biodegradable, and non-cytotoxic, it is one of the most promising polymers for the development of vaccines or parenteral treatment in different types of systemic infections (Sharma et al., 2015; Frank et al., 2020).

PLGA is a synthetic co-polymer produced from the linkage of glycolic acid (GA) and lactic acid (LA) monomers, the

same molecules produced by PLGA biodegradation (Amaral et al., 2009; Souza et al., 2015). The properties of PLGA are directly related to the molecular weight and proportions of the monomers. Therefore, the mechanical resistance, biodegradation rate, and the hydrolysis of the nanocarrier are influenced by the degree of crystallinity of the PLGA, which depends on the molar ratio between GA and LA. The most commonly used concentration being 50% poly lactic acid (PLA) and 50% poly glycolic acid (PGA) (Danhier et al., 2012). In addition, alkaline or strongly acidic pHs can accelerate the biodegradation of the polymer. Due to its biocompatibility, low cytotoxicity, and biodegradability, PLGA is one of the few Food and Drug Administration (FDA) approved polymers for use in complexing drugs or immunogenic molecules (Danhier et al., 2012). The production of PLGA NPs requires different techniques depending on the polarity of the molecules to be complexed (Amaral et al., 2010). PLGA NPs can be used for delivery of molecules via the enteral and parenteral routes, both followed by rapid body clearance (Semete et al., 2010). Pegylation, or the incorporation of polyethylene glycol (PEG) molecules on the NP surface, can make the NPs “invisible” to phagocytic cells and extend their half-life (Semete et al., 2010).

Amphiphilic block-copolymers, with hydrophilic shell and hydrophobic core, are used to form polymeric micelles, and these micelles can successfully deliver hydrophobic compounds. Polymeric micelles can improve drug administration and penetration, promoting drug accumulation in the target tissue. For these reasons, this type of nanocarrier has been explored to target drugs to the central nervous system, which is further discussed below in the topic on *Cryptococcus* sp. (Shao et al., 2012).

Phospholipid-Based Vesicles: Liposomes

Liposomes are lipid particles formed in a bilayer with a hydrophobic interior layer and a hydrophilic exterior, similar to the structure of a cellular plasma membrane (Nisini et al., 2018). Liposomes can be unilamellar (one bilayer) or multilamellar (several bilayers separated by some hydrophilic fluid). The feature of hydrophilic, hydrophobic, and hydrophilic spaces makes liposomes the most versatile particles for transporting molecules, which can be dispersed inside the lipid bilayer to interact with hydrophobic molecules or dispersed in the aqueous nucleus thus interacting with hydrophilic molecules. These features allow liposomes to carry large amounts of molecules and permits improved control over the release of these payload molecules (Lila and Ishida, 2017; Nisini et al., 2018).

Their similarity to plasma membranes provides another interesting facet of liposomes in that sterols can be added to modify the stiffness of the bilayer and liposomes can be used to anchor molecules that can direct and facilitate delivery of charged payloads. Liposomes can also be functionalized to simulate an infection; thereby an immune-like response can be stimulated reducing the need for adjuvants (Rukavina and Vanić, 2016; Kube et al., 2017; Lila and Ishida, 2017).

Several drugs have been incorporated into liposomes. Currently, formulations carrying AmB are commercially available as AmBisome[®] and Abelcet[®]. AmBisome[®] is a

liposomal formulation of unicellular vesicles, formed from hydrogenated phosphatidylcholine from soy, cholesterol, distethylphosphatidylglycerol (DMPG) and AmB in the ratio 2:1:0.8:0.4. Abelcet[®] is a lipid complex with a multilamellar structure, formed of diesteroylphosphatidylcholine (DMPC) and DMPG in a 7:3 ratio, carrying 36 mol% of AmB. These formulations are administered worldwide to treat fungal infections (Newton et al., 2016; Godet et al., 2017).

Nanostructured Lipid Carriers (NLCs)

NLCs are a mixture of solid lipid and a fraction of liquid lipid from natural sources, which make them biodegradable and biocompatible particles (Gartziandia et al., 2015; Khan et al., 2015). NLCs are second generation carriers that may overcome the disadvantages of solid lipid NPs (SLNs), which present low drug loading capacity and drug loss due to reorganization and formation of highly ordered crystalline arrangements during storage (Soliman, 2017). Thus, NLCs have improved characteristics due to the incorporation of a liquid lipid fraction that offers greater drug retention capacity and long-term stability, making this type of system more effective in drug delivery since most drugs are lipophilic in nature (Salvi and Pawar, 2019). ITZ incorporated into NLCs has shown more than 98% encapsulation efficiency in different studies and remained stable after 6-month storage (Pardeike et al., 2016; El-Sheridy et al., 2019). Beloqui et al. (2013) evaluated the tissue distribution of NLCs after intravenous administration in rats and confirmed that radiolabeled NLCs remain in circulation up to 24 h after administration. In addition, nanocarrier biodistribution is influenced by the particle size and charge. Large particles are captured by the lung and small particles by the liver and bone marrow, whereas positive NPs are observed in the kidney and negative NPs home to the liver. Therefore, NLCs have become valuable alternatives in drug delivery studies.

Dendrimers

Dendrimers are highly branched polymeric NPs consisting of a multifunctional central core, branches, and end groups that allow functionalization (Sherje et al., 2018). Dendrimers can be constructed convergently (from edges to center) or divergently (from center to edges), and the form of construction is made in stages (generations) where each stage promotes uniform growth in size and shape because binding of branches is mirrored (Ahmed et al., 2016). Dendrimers are widely studied for the transport of drugs active against infections, inflammation, and cancer, or for the transport of genetic material such as DNA, RNA, or plasmids (Mendes et al., 2017). The main chemical components used for core construction are poly (amidoamine) (PAMAM), poly (propylene imine) (DAB or PPI), and poly (ether hydroxylamine) (PEHAM) (Voltan et al., 2016; Sherje et al., 2018).

Despite their wide range of applications, dendrimers may cause relevant cytotoxicity due to their composition, because the vast majority of dendrimers have a strong cationic characteristic that can cause membrane destabilization (Ghaffari et al., 2018; Sherje et al., 2018). However, various additions to these dendrimers have been introduced, which reduce the cytotoxic

effects and prolong the body circulation time (Ghaffari et al., 2018).

Nano-Emulsions (NE)

NE consist of isotropic mixtures of drugs, lipids, hydrophilic surfactants, and co-solvents, with droplet sizes ranging from 10 to 500 nm (Mundada et al., 2016). In general, they are kinetically stable and can replace less stable nanocarriers such as liposomes (Mahtab et al., 2016; Hussain et al., 2017). NE are of great interest as antifungal drug-delivery vehicles, since the lipophilic nature of the formulation permits the solubilization of drugs, which, coupled to the small size of the droplets, make them easily absorbed through biological membranes such as the intranasal mucosa (Thakkar et al., 2015; Hussain et al., 2016). Other authors have discussed intranasally administered NE as an efficient alternative for brain targeting drugs (Kumar et al., 2016; Chatterjee et al., 2019; Iqbal et al., 2019), including the analgesic Tramadol (Lalani et al., 2015) and the anti-depressive Paroxetine (Pandey et al., 2016). This approach is potentially relevant for the treatment of meningitis caused by *Cryptococcus* spp. Due to the versatility of NE in formulating gels, creams and foams, this approach has become widely explored in topical mycosis therapy (Jaiswal et al., 2015; Mahtab et al., 2016).

Metallic and Magnetic Nanoparticles

Metallic NPs are extremely interesting, since, apart from acting as drug carriers, they represent an alternative to the treatment of infectious diseases via their intrinsic antimicrobial activity, which is well described for metals such as zinc, silver (Ag), and copper (Seil and Webster, 2012). Several studies have validated the intrinsic potential of metallic NPs in antimicrobial therapy (Franci et al., 2015; Malekhaiaf Häfner and Malmsten, 2017; Majid et al., 2018) and demonstrated their biocompatibility (Zhao et al., 2018). Silver is one of the noble metals most commonly used to generate NPs due to its unique properties such as chemical stability, good conductivity, and antimicrobial, antiviral, and antifungal potential as well as displaying anti-inflammatory activity (Ahmad et al., 2003). Metallic NPs have been widely explored in the literature for their synthesis from biological sources (Dipankar and Murugan, 2012; Thangamani and Bhuvaneshwari, 2019; Kischkel et al., 2020). The synthesis of NPs from plants or microorganisms is possible based on metabolites and proteins present in the extracts. These metabolites are essential for green synthetic pathways as they act to reduce metal and stabilize NPs (Khanna et al., 2019). Flavonoids, phenolic compounds, terpenoids, heterocyclic compounds, enzymes, and tannic acid are among the most commonly used compounds (Akhtar et al., 2013). Therefore, biologically synthesized NPs have the advantage of bringing together properties of the metal and the molecules used for synthesis (Dipankar and Murugan, 2012). Magnetic NPs can be formed from other metals such as iron, gold (Au), nickel, cobalt, and metal oxides (Huang et al., 2014). An advantage of using magnetic NPs is the ability to target their accumulation in the body, as magnetic NPs can be directed through a magnetic field generated by an external magnet to the specific site of drug delivery (Hussein-Al-Ali et al., 2014). This approach

theoretically decreases the amount of drug needed for treatment and reduces drug concentration in non-target organs, which minimizes the incidence of serious side effects (Chomoucka et al., 2010; Rózsalska et al., 2018; Rodrigues et al., 2019). In particular, superparamagnetic iron oxide NPs are a promising alternative for antifungal delivery, since they are highly responsive to external magnetic fields (Souza and Amaral, 2017).

A schematic representation of the nanocarrier types described above can be seen in **Figure 2**.

CURRENT SCENARIO OF NANOTECHNOLOGY IN THE TREATMENT AND VACCINATION OF FUNGAL INFECTIONS

Candidiasis

Species of the genus *Candida* are part of the human microbiota. However, under conditions of immunosuppression or lowering biological barriers, these microorganisms cause serious infections. Among *Candida* species, *C. albicans* is the species most associated with superficial and systemic infections (Pfaller and Diekema, 2010). Among the other species, *C. auris*, has emerged as a major threat due to its remarkable tendency for intrinsic multidrug-resistance (Kordalewska and Perlin, 2019). Treatment of invasive candidiasis is based on three classes of antifungals: polyenes, azoles and echinocandins. However, these drugs have variable effectiveness in the setting of biofilms (Tumbarello et al., 2007; Sawant and Khan, 2017).

Diverse NPs have been studied for their activity against *Candida*. For example, gold NPs (AuNPs) have been studied aiming at their antifungal activity in *C. albicans* biofilms, since in conjunction with photosensitizer, AuNPs can increase the effectiveness of photodynamic therapy (Khan et al., 2012; Sherwani et al., 2015; Maliszewska et al., 2017). AuNPs can destabilize the cell membrane of the pathogen through direct interaction with proteins and lipids. In addition, the association of photosensitizers with metallic nanoparticles can reduce the risk of pathogens developing resistance to photodynamic therapy (Maliszewska et al., 2017).

The effect of AgNPs against *Candida* spp. have also been widely studied, both against planktonic cells and biofilms (Monteiro et al., 2011; Lara et al., 2015). Kischkel et al. (2020) evaluated the efficacy of AgNPs carried with propolis extract (PE) against mature biofilms of *Candida* species and other fungi and observed that the concentration required for the fungicidal activity of the formulation was below the cytotoxic concentration.

Curcumin has broad antimicrobial activity and it is nontoxic. However, due to several factors, such as degradation and rapid systemic elimination, curcumin has had limited applications as a therapeutic due to its low bioavailability in the blood (Anand et al., 2007). AgNPs have been created to enhance curcumin delivery. The Curcumin—AgNPs significantly inhibit fluconazole resistant *C. albicans* and *C. glabrata*, and the inhibition depended on the concentration of curcumin used (Paul et al., 2018).

Rózsalska et al. (2018) studied biogenic AgNPs against reference strains of *C. albicans*, *C. glabrata*, and *C. parapsilosis*

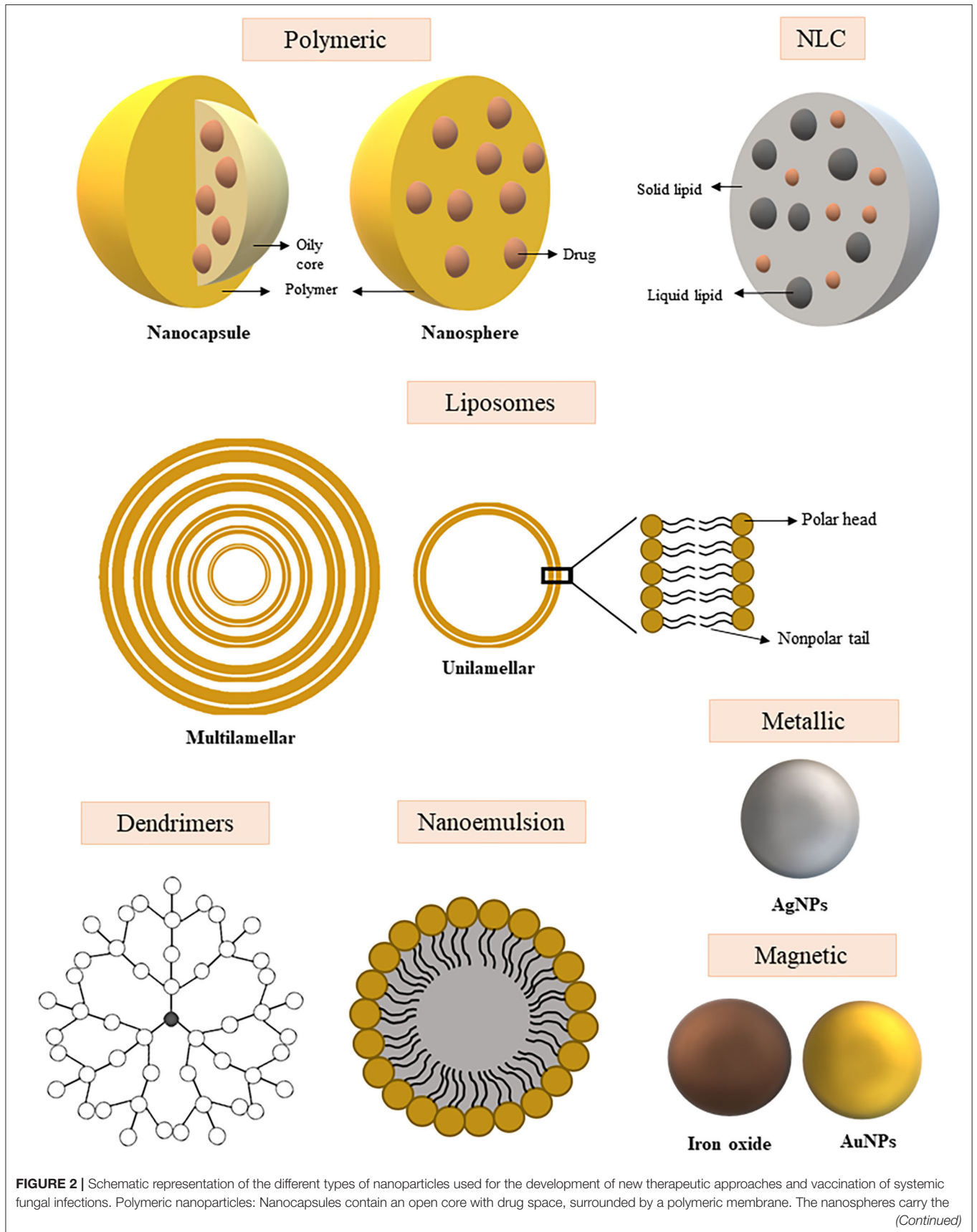


FIGURE 2 | Schematic representation of the different types of nanoparticles used for the development of new therapeutic approaches and vaccination of systemic fungal infections. Polymeric nanoparticles: Nanocapsules contain an open core with drug space, surrounded by a polymeric membrane. The nanospheres carry the (Continued)

FIGURE 2 | drugs evenly distributed over a polymeric matrix. NLC (Nanostructured lipid carriers): Structure composed of a solid lipid and liquid lipid fraction into which the drug may be incorporated within the structure. Liposomes: Nanoparticle with unilamellar or multilamellar structure with space for drug transport between layers and/or core. Dendrimers: Complex structure branched and highly organized around the nucleus, the drug can be incorporated between the layers or on the surface of the structure. Nanoemulsion: Colloidal dispersion composed of an oil and water phase that promotes drug encapsulation. Metallic nanoparticle: Nanoparticle of metal core and intrinsic antimicrobial activity. Magnetic nanoparticle: Nanoparticle of metal core with magnetic properties.

and found that the particles were effective at a low minimum inhibitory concentration (MIC) range (1.56–6.25 $\mu\text{g/mL}$), which did not concomitantly show cytotoxicity. Notably, the biogenic AgNPs were stable *in vitro* for long periods. In addition, AgNPs used in combination with fluconazole were able to decrease the biological activity of *C. albicans* biofilms, which was attributed to the ability of the NPs to enhance the penetration of the azole disturbing the cell membrane, while Ag destabilized efflux transporter efficacy. However, despite the advantages of biomolecule synthesis, AgNPs have a tendency to aggregate and this effect impairs their antimicrobial activity (Rózsalska et al., 2018).

Vazquez-Muñoz et al. (2014) observed that AgNPs did not penetrate the intracellular environment and that fungal cell death may have occurred due to the release of silver ions from AgNPs accumulated outside the cells, resulting in smaller NPs located throughout the cytoplasm. In another publication, ROS production, changes in ergosterol levels, and other effects acted together to enhance the effect of AgNPs against *C. albicans* (Radhakrishnan et al., 2018b). In addition, intracellular ROS levels could be reversed by ascorbic acid antioxidant without altering the effectiveness of AgNPs against *C. albicans* (Radhakrishnan et al., 2018a).

The antifungal effects of AmB and nystatin coupled to magnetic NPs (MNP-AmB and MNP-Nystatin) have been studied against clinical isolates of *C. albicans*. Niemirowicz et al. (2016) observed that MNP-AmB and MNP-Nystatin showed significant fungicidal effect and prevented biofilm formation. The observed effect could be due to catalase inactivation (Cat1) in cells exposed to nanosystem treatment, since disturbance of the redox balance could lead to inhibition of *C. albicans* growth. Subsequently, magnetic NPs coated with peptide LL-37 and ceragenin CSA-13 also showed fungicidal effects against *Candida* sp. due to increased ROS production associated to pore formation in the cell membrane, thus assisting NPs penetration into the yeast cells (Niemirowicz et al., 2017b).

Using encapsulated AmB in PLGA-PEG NPs (PLGA-PEG-AmB), the efficacy, toxicity, and oral bioavailability of these formulations were evaluated, *in vivo* and *in vitro*. Compared to free AmB, the PLGA-PEG-AmB NPs decreased MIC against *C. albicans* cells. Using a hemolysis assay, NP formulations had lower toxicities compared with Fungizone[®]. *In vivo*, blood urea nitrogen, and plasma creatinine measurements remained normal after a week of oral administration of PLGA-PEG-AmB NPs in rats. Finally, bioavailability of the PLGA-PEG-AmB NPs was further enhanced with the addition of glycyrrhizin acid (GA) (Radwan et al., 2017).

NPs of PLGA with chitosan containing AmB (PLGA-CHI-AmB) were synthesized and the derived NPs achieved nanometer size, low polydispersity, positive surface charge, and good encapsulation capacity for AmB. Notably, chitosan, in addition to having mucoadhesive properties, helps maintain the stability of nanoparticles and increases their biocompatibility. However, the PLGA-CHI-AmB showed variable MICs against with different *Candida* sp.. This result can be explained by the prolonged release of AmB, resulting in less activity *in vitro*. Although AmB is available to act on the target, the release kinetics of the NPs of PLGA with chitosan needs to be more controlled to achieve efficacy (Ludwig et al., 2018).

Among the virulence factors of *C. albicans*, the transition from yeast to hyphae represents an important factor in its pathogenicity. Farnesol is a molecule produced by *C. albicans* and it is an important quorum-sensing molecule that inhibits the growth of hyphae (Kruppa, 2009). Chitosan NPs were formulated to encapsulate farnesol and miconazole, which were then evaluated in a murine model of vulvovaginal candidiasis. Interestingly, no *in vitro* synergism between miconazole and farnesol was found. Farnesol-containing chitosan NPs, however, were effective in reducing the pathogenicity in mice, and farnesol-containing NPs inhibited hyphal growth in *C. albicans*. Additionally, the NPs tested showed no toxicity in cultured fibroblasts (Fernandes Costa et al., 2019).

SLNs and NLCs were created that were easily loaded with AmB and the NPs displayed lower hemolytic activity compared with Fungizone[®]. The AmB SLNs and NLCs were also more effective than free AmB or Fungizone[®] against *C. albicans*. The data suggest that these formulations may increase antifungal activity, increase AmB solubility, and decrease the toxic effect of treatment. This effect may be due to by the sustained release of AmB in the formulations and by its monomeric state, since AmB with a low degree of aggregation is more selective and binds mainly to ergosterol (Jansook et al., 2018).

Antifungal SLNs have been studied with drug resistant *Candida*. Fluconazole loaded SLNs (FLZ-SLNs) were more effective than free fluconazole against the species tested. The FLZ-SLNs displayed fast drug release in the first 30 min followed by sustained release over 24 h (Moazeni et al., 2016; Kelidari et al., 2017). One of the main resistance mechanisms in yeasts is the overexpression of efflux pumps, reducing the levels of azoles within the cell. The increased susceptibility to antifungals, in this case, may be related to the protection that NLCs provided to FLZ, protecting the drug from being discharged from the cell. In addition, the hydrophobic surface of FLZ-NLCs can increase the penetration of the drug into yeast (Kelidari et al., 2017).

Lipid core NPs and fluconazole containing NLCs were evaluated in fluconazole resistant *Candida*. Although the NLCs were not effective, the lipid nucleus NPs were active at reduced fluconazole concentrations. Additionally, the lipid nucleus-fluconazole NPs prevented fluconazole recognition by efflux pumps in fungal cells (Domingues Bianchin et al., 2019).

To reduce the toxicity reported for miltefosine and maintain its antifungal effect, Spadari et al. (2019) evaluated the activity of miltefosine-loaded alginate NPs against *Candida* and *Cryptococcus* species. Miltefosine encapsulation in 80% alginate NPs significantly reduced the toxic effects compared to free miltefosine in an *in vitro* system as well as in *Galleria mellonella*. Moreover, the treatment of *G. mellonella* infected with *C. albicans* with miltefosine-alginate NPs significantly extended larval survival time. The effect obtained may be associated with the controlled release of the drug, since alginate-based nanocarriers allow for the constant release of the drug, which can maintain its bioavailability and reduce potential adverse effects. Another advantage described is the size of the nanoparticles obtained in this study (average size of 279.1 ± 56.7 nm), which are favorable for mucosal and oral administration (Spadari et al., 2019).

The first study involving NPs as a *C. albicans* vaccine was published by Han and Cutler (1995), in which they used phosphatidylcholine and cholesterol liposomes to carry manganese extracted from *C. albicans*. Vaccination provided protection against widespread infection and the antiserum from infected animals was able to protect BALB/cByJ and SCID mice against *C. albicans* and *C. tropicalis*. Also, in this study, a specific monoclonal antibody was obtained, MAb B6.1, which protected against widespread infection. Subsequently, the vaccine potential of this mAb against vaginal candidiasis was evaluated (Han et al., 1998). Concurrently, another study evaluated vaccine potential of *C. albicans* ribosomes incorporated into liposomes composed of dimyristoyl phosphatidyl choline (DMPC) and dimyristoyl phosphatidyl glycerol (DMPG). Immunization of mice with these liposomes resulted in 60% survival rate of animals with disseminated candidiasis (Eckstein et al., 1997).

Heat shock protein 90 represents a highly conserved *C. albicans* chaperone that is also an immunogenic protein abundantly present in the fungal cell wall, which has been studied as a potential vaccine candidate (Matthews et al., 1987). Mašek et al. (2011), incorporated rHSP90 into the surface of nickel chelating liposomes associated with norAbuMDP pyrogen adjuvant, a compound of lipophilic derivatives of muramyl dipeptide (MDP), for intradermal vaccination of BALB/c mice and observed comparable Th1 and Th2 response to Freund's complete adjuvant vaccine. Later, Knotigová et al. (2015), evaluated the vaccine efficacy of rHSP90 in nickel-chelating liposomes associated with two pyrogen-free adjuvants (norAbuMDP and norAbuGMDPs) in ICR mice and rabbits, and showed stimulation of innate and adaptive immune response against the rHSP90-containing nano formulation.

More recently, Carneiro et al. (2015, 2016) employed dimethyldioctadecylammonium bromide (DODAB) monoolein-based liposomes for delivery of *C. albicans* wall proteins. In the first study, prophylactic vaccination using the NPs in BALB/c mice stimulated humoral and cellular immune response with

production of IgG antibodies against two specific proteins found in the cell wall, Cht3p and Xog1p. Additionally, there was no apparent toxicity of the NPs. In a second study, two formulations with different lipid concentrations for protein loading, called ADS1 and ADS2, each containing a total lipid concentration of 1,774 and 266 $\mu\text{g/ml}$, respectively, were evaluated. The results showed that only the administration of ADS1 was able to confer protection against infection in mice, with a high production of specific antibodies that increased fungal phagocytosis. There was also an increased production of IL-4, IL-17, and IL-10 cytokines, demonstrating a mixed Th1, Th2, and anti-inflammatory response.

Studies involving NPs for treatment of candidiasis are shown in **Table 1** and for vaccination in **Table 4**.

Cryptococcosis

Cryptococcosis is a systemic mycosis caused by *C. neoformans/C. gattii* species complexes (Hagen et al., 2015), associated with high morbidity and mortality rates, especially in immunocompromised individuals and low-income countries (reviewed in Mourad and Perfect, 2018). The infection begins with inhalation of fungal propagules and in healthy individuals can be eliminated without significant symptoms. Asymptomatic spread frequently occurs, which can also lead to disease relapse in immunosuppressed infected individuals. Immunocompromised hosts can develop the primary infection. In either situation, the mycosis frequently affects the central nervous system as a meningoencephalitis (Kwon-Chung et al., 2014). Although individuals infected with human immunodeficiency virus (HIV) are the main risk group affected by *C. neoformans*, patients receiving immunosuppressive drugs and chemotherapy are also at risk (Sloan and Parris, 2014). Notably, *C. gattii* is mostly associated with immunocompetent individuals, although some other risk factors may contribute to the development of the disease (Marr et al., 2012; Chen et al., 2014; Saijo et al., 2014).

The choice treatment of cryptococcosis presented as cryptococcal meningitis or severe pulmonary cryptococcosis, is based on the administration of AmB in combination with 5-fluorocytosine, followed by fluconazole as a maintenance drug, for weeks to lifetime (Perfect et al., 2010). In countries where 5-fluorocytosine is not available fluconazole can be used as a replacement in conjunction with AmB (Perfect et al., 2010). In little resourced areas, high doses fluconazole may be used as primary therapy.

AmB deoxycholate remains an important drug for the treatment of deep fungal infections. However, its use for the treatment of cryptococcal meningitis is limited due to the inability of the drug to cross the blood-brain barrier (Xu et al., 2011). Searching for a brain drug delivery system, some nanocarriers have been studied and interesting results against *Cryptococcus* sp. have been reported (Ren et al., 2009; Xu et al., 2011; Pedroso et al., 2018). Early nanocarrier studies used polysorbate 80, a surfactant and emulsifier that improves NP uptake by human and bovine primary brain capillary endothelial cells. Polysorbate 80 coated particles can increase the concentration of drug in the brain by up to 20 times 1 hour after the injection and are therefore considered an efficient

TABLE 1 | Nanoformulations studied for the treatment of fungal infections caused by *Candida* and *Cryptococcus* yeasts.

Nanoparticle	Drug (*)	Fungi	In vitro/in vivo	References
AuNP	–	<i>C. albicans</i>	<i>in vitro</i> and <i>in vivo</i> (mice)	Khan et al., 2012; Sherwani et al., 2015; Maliszewska et al., 2017
AgNP	FLZ	<i>C. albicans</i> <i>C. glabrata</i> <i>C. parapsilosis</i> <i>C. tropicalis</i> <i>Candida kefyr</i>	<i>In vitro</i>	Monteiro et al., 2011; Vazquez-Muñoz et al., 2014; Lara et al., 2015; Paul et al., 2018; Radhakrishnan et al., 2018a,b; Rózsalska et al., 2018
	Propolis	<i>C. albicans</i> <i>C. glabrata</i> <i>C. parapsilosis</i> <i>C. tropicalis</i> <i>C. krusei</i> <i>F. oxysporum</i> <i>T. interdigitale</i> <i>T. rubrum</i> <i>M. canis</i>	<i>In vitro</i>	Kischkel et al., 2020.
Magnetic PLGA-PEG PLGA-CHI	AmB/NYS AmB	<i>C. albicans</i> <i>C. albicans</i> <i>C. glabrata</i> <i>C. tropicalis</i> <i>Trichosporon asahii</i> <i>C. guilhermondii</i>	<i>In vitro</i> <i>In vitro</i> and <i>in vivo</i> (rats)	Niemirowicz et al., 2016, 2017b. Radwan et al., 2017; Ludwig et al., 2018
Chitosan Solid lipid	farnesol/miconazole AmB/FLZ	<i>C. albicans</i> <i>C. albicans</i> <i>C. glabrata</i> <i>C. parapsilosis</i> <i>C. neoformans fumigatus</i> <i>Penicillium marneffeii</i>	<i>In vitro</i> and <i>in vivo</i> (mice) <i>In vitro</i>	Fernandes Costa et al., 2019 Moazeni et al., 2016; Jansook et al., 2018
Nanostructured lipid carrier	AmB/FLZ	<i>C. neoformans</i> <i>C. tropicalis</i> <i>C. krusei</i> <i>C. parapsilosis</i> <i>C. glabrata</i> <i>C. kefyre</i> <i>fumigatus</i> <i>Penicillium marneffeii</i>	<i>In vitro</i>	Kelidari et al., 2017; Jansook et al., 2018; Domingues Bianchin et al., 2019
Core-shell architecture of silver nanostructure (Pd@AgNSs)	AmB	<i>Cryptococcus spp.</i>	<i>In vitro</i>	Zhang C. et al., 2016
AgNPs and AuNPs	–	<i>C. neoformans</i> <i>C. gattii</i> <i>Candida spp.</i> <i>Dermatophytes</i>	<i>In vitro</i>	Ishida et al., 2014; Rónavári et al., 2018
Chloroaluminum phthalocyanine nanoemulsion (CIAIP/NE)	–	<i>C. neoformans</i>	<i>In vitro</i> photodynamic antimicrobial chemotherapy (PACT)	Rodrigues et al., 2012
PLA-b-PEG coated with polysorbate 80 (Tween-80)	AmB	<i>C. neoformans</i>	<i>In vivo</i>	Ren et al., 2009
Polybutylcyanoacrylate (PBCA)	AmB	<i>C. neoformans</i>	<i>In vivo</i> (mice)	Xu et al., 2011
Angiopep-PEG-PE polymeric micelles	AmB	<i>C. neoformans</i>	<i>In vitro</i> and <i>in vivo</i> (mice)	Shao et al., 2012
BSA nanoparticles coated with polysorbate- 80	AmB	<i>C. neoformans</i>	<i>In vitro</i>	Pedroso et al., 2018
Nanoparticle crystal encapsulated (encochleated)	AmB/5FC	<i>C. neoformans</i>	<i>In vivo</i> (mice)	Lu et al., 2019
PLGA/PLGA-PEG	ITZ/AmB	<i>C. neoformans</i> <i>C. albicans</i>	<i>In vitro</i> and <i>in vivo</i> (mice)	Moraes Moreira Carraro et al., 2017; Tang et al., 2018
SDCS nanomicelles	AmB	<i>C. neoformans</i> , <i>C. albicans</i>	<i>In vitro</i>	Usman et al., 2018
PAMAM-sulfonamide dendrimers	-	<i>C. neoformans</i> <i>C. glabrata</i>	<i>In vitro</i>	Carta et al., 2015

(*) Drugs: AmB, Amphotericin B; ITZ, Itraconazole; NYS, Nystatin; FLZ, Fluconazole; 5FC, 5 fluorocytosine.

brain “driver” (Ramge et al., 2000). Xu et al. (2011) developed AmB-polybutylcyanoacrylate NPs and polysorbate coated (AmB-PBCA-NPs) for systemic administration in a mouse model. According to the authors, NPs of ~69 nm were detected in the brain 30 min after injection and in a higher concentration than liposomal AmB. Interestingly, AmB deoxycholate was not detected in the brain; however, survival rates were 80, 60, and 0% for AmB-PBCA-NPs, Liposomal AmB, and AmB deoxycholate, respectively. According to Ren et al. (2009), polysorbate 80 also improves the trapping effectiveness of AmB in the polymeric system as PLA-b-PEG. In *in vitro* tests, 100% of the AmB was released between 35 and 40 h. In NPs containing the polysorbate, almost 100% of AmB was released between 60 and 70 h.

Lipid based AmB cochleates (CAMB) is a new type of AmB nanocarrier with potential for oral administration, showing greater stability and resistance to gastrointestinal degradation (Santangelo et al., 2000). Lu et al. (2019) recently studied the administration of CAMB in combination with 5-fluorocytosine and found it to be highly effective in a murine model of cryptococcal meningoencephalitis. *In vivo* data also showed that CAMB doses up to 90 mg/kg/day appeared to be non-toxic. A particular benefit of the CAMB formulation is that the release of the drug is calcium dependent and can thus maintain its stability until reaching the intracellular environment. This provides a mechanism for controlling drug release as well as enhancing CNS drug levels (Lu et al., 2019).

Several studies, therefore, have focused on the development of safe, effective, and less expensive alternatives for the use of AmB. Liposomal, colloidal dispersion, and lipid complexes are examples of nano formulations that have been shown to attenuate toxic effects in therapy (Reviewed in Spadari et al., 2017).

Formulations with nanomicelles of AmB using sodium deoxycholate sulfate (SDCS) have been developed for targeted pulmonary delivery through inhalation of nanoformulation. According to Usman et al. (2018), the AmB-SDCS is equivalent in efficacy to Fungizone[®], but the NPs does not cause toxic effects in respiratory and kidney cell lines. AmB-SDCS formulations showed activity against *C. neoformans*, *C. albicans*, and *S. cerevisiae*. A phagocytosis assay using NR8383 cells revealed that AmB-SDCS accumulated within the host effector cells without evidence of phagocytic cell damage. As we have already discussed, macrophages internalize particles of 0.5–5 μ m. AmB-SDCS have a diameter of 0.9–1.6 μ m. In addition to size, the surface chemistry of NPs can also influence uptake by macrophages as hydrophobic particles can stick to the cell surface (Xiang et al., 2006; Usman et al., 2018). This study demonstrated the effectiveness of an aerosolized lipid formulation in the delivery of AmB to alveolar macrophages *in vitro*, one of the main reservoirs of fungi such as *Cryptococcus* and *Aspergillus*. However, further studies are needed to validate the method *in vivo*.

Nanotechnology can overcome certain limitations of current antifungal drugs (Niemirowicz et al., 2017a). Similar to AmB, the hydrophobic character of ITZ causes the drug to have poor tissue penetration. Nanocarriers used for controlled drug release could help increase ITZ levels. Curić et al. (2017) incorporated ITZ into poly (butyl cyanoacrylate) nanocapsules, helping the drug stability and targeting. Aiming at oral administration, a system

using PLGA and chitosan NPs was developed and analyzed for efficacy against *C. neoformans* pulmonary infection. A chitosan-binding peptide, screened by phage display, was conjugated to PLGA NPs (CP-NPs) with or without free chitosan (C-CP-NPs) and ITZ was incorporated in the NP. Notably, free chitosan (C-CP-NPs/ITZ) did not influence the efficiency of drug incorporation and it did not impact drug release. Both CP-NPs/ITZ and C-CP-NPs/ITZ prolonged the survival of mice with pulmonary cryptococcosis, although C-CP-NPs/ITZ was more effective (Tang et al., 2018).

Antimicrobial activity of some nanomaterials, such as Ag and Au, is commonly reported, inhibiting or killing both eukaryotic and prokaryotic pathogens (Musarrat et al., 2010; Yu et al., 2016). Although safety uncertainty of AgNPs causes conflicting information, the therapeutic effect against some pathogens is unquestionable (Vazquez-Muñoz et al., 2017).

Zhang C. et al. (2016) conducted a study using core-shell architecture of Ag nanostructure (Pd@AgNSs), to evaluate the antifungal activity against invasive fungi. This nanostructured Ag was obtained through deposition techniques based on palladium seeds that generated NPs with a high degree of biocompatibility due to the uniform size and shape. Pd@AgNSs displayed broad activity against ascomycetes and basidiomycetes, including strains considered resistant to fluconazole. The antifungal effect of the Pd@AgNSs was independent on the size of the nanoparticles. The authors speculate that the hexagonal shape of the NPs had a greater influence on antifungal properties and that this potent activity masked the expected size effects. Pd@AgNSs were cidal to fungi through mechanisms that included alterations in protein synthesis and energy metabolism. In addition, Pd@AgNSs induced increased numbers of vacuoles, which may be associated with survival strategies of the fungus itself to improve protein transport, since cell stress can increase energy demand and therefore result in increased numbers of mitochondria. Pd@AgNSs also acted synergistically with AmB, reducing the effective AmB concentration to 0.125 μ g/mL.

NPs synthesized by biological routes have been explored for efficacy against cryptococcosis. In this type of synthesis, we emphasize that it is necessary to take into account the source of obtaining secondary metabolites. The source must offer a toxin-free extract that is rich in substances such as flavonoids, terpenoids, among others, which are mainly responsible for the synthesis and stabilization of metal ions that influence the final cytotoxicity of the nanoformulation (Ahmed et al., 2018; Lakshmeesha et al., 2019).

Ag and Au NPs were synthesized using cell-free extract of *Phaffia rhodozyma*, the red yeast containing astaxanthin, a type of natural antioxidant that aids in the formation of metallic NPs. These biologically synthesized AgNPs and AuNPs showed no toxicity to human HaCat keratinocytes. Although the AgNPs were broadly effective against basidiomycetes and ascomycetes, the AuNPs were also able to inhibit *C. neoformans* (Rónavári et al., 2018). Ishida et al. (2014) created Ag nanostructures using an aqueous extract of *Fusarium oxysporum* that was effective against *Candida* and *Cryptococcus* species, particularly *C. gatti*. The AgNPs induced changes in the cytoplasmic membrane and wall of *Cryptococcus* spp. strains, but not of *Candida* spp..

Photodynamic antimicrobial chemotherapy is a method that can be combined with nanocarriers (Rodrigues et al., 2012). In this case, the nanocarrier is called a photosensitizer and can be applied to the skin lesion caused by the fungus where it can bind fungal cells and accumulate at the infection site. The photosensitizer is then exposed to visible light at appropriate wavelengths to induce the production of ROS resulting in the death of the fungus (Donnelly et al., 2008). Therefore, the photosensitizer must be an agent that is directed at the fungal cell while the light focuses on the lesion. Photodynamic antimicrobial therapy was evaluated in melanized *C. neoformans* cells using chloroaluminum phthalocyanine incorporated into NE (CIAIP/NE). CIAIP/NE effected the viability of *C. neoformans* cells in a dose dependent manner according to both the amount of the particle and the intensity of the light applied. The use of this alternative was helpful in the treatment of skin lesions caused by *C. neoformans* and other fungi (Rodrigues et al., 2012).

The studies involving NPs for cryptococcosis treatment are summarized in **Table 1**.

Aspergillosis

The members of the genus *Aspergillus* are described as opportunistic pathogens capable of inducing allergic reactions to systemic infections in humans. *A. fumigatus* is the most predominant species, responsible for 90% of invasive infections (Paulussen et al., 2017). It is a globally ubiquitous organism and dominant in different habitats due to various morphological and physiological factors (Cray et al., 2013). Importantly, azole resistance is an emerging problem in *A. fumigatus*, which has resulted in treatment failures (Seyedmousavi et al., 2014).

Different types of polymeric NPs have been explored as carriers of AmB for the treatment of experimental aspergillosis (Shirkhani et al., 2015; Salama et al., 2016; Yang et al., 2018). Among them, Italia et al. (2011) reported the efficacy of PLGA NPs for oral administration of AmB. The oral administration of PLGA NPs was superior to parenteral Ambisome[®] and Fungizone[®] in neutropenic murine models of disseminated and invasive aspergillosis. Notably, conventional AmB (Fungizone[®]) is ineffective in this model. The AmB PLGA NPs promoted greater oral absorption of AmB compared to AmB alone. The NPs were able to protect the drug from degradation by pH and gastrointestinal enzymes, thereby overcoming incoming metabolism and allowing more NPs to be captured by lymph nodes (Italia et al., 2011). Therefore, oral administration of AmB may represent a promising strategy for the treatment of disseminated fungal infections, or at least azole refractory oral thrush. Similarly, Van de Ven et al. (2012) found that a PLGA and nanosuspension NPs containing AmB administered by intraperitoneal route in mice were two and four times more effective in reducing fungal load, respectively, than Ambisome[®] and Fungizone[®] in disseminated aspergillosis models. In this case, the authors hypothesized that the state of aggregation of AmB in the delivery system may influence the interaction of NPs with ergosterol present in fungal membranes. These differences in the aggregation states of the particles in solution were confirmed by analyzing the UV/VIS spectra of the evaluated formulations. In addition, the authors speculated that PLGA and

nanosuspension NPs may have transported the drug directly to the tissue compartment, since the nanoformulation has an ideal size for blood circulation (≤ 100 nm) and may promote rapid uptake by the reticuloendothelial system, as is the case of formulations like Abelcet[®] and Amphocil[®] (Van de Ven et al., 2012).

Some nanoformulations, besides being effective in the treatment of aspergillosis *in vitro* and *in vivo*, may have reduced side effects in relation to some commercially available formulations. mPEG-b-P(Glu-co-Phe) carrying AmB is stable in plasma and has lower nephrotoxicity than free AmB (Yang et al., 2018). A PEG-Lipid NPS carrying AmB showed low cytotoxicity against human kidney cells than Fungizone[®] and Ambisome[®], in addition to lower hematotoxicity compared to Fungizone[®] (Jung et al., 2009). PEG/PLA with ITZ caused moderate hemolysis, although it showed superior *in vitro* antifungal activity compared to free ITZ (Essa et al., 2013). The increased toxicity of Fungizone[®] or free ITZ can be explained by the faster release of the drug compared to studied NP and/or Ambisome[®] formulations. The strong interactions between AmB and the lipids, phospholipids or polymers present in these formulations can delay the release of the drug, and, consequently, reduce the cytotoxic effects. On the other hand, a lower toxicity of PEG-LNPs compared to Ambisome[®] suggests that nanoformulation may be more efficient (Jung et al., 2009).

Some studies have considered evaluating the efficacy of inhaled formulations in the prophylaxis of aspergillosis, since infection by *Aspergillus* sp. starts from inhalation of infectious spores (Rodríguez-Cerdeira et al., 2014). A lipid complex of AmB (Abelcet[®]) was administered as an aerosol for prophylaxis for pulmonary aspergillosis model in rats. Through this technique it was possible to observe higher and prolonged levels of the compound in the lungs, and higher survival rates after 2 and 10 days of infection compared to aero-AmB (Fungizone[®]) (Cicogna et al., 1997). In 12 human lung transplant recipients, the nebulized Abelcet[®] was well distributed in the lungs, but the deposition rate was below expectations (Corcoran et al., 2006). Shirkhani et al. (2015) explored the efficacy of PMA, delivered via nebulizer to prevent *Aspergillus* infection in a mouse transplant immunosuppression model, in which 3 days of prophylactic treatment were sufficient to deposit the AmB NPs in the lung and prevent fungal growth. In this case, a polymethacrylic acid was used to transform the insoluble AmB into a 78–9 nm particle of water-soluble AmB-PMA and with a UV/VIS spectrum identical to the liposomal AmB. PMA does not have immunomodulatory properties, so the administration of AmB-PMA by nebulization would constitute a pre-transplant prophylactic therapy approach capable of effectively delivering the drug to the lung and protecting against the development of fungal infections that initially come into contact with the lung.

Different AmB formulations have been tested to treat eye complications caused by *A. fumigatus* (Zhao et al., 2015; Khames et al., 2019). The development of nanostructured systems for delivering medication to the cornea consists of advantages such as improving the penetration of the drug into the cornea, improving mucoadhesive properties and prolonged residence time. SLNs represent an efficient delivery system for this purpose

due to the lipophilic nature and the small size that allows the penetration of physiological barriers and the sustained release of drugs without impairing vision. In order to improve the penetration of natamycin (NAT) into the cornea, Khames et al. (2019) incorporated the drug into SLNs. The NAT-SLNs effectively released NAT for 10-h and improved the corneal permeation compared to a free drug. The NAT-SLNs were more potent than free NAT *in vitro*. Furthermore, the NAT-SLNs showed no cytotoxic effect in corneal tissues obtained from goats.

On the other hand, Zhao et al. (2015) compared voriconazole and liposomal AmB in guinea pig endophthalmitis model. Both drugs were able to treat endophthalmitis. However, voriconazole was more effective than liposomal AmB using a similar dose (20 µg) in the initial treatment period, since the group treated with voriconazole after induction of endophthalmitis, showed lower inflammation in the early and middle stages. The retinal histopathology was normal after administration of both drugs. A lower performance of liposomal AmB in the initial stage of treatment can be explained due to the presence of cholesterol, acting as a stabilizer in NPs, as well as the controlled release of the drug that occurs when the fungus comes into contact with liposomal AmB and the drug is released liposome. Thus, resulting in a delayed efficacy compared to free voriconazole.

Nanoformulations for AmB delivery are the most studied, considering that it is a first line antifungal in the treatment of fungal infections. Side effects of AmB deoxycholate have been reduced with the development of several liposomal formulations. However, these formulations are not produced under the same conditions and/or in the same concentration of lipids and drugs, for example, as mentioned in topic 2.2 on the composition of Abelcet[®] and Ambisome[®]. On the other hand, two formulations with similar chemical composition can result in particles of different sizes, such as AmBisome[®] (77.8 nm) and Lambin[®] (122.2 nm). These differences can influence the physical-chemical properties as well as the biological activity of these formulations (Olson et al., 2015). AmBisome[®], for example, is one of the most commonly reported AmB formulations referenced in articles to compare the efficiency of other nanoformulations (Clemons et al., 2005; Jung et al., 2009; Sheikh et al., 2010; Italia et al., 2011). Below, we cite some articles that show some differences in the biological activity of these commercial liposomal formulations that can be explained by differences in the synthesis and composition of the final formulation.

A study compared the toxicity and efficacy of two AmB lipid formulations, AmBisome[®] and Lambin[®], in mice. The application of a single dose of 50 mg/kg of the drugs led to 80% mortality with Lambin[®] and 0% with AmBisome[®]. After daily intravenous administration of 5 mg/kg of the drugs, tubular renal changes were observed in mice that received Lambin[®]. Although both drugs significantly decreased fungal burden in the lungs of mice treated after *A. fumigatus* infection, survival rates were 30% with Lambin[®] and 60% with AmBisome[®]. The histopathology showed that treated animals with AmBisome[®] presented fewer fungal elements and less tissue damage (Olson et al., 2015).

Olson et al. (2006) established the ideal concentration for treatment of pulmonary aspergillosis taking into

consideration the toxicity and efficacy of AmBisome[®] and Abelcet[®] formulations in a murine model. Both formulations showed prolonged survival at 12 mg/kg. Due to the reduced nephrotoxicity of AmBisome[®], increased doses of 15 or 20 mg/kg can be used safely. Seyedmousavi et al. (2013) demonstrated that AmBisome[®] is able to prolong the survival of the mouse regardless of the mechanism of azole resistance displayed in isolates used for infection.

Lewis et al. (2007) compared the accumulation kinetics of AmBisome[®] and Abelcet in the lungs of immunosuppressed mice and with invasive pulmonary aspergillosis. In conclusion, Abelcet[®] at 5 mg/kg/day conveys active AmB in the lung faster than AmBisome[®], leading to a more rapid reduction in fungal burden. At concentrations higher than 10 mg/kg/day there was no pharmacodynamic difference between the formulations. Regarding neutropenia, Siopi et al. (2019), demonstrated in mice that the appropriate doses of AmBisome[®] range 1–3 mg/kg for non-neutropenic patients and 7.5–10 mg/kg for neutropenic patients with isolates of *A. fumigatus* with MIC from 0.5 to 1 mg/L.

Patients were evaluated for responsiveness to AmBisome[®] in chronic pulmonary aspergillosis therapy. Seventy-one patients were included in the study, in which all responded to long-term therapy; however, 25% patients developed acute kidney injury, indicating that these drugs should be used with caution (Newton et al., 2016).

Combination therapy for the treatment of invasive fungal infections can be explored in an attempt to lessen the side effects of more potent drugs like AmB by combining it with other less toxic antifungals. Thus, promoting the reduction of the concentration of AmB used in a monotherapy. In addition, some studies based on the combination of antifungals aim to assess whether there is synergistic or additive potential between specific antifungals (Olson et al., 2010). In murine models of disseminated aspergillosis, combined therapy of AmBisome[®] prior to echinocandin or both drugs administered together were as effective as AmBisome[®] alone. Both classes of drugs target the cell membrane, as we mentioned earlier. The authors support the use of AmBisome[®] before echinocandins due to the greater reduction in fungal burden observed in the study (Olson et al., 2010). The combination of AmBisome[®] with voriconazole was effective for treatment of CNS aspergillosis, while the combination of AmBisome[®] with micafungin or caspofungin did not show much benefit in CNS disease treatment (Clemons et al., 2005).

The oligosaccharide OligoG, an alginate derived from seaweed, inhibited the growth of *Candida* and *Aspergillus* strains *in vitro*, in a dose dependent manner. In addition, it inhibited hyphal growth depending on the strain and disrupted biofilm formation. OligoG was also associated with other antifungals such as nystatin, AmB, fluconazole, miconazole, voriconazole and terbinafine, which potentiated their inhibitory effects *in vitro*. The combination of drugs led to a decrease of up to 4 times in MIC, with nystatin being the best association, promoting a reduction of up to 16 times in MIC (Tøndervik et al., 2014).

Salama et al. (2016) evaluated the activity of cross-linked chitosan biguanidine (CChG) loaded with AgNPs. The thermal

TABLE 2 | Nanoformulations studied for the treatment of fungal infections caused by the *Aspergillus* sp..

Nanoparticle	Drug (*)	Fungi	In vitro/in vivo	References
PLGA/vv	AmB VOR	<i>A. fumigatus</i>	<i>In vivo</i> (mice) <i>In vivo</i> (rabbits)	Italia et al., 2011; Van de Ven et al., 2012 Yang et al., 2011
Chitosan biguanidine	Silver	<i>A. fumigatus</i> <i>G. candidum</i> <i>S. recemosum</i>	<i>In vitro</i>	Salama et al., 2016
PMA	AmB	<i>A. fumigatus</i>	<i>In vitro/in vivo</i> (mice)	Shirkhani et al., 2015
PEG/PLA	ITZ	<i>A. fumigatus</i>	<i>In vitro</i>	Essa et al., 2013
PEG-LNPs	AmB	<i>C. albicans</i>	<i>In vitro/in vivo</i> (rats and mice)	Jung et al., 2009
Alginate oligosaccharides (OligoG)	–	<i>C. albicans</i> <i>C. parapsilosis</i> <i>C. Krusei</i> <i>C. lusitaniae</i> <i>C. tropicalis</i> <i>C. glabrata</i> <i>niger</i> <i>A. fumigatus</i> <i>A. flavus</i>	<i>In vitro</i>	Tøndervik et al., 2014
mPEG- <i>b</i> -P-(Glu-co-Phe)	AmB	<i>A. fumigatus</i>	<i>in vivo</i> (mice)	Yang et al., 2018
Nanosuspension	AmB	<i>C. albicans</i> <i>A. fumigatus</i> <i>T. rubrum</i>	<i>In vitro/in vivo</i> (mice)	Van de Ven et al., 2012
Liposomal (AmBisome®)	ITZ	<i>A. fumigatus</i>	<i>In vivo</i> (quails)	Wlaz et al., 2015
	AmB	<i>A. fumigatus</i>	<i>In vivo</i> (mice) <i>In vivo</i> (rabbits and mice) <i>In vivo</i> (human)	Clemons et al., 2005; Olson et al., 2006, 2010, 2015; Lewis et al., 2007; Jung et al., 2009; Italia et al., 2011; Seyedmousavi et al., 2013; Siopi et al., 2019 Sheikh et al., 2010. Newton et al., 2016; Godet et al., 2017
Liposomal	AmB	<i>A. fumigatus</i>	<i>In vitro/in vivo</i> (guinea pig)	Zhao et al., 2015
Liposomal—Lambin® (Lbn)	AmB	<i>A. fumigatus</i>	<i>In vivo</i> (mice)	Olson et al., 2015
Liposomal (Abelcet®)	AmB	<i>A. fumigatus</i>	<i>In vivo</i> (mice) <i>In vivo</i> (rats)	Olson et al., 2006; Lewis et al., 2007 Cicogna et al., 1997
SLNs	NAT	<i>A. fumigatus</i> and <i>C. albicans</i>	<i>In vitro/ex vivo</i> (goat corneas)	Khames et al., 2019

(*) Drugs: AmB, Amphotericin B; VOR, voriconazole; ITZ, Itraconazole; NYS, Nystatin.

stability of the polymer was improved due to silver incorporation, resulting in NPs with lower cytotoxicity for MCF-7 cells (human breast adenocarcinoma cell line) and improved antimicrobial activity against bacteria and fungi compared to chitosan or CChG. In this case, the association of polymers with AgNPs is mainly aimed at improving antimicrobial activity due to the intrinsic properties of Ag in association with sustained delivery through polymers. The degradation of the nanocomposite at higher temperatures after the association of CChG and AgNPs, is due to the interaction of these compounds that promoted an enhanced stabilization of the structure.

The studies involving NPs in aspergillosis treatment are summarized in **Table 2**.

PCM

PCM is a systemic mycosis caused by thermo-dimorphic fungi of the genus *Paracoccidioides* (Taborda et al., 2015). PCM has two clinical forms, acute/subacute form (juvenile) and chronic form

(adult) (Shikanai-Yasuda and Mendes, 2007). PCM treatment is based on chemotherapy, the chief ones being azole agents such as fluconazole, polyenes such as AmB and sulfonamides such as Bactrim® (Shikanai-Yasuda and Mendes, 2007; Amaral et al., 2009; Souza and Amaral, 2017).

The targeting of NPs commonly can be achieved by adding antibodies to the surface of the particle. However, additional molecules also have this potential to target NPs to specific tissues. Just as polysorbate 80 assists in targeting drugs to the brain, the incorporation of dimercaptosuccinic acid (DMSA) in nanocarrier systems directs NPs mainly to the lung. However, the mechanisms by which this tropism occurs has not been well-established (Amaral et al., 2009). PLGA and DMSA NPs carrying AmB (Nano-D-AMB) were evaluated for treatment efficacy of chronic PCM caused by *P. brasiliensis*. After 30 days of infection, BALB/c mice were treated with 6 mg/kg Nano-D-AMB at 72 h intervals. Treated mice had reduced body weight loss, absence of stress (piloerection and hypotrichosis) and renal or hepatic

TABLE 3 | Nanoformulations studied for the treatment of fungal infections caused by dimorphic fungi *Coccidioides* sp., *Paracoccidioides* sp. and *Histoplasma* spp..

Nanoparticle	Drug (*)	Fungi	In vitro/in vivo	References
Lipid complex; colloidal dispersion and liposomal	AmB and NYS	<i>C. immitis</i>	<i>In vitro</i>	González et al., 2002
Liposomal (AmBisome)	AmB	<i>C. immitis</i>	<i>In vivo</i> (human)	Antony et al., 2003; Rangel et al., 2010; Nakhla, 2018; Sidhu et al., 2018
			<i>In vivo</i> (rabbits)	Clemons et al., 2002
		<i>C. posadasii</i>	<i>In vivo</i> (rabbits)	Clemons et al., 2009
		<i>Coccidioides</i> spp.	<i>In vivo</i> (human)	Stewart et al., 2018
		<i>H. capsulatum</i>	<i>In vivo</i> (human)	Johnson et al., 2002
Lipid complex (Abelcet)	AmB	<i>C. immitis</i>	<i>In vivo</i> (human)	Koehler et al., 1998; Sidhu et al., 2018
		<i>C. posadasii</i>	<i>In vivo</i> (rabbits)	Capilla et al., 2007; Clemons et al., 2009
PLGA-DMSA	AmB	<i>P. brasiliensis</i>	<i>In vivo</i> (mice)	Amaral et al., 2009; Souza et al., 2015
	ITZ		<i>In vitro</i>	Cunha-Azevedo et al., 2011
Nanostructured lipid system (NLS)	Dodecyl gallate (DOD)	<i>P. brasiliensis</i> and <i>P. lutzii</i>	<i>In vitro/in vivo</i>	Singulani et al., 2018

(*) Drugs: AmB, Amphotericin B; ITZ, Itraconazole; NYS, Nystatin.

abnormalities compared to the AmB deoxycholate treated group. In addition, the formulation raised no genotoxic and cytotoxic effects (Amaral et al., 2009). A subsequent study showed that the nano-D-AMB is highly captured in the lungs, liver, and spleen of mice (Souza et al., 2015). DMSA-PLGA NPs loaded with ITZ have also been studied against *P. brasiliensis* and the PLGA-ITZ had lower MICs compared to ITZ alone with less cytotoxicity compared to the free drug (Cunha-Azevedo et al., 2011).

Gallic acid is a secondary metabolite derived from plants such as *Paeonia rockii*, *Astronium* sp., and *Syzygium cumini*, among others. Interestingly, reversed gallic acid, or dodecyl gallate (DOD) has antifungal activity (Singulani et al., 2018). A recent study evaluated the antifungal efficacy of DOD associated with NLS (DOD + NLS) *in vitro* and *in vivo*. The results showed that the formulation exhibited good *in vitro* activity against *P. brasiliensis* and *P. lutzii* (0.24 and 0.49 mg/L, respectively), low toxicity in pulmonary fibroblasts (>250 mg/L) and zebrafish embryos (>125 mg/L). In addition, DOD + NLS reduced the fungal load in mouse lungs at a concentration of 10 mg/kg (Singulani et al., 2018).

Although promising, vaccines that have been studied against PCM have shown a rapid degradation of the immunogen (Travassos and Tabora, 2012). The most efficient way to protect the immunogenic molecule, reduce its concentration and reduce the number of doses was achieved by complexing it into NPs, as shown by Amaral et al. (2010), Jannuzzi et al. (2018), and Ribeiro et al. (2013). For example, the immunomodulatory peptide P10 trapped in PLGA NPs was effective in treating chronic murine PCM after 90 days of treatment with 5 or 10 50 μL^{-1} , and the P10-PLGA NPs induced a robust, protective Th1 immune response (Amaral et al., 2010).

Variable single-chain fragments (scFv) obtained from the monoclonal antibody (mAb) 7.B12 that mimics gp43, the main *P. brasiliensis* antigen was incorporated into PLGA. After scFv-PLGA treatment of infected mice, a reduction in fungal load and

increased production of IFN- γ and IL-12 cytokines was observed, as well as an abundance of macrophages and dendritic cells was seen in the lung tissue (Jannuzzi et al., 2018).

Ribeiro et al. (2013) used liposomes and PLGA to deliver plasmids containing the genetic information necessary for the expression of *Mycobacterium leprae* heat shock proteins (DNAhsp65). Both formulations were able to promote immune response modulation and fungal load reduction with the advantage of nasal administration of the liposomal formulation that could be more easily accepted by patients.

The studies involving NPs for PCM treatment are summarized in **Table 3** and for vaccination in **Table 4**.

Histoplasmosis

Histoplasmosis is an invasive endemic mycosis caused by the thermo dimorphic fungus *H. capsulatum* (Kauffman, 2007). Histoplasmosis is considered the most common respiratory fungal infection with a worldwide distribution of an asymptomatic infection to deep pulmonary mycosis and/or systemic disease, depending on the infectious inoculum and the immunologic condition of the host (Sepúlveda et al., 2017). The yeast form of *H. capsulatum* has mechanisms to prevent intracellular death by phagocytes. In addition, the intracellular localization of the fungus makes it difficult to treat the infection, as macrophages can act as a barrier, preventing the antifungal drug from interacting with its target in the cell (Edwards et al., 2013).

Currently, only AmBisome[®] has been evaluated in the treatment of histoplasmosis. A study compared the efficacy of AmB deoxycholate and AmBisome[®] in the treatment of 81 patients with moderate and severe histoplasmosis associated with AIDS. The AmB deoxycholate achieved clinical success in 14 of 22 patients (64%), with death of 3. Side effects developed in 63%, with nephrotoxicity in 37%. AmBisome[®] was effective in 45 of 51

TABLE 4 | Studies reporting the use of nanoformulations as an antigen delivery vehicle for *Candida albicans* and *Paracoccidioides brasiliensis* vaccine.

Fungi	Nanoformulation + adjuvant	Antigen	Animal model	Route of administration	References
<i>Candida albicans</i> and <i>C. tropicalis</i>	PC/Chol liposomes	Fraction of <i>C. albicans</i> mannan	BALB/cByJ mice	Intravenous	Han and Cutler, 1995
<i>Candida albicans</i>	DMPC/DMPGLiposomes + LA	Ribosomes of <i>C. albicans</i>	ICR mice	Subcutaneous	Eckstein et al., 1997
	Metallochelating liposomes + MDP	rHSP90	BALB/c mice	Intradermal	Mašek et al., 2011
	Metallochelating liposomes + MDP and GMDP	rHSP90	ICR mice	Intradermal	Knotigová et al., 2015
	MO liposomes + DODAB	<i>C. albicans</i> wall proteins	BALB/c mice	Subcutaneous	Carneiro et al., 2015, 2016
<i>Paracoccidioides brasiliensis</i>	PLGA	P10 peptide	BALB/c mice	–	Amaral et al., 2010
		Single-chain Variable fragments (scFv)	BALB/c mice	Intramuscular	Jannuzzi et al., 2018
	PLGA e Liposomes	DNAhsp65	BALB/c mice	Intramuscular or intranasally	Ribeiro et al., 2013

patients (88%), although one patient died, 25% experienced drug-related side effects with 9% developing nephrotoxicity (Johnson et al., 2002) (Table 3).

Although the design of nanoparticles for delivery to specific cells is critical (as mentioned in topic 1), we believe that it is only a matter of time before these strategies are more deeply explored and improved upon in relation to fungal infections caused by pathogens such as *H. capsulatum*. These strategies can enhance the efficacy of treatment and, potentially, reduce occurrences of the disease.

There is no NP-based strategy for vaccination against *H. capsulatum*, although there are studies based on glucan particles extracted from *S. cerevisiae* (Wüthrich et al., 2015; Deepe et al., 2018).

Coccidioidomycosis

Coccidioidomycosis is caused by inhalation of infectious propagules of the dimorphic fungus *C. immitis* or *C. posadasii*. It is an endemic mycosis in the southwestern USA, Mexico, and some regions of South America (Stockamp and Thompson, 2016). Studies indicated that 17–29% cases of pneumonia acquired in highly endemic areas were caused by *Coccidioides* spp. (Thompson, 2011). Patients may have varying complications of the disease, from pulmonary to widespread infections reaching bones, joints, meninges, and skin (Thompson, 2011; McConnell et al., 2017).

Prior to nanoformulations, it was believed that the use of AmB to treat meningitis was not possible due to the low concentration of drugs reaching the brain. However, AmBisome[®], was effective in animal models (Clemons et al., 2002). The increased ability of liposomal AmB to reach the disease site is due to the transport by infiltrating monocytic cells (Clemons et al., 2009). The authors compared the efficacy of liposomal AmB formulation of Abelcet[®] and AmBisome[®] in the treatment of meningitis caused by *C. posadasii* in New Zealand white rabbits. The treated animals showed a reduction in fungal burden on the brain and

spinal cord, 100–10,000 times lower than the untreated group. Statistically, both formulations were considered equally efficient. However, as we described, a formulation with higher liposomal effects has been described for drug delivery to the brain for the treatment of cryptococcal meningitis (Xu et al., 2011).

To evaluate the efficacy and toxicity of Abelcet[®] and AmBisome[®] in the treatment of severe coccidioidomycosis in human patients, a retrospective review was conducted in patients between 2005 and 2014. Both formulations were equally effective in the treatment without significant difference, however, due to acute kidney injury, the treatment had to be discontinued in 10 patients treated with Abelcet[®] and in only one with AmBisome[®] (Sidhu et al., 2018). The toxicity of the Abelcet[®] has previously been discussed (Koehler et al., 1998).

AmBisome[®] is effective in treating coccidioidomycosis in human patients (Stewart et al., 2018). During treatment of coccidioidal meningitis for a period of 9 months, AmBisome[®] did not present clinical or laboratory data suggestive of toxicity (Rangel et al., 2010). In addition, AmBisome[®] has been successful in treating disseminated coccidioidomycosis in patients undergoing steroid therapy (Antony et al., 2003). It was employed in case of rare dissemination to the spine that required surgical intervention, being associated with continuous therapy with other azoles (Nakhla, 2018).

The studies involving NPs in the treatment of coccidioidomycosis are summarized in Table 3.

Blastomyces sp. and *Pneumocystis* sp. are important pathogens that cause systemic infections. The effectiveness of nanoformulations against these genera has not yet been discussed in the literature.

CONCLUDING REMARKS

The search for new and more effective therapeutic options for the treatment of fungal infections has advanced continuously

with the use of new technologies such as the development of NPs. Different types of nanoformulations have been studied and greater efficacy and less toxicity have been achieved in the administration of conventional antifungal drugs, such as AmB, compared to the free drug available in today's market. In this way, nanotechnology allows for the development of formulations that can improve not only the effectiveness of the treatment, but also the quality of life of the patient by reducing side effects, especially during prolonged therapies. In addition, we emphasize here the importance of developing new drugs that can overcome resistance and that can be combined with NPs in the development of improved therapies. Nanotechnology is still an expanding field in vaccinology and pharmacology. The application of NPs for antigen delivery is at an early stage of development, but the first studies already show the advantages of this system, as described in this review. In addition, NPs can be obtained by different synthetic methods that allow for the adaptation of production according to the needs of the manufacturer. Obstacles, however,

such as the standardization of NPs still need to make progress in this field.

AUTHOR CONTRIBUTIONS

BK conceived, designed, did the literature review, provided, and wrote the manuscript. SR and SS did the literature review, provided, and wrote the manuscript. JN, LT, and CT assisted in the preparation, final review, and co-wrote the manuscript. All authors listed approved it for publication.

FUNDING

This research was funded by São Paulo Research Foundation (FAPESP) grants 2016/08730-6, 2018/26402-1, and 2017/25780-0. CNPq (grant 420480/2018-8) and CAPES-Education Ministry, Brazil. CT and LT are research fellows of the CNPq.

REFERENCES

- Ahmad, A., Mukherjee, P., Senapati, S., Mandal, D., Khan, M. I., Kumar, R., et al. (2003). Extracellular biosynthesis of silver nanoparticles using the fungus *Fusarium oxysporum*. *Colloids Surf. B Biointerfaces* 28, 313–318. doi: 10.1016/S0927-7765(02)00174-1
- Ahmed, A.-A., Hamzah, H., and Maarooof, M. (2018). Analyzing formation of silver nanoparticles from the filamentous fungus *Fusarium oxysporum* and their antimicrobial activity. *Turk. J. Biol.* 42, 54–62. doi: 10.3906/biy-1710-2
- Ahmed, S., Vepuri, S. B., Kalhapure, R. S., and Govender, T. (2016). Interactions of dendrimers with biological drug targets: reality or mystery - a gap in drug delivery and development research. *Biomater. Sci.* 4, 1032–1050. doi: 10.1039/C6BM00090H
- Ahmed, T. A., and Aljaeid, B. M. (2016). Preparation, characterization, and potential application of chitosan, chitosan derivatives, and chitosan metal nanoparticles in pharmaceutical drug delivery. *Drug Des. Devel. Ther.* 10, 483–507. doi: 10.2147/DDDT.S99651
- Akhtar, M. S., Panwar, J., and Yun, Y. S. (2013). Biogenic synthesis of metallic nanoparticles by plant extracts. *ACS Sustain. Chem. Eng.* 1, 591–602. doi: 10.1021/sc300118u
- Amaral, A. C., Bocca, A. L., Ribeiro, A. M., Nunes, J., Peixoto, D. L. G., Simioni, A. R., et al. (2009). Amphotericin B in poly(lactic-co-glycolic acid) (PLGA) and dimercaptosuccinic acid (DMSA) nanoparticles against paracoccidiodomycosis. *J. Antimicrob. Chemother.* 63, 526–533. doi: 10.1093/jac/dkn539
- Amaral, A. C., Marques, A. F., Muñoz, J. E., Bocca, A. L., Simioni, A. R., Tedesco, A. C., et al. (2010). Poly(lactic acid-glycolic acid) nanoparticles markedly improve immunological protection provided by peptide P10 against murine paracoccidiodomycosis. *Br. J. Pharmacol.* 159, 1126–1132. doi: 10.1111/j.1476-5381.2009.00617.x
- Ambrosio, J. A. R., Pinto, B. C. D. S., da Silva, B. G. M., Passos, J. C. D. S., Beltrame Junior, M., Costa, M. S., et al. (2019). Gelatin nanoparticles loaded methylene blue as a candidate for photodynamic antimicrobial chemotherapy applications in *Candida albicans* growth. *J. Biomater. Sci. Polym. Ed.* 30, 1356–1373. doi: 10.1080/09205063.2019.1632615
- Anand, P., Kunnumakkara, A. B., Newman, R. A., and Aggarwal, B. B. (2007). Bioavailability of curcumin: problems and promises. *Mol. Pharm.* 4, 807–818. doi: 10.1021/mp700113r
- Antony, S., Dominguez, D. C., and Sotelo, E. (2003). Use of liposomal amphotericin B in the treatment of disseminated coccidiodomycosis. *J. Natl. Med. Assoc.* 95, 982–5.
- Armstead, A. L., and Li, B. (2011). Nanomedicine as an emerging approach against intracellular pathogens. *Int. J. Nanomed.* 6, 3281–3293. doi: 10.2147/IJN.S27285
- Armstrong-James, D., Brown, G. D., Netea, M. G., Zelante, T., Gresnigt, M. S., van de Veerdonk, F. L., et al. (2017). Immunotherapeutic approaches to treatment of fungal diseases. *Lancet Infect. Dis.* 17, e393–e402. doi: 10.1016/S1473-3099(17)30442-5
- Ashley, E. D., Drew, R., Johnson, M., Danna, R., Dabrowski, D., Walker, V., et al. (2012). Cost of invasive fungal infections in the era of new diagnostics and expanded treatment options. *Pharmacother. J. Hum. Pharmacol. Drug Ther.* 32, 890–901. doi: 10.1002/j.1875-9114.2012.01124
- Beloqui, A., Solinis, M. A., Delgado, A., Évora, C., del Pozo-Rodríguez, A., and Rodríguez-Gascón, A. (2013). Biodistribution of Nanostructured Lipid Carriers (NLCs) after intravenous administration to rats: influence of technological factors. *Eur. J. Pharm. Biopharm.* 84, 309–314. doi: 10.1016/j.ejpb.2013.01.029
- Benedict, K., Jackson, B. R., Chiller, T., and Beer, K. D. (2019). Estimation of direct healthcare costs of fungal diseases in the United States. *Clin. Infect. Dis.* 68, 1791–1797. doi: 10.1093/cid/ciy776
- Bicanic, T. A. (2014). Systemic fungal infections. *Medicine* 42, 26–30. doi: 10.1016/j.mpmed.2013.10.006
- Bolhassani, A., Javanad, S., Saleh, T., Hashemi, M., Aghasadeghi, M. R., and Sadat, S. M. (2014). Polymeric nanoparticles: potent vectors for vaccine delivery targeting cancer and infectious diseases. *Hum. Vaccin. Immunother.* 10, 321–332. doi: 10.4161/hv.26796
- Bongomin, F., Gago, S., Oladele, R. O., and Denning, D. W. (2017). Global and multi-national prevalence of fungal diseases-estimate precision. *J. Fungi* 3:57. doi: 10.3390/jof3040057
- Brown, G. D., Denning, D. W., Gow, N. A. R., Levitz, S. M., Netea, M. G., and White, T. C. (2012). Hidden killers: human fungal infections. *Sci. Transl. Med.* 4:165rv13. doi: 10.1126/science.1222236
- Brown, G. D., Taylor, P. R., Reid, D. M., Willment, J. A., Williams, D. L., Martinez-Pomares, L., et al. (2002). Dectin-1 is a major β -Glucan receptor on macrophages. *J. Exp. Med.* 196, 407–412. doi: 10.1084/jem.20020470
- Brunet, K., Alanio, A., Lortholary, O., and Rammaert, B. (2018). Reactivation of dormant/latent fungal infection. *J. Infect.* 77, 463–468. doi: 10.1016/j.jinf.2018.06.016
- Capilla, J., Clemons, K. V., Sobel, R. A., and Stevens, D. A. (2007). Efficacy of amphotericin B lipid complex in a rabbit model of coccidiodal meningitis. *J. Antimicrob. Chemother.* 60, 673–676. doi: 10.1093/jac/dkm264
- Carlson, C., Hussain, S. M., Schrand, A. M., K., Braydich-Stolle, L. K., Hess, K. L., Jones, R. L., et al. (2008). Unique cellular interaction of silver nanoparticles: size-dependent generation of reactive oxygen species. *J. Phys. Chem. B* 112, 13608–13619. doi: 10.1021/jp712087m
- Carmona, E. M., and Limper, A. H. (2017). Overview of treatment approaches for fungal infections. *Clin. Chest Med.* 38, 393–402. doi: 10.1016/j.ccm.2017.04.003

- Carneiro, C., Correia, A., Collins, T., Vilanova, M., Pais, C., Gomes, A. C., et al. (2015). DODAB:monoolein liposomes containing *Candida albicans* cell wall surface proteins: a novel adjuvant and delivery system. *Eur. J. Pharm. Biopharm.* 89, 190–200. doi: 10.1016/j.ejpb.2014.11.028
- Carneiro, C., Correia, A., Lima, T., Vilanova, M., Pais, C., Gomes, A. C., et al. (2016). Protective effect of antigen delivery using monoolein-based liposomes in experimental hematogenously disseminated candidiasis. *Acta Biomater.* 39, 133–145. doi: 10.1016/j.actbio.2016.05.001
- Carta, F., Osman, S. M., Vullo, D., AlOthman, Z., Del Prete, S., Capasso, C., et al. (2015). Poly(amidoamine) dendrimers show carbonic anhydrase inhibitory activity against α -, β -, γ - and η -class enzymes. *Bioorg. Med. Chem.* 23, 6794–6798. doi: 10.1016/j.bmc.2015.10.006
- Cassone, A., and Casadevall, A. (2012). Recent progress in vaccines against fungal diseases. *Curr. Opin. Microbiol.* 15, 427–433. doi: 10.1016/j.mib.2012.04.004
- Chatterjee, B., Gorain, B., Mohanaidu, K., Sengupta, P., Mandal, U. K., and Choudhury, H. (2019). Targeted drug delivery to the brain via intranasal nanoemulsion: Available proof of concept and existing challenges. *Int. J. Pharm.* 565, 258–268. doi: 10.1016/j.ijpharm.2019.05.032
- Chen, S. C.-A., Meyer, W., and Sorrell, T. C. (2014). *Cryptococcus gattii* infections. *Clin. Microbiol. Rev.* 27, 980–1024. doi: 10.1128/CMR.00126-13
- Chomoucka, J., Drbohlavova, J., Huska, D., Adam, V., Kizek, R., and Hubalek, J. (2010). Magnetic nanoparticles and targeted drug delivering. *Pharmacol. Res.* 62, 144–149. doi: 10.1016/j.phrs.2010.01.014
- Cicogna, C. E., White, M. H., Bernard, E. M., Ishimura, T., Sun, M., Tong, W. P., et al. (1997). Efficacy of prophylactic aerosol amphotericin B lipid complex in a rat model of pulmonary aspergillosis. *Antimicrob. Agents Chemother.* 41, 259–61. doi: 10.1128/AAC.41.2.259
- Clemons, K. V., Capilla, J., Sobel, R. A., Martinez, M., Tong, A.-J., and Stevens, D. A. (2009). Comparative efficacies of lipid-complexed amphotericin B and liposomal amphotericin B against coccidioidal meningitis in rabbits. *Antimicrob. Agents Chemother.* 53, 1858–1862. doi: 10.1128/AAC.01538-08
- Clemons, K. V., Espiritu, M., Parmar, R., and Stevens, D. A. (2005). Comparative efficacies of conventional amphotericin b, liposomal amphotericin B (AmBisome), caspofungin, micafungin, and voriconazole alone and in combination against experimental murine central nervous system aspergillosis. *Antimicrob. Agents Chemother.* 49, 4867–4875. doi: 10.1128/AAC.49.12.4867-4875.2005
- Clemons, K. V., Sobel, R. A., Williams, P. L., Pappagianis, D., and Stevens, D. A. (2002). Efficacy of intravenous liposomal amphotericin B (AmBisome) against coccidioidal meningitis in rabbits. *Antimicrob. Agents Chemother.* 46, 2420–2426. doi: 10.1128/AAC.46.8.2420-2426.2002
- Coelho, C., and Casadevall, A. (2016). Cryptococcal therapies and drug targets: the old, the new and the promising. *Cell. Microbiol.* 18, 792–799. doi: 10.1111/cmi.12590
- Colombo, A. L., de Almeida Júnior, J. N., Slavin, M. A., Chen, S. C.-A., and Sorrell, T. C. (2017). *Candida* and invasive mould diseases in non-neutropenic critically ill patients and patients with haematological cancer. *Lancet Infect. Dis.* 17, e344–e356. doi: 10.1016/S1473-3099(17)30304-3
- Corcoran, T. E., Venkataraman, R., Mihelc, K. M., Marcinkowski, A. L., Ou, J., McCook, B. M., et al. (2006). Aerosol deposition of lipid complex amphotericin-B (Abelcet) in lung transplant recipients. *Am. J. Transplant.* 6, 2765–2773. doi: 10.1111/j.1600-6143.2006.01529.x
- Couvreux, P. (2013). Nanoparticles in drug delivery: past, present and future. *Adv. Drug Deliv. Rev.* 65, 21–23. doi: 10.1016/j.addr.2012.04.010
- Cray, J. A., Bell, A. N. W., Bhaganna, P., Mswaka, A. Y., Timson, D. J., and Hallsworth, J. E. (2013). The biology of habitat dominance; can microbes behave as weeds? *Microb. Biotechnol.* 6, 453–492. doi: 10.1111/1751-7915.12027
- Cunha-Azevedo, E. P., Silva, J. R., Martins, O. P., Siqueira-Moura, M. P., Bocca, A. L., Felipe, M. S. S., et al. (2011). *In vitro* antifungal activity and toxicity of itraconazole in DMSA-PLGA nanoparticles. *J. Nanosci. Nanotechnol.* 11, 2308–2314. doi: 10.1166/jnn.2011.3576
- Curic, A., Möschwitzer, J. P., and Fricker, G. (2017). Development and characterization of novel highly-loaded itraconazole poly(butyl cyanoacrylate) polymeric nanoparticles. *Eur. J. Pharm. Biopharm.* 114, 175–185. doi: 10.1016/j.ejpb.2017.01.014
- Dai, T., Tanaka, M., Huang, Y. Y., and Hamblin, M. R. (2011). Chitosan preparations for wounds and burns: antimicrobial and wound-healing effects. *Expert Rev. Anti. Infect. Ther.* 9, 857–879. doi: 10.1586/eri.11.59
- Danhier, F., Ansorena, E., Silva, J. M., Coco, R., Le Breton, A., and Préat, V. (2012). PLGA-based nanoparticles: an overview of biomedical applications. *J. Control. Release* 161, 505–522. doi: 10.1016/j.jconrel.2012.01.043
- Deepe, G. S., Buesing, W. R., Ostroff, G. R., Abraham, A., Specht, C. A., Huang, H., et al. (2018). Vaccination with an alkaline extract of *Histoplasma capsulatum* packaged in glucan particles confers protective immunity in mice. *Vaccine* 36, 3359–3367. doi: 10.1016/j.vaccine.2018.04.047
- Del Poeta, M., and Casadevall, A. (2012). Ten Challenges on *Cryptococcus* and *Cryptococcosis*. *Mycopathologia* 173, 303–310. doi: 10.1007/s11046-011-9473-z
- Di Mambro, T., Guerriero, I., Aurisicchio, L., Magnani, M., and Marra, E. (2019). The yin and yang of current antifungal therapeutic strategies: how can we harness our natural defenses? *Front. Pharmacol.* 10:80. doi: 10.3389/fphar.2019.00080
- Dipankar, C., and Murugan, S. (2012). The green synthesis, characterization and evaluation of the biological activities of silver nanoparticles synthesized from *Iresine herbstii* leaf aqueous extracts. *Colloids Surf. B. Biointerfaces* 98, 112–119. doi: 10.1016/j.colsurfb.2012.04.006
- Domingues Bianchin, M., Borowicz, S. M., da Rosa Monte Machado, G., Pippi, B., Stanisquaski Guterres, S., Raffin Pohlmann, A., et al. (2019). Lipid core nanoparticles as a broad strategy to reverse fluconazole resistance in multiple *Candida* species. *Colloids Surf. B Biointerfaces* 175, 523–529. doi: 10.1016/j.colsurfb.2018.12.011
- Donnelly, R. F., McCarron, P. A., and Tunney, M. M. (2008). Antifungal photodynamic therapy. *Microbiol. res.* 163, 1–12. doi: 10.1016/j.micres.2007.08.001
- Dube, A., Reynolds, J. L., Law, W.-C., Maponga, C. C., Prasad, P. N., and Morse, G. D. (2014). Multimodal nanoparticles that provide immunomodulation and intracellular drug delivery for infectious diseases. *Nanomed. Nanotechnol. Biol. Med.* 10, 831–838. doi: 10.1016/j.nano.2013.11.012
- Eckstein, M., Barenholz, Y., Bar, L. K., and Segal, E. (1997). Liposomes containing *Candida albicans* ribosomes as a prophylactic vaccine against disseminated candidiasis in mice. *Vaccine* 15, 220–224. doi: 10.1016/S0264-410X(96)00137-5
- Edwards, J. A., Kemski, M. M., and Rappleye, C. A. (2013). Identification of an aminothiazole with antifungal activity against intracellular *Histoplasma capsulatum*. *Antimicrob. Agents Chemother.* 57, 4349–4359. doi: 10.1128/AAC.00459-13
- El-Sheridy, N. A., Ramadan, A. A., Eid, A. A., and El-Khordagui, L. K. (2019). Itraconazole lipid nanocapsules gel for dermatological applications: *in vitro* characteristics and treatment of induced cutaneous candidiasis. *Colloids Surf. B Biointerfaces* 181, 623–631. doi: 10.1016/j.colsurfb.2019.05.057
- Essa, S., Louhichi, F., Raymond, M., and Hildgen, P. (2013). Improved antifungal activity of itraconazole-loaded PEG/PLA nanoparticles. *J. Microencapsul.* 30, 205–217. doi: 10.3109/02652048.2012.714410
- Fernandes Costa, A., Evangelista Araujo, D., Santos Cabral, M., Teles Brito, I., Borges de Menezes Leite, L., Pereira, M., et al. (2019). Development, characterization, and *in vitro-in vivo* evaluation of polymeric nanoparticles containing miconazole and farnesol for treatment of vulvovaginal candidiasis. *Med. Mycol.* 57, 52–62. doi: 10.1093/mmy/myx155
- Fontes, A. C., Bretas Oliveira, D., Santos, J. R., Carneiro, H. C., Ribeiro, NQ., Oliveira, L. V., et al. (2017). A subdose of fluconazole alters the virulence of *Cryptococcus gattii* during murine cryptococcosis and modulates type I interferon expression. *Med. Mycol.* 55, 203–212. doi: 10.1093/mmy/myw056
- Franci, G., Falanga, A., Galdiero, S., Palomba, L., Rai, M., Morelli, G., et al. (2015). Silver nanoparticles as potential antibacterial agents. *Molecules* 20, 8856–8874. doi: 10.3390/molecules20058856
- Frank, L. A., Onzi, G. R., Morawski, A. S., Pohlmann, A. R., Guterres, S. S., and Contri, R. V. (2020). Chitosan as a coating material for nanoparticles intended for biomedical applications. *React. Funct. Polym.* 147:104459. doi: 10.1016/j.reactfunctpolym.2019.104459
- Gartzandia, O., Herran, E., Pedraz, J. L., Carro, E., Igartua, M., and Hernandez, R. M. (2015). Chitosan coated nanostructured lipid carriers for brain delivery of proteins by intranasal administration. *Colloids Surf. B Biointerfaces* 134, 304–313. doi: 10.1016/j.colsurfb.2015.06.054
- Ghaffari, M., Dehghan, G., Abedi-Gaballu, F., Kashanian, S., Baradaran, B., Ezzati Nazhad Dolatabadi, J., et al. (2018). Surface functionalized dendrimers as controlled-release delivery nanosystems for tumor targeting. *Eur. J. Pharm. Sci.* 122, 311–330. doi: 10.1016/j.ejps.2018.07.020

- Giacomazzi, J., Baethgen, L., Carneiro, L. C., Millington, M. A., Denning, D. W., Colombo, A. L., et al. (2016). The burden of serious human fungal infections in Brazil. *Mycoses* 59, 145–150. doi: 10.1111/myc.12427
- Gintjee, T. J., Donnelly, M. A., and Thompson, G. R. (2020). Aspiring antifungals: review of current antifungal pipeline developments. *J. Fungi* 6:28. doi: 10.3390/jof6010028
- Godet, C., Couturaud, F., Ragot, S., Laurent, F., Brun, A. L., Bergeron, A., et al. (2017). Aspergillose bronchopulmonaire allergique: évaluation d'un traitement d'entretien par Ambisome® nébulisé [Allergic bronchopulmonary aspergillosis: evaluation of a maintenance therapy with nebulized Ambisome®]. *Rer. Mal. Respir.* 34, 581–587. doi: 10.1016/j.rmr.2017.04.001
- Gondim, B. L. C., Castellano, L. R. C., de Castro, R. D., Machado, G., Carlo, H. L., Valença, A. M. G., et al. (2018). Effect of chitosan nanoparticles on the inhibition of *Candida* spp. biofilm on denture base surface. *Arch. Oral Biol.* 94, 99–107. doi: 10.1016/j.archoralbio.2018.07.004
- González, G. M., Tijerina, R., Sutton, D. A., Graybill, J. R., and Rinaldi, M. G. (2002). *In vitro* activities of free and lipid formulations of amphotericin B and nystatin against clinical isolates of *Coccidioides immitis* at various saprobic stages. *Antimicrob. Agents Chemother.* 46, 1583–1585. doi: 10.1128/AAC.46.5.1583-1585.2002
- Goodridge, H. S., Wolf, A. J., and Underhill, D. M. (2009). β -glucan recognition by the innate immune system. *Immunol. Rev.* 230, 38–50. doi: 10.1111/j.1600-065X.2009.00793.x
- Hagen, F., Khayhan, K., Theelen, B., Kolecka, A., Polacheck, I., Sionov, E., et al. (2015). Recognition of seven species in the *Cryptococcus gattii/Cryptococcus neoformans* species complex. *Fungal Genet. Biol.* 78, 16–48. doi: 10.1016/j.fgb.2015.02.009
- Hagiwara, D., Watanabe, A., Kamei, K., and Goldman, G. H. (2016). Epidemiological and genomic landscape of azole resistance mechanisms in *Aspergillus* fungi. *Front. Microbiol.* 7:1382. doi: 10.3389/fmicb.2016.01382
- Han, Y., and Cutler, J. E. (1995). Antibody response that protects against disseminated candidiasis. *Infect. Immun.* 63, 2714–2719. doi: 10.1128/IAI.63.7.2714-2719.1995
- Han, Y., Morrison, R. P., and Cutler, J. E. (1998). A vaccine and monoclonal antibodies that enhance mouse resistance to *Candida albicans* vaginal infection. *Infect Immun.* 66, 5771–5776. doi: 10.1128/IAI.66.12.5771-5776.1998
- Haroon Anwar, S. (2018). A brief review on nanoparticles: types of platforms, biological synthesis and applications. *Res. Rev. J. Mater. Sci.* 6, 109–116. doi: 10.4172/2321-6212.1000222
- Huang, K.-S., Shieh, D.-B., Yeh, C.-S., Wu, P.-C., and Cheng, F.-Y. (2014). Antimicrobial applications of water-dispersible magnetic nanoparticles in biomedicine. *Curr. Med. Chem.* 21, 3312–3122. doi: 10.2174/0929867321666140304101752
- Huang, W., Liao, G., Baker, G. M., Wang, Y., Lau, R., Paderu, P., et al. (2016). Lipid flippase subunit Cdc50 mediates drug resistance and virulence in *Cryptococcus neoformans*. *mBio* 7, e00478–e00416. doi: 10.1128/mBio.00478-16
- Hussain, A., Samad, A., Singh, S. K., Ahsan, M. N., Haque, M. W., Faruk, A., et al. (2016). Nanoemulsion gel-based topical delivery of an antifungal drug: *in vitro* activity and *in vivo* evaluation. *Drug Deliv.* 23, 642–657. doi: 10.3109/10717544.2014.933284
- Hussain, A., Singh, S., Webster, T. J., and Ahmad, F. J. (2017). New perspectives in the topical delivery of optimized amphotericin B loaded nanoemulsions using excipients with innate anti-fungal activities: a mechanistic and histopathological investigation. *Nanomed. Nanotechnol. Biol. Med.* 13, 1117–1126. doi: 10.1016/j.nano.2016.12.002
- Hussein-Al-Ali, S. H., El Zowalaty, M. E., Hussein, M. Z., Geilich, B. M., and Webster, T. J. (2014). Synthesis, characterization, and antimicrobial activity of an ampicillin-conjugated magnetic nanoantibiotic for medical applications. *Int. J. Nanomed.* 9, 3801–3814. doi: 10.2147/IJN.S61143
- Illum, L. (2003). Nasal drug delivery - possibilities, problems and solutions. *J. Controlled Release* 87, 187–198. doi: 10.1016/S0168-3659(02)00363-2
- Iqbal, R., Ahmed, S., Jain, G. K., and Vohora, D. (2019). Design and development of letrozole nanoemulsion: a comparative evaluation of brain targeted nanoemulsion with free letrozole against status epilepticus and neurodegeneration in mice. *Int. J. Pharm.* 565, 20–32. doi: 10.1016/j.ijpharm.2019.04.076
- Ishida, K., Cipriano, T. F., Rocha, G. M., Weissmüller, G., Gomes, F., Miranda, K., et al. (2014). Silver nanoparticle production by the fungus *Fusarium oxysporum*: nanoparticle characterisation and analysis of antifungal activity against pathogenic yeasts. *Mem. Inst. Oswaldo Cruz* 109, 220–228. doi: 10.1590/0074-0276130269
- Italia, J. L., Sharp, A., Carter, K. C., Warn, P., and Kumar, M. N. V. R. (2011). Peroral amphotericin B polymer nanoparticles lead to comparable or superior *in vivo* antifungal activity to that of intravenous Ambisome® or Fungizone™. *PLoS ONE* 6:e25744. doi: 10.1371/journal.pone.0025744
- Jain, D., and Bar-Shalom, D. (2014). Alginate drug delivery systems: Application in context of pharmaceutical and biomedical research. *Drug Dev. Ind. Pharm.* 40, 1576–1584. doi: 10.3109/03639045.2014.917657
- Jaiswal, M., Dudhe, R., and Sharma, P. K. (2015). Nanoemulsion: an advanced mode of drug delivery system. *3 Biotech* 5, 123–127. doi: 10.1007/s13205-014-0214-0
- Jannuzzi, G. P., Souza, N., Françoso, K. S., Pereira, R. H., Santos, R. P., Kaihami, G. H., et al. (2018). Therapeutic treatment with scFv-PLGA nanoparticles decreases pulmonary fungal load in a murine model of paracoccidioidomycosis. *Microb. Infect.* 20, 48–56. doi: 10.1016/j.micinf.2017.09.003
- Jansook, P., Pichayakorn, W., and Ritthidej, G. C. (2018). Amphotericin B-loaded solid lipid nanoparticles (SLNs) and nanostructured lipid carrier (NLCs): effect of drug loading and biopharmaceutical characterizations. *Drug Dev. Ind. Pharm.* 44, 1693–1700. doi: 10.1080/03639045.2018.1492606
- Johnson, P. C., Wheat, L. J., Cloud, G. A., Goldman, M., Lancaster, D., Bamberger, D. M., et al. (2002). Safety and efficacy of liposomal amphotericin B compared with conventional amphotericin B for induction therapy of histoplasmosis in patients with AIDS. *Ann. Intern. Med.* 137, 105–109. doi: 10.7326/0003-4819-137-2-200207160-00008
- Jukic, E., Blatzer, M., Posch, W., Steger, M., Binder, U., Lass-Flörl, C., et al. (2017). Oxidative stress response tips the balance in *Aspergillus terreus* Amphotericin B Resistance. *Antimicrob. Agents Chemother.* 61:AAC00670-17. doi: 10.1128/AAC.00670-17
- Jung, S. H., Lim, D. H., Jung, S. H., Lee, J. E., Jeong, K. S., Seong, H., et al. (2009). Amphotericin B-entrapping lipid nanoparticles and their *in vitro* and *in vivo* characteristics. *Eur. J. Pharm. Sci.* 37, 313–320. doi: 10.1016/j.ejps.2009.02.021
- Kauffman, C. A. (2007). Histoplasmosis: a clinical and laboratory update. *Clin. Microbiol. Rev.* 20, 115–132. doi: 10.1128/CMR.00027-06
- Kelidari, H. R., Moazeni, M., Babaei, R., Saedi, M., Akbari, J., Parkoobi, P. I., et al. (2017). Improved yeast delivery of fluconazole with a nanostructured lipid carrier system. *Biomed. Pharmacother.* 89, 83–88. doi: 10.1016/j.biopha.2017.02.008
- Khames, A., Khaleel, M. A., El-Badawy, M. F., and El-Nezhawy, A. O. H. (2019). Natamycin solid lipid nanoparticles - sustained ocular delivery system of higher corneal penetration against deep fungal keratitis: preparation and optimization. *Int. J. Nanomed.* 14, 2515–2531. doi: 10.2147/IJN.S190502
- Khan, S., Alam, F., Azam, A., and Khan, A. U. (2012). Gold nanoparticles enhance methylene blue-induced photodynamic therapy: a novel therapeutic approach to inhibit *Candida albicans* biofilm. *Int. J. Nanomed.* 7, 3245–3257. doi: 10.2147/IJN.S31219
- Khan, S., Baboota, S., Ali, J., Khan, S., Narang, R. S., and Narang, J. K. (2015). Nanostructured lipid carriers: an emerging platform for improving oral bioavailability of lipophilic drugs. *Int. J. Pharm. Invest.* 5, 182–191. doi: 10.4103/2230-973X.167661
- Khanna, P., Kaur, A., and Goyal, D. (2019). Algae-based metallic nanoparticles: synthesis, characterization and applications. *J. Microbiol. Methods* 163:105656. doi: 10.1016/j.mimet.2019.105656
- Kischkel, B., Castilho, P. F., de Oliveira, K. M. P., de Bruschi, M. L., Svidzinski, T. I. E., et al. (2020). Silver nanoparticles stabilized with propolis shows reduced toxicity and potential activity against fungal infections. *Future Microbiol.* 15, 521–539. doi: 10.2217/fmb-2019-0173
- Knotigová, P. T., Zyka, D., Mašek, J., Kovalová, A., Krupka, M., Bartheldyová, E., et al. (2015). Molecular adjuvants based on nonpyrogenic lipophilic derivatives of norAbuMDP/GMDP formulated in nanoliposomes: stimulation of innate and adaptive immunity. *Pharm. Res.* 32, 1186–1199. doi: 10.1007/s11095-014-1516-y
- Koehler, A. P., Cheng, A. F., Chu, K. C., Chan, C. H., Ho, A. S., and Lyon, D. J. (1998). Successful treatment of disseminated

- coccidioidomycosis with amphotericin B lipid complex. *J. Infect.* 36, 113–115. doi: 10.1016/S0163-4453(98)93522-8
- Kordalewska, M., and Perlin, D. S. (2019). Identification of drug resistant *Candida auris*. *Front. Microbiol.* 10:1918. doi: 10.3389/fmicb.2019.01918
- Kriesel, J. D., Sutton, D. A., Schulman, S., Fothergill, A. W., and Rinaldi, M. G. (2008). Persistent pulmonary infection with an azole-resistant *Coccidioides* species. *Med. Mycol.* 46, 607–610. doi: 10.1080/13693780802140923
- Kruppa, M. (2009). Quorum sensing and *Candida albicans*. *Mycoses* 52, 1–10. doi: 10.1111/j.1439-0507.2008.01626.x
- Kube, S., Hersch, N., Naumovska, E., Gensch, T., Hendriks, J., Franzen, A., et al. (2017). Fusogenic liposomes as nanocarriers for the delivery of intracellular proteins. *Langmuir* 33, 1051–1059. doi: 10.1021/acs.langmuir.6b04304
- Kumar, A., Pandey, A. N., and Jain, S. K. (2016). Nasal-nanotechnology: revolution for efficient therapeutics delivery. *Drug Deliv.* 23, 671–683. doi: 10.3109/10717544.2014.920431
- Kwon-Chung, K. J., Fraser, J. A., Doering, T. L., Wang, Z., Janbon, G., Idnurm, A., et al. (2014). *Cryptococcus neoformans* and *Cryptococcus gattii*, the etiologic agents of cryptococcosis. *Cold Spring Harb. Perspect. Med.* 4:a019760. doi: 10.1101/cshperspect.a019760
- Lakshmeesha, T. R., Kalagatur, N. K., Mudili, V., Mohan, C. D., Rangappa, S., Prasad, B. D., et al. (2019). Biofabrication of zinc oxide nanoparticles with syzygium aromaticum flower buds extract and finding its novel application in controlling the growth and mycotoxins of *Fusarium graminearum*. *Front. Microbiol.* 10:1244. doi: 10.3389/fmicb.2019.01244
- Lalani, J., Baradia, D., Lalani, R., and Misra, A. (2015). Brain targeted intranasal delivery of tramadol: comparative study of microemulsion and nanoemulsion. *Pharm. Dev. Technol.* 20, 992–1001. doi: 10.3109/10837450.2014.959177
- Lara, H. H., Romero-Urbina, D. G., Pierce, C., Lopez-Ribot, J. L., Arellano-Jiménez, M. J., and Jose-Yacamán, M. (2015). Effect of silver nanoparticles on *Candida albicans* biofilms: an ultrastructural study. *J. Nanobiotechnol.* 13:91. doi: 10.1186/s12951-015-0147-8
- LaSenna, C. E., and Tosti, A. (2015). Patient considerations in the management of toe onychomycosis - role of efinaconazole. *Patient Prefer. Adherence* 9, 887–891. doi: 10.2147/PPA.S72701
- Lewis, R. E. (2011). Current concepts in antifungal pharmacology. *Mayo Clin. Proc.* 86, 805–817. doi: 10.4065/mcp.2011.0247
- Lewis, R. E., Liao, G., Hou, J., Chamilos, G., Prince, R. A., and Kontoyiannis, D. P. (2007). Comparative analysis of amphotericin B lipid complex and liposomal amphotericin B kinetics of lung accumulation and fungal clearance in a murine model of acute invasive pulmonary aspergillosis. *Antimicrob. Agents Chemother.* 51, 1253–1258. doi: 10.1128/AAC.01449-06
- Lila, A. S. A., and Ishida, T. (2017). Liposomal delivery systems: design optimization and current applications. *Biol. Pharm. Bull.* 40, 1–10. doi: 10.1248/bpb.b16-00624
- Limper, A. H., Adenis, A., Le, T., and Harrison, T. S. (2017). Fungal infections in HIV/AIDS. *Lancet Infect. Dis.* 17, e334–e343. doi: 10.1016/S1473-3099(17)30303-1
- Lin, P.-C., Lin, S., Wang, P., Cui, C., and Sridhar, R. (2014). Techniques for physicochemical characterization of nanomaterials. *Biotechnol. Adv.* 32, 711–726. doi: 10.1016/j.biotechadv.2013.11.006
- Lockhart, S. R. (2019). Emerging and reemerging fungal infections. *Semin. Diagn. Pathol.* 36, 177–181. doi: 10.1053/j.semmp.2019.04.010
- Lopes, M., Abraham, B., Veiga, F., Seica, R., Cabral, L. M., Arnaud, P., et al. (2017). Preparation methods and applications behind alginate-based particles. *Expert Opin. Drug Deliv.* 14, 769–782. doi: 10.1080/17425247.2016.1214564
- Lu, R., Hollingsworth, C., Qiu, J., Wang, A., Hughes, E., Xin, X., et al. (2019). Efficacy of oral encochleated amphotericin b in a mouse model of cryptococcal meningoencephalitis. *MBio* 10:e00724-19. doi: 10.1128/mBio.00724-19
- Ludwig, D. B., de Camargo, L. E. A., Khalil, N. M., Auler, M. E., and Mainardes, R. M. (2018). Antifungal Activity of Chitosan-Coated Poly(lactic-co-glycolic) Acid Nanoparticles Containing Amphotericin B. *Mycopathologia* 183, 659–668. doi: 10.1007/s11046-018-0253-x
- Mahtab, A., Anwar, M., Mallick, N., Naz, Z., Jain, G. K., and Ahmad, F. J. (2016). Transungual delivery of ketoconazole nanoemulgel for the effective management of onychomycosis. *AAPS PharmSciTech.* 17, 1477–1490. doi: 10.1208/s12249-016-0488-0
- Majid, A., Ahmed, W., Patil-Sen, Y., and Sen, T. (2018). "Synthesis and characterisation of magnetic nanoparticles in medicine," in *Micro and Nanomanufacturing*. Vol. II (Cham: Springer International Publishing), 413–442. doi: 10.1007/978-3-319-67132-1_14
- Malekhaia Häfner, S., and Malmsten, M. (2017). Membrane interactions and antimicrobial effects of inorganic nanoparticles. *Adv. Colloid Interface Sci.* 248, 105–128. doi: 10.1016/j.cis.2017.07.029
- Maliszewska, I., Lisiak, B., Popko, K., and Matczyszyn, K. (2017). Enhancement of the efficacy of photodynamic inactivation of *Candida albicans* with the use of biogenic gold nanoparticles. *Photochem. Photobiol.* 93, 1081–1090. doi: 10.1111/php.12733
- Marques, M. R. C., Choo, Q., Ashtikar, M., Rocha, T. C., Bremer-Hoffmann, S., and Wacker, M. G. (2019). Nanomedicines - tiny particles and big challenges. *Adv. Drug Deliv. Rev.* 151–152, 23–43. doi: 10.1016/j.addr.2019.06.003
- Marr, K. A., Datta, K., Pirofski, L., and Barnes, R. (2012). *Cryptococcus gattii* infection in healthy hosts: a sentinel for subclinical immunodeficiency? *Clin. Infect. Dis.* 54, 153–154. doi: 10.1093/cid/cir756
- Mašek, J., Bartheldyová, E., Turánek-Knotigová, P., Skrabalová, M., Korvasová, Z., Plocková, J., et al. (2011). Metallochelating liposomes with associated lipophilised norAbuMDP as biocompatible platform for construction of vaccines with recombinant His-tagged antigens: preparation, structural study and immune response towards rHsp90. *J. Control. Release* 151, 193–201. doi: 10.1016/j.jconrel.2011.01.016
- Matthews, R. C., Burnie, J. P., and Tabaqchali, S. (1987). Isolation of immunodominant antigens from sera of patients with systemic candidiasis and characterization of serological response to *Candida albicans*. *J. Clin. Microbiol.* 25, 230–237. doi: 10.1128/JCM.25.2.230-237.1987
- McConnell, M. F., Shi, A., Lasco, T. M., and Yoon, L. (2017). Disseminated coccidioidomycosis with multifocal musculoskeletal disease involvement. *Radiol. Case Rep.* 12, 141–145. doi: 10.1016/j.radcr.2016.11.017
- Medici, N. P., Del Poeta, M., Medici, N. P., and Del Poeta, M. (2015). New insights on the development of fungal vaccines: from immunity to recent challenges. *Mem. Inst. Oswaldo Cruz* 110, 966–973. doi: 10.1590/0074-02760150335
- Mehta, R. T., Poddar, S., Kalidas, M., Gomez-Flores, R., and Dulski, K. (1997). Role of macrophages in the candidacidal activity of liposomal amphotericin B. *J. Infect. Dis.* 175, 214–217. doi: 10.1093/infdis/175.1.214
- Mendes, L. P., Pan, J., and Torchilin, V. P. (2017). Dendrimers as nanocarriers for nucleic acid and drug delivery in cancer therapy. *Molecules* 22:1401. doi: 10.3390/molecules22091401
- Moazeni, M., Kelidari, H. R., Saeedi, M., Morteza-Semnani, K., Nabili, M., Gohar, A. A., et al. (2016). Time to overcome fluconazole resistant *Candida* isolates: solid lipid nanoparticles as a novel antifungal drug delivery system. *Colloids Surf. B. Biointerfaces* 142, 400–407. doi: 10.1016/j.colsurfb.2016.03.013
- Mohammed Fayaz, A., Ao, Z., Girilal, M., Chen, L., Xiao, X., Kalaichelvan, P., et al. (2012). Inactivation of microbial infectiousness by silver nanoparticles-coated condom: a new approach to inhibit HIV- and HSV-transmitted infection. *Int. J. Nanomed.* 7, 5007–5018. doi: 10.2147/IJN.S34973
- Monteiro, D. R., Gorup, L. F., Silva, S., Negri, M., de Camargo, E. R., Oliveira, R., et al. (2011). Silver colloidal nanoparticles: antifungal effect against adhered cells and biofilms of *Candida albicans* and *Candida glabrata*. *Biofouling* 27, 711–719. doi: 10.1080/08927014.2011.599101
- Moraes Moreira Carraro, T. C., Altmeyer, C., Maissar Khalil, N., and Mara Mainardes, R. (2017). Assessment of *in vitro* antifungal efficacy and *in vivo* toxicity of Amphotericin B-loaded PLGA and PLGA-PEG blend nanoparticles. *J. Mycol. Med.* 27, 519–529. doi: 10.1016/j.mycmed.2017.07.004
- Moriyama, B., Gordon, L. A., McCarthy, M., Henning, S. A., Walsh, T. J., and Penzak, S. R. (2014). Emerging drugs and vaccines for Candidemia. *Mycoses* 57, 718–733. doi: 10.1111/myc.12265
- Mourad, A., and Perfect, J. R. (2018). The war on cryptococcosis: a review of the antifungal arsenal. *Mem. Inst. Oswaldo Cruz* 113:e170391. doi: 10.1590/0074-02760170391
- Mundada, V., Patel, M., and Sawant, K. (2016). Submicron emulsions and their applications in oral delivery. *Crit. Rev. Ther. Drug Carr. Syst.* 33, 265–308. doi: 10.1615/CritRevTherDrugCarrierSyst.2016017218
- Murdock, R. C., Braydich-Stolle, L., Schrand, A. M., Schlager, J. J., and Hussain, S. M. (2008). Characterization of nanomaterial dispersion in solution prior to *in vitro* exposure using dynamic light scattering technique. *Toxicol. Sci.* 101, 239–253. doi: 10.1093/toxsci/kfm240
- Musarrat, J., Dwivedi, S., Singh, B. R., Al-Khedhairi, A. A., Azam, A., and Naqvi, A. (2010). Production of antimicrobial silver nanoparticles in water extracts of the

- fungus *Amylomyces rouxii* strain KSU-09. *Bioresour. Technol.* 101, 8772–8776. doi: 10.1016/j.biortech.2010.06.065
- Nakhla, S. G. (2018). Complications and management of a rare case of disseminated coccidioidomycosis to the vertebral spine. *Case Rep. Infect. Dis.* 2018, 1–3. doi: 10.1155/2018/8954016
- Nel, A., Xia, T., Mädler, L., and Li, N. (2006). Toxic potential of materials at the nanolevel. *Science* 311, 622–627. doi: 10.1126/science.1114397
- Newton, P. J., Harris, C., Morris, J., and Denning, D. W. (2016). Impact of liposomal amphotericin B therapy on chronic pulmonary aspergillosis. *J. Infect.* 73, 485–495. doi: 10.1016/j.jinf.2016.06.001
- Niemirowicz, K., Durnaś, B., Piktel, E., and Bucki, R. (2017a). Development of antifungal therapies using nanomaterials. *Nanomedicine* 12, 1891–1905. doi: 10.2217/nnm-2017-0052
- Niemirowicz, K., Durnaś, B., Tokajuk, G., Gluszek, K., Wilczewska, A. Z., Myształewska, I., et al. (2016). Magnetic nanoparticles as a drug delivery system that enhance fungicidal activity of polyene antibiotics. *Nanomed. Nanotechnol. Biol. Med.* 12, 2395–2404. doi: 10.1016/j.nano.2016.07.006
- Niemirowicz, K., Durnaś, B., Tokajuk, G., Piktel, E., Michalak, G., Gu, X., et al. (2017b). Formulation and candidacidal activity of magnetic nanoparticles coated with cathelicidin LL-37 and ceragenin CSA-13. *Sci. Rep.* 7:4610. doi: 10.1038/s41598-017-04653-1
- Nisini, R., Poerio, N., Mariotti, S., De Santis, F., and Fraziano, M. (2018). The multirole of liposomes in therapy and prevention of infectious diseases. *Front. Immunol.* 9:155. doi: 10.3389/fimmu.2018.00155
- Oberdörster, G., Oberdörster, E., and Oberdörster, J. (2005). Nanotoxicology: an emerging discipline evolving from studies of ultrafine particles. *Environ. Health Perspect.* 113, 823–839. doi: 10.1289/ehp.7339
- Olson, J. A., Adler-Moore, J. P., Schwartz, J., Jensen, G. M., and Proffitt, R. T. (2006). Comparative efficacies, toxicities, and tissue concentrations of amphotericin B lipid formulations in a murine pulmonary aspergillosis model. *Antimicrob. Agents Chemother.* 50, 2122–2131. doi: 10.1128/AAC.00315-06
- Olson, J. A., George, A., Constable, D., Smith, P., Proffitt, R. T., and Adler-Moore, J. P. (2010). Liposomal amphotericin B and echinocandins as monotherapy or sequential or concomitant therapy in murine disseminated and pulmonary *Aspergillus fumigatus* infections. *Antimicrob. Agents Chemother.* 54, 3884–3894. doi: 10.1128/AAC.01554-09
- Olson, J. A., Schwartz, J. A., Hahka, D., Nguyen, N., Bunch, T., Jensen, G. M., et al. (2015). Toxicity and efficacy differences between liposomal amphotericin B formulations in uninfected and *Aspergillus fumigatus* infected mice. *Med. Mycol.* 53, 107–118. doi: 10.1093/mmy/myu070
- Palacios, D. S., Dailey, I., Siebert, D. M., Wilcock, B. C., and Burke, M. D. (2011). Synthesis-enabled functional group deletions reveal key underpinnings of amphotericin B ion channel and antifungal activities. *Proc. Natl. Acad. Sci. U.S.A.* 108, 6733–6738. doi: 10.1073/pnas.1015023108
- Pandey, Y. R., Kumar, S., Gupta, B. K., Ali, J., and Baboota, S. (2016). Intranasal delivery of paroxetine nanoemulsion via the olfactory region for the management of depression: formulation, behavioural and biochemical estimation. *Nanotechnology* 27:025102. doi: 10.1088/0957-4484/27/2/025102
- Pardeike, J., Weber, S., Zarfl, H. P., Pagitz, M., and Zimmer, A. (2016). Itraconazole-loaded nanostructured lipid carriers (NLC) for pulmonary treatment of aspergillosis in falcons. *Eur. J. Pharm. Biopharm.* 108, 269–276. doi: 10.1016/j.ejpb.2016.07.018
- Park, B. J., Wannemuehler, K. A., Marston, B. J., Govender, N., Pappas, P. G., and Chiller, T. M. (2009). Estimation of the current global burden of cryptococcal meningitis among persons living with HIV/AIDS. *AIDS* 23, 525–530. doi: 10.1097/QAD.0b013e328322ffac
- Paul, S., Mohanram, K., and Kannan, I. (2018). Antifungal activity of curcumin-silver nanoparticles against fluconazole-resistant clinical isolates of *Candida* species. *AYU* 39:182. doi: 10.4103/ayu.AYU_24_18
- Paulussen, C., Hallsworth, J. E., Álvarez-Pérez, S., Nierman, W. C., Hamill, P. G., Blain, D., et al. (2017). Ecology of aspergillosis: insights into the pathogenic potency of *Aspergillus fumigatus* and some other *Aspergillus* species. *Microb. Biotechnol.* 10, 296–322. doi: 10.1111/1751-7915.12367
- Pedroso, L. S., Khalil, N. M., and Mainardes, R. M. (2018). Preparation and *in vitro* evaluation of efficacy and toxicity of Polysorbate 80-coated bovine serum albumin nanoparticles containing Amphotericin B. *Curr. Drug Deliv.* 15, 1055–1063. doi: 10.2174/1567201815666180409103028
- Perfect, J. R., Dismukes, W. E., Dromer, F., Goldman, D. L., Graybill, J. R., Hamill, R. J., et al. (2010). Clinical practice guidelines for the management of cryptococcal disease: 2010 update by the infectious diseases society of America. *Clin. Infect. Dis.* 50, 291–322. doi: 10.1086/649858
- Perlroth, J., Choi, B., and Spellberg, B. (2007). Nosocomial fungal infections: epidemiology, diagnosis, and treatment. *Med. Mycol.* 45, 321–346. doi: 10.1080/13693780701218689
- Pfaller, M. A., and Diekema, D. J. (2010). Epidemiology of invasive mycoses in North America. *Crit. Rev. Microbiol.* 36, 1–53. doi: 10.3109/10408410903241444
- Polvi, E. J., Li, X., O'Meara, T. R., Leach, M. D., and Cowen, L. E. (2015). Opportunistic yeast pathogens: reservoirs, virulence mechanisms, and therapeutic strategies. *Cell. Mol. Life Sci.* 72, 2261–2287. doi: 10.1007/s00018-015-1860-z
- Radhakrishnan, V. S., Dwivedi, S. P., Siddiqui, M. H., and Prasad, T. (2018a). *In vitro* studies on oxidative stress-independent, Ag nanoparticles-induced cell toxicity of *Candida albicans*, an opportunistic pathogen. *Int. J. Nanomed.* 13, 91–96. doi: 10.2147/IJN.S125010
- Radhakrishnan, V. S., Reddy Mudiam, M. K., Kumar, M., Dwivedi, S. P., Singh, S. P., and Prasad, T. (2018b). Silver nanoparticles induced alterations in multiple cellular targets, which are critical for drug susceptibilities and pathogenicity in fungal pathogen (*Candida albicans*). *Int. J. Nanomed.* 13, 2647–2663. doi: 10.2147/IJN.S150648
- Radwan, M. A., AlQuadeib, B. T., Šiller, L., Wright, M. C., and Horrocks, B. (2017). Oral administration of amphotericin B nanoparticles: antifungal activity, bioavailability and toxicity in rats. *Drug Deliv.* 24, 40–50. doi: 10.1080/10717544.2016.1228715
- Rajasingham, R., Smith, R. M., Park, B. J., Jarvis, J. N., Govender, N. P., Chiller, T. M., et al. (2017). Global burden of disease of HIV-associated cryptococcal meningitis: an updated analysis. *Lancet Infect. Dis.* 17, 873–881. doi: 10.1016/S1473-3099(17)30243-8
- Ramage, P., Unger, R. E., Oltrogge, J. B., Zenker, D., Begley, D., Kreuter, J., et al. (2000). Polysorbate-80 coating enhances uptake of polybutylcyanoacrylate (PBCA)-nanoparticles by human and bovine primary brain capillary endothelial cells. *Eur. J. Neurosci.* 12, 1931–1940. doi: 10.1046/j.1460-9568.2000.00078.x
- Rangel, M. A. C., Rivera, N. G., Castillo, R. D., Soto, J. C., and Talamante, S. (2010). Tratamiento de coccidioidomycosis meníngea con anfotericina liposomal: presentación de un caso. *Boletín Médico del Hospital Infantil de México.* 67, 142–146. Available online at: http://www.scielo.org.mx/scielo.php?script=sci_arttext&pid=S1665-11462010000200008&lng=es&tlng=es
- Rautema-Richardson, R., and Richardson, M. D. (2017). Systemic fungal infections. *Medicine* 45, 757–762. doi: 10.1016/j.mpmed.2017.09.007
- Reddy, L. H., Arias, J. L., Nicolas, J., and Couvreur, P. (2012). Magnetic nanoparticles: design and characterization, toxicity and biocompatibility, pharmaceutical and biomedical applications. *Chem. Rev.* 112, 5818–5878. doi: 10.1021/cr300068p
- Ren, T., Xu, N., Cao, C., Yuan, W., Yu, X., Chen, J., et al. (2009). Preparation and therapeutic efficacy of polysorbate-80-coated amphotericin B/PLA-b-PEG nanoparticles. *J. Biomater. Sci. Polym. Ed.* 20, 1369–1380. doi: 10.1163/092050609X12457418779185
- Ribeiro, A. M., Souza, A. C. O., Amaral, A. C., Vasconcelos, N. M., Jerônimo, M. S., Carneiro, F. P., et al. (2013). Nanobiotechnological approaches to delivery of DNA vaccine against fungal infection. *J. Biomed. Nanotechnol.* 9, 221–230. doi: 10.1166/jbn.2013.1491
- Riteau, N., and Sher, A. (2016). Chitosan: an adjuvant with an unanticipated STING. *Immunity* 44, 522–524. doi: 10.1016/j.immuni.2016.03.002
- Rodrigues, G. B., Primo, F. L., Tedesco, A. C., and Braga, G. U. L. (2012). *In vitro* photodynamic inactivation of *Cryptococcus neoformans* melanized cells with chloroaluminum phthalocyanine nanoemulsion. *Photochem. Photobiol.* 88, 440–447. doi: 10.1111/j.1751-1097.2011.01055.x
- Rodrigues, G. R., López-Abarrategui, C., de la Serna Gómez, I., Dias, S. C., Otero-González, A. J., and Franco, O. L. (2019). Antimicrobial magnetic nanoparticles based-therapies for controlling infectious diseases. *Int. J. Pharm.* 555, 356–367. doi: 10.1016/j.ijpharm.2018.11.043
- Rodriguez-Cerdeira, C., Arenas, R., Moreno-Coutiño, G., Vázquez, E., Fernández, R., and Chang, P. (2014). Systemic fungal infections in patients

- with human immunodeficiency virus. *Actas Dermo-Sifiliográfica*. 105, 5–17. doi: 10.1016/j.adengl.2012.06.032
- Rónavári, A., Igaz, N., Gopisetty, M. K., Szerencsés, B., Kovács, D., Papp, C., et al. (2018). Biosynthesized silver and gold nanoparticles are potent antimicrobials against opportunistic pathogenic yeasts and dermatophytes. *Int. J. Nanomed.* 13, 695–703. doi: 10.2147/IJN.S152010
- Rózalska, B., Sadowska, B., Budzyńska, A., Bernat, P., and Rózalska, S. (2018). Biogenic nanosilver synthesized in *Metarhizium robertsii* waste mycelium extract - as a modulator of *Candida albicans* morphogenesis, membrane lipidome and biofilm. *PLoS ONE* 13:e0194254. doi: 10.1371/journal.pone.0194254
- Rukavina, Z., and Vanić, Ž. (2016). Current trends in development of liposomes for targeting bacterial biofilms. *Pharmaceutics* 8:18. doi: 10.3390/pharmaceutics8020018
- Sahoo, S. K., Parveen, S., and Panda, J. J. (2007). The present and future of nanotechnology in human health care. *Nanomedicine* 3, 20–31. doi: 10.1016/j.nano.2006.11.008
- Saijo, T., Chen, J., Chen, S. C.-A., Rosen, L. B., Yi, J., Sorrell, T. C., et al. (2014). Anti-granulocyte-macrophage colony-stimulating factor autoantibodies are a risk factor for central nervous system infection by *Cryptococcus gattii* in otherwise immunocompetent patients. *MBio* 5, e00912–e00914. doi: 10.1128/mBio.00912-14
- Salama, H. E., Saad, G. R., and Sabaa, M. W. (2016). Synthesis, characterization, and biological activity of cross-linked chitosan biguanidine loaded with silver nanoparticles. *J. Biomater. Sci. Polym. Ed.* 27, 1880–1898. doi: 10.1080/09205063.2016.1239950
- Salvi, V. R., and Pawar, P. (2019). Nanostructured lipid carriers (NLC) system: A novel drug targeting carrier. *J. Drug Deliv. Sci. Technol.* 51, 255–267. doi: 10.1016/j.jddst.2019.02.017
- Santangelo, R., Paderu, P., Delmas, G., Chen, Z. W., Mannino, R., Zarif, L., et al. (2000). Efficacy of oral coxleate-amphotericin B in a mouse model of systemic candidiasis. *Antimicrob. Agents Chemother.* 44, 2356–2360. doi: 10.1128/AAC.44.9.2356-2360.2000
- Sav, H., Rafati, H., Öz, Y., Dalyan-Cilo, B., Ener, B., Mohammadi, F., et al. (2018). Biofilm formation and resistance to fungicides in clinically relevant members of the fungal genus *Fusarium*. *J. Fungi* 4:16. doi: 10.3390/jof4010016
- Sawant, B., and Khan, T. (2017). Recent advances in delivery of antifungal agents for therapeutic management of candidiasis. *Biomed. Pharmacother.* 96, 1478–1490. doi: 10.1016/j.biopha.2017.11.127
- Seil, J. T., and Webster, T. J. (2012). Antimicrobial applications of nanotechnology: methods and literature. *Int. J. Nanomed.* 7, 2767–2781. doi: 10.2147/IJN.S24805
- Semete, B., Booysen, L. I. J., Kalombo, L., Venter, J. D., Katata, L., Ramalapa, B., et al. (2010). *In vivo* uptake and acute immune response to orally administered chitosan and PEG coated PLGA nanoparticles. *Toxicol. Appl. Pharmacol.* 249, 158–165. doi: 10.1016/j.taap.2010.09.002
- Sepúlveda, V. E., Márquez, R., Turissini, D. A., Goldman, W. E., and Matute, D. R. (2017). Genome sequences reveal cryptic speciation in the human pathogen *Histoplasma capsulatum*. *MBio* 8:e01339-17. doi: 10.1128/mBio.01339-17
- Seyedmousavi, S., Melchers, W. J. G., Mouton, J. W., and Verweij, P. E. (2013). Pharmacodynamics and dose-response relationships of liposomal amphotericin B against different azole-resistant *Aspergillus fumigatus* isolates in a murine model of disseminated aspergillosis. *Antimicrob. Agents Chemother.* 57, 1866–1871. doi: 10.1128/AAC.02226-12
- Seyedmousavi, S., Mouton, J. W., Melchers, W. J. G., Brüggemann, R. J. M., and Verweij, P. E. (2014). The role of azoles in the management of azole-resistant aspergillosis: From the bench to the bedside. *Drug Resist. Updat.* 17, 37–50. doi: 10.1016/j.drup.2014.06.001
- Shao, K., Wu, J., Chen, Z., Huang, S., Li, J., Ye, L., et al. (2012). A brain- vectored angioprep-2 based polymeric micelles for the treatment of intracranial fungal infection. *Biomaterials* 33, 6898–6907. doi: 10.1016/j.biomaterials.2012.06.050
- Sharma, R., Agrawal, U., Mody, N., and Vyas, S. P. (2015). Polymer nanotechnology based approaches in mucosal vaccine delivery: challenges and opportunities. *Biotechnol. Adv.* 33, 64–79. doi: 10.1016/j.biotechadv.2014.12.004
- Sheikh, S., Ali, S. M., Ahmad, M. U., Ahmad, A., Mushtaq, M., Paithankar, M., et al. (2010). Nanosomal Amphotericin B is an efficacious alternative to Ambisome® for fungal therapy. *Int. J. Pharm.* 397, 103–108. doi: 10.1016/j.ijpharm.2010.07.003
- Sherje, A. P., Jadhav, M., Dravyakar, B. R., and Kadam, D. (2018). Dendrimers: a versatile nanocarrier for drug delivery and targeting. *Int. J. Pharm.* 548, 707–720. doi: 10.1016/j.ijpharm.2018.07.030
- Sherwani, M. A., Tufail, S., Khan, A. A., and Owais, M. (2015). Gold nanoparticle-photosensitizer conjugate based photodynamic inactivation of biofilm producing cells: potential for treatment of *C. albicans* infection in BALB/c Mice. *PLoS ONE* 10:e0131684. doi: 10.1371/journal.pone.0131684
- Shikanai-Yasuda, M. A., and Mendes, R. P. (2007). Consensus Brazilian guidelines for the clinical management of paracoccidioidomycosis. *Rev. Soc. Bras. Med. Trop.* 50, 715–740. doi: 10.1590/0037-8682-0230-2017
- Shirkhani, K., Teo, I., Armstrong-James, D., and Shaunak, S. (2015). Nebulised amphotericin B-polymethacrylic acid nanoparticle prophylaxis prevents invasive aspergillosis. *Nanomedicine* 11, 1217–1226. doi: 10.1016/j.nano.2015.02.012
- Sidhu, R., Lash, D. B., Heidari, A., Natarajan, P., and Johnson, R. H. (2018). Evaluation of amphotericin B lipid formulations for treatment of severe coccidioidomycosis. *Antimicrob. Agents Chemother.* 62:e02293-17. doi: 10.1128/AAC.02293-17
- Silva, L., Dias, L. S., Rittner, G., Muñoz, J. E., Souza, A., Nosanchuk, J. D., et al. (2017). Dendritic cells primed with *Paracoccidioides brasiliensis* Peptide P10 are therapeutic in immunosuppressed mice with paracoccidioidomycosis. *Front. Microbiol.* 8:1057. doi: 10.3389/fmicb.2017.01057
- Singulani, J., Scorzoni, L., Lourencetti, N. M. S., Oliveira, L. R., Conçolaro, R. S., da Silva, P. B., et al. (2018). Potential of the association of dodecyl gallate with nanostructured lipid system as a treatment for paracoccidioidomycosis: *in vitro* and *in vivo* efficacy and toxicity. *Int. J. Pharm.* 547, 630–636. doi: 10.1016/j.ijpharm.2018.06.013
- Siopi, M., Mouton, J. W., Pournaras, S., and Meletiadis, J. (2019). *In vitro* and *in vivo* exposure-effect relationship of liposomal amphotericin b against *aspergillus fumigatus*. *Antimicrob. Agents Chemother.* 63:e02673-18. doi: 10.1128/AAC.02673-18
- Sloan, D. J., and Parris, V. (2014). Cryptococcal meningitis: epidemiology and therapeutic options. *Clin. Epidemiol.* 6, 169–182. doi: 10.2147/CLEP.S38850
- Snelders, E., Karawajczyk, A., Verhoeven, R. J. A., Venselaar, H., Schaftenaar, G., Verweij, P. E., et al. (2011). The structure–function relationship of the *Aspergillus fumigatus* cyp51A L98H conversion by site-directed mutagenesis: the mechanism of L98H azole resistance. *Fungal Genet. Biol.* 48, 1062–1070. doi: 10.1016/j.fgb.2011.08.002
- Soliman, G. M. (2017). Nanoparticles as safe and effective delivery systems of antifungal agents: Achievements and challenges. *Int. J. Pharm.* 523, 15–32. doi: 10.1016/j.ijpharm.2017.03.019
- Souza, A. C. O., and Amaral, A. C. (2017). antifungal therapy for systemic mycosis and the nanobiotechnology era: improving efficacy, biodistribution and toxicity. *Front. Microbiol.* 8:336. doi: 10.3389/fmicb.2017.00336
- Souza, A. C. O., Nascimento, A. L., De Vasconcelos, N. M., Jerônimo, M. S., Siqueira, I. M., R-Santos, L., et al. (2015). Activity and *in vivo* tracking of Amphotericin B loaded PLGA nanoparticles. *Eur. J. Med. Chem.* 95, 267–276. doi: 10.1016/j.ejmech.2015.03.022
- Spadari, C., de, C., Lopes, L. B., and Ishida, K. (2017). Potential use of alginate-based carriers as antifungal delivery system. *Front. Microbiol.* 8:97. doi: 10.3389/fmicb.2017.00097
- Spadari, C. C., de Bastiani, F. W. M., S., Lopes, L. B., and Ishida, K. (2019). Alginate nanoparticles as non-toxic delivery system for miltefosine in the treatment of candidiasis and cryptococcosis. *Int. J. Nanomed.* 14, 5187–5199. doi: 10.2147/IJN.S205350
- Spellberg, B. (2011). Vaccines for invasive fungal infections. *F1000 Med. Rep.* 3:13. doi: 10.3410/M3-13
- Stewart, E. R., Eldridge, M. L., McHardy, I., Cohen, S. H., and Thompson, G. R. (2018). Liposomal amphotericin B as monotherapy in relapsed coccidioid meningitis. *Mycopathologia* 183, 619–622. doi: 10.1007/s11046-017-0240-7
- Stockamp, N. W., and Thompson, G. R. (2016). Coccidioidomycosis. *Infect. Dis. Clin. North Am.* 30, 229–246. doi: 10.1016/j.idc.2015.10.008
- Stop neglecting fungi (2017). *Nat. Microbiol.* 2:17120. doi: 10.1038/nmicrobiol.2017.120
- Taborda, C. P., Urán, M. E., Nosanchuk, J. D., and Travassos, L. R. (2015). Paracoccidioidomycosis: challenges in the development of a vaccine against an

- endemic mycosis in the Americas. *Rev. Inst. Med. Trop. São Paulo* 57, 21–24. doi: 10.1590/S0036-46652015000700005
- Tang, Y., Wu, S., Lin, J., Cheng, L., Zhou, J., Xie, J., et al. (2018). Nanoparticles targeted against cryptococcal pneumonia by interactions between chitosan and its peptide ligand. *Nano Lett.* 18, 6207–6213. doi: 10.1021/acs.nanolett.8b02229
- Thakkar, H. P., Khunt, A., Dhande, R. D., and Patel, A. A. (2015). Formulation and evaluation of Itraconazole nanoemulsion for enhanced oral bioavailability. *J. Microencapsul.* 32, 559–569. doi: 10.3109/02652048.2015.1065917
- Thangamani, N., and Bhuvaneshwari, N. (2019). Green synthesis of gold nanoparticles using *Simarouba glauca* leaf extract and their biological activity of micro-organism. *Chem. Phys. Lett.* 732:136587. doi: 10.1016/j.cplett.2019.07.015
- Thompson, G. R. (2011). Pulmonary coccidioidomycosis. *Semin. Respir. Crit. Care Med.* 32, 754–763. doi: 10.1055/s-0031-1295723
- Tiew, P. Y., Mac Aogain, M., Ali, N. A. B. M., Thng, K. X., Goh, K., Lau, K. J. L., et al. (2020). The mycobiome in health and disease: Emerging concepts, methodologies and challenges. *Mycopathologia* 185, 207–231. doi: 10.1007/s11046-019-00413-z
- Tøndervik, A., Sletta, H., Klinkenberg, G., Emanuel, C., Powell, L. C., Pritchard, M. F., et al. (2014). Alginate oligosaccharides inhibit fungal cell growth and potentiate the activity of antifungals against *Candida* and *Aspergillus* spp. *PLoS ONE* 9:e112518. doi: 10.1371/journal.pone.0112518
- Travassos, L. R., and Taborda, C. P. (2012). Paracoccidioidomycosis vaccine. *Hum. Vaccines Immunother.* 8, 1450–1453. doi: 10.4161/hv.21283
- Travassos, L. R., and Taborda, C. P. (2017). Linear epitopes of paracoccidioides brasiliensis and other fungal agents of human systemic mycoses as vaccine candidates. *Front. Immunol.* 8:224. doi: 10.3389/fimmu.2017.00224
- Tukulula, M., Gouveia, L., Paixao, P., Hayeshi, R., Naicker, B., and Dube, A. (2018). Functionalization of PLGA Nanoparticles with 1,3- β -glucan Enhances the Intracellular Pharmacokinetics of Rifampicin in Macrophages. *Pharm. Res.* 35:111. doi: 10.1007/s11095-018-2391-8
- Tukulula, M., Hayeshi, R., Fonteh, P., Meyer, D., Ndamase, A., Madziva, M. T., et al. (2015). Curdlan-conjugated PLGA nanoparticles possess macrophage stimulant activity and drug delivery capabilities. *Pharm. Res.* 32, 2713–2726. doi: 10.1007/s11095-015-1655-9
- Tumbarello, M., Posteraro, B., Trecarichi, E. M., Fiori, B., Rossi, M., Porta, R., et al. (2007). Biofilm production by *Candida* species and inadequate antifungal therapy as predictors of mortality for patients with candidemia. *J. Clin. Microbiol.* 45, 1843–1850. doi: 10.1128/JCM.00131-07
- Usman, F., Khalil, R., Ul-Haq, Z., Nakpheng, T., and Srichana, T. (2018). Bioactivity, safety, and efficacy of Amphotericin B Nanomicellar aerosols using sodium deoxycholate sulfate as the lipid carrier. *AAPS PharmSciTech.* 19, 2077–2086. doi: 10.1208/s12249-018-1013-4
- Van de Ven, H., Paulussen, C., Feijens, P. B., Matheeußen, A., Rombaut, P., Kayaert, P., et al. (2012). PLGA nanoparticles and nanosuspensions with amphotericin B: potent *in vitro* and *in vivo* alternatives to Fungizone and AmBisome. *J. Control Release* 161, 795–803. doi: 10.1016/j.jconrel.2012.05.037
- Vazquez-Muñoz, R., Avalos-Borja, M., and Castro-Longoria, E. (2014). Ultrastructural analysis of *Candida albicans* when exposed to silver nanoparticles. *PLoS ONE* 9:e108876. doi: 10.1371/journal.pone.0108876
- Vazquez-Muñoz, R., Borrego, B., Juárez-Moreno, K., García-García, M., Mota Morales, J. D., Bogdanchikova, N., et al. (2017). Toxicity of silver nanoparticles in biological systems: does the complexity of biological systems matter? *Toxicol. Lett.* 276, 11–20. doi: 10.1016/j.toxlet.2017.05.007
- Venkatesan, J., Jayakumar, R., Mohandas, A., Bhatnagar, I., and Kim, S.-K. (2014). Antimicrobial activity of chitosan-carbon nanotube hydrogels. *Materials* 7, 3946–3955. doi: 10.3390/ma7053946
- Vincent, B. M., Lancaster, A. K., Scherz-Shouval, R., Whitesell, L., and Lindquist, S. (2013). Fitness trade-offs restrict the evolution of resistance to amphotericin B. *PLoS Biol.* 11:e1001692. doi: 10.1371/journal.pbio.1001692
- Voltan, A. R., Quindós, G., Alarcón, K. P. M., Fusco-Almeida, A. M., Mendes-Giannini, M. J. S., and Chorilli, M. (2016). Fungal diseases: could nanostructured drug delivery systems be a novel paradigm for therapy? *Int. J. Nanomed.* 11, 3715–3730. doi: 10.2147/IJN.S93105
- Wagner, V., Dullaart, A., Bock, A.-K., and Zweck, A. (2006). The emerging nanomedicine landscape. *Nat. Biotechnol.* 24, 1211–1217. doi: 10.1038/nbt1006-1211
- Westerberg, D. P., and Voyack, M. J. (2013). Onychomycosis: current trends in diagnosis and treatment. *Am. Fam. Phys.* 88, 762–770.
- Wheat, L. J., Connolly, P., Smedema, M., Brizendine, E., Hafner, R., AIDS Clinical Trials Group, and the Mycoses Study Group of the National Institute of Allergy and Infectious Diseases (2001). Emergence of resistance to fluconazole as a cause of failure during treatment of histoplasmosis in patients with acquired immunodeficiency disease syndrome. *Clin. Infect. Dis.* 33, 1910–1913. doi: 10.1086/323781
- Wlaz, P., Knaga, S., Kasperek, K., Wlaz, A., Poleszak, E., Jezewska-Witkowska, G., et al. (2015). Activity and safety of inhaled itraconazole nanosuspension in a model pulmonary aspergillus fumigatus infection in inoculated young quails. *Mycopathologia* 180, 35–42. doi: 10.1007/s11046-015-9885-2
- Wojtyczka, R., Dziedzic, A., Idzik, D., Kepa, M., Kubina, R., Kabała-Dzik, A., et al. (2013). Susceptibility of staphylococcus aureus clinical isolates to propolis extract alone or in combination with antimicrobial drugs. *Molecules* 18, 9623–9640. doi: 10.3390/molecules18089623
- Wüthrich, M., Brandhorst, T. T., Sullivan, T. D., Filutowicz, H., Sterkel, A., Stewart, D., et al. (2015). Calnexin induces expansion of antigen-specific CD4(+) T cells that confer immunity to fungal ascomycetes via conserved epitopes. *Cell Host Microbe* 17, 452–465. doi: 10.1016/j.chom.2015.02.009
- Xiang, S. D., Scholzen, A., Minigo, G., David, C., Apostolopoulos, V., Mottram, P. L., et al. (2006). Pathogen recognition and development of particulate vaccines: does size matter? *Methods* 40, 1–9. doi: 10.1016/j.ymeth.2006.05.016
- Xu, N., Gu, J., Zhu, Y., Wen, H., Ren, Q., and Chen, J. (2011). Efficacy of intravenous amphotericin B-polybutylcyanoacrylate nanoparticles against cryptococcal meningitis in mice. *Int. J. Nanomed.* 6, 905–913. doi: 10.2147/IJN.S17503
- Xue, B., Zhang, Y., Xu, M., Wang, C., Huang, J., Zhang, H., et al. (2019). Curcumin-silk fibroin nanoparticles for enhanced anti-*Candida albicans* activity *in vitro* and *in vivo*. *J. Biomed. Nanotechnol.* 15, 769–778. doi: 10.1166/jbn.2019.2722
- Yah, C. S., and Simate, G. S. (2015). Nanoparticles as potential new generation broad spectrum antimicrobial agents. *Daru* 23:43. doi: 10.1186/s40199-015-0125-6
- Yang, C., Xue, B., Song, W., Kan, B., Zhang, D., Yu, H., et al. (2018). Reducing the toxicity of amphotericin B by encapsulation using methoxy poly(ethylene glycol)-b-poly(l-glutamic acid-co-l-phenylalanine). *Biomater. Sci.* 6, 2189–2196. doi: 10.1039/C8BM00506K
- Yang, L., Dong, X., Wu, X., Xie, L., and Min, X. (2011). Intravitreally implantable voriconazole delivery system for experimental fungal endophthalmitis. *Retina* 31, 1791–1800. doi: 10.1097/IAE.0b013e31820d3cd2
- Yang, M., Du, K., Hou, Y., Xie, S., Dong, Y., Li, D., et al. (2019). Synergistic antifungal effect of Amphotericin B-Loaded Poly(Lactic-Co-Glycolic Acid) nanoparticles and ultrasound against *Candida albicans* biofilms. *Antimicrob. Agents Chemother.* 63:e02022-18. doi: 10.1128/AAC.02022-18
- Yehia, S., El-Gazayerly, O., and Basalious, E. (2009). Fluconazole mucoadhesive buccal films: *in vitro/in vivo* performance. *Curr. Drug Deliv.* 6, 17–27. doi: 10.2174/156720109787048195
- Yu, Q., Li, J., Zhang, Y., Wang, Y., Liu, L., and Li, M. (2016). Inhibition of gold nanoparticles (AuNPs) on pathogenic biofilm formation and invasion to host cells. *Sci. Rep.* 6:26667. doi: 10.1038/srep26667
- Zhang, C., Chen, M., Wang, G., Fang, W., Ye, C., Hu, H., et al. (2016). Pd@Ag nanosheets in combination with Amphotericin B exert a potent anti-cryptococcal fungicidal effect. *PLoS ONE* 11:e0157000. doi: 10.1371/journal.pone.0157000


- Zhang, X.-F., Liu, Z.-G., Shen, W., and Gurunathan, S. (2016). Silver nanoparticles: synthesis, characterization, properties, applications, and therapeutic approaches. *Int. J. Mol. Sci.* 17, 1534. doi: 10.3390/ijms17091534
- Zhao, J., Cheng, Y., Song, X., Wang, C., Su, G., and Liu, Z. (2015). A comparative treatment study of intravitreal voriconazole and liposomal Amphotericin B in an aspergillus fumigatus endophthalmitis model. *Invest. Ophthalmol. Vis. Sci.* 56, 7369–7376. doi: 10.1167/iops.15-17266
- Zhao, L., Seth, A., Wibowo, N., Zhao, C.-X., Mitter, N., Yu, C., et al. (2014). Nanoparticle vaccines. *Vaccine* 32, 327–337. doi: 10.1016/j.vaccine.2013.11.069
- Zhao, W., Liu, Q., Zhang, X., Su, B., and Zhao, C. (2018). Rationally designed magnetic nanoparticles as anticoagulants for blood purification. *Colloids Surf B Biointerfaces* 164, 316–323. doi: 10.1016/j.colsurfb.2018.01.050

Conflict of Interest: The authors declare that the research was conducted in the absence of any commercial or financial relationships that could be construed as a potential conflict of interest.

Copyright © 2020 Kischkel, Rossi, Santos Junior, Nosanchuk, Travassos and Taborda. This is an open-access article distributed under the terms of the Creative Commons Attribution License (CC BY). The use, distribution or reproduction in other forums is permitted, provided the original author(s) and the copyright owner(s) are credited and that the original publication in this journal is cited, in accordance with accepted academic practice. No use, distribution or reproduction is permitted which does not comply with these terms.



Bionized Nanoferrite Particles Alter the Course of Experimental *Cryptococcus neoformans* Pneumonia

Livia C. Liporagi Lopes,^{a,b} Preethi Korangath,^c Samuel R. dos Santos, Jr.,^{a,d} Kathleen L. Gabrielson,^{e,f,g} Robert Ivkov,^{c,g,h,i}
 Arturo Casadevall^a

^aDepartment of Molecular Microbiology and Immunology, Johns Hopkins Bloomberg School of Public Health, Baltimore, Maryland, USA

^bDepartamento de Análises Clínicas e Toxicológicas, Faculdade de Farmácia, Universidade Federal do Rio de Janeiro, Rio de Janeiro, Brazil

^cDepartment of Radiation Oncology and Molecular Radiation Sciences, Johns Hopkins University School of Medicine, Baltimore, Maryland, USA

^dDepartamento de Microbiologia, Instituto de Ciências Biomédicas, Universidade de São Paulo, São Paulo, Brazil

^eDepartment of Molecular and Comparative Pathobiology, Johns Hopkins University School of Medicine, Baltimore, Maryland, USA

^fDepartment of Pathology, Johns Hopkins University School of Medicine, Baltimore, Maryland, USA

^gDepartment of Oncology, Johns Hopkins University School of Medicine, Baltimore, Maryland, USA

^hDepartment of Mechanical Engineering, Whiting School of Engineering, Johns Hopkins University, Baltimore, Maryland, USA

ⁱDepartment of Materials Science and Engineering, Whiting School of Engineering, Johns Hopkins University, Baltimore, Maryland, USA

Livia C. Liporagi Lopes and Preethi Korangath contributed equally to this article as first authors. Author order was determined on the basis that Livia C. Liporagi Lopes carried out many of the mouse experiments.

Robert Ivkov and Arturo Casadevall contributed equally to this article as senior authors. Author order was determined on the basis of mutual agreement given that this paper dealt primarily with *Cryptococcus neoformans*.

ABSTRACT Cryptococcosis is a devastating fungal disease associated with high morbidity and mortality even when treated with antifungal drugs. Bionized nanoferrite (BNF) nanoparticles are powerful immunomodulators, but their efficacy for infectious diseases has not been investigated. Administration of BNF nanoparticles to mice with experimental cryptococcal pneumonia altered the outcome of infection in a dose response manner as measured by CFU and survival. The protective effects were higher at lower doses, with reductions in IL-2, IL-4, and TNF- α , consistent with immune modulation whereby reductions in inflammation translate into reduced host damage, clearance of infection, and longer survival.

KEYWORDS cryptococcal pneumonia, iron oxide nanoparticles, immune system

Cryptococcus *neoformans* is a fungal pathogen with a worldwide distribution. Serological studies of human populations show a high prevalence of human infection, which rarely progresses to disease in immunocompetent hosts (1, 2). However, decreased host immunity places individuals at high risk for cryptococcal disease. The disease can result from acute infection or reactivation of latent infection, in which yeasts within granulomas and host macrophages emerge to cause disease (3). In both immunocompetent and immunosuppressed patients, cryptococcosis has high morbidity and mortality, even with aggressive antifungal drug therapy (1). Current therapies can require antifungal drugs for several months, and treatment can be complicated by rising antimicrobial drug resistance (4, 5). Consequently, development of new therapeutics against *C. neoformans* infections is urgently required.

Magnetic iron oxide nanoparticles (MNPs) have proven useful for the diagnosis and therapy of various conditions because they display generally favorable biocompatibility and varied responsiveness to magnetic fields (6–10). When injected into the bloodstream, nanoparticles encounter a complex fluid environment that can modify the initial particle surface to one having a molecular signature that produces specific interactions with host biology (11–13). Ultimately, although indirectly, the interactions

Copyright © 2022 American Society for Microbiology. All Rights Reserved.

Address correspondence to Arturo Casadevall, acasade1@jhu.edu.

The authors declare no conflict of interest.

Received 20 December 2021

Returned for modification 23 January 2022

Accepted 12 February 2022

Published 16 March 2022

of nanoparticles with the complex host environment can lead to their deposition in organs or tissues that depends upon the initial physical and chemical properties of the injected construct (14). The immune system's function in the maintenance of tissue homeostasis is to protect the host from environmental agents such as microbes or chemicals, and thereby preserve the integrity of the body. The study of the interactions between nanoparticles and various components of the immune system is an active area of research in bio- and nanotechnology because the benefits of using nanotechnology in industry and medicine are often questioned over concerns regarding the safety of these novel materials (11, 15, 16). The last decade of research has shown that, while in certain situations nanoparticles can be toxic, nanotechnology engineering can modify these materials to either avoid or target the immune system. Depending on the nanoparticle composition and physicochemical properties, nanoparticle interactions with host biology can induce or increase inflammation (17, 18) or mediate immunosuppression (19, 20). Either of these responses can be used to enhance efficacy in specific disease contexts, and which response is desired depends on specific features of both the disease and nanoparticle. For a nanoparticle to induce both inflammation and immunosuppression in the same disease context, however, is unusual. Specific targeting of the immune system, on the other hand, provides an attractive option for vaccine delivery, as well as for improving the quality of anti-inflammatory, anticancer, and antiviral therapies (21–24). Macrophages utilize multiple routes to ingest the same types of nanoparticles (25). Several studies reported that smaller particles (20–200 nm) elicit stronger immune responses than their larger counterparts (11, 26–29).

Previous studies have shown that injection of nanoparticles into experimental animals elicited pseudo infection-like response or local inflammation or systemic immune response leading to immunological changes in tumor microenvironment in mouse models of cancer (30, 31). When delivered systemically, BNF nanoparticles can trigger an immune response that resembles infection, leading to downstream signaling that engages effector antitumor CD8⁺ T cell function (31). The effect of nanoparticles on tumor biology has attracted considerable attention, but there has been no comparable effort to study their effect on infectious diseases. Like other engineered nanoparticles (NPs), BNF NPs inherently possess physical features resembling viruses and elicit an antitumor immune response when injected into immunocompetent mouse models of breast cancer (31).

In this study we tested the effect of BNF in a mouse model of cryptococcal pneumonia. Our results show that BNF nanoparticles have a profound effect on the inflammatory response to *C. neoformans* infection that is associated with altered outcomes depending on the nanoparticle dose used.

RESULTS

The fungal burden was assessed from the removed lungs, and mice treated with BNF at high dose had higher CFU (Fig. 1A); CFU numbers between groups were not statistically significant, but there was a trend toward higher fungal burden in the BNF-treated groups, with higher numbers in groups that received BNF 24 h after the challenge with *C. neoformans* (Fig. 1A). Histological slides of lungs showed that PBS-treated group had some inflammation (Fig. 1B), whereas nanoparticle injection (5 mg Fe/mouse) before (Fig. 1C) or after 24 h (Fig. 1D) of infection had increased inflammation seen by hematoxylin and eosin (H&E). It is possible to observe in the slides an increased number of yeasts in both nanoparticle-treated groups (Fig. 1F and G) compared to control (Fig. 1E), as shown by periodic acid-Schiff stain (PAS) of lungs. This aggravated reaction could be due to the very high concentration of nanoparticle used in this initial study.

Given the results from the high dose BNF experiment in FVB/N mice, we evaluated whether lower doses of BNF nanoparticles in the same model of FVB/N mice would produce different outcomes. A significant decrease ($P < 0.05$) of fungal CFU from the recovered lungs was observed in mice treated with lowest dose of BNF (0.005 mg) (Fig. 2A),

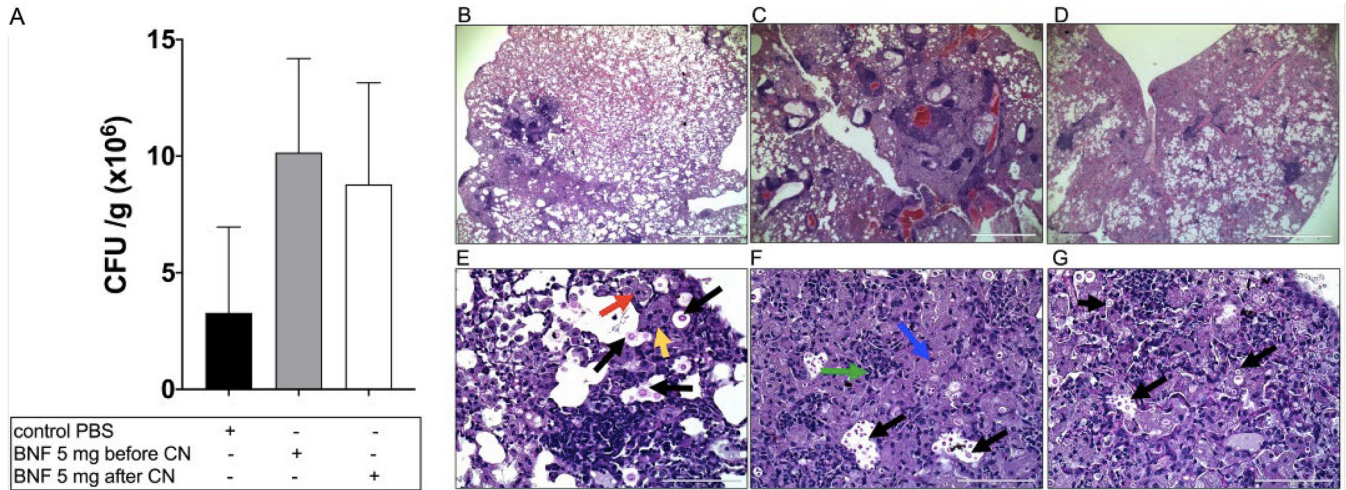


FIG 1 Higher recovery of lungs CFU 60 days after challenge with *C. neoformans* strain 24067 from the BNF-treated groups compared with the PBS control group (A). Intense immune reaction with numerous yeast organisms was seen following treatment with higher concentrations of nanoparticles in FVB/NJ mice. Representative histology images after 60 days of infection in PBS treated group (B), and nanoparticle injection (5 mg Fe/mouse) before 24 h (C) or after 24 h (D) by H&E. It is possible to observe an increased amount of yeast in nanoparticle treated groups (F, G) compared to control (E), by PAS. Black arrows in E-G indicate yeast, red arrows indicate foamy macrophages, and yellow indicates multinucleated giant cells. Blue arrow in F indicate organism inside a macrophage, and green indicates neutrophils.

demonstrating that at lower doses, BNF NPs (as 0.005 mg) could protect against *C. neoformans* infection. Corroborating with CFU data, H&E-stained lung sections show inflammatory cells surrounding *Cryptococcus* yeast in FVB/NJ mice treated with PBS, with numerous macrophages and multinucleated giant cells (blue arrow) and neutrophils (green arrow; Fig. 2B and C). BNF (0.005 mg) treated lungs had fewer inflammatory cells (Fig. 2D and 2E). PAS staining showed presence of multiple fungal yeasts in PBS treated mice (Fig. 2F), whereas

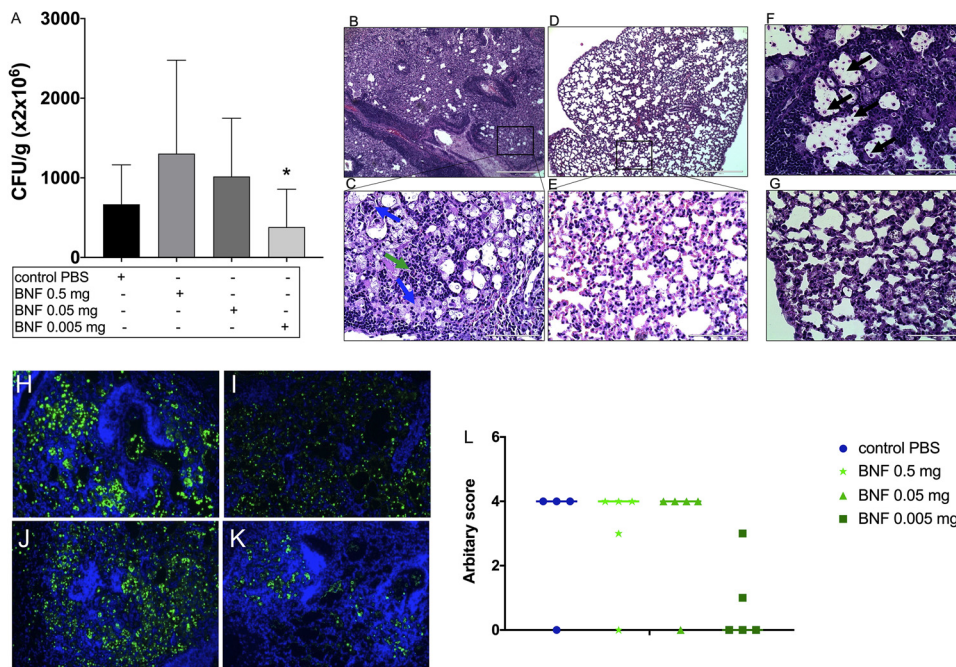


FIG 2 BNF 0.005 mg doses showed a significant decrease ($P < 0.05$) of fungal CFU from recovered lungs (A), indicating a protective profile in lungs 14 days after challenge with *C. neoformans* strain 24067. H&E-stained lung in FVB/NJ mice treated with PBS showing numerous macrophages and multinucleated giant cells (blue arrow) and neutrophils (green arrow) (B, C). BNF (0.005 mg) treated lungs (D, E). PAS staining in PBS treated mouse (F) and in nanoparticle treated lungs (G). Tissues were stained with monoclonal antibody 18B7 conjugated with Oregon green and counterstained with DAPI. Control PBS (H), BNF 0.5 mg (I), BNF 0.05 mg (J), BNF 0.005 mg (K) $\times 10$ magnification. Representative graph showing the IF score generated by the IF slides (L). Black arrows show fungal yeast cells. *, $P < 0.05$.

lower concentration (BNF 0.005 mg) of nanoparticle treated lungs showed no positive staining for yeast (Fig. 2G). Prussian blue staining for nanoparticles in lungs also showed no evidence of iron (BNF) deposits (data not shown).

To further analyze the protective effect observed in FVB/N mice treated with lower dose of BNF, we carried out a survival study in A/J mice. A/J mice were chosen to test whether the high innate resistance of FVB/N mice to cryptococcal infection, which survived a high *C. neoformans* inoculum such that none died after 60 days, was responsible for the observed effects. In this experiment, we analyzed both mouse survival and lung fungal burden in different groups. Mice receiving the lowest dose of BNF (0.0005 mg) showed a significant increase ($P < 0.05$) in the survival, with no deaths (survival of 100%) after 60 days, in comparison with the control group (PBS injected), with a survival of only 20% (Fig. 3A). To analyze the fungal burden, lungs were removed 14 days after infection and CFU numbers were determined. Similarly, a significant decrease ($P < 0.05$) in the number of recovered lung CFUs was observed in the group that received the BNF at 0.0005 mg (Fig. 3B). These data suggest that at lower dose, systemic treatment with BNF NPs can stimulate a protective response when challenged by two different strains of *C. neoformans* in two different mouse strains. We observed nearly complete remission of disease following a single treatment with low dose BNF NPs in A/J mice. Analysis of H&E-stained lung sections revealed numerous and varied inflammatory cells surrounding *Cryptococcus* yeast indicative of a robust and organized immune response (blue arrow) (Fig. 3C and D). Additionally, BNF nanoparticle (0.0005 mg Fe/mouse) treated mouse lungs had fewer inflammatory cells in lungs (Fig. 3E and 3F). PAS staining showed presence of numerous *Cryptococcus* in PBS treated control mouse lungs (Fig. 3G, black arrow). BNF nanoparticle (0.0005 mg Fe) treated mouse lungs showed no positive staining for yeast (H). We noted less MAb 18B7 immunofluorescence in mouse tissues treated with low dose nanoparticles (0.0005 mg) (Fig. 3K and 3L). Mice treated with higher nanoparticle doses (0.005 mg) (Fig. 3J and 3L) had *C. neoformans* similar to that of the control group (Fig. 3I and 3L). In the lungs and spleens of mice given the lower doses of BNF, the levels of the proinflammatory cytokines tumor necrosis factor- α (TNF- α) was decreased after 14 days of infection of the BNF 0.005 mg group relative to control mice infected with *C. neoformans* ($P < 0.05$) (Fig. 3M). Additionally, interleukin-2 (IL-2), interleukin-4 (IL-4), interleukin-10 (IL-10), and interferon-gamma (IFN- γ) were analyzed, but no statistical differences were observed between the groups (Fig. 3M). We focused on the low BNF doses since these were associated with better control of infection.

Lab culture passages can affect the pathogenicity of cultured *Cryptococcus* strains (32). To test the potential effects of lab strain variability, we thawed a second vial of strain H99 to infect mice in Study IV to compare the effects with assays of fungal burden and cytokines from lung and spleen in A/J mice. In contrast to results obtained from Study III (Fig. 3B), there was no statistically significant difference in the number of recovered CFU measured in lungs between PBS control and BNF 0.0005 mg groups (Fig. 4A). There was, however, a slight decrease in the CFU number measured in the BNF 0.0005 mg Fe group from spleen, but this was not statistically significant (Fig. 4A). From the lung and spleen cytokines analysis, levels of proinflammatory cytokines, including interleukin-2 (IL-2), interleukin-4 (IL-4), tumor necrosis factor- α (TNF- α), and interferon-gamma (IFN- γ), were decreased after 14 days of infection relative to control mice infected with *C. neoformans* (Fig. 4B), but this difference was statistically significant only for IL-2 ($P < 0.005$). Interleukin-10 (IL-10) and interferon-gamma (IFN- γ) were analyzed by no statistically significant differences were observed between both groups (Fig. 4B).

Table 1 summarizes all the parameters accessed and analyzed between Study I and Study IV. The four independent experiments reported here each differs in several variables, and they represent our experience as we modified the conditions sequentially in an effort to find a set of parameters that resulted in benefit to the mice. Clearly, changes in such variables as mouse background, inoculum, cryptococcal strain, and BNF dose can each have large effects on the outcome of individual experiments.

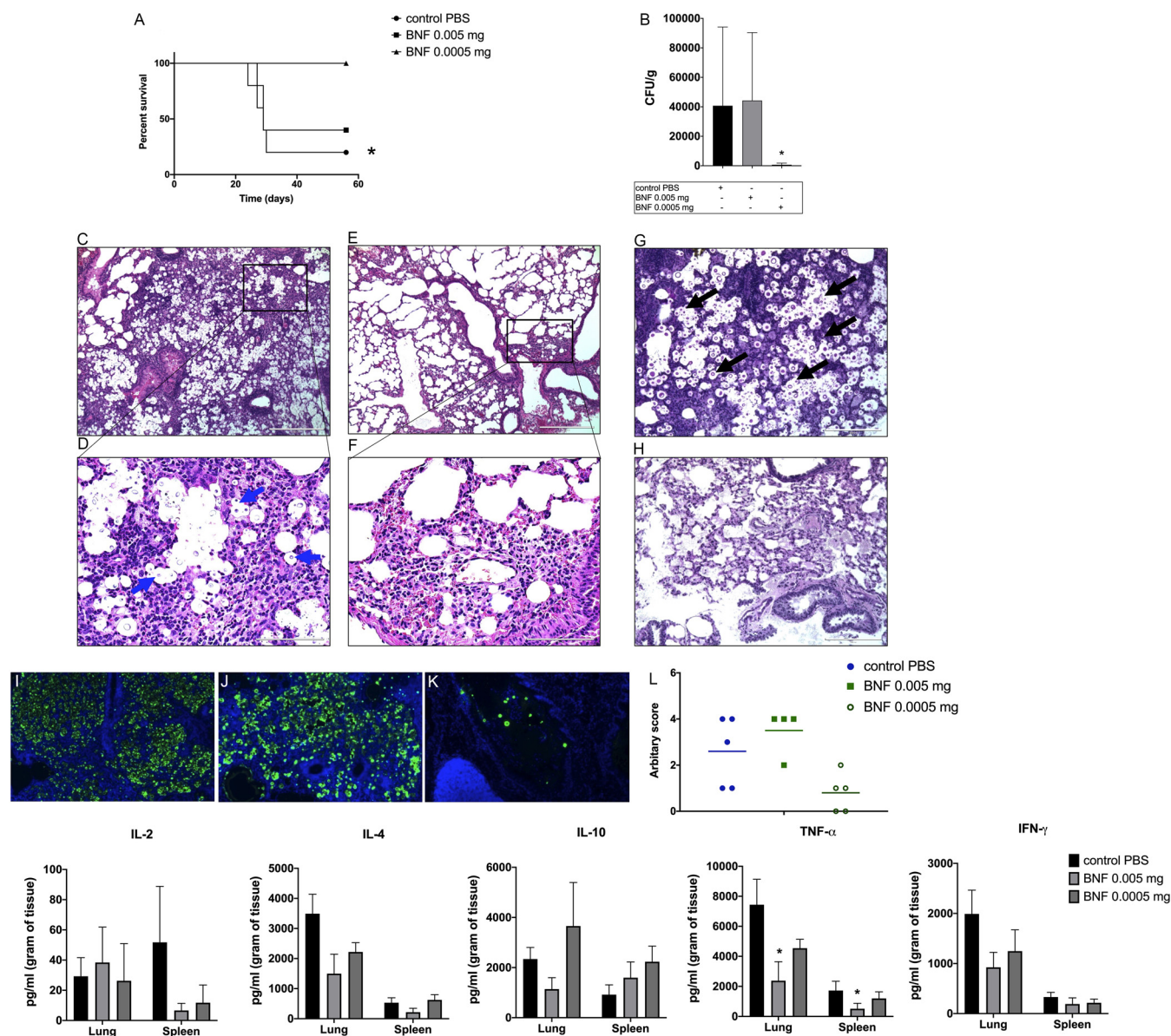


FIG 3 A/J mice injected with lower doses of BNF showed a protective profile in lungs 14 days after challenge with *C. neoformans* strain H99. Mice injected with the lower doses of BNF nanoparticles (0.0005 mg) showed a survival of 100% in comparison with the control group (no BNF nanoparticle injection) with a survival of only 20% ($P < 0.05$) (A). Lung fungal burden showed a significant decrease ($P < 0.05$) in the number of recovered CFU in the mice that received the BNF 0.0005 mg (B). H&E-stained lung sections showed numerous inflammatory cells surrounding *Cryptococcus* yeast (blue arrow) (C, D). BNF nanoparticle (0.0005 mg Fe/mouse) treated mouse (E, F). PAS staining showed presence of numerous *Cryptococcus* in PBS treated control mouse lung (G, black arrow). BNF nanoparticle (0.0005 mg Fe) treated (H). Tissues were stained with monoclonal antibody 18B7 conjugated with Oregon green with DAPI ($\times 10$ magnification). Control PBS (I), BNF 0.005 mg (J), and BNF 0.0005 mg (K). Representative graph showing the IF score generated by the IF slides (L). Lung and spleen cytokine levels during the course of infection (M). *, $P < 0.05$.

Hence, we caution about interpretations from individual experiments and instead stress that the common result across all the experiments was that BNF administration affected the outcome of *C. neoformans* infection in mice. These exploratory studies provide encouragement for future additional work to delineate the conditions where BNF particles can be used to modify the outcome of infection.

DISCUSSION

Clinically, Cryptococcosis is most prevalent in immunocompromised patients, but a significant proportion of cases occur in patients with no apparent immune deficit. One of the confounding paradoxes of this disease is that the prognosis is better in patients

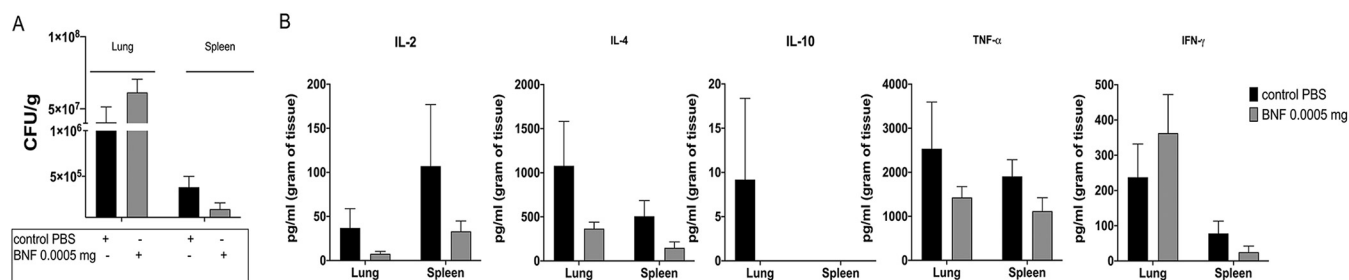


FIG 4 Fungal burden from lungs and spleens of A/J mice 14 days after challenge with recently thawed *C. neoformans* strain H99 showed a slight decrease from spleens of BNF 0.0005 mg group compared with PBS control groups (A). Lung and spleen cytokine levels were also analyzed (B).

with AIDS, possibly because host damage is a function of both fungal processes such as increased intracranial pressure and also tissue damaging effects inflammation (reviewed in reference 33). Consequently, a common denominator in human cryptococcosis, whether it occurs in immunosuppressed or immunologically intact individuals, is dysregulated inflammatory responses, that are ineffective to contain the infection. Since deficits in immune function appear to be major contributors to the outcome of cryptococcosis, it is reasonable to posit that future improvements in therapy will require immune modulators, rather than immune stimulating or immune suppressing treatments (34). In the present study, BNF nanoparticles altered the outcome of infection in a dose response manner, with the best effects observed with low nanoparticle doses, consistent with downregulation of the inflammatory response, possibly associated with immune modulation. Higher doses of BNF particles were associated with stronger inflammation and a trend toward higher fungal burden, suggesting they triggered exuberant immune responses that aggravated infection and damaged host tissue. The association of stronger inflammatory response with lower efficacy is consistent with emerging evidence that host damage in cryptococcosis can have a strong immune mediated component (33).

In summary, our results show that administration of BNF nanoparticles before and after experimental cryptococcal pneumonia infection in mice alters the outcome of infection. Taken together, these preliminary results indicate that iron oxide nanoparticles may harbor immune modulating capabilities to increase/induce and to suppress/reduce inflammation, depending on dose. In this context, nanoparticles comprise important characteristics that make them attractive for a variety of biomedical applications (35). Specifically, iron oxide nanoparticles are physically and chemically stable, biocompatible, and environmentally safe (35), thus presenting unique characteristics for clinical applications. To our knowledge, this is the first exploration of BNF nanoparticles in an infectious disease model, and our results establish the proof of principle that BNF nanoparticles can affect the course of infectious diseases in a manner similar to the experience with cancer and inflammatory diseases. Our results encourage further studies to determine whether they can be used for immunotherapy of cryptococcosis as an adjuvant of standard antifungal therapy.

MATERIALS AND METHODS

C. neoformans serotype D strain 24067 was used in all FVB/N mouse experiments. *C. neoformans* var. *grubii* serotype A strain H99 (ATCC 208821) was used in all A/J mice. The yeast cells were kept frozen in 10% glycerol. Sabouraud dextrose broth (SAB, from Gibco) medium was used for standard growth of yeast cells at 30°C with moderate shaking (120 rpm) overnight.

BNF NPs are commercially available as aqueous suspensions of hydroxyethyl starch-coated magnetite (Fe₃O₄) core-shell nanoparticles (Micromod Partikeltechnologie, GmbH, Rostock, Germany). Their synthesis and physical and biological characterization have been extensively documented by us (31, 36–39). BNF NPs are synthesized by precipitating ferric and ferrous sulfate salts from solution at high pH in a high-pressure-homogenization reaction vessel. According to the manufacturer, they have a mean hydrodynamic diameter of ~100 nm (polydispersity index < 0.25); approximately neutral zeta potential (~–2 mV @ pH = 7.4); and, Fe content >50% wt/wt (or iron oxide >70% wt/wt) (31).

All animal procedures were performed with prior approval from Johns Hopkins University (JHU) Animal Care and Use Committee (IACUC), under approved protocol number MO18H152. JHU Animal

TABLE 1 Summary of all the parameters from Study I, Study II, Study III and Study IV^a

Expt	BNF doses and before fungal challenge)	Mice strain	No. of mice	Fungal strain	Time of mice infection	Parameters assessed (H&E, PAS)	CFU data (lung)	CFU data (spleen)	Survival curve (60 days)	Histology (lung)	IF (lung)	IL-2	IL-4	IL-10	IFN- γ	TNF- α
Study I	5 mg (24 h after and before fungal challenge)	FVB/N	5 per group	24067	60 days	CFU, histology (H&E, PAS)	No difference between groups	X	No difference between groups	No difference between groups	X	X	X	HX	X	X
Study II	0.5/0.05/0.005 mg	FVB/N	5 per group	24067	14 days	CFU, histology (H&E, PAS, IF)	Lower CFU no. on 0.005 mg ($P < 0.05$)	X	X	Less yeasts and inflammation on 0.0005 mg mice group	Less yeasts on 0.0005 mg mice group	X	X	X	X	X
Study III	0.005/0.0005 mg	A/J	10 per group	H99	14 days to sacrifice/60 days survival	CFU, histology (H&E, PAS, IF), survival, cytokine	Lower CFU no. on 0.0005 mg ($P < 0.05$)	X	Higher survival on both 0.005 & 0.0005 mg groups, ($P < 0.05$ on 0.0005 mg group)	Less yeasts and inflammation on 0.0005 mg mice group	Less yeasts on 0.0005 mg mice group	Tendency to decrease (lung)	Tendency to decrease (lung)	No difference	Tendency to decrease (lung and spleen)	Decreased (lung and spleen) on 0.0005 mg group ($P < 0.005$)
Study IV	0.0005 mg	A/J	10 per group	H99	14 days	CFU, cytokine	No difference between groups	Lower CFU no. on 0.0005 mg	X	X	Decreased (lung and spleen) on 0.0005 mg group ($P < 0.005$)	Tendency to decrease (lung and spleen)	Tendency to decrease (lung and spleen)	No difference	Tendency to decrease (lung and spleen)	Tendency to decrease (lung and spleen)

^aBNF, bionized nanoferrite; CFU, colony-forming unit; H&E, hematoxylin and eosin; PAS, periodic acid-Schiff; IF, immunofluorescence; IL, interleukin; TNF- α , tumor necrosis factor alpha; IFN- γ , interferon gamma.

Welfare Assurance Number is D16-00173 (A3272-01). Two mouse strains were used to perform the experiments: 6-week-old female A/J mice (from Jackson Laboratory; JAX stock #000646) and 6- to 8-week-old female FVB/N (from Jackson Laboratory; JAX stock #001800). A/J mice were used because they are highly susceptible to cryptococcal infection (40), whereas our use of FVB/N mice was motivated by our previously reported findings of anticancer immune modulation by BNF NPs in this mouse strain (31). Four different murine experiments were performed as described below. In all experiments, each mouse received a single intravenous injection of either PBS (150 μ l/mouse) or BNF at the described dose, according to its group assignment as follows.

Experiment I: Fifteen female FVB/N mice were divided into three groups ($n = 5$ animals per group): Group 1, PBS 24 h after *C. neoformans* infection (control PBS); Group 2, BNF 5 mg Fe in 150 μ l/mouse 24 h after *C. neoformans* infection (BNF 5 mg after CN); and Group 3, BNF 5 mg Fe in 150 μ l/mouse 24 h before *C. neoformans* infection (BNF 5 mg before CN). Sixty days after infection, surviving animals were euthanized and tissues extracted for fungal burden and histology analysis.

Experiment II: Experimental design was modeled from Study I, but with de-escalating BNF dose to determine dose-response. Analysis of Study I results indicated potent immune responses, motivating a dose de-escalation study. Another 20 female FVB/N mice were divided into four groups ($n = 5$ animals per group), representing PBS control and BNF dose: Group 1, PBS 24 h before *C. neoformans* infection (control PBS); Group 2, BNF 0.5 mg Fe in 100 μ l/animal 24 h before *C. neoformans* infection (BNF 0.5 mg); Group 3, BNF 0.05 mg Fe in 100 μ l/animal 24 h before *C. neoformans* infection (BNF 0.05 mg); and Group 4, BNF 0.005 mg Fe in 100 μ l/animal 24 h before *C. neoformans* infection (BNF 0.005 mg). Animals were observed daily for 14 days, surviving animals were euthanized, and tissues were extracted for fungal burden and histology analysis on 14 days after infection.

Experiment III: Study II results showed lower dose of BNF nanoparticles protected FVB/N mice from *C. neoformans* infection, motivating further study in the A/J strain with established susceptibility to *C. neoformans* infection. Thirty A/J mice ($n = 10$ animals per group) were divided into three groups: Group 1, PBS 24 h before *C. neoformans* infection (control PBS); Group 2, BNF 0.005 mg Fe in 100 μ l/animal 24 h before *C. neoformans* infection (BNF 0.005 mg); and Group 3, BNF 0.0005 mg Fe in 100 μ l/animal 24 h before *C. neoformans* infection (BNF 0.0005 mg). Five animals from each group were euthanized 14 days after infection for fungal burden, histology, and cytokine analysis, and the other five were followed for survival until 60 days.

Experiment IV: Another cohort of 20 A/J mice ($n = 10$ animals per group) were divided into two groups: Group 1, PBS 24 h before *C. neoformans* infection (control PBS); and Group 2, BNF 0.0005 mg Fe in 100 μ l/animal 24 h before *C. neoformans* infection (BNF 0.0005 mg). All animals were sacrificed on day 14 for fungal burden and cytokine analysis from lung and spleen.

All mice challenged with *C. neoformans* were intranasally infected with 1×10^7 *C. neoformans* yeast per animal, in a total volume of 20 μ l (10 μ l in each nasal cavity of the mouse). This model produces a pulmonary infection that rapidly disseminates to brain and other organs (41). Mice were anesthetized with 60 μ L xylazine/ketamine solution intraperitoneally (95 mg of ketamine and 5 mg of xylazine per kilogram of animal body weight) to perform intranasal infection.

The fungal burden in lungs was measured in surviving mice by counting CFU (41, 42). At the end-point of each experiment (as described above), mice were euthanized and the lungs (left lobe) were removed. Organ sections were weighed and homogenized in 1 mL of PBS. After serial dilutions, homogenates were inoculated on Sabouraud agar plates with 10 U/mL of streptomycin/penicillin. The plates were incubated at room temperature, and colonies counted after 48–72 h.

A piece of the right lung and a piece of the spleen were fixed in 10% formalin for 48 h before embedding in paraffin. Tissue slides were stained with hematoxylin and eosin (H&E), periodic acid-Schiff (PAS) for *C. neoformans*, and Prussian blue to visualize nanoparticles. The remaining right lungs and spleens of each A/J mouse treated with PBS or BNF 0.0005 mg were macerated with protease inhibitor (complete, EDTA-free, Roche Life Science, IN, USA) and centrifuged; supernatants of these samples were used for cytokine detection by sandwich-ELISA with commercial kits (BD OptEIA, BD Franklin Lakes, NJ, USA) for the following cytokines: IL-2 (#555148), IL-4 (#555232), IL-10 (#555252), IFN- γ (#551866), and TNF- α (#555268). The protocol was followed according to the manufacturer's recommendations. Readings were performed in a plate spectrophotometer at 450 and 570 nm.

Immunofluorescence (IF) staining was performed on lung tissues to analyze the capsular polysaccharide covering *Cryptococcus* yeasts. Briefly, slides were deparaffinized on a slide warmer at 58°C 10 min followed by serial washing in 2 changes of xylene and in 100%, 95%, and 70% alcohol. Slides were dehydrated in deionized water and then treated with the antibody in a blocking solution for 30 min. The slides were then stained with the antibody (18B7) (43) conjugated with Oregon green during 16 h at 4°C. On the next day, all slides were washed with at least 5 changes of PBS and mounted with DAPI (4',6-diamidino-2-phenylindole) containing mounting media (ProLong Gold Antifade Mountant, ThermoFisher Scientific, MA, USA). Slides were then visualized and imaged with a Zeiss microscope with $\times 100$ magnification.

Statistical analyses were done using GraphPad Prism version 8.00 for Mac OS X (GraphPad Software, San Diego, CA, USA). One-way analysis of variance using a Kruskal-Wallis nonparametric test was used to compare the differences between groups, and individual comparisons of groups were performed using a Bonferroni posttest. The Student's *t* test was used to compare the number of CFU for different groups. The 90–95% confidence interval was determined in all experiments. Unpaired *t* test (F test to compare variances) was performed to compare cytokines data.

ACKNOWLEDGMENTS

A.C. was supported in part by NIH grants AI052733, AI15207, and HL059842. This work was supported in part by Johns Hopkins Discovery Award.

REFERENCES

- Coelho C, Bocca AL, Casadevall A. 2014. The intracellular life of *Cryptococcus neoformans*. *Annu Rev Pathol* 9:219–238. <https://doi.org/10.1146/annurev-pathol-012513-104653>.
- Goldman DL, Khine H, Abadi J, Lindenberg DJ, Pirofski L, Niang R, Casadevall A. 2001. Serologic evidence for *Cryptococcus neoformans* infection in early childhood. *Pediatrics* 107:E66. <https://doi.org/10.1542/peds.107.5.e66>.
- Garcia-Hermoso D, Janbon G, Dromer F. 1999. Epidemiological evidence for dormant *Cryptococcus neoformans* infection. *J Clin Microbiol* 37:3204–3209. <https://doi.org/10.1128/JCM.37.10.3204-3209.1999>.
- Kwon-Chung KJ, Fraser JA, Doering TL, Wang Z, Janbon G, Idnurm A, Bahn YS. 2014. *Cryptococcus neoformans* and *Cryptococcus gattii*, the etiologic agents of cryptococcosis. *Cold Spring Harb Perspect Med* 4:a019760. <https://doi.org/10.1101/cshperspect.a019760>.
- Ghannoum MA, Rice LB. 1999. Antifungal agents: mode of action, mechanisms of resistance, and correlation of these mechanisms with bacterial resistance. *Clin Microbiol Rev* 12:501–517. <https://doi.org/10.1128/CMR.12.4.501>.
- Sharma A, Cornejo C, Mihalic J, Geyh A, Bordelon DE, Korangath P, Westphal F, Gruettner C, Ivkov R. 2018. Physical characterization and in vivo organ distribution of coated iron oxide nanoparticles. *Sci Rep* 8:4916. <https://doi.org/10.1038/s41598-018-23317-2>.
- Weinstein JS, Varallyay CG, Dosa E, Gahramanov S, Hamilton B, Rooney WD, Muldoon LL, Neuwelt EA. 2010. Superparamagnetic iron oxide nanoparticles: diagnostic magnetic resonance imaging and potential therapeutic applications in neurooncology and central nervous system inflammatory pathologies, a review. *J Cereb Blood Flow Metab* 30:15–35. <https://doi.org/10.1038/jcbfm.2009.192>.
- Marchal S, El Hor A, Millard M, Gillon V, Bezdetnaya L. 2015. Anticancer drug delivery: an update on clinically applied nanotherapeutics. *Drugs* 75:1601–1611. <https://doi.org/10.1007/s40265-015-0453-3>.
- Gobbo OL, Sjaastad K, Radomski MW, Volkov Y, Prina-Mello A. 2015. Magnetic nanoparticles in cancer theranostics. *Theranostics* 5:1249–1263. <https://doi.org/10.7150/thno.11544>.
- Soetaert F, Korangath P, Serantes D, Fiering S, Ivkov R. 2020. Cancer therapy with iron oxide nanoparticles: agents of thermal and immune therapies. *Adv Drug Deliv Rev* 163–164:65–83. <https://doi.org/10.1016/j.addr.2020.06.025>.
- Dobrovolskaia MA, Shurin M, Shvedova AA. 2016. Current understanding of interactions between nanoparticles and the immune system. *Toxicol Appl Pharmacol* 299:78–89. <https://doi.org/10.1016/j.taap.2015.12.022>.
- Blanco E, Shen H, Ferrari M. 2015. Principles of nanoparticle design for overcoming biological barriers to drug delivery. *Nat Biotechnol* 33:941–951. <https://doi.org/10.1038/nbt.3330>.
- Bertrand N, Grenier P, Mahmoudi M, Lima EM, Appel EA, Dormont F, Lim JM, Karnik R, Langer R, Farokhzad OC. 2017. Mechanistic understanding of in vivo protein corona formation on polymeric nanoparticles and impact on pharmacokinetics. *Nat Commun* 8:777. <https://doi.org/10.1038/s41467-017-00600-w>.
- Lundqvist M, Stigler J, Elia G, Lynch I, Cedervall T, Dawson KA. 2008. Nanoparticle size and surface properties determine the protein corona with possible implications for biological impacts. *Proc Natl Acad Sci U S A* 105:14265–14270. <https://doi.org/10.1073/pnas.0805135105>.
- Kim CS, Nguyen HD, Ignacio RM, Kim JH, Cho HC, Maeng EH, Kim YR, Kim MK, Park BK, Kim SK. 2014. Immunotoxicity of zinc oxide nanoparticles with different size and electrostatic charge. *Int J Nanomedicine (Lond)* 9(Suppl 2):195–205. <https://doi.org/10.2147/IJN.S57935>.
- Mocan T, Matea CT, Iancu C, Agoston-Coldea L, Mocan L, Orasan R. 2016. Hypersensitivity and nanoparticles: update and research trends. *Clujul Med* 89:216–219. <https://doi.org/10.15386/cjmed-574>.
- Kharazian B, Lohse SE, Ghasemi F, Raoufi M, Saei AA, Hashemi F, Farvadi F, Alimohamadi R, Jalali SA, Shokrogozar MA, Hadipour NL, Eftehadi MR, Mahmoudi M. 2018. Bare surface of gold nanoparticle induces inflammation through unfolding of plasma fibrinogen. *Sci Rep* 8:12557. <https://doi.org/10.1038/s41598-018-30915-7>.
- Deng Z, Jin J, Wang Z, Wang Y, Gao Q, Zhao J. 2017. The metal nanoparticle-induced inflammatory response is regulated by SIRT1 through NF- κ B deacetylation in aseptic loosening. *Int J Nanomedicine (Lond)* 12:3617–3636. <https://doi.org/10.2147/IJN.S124661>.
- Ilinskaya AN, Dobrovolskaia MA. 2016. Understanding the immunogenicity and antigenicity of nanomaterials: past, present and future. *Toxicol Appl Pharmacol* 299:70–77. <https://doi.org/10.1016/j.taap.2016.01.005>.
- Ngobil TA, Daniele MA. 2016. Nanoparticles and direct immunosuppression. *Exp Biol Med (Maywood)* 241:1064–1073. <https://doi.org/10.1177/1535370216650053>.
- Mallipeddi R, Rohan LC. 2010. Progress in antiretroviral drug delivery using nanotechnology. *Int J Nanomedicine (Lond)* 5:533–547.
- Gonzalez-Aramundiz JV, Cordeiro AS, Csaba N, de la Fuente M, Alonso MJ. 2012. Nanovaccines: nanocarriers for antigen delivery. *Biol Aujourdhui* 206:249–261. <https://doi.org/10.1051/jbio/2012027>.
- Zaman M, Good MF, Toth I. 2013. Nanovaccines and their mode of action. *Methods* 60:226–231. <https://doi.org/10.1016/j.jymeth.2013.04.014>.
- Tran TH, Amiji MM. 2015. Targeted delivery systems for biological therapies of inflammatory diseases. *Expert Opin Drug Deliv* 12:393–414. <https://doi.org/10.1517/17425247.2015.972931>.
- Franca A, Aggarwal P, Barsov EV, Kozlov SV, Dobrovolskaia MA, Gonzalez-Fernandez A. 2011. Macrophage scavenger receptor A mediates the uptake of gold colloids by macrophages in vitro. *Nanomedicine (Lond)* 6:1175–1188. <https://doi.org/10.2217/nnm.11.41>.
- O'Hagan DT, MacKichan ML, Singh M. 2001. Recent developments in adjuvants for vaccines against infectious diseases. *Biomol Eng* 18:69–85. [https://doi.org/10.1016/S1389-0344\(01\)00101-0](https://doi.org/10.1016/S1389-0344(01)00101-0).
- Fifis T, Mottram P, Bogdanoska V, Hanley J, Plebanski M. 2004. Short peptide sequences containing MHC class I and/or class II epitopes linked to nano-beads induce strong immunity and inhibition of growth of antigen-specific tumor challenge in mice. *Vaccine* 23:258–266. <https://doi.org/10.1016/j.vaccine.2004.05.022>.
- Minigo G, Scholzen A, Tang CK, Hanley JC, Kalkanidis M, Pietersz GA, Apostolopoulos V, Plebanski M. 2007. Poly-L-lysine-coated nanoparticles: a potent delivery system to enhance DNA vaccine efficacy. *Vaccine* 25:1316–1327. <https://doi.org/10.1016/j.vaccine.2006.09.086>.
- Manolova V, Flace A, Bauer M, Schwarz K, Saudan P, Bachmann MF. 2008. Nanoparticles target distinct dendritic cell populations according to their size. *Eur J Immunol* 38:1404–1413. <https://doi.org/10.1002/eji.200737984>.
- Zanganeh S, Hutter G, Spitler R, Lenkov O, Mahmoudi M, Shaw A, Pajarinen JS, Nejadnik H, Goodman S, Moseley M, Coussens LM, Daldrop-Link HE. 2016. Iron oxide nanoparticles inhibit tumour growth by inducing pro-inflammatory macrophage polarization in tumour tissues. *Nat Nanotechnol* 11:986–994. <https://doi.org/10.1038/nnano.2016.168>.
- Korangath P, Barnett JD, Sharma A, Henderson ET, Stewart J, Yu SH, Kandala SK, Yang CT, Caserto JS, Hedayati M, Armstrong TD, Jaffee E, Gruettner C, Zhou XC, Fu W, Hu C, Sukumar S, Simons BW, Ivkov R. 2020. Nanoparticle interactions with immune cells dominate tumor retention and induce T cell-mediated tumor suppression in models of breast cancer. *Sci Adv* 6:eaay1601. <https://doi.org/10.1126/sciadv.aay1601>.
- Franzot SP, Mukherjee J, Cherniak R, Chen LC, Hamdan JS, Casadevall A. 1998. Microevolution of a standard strain of *Cryptococcus neoformans* resulting in differences in virulence and other phenotypes. *Infect Immun* 66:89–97. <https://doi.org/10.1128/IAI.66.1.89-97.1998>.
- Pirofski LA, Casadevall A. 2017. Immune-mediated damage completes the parabola: *Cryptococcus neoformans* pathogenesis can reflect the outcome of a weak or strong immune response. *mBio* 8:e02063-17. <https://doi.org/10.1128/mBio.02063-17>.
- Panackal AA, Williamson KC, van de Beek D, Boulware DR, Williamson PR. 2016. Fighting the monster: applying the host damage framework to human central nervous system infections. *mBio* 7:e01906-15–e01915. <https://doi.org/10.1128/mBio.01906-15>.
- Arias LS, Pessan JP, Vieira APM, Lima TMT, Delbem ACB, Monteiro DR. 2018. Iron oxide nanoparticles for biomedical applications: a perspective on synthesis, drugs, antimicrobial activity, and toxicity. *Antibiotics (Basel)* 7:46. <https://doi.org/10.3390/antibiotics7020046>.

36. Grüttner C, Müller K, Teller J, Westphal F, Foreman A, Ivkov R. 2007. Synthesis and antibody conjugation of magnetic nanoparticles with improved specific power absorption rates for alternating magnetic field cancer therapy. *J Magnetism and Magnetic Materials* 311:181–186. <https://doi.org/10.1016/j.jmmm.2006.10.1151>.
37. Natarajan A, Gruettner C, Ivkov R, DeNardo GL, Mirick G, Yuan A, Foreman A, DeNardo SJ. 2008. NanoFerrite particle based radioimmunonanoparticles: binding affinity and in vivo pharmacokinetics. *Bioconjugate Chem* 19:1211–1218. <https://doi.org/10.1021/bc800015n>.
38. Dennis CL, Jackson AJ, Borchers JA, Hoopes PJ, Strawbridge R, Foreman AR, van Lierop J, Gruttner C, Ivkov R. 2009. Nearly complete regression of tumors via collective behavior of magnetic nanoparticles in hyperthermia. *Nanotechnology* 20:395103. <https://doi.org/10.1088/0957-4484/20/39/395103>.
39. Dennis CL, Krycka LK, Borchers JA, Desautels RD, van Lierop J, Huls NF, Jackson AJ, Gruettner C, Ivkov R. 2015. Internal magnetic structure of nanoparticles dominates time-dependent relaxation processes in a magnetic field. *Adv Funct Mater* 25:4300–4311. <https://doi.org/10.1002/adfm.201500405>.
40. Rhodes JC, Wicker LS, Urba WJ. 1980. Genetic control of susceptibility to *Cryptococcus neoformans* in mice. *Infect Immun* 29:494–499. <https://doi.org/10.1128/iai.29.2.494-499.1980>.
41. Coelho C, Camacho E, Salas A, Alanio A, Casadevall A. 2019. Intranasal inoculation of *Cryptococcus neoformans* in mice produces nasal infection with rapid brain dissemination. *mSphere* 4:e00483-19. <https://doi.org/10.1128/mSphere.00483-19>.
42. Muhammed M, Feldmesser M, Shubitz LF, Lionakis MS, Sil A, Wang Y, Glavis-Bloom J, Lewis RE, Galgiani JN, Casadevall A, Kontoyiannis DP, Mylonakis E. 2012. Mouse models for the study of fungal pneumonia: a collection of detailed experimental protocols for the study of *Coccidioides*, *Cryptococcus*, *Fusarium*, *Histoplasma* and combined infection due to *Aspergillus-Rhizopus*. *Virulence* 3:329–338. <https://doi.org/10.4161/viru.20142>.
43. Casadevall A, Cleare W, Feldmesser M, Glatman-Freedman A, Goldman DL, Koziel TR, Lendvai N, Mukherjee J, Pirofski LA, Rivera J, Rosas AL, Scharff MD, Valadon P, Westin K, Zhong Z. 1998. Characterization of a murine monoclonal antibody to *Cryptococcus neoformans* polysaccharide that is a candidate for human therapeutic studies. *Antimicrob Agents Chemother* 42:1437–1446. <https://doi.org/10.1128/AAC.42.6.1437>.



Amoeba Predation of *Cryptococcus neoformans* Results in Pleiotropic Changes to Traits Associated with Virulence

Man Shun Fu,^a Livia C. Liporagi-Lopes,^{a,b} Samuel R. dos Santos Júnior,^{a,c} Jennifer L. Tenor,^d John R. Perfect,^d
 Christina A. Cuomo,^e Arturo Casadevall^a

^aDepartment of Molecular Microbiology and Immunology, Johns Hopkins Bloomberg School of Public Health, Baltimore, Maryland, USA

^bDepartamento de Análises Clínicas e Toxicológicas, Faculdade de Farmácia, Universidade Federal do Rio de Janeiro, Rio de Janeiro, Brazil

^cDepartamento de Microbiologia, Instituto de Ciências Biomédicas, Universidade de São Paulo, São Paulo, Brazil

^dDivision of Infectious Diseases, Department of Medicine and Department of Molecular Genetics and Microbiology, Duke University, Durham, North Carolina, USA

^eInfectious Disease and Microbiome Program, Broad Institute, Cambridge, Massachusetts, USA

ABSTRACT Amoeboid predators, such as amoebae, are proposed to select for survival traits in soil microbes such as *Cryptococcus neoformans*; these traits can also function in animal virulence by defeating phagocytic immune cells, such as macrophages. Consistent with this notion, incubation of various fungal species with amoebae enhanced their virulence, but the mechanisms involved are unknown. In this study, we exposed three strains of *C. neoformans* (1 clinical and 2 environmental) to predation by *Acanthamoeba castellanii* for prolonged times and then analyzed surviving colonies phenotypically and genetically. Surviving colonies comprised cells that expressed either pseudohyphal or yeast phenotypes, which demonstrated variable expression of traits associated with virulence, such as capsule size, urease production, and melanization. Phenotypic changes were associated with aneuploidy and DNA sequence mutations in some amoeba-passaged isolates, but not in others. Mutations in the gene encoding the oligopeptide transporter (CNAG_03013; *OPT1*) were observed among amoeba-passaged isolates from each of the three strains. Isolates derived from environmental strains gained the capacity for enhanced macrophage toxicity after amoeba selection and carried mutations on the CNAG_00570 gene encoding Pkr1 (AMP-dependent protein kinase regulator) but manifested reduced virulence in mice because they elicited more effective fungal-clearing immune responses. Our results indicate that *C. neoformans* survival under constant amoeba predation involves the generation of strains expressing pleiotropic phenotypic and genetic changes. Given the myriad potential predators in soils, the diversity observed among amoeba-selected strains suggests a bet-hedging strategy whereby variant diversity increases the likelihood that some will survive predation.

IMPORTANCE *Cryptococcus neoformans* is a ubiquitous environmental fungus that is also a leading cause of fatal fungal infection in humans, especially among immunocompromised patients. A major question in the field is how an environmental yeast such as *C. neoformans* becomes a human pathogen when it has no need for an animal host in its life cycle. Previous studies showed that *C. neoformans* increases its pathogenicity after interacting with its environmental predator amoebae. Amoebae, like macrophages, are phagocytic cells that are considered an environmental training ground for pathogens to resist macrophages, but the mechanism by which *C. neoformans* changes its virulence through interactions with protozoa is unknown. Our study indicates that fungal survival in the face of amoeba predation is associated with the emergence of pleiotropic phenotypic and genomic changes that increase the chance of fungal survival, with this diversity suggesting a bet-hedging strategy to ensure that some forms survive.

Citation Fu MS, Liporagi-Lopes LC, dos Santos SR, Júnior, Tenor JL, Perfect JR, Cuomo CA, Casadevall A. 2021. Amoeba predation of *Cryptococcus neoformans* results in pleiotropic changes to traits associated with virulence. mBio 12:e00567-21. <https://doi.org/10.1128/mBio.00567-21>.

Invited Editor Michal A. Olszewski, University of Michigan and VA Ann Arbor Health Systems

Editor Floyd L. Wormley, Texas Christian University

Copyright © 2021 Fu et al. This is an open-access article distributed under the terms of the [Creative Commons Attribution 4.0 International license](https://creativecommons.org/licenses/by/4.0/).

Address correspondence to Arturo Casadevall, acasade1@jhu.edu.

Received 1 March 2021

Accepted 30 March 2021

Published 27 April 2021

KEYWORDS *Acanthamoeba castellanii*, amoeba, *Cryptococcus neoformans*, evolution, host-pathogen interactions, macrophages, opportunistic fungi

C*ryptococcus neoformans* is a major, life-threatening fungal pathogen that predominantly infects severely immunocompromised patients and causes over 180,000 deaths per year worldwide (1). *C. neoformans* expresses virulence factors that promote its pathogenicity in humans, including formation and enlargement of a polysaccharide capsule that interferes with the host immune system in varied ways, melanin production that protects against oxidative stress (2–5), and extracellular secretion of various enzymes, including phospholipase and urease (6, 7). *C. neoformans* is found primarily and ubiquitously in environments such as soils contaminated with bird excreta or from trees (8–11). It is a saprophyte and does not require an animal host for survival and reproduction. Besides, there is rare evidence of human-to-human transmission and thus it is unlikely that its virulence traits were selected for causing disease in humans or animals. That raises the fundamental question of how *C. neoformans* acquired those traits, which are essential for pathogenesis of cryptococcosis in human.

To explain this enigma, the “amoeboid predator-fungal animal virulence” hypothesis posits that virulence emerges accidentally from coincident selection resulting from selective pressures in both natural environmental and animal niches such as predatory amoebae and nematodes (12). According to this view, microbial traits selected for environmental survival also confer the capacity for virulence by promoting survival in animal hosts (12, 13). For example, the capsule can protect the fungi from desiccation and against predatory amoebae (14, 15), while melanin may reduce damage of fungi from exposure to UV radiation, osmotic stresses, or extreme temperatures (16–19). Urease plays a nutritional role in nitrogen acquisition in the environment (20). Moreover, it is striking that *C. neoformans* isolates from the soil are virulent for animal hosts (21). Understanding the evolutionary adaptation of *C. neoformans* in nature will help us to understand further the origin of virulence and pathogenesis of cryptococcosis.

Amoebae are one of the major sources of selective pressure in nature for a broad range of soil microorganisms that have pathogenic potential for humans, including bacteria such as *Legionella pneumophila* and *Mycobacterium* spp. and fungi such as *Cryptococcus neoformans*, *Aspergillus fumigatus*, and *Paracoccidioides* spp. (13, 15, 22–24). Similarly to human macrophages, amoebae ingest microorganisms; undergo a respiratory burst, phagosome maturation, and acidification; and express cell surface receptors and expel undigested materials (25–31). However, many bacteria and fungi have strategies to survive in amoebae that function in parallel for survival in mammalian phagocytic cells. For example, *L. pneumophila* utilizes similar cellular and molecular mechanisms of invasion, survival, and replication inside both amoebae and macrophages (32–37). Amoeba-grown *L. pneumophila* bacteria are more invasive for epithelial cells and macrophages (22). After passage in amoebae, *Mycobacterium avium* enhances both entry and intracellular replication in epithelial cells and is more virulent in the macrophage and mouse models of infection (23). Among fungal pathogens, concordance of virulence factor function for amoebae and animals was also demonstrated for *A. fumigatus* (13). For example, the mycotoxin fumagillin can inhibit the growth of *Entamoeba histolytica*, and it can also cause mammalian epithelial cell damage (38). Many studies have been done to explore amoeba-*C. neoformans* interaction and have shown evidence that amoebae influence the virulence of *C. neoformans* for mammalian infection (39, 40).

Acanthamoeba castellanii was originally isolated from cultures of a *Cryptococcus* sp. and, like other amoeba species, it preys on *Cryptococcus* spp. (41, 42). There is evidence that amoebae are natural predators of *C. neoformans* in the natural environment (43). On the other hand, *C. neoformans* is able to resist destruction by amoebae, especially in nutrient-poor conditions (44) without metal cations (45). Several studies have shown that the virulence factors and the cellular process that fungi use for defending against amoeba predation are remarkably similar to those employed for mammalian virulence.

For example, capsule formation and melanin production are important for *C. neoformans* to resist predation by *A. castellanii* and play important roles for pathogenicity in mammalian infection (15, 39). Interestingly, the phospholipids that are secreted by both macrophages and amoebae trigger capsule enlargement (40). The nonlytic exocytosis process which is found in macrophage-containing *C. neoformans* can be also observed in *A. castellanii* and *Dictyostelium discoideum* through the similar action of actin polymerization (46, 47). Transcriptional studies showed a conserved metabolic response of *C. neoformans* to the microenvironments of both macrophages and amoebae (48). All of those common strategies found to adapt to both amoebae and macrophages support the hypothesis that cryptococcal pathogenesis is derived from the interaction with amoebae in the natural environment. More direct evidence comes from an experiment on the passage of an attenuated cryptococcal strain to *D. discoideum* cultures that showed enhancement of fungal virulence in a murine infection model (39). Passaged *C. neoformans* also exhibits capsule enlargement and rapid melanization, suggesting that those are mechanisms to enhance the survival of fungus in mice. However, the underlying mechanism of how these phenotypic changes occur is still unclear.

In this study, we sought to determine the long-term evolutionary adaptation of *C. neoformans* when interacting with amoebae and whether the adaptation affected virulence traits for animal hosts. Our results show that persistent amoeba predation was associated with the emergence of pleiotropic phenotypic changes of *C. neoformans*.

RESULTS

Selection of amoeba resistance strains. We studied the interaction between *C. neoformans* and *Acanthamoeba castellanii* by culturing them together on Sabouraud agar. For the initial experiments, we used the well-studied common laboratory strain H99. The experimental setup involved spreading approximately 200 cryptococcal cells on agar, followed by placing approximately 5,000 *A. castellanii* cells on the plate (Fig. 1A). After approximately 1 month of coinoculation, small colonies emerged within the predation zone of *A. castellanii* (Fig. 1A and B), sometimes under the mat of amoebae. Microscopic morphological analysis of cells in those colonies revealed pseudohyphal and hyphal forms of *C. neoformans* (Fig. 1C and D). We selected 20 single hyphal cells from two colonies (10 hyphae from each colony), and these were transferred to a fresh Sabouraud agar plate without amoeba (Fig. 1A, E, and I). After 24 h, microcolonies composed exclusively of yeast cells emerged on the agar (Fig. 1F and J), which manifested two distinct colony morphologies, smooth and serrated, after 2 days of agar growth (Fig. 1G and K). All of the cells from these colonies were yeasts (Fig. 1H and L). The same experiment was then repeated with two environmental *C. neoformans* strains, A1-35-8 and Ftc555-1. A1-35-8 with a genotype of the VN1 molecular type was isolated from pigeon guano in the United States, while Ftc555-1 was isolated from a mopane tree in Botswana and had the VNB molecular type. Both strains were avirulent in mouse model (49–51). A total of 20 single hyphae were picked from four surviving colonies (five hyphae from each colony) to a fresh agar plate. Like the experience with H99, these strains responded to the presence of amoebae by generating cells that formed colonies with various cellular and colony morphologies, of which some (isolates A4 to A6) were slightly serrated, with pseudohyphal cells (Fig. 1M). We also observed some hyphal colonies formed by Ftc555-1 cells, but these eventually converted back to yeast cells when streaked on fresh agar medium (Fig. 1N). The results showed that after interacting with amoebae, *C. neoformans* can develop a large variety of cellular and colony morphologies even in amoeba-free medium.

Six colonies from each strain were selected together with three controls, which were colonies on the same plate with isolates but without interacting with amoebae, for further phenotypic characterization (Fig. 1A). These will be referred to here as amoeba-passaged isolates with numbers preceded by the letters H, A, and F to indicate their origins from strains H99, A1-35-8, and Ftc555-1, respectively. Controls will be

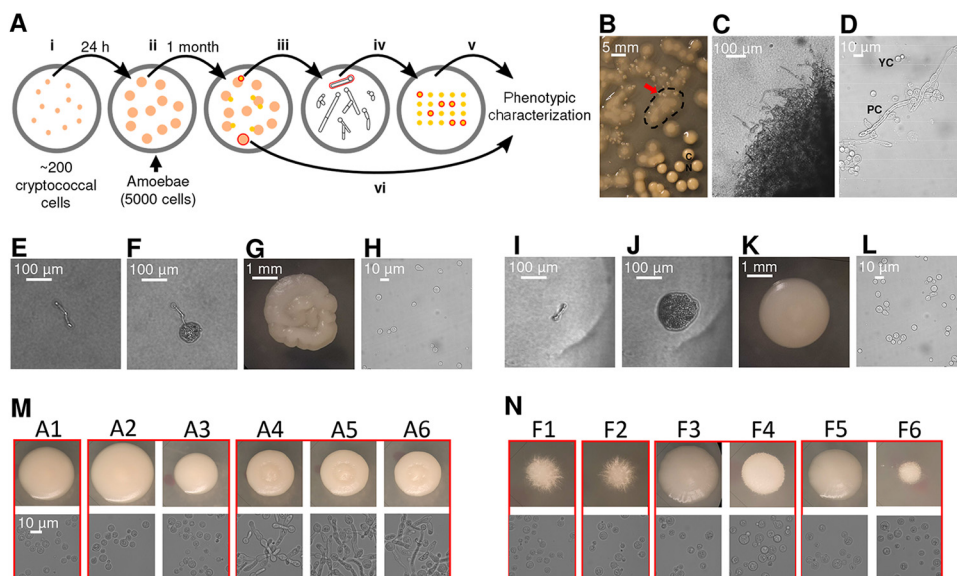


FIG 1 *C. neoformans* colonies exhibit various cellular and colony morphologies after coincubation with amoebae in Sabouraud agar. (A) Schematic representation of experimental setup for amoeba resistance strain selection. (i) Approximately 200 cryptococcal cells were spread on agar. (ii) After 24 h, approximately 5,000 *A. castellanii* cells were placed on agar with cryptococcal colonies. (iii) After approximately 1 month of coincubation, small colonies emerged within the predation zone of *A. castellanii*. Surviving colonies were picked using pipette tips and transferred to phosphate-buffered saline (PBS) in a 3-mm culture dish. (iv) A total of 20 individual hyphae from 2 to 4 colonies were selected under a microscope and transferred to fresh Sabouraud agar. Plates were incubated at 30°C to generate colonies. (v) Six colonies were then selected for further phenotypic characterization. (vi) Control colonies were also picked from the same plate of hyphal isolates but without interaction with amoeba. (B) Small colonies of H99 cells (red arrow) surviving in a mat of amoebae that appears as a hazy, cloudy area (denoted by dashed line). Typical *C. neoformans* colonies (CN) are visible on the bottom right of the image. (C) Cells in the surviving colony exhibit hyphal or pseudohyphal morphology ($\times 100$ magnification). (D) Both pseudohyphae and yeast cells were identified on a wet mount of samples taken from the surviving colony ($\times 400$). (E) Single pseudohyphal cell isolated from the surviving colonies and transferred onto a fresh amoeba-free solid medium, where it formed new colonies. (F) Microcolony with primarily yeast cells, formed from a single pseudohyphal cell in 24 h. (G) The colony developed a serrated appearance after 2 days. (H) Yeast cells were identified on a wet mount of samples taken from the serrated colony. (I to L) Images show another example of single pseudohyphal cell isolation. A smooth colony was formed from this particular pseudohyphal cell. (M and N) The same experiment was performed on environmental strains A1-35-8 and Ftc-555-1. Various cellular and colony morphologies have been identified among isolates A1 to A6 and F1 to F6 in backgrounds of A1-35-8 and Ftc555-1, respectively. Colonies grown from individual hyphae that were isolated from the same surviving colony are grouped in red boxes.

referred to as HC, AC, and FC, and parental strains will be referred to as HP, AP, and FP. Amoeba-passaged isolates, their parental strains, and controls are listed in Table S1 in the supplemental material. To test if amoebae exert selection pressure that resulted in amoeba-resistant cells, we examined if those isolates increased their survival during amoeba interaction. Isolates were then coincubated with amoebae in the agar medium again, with *C. neoformans* streaked into a cross pattern, and amoebae were spotted in the center, at the intersection of the two perpendicular streaks (Fig. 2A and B). The radii of clear zones were measured as a function of time, and these represented how well the amoebae cleared the culture of *C. neoformans*. All of the amoeba-passaged isolates derived from H99 had a reduced size of predation zone compared to those of their controls and parental strain (Fig. 2C). In particular, the isolates that formed smooth colonies (H13, H16, and H17) had the smallest predation zone (Fig. 2C). This result implies that amoeba passage resulted in *C. neoformans* strains with an increased ability to subsequently resist predation by amoebae. Next, we investigated the mechanism of the resistance. Samples were taken at the edge of the predation zone at the early stage of the interaction (week 1), and observed under microscope. Isolates H13, H16, and H17 formed pseudohyphae, while most of the cells in isolates H1, H2, and H14 were in yeast form, with some displaying pseudohyphae (Fig. 2D). However, no pseudohyphae were found in cells from controls and H99 parental colonies, although pseudohyphae were

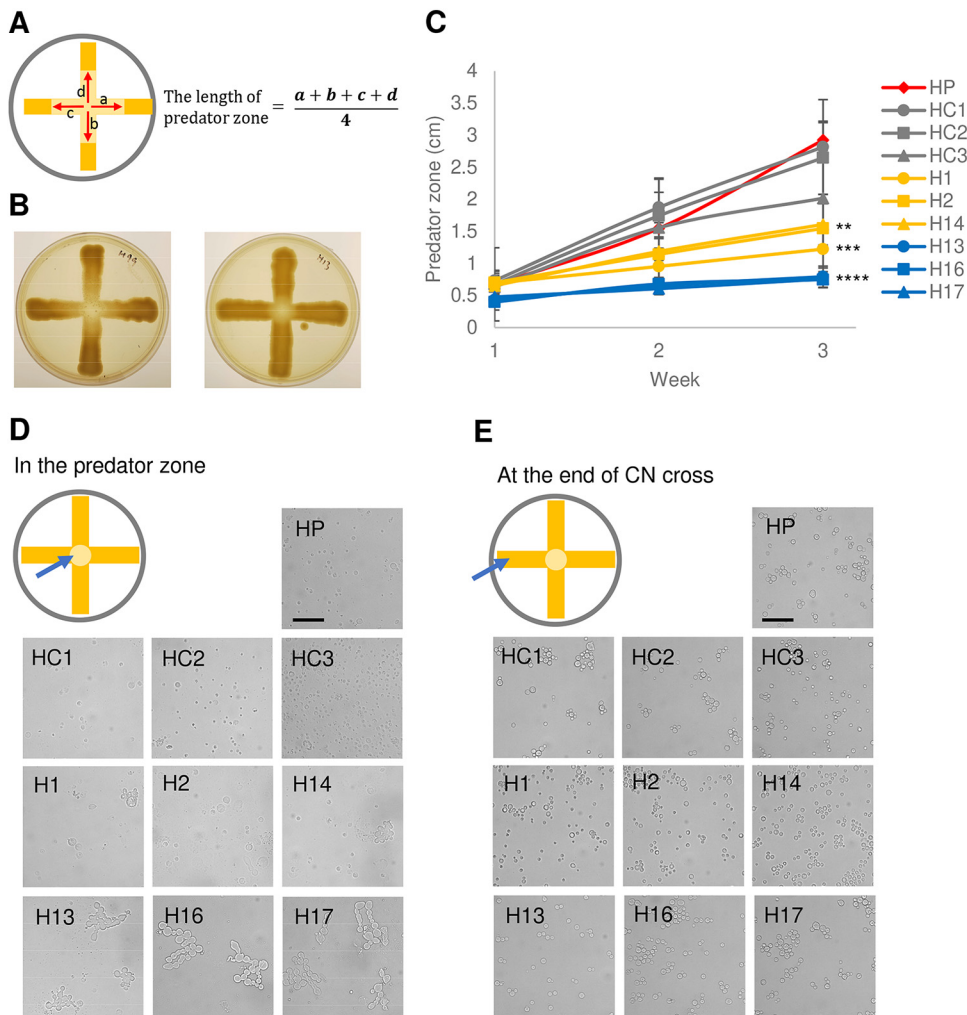


FIG 2 Isolates in H99 background derived from exposure to amoebae demonstrated increased resistance to amoeba killing by rapid pseudohyphal formation. (A) Scheme of amoeba killing assay. *C. neoformans* was streaked in a cross, while *A. castellanii* was dropped at the intersection of the cross on Sabouraud agar. Data shown are the average of the distance between boundary and center of the clear predation zone in four indicated directions (a and b), with the area being the predation zone. (B) Representative images of amoeba killing assay on agar plates. Images were taken 3 weeks after *A. castellanii* was dropped at the intersection of *C. neoformans* culture. Left, H99; right, H13. (C) All of the isolates that had prior exposure to amoebae had smaller clear zones than those of their parental strain and controls, consistent with enhanced resistance. HP, parental strain; HC1-3, controls; H, isolates derived from H99 after exposure to amoeba. Data are means from three biological replicates, and error bars are standard deviation (SD). **, $P < 0.01$; ***, $P < 0.001$; ****, $P < 0.0001$, compared to parental strain by one-way analysis of variance (ANOVA) and followed by Tukey's multiple-comparison test. (D) Samples were taken from the peripheral areas of the predation zone after 1 week of coinubation with amoebae and visualized under a microscope. All of the isolates showed pseudohyphal formation, but the parental strain and the controls did not. (E) Sample were taken from the end of the cross, where *C. neoformans* have not yet contacted *A. castellanii*. All of the isolates manifested yeast cell morphology.

eventually formed at the late stage of the interaction. Samples were also taken at a distance from the predation zone, where cryptococcal cells had no contact with amoebae, and in each of these regions all cells were in yeast form (Fig. 2E). These results showed that pseudohyphal cells emerged rapidly from each of the amoeba-passaged strains, even though their cells were yeast prior to the incubation with amoebae, and that pseudohyphal formation is a major mechanism of increased ability to resist predation.

When the isolates derived from A1-35-8 and Ftc555-1 strains were again exposed to *A. castellanii*, some but not all exhibited increased resistance to amoebae (Fig. 3A and B). Isolates derived from A1-35-8 (A4 to A6) were significantly more resistant than the

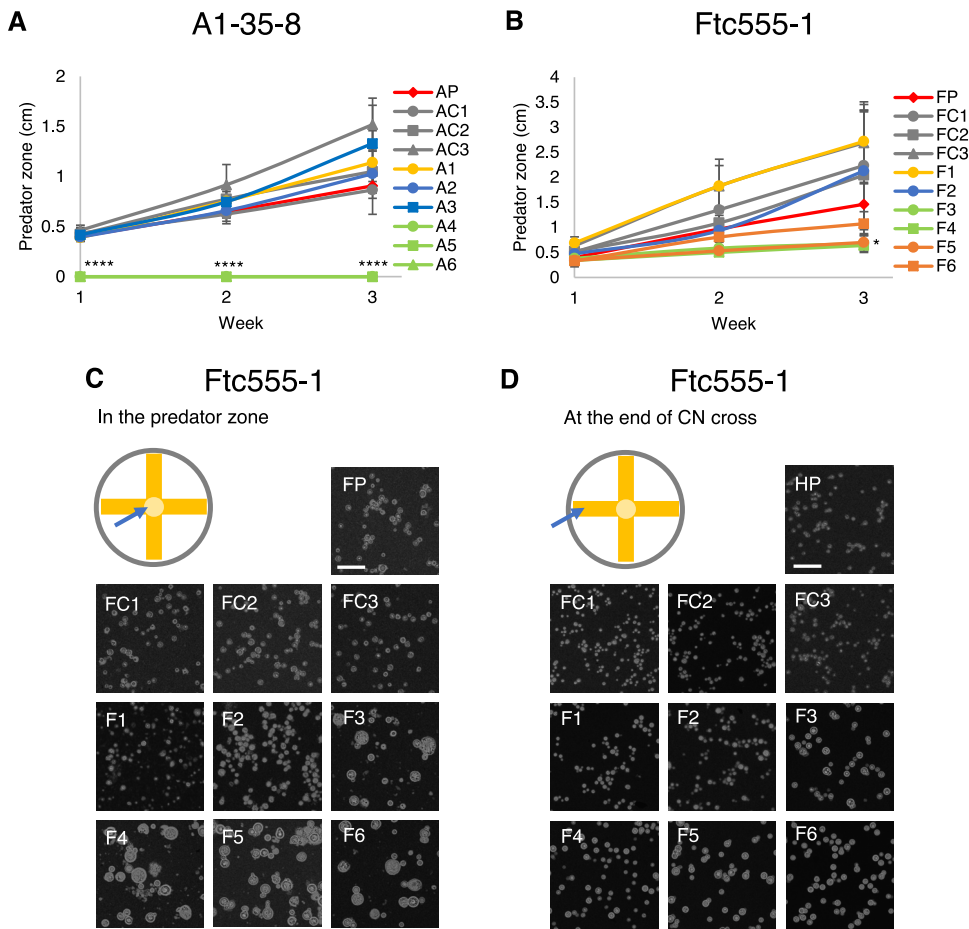


FIG 3 Some of the isolates recovered from the environmental strains A1-35-8 and Ftc-555-1 exhibited increased resistance to *A. castellanii*. (A) No clear predation zone of clearance was apparent with isolates A4 to A6, while larger predation zones were apparent for isolates A1 to A3 compared to those of their parental strains. AP, parental strain; AC1 to AC3, controls; A1 to A6, isolates derived from A1-35-8 after exposure to amoebae. ****, $P < 0.0001$, compared to parental strain by one-way ANOVA and followed by Tukey's multiple-comparison test. (B) Isolates F3 to F5 showed a smaller predation zone than that of their parental strain. Data are means from three biological replicates, and error bars are SD. FP, parental strain; FC1 to FC3, controls; F1 to F6, isolates derived from Ftc555-1 after exposure to amoebae. *, $P < 0.1$, compared to parental strain by one-way ANOVA and followed by Tukey's multiple-comparison test. (C) Ftc555-1 samples were collected from the predation zone after 1 week of coinubation. Isolates F3 to F6 formed larger-sized cells than those of their parental strain and controls. (D) The cell size of isolates F3 to F6 from the end of the cross is slightly larger than those of parental strain and controls, but they are not as large as the cells taken from the predation zone.

others (Fig. 3A). That may be due to maintenance of pseudohyphal cell morphology by isolates A4 to A6 even in the amoeba-free medium. Isolates F3 to F5 manifested increased resistance to amoeba but, unlike the H99-derived isolates, displayed no pseudohyphal formation but had larger cells compared to their parental strain (Fig. 3C and D) at the early stage of interaction, which may be another survival strategy for *C. neoformans* against amoebae. In this regard, phagocytosis of *C. neoformans* by macrophage was reduced by cell enlargement of *C. neoformans* (52–54). The resistance of isolates F3 to F5 to amoebae may reflect their larger cell size.

Effects of amoeba selection on known virulence factors. *C. neoformans* expresses virulence factors that promote its pathogenicity, including formation and enlargement of a polysaccharide capsule, melanin production, extracellular secretion of urease, and cell enlargement. To evaluate whether the emergence of variant forms of *C. neoformans* was accompanied by changes to known virulence factors, we analyzed the virulence-related phenotypic characteristics of the isolates derived from the three strains. Isolates H13, H16, and H17 and each of the isolates derived from the A1-35-8 strain

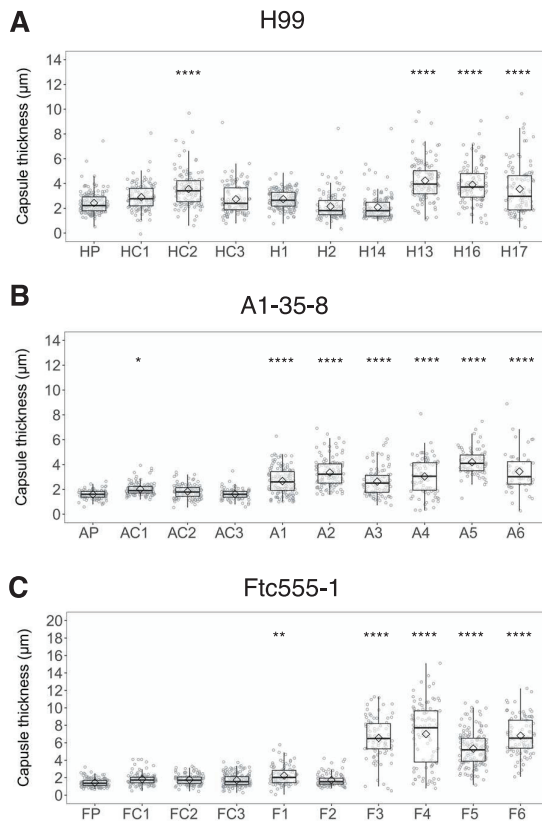


FIG 4 Capsule thickness for cells of the parent strain and amoeba-selected strains. (A) H99 isolates (B), A1-35-8 isolates, and (C) Ftc555-1 isolates were cultured in minimal medium at 30°C for 3 days. Capsule was visualized by counterstaining with India ink. HP, AP, FP: parental strains; HC, AC, FC: controls. Boxes indicate the 25th and 75th percentiles; bars show the 5th and 95th percentiles. The line and diamond within each box indicate the median and mean, respectively. *, $P < 0.1$; **, $P < 0.01$; ****, $P < 0.0001$; one-way ANOVA, followed by Tukey's multiple-comparison test.

had larger capsule thickness relative to those of their parental strain when cultured in minimal medium but cell sizes were similar, while isolates F3 to F6 increased both their capsule and cell sizes (Fig. 4 and 5). Isolates F3 to F6 also had more cells with a size larger than $10\ \mu\text{m}$ inside macrophages (Fig. 5E; see also Fig. S1 in the supplemental material). Time-lapse imaging was also done to confirm that evolved strain of Ftc-555-1 was able to increase its cell size after engulfment by macrophages (see Movies S1 and S2 in the supplemental material). Cell enlargement of isolates F3 to F6 has been also observed extracellularly in macrophage medium at 37°C and 9.5% CO_2 (Fig. 5D and F and Fig. S1), showing that this response is not specific to ingestion by macrophages. All of the isolates had increased urease activity compared to that of their parental strain (Fig. 6). Isolates H1, H2, and H14 and all of the isolates of A1-35-8 and Ftc555-1 manifested less melanin production (Fig. 7).

We further characterized the isolates under in stress conditions by analyzing their growth under thermal stress and exposure to the antifungal drug fluconazole (Fig. 8). Isolates H13, H16, and H17 had reduced growth at 40°C and in the presence of fluconazole, while H1, H2, and H14 had slightly increased their resistance to fluconazole compared to that of their ancestral strain. Isolates A4 to A6 and F3 to F6 displayed defects in growth at high temperature and after exposure to fluconazole.

Overall, the data show that the phenotypic changes were broad and diverse among isolates. A summary table with all isolates and their virulence factor phenotypes is provided in Fig. S2 in the supplemental material.

Genomic analysis and sequencing results. A prior study showed that DNA mutation was involved in pseudohyphal formation during amoeba interaction (55). To find

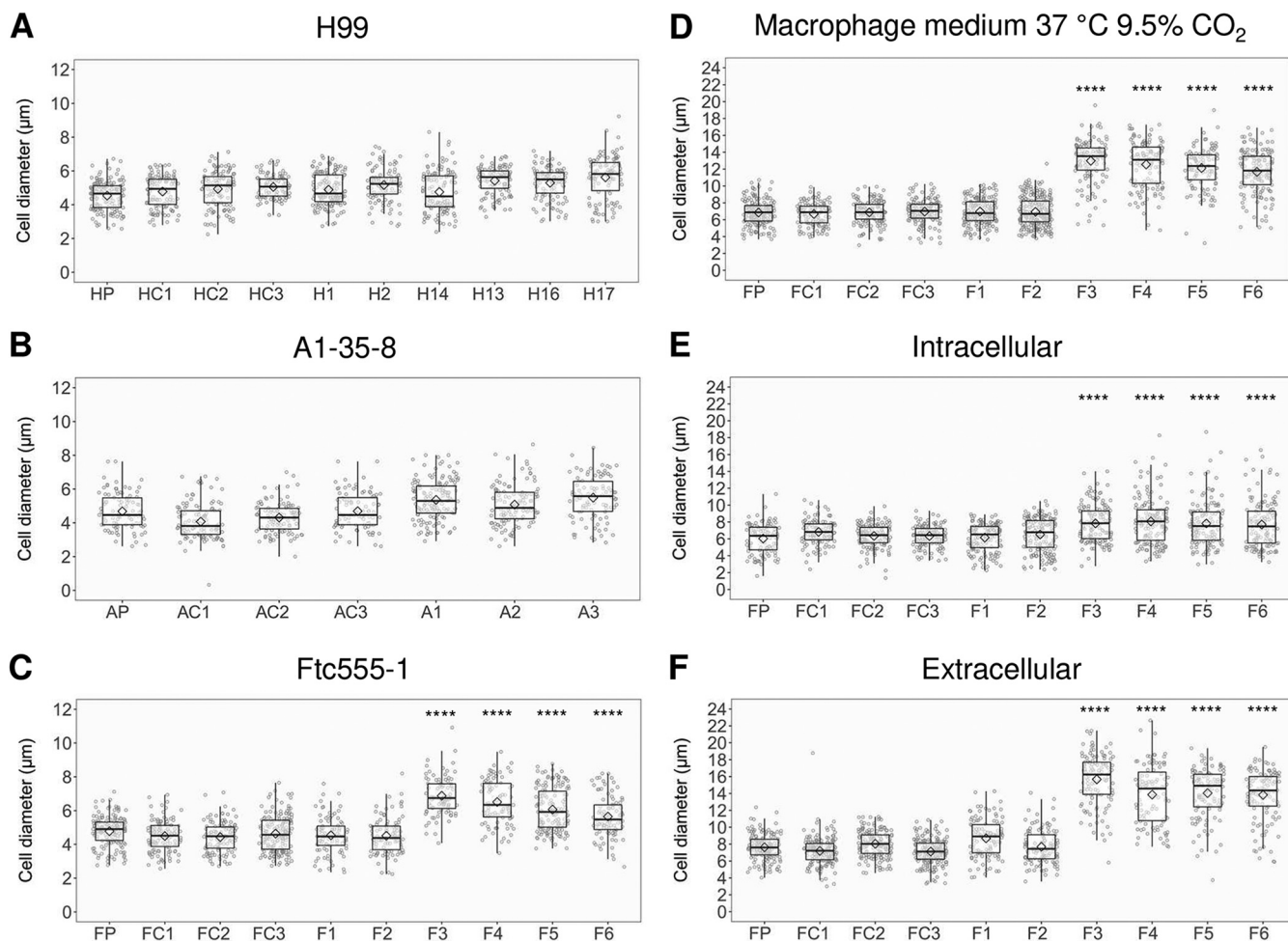


FIG 5 Cellular dimensions for cells of parent strain and amoeba-selected strains. (A) H99 isolates (B), A1-35-8 isolates, and (C) Ftc555-1 isolates were cultured in minimal medium for 3 days. HP, AP, FP: parental strains; HC, AC, FC: controls. (D to E) Ftc555-1 isolates were also cultured in macrophage medium and with bone marrow-derived macrophages (BMDMs) at 37°C and 9.5% CO₂ for 24 h. Extracellular cryptococcal cells were collected from the culture supernatant, while intracellular cells were retrieved from lysing the BMDMs. HP, AP, FP: parental strains; HC, AC, FC: controls. Boxes indicate the 25th and 75th percentiles; bars show the 5th and 95th percentiles. The line and diamond within each box indicate the median and mean, respectively. ****, $P < 0.0001$; one-way ANOVA, followed by Tukey's multiple-comparison test.

out if there are any such mutations or other mutations in our experiments, the genomes of all isolates were sequenced. Single-nucleotide polymorphisms (SNPs) and indels were identified compared to the H99 reference genome (Table 1; see also Table S2 in the supplemental material). Genome sequencing revealed that H and A isolates acquired only small numbers of SNPs and indels during amoeba passage, whereas the rate of mutations in the Ftc555-1 isolates was 10 times higher, ranging from 22 to 77 SNPs (total of 225 SNPs) and 7 to 15 indels (total of 34 indels) in these isolates. Among those SNPs, three SNPs were annotated as high-impact mutations resulting in disruption of the coding region (early stop codons and splice site mutations) (Table 1). Nonsynonymous SNP changes and indels were identified in CNAG_03013 (*OPT1*), which encode an oligopeptide transporter, commonly in all three strain backgrounds. These SNPs contributes to the changes in the sequence of *OPT1*, which include a missense mutation resulting in the replacement of methionine 484 with arginine in H1, H2, and H14, a single-nucleotide deletion causing a frameshift at P358 in A1, a nonsense mutation in A2 and A3, and a splice site mutation in F1. *Opt1* has been shown to be required for transporting Qsp1, a quorum-sensing peptide, into the receiving cells (56). Another SNP results in a nonsense mutation (G407*) in CNAG_00570, which encodes Pkr1 (AMP-dependent protein kinase regulator) in F5 and F6 isolates. In addition, F3 and F4 isolates carry a single-nucleotide deletion in CNAG_00570 that leads to a

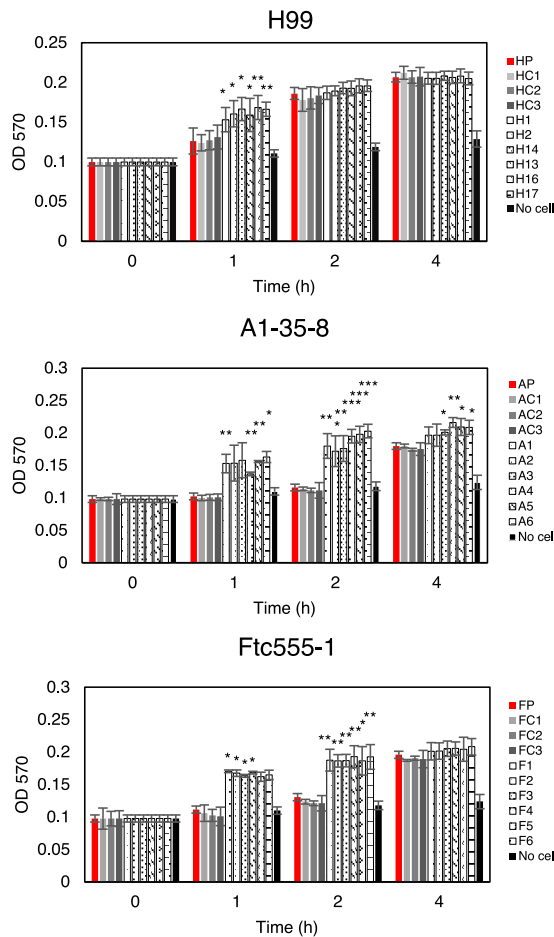


FIG 6 Urease activity for cells of the parent strain and amoeba-selected strains. The urease activity of cryptococcal cells were detected by using the rapid urea broth (RUH) method. Amoeba-passaged isolates are labeled with numbers preceded by the letters H, A, and F to indicate their origin from strains H99, A1-35-8, and Ftc555-1, respectively. HP, AP, FP: parental strains; HC, AC, FC: controls. The assay was performed in triplicate for each time point. Error bars represent SD. *, $P < 0.1$; **, $P < 0.01$; ***, $P < 0.001$; unpaired t test. OD₅₇₀, optical density at 570 nm.

frameshift at residue 194 of 482. Pkr1 is one of the important components of cAMP/protein kinase A (PKA) pathway and negatively regulates Pka activity, which is involved in morphogenesis, nutrient acquisition, stress responses, and virulence in *C. neoformans* (57). An SNP found in H1, H2, and H14 isolates causes an intron variant in a gene encoding a protein kinase (CNAG_02531; *CPK2*) as part of the MAPK protein kinase family. Loss of *CPK2* reduces melanin production in Niger seed medium (58). In A1, one missense SNP was found in CNAG_01101, which encodes a hypothetical protein with a centrosomin N-terminal motif. SNPs were also identified in A2 and A3 isolates, resulting in a missense mutation in CNAG_02858, which encodes adenylysuccinate synthetase. Another SNP in the A2 isolate was found in an intergenic region, a site with a high fraction of ambiguous calls. Isolates A4 to A6 had a single-nucleotide deletion at gene CNAG_03622 (*TAO3*), which led to a frameshift at residue 150 of 2,392. This mutation is consistent with the finding in a previous study that *TAO3* mutation led to the pseudohyphal phenotype (55). In summary, there are three noteworthy observations in the sequence data, as follows: (i) the gene CNAG_03013 (*OPT1*) was affected by nonsynonymous SNP changes in all three strain backgrounds, (ii) the previously described *TAO3* mutation responsible for pseudohyphal or hyphal formation was found in our isolates A4, A5, and A6 (55), and (iii) no SNPs or indels were found in some of the isolates,

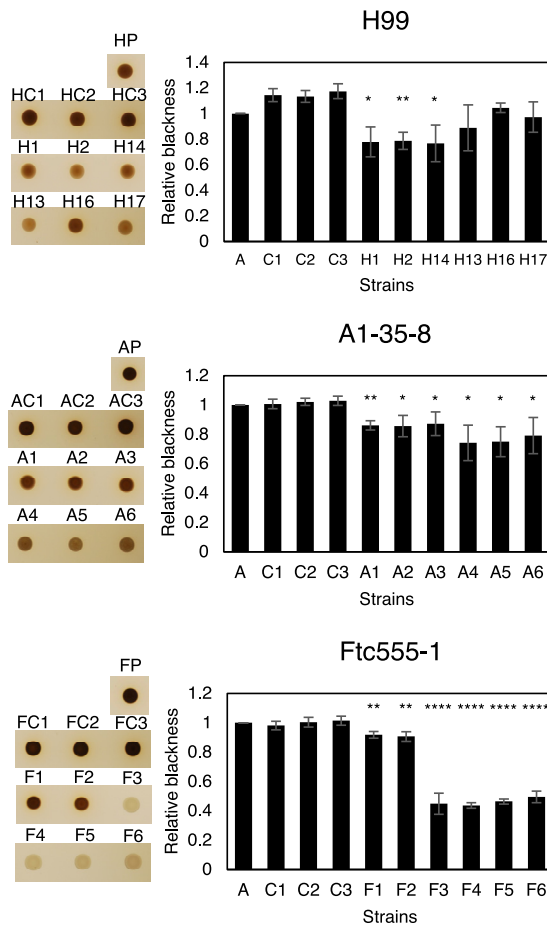


FIG 7 Melanization for cells of parent strain and amoeba-selected strains. Melanization was analyzed by spotting the 10^6 cryptococcal cells on minimal medium agar with L-3,4-dihydroxyphenylalanine (L-DOPA) for 24 h. The pigmentation of colonies was measured through grayscale pixel quantification using the software ImageJ. Relative blackness was calculated as a ratio of grayscale quantification between isolates, their parental strains (HP, AP, and FP), and controls (HC, AC, and FC). Error bars represent SD. *, $P < 0.1$; **, $P < 0.01$; ****, $P < 0.0001$; unpaired t test.

including H13, H16, and H17, suggesting that the phenotypic changes observed did not originate from single-nucleotide variants in the genome.

To determine if the high-impact mutations we identified in genes *PKR1*, *OPT1*, *CNAG_02531*, and *CNAG_01506* are responsible for resistance to the killing of amoebae, deletion mutants of the candidate genes in the H99 background were coincubated with amoebae on solid medium. However, the predation zones from these mutants were comparable with those of the parental strain (see Fig. S3 in the supplemental material).

Aneuploidy. We next hypothesized that emergence of aneuploidy could be a source of evolutionary adaptation because aneuploidies are frequent in *C. neoformans* and have been shown to play crucial roles in stress resistance (59, 60). To this end, the chromosomal copy numbers of the isolates evolved from all three strain backgrounds were defined based on the normalized depth of sequence coverage. The analysis revealed that there were duplications of chromosome 8 in isolates H13, H16, and H17, but no chromosomal duplication has been found in other isolates (Fig. 9A). The results were confirmed by quantitative (qPCR) with two selected isolates, H14 and H17 (Fig. 9B and C). We next investigated if this chromosomal duplication was responsible for the pseudohyphal formation and other phenotypic changes. In order to do so, H17 was passaged in fresh rich medium every day for 30 days to eliminate the duplication. The elimination was confirmed by qPCR (Fig. 9D). The H17 euploid strain (H17^{eu}) was

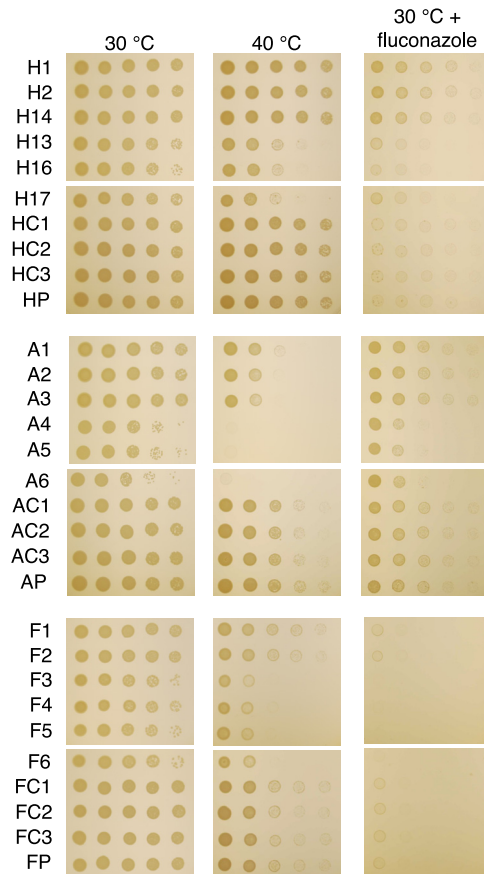


FIG 8 The growth of parent strains and isolates under stress conditions. Cells were 10-fold serially diluted and spotted onto Sabouraud medium with or without fluconazole (16 $\mu\text{g}/\text{ml}$) and grown for 2 days at 30°C or 40°C. Amoeba-passaged isolates are labeled with numbers preceded by the letters H, A, and F to indicate their origin from strains H99, A1-35-8, and Ftc555-1, respectively. HP, AP, FP: parental strains; HC, AC, FC: controls.

then coincubated with amoeba culture in solid medium, and samples were taken from the edge of the predation zone and visualized under a microscope. No pseudohyphae could be observed in H17^{eu} (Fig. 9E). In this case, the observation was similar to what we found in H99, but distinct from that in the H17 aneuploid strain (H17^{aneu}), which primarily formed pseudohyphae after 1 week of coincubation (Fig. 9E). Not surprisingly, H17^{eu} had a decreased ability for amoeba resistance, having a similar size of the predation zone to that of H99, while H17^{aneu} had a smaller predation zone (Fig. 9F). The capsule size of H17^{eu} was smaller than that of H17^{aneu} and was similar to that of H99, suggesting that the duplication of chromosome 8 results in a larger capsule size (Fig. 9G). After 1 h, H17^{eu} had lower urease activity than that of H17^{aneu} but a comparable level to that of H99 (Fig. 9H). However, the urease activity of H17^{eu} increased more quickly than that of H99 after 1.5 h. The result implied that the chromosomal duplication may be responsible in part for the high urease activity found in H17^{aneu}.

Aneuploidy can arise from a multinucleate state through transient polyploidization after failed cytokinesis or cell fusion. The filamentous multinucleate fungus *Ashbya gossypii* frequently exhibits both polyploidy and aneuploidy after cell division (61). Since pseudohyphae have a cytokinesis defect and multiple nuclei within a common cytosol, we asked if the pseudohyphal formation might lead to ploidy variation and thus could become one of the sources of phenotypic variation. Consequently, H99 cells expressing green fluorescent protein-labeled histone-2 (GFP-H2B) that were passaged through amoebae were visualized by time-lapse imaging, and a nucleus fusion was observed in one of the pseudohyphae after nuclei separation (Fig. 10 and Movie S1). This event

TABLE 1 High- and moderate-impact SNPs and indels found in passaged isolates

Gene identifier	Gene function	Isolates	Chromosome	Position	Reference	Alternate	Effect of mutation
CNAG_03013	Oligopeptide transporter	H1, H2, H14	3	211613	T	G	M484R
		A1	3	211137	GC	G	Frameshift at P358
		A2, A3	3	213165	G	A	Nonsense mutation W932 ^b
		F1 ^a	3	213566	G	T	Splice site mutation
CNAG_00570	cAMP-dependent protein kinase regulator	F5, F6 ^a	1	1469244	C	A	Nonsense mutation G407 ^b
		F3, F4 ^b	1	1469985	GT	G	Frameshift at N194
CNAG_02531	Calcium-dependent protein kinase	H1, H2, H14	6	68953	C	A	Intron variant
CNAG_01101	Hypothetical protein	A1	5	1208219	T	C	R478G
CNAG_02858	Adenylsuccinate synthetase	A2, A3	3	594765	A	G	I346V
Intergenic region		A2	13	592173	C	T	
CNAG_03622	Cell polarity	A4, A5, A6	2	363200	CA	C	Frameshift at N150
CNAG_01506	Hypothetical protein	FC2 ^a	11	136455	T	G	Splice site mutation

^aOnly high-impact mutations of passaged Ftc555-1 isolates are shown.

^bOnly selected high-impact indels of passaged Ftc555-1 isolates are shown here. Others are shown in Table S2 in the supplemental material.

provides evidence that polyploidization can exist in pseudohyphae and thus may have a high chance of leading to aneuploidy and phenotypic variation.

Effects of amoeba selection on interactions with murine macrophages. Based on the changes of multiple virulence-related phenotypes, we expected that some of the isolates would have a better survival when interacting with macrophages. However, there was no significant change in intracellular survival among all the isolates (Fig. 11A to C). Nevertheless, we cannot rule out the possibility that isolates may cause damage to macrophages. Since isolates F3 to F6 underwent cell enlargement inside macrophages, we hypothesize that the increased cell size may physically rupture macrophages. Therefore, we measured the release of lactate dehydrogenase (LDH) from the macrophages when they were infected with Ftc555-1 isolates. Indeed, it was found that LDH release was significantly induced from the macrophages containing F3 to F6 compared to that from those containing the ancestral strain (Fig. 11D), suggesting that F3 to F6 and their enlarged yeast cells cause damage to their host cells. While it may seem paradoxical that incubation of F isolates with macrophages resulted in no major changes in CFU of F isolates while increasing phagocytic cell damage, we note that these can be independent effects. For example, differences in cryptococcal cell proliferation rate could change CFU, whereas cell enlargement, which can disrupt the phagosome through physical stress (62), can be associated with elongated cell cycle phases (63).

Virulence in mice and moth larvae. The deletion of PKR1 was reported to be hypervirulent in mice (64). Since isolates F5 and F6 were more cytotoxic to macrophages and contained loss of function mutations in *PKR1*, we investigated their virulence and their parental strain Ftc555-1 in a murine infection model. However, all animals survived for 60 days after intranasal inoculation (data not shown). Lung fungal burden was determined by enumerating CFU. Only the cells of the initial isolate (Ftc555-1) were detected in the mouse lung after this incubation period, and there was considerable mouse-to-mouse variation in CFU. Hence, the two isolates carrying *PKR1* mutations were cleared from the lungs 60 days after inoculation (Fig. 12). Consequently, we explored early times of infection and noted that at day 5 after challenge, both Ftc555-1 and F5 had comparable fungal burdens, while that of F6 was reduced (Fig. 12). Hence, all three strains were able to establish themselves in mice initially and avoid clearance by innate immunity, but the F5 and F6 strains were subsequently cleared, presumably by the development of acquired immunity, which normally occurs at a later stage of the infection.

To gain more insight into the immune responses elicited by Ftc555-1, F5, and F6 in the lung, we studied several cytokine responses. In the lungs, the levels of proinflammatory cytokines, including tumor necrosis factor alpha (TNF- α) and interferon gamma (IFN- γ), were increased and remained high after 60 days postinfection with F5 and F6 strains (Fig. 12). F5 and F6 elicited lower lung levels than Ftc555-1 of interleukin 10 (IL-

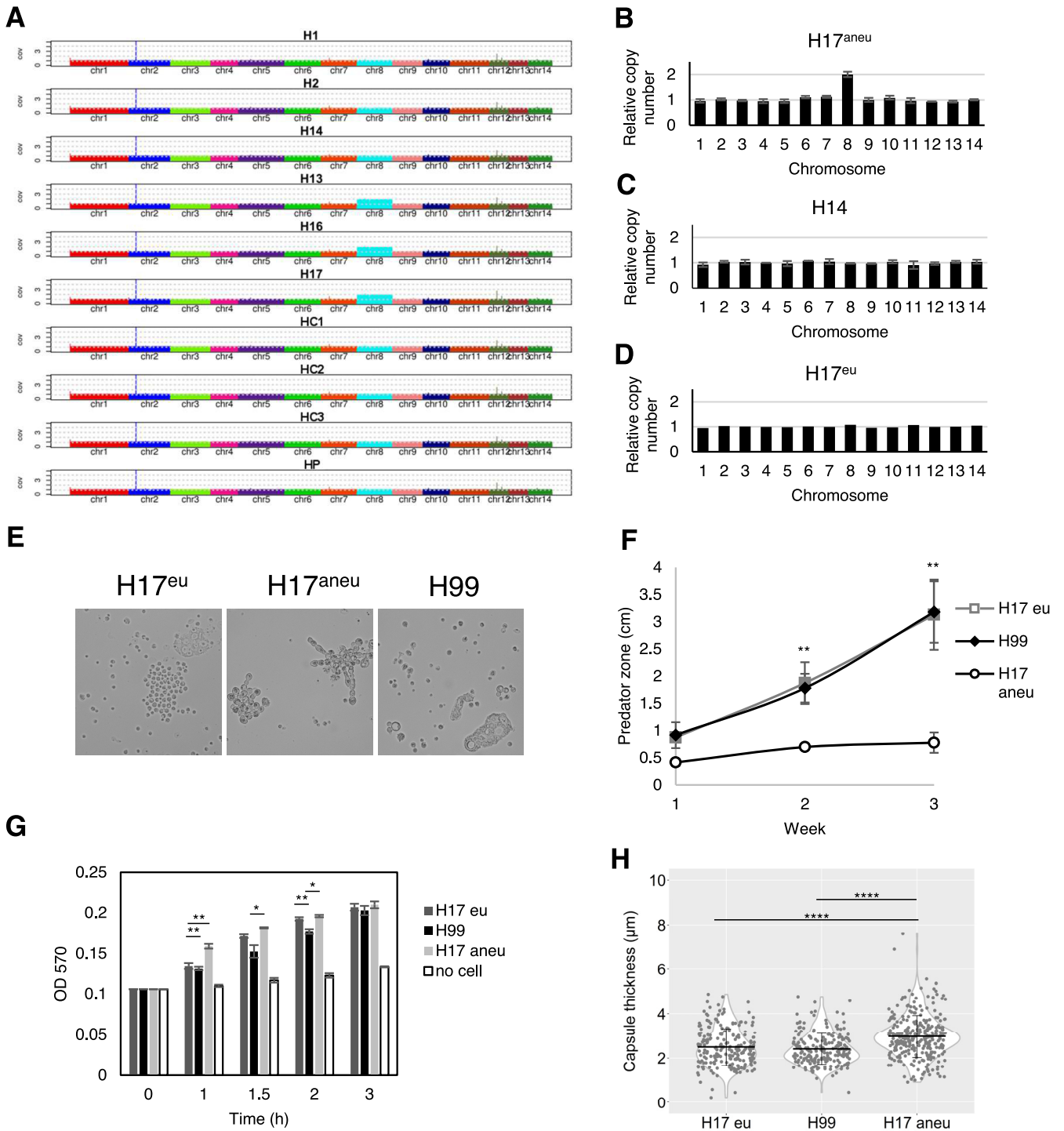


FIG 9 Aneploidy plays a role in pseudohyphal formation. (A) Chromosomal copy numbers of H99 isolates were determined based on depth of sequence coverage normalized by the average genome-wide sequence depth. (B) The relative chromosome copy number of isolate H17 was obtained by quantitative PCR (qPCR). H17 has duplication of chromosome 8. (C) No aneploidy was found in isolate H14. (D) Chromosome duplication in H17 is eliminated by passing H17 in fresh Sabouraud medium for 30 days. (E) The H17 euploid (H17^{eu}) strain did not form pseudohyphae as rapidly as the H17 aneuploid strain. (F) The H17^{eu} euploid strain has larger predation zone than that of H17^{aneu}. Data represent the mean of three biological replicates per biological sample, and error bars are SD. **, $P < 0.01$, compared to H17^{aneu} by one-way ANOVA and followed by Tukey's multiple-comparison test. (G) The H17^{eu} strain has lower urease activity than that of H17^{aneu} and comparable urease activity to that of H99 at an early time point (1 h). Data represent the mean of two biological replicates per biological sample, and error bars are SD. (H) H17^{eu} has smaller capsule size than that of H17^{aneu}, but a similar capsule size to that of H99.

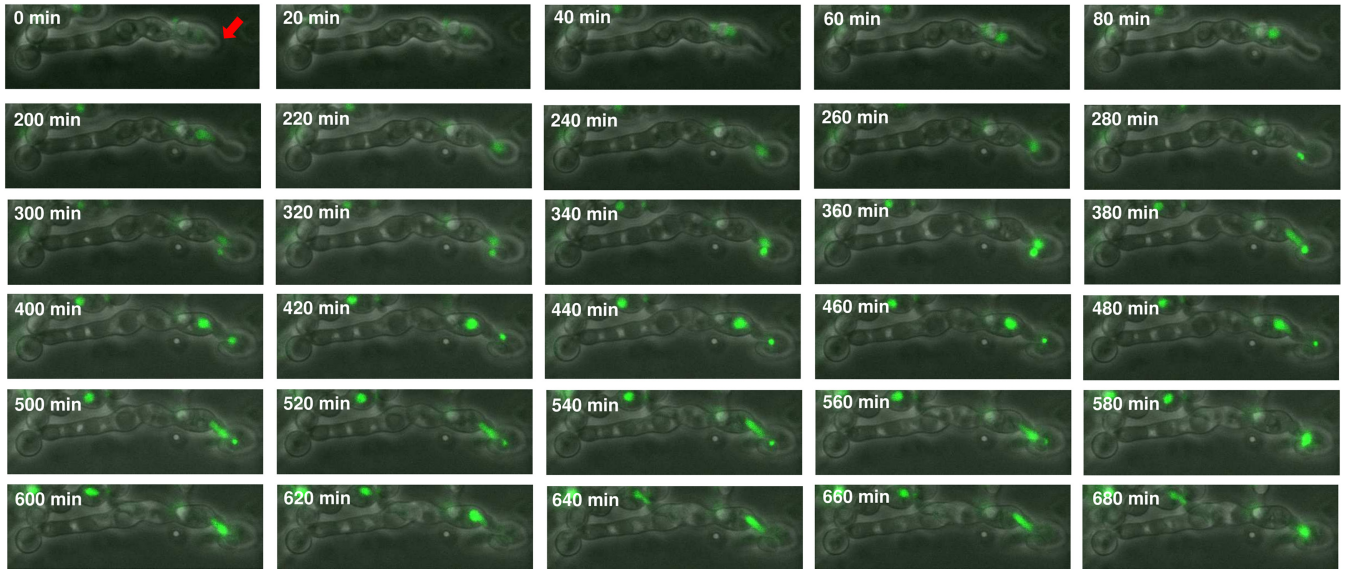


FIG 10 Time-lapse imaging showing nuclear division of pseudohyphae. The images of pseudohyphae of amoeba-passaged H99 GFP-H2B strain were taken by phase-contrast and fluorescence microscopy. Buds (red arrow) formed between 0 and 220 min. The nuclei migrated into the daughter cells at 240 min and separated at 300 min. Nuclear division was completed at 400 min. However, the nuclei from mother cells reentered the daughter cells at 500 min and underwent fusion at 580 min.

10), which could help their clearance from lung tissue relative to that of Ftc555-1, since reduction of this anti-inflammatory cytokine is associated with increased resistance to cryptococcal infection in mice (65). Interestingly, the levels of the same molecules were different when we analyzed the systemic immune response as measured by cytokines in their spleens (see Fig. S4 in the supplemental material). These results suggest that eliciting high levels of these cytokines may stimulate an inflammatory reaction, which

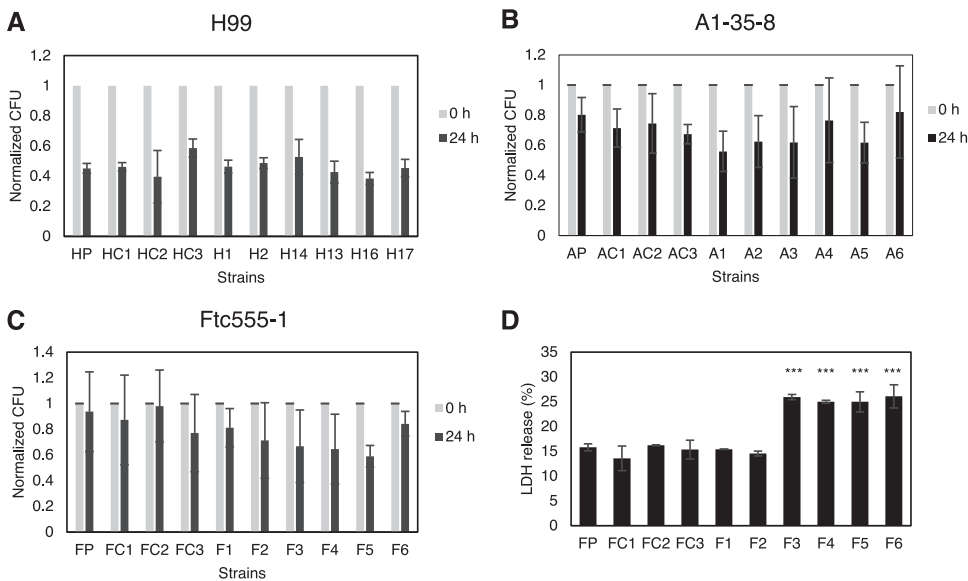


FIG 11 (A to C) The survival of parent strains and isolates in culture with BMDMs. The survival of (A) H99, (B) A1-35-8, and (C) Ftc555-1 isolates was determined by CFU after 0 and 24 h phagocytosis. The percentage of survival was calculated by normalizing the CFU value of 24 h infection to time zero. HP, AP, FP: parental strains; HC, AC, FC: controls. Data represent the mean of three biological replicates, and error bars are SD. There was no statistically significant difference between isolates and their parental strains as determined by one-way ANOVA followed by Tukey's multiple-comparison test. (D) BMDMs were infected with Ftc555-1 isolates for 48 h. Lactate dehydrogenase (LDH) release from damaged BMDMs into culture supernatant was assayed. ***, $P < 0.001$; one-way ANOVA followed by Tukey's multiple-comparison test.

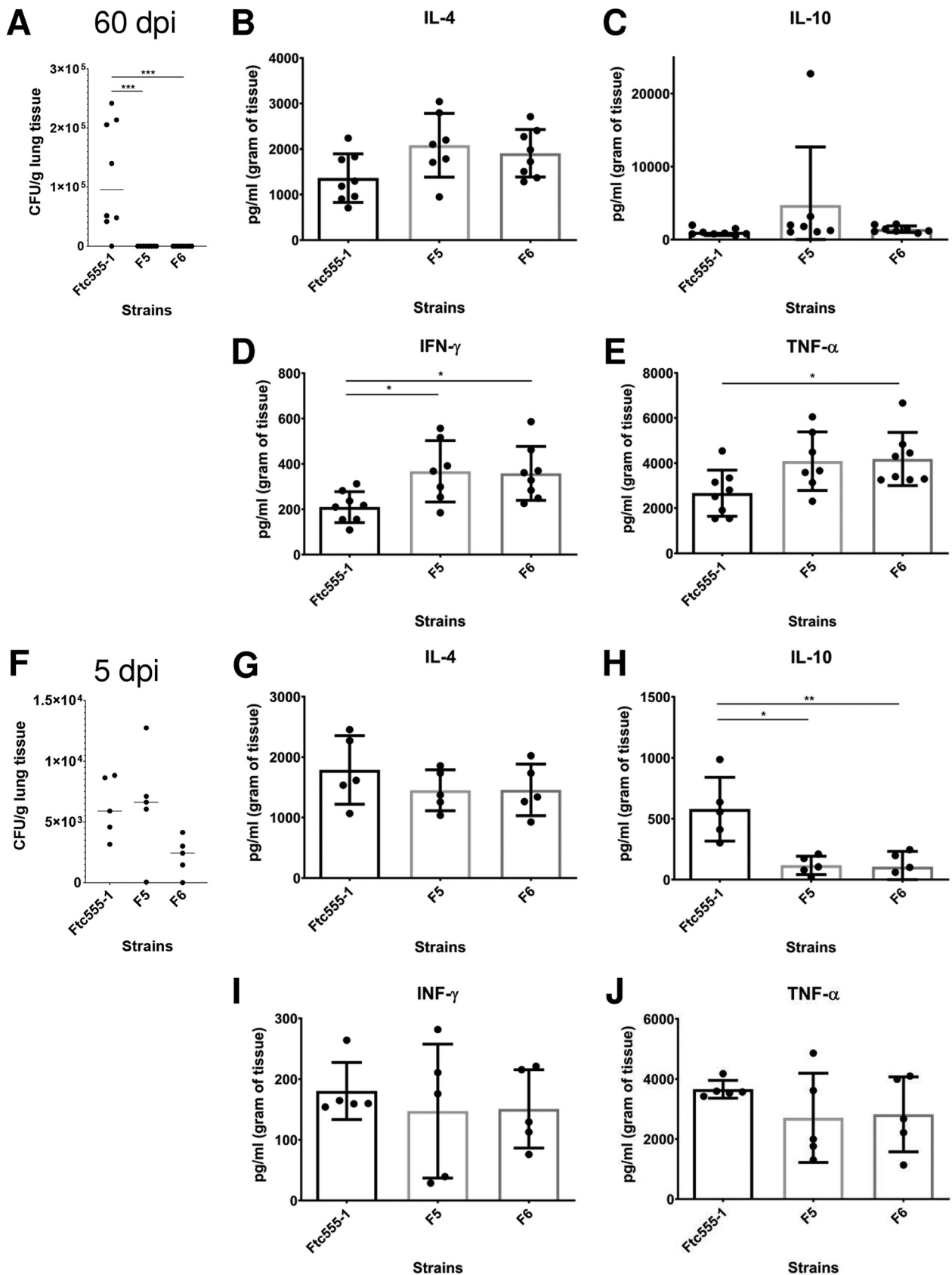


FIG 12 Fungal burden and cytokine production in the lung after infection with Ftc555-1, as well as its isolates F5 and F6. After 60 days of infection, mice were sacrificed, and fungal burden in the lung was determined by CFU counting (A). The levels of cytokines (B) interleukin 4 (IL-4), (C) IL-10, (D) interferon (Continued on next page)

could be associated with resolution of the infection of the F5 and F6 strains. These cytokine results show that F5 and F6 strains elicited quantitatively different immune responses from the parent strain Ftc555-1, consistent with the notion that the differences in virulence observed for these strains reflect differences in the effectiveness of the immune responses triggered.

We also examined the virulence of the isolates using a wax moth larval model, and isolates H13, H16, and H17 were less virulent than their parental strain (see Fig. S5A in the supplemental material). This may be due to the fact that these isolates can rapidly form pseudohyphae in the larvae, and pseudohyphal *C. neoformans* cells are attenuated for virulence in wax moth larvae (55).

DISCUSSION

In the past 2 decades, the concept that amoebae act as a selective pressure for virulence traits of environmental microbes has gained considerable traction. For fungal pathogens, concordance between virulence factor function in amoebae and macrophages has been demonstrated for *C. neoformans* (15, 40), *Aspergillus fumigatus* (13, 66), and *Paracoccidioides* spp. (24), but many questions remain regarding how fungal-protozoal interactions select for mammalian virulence. In this study, we investigated how interactions with amoebae affected the phenotype and genotype of *C. neoformans* to explore the mechanisms behind this long-term evolutionary adaptation. Our results provide new insights on how amoeba predation can drive the evolution of *C. neoformans*, since survivors emerge that show major phenotypic and genetic differences from the founder strain. This phenotypic diversity may facilitate *C. neoformans* adaptation to different hosts and alter its virulence.

Pseudohyphal formation was the most common response to *C. neoformans* survival when faced with amoeba predation. This result confirms an older observation that pseudohyphal formation was an “escape hatch” for *C. neoformans* survival when preyed upon by amoebae (67). Different fungal morphologies are reported to trigger different killing mechanisms by amoebae (68), and the *C. neoformans* filamentous form may be more resistant to killing. Similarly to our observation, Nielson et al. (67) reported that when *C. neoformans* was cocultured with amoebae, most of the fungal cells were killed, with survivors forming colonies that contained pseudohyphae. Most of their isolates remained pseudohyphal, with only one out of eight isolates reverting back to the yeast form. That result differed from ours, since most of the pseudohyphal isolates in this study reverted to yeast forms after removal from the amoeba culture, such that only 3 of 18 isolates studied in detail maintained a stable pseudohyphal phenotype. Those three isolates (A4 to A6) have a single-nucleotide deletion in the *TAO3* gene, shown by whole-genome sequencing, which is consistent with mutations in the RAM/MOR (regulation of Ace2 and morphogenesis/morphogenesis-related NDR kinase) pathway of the pseudohyphal variants reported in a previous study (55).

Previous studies have focused primarily on cryptococcal isolates with pseudohyphal phenotypes derived from amoeba, but in this study, we investigated in detail those amoeba-resistant isolates with unstable pseudohyphal phenotypes. We found that although some of the isolates (H13, H16, and H17) reverted to yeast, they were able to form pseudohyphae more quickly than their parental strain when they were exposed to amoebae again. These isolates were less virulent in a *Galleria* infection model, a finding consistent with prior reports that the pseudohyphal strains were less virulent in animal models. Interaction with amoebae also resulted in measurable virulence-related phenotypic changes in *C. neoformans*, confirming that amoebae can play a powerful role in the selection of virulence factors, which are related to the pathogenesis of

FIG 12 Legend (Continued)

gamma (IFN- γ), and (E) tumor necrosis factor alpha (TNF- α) in the lung were measured by enzyme-limited immunosorbent assay (ELISA). At 5 days postinfection, (F) fungal burden and the amounts of cytokines (G) IL-4, (H) IL-10, (I) IFN- γ , and (J) TNF- α in the lung were also measured. All data represent the mean of eight mice per group, and errors bars are SD. One-way ANOVA with Kruskal-Wallis nonparametric test was used and followed by Bonferroni's multiple-comparison test. *, $P < 0.1$; **, $P < 0.01$; ***, $P < 0.001$.

human disease. It is of note that we selected only six isolates from each strain for further characterization, but all of them had changes, suggesting that the microevolution occurs frequently and rapidly when isolates are exposed to amoebae. Moreover, the changes were pleiotropic and included differences in colony morphology, capsule size, cell size, urease activity, melanin production, and susceptibility to thermal stress and an antifungal drug. However, isolates studied revealed a different configuration of phenotypic changes, although they tended to cluster in groups from the same surviving pseudohyphal colony (see Fig. S1 in the supplemental material). Overall, the interaction of *C. neoformans* with amoeba-passaged isolates increased phenotypic diversity. Since there are many types of amoeboid predators in the soil and *Cryptococcus* species do not know the identity of the phagocytic predator, generating great diversity in strains could provide this fungus with insurance that some will survive. Hence, the diversity observed among isolates that survived amoeba predation suggests a bet-hedging strategy for survival based on the generation of phenotypic diversity.

To identify the mechanism for the phenotypic changes, we compared the whole-genome sequencing of isolates and ancestral strains using deep sequencing to identify point mutations, amplification or deletion of chromosomal segments, and whole-chromosome aneuploidy. We found that there were only two SNPs in H99-derived isolates and four SNPs and two indels in the A1-35-8-derived isolates. Isolates from the same surviving pseudohyphal colonies had similar SNPs, which is consistent with the similarity of their phenotypic changes, suggesting that the point mutations may be associated with some of the phenotypic changes. Interestingly, there were in total 252 SNPs in Ftc555-1-derived isolates, with an average of 48 SNPs among isolates (range of 22 to 80), a rate approximately 10 times higher than those for H99 and A1-35-8. That may be explained by the fact that the ancestral Ftc555-1 strain contains a splice donor site mutation in *MLH1*, a gene involved in mismatch repair of nuclear DNA. This predicted high-impact loss-of-function mutation (G-to-A change at position 1270268 of chromosome 6) is also found in all sequenced Ftc555-1 progeny isolates. Since the Idnum laboratory has previously reported that the loss of *MLH1* results in elevated mutation rates (69), Ftc555-1 is likely to be a hypermutator strain. Increased mutation rates will drive phenotypic variations, and some of those may be adaptive for survival in stressful environments, leading to rapid microevolution. On the other hand, the sequencing revealed that one gene (CNAG_03013; *OPT1*) was impacted by nonsynonymous SNP changes and single-nucleotide deletion in all three strain backgrounds. *OPT1* has been identified by the Madhani group as an oligopeptide transporter required for transporting Qsp1, a quorum-sensing peptide, into the receiving cells (56). Deletion of *OPT1* produces phenotypes similar to those of our isolates, including increased capsule size and reduced melanin production, suggesting that this mutation may cause some of the phenotypic changes in our isolates. Increased capsule size can protect *C. neoformans* against amoeba phagocytosis (46). Moreover, amoebae are known to produce antimicrobial pore-forming peptides (70), and it is conceivable that mutation of *OPT1* could reduce their importance and protect *C. neoformans*. By reviewing the published sequences of 387 clinical and environmental strains (71), we found that 6 of 287 clinical isolates had high-impact potential loss-of-function mutations in *OPT1*, but there were no *OPT1* mutations in the 100 environmental isolates. The Fraser laboratory also reported that one of the clinical isolates in their study contains an inversion in chromosome 3 that affect two genes, one of them being *OPT1* (72). The relatively high frequency of mutations in *OPT1* among clinical isolates suggests that this gene may be under particular selection during human infection. Another interesting mutation found in Ftc555-1 isolates was in the gene *PKR1*. This was a high-impact mutation in F3, F4, F5, and F6, which exhibited phenotypes of titan cells and enlarged capsules inside macrophages and in macrophage medium. Pkr1 is known to be a negative regulator of titan cell formation and capsule enlargement in laboratory strains and clinical isolates (64, 73). A *pk1* deletion mutant exhibits both enlarged capsule and titan cell production. It is also hypervirulent in a murine infection model (64).

The relatively small number of SNPs raises the question of how some of these

strains changed rapidly in response to amoeba predation, resulting in broad and rapid phenotypic changes. Therefore, we also investigated the impact of whole-chromosome aneuploidy on isolates. An extra copy of chromosome 8 has been found in three isolates (H13, H16, and H17) which were isolated from the same surviving pseudohyphal colony. Aneuploidy is caused by abnormal chromosomal segregation and can happen within even a single mitotic division, so this type of mutant can occur rapidly. This drastic DNA structural change often results in decreased fitness (74). However, when fungi are exposed to stressors, such as antifungal drugs, specific chromosomal aneuploidies can be advantageous through selection for increased gene expression of a subset of genes (60, 75–79). In *Candida albicans* and *C. neoformans*, extra copies of specific chromosomes containing drug resistance genes have been frequently found in antifungal drug resistance strains (60, 77, 78). Likewise, *C. neoformans* could gain an extra chromosome as a solution for adaptation when the fungi encounter threats from amoebae. For instance, chromosome 8 contains one gene (*ZNF2*) that encodes a zinc finger transcription factor that drives hyphal growth upon overexpression (80). Chromosome 8 also contains another gene (*CBK1*) that is responsible for pseudohyphal formation (55, 81). *CBK1* encodes a serine/threonine protein kinase, which is one of the components of the RAM pathway. Mutants in the RAM pathway have a pseudohyphal phenotype, but we are not aware of any reports showing the effect of the overexpression of *CBK1* on pseudohyphal morphology. Since filamentous morphologies are important for resistance to phagocytosis by amoebae, it is possible that duplication of chromosome 8 could rapidly increase cryptococcal fitness after exposure to amoebae. Indeed, when we reintroduced those aneuploid strains to amoebae, they could switch to filamentous forms more quickly than their parental strain and efficiently resisted killing by amoebae. When we eliminated the chromosomal duplication, the phenotypes were restored back to the wild-type level, supporting a strong link between duplication of chromosome 8, amoeba resistance and other changes in virulence phenotypes such as capsule size and urease activity. In addition, there are no point mutations or structural changes, such as amplification or deletion of chromosomal segments, in these isolates. Therefore, aneuploidy may be the major source of the phenotypic change in that particular group of isolates. However, aneuploidy was not found in isolates from other two strain backgrounds (A1-35-8 and Ftc555-1), so it may not be a general resistance trait.

Pseudohyphae are chains of elongated yeast cells that are unable to undergo complete cytokinesis, leading to multiple nuclei. Multinucleated cells showed a high level of chromosome instability, resulting in polyploidy and aneuploidy in eukaryotic cells (61). Previous study of live-cell imaging on *Candida albicans* showed that hyphal cells occasionally generated multinucleated yeast cells (82) with polyploidy and/or aneuploidy but there are very limited studies on whether pseudohyphal or hyphal formation may directly affect the ploidy variation. In this study, nuclear division, detected with GFP-H2B, was observed in cryptococcal pseudohyphae isolated from amoeba culture. Time-lapse imaging detected a nuclear fusion event, suggesting the cell experienced atypical nuclear division and may potentially undergo polyploidization, which frequently generates offspring with amplification of chromosomal segments or whole-chromosome aneuploidy. This result implies that interaction with amoebae not only contributes to the selection and maintenance of traits in *C. neoformans*, but also may drive heritable variation through pseudohyphae formation. However, a single event was observed, so this may not be a common escape strategy of *C. neoformans*.

The “amoeboid predator-fungal animal virulence hypothesis” posits that the capacity for virulence in soil fungi with no need for an animal host arose accidentally from the selection of traits that promote survival against amoeboid predators, which also function as virulence factors for animal infection (12). Consistent with this notion, there is a remarkable concordance between fungal phenotypes that promote survival against amoebae and in animal hosts (13, 15), and passage in amoeba is associated with increased virulence for several fungal species (24, 39, 83). Analysis of virulence for

the amoeba-selected strains described in our study in wax moths revealed no major changes in virulence from the parental strains. It is possible that this host does not discriminate between passaged and nonpassaged *C. neoformans* cells, or that none of the isolates tested gained or lost traits associated with virulence in that particular host. It is also possible that these strains already had the maximum pathogenic potential (84) for these animal hosts, which could not be further increased by amoeba interactions. However, we did observe that some amoeba-passaged strains were significantly more cytotoxic for macrophages *in vitro*. This result is consistent with the finding that those strains also had great resistance to amoeba killing. The mechanism behind that is still unclear. However, those particular amoeba-passaged strains can form larger-sized cells and capsules in both amoeba and macrophage culture, which may help them escape from, and damage host cells. These results fit the hypothesis that amoebae are the training grounds for macrophage resistance of pathogens, since the hostile environments in amoebae and macrophages are similar. Among these strains, the virulence of isolates F5 and F6 were further tested in a murine infection model. These particular strains were picked because they acquired a mutation in *PKR1*, and deletion of *PKR1* has been shown to increase virulence (64). However, neither F5 and F6 exhibited a hypervirulence phenotype during murine infection, and instead were cleared faster than their parental isolate. It is noteworthy that the nonsense mutation found in F5 and F6 is located in codon 407, which is only 75 codons prior to the original stop codon of *PKR1*. It is possible that the mutation results in altered function rather than loss of function and that this is not sufficient to reproduce the hypovirulence phenotype caused by full *PKR1* knockout. Microbial virulence is a complex property that is expressed only in a susceptible host, and host damage can come from the microbe or the immune response (85). Both F5 and F6 were able to establish themselves in the lung but triggered a more effective immune responses that cleared them. This finding implies the occurrence of other amoeba-selected changes that affect the immune response, including overriding of the hypervirulence phenotype caused from the mutation of *PKR1* by compensation from other mutations or changes.

The amoeba-passaged *C. neoformans* isolates selected in our study differ from those reported in prior studies (24, 39, 83) in that they did not increase in virulence. Instead, we observed reductions in murine virulence from their long interaction with amoeba for two of the isolates studied, despite increased capacity to damage macrophages. Given the pleiotropic changes observed in our isolate set, it is possible that we did not sample sufficient numbers to observe more virulent strains. Our study also differs from prior amoeba-*C. neoformans* studies (39) in that it involved prolonged selection on a semisolid agar surface under conditions that favored amoeba by the presence of cations. Under these conditions, amoeba dominance is manifested by a zone of fungal growth clearance where only occasional *C. neoformans* colonies emerged after several weeks. These colonies presumably emerged from resistant cells that survived the initial amoeba onslaught and gave rise to the variant strains that were analyzed in this study. We suggest that these amoeba-resistant cells were very rare in the initial parental population and emerged from the mechanisms discussed above, namely, mutation and aneuploidy, which by chance conferred amoeba resistance upon those cells. Alternatively, these colonies represent rare cells that were able to sense the amoeba danger and turn on diversity-generating mechanisms that occasionally produced amoeba-resistant strains. In this regard, *C. neoformans* can sense amoebae and respond by increasing the size of its capsule by sensing protozoal phospholipids (40), but this process takes time, and fungal cell survival probably depends on the race between adaptation and predation. The selection versus adaptation explanations for the origin of these are not mutually exclusive, and both could have been operational in these experiments. These survivor cells then grew into a colony under constant amoeba selection where they gave rise to progeny cells where these phenotypic diversity-generating mechanisms were maintained and amplified, thus accounting for the phenotypic diversity observed in this study.

In summary, amoeba predation places selective pressure in *C. neoformans*, resulting

in the rapid emergence of new phenotypes associated with mutations and aneuploidy, which combine to create great phenotypic diversity. The effect of phenotype diversification on the fitness of the fungi differs within the same or different hosts, suggesting a bet-hedging strategy by *C. neoformans* that spreads the risk in situations where the environmental threat is unpredictable. Given that human infection also results in rapid fungal microevolution in this host (86, 87), it is possible that similar mechanisms occur *in vivo* when this fungus comes under attack by immune cells. Indeed, macrophages appear to also use a bet-hedging strategy in phagosomal acidification to control microbes (88), and several studies have shown microevolution of *Cryptococcus* during mammalian infection (72, 87, 89, 90). A bet-hedging strategy that generates a prodigious number of phenotypes would increase survival in the face of unknown threats and could represent a general mechanism for survival in soils. Interference with the mechanism responsible for generating this plasticity could in turn result in new antimicrobial strategies that would reduce the emergence of diversity and thus simplify the problem for the immune response. Hence, it is interesting to hypothesize that amoeba predation in *C. neoformans* pushes a trigger that sets forth a series of events that generate diversity and that similar mechanisms exist in other soil fungi that must routinely confront similar stresses.

MATERIALS AND METHODS

Ethics statement. All animal procedures were performed with prior approval from Johns Hopkins University (JHU) Animal Care and Use Committee (IACUC), under approved protocol number MO18H152. Mice were handled and euthanized with CO₂ in an appropriate chamber followed by thoracotomy as a secondary means of death in accordance with guidelines on Euthanasia of the American Veterinary Medical Association. JHU is accredited by AAALAC International, in compliance with Animal Welfare Act regulations and Public Health Service (PHS) policy, and has a PHS Approved Animal Welfare Assurance with the NIH Office of Laboratory Animal Welfare. The JHU Animal Welfare assurance number is D16-00173 (A3272-01). JHU utilizes U.S. Government laws and policies for the utilization and care of vertebrate animals used in testing, research, and training guidelines for appropriate animal use in a research and teaching setting. Mice were maintained in a 12-h:12-h light-dark (LD) cycle and at constant temperature (22°C ± 1°C). They were allowed to free access to water and food. Mice were kept under these conditions for 1 week before and during the experiments.

Cell culture. *Acanthamoeba castellanii* strain 30234 was obtained from the American Type Culture Collection (ATCC). Cultures were maintained in yeast-peptone-glucose (YPG) broth (ATCC medium 712) at 25°C according to instructions from ATCC. *C. neoformans* var. *grubii* serotype A strain H99 and two environmental isolates, A1-35-8 and Ftc555-1, were used for the interaction with amoebae. The histone 2B-GFP-tagged (C1746) H99 strain that was used for visualization of nuclear division of pseudohyphae was obtained from Kyung Kwon-Chung (Bethesda, MD) (91). Cryptococcal cells were cultivated in Sabouraud dextrose broth with shaking (120 rpm) at 30°C overnight (16 h) prior to use in all experiments.

Bone marrow-derived macrophages (BMDMs) were isolated from the marrow of hind leg bones of 5- to 8-week-old C57BL/6J female mice (Jackson Laboratory, Bar Harbor, ME). For differentiation, cells were seeded in 100-mm tissue culture (TC)-treated cell culture dishes (Corning, Corning, NY) in Dulbecco's modified Eagle medium (DMEM; Corning) with 20% L-929 cell-conditioned medium, 10% fetal bovine serum (FBS; Atlanta Biologicals, Flowery Branch, GA), 2 mM Glutamax (Gibco, Gaithersburg MD), 1% nonessential amino acids (Cellgro, Manassas, VA), 1% HEPES buffer (Corning), 1% penicillin-streptomycin (Corning), and 0.1% 2-mercaptoethanol (Gibco) for 6 to 7 days at 37°C with 9.5% CO₂. Fresh medium (3 ml) was supplemented on day 3, and the medium were replaced on day 6. Differentiated BMDMs were used for experiments within 5 days after completed differentiation.

Assay of *A. castellanii* and *C. neoformans* interaction. Two hundred *C. neoformans* yeast cells were spread on Sabouraud agar and incubated at 30°C overnight. *A. castellanii* cells (5×10^3) were dropped randomly at several locations on the agar plate containing *C. neoformans*. Plates were sealed with parafilm and incubated at 25°C for 3 to 4 weeks until surviving colonies of *C. neoformans* emerged.

To isolate an individual cell (in this case, hyphae or pseudohyphae) from the colony (Fig. 1D), surviving colonies were randomly picked from the plate to a 3-cm culture dish with phosphate-buffered saline (PBS) using pipette tips. Individual cells were picked under a light microscope using a pipette and transferred into fresh Sabouraud agar. The plates were incubated at 30°C. After 24 h of incubation, the morphologies of microcolonies were visualized using a Zeiss Axiovert 200M inverted microscope with a 10× phase objective. After 72 h of incubation, colony morphologies were examined using Olympus SZX9 microscope with a 1× objective and a 32× zoom range. Morphologies of cells from colonies were visualized using an Olympus AX70 microscope with a 20× objective using the QCapture Suite v2.46 software (QImaging, Surrey, Canada).

Amoebae killing assay. *C. neoformans* cells (5×10^5 cells) were spread as a cross onto Sabouraud agar and incubated at 30°C for overnight. *A. castellanii* cells (10^4) were dropped at the center of the *C. neoformans* cross. The plates were sealed in parafilm and incubated at 25°C. The distance from center to

the edge of the clear predation zones in four directions was measured after 1 to 3 weeks incubation. Data are represented as the average of the distances of the clear zone from four direction.

C. neoformans cells were also taken from the edge of the clear zone and at the end of the cross after 1 week of incubation and visualized using an Olympus AX70 microscope with 20× objective. For samples of Ftc555-1 strains, the cells were counterstained with India ink.

Capsule and cell size. *C. neoformans* cells were incubated in minimal medium (15 mM dextrose, 10 mM MgSO₄, 29.4 mM KH₂PO₄, 13 mM glycine, and 3 μM thiamine-HCl) at 30°C for 72 h. In addition, Ftc555-1 and its isolates were incubated in medium for BMDMs at 37°C for 24 h. BMDMs (1.5 × 10⁶ cells) were also infected with Ftc555-1 and its isolates (1.5 × 10⁶ cells) in 6-well plates. After 24 h of infection, the culture supernatant was collected, and the plates were washed once to collect the extracellular *C. neoformans*. Intracellular *C. neoformans* was collected by lysing the host cell with sterile water. The cells were stained with 0.1% Uvitex 2B (Polysciences, Warrington, PA) for 10 min and washed two times with PBS. The capsule was visualized by India ink negative staining by mixing cell samples with equal volumes of India ink on glass slides and spreading the smear evenly with coverslips. Images with a minimum of 100 randomly chosen cells were taken using an Olympus AX70 microscope with 40× objective using bright-field illumination and the 4',6-diamidino-2-phenylindole (DAPI) channel. The areas of the cell body and the whole cell (cell body plus capsule) were measured using ImageJ software. Capsule thickness was calculated by subtracting the diameter of the whole cell from that of the cell body. Cell size is presented as the diameter of the cell body without the capsule. Three biological independent experiments were performed for each sample.

Lactate dehydrogenase release assay. BMDM cells (5 × 10⁴ cells/well) were seeded in 96-well plates with BMDM medium for overnight. To initiate the phagocytosis, BMDMs was infected with *C. neoformans* (5 × 10⁵ cells) opsonized with 18B7 monoclonal antibody (MAb), which binds capsular glucuronoxylomannan, at a concentration of 10 μg/ml. The culture plates were centrifuged at 1,200 rpm for 1 min to settle yeast cells on the monolayer of macrophage culture. After 48 h of infection, lactate dehydrogenase (LDH) release was assessed using the CytoTox-One homogeneous membrane integrity assay kit (Promega, Madison, WI) according to the manufacturer's instructions.

Urease activity. *C. neoformans* cells (10⁹) were incubated in 1 ml of rapid urea broth (RUH) developed by Roberts et al. (92) and adapted by Kwon-Chung et al. (93) at 30°C. After 1 to 4 h of incubation, cells were collected by centrifugation, and 100 μl of supernatant was transferred to a 96-well plate. The absorbance of the supernatant was measured at 570 nm using an EMax Plus microplate reader (Molecular Devices, San Jose, CA). The assay was performed in triplicate for each time interval.

Melanin quantification. *C. neoformans* in 10⁴, 10⁵, 10⁶, and 10⁷ cells were spotted on minimal medium agar supplemented with 1 mM L-3,4-dihydroxyphenylalanine (L-DOPA; Sigma-Aldrich, St. Louis, MO). The plates were incubated at 30°C without light. Photos were taken after 1 to 3 days of incubation on a white light illuminator. Photos of samples were always taken together with their parental strains under the same condition in order to avoid different exposure times or light adjusted by the camera. The obtained photos were then converted to greyscale using ImageJ software. The regions of the colonies were selected and the pixels of each selected region were quantified in grayscale. The relative gray-scales of the colonies from samples were normalized by the gray-scales of the colonies of parental strains. The representative data shown in this paper are from the cell number of 10⁶ cells and at the time point of 24 h. Three biological independent experiments were performed for each sample.

Macrophage killing assay. BMDM cells (5 × 10⁴ cells/well) were infected with *C. neoformans* (5 × 10⁴ cells) in the presence of 10 μg/ml 18B7 MAb. The culture plates were centrifuged at 1,200 rpm for 1 min to settle yeast cells on the monolayer of macrophage culture. After 24 h of infection, phagocytized cryptococcal cells were released by lysing the macrophages with sterilized water. The lysates were serially diluted, plated onto Sabouraud agar, and incubated at 30°C for 48 h for CFU determination. This experiment was performed in triplicate for each strain.

Virulence assay in *Galleria mellonella*. *Galleria mellonella* larvae were purchased from Vanderhorst Wholesale (Saint Mary's, OH). Larvae were picked based on weight (175 to 225 mg) and appearance (creamy white in color). Larvae were starved overnight at room temperature. The next day, overnight cultures of *C. neoformans* that grew in Sabouraud broth were washed three times with PBS and diluted to 1 × 10⁵ cells/ml. Cells in 10 μl PBS were injected into the larva via the second-to-last left proleg paw with 31-gauge needles. Infected larvae were incubated at 30°C, and the number of dead larvae was scored daily until all the larvae infected with *C. neoformans* ancestral strains in this study were dead. Control groups of larvae were inoculated with 10 μl of sterile PBS. Experiments were repeated at least two times with experimental groups of 15 larvae at a time.

Whole-genome sequencing and variant identification. Genomic DNA was prepared using cetyltrimethylammonium bromide (CTAB) phenol-chloroform extraction as described previously (94). Genomic DNA was further purified using a PowerClean DNA cleanup kit (Qiagen, Hilden, Germany). Libraries were constructed using the Illumina DNA Flex library kit and were sequenced on an Illumina HiSeq 2500 instrument to generate paired 150-base reads. An average of 145× sequence depth (range, 69 to 176×) was generated for each sample.

Reads were aligned to the *C. neoformans* H99 assembly (95) using BWA-MEM v0.7.12 (96). Variants were identified using GATK v3.7 (97); HaplotypeCaller was invoked in genomic variant call format (GVCF) mode with ploidy = 1, and GenotypeGVCFs was used to predict variants in each strain. The workflow used to execute these steps on Terra (terra.bio) is available on GitHub (https://github.com/broadinstitute/fungal-wdl/blob/master/gatk3/workflows/fungal_variant_calling_gatk3.wdl). Sites were filtered with variant filtration using variant annotations QD of <2.0, an FS of >60.0, and an MQ of <40.0 (QD = QualByDepth, FS = FisherStrand, and MQ = RMSMappingQuality). Genotypes were filtered if the minimum genotype quality was

<50, percent alternate alleles was <0.8, or depth was <10 (<https://github.com/broadinstitute/broad-fungalgroup/blob/master/scripts/SNPs/filterGatkGenotypes.py>). Genomic variants were annotated and the functional effect was predicted using SnpEff v4.1g (98).

Cryptococcal cell karyotyping. Cell karyotypes were analyzed by quantitative PCR. qPCR primers used in this study have been published in Gerstein et al. (59). qPCRs were performed in a StepOnePlus real-time PCR system (Applied BioSciences, Beverly Hills, CA) using 20- μ l reaction volumes. All reactions were set up in technical triplicate. Each reaction mixture contained PowerUp SYBR green mastermix (Applied BioSciences), 300 nM each primer, 10 ng genomic DNA from CTAB extraction, and distilled water (dH₂O). Cycling conditions were 95°C for 5 min, followed by 40 cycles of 95°C for 15 s and 55°C for 1 min. Melt curve analysis was performed in 0.5°C increments from 55 to 95°C for 5 s for each step to verify that no primer dimers or products from misannealed primers had been amplified. Threshold cycle (C_T) values were obtained using StepOnePlus software v2.3 (Applied BioSciences), where the threshold was adjusted to be within the geometric (exponential) phase of the amplification curve. Chromosome copy numbers were determined using a modified version of the classical C_T method as described by Pavelka et al. (76).

Visualization of nuclear division in pseudohyphae. Histone 2B-GFP-tagged H99 (C1746) was allowed to interact with *A. castellanii* on Sabouraud agar as described above until surviving colonies with pseudohyphae emerged. The colonies were transferred to the wells of 18B7 antibody (Ab)-coated-coverslip-bottomed petri dishes with 14-mm microwells (MatTek Brand Corporation, Ashland, MA) in minimal medium. After 30 min of incubation to allow for settling down the cells, 2 ml of minimal medium was added. Images were taken every 10 min for 24 h using a Zeiss Axiovert 200M inverted microscope with a 10 \times phase objective and GFP channel in an enclosed chamber under 30°C conditions.

Stress sensitivity test. The overnight cultures were diluted in Sabouraud broth to an OD₆₀₀ of 2 and further diluted 10⁻¹, 10⁻², 10⁻³, 10⁻⁴, and 10⁻⁵-fold. The dilutions (5 μ l) were spotted onto Sabouraud agar plates supplemented with 16 μ g/ml fluconazole and incubated for 48 h at 30°C. Plates without fluconazole were also incubated for 48 h at either 30°C or 37°C.

Growth curve. *C. neoformans* strains Ftc555-1, F5, and F6 were grown in Sabouraud medium at 30°C with orbital shaker (120 rpm) for 7 days, with data measurements each 24 h. The assay was performed in a 96-well plate, and some serial dilutions were done, with a cell concentration range between 1.0 \times 10⁷ to 5.0 \times 10³/well. Each condition was carried out in triplicate. The growth was measured by optical density at 600 nm.

Murine infection. Six-week-old female A/J mice (JAX stock no. 000646; Jackson Laboratory) were infected intranasally with 1.0 \times 10⁷ yeast cells of each *C. neoformans* strain used in this study. Three groups of mice (n = 8 animals per group) were infected, and animals were observed daily for 60 days and euthanized at any time if showing more than 20% weight loss, appearance of moribundity, pain, or inability to feed. Surviving animals after 60 days were euthanized and tissues extracted for fungal burden and cytokine level determination.

A second experimental infection was performed with some modifications. Six-week-old female A/J mice were infected intranasally with 1.0 \times 10⁷ yeast cells of each *C. neoformans* strain (n = 5 animal per group) and then euthanized after 5 days. The organs were also removed for fungal burden and cytokine level evaluation.

In all of the mouse experiments, animals were intranasally infected with *C. neoformans* yeasts, in a total volume of 20 μ l (10 μ l in each nasal cavity of the mouse). Mice were anesthetized with 60 μ l xylazine-ketamine solution intraperitoneally (95 mg of ketamine and 5 mg of xylazine per kg of animal body weight) to perform intranasal infection.

Fungal burden assessment. The fungal burden was measured by counting CFU. After animals were euthanized, the lungs were removed, weighed, and homogenized in 1 ml of PBS. After serial dilutions, homogenates were inoculated onto Sabouraud agar plates with 10 U/ml of streptomycin-penicillin. The plates were incubated at room temperature, and the colonies were counted after 48 to 72 h.

Determination of cytokine levels in the organs. The spleen and lungs of each mouse were macerated with protease inhibitor (complete, EDTA-free; Roche Life Science, IN, United States) and centrifuged; supernatants of these samples were used for cytokine detection by a sandwich enzyme-limited immunosorbent assay (ELISA) using commercial kits (BD OptEIA; BD Franklin Lakes, NJ, US) for the following cytokines: IL-2 (catalog no. 555148), IL-4 (catalog no. 555232), IL-10 (catalog no. 555252), IFN- γ (catalog no. 551866), and TNF- α (catalog no. 555268). The protocol was followed according to the manufacturer's recommendations. The reading was performed in a plate spectrophotometer at 450 nm and 570 nm.

Data availability. All sequences for this project are available in the NCBI database under BioProject accession number [PRJNA640358](https://www.ncbi.nlm.nih.gov/bioproject/PRJNA640358).

SUPPLEMENTAL MATERIAL

Supplemental material is available online only.

VIDEO S1, AVI file, 19.4 MB.

VIDEO S2, AVI file, 19.2 MB.

VIDEO S3, AVI file, 0.2 MB.

FIG S1, PDF file, 2 MB.

FIG S2, PDF file, 0.1 MB.

FIG S3, PDF file, 0.04 MB.

FIG S4, PDF file, 0.2 MB.

FIG S5, PDF file, 0.1 MB.

TABLE S1, DOCX file, 0.01 MB.

TABLE S2, DOCX file, 0.02 MB.

ACKNOWLEDGMENTS

We thank the Broad Institute Microbial Omics Core for generating the DNA libraries and the Genomics Platform for the sequencing for this study. We thank H. J. Tsai for advice on figure design.

A.C. is supported by National Institutes of Health grants AI052733, AI15207, and HL059842. C.A.C. is supported by National Institute of Allergy and Infectious Diseases, National Institutes of Health, award U19AI110818. J.R.P. is supported by Public Health Services grants AI73896 and AI93257.

REFERENCES

- Rajasingham R, Smith RM, Park BJ, Jarvis JN, Govender NP, Chiller TM, Denning DW, Loyse A, Boulware DR. 2017. Global burden of disease of HIV-associated cryptococcal meningitis: an updated analysis. *Lancet Infect Dis* 17:873–881. [https://doi.org/10.1016/S1473-3099\(17\)30243-8](https://doi.org/10.1016/S1473-3099(17)30243-8).
- Cross CE, Bancroft GJ. 1995. Ingestion of acapsular *Cryptococcus neoformans* occurs via mannose and beta-glucan receptors, resulting in cytokine production and increased phagocytosis of the encapsulated form. *Infect Immun* 63:2604–2611. <https://doi.org/10.1128/IAI.63.7.2604-2611.1995>.
- Johnston SA, May RC. 2013. *Cryptococcus* interactions with macrophages: evasion and manipulation of the phagosome by a fungal pathogen. *Cell Microbiol* 15:403–411. <https://doi.org/10.1111/cmi.12067>.
- Kozel TR. 1977. Non-encapsulated variant of *Cryptococcus neoformans*. II. Surface receptors for cryptococcal polysaccharide and their role in inhibition of phagocytosis by polysaccharide. *Infect Immun* 16:99–106. <https://doi.org/10.1128/IAI.16.1.99-106.1977>.
- Vecchiarelli A. 2000. Immunoregulation by capsular components of *Cryptococcus neoformans*. *Med Mycol* 38:407–417. <https://doi.org/10.1080/mmy.38.6.407.417>.
- Cox GM, Mukherjee J, Cole GT, Casadevall A, Perfect JR. 2000. Urease as a virulence factor in experimental cryptococcosis. *Infect Immun* 68:443–448. <https://doi.org/10.1128/iai.68.2.443-448.2000>.
- Cox GM, McDade HC, Chen SC, Tucker SC, Gottfredsson M, Wright LC, Sorrell TC, Leidich SD, Casadevall A, Ghannoum MA, Perfect JR. 2001. Extracellular phospholipase activity is a virulence factor for *Cryptococcus neoformans*. *Mol Microbiol* 39:166–175. <https://doi.org/10.1046/j.1365-2958.2001.02236.x>.
- Emmons CW. 1951. Isolation of *Cryptococcus neoformans* from soil. *J Bacteriol* 62:685–690. <https://doi.org/10.1128/JB.62.6.685-690.1951>.
- Emmons CW. 1955. Saprophytic sources of *Cryptococcus neoformans* associated with the pigeon (*Columba livia*). *Am J Hyg* 62:227–232. <https://doi.org/10.1093/oxfordjournals.aje.a119775>.
- Lazera MS, Salmito Cavalcanti MA, Londero AT, Trilles L, Nishikawa MM, Wanke B. 2000. Possible primary ecological niche of *Cryptococcus neoformans*. *Med Mycol* 38:379–383. <https://doi.org/10.1080/mmy.38.5.379.383>.
- Castro e Silva DM, Santos DCS, Martins MA, Oliveira L, Szesz MW, Melhem MSC. 2016. First isolation of *Cryptococcus neoformans* genotype VNI MAT-alpha from wood inside hollow trunks of *Hymenaea courbaril*. *Med Mycol* 54:97–102. <https://doi.org/10.1093/mmy/myv066>.
- Casadevall A, Fu MS, Guimaraes AJ, Albuquerque P. 2019. The ‘amoeboid predator-fungal animal virulence’ hypothesis. *J Fungi* 5:10. <https://doi.org/10.3390/jof5010010>.
- Novohradská S, Ferling I, Hillmann F. 2017. Exploring virulence determinants of filamentous fungal pathogens through interactions with soil amoebae. *Front Cell Infect Microbiol* 7:497. <https://doi.org/10.3389/fcimb.2017.00497>.
- Ophir T, Gutnick DL. 1994. A role for exopolysaccharides in the protection of microorganisms from desiccation. *Appl Environ Microbiol* 60:740–745. <https://doi.org/10.1128/AEM.60.2.740-745.1994>.
- Steenbergen JN, Shuman HA, Casadevall A. 2001. *Cryptococcus neoformans* interactions with amoebae suggest an explanation for its virulence and intracellular pathogenic strategy in macrophages. *Proc Natl Acad Sci U S A* 98:15245–15250. <https://doi.org/10.1073/pnas.261418798>.
- Jacobson ES, Emery HS. 1991. Catecholamine uptake, melanization, and oxygen toxicity in *Cryptococcus neoformans*. *J Bacteriol* 173:401–403. <https://doi.org/10.1128/jb.173.1.401-403.1991>.
- Wang Y, Aisen P, Casadevall A. 1995. *Cryptococcus neoformans* melanin and virulence: mechanism of action. *Infect Immun* 63:3131–3136. <https://doi.org/10.1128/IAI.63.8.3131-3136.1995>.
- Rosas ÁL, Casadevall A. 1997. Melanization affects susceptibility of *Cryptococcus neoformans* to heat and cold. *FEMS Microbiol Lett* 153:265–272. <https://doi.org/10.1111/j.1574-6968.1997.tb12584.x>.
- Wang Y, Casadevall A. 1994. Decreased susceptibility of melanized *Cryptococcus neoformans* to UV light. *Appl Environ Microbiol* 60:3864–3866. <https://doi.org/10.1128/AEM.60.10.3864-3866.1994>.
- Fu MS, Coelho C, De Leon-Rodriguez CM, Rossi DCP, Camacho E, Jung EH, Kulkarni M, Casadevall A. 2018. *Cryptococcus neoformans* urease affects the outcome of intracellular pathogenesis by modulating phagolysosomal pH. *PLoS Pathog Pathogens* 14:e1007144. <https://doi.org/10.1371/journal.ppat.1007144>.
- Casadevall A, Perfect JR. 1998. *Cryptococcus neoformans*. American Society of Microbiology, Washington, DC. <https://doi.org/10.1128/9781555818241>.
- Cirillo JD, Falkow S, Tompkins LS. 1994. Growth of *Legionella pneumophila* in *Acanthamoeba castellanii* enhances invasion. *Infect Immun* 62:3254–3261. <https://doi.org/10.1128/IAI.62.8.3254-3261.1994>.
- Cirillo JD, Falkow S, Tompkins LS, Bermudez LE. 1997. Interaction of *Mycobacterium avium* with environmental amoebae enhances virulence. *Infect Immun* 65:3759–3767. <https://doi.org/10.1128/IAI.65.9.3759-3767.1997>.
- Albuquerque P, Nicola AM, Magnabosco DAG, Derengowski LDS, Crisóstomo LS, Xavier LCG, Frazão SDO, Guilhelmelli F, de Oliveira MA, Dias JDN, Hurtado FA, Teixeira MDM, Guimarães AJ, Paes HC, Bagagli E, Felipe MSS, Casadevall A, Silva-Pereira I. 2019. A hidden battle in the dirt: soil amoebae interactions with *Paracoccidioides* spp. *PLoS Negl Trop Dis* 13:e0007742. <https://doi.org/10.1371/journal.pntd.0007742>.
- Davies B, Chattings LS, Edwards SW. 1991. Superoxide generation during phagocytosis by *Acanthamoeba castellanii*: similarities to the respiratory burst of immune phagocytes. *Microbiology* 137:705–710. <https://doi.org/10.1099/00221287-137-3-705>.
- Davies B, Edwards SW. 1991. Chemiluminescence and superoxide production in *Acanthamoeba castellanii*: free radicals generated during oxidative stress. *Microbiology* 137:1021–1027. <https://doi.org/10.1099/00221287-137-5-1021>.
- Allen PG, Dawidowicz EA. 1990. Phagocytosis in *Acanthamoeba*: I. A mannose receptor is responsible for the binding and phagocytosis of yeast. *J Cell Physiol* 145:508–513. <https://doi.org/10.1002/jcp.1041450317>.
- Allen PG, Dawidowicz EA. 1990. Phagocytosis in *Acanthamoeba*: II. Soluble and insoluble mannose-rich ligands stimulate phosphoinositide metabolism. *J Cell Physiol* 145:514–521. <https://doi.org/10.1002/jcp.1041450318>.
- Brown RC, Bass H, Coombs JP. 1975. Carbohydrate binding proteins involved in phagocytosis by *Acanthamoeba*. *Nature* 254:434–435. <https://doi.org/10.1038/254434a0>.
- Lock R, Öhman L, Dahlgren C. 1987. Phagocytic recognition mechanisms in human granulocytes and *Acanthamoeba castellanii* using type 1 fimbriated *Escherichia coli* as phagocytic prey. *FEMS Microbiol Lett* 44:135–140. <https://doi.org/10.1111/j.1574-6968.1987.tb02257.x>.

31. Gotthardt D, Warnatz HJ, Henschel O, Brückert F, Schleicher M, Soldati T. 2002. High-resolution dissection of phagosome maturation reveals distinct membrane trafficking phases. *Mol Biol Cell* 13:3508–3520. <https://doi.org/10.1091/mbc.e02-04-0206>.
32. Kwaik YA. 1996. The phagosome containing *Legionella pneumophila* within the protozoan *Hartmannella vermiformis* is surrounded by the rough endoplasmic reticulum. *Appl Environ Microbiol* 62:2022–2028.
33. Bozue JA, Johnson W. 1996. Interaction of *Legionella pneumophila* with *Acanthamoeba castellanii*: uptake by coiling phagocytosis and inhibition of phagosome-lysosome fusion. *Infect Immun* 64:6.
34. Horwitz MA. 1983. The Legionnaires' disease bacterium (*Legionella pneumophila*) inhibits phagosome-lysosome fusion in human monocytes. *J Exp Med* 158:2108–2126. <https://doi.org/10.1084/jem.158.6.2108>.
35. Horwitz MA, Silverstein SC. 1980. Legionnaires' disease bacterium (*Legionella pneumophila*) multiplies intracellularly in human monocytes. *J Clin Invest* 66:441–450. <https://doi.org/10.1172/JCI109874>.
36. Rowbotham TJ. 1980. Preliminary report on the pathogenicity of *Legionella pneumophila* for freshwater and soil amoebae. *J Clin Pathol* 33:1179–1183. <https://doi.org/10.1136/jcp.33.12.1179>.
37. Swanson MS, Isberg RR. 1995. Association of *Legionella pneumophila* with the macrophage endoplasmic reticulum. *Infect Immun* 63:3609–3620. <https://doi.org/10.1128/IAI.63.9.3609-3620.1995>.
38. Arico-Muendel C, Centrella PA, Contonio BD, Morgan BA, O'Donovan G, Paradise CL, Skinner SR, Sluboski B, Svendsen JL, White KF, Debnath A, Gut J, Wilson N, McKerrrow JH, DeRisi JL, Rosenthal PJ, Chiang PK. 2009. Antiparasitic activities of novel, orally available fumagillin analogs. *Bioorg Med Chem Lett* 19:5128–5131. <https://doi.org/10.1016/j.bmcl.2009.07.029>.
39. Steenbergen JN, Nosanchuk JD, Malliaris SD, Casadevall A. 2003. *Cryptococcus neoformans* virulence is enhanced after growth in the genetically malleable host *Dictyostelium discoideum*. *Infect Immun* 71:4862–4872. <https://doi.org/10.1128/iai.71.9.4862-4872.2003>.
40. Chrisman CJ, Albuquerque P, Guimaraes AJ, Nieves E, Casadevall A. 2011. Phospholipids trigger *Cryptococcus neoformans* capsular enlargement during interactions with amoebae and macrophages. *PLoS Pathog* 7:e1002047. <https://doi.org/10.1371/journal.ppat.1002047>.
41. Castellani A. 1930. An amoeba growing in cultures of a yeast I, II, III, IV. *Jour Trop Med Hyg* 33:160, 188–191, 221–222, 237.
42. Castellani A. 1955. [Phagocytic and destructive action of *Hartmannella castellanii* (*Amoeba castellanii*) on pathogenic encapsulated yeast-like fungi *Torulopsis neoformans* (*Cryptococcus neoformans*)]. *Ann Inst Pasteur (Paris)* 89:1–7. (In French)
43. Ruiz A, Neilson JB, Bulmer GS. 1982. Control of *Cryptococcus neoformans* in nature by biotic factors. *Sabouraudia* 20:21–29.
44. Garcia-Solache MA, Izquierdo-Garcia D, Smith C, Bergman A, Casadevall A. 2013. Fungal virulence in a lepidopteran model is an emergent property with deterministic features. *mBio* 4:e00100-13–e00113. <https://doi.org/10.1128/mBio.00100-13>.
45. Fu MS, Casadevall A. 2017. Divalent metal cations potentiate the predatory capacity of amoeba for *Cryptococcus neoformans*. *Appl Environ Microbiol* 84:e01717-17. <https://doi.org/10.1128/AEM.01717-17>.
46. Chrisman CJ, Alvarez M, Casadevall A. 2010. Phagocytosis of *Cryptococcus neoformans* by, and nonlytic exocytosis from, *Acanthamoeba castellanii*. *Appl Environ Microbiol* 76:6056–6062. <https://doi.org/10.1128/AEM.00812-10>.
47. Watkins RA, Andrews A, Wynn C, Barisch C, King JS, Johnston SA. 2018. *Cryptococcus neoformans* escape from *Dictyostelium* amoeba by both WASH-mediated constitutive exocytosis and vomocytosis. *Front Cell Infect Microbiol* 8:108. <https://doi.org/10.3389/fcimb.2018.00108>.
48. Derengowski LDS, Paes HC, Albuquerque P, Tavares AHFP, Fernandes L, Silva-Pereira I, Casadevall A. 2013. The transcriptional response of *Cryptococcus neoformans* to ingestion by *Acanthamoeba castellanii* and macrophages provides insights into the evolutionary adaptation to the mammalian host. *Eukaryot Cell* 12:761–774. <https://doi.org/10.1128/EC.00073-13>.
49. Litvintseva AP, Mitchell TG. 2009. Most environmental isolates of *Cryptococcus neoformans* var. *grubii* (serotype A) are not lethal for mice. *Infect Immun* 77:3188–3195. <https://doi.org/10.1128/IAI.00296-09>.
50. Litvintseva AP, Thakur R, Vilgalys R, Mitchell TG. 2006. Multilocus sequence typing reveals three genetic subpopulations of *Cryptococcus neoformans* var. *grubii* (serotype A), including a unique population in Botswana. *Genetics* 172:2223–2238. <https://doi.org/10.1534/genetics.105.046672>.
51. Chen Y, Litvintseva AP, Frazzitta AE, Haverkamp MR, Wang L, Fang C, Muthoga C, Mitchell TG, Perfect JR. 2015. Comparative analyses of clinical and environmental populations of *Cryptococcus neoformans* in Botswana. *Mol Ecol* 24:3559–3571. <https://doi.org/10.1111/mec.13260>.
52. Okagaki LH, Strain AK, Nielsen JN, Charlier C, Baltes NJ, Chrétien F, Heitman J, Dromer F, Nielsen K. 2010. Cryptococcal cell morphology affects host cell interactions and pathogenicity. *PLoS Pathog* 6:e1000953. <https://doi.org/10.1371/journal.ppat.1000953>.
53. Zaragoza O, García-Rodas R, Nosanchuk JD, Cuenca-Estrella M, Rodríguez-Tudela JL, Casadevall A. 2010. Fungal cell gigantism during mammalian infection. *PLoS Pathog* 6:e1000945. <https://doi.org/10.1371/journal.ppat.1000945>.
54. Okagaki LH, Nielsen K. 2012. Titan cells confer protection from phagocytosis in *Cryptococcus neoformans* infections. *Eukaryot Cell* 11:820–826. <https://doi.org/10.1128/EC.00121-12>.
55. Magditch DA, Liu T-B, Xue C, Idnurm A. 2012. DNA mutations mediate microevolution between host-adapted forms of the pathogenic fungus *Cryptococcus neoformans*. *PLoS Pathog* 8:e1002936. <https://doi.org/10.1371/journal.ppat.1002936>.
56. Homer CM, Summers DK, Goranov AI, Clarke SC, Wiesner DL, Diedrich JK, Moresco JJ, Toffaletti D, Upadhyay R, Caradonna I, Petnic S, Pessino V, Cuomo CA, Lodge JK, Perfect J, Yates JR, Nielsen K, Craik CS, Madhani HD. 2016. Intracellular action of a secreted peptide required for fungal virulence. *Cell Host Microbe* 19:849–864. <https://doi.org/10.1016/j.chom.2016.05.001>.
57. Choi J, Vogl AW, Kronstad JW. 2012. Regulated expression of cyclic AMP-dependent protein kinase A reveals an influence on cell size and the secretion of virulence factors in *Cryptococcus neoformans*. *Mol Microbiol* 85:700–715. <https://doi.org/10.1111/j.1365-2958.2012.08134.x>.
58. Lee K-T, So Y-S, Yang D-H, Jung K-W, Choi J, Lee D-G, Kwon H, Jang J, Wang LL, Cha S, Meyers GL, Jeong E, Jin J-H, Lee Y, Hong J, Bang S, Ji J-H, Park G, Byun H-J, Park SW, Park Y-M, Adedoyin G, Kim T, Averette AF, Choi J-S, Heitman J, Cheong E, Lee Y-H, Bahn Y-S. 2016. Systematic functional analysis of kinases in the fungal pathogen *Cryptococcus neoformans*. *Nat Commun* 7:12766. <https://doi.org/10.1038/ncomms12766>.
59. Gerstein AC, Fu MS, Mukaremera L, Li Z, Ormerod KL, Fraser JA, Berman J, Nielsen K. 2015. Polyploid titan cells produce haploid and aneuploid progeny to promote stress adaptation. *mBio* 6:e01340-15. <https://doi.org/10.1128/mBio.01340-15>.
60. Sionov E, Lee H, Chang YC, Kwon-Chung KJ. 2010. *Cryptococcus neoformans* overcomes stress of azole drugs by formation of disomy in specific multiple chromosomes. *PLoS Pathog* 6:e1000848. <https://doi.org/10.1371/journal.ppat.1000848>.
61. Anderson CA, Roberts S, Zhang H, Kelly CM, Kendall A, Lee C, Gerstenberger J, Koenig AB, Kabeche R, Gladfelter AS. 2015. Ploidy variation in multinucleate cells changes under stress. *Mol Biol Cell* 26:1129–1140. <https://doi.org/10.1091/mbc.E14-09-1375>.
62. De Leon-Rodríguez CM, Rossi DCP, Fu MS, Dragotakes Q, Coelho C, Guerrero Ros I, Caballero B, Nolan SJ, Casadevall A. 2018. The outcome of the *Cryptococcus neoformans*-macrophage interaction depends on phagolysosomal membrane integrity. *J Immunol* 201:583–603. <https://doi.org/10.4049/jimmunol.1700958>.
63. García-Rodas R, Cordero RJB, Trevijano-Contador N, Janbon G, Moyrand F, Casadevall A, Zaragoza O. 2014. Capsule growth in *Cryptococcus neoformans* is coordinated with cell cycle progression. *mBio* 5:e00945-14. <https://doi.org/10.1128/mBio.00945-14>.
64. D'Souza CA, Alspaugh JA, Yue C, Harashima T, Cox GM, Perfect JR, Heitman J. 2001. Cyclic AMP-dependent protein kinase controls virulence of the fungal pathogen *Cryptococcus neoformans*. *Mol Cell Biol* 21:3179–3191. <https://doi.org/10.1128/MCB.21.9.3179-3191.2001>.
65. Beenhouwer DO, Shapiro S, Feldmesser M, Casadevall A, Scharff MD. 2001. Both Th1 and Th2 cytokines affect the ability of monoclonal antibodies to protect mice against *Cryptococcus neoformans*. *Infect Immun* 69:6445–6455. <https://doi.org/10.1128/IAI.69.10.6445-6455.2001>.
66. Van Waeyenberghe L, Baré J, Pasmans F, Claeys M, Bert W, Haesebrouck F, Houf K, Martel A. 2013. Interaction of *Aspergillus fumigatus* conidia with *Acanthamoeba castellanii* parallels macrophage-fungus interactions. *Environ Microbiol Rep* 5:819–824. <https://doi.org/10.1111/1758-2229.12082>.
67. Neilson JB, Ivey MH, Bulmer GS. 1978. *Cryptococcus neoformans*: pseudohyphal forms surviving culture with *Acanthamoeba polyphaga*. *Infect Immun* 20:262–266. <https://doi.org/10.1128/IAI.20.1.262-266.1978>.
68. Radosa S, Ferling I, Sprague JL, Westermann M, Hillmann F. 2019. The different morphologies of yeast and filamentous fungi trigger distinct killing and feeding mechanisms in a fungivorous amoeba. *Environ Microbiol* 21:1809–1820. <https://doi.org/10.1111/1462-2920.14588>.
69. Billmyre RB, Clancey SA, Heitman J. 2017. Natural mismatch repair mutations mediate phenotypic diversity and drug resistance in *Cryptococcus deuterogattii*. *Elife* 6:e28802. <https://doi.org/10.7554/eLife.28802>.

70. Leippe M, Ebel S, Schoenberger OL, Horstmann RD, Müller-Eberhard HJ. 1991. Pore-forming peptide of pathogenic *Entamoeba histolytica*. Proc Natl Acad Sci U S A 88:7659–7663. <https://doi.org/10.1073/pnas.88.17.7659>.
71. Desjardins CA, Giamberardino C, Sykes SM, Yu C-H, Tenor JL, Chen Y, Yang T, Jones AM, Sun S, Haverkamp MR, Heitman J, Litvintseva AP, Perfect JR, Cuomo CA. 2017. Population genomics and the evolution of virulence in the fungal pathogen *Cryptococcus neoformans*. Genome Res 27:1207–1219. <https://doi.org/10.1101/gr.218727.116>.
72. Ormerod KL, Morrow CA, Chow EWL, Lee IR, Arras SDM, Schirra HJ, Cox GM, Fries BC, Fraser JA. 2013. Comparative genomics of serial isolates of *Cryptococcus neoformans* reveals gene associated with carbon utilization and virulence. G3 (Bethesda) 3:675–686. <https://doi.org/10.1534/g3.113.005660>.
73. Hommel B, Mukaremera L, Cordero RJB, Coelho C, Desjardins CA, Sturny-Leclère A, Janbon G, Perfect JR, Fraser JA, Casadevall A, Cuomo CA, Dromer F, Nielsen K, Alanio A. 2018. Titan cells formation in *Cryptococcus neoformans* is finely tuned by environmental conditions and modulated by positive and negative genetic regulators. PLoS Pathog 14:e1006982. <https://doi.org/10.1371/journal.ppat.1006982>.
74. Torres EM, Sokolsky T, Tucker CM, Chan LY, Boselli M, Dunham MJ, Amon A. 2007. Effects of aneuploidy on cellular physiology and cell division in haploid yeast. Science 317:916–924. <https://doi.org/10.1126/science.1142210>.
75. Rancati G, Pavelka N, Fleharty B, Noll A, Trimble R, Walton K, Perera A, Staehling-Hampton K, Seidel CW, Li R. 2008. Aneuploidy underlies rapid adaptive evolution of yeast cells deprived of a conserved cytokinesis motor. Cell 135:879–893. <https://doi.org/10.1016/j.cell.2008.09.039>.
76. Pavelka N, Rancati G, Zhu J, Bradford WD, Saraf A, Florens L, Sanderson BW, Hattem GL, Li R. 2010. Aneuploidy confers quantitative proteome changes and phenotypic variation in budding yeast. Nature 468:321–325. <https://doi.org/10.1038/nature09529>.
77. Selmecki A, Forche A, Berman J. 2006. Aneuploidy and isochromosome formation in drug-resistant *Candida albicans*. Science 313:367–370. <https://doi.org/10.1126/science.1128242>.
78. Selmecki A, Gerami-Nejad M, Paulson C, Forche A, Berman J. 2008. An isochromosome confers drug resistance *in vivo* by amplification of two genes, *ERG11* and *TAC1*. Mol Microbiol 68:624–641. <https://doi.org/10.1111/j.1365-2958.2008.06176.x>.
79. Sunshine AB, Payen C, Ong GT, Liachko I, Tan KM, Dunham MJ. 2015. The fitness consequences of aneuploidy are driven by condition-dependent gene effects. PLoS Biol 13:e1002155. <https://doi.org/10.1371/journal.pbio.1002155>.
80. Lin J, Idnurm A, Lin X. 2015. Morphology and its underlying genetic regulation impact the interaction between *Cryptococcus neoformans* and its hosts. Med Mycol 53:493–504. <https://doi.org/10.1093/mmy/myv012>.
81. Walton FJ, Heitman J, Idnurm A. 2006. Conserved elements of the RAM signaling pathway establish cell polarity in the basidiomycete *Cryptococcus neoformans* in a divergent fashion from other fungi. Mol Biol Cell 17:3768–3780. <https://doi.org/10.1091/mbc.e06-02-0125>.
82. Thomson DD, Berman J, Brand AC. 2016. High frame-rate resolution of cell division during *Candida albicans* filamentation. Fungal Genet Biol 88:54–58. <https://doi.org/10.1016/j.fgb.2016.02.001>.
83. Gonçalves D, d S, Ferreira M, d S, Gomes KX, Rodríguez-de La Noval C, Liedke SC, da Costa GCV, Albuquerque P, Cortines JR, Saramago Peralta RH, Peralta JM, Casadevall A, Guimarães AJ. 2019. Unravelling the interactions of the environmental host *Acanthamoeba castellanii* with fungi through the recognition by mannose-binding proteins. Cell Microbiol 21:e13066. <https://doi.org/10.1111/cmi.13066>.
84. Casadevall A. 2017. The pathogenic potential of a microbe. mSphere 2:e00015-17. <https://doi.org/10.1128/mSphere.00015-17>.
85. Casadevall A, Pirofski L. 2001. Host-pathogen interactions: the attributes of virulence. J Infect Dis 184:337–344. <https://doi.org/10.1086/322044>.
86. Fernandez KE, Brockway A, Haverkamp M, Cuomo CA, van Ogtrop F, Perfect JR, Carter DA. 2018. Phenotypic variability correlates with clinical outcome in *Cryptococcus* isolates obtained from Botswana HIV/AIDS patients. mBio 9:e02016-18. <https://doi.org/10.1128/mBio.02016-18>.
87. Chen Y, Farrer RA, Giamberardino C, Sakthikumar S, Jones A, Yang T, Tenor JL, Wagih O, Van Wyk M, Govender NP, Mitchell TG, Litvintseva AP, Cuomo CA, Perfect JR. 2017. Microevolution of serial clinical isolates of *Cryptococcus neoformans* var. *grubii* and *C. gattii*. mBio 8:e00166-17. <https://doi.org/10.1128/mBio.00166-17>.
88. Dragotakes Q, Stouffer KM, Fu MS, Sella Y, Youn C, Yoon OI, De Leon-Rodriguez CM, Freij JB, Bergman A, Casadevall A. 2020. Macrophages use a bet-hedging strategy for antimicrobial activity in phagolysosomal acidification. J Clin Invest 130:3805–3819. <https://doi.org/10.1172/JCI133938>.
89. Blasi E, Brozzetti A, Francisci D, Neglia R, Cardinali G, Bistoni F, Vidotto V, Baldelli F. 2001. Evidence of microevolution in a clinical case of recurrent *Cryptococcus neoformans* meningoencephalitis. Eur J Clin Microbiol Infect Dis 20:535–543. <https://doi.org/10.1007/s100960100549>.
90. Sullivan D, Haynes K, Moran G, Shanley D, Coleman D. 1996. Persistence, replacement, and microevolution of *Cryptococcus neoformans* strains in recurrent meningitis in AIDS patients. J Clin Microbiol 34:1739–1744. <https://doi.org/10.1128/JCM.34.7.1739-1744.1996>.
91. Chang YC, Khanal Lamichhane A, Kwon-Chung KJ. 2018. *Cryptococcus neoformans*, unlike *Candida albicans*, forms aneuploid clones directly from uninucleated cells under fluconazole stress. mBio 9:e01290-18. <https://doi.org/10.1128/mBio.01290-18>.
92. Roberts GD, Horstmeier CD, Land GA, Foxworth JH. 1978. Rapid urea broth test for yeasts. J Clin Microbiol 7:584–588.
93. Kwon-Chung KJ, Wickes BL, Booth JL, Vishniac HS, Bennett JE. 1987. Urease inhibition by EDTA in the two varieties of *Cryptococcus neoformans*. Infect Immun 55:1751–1754. <https://doi.org/10.1128/IAI.55.8.1751-1754.1987>.
94. Velegraki A, Kambouris M, Kostourou A, Chalevelakis G, Legakis NJ. 1999. Rapid extraction of fungal DNA from clinical samples for PCR amplification. Med Mycol 37:69–73. <https://doi.org/10.1046/j.1365-280X.1999.00193.x>.
95. Janbon G, Ormerod KL, Paulet D, Byrnes EJ, Yadav V, Chatterjee G, Mullanpudi N, Hon C-C, Billmyre RB, Brunel F, Bahn Y-S, Chen W, Chen Y, Chow EWL, Coppée J-Y, Floyd-Averette A, Gaillardin C, Gerik KJ, Goldberg J, Gonzalez-Hilarion S, Gujja S, Hamlin JL, Hsueh Y-P, Ianiri G, Jones S, Kodira CD, Kozubowski L, Lam W, Marra M, Mesner LD, Mieczkowski PA, Moyrand F, Nielsen K, Proux C, Rossignol T, Schein JE, Sun S, Wollschlaeger C, Wood IA, Zeng Q, Neuvéglise C, Newlon CS, Perfect JR, Lodge JK, Idnurm A, Stajich JE, Kronstad JW, Sanyal K, Heitman J, Fraser JA, et al. 2014. Analysis of the genome and transcriptome of *Cryptococcus neoformans* var. *grubii* reveals complex RNA expression and microevolution leading to virulence attenuation. PLoS Genet 10:e1004261. <https://doi.org/10.1371/journal.pgen.1004261>.
96. Li H. 2013. Aligning sequence reads, clone sequences and assembly contigs with BWA-MEM. arXiv 13033997 [q-bio.GN]. <http://arXiv.org/abs/1303.3997>.
97. McKenna A, Hanna M, Banks E, Sivachenko A, Cibulskis K, Kernytsky A, Garimella K, Altshuler D, Gabriel S, Daly M, DePristo MA. 2010. The Genome Analysis Toolkit: a MapReduce framework for analyzing next-generation DNA sequencing data. Genome Res 20:1297–1303. <https://doi.org/10.1101/gr.107524.110>.
98. Cingolani P, Platts A, Wang LL, Coon M, Nguyen T, Wang L, Land SJ, Lu X, Ruden DM. 2012. A program for annotating and predicting the effects of single nucleotide polymorphisms, SnpEff: SNPs in the genome of *Drosophila melanogaster* strain w1118; iso-2; iso-3. Fly (Austin) 6:80–92. <https://doi.org/10.4161/fly.19695>.